COST STUDIES OF MULTIPURPOSE LARGE LAUNCH VEHICLES
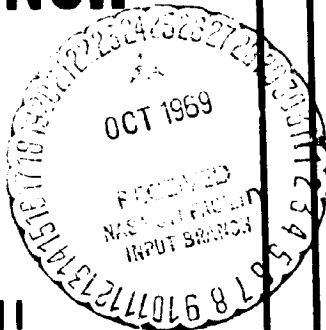
OCT 1969

RECEIVED
NASA STI FACILITY
INPUT BRANCH

VOLUME II

HALF SIZE (MLLV)

CONCEPTUAL DESIGN

NASA

FINAL REPORT

SEPTEMBER 15, 1969

FINAL REPORT
FOR
COST STUDIES OF MULTIPURPOSE
LARGE LAUNCH VEHICLES

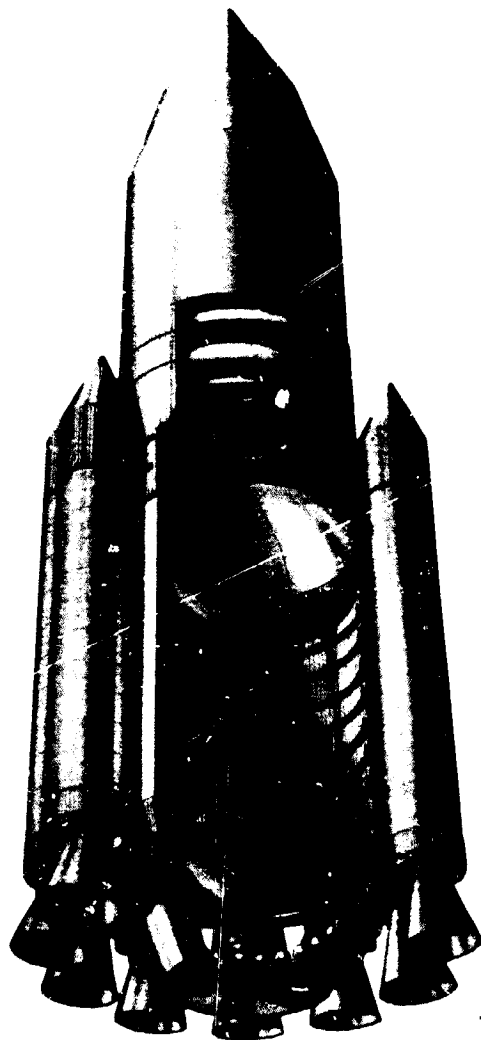
VOLUME II
HALF SIZE VEHICLE (MLLV) CONCEPTUAL DESIGN

PREPARED UNDER CONTRACT NAS2-5056
FOR
NATIONAL AERONAUTICS AND SPACE ADMINISTRATION
OFFICE OF ADVANCE RESEARCH AND TECHNOLOGY
MISSION ANALYSIS DIVISION

PREPARED BY

CHARLES J. CORSO

APPROVED BY

JOSEPH W. MONROE

THE BOEING COMPANY
SOUTHEAST DIVISION
HUNTSVILLE OPERATION
HUNTSVILLE, ALABAMA

ABSTRACT

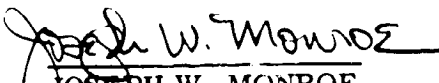Nine volumes including this volume present the final report documentation
outlining the accomplishments for the "Cost Studies of the Multipurpose Large
Launch Vehicles" (MLLV), NASA/OART Contract NAS2-5056. This volume
presents the Multipurpose Large Launch Vehicle (MLLV) design trades, ground
and flight environments and the baseline vehicle design.

The MLLV family will consist of a single-stage-to-orbit configuration plus
other configurations consisting of a main stage (as used for the single-stage-to-
orbit configuration) with various quantities of 260 inch diameter solid rocket
motor (SRM) strap-on stages and/or injection stage modules. The main stage
will employ LOX/LH$_2$ propellant with either a multichamber/plug or toroidal/
aerospike engine system. The single-stage-to-orbit configuration will have a
payload capability of approximately 500,000 pounds to a 100 nautical mile earth
orbit. With the addition of the strap-on SRM stages and/or LOX/LH$_2$ injection
stage modules, this payload capability can be increased incrementally to as
much as 1,850,000 pounds.

The contract consisted of four study phases. The Phase I activity was a detailed
cost analysis of an Advanced Multipurpose Large Launch Vehicle (AMLLV)
family as previously defined in NASA/OART Contract NAS2-4079. Costs for
vehicle design, test, transportation, manufacture and launch were defined.
Resource implications for the AMLLV configurations were determined to support
the cost analysis.

The Phase II study activity consisted of the conceptual design and resource analysis
of a smaller or half size Multipurpose Large Launch Vehicle (MLLV) family.

The Phase III activity consisted of a detailed cost analysis of the smaller
Multipurpose Large Launch Vehicle configurations as defined in Phase II. Costs
for vehicle design, test, transportation, manufacture and launch were determined.

The Phase IV activity assessed the results of the study including the implications
on performance, resources and cost of vehicle size, program options, and vehicle
configuration options. The study results provided data in sufficient depth to
permit analysis of the cost/performance potential of the various options and/or
advanced technologies.

ABSTRACT (Continued)

KEY WORDS

Advanced Multipurpose Large Launch Vehicles (AMLLV)

Half Size Multipurpose Large Launch Vehicles (MLLV)

Single-Stage-to-Orbit

Multichamber/Plug Engine System

Toroidal/Aerospike Engine System

260 Inch Solid Propellant Rocket Motor (SRM)

Orbital Injection Stage

Contract NAS2-4079

Contract NAS''-5056

Payload to 100 NM Orbit

Cost

Resources

Zero Stage Vehicles

Parallel Stage Vehicles

Main Stage Throttling

iv

TABLE OF CONTENTS

CONTENTS (Continued)

CONTENTS (Continued)

vii

FOREWORD

This volume, Half-Size Vehicle (MLLV) Conceptual Design, is one of nine volumes documenting the results of a twelve month study program "Cost Studies of Multi-purpose Large Launch Vehicles" NASA/OART Contract NAS2-5056. The objective of this study was to define cost, cost sensitivities, and cost/size sensitivities of potential future launch vehicles to aid in the guidance of current and future technology programs. The baseline vehicles utilized to make this assessment were:

1. The Advanced Multipurpose Large Launch Vehicles (AMLLV) as defined under NASA/OART Contract NAS2-4079.

2. The Multipurpose Large Launch Vehicles (MLLV) as defined under this contract and described in this volume, "Half Size Vehicle (MLLV) Conceptual Design".

The program documentation includes this Design Volume, plus a Summary Volume, a Resources Volume, Cost Volumes, Cost Implications Volume, Advanced Technology Implications Volume, and Appendices Volumes. Individual designations for these volumes are as follows:

Volume I	Summary
Volume II	Half Size Vehicle (MLLV) Conceptual Design
Volume III	Resource Implications
Volume IV	Baseline AMLLV Costs
Volume V	Baseline MLLV Costs
Volume VI	Cost Implications of Vehicle Size, Technology Configurations, and Program Options
Volume VII	Advanced Technology Implications
Volume VIII	Flight Control and Separation, and Stress Analysis (Unclassified Appendices)
Volume IX	Propulsion Data and Trajectories (Classified Appendices)

Data on the 260 inch diameter solid propellant rocket motor were obtained from the Aerojet General Corporation. Data on the multichamber/plug propulsion system were obtained from the Pratt and Whitney Division of the United Aircraft Corporation and the Rocketdyne Division of the North American Rockwell Corporation. Data on

FOREWORD (Continued)

the toroidal/aerospike propulsion system were obtained from the Rocketdyne
Division of the North American Rockwell Corporation.

These propulsion data were obtained from the propulsion contractors at no cost
to the contract. The material received encompassed not only the technical data,
but resources, schedules cost and advanced technology information. This support
materially aided The Boeing Company in the preparation of a complete and
meaningful study and is gratefully acknowledged.

This study was administered under the direction of NASA/OART Mission Analysis
Division, Ames Research Center, Moffett Field, California under the direction
of the technical monitor, Mr. Edward W. Gomersall.

1.0 INTRODUCTION

Manned planetary space missions, extended lunar exploration, and large orbital space stations are potential future space activities. These activities may require uprating of existing launch systems or development of new launch systems. Under the auspices of NASA/OART, studies have been and are currently being conducted to develop large launch vehicle configuration concepts. The purpose of these efforts is to provide effective data and trade-offs for guidance of on-going technology programs and for planning of future launch vehicle developments.

A previous study for the National Aeronautics and Space Administration on Contract NAS2-4079, "Advanced Multipurpose Large Launch Vehicles, (AMLLV)" defined an attractive large launch vehicle family in terms of performance and payload capability. (See Reference 1.0.0.0-1.) The overall attractiveness of the design concepts were not, however, assessed in terms of their economic potential. Economic analyses were required to assure that the technological advantages can justify the required expenditures.

The objectives of this study, "Cost Studies of Multipurpose Large Launch Vehicles (NAS2-5056), were to define costs, cost sensitivities and cost/size sensitivities such that with both technological and economic aspects determined, NASA will be better able to identify additional technology needs and to effectively guide current and future technology programs. To meet these objectives, the study activity was directed to provide the following results:

a. Cost for development, procurement and operation of the <u>baseline</u> (AMLLV) vehicle family as defined by the aforementioned NAS2-4079. (Note: This prior contract is hereinafter referred to as the reference contract.)

b. Conceptual design, resource implications and cost for development, procurement and operation of a similar half size vehicle (MLLV) family.

c. The relationship of cost to overall system size.

d. Cost-effectiveness of program and feasible configuration options.

e. Cost-effectiveness of advanced technology applications to the vehicle systems.

f. Modularized cost data and methodology which can be applied to assess varying future space program philosophy and/or options

---

Reference: 1.0.0.0-1 - NAS CR 73154, "Study of Advanced Multipurpose Large Launch Vehicles", The Boeing Company, January 1968.

1

1.1 STUDY PHASING

Figure 1.1.0.0-1 shows the study logic and the relationship of the four phases of the study.

The Phase I activity, Detailed Cost Analyses of the previously defined (AMLLV) Vehicle family, was divided into three tasks:

Task I - Non-recurring and recurring costs for implementation and launch of the baseline (AMLLV) vehicle family (See Volume IV).

Task II - Cost effectiveness of configuration and program options considering all potential operational combinations of the elements of the baseline vehicle family, its configuration options and the effects of the overall quantity of vehicles produced (number of operational vehicles required to effectively amortize development costs). (See Volume VI.)

Task III - Cost sensitivity to alternative, operational or advanced technology applications. (See Volume VI.)

The Phase II activity, Half Size (MLLV) Vehicle Conceptual Design and Resources Implications, was divided into two tasks:

Task I - Conceptual vehicle design - Design and performance trades of design concepts for selection of a baseline MLLV vehicle family for follow-on study. The half-size (MLLV) vehicle is similar in concept to that defined by the reference contract except for those changes necessary to provide the effective half size (i.e., one half the AMLLV payload) configuration. (See Section 4.1 of this Volume).

Task II - Design, resource and technology data for the baseline (MLLV) vehicle, include:

1. Flight environment and performance (See Section 4.2 of this volume).

2. Basic design features and attractive configuration alternatives (See Section 4.3 of this volume).

3. Required development, manufacturing, and operational resources (See Volume III).

4. An assessment of the technologies required to develop the systems (See Volume VII).

2
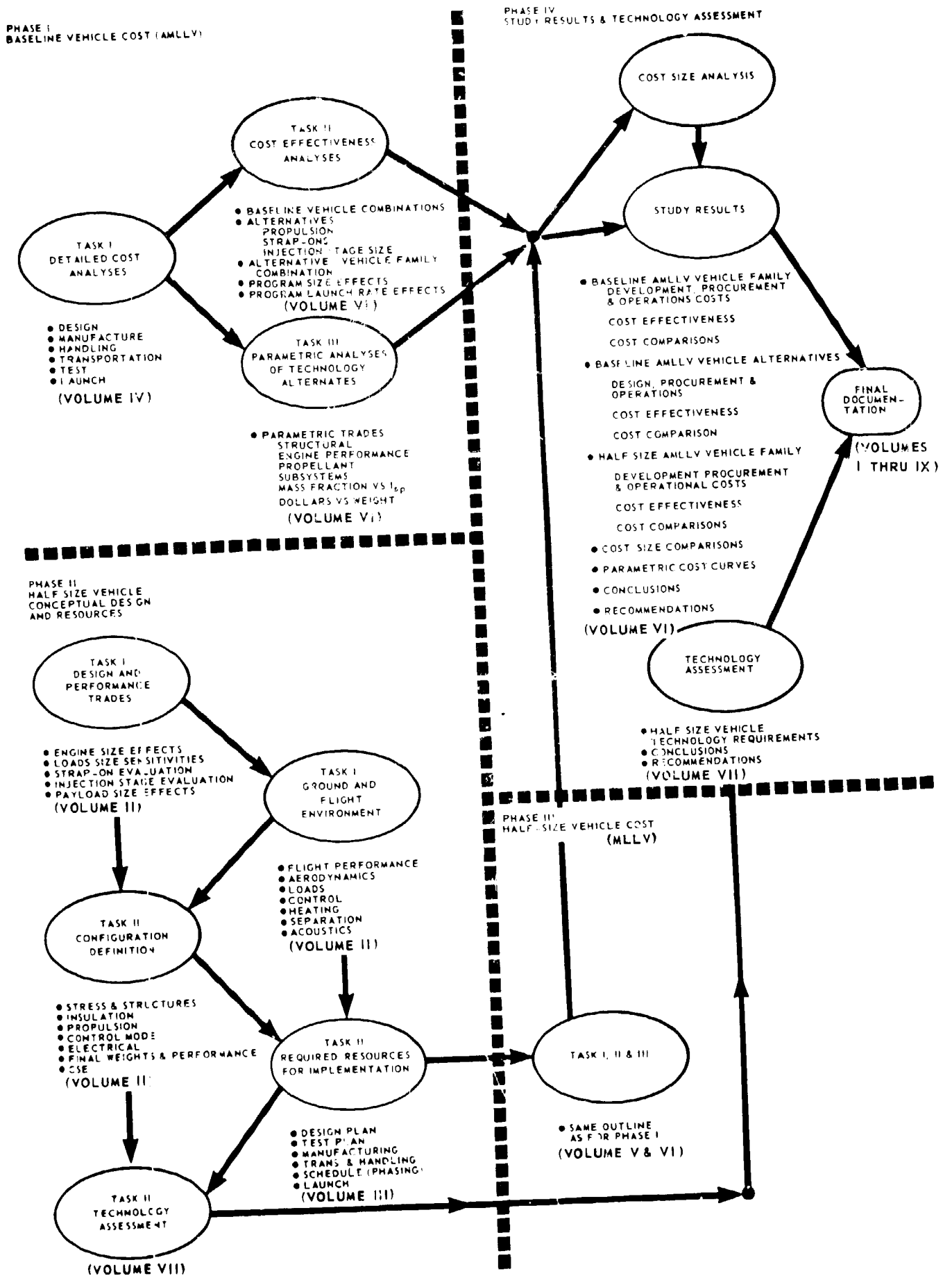
FIGURE 1.1.0.0-1 STUDY LOGIC AND PHASING

3

1.1   (Continued)

The Phase III activity, Detailed Cost Analyses of the Half Size (MLLV) Vehicle Family consisted of the same three tasks as outlined for Phase I above. (This phase is reported in Volume V.)

The Phase IV activity correlated and compared the results of Phases I through III to define the cost/size relationships and technology implications for multi-purpose large launch vehicle families. The configuration alternatives and relative cost-effectiveness as defined in the prior phases were reviewed and significant conclusions noted. Similarly the impact of advanced technologies as applied to both systems was investigated. Where indicated, recommendations were made regarding specific technology advancements which can improve the cost/performance potential of these vehicles for future space programs. (This phase is reported in Volume VI.)

1.2   BASELINE AMLLV VEHICLE FAMILY

The baseline AMLLV vehicle family, costed in Phase I, is illustrated in Figure 1.2.0.0-1. Four representative configurations for the overall vehicle family are shown. A total of twenty six configurations can be developed from the main stage, injection stage modules, and strap-on stages to provide a range of payload capability, for the 100 nautical mile earth orbit mission, from one million to 3.74 million pounds.

The AMLLV main stage, sized to orbit one million pounds to low Earth orbit, has 16.0 million pounds of sea level thrust (provided by either a toroidal/aero-spike or a multichamber/plug engine system) with 11.1 million pounds of propellant. The main stage inert weight (stage drop weight) of 634,000 pounds will result in a stage mass fraction of approximately 0.946 (numbers quoted are for the toroidal/aerospike main stage). The structure will principally employ conventional skin-stringer-frame construction using 2219-T87 aluminum for the propellant tanks and 7075-T6 aluminum for the forward skirt and thrust structure. The design has a forward LOX tank separated from the LH_2 tank by a common bulkhead of sandwich aluminum construction. The thrust skirt, bulkheads and tank walls are designed for the "worst condition" load envelope of the overall vehicle family. The forward skirt will be used for vehicle support and/or solid motor thrust take-out. The forward skirt will, therefore, be subjected to a significant range of loads for the various configurations of the vehicle family (from 4,000 pounds to 16,000 pounds per inch), two interchangeable forward skirts will be provided to minimize the weight penalties. A light-weight forward skirt assembly will be provided for configurations without strap-ons and a heavier skirt assembly will be used with the strap-on configurations. Vehicle control will be provided by tilting the hinged multichamber/plug engine system modules or by a LOX injection system for the toroidal/aerospike engine system. Roll control will be provided by deflection of the turbo-pump exhaust

4

GROSS PAYLOAD ≈ 1.0M LBS. WITH EITHER PROPULSION SYSTEM

LIGHT WEIGHT SKIRT

T_O = 16M LBS.
T/W = 1.25
W_O = 12.8M LBS.
W_P TOTAL = 11.1M LBS.

MULTICHAMBER/PLUG

PRATT & WHITNEY HIGH PRESSURE WITH HINGED MODULES
λ' = .94

OR

TOROIDAL AEROSPIKE

ROCKETDYNE
P_C = 2000 PSI
λ' = .946

GROSS PAYLOAD = 1.18 M LBS.

T/W_O = 1.18
LIGHT WEIGHT SKIRT

INJECTION STAGE

$W_{I.S.}$ = 550,000 LBS.
W_P = 450,000 LBS.
$\lambda'_{I.S.}$ = .82
THRUST = 500K LBS. (2 ENGINES)
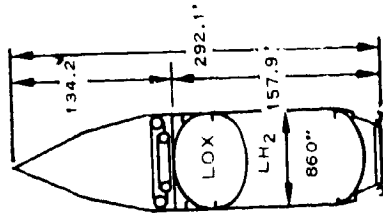
GROSS PAYLOAD - 3.52 M LBS. (12 STRAP-ONS)

HEAVY WEIGHT SKIRT

W_O = 15.36 M LBS.

260" STRAP-ONS λ's = .90
(INCL. STAGE COMPONENTS)

NO.	W_F (M LBS.)	T_O (M LBS.)	T_O/W_O
12	45.7	108	1.63
8	30.5	72	1.49
4	15.2	36	1.18

260" MOTOR PERFORMANCE (EACH)
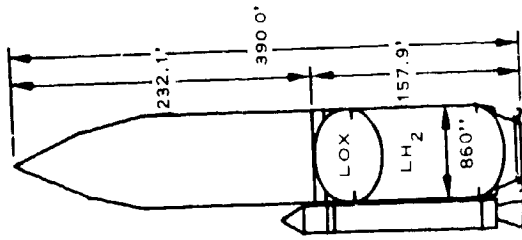
W_P = 3.81 M LBS.
F = 9.0 M LBS.

GROSS PAYLOAD - 3.74 M LBS.

HEAVY WEIGHT SKIRT

STRAP-ON MOTORS λ's = .90

NO	W_P	T	T_O/W_O
12	45.7M	108M	1.59

INJECTION STAGE

$W_{I.S.}$ = 1.614 M LBS.
W_P = 1.350 M LBS.
$\lambda'_{I.S.}$ = .87
T = 1.50 M LBS. (6 ENGINES)

CORE VEHICLE

CORE + INJECTION STAGE
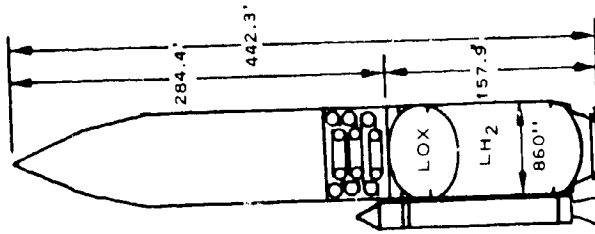
CORE + STRAP-ON'S

CORE + STRAP-ON'S + INJECTION STAGE

* ALL PAYLOADS SHOWN FOR ρ = 5 LBS/FT³ 100 NAUTICAL MILE CIRCULAR ORBIT

FIGURE 1.2.0.0-1 ADVANCED MULTIPURPOSE LARGE LAUNCH VEHICLE BASELINE FAMILY

1.2   (Continued)

(toroidal/aerospike) or by deflection of the base plug gas generator exhaust (multichamber/plug).

The main stage can be augmented with either solid or liquid propulsion strap-on stages. The AMLLV baseline family, as shown, will use from two to twelve strap-on 260-inch solid motors having 9,000,000 pounds of thrust and 3,810,000 pounds of propellant each (with a fifty percent regressive thrust-time trace). A zero stage flight mode (i.e., the solid motors burn as a first stage with the main stage igniting during solid motor tailoff) will provide the maximum payload and minimum flight load conditions as compared to parallel burn flight mode where the main stage and the strap-on stages operate together. (This applies to all configurations except the configuration employing two strap-on stages. The solid thrust for this configuration is too low for lift-off and, therefore, necessitates a parallel burn launch mode).

To minimize the side wall structural increase for strap-on configurations, solid motor thrust will be reacted in the forward skirt rather than in the aft thrust structure. Other weight penalties associated with the use of the strap-on stages, such as thicker tank skins to contain the higher fluid pressures, are independent of the attachment concept used.

Injection stage modules, to provide payload versatility and reduce configuration sensitivities, can be used with both the main stage and the main stage plus strap-on configurations. The modules will each have 450,000 pounds of LOX/LH$_2$ propellant contained within the toroidal propellant tanks and will have extendible nozzle high-pressure bell engines. The design is flexible as it has modular capability where additional propellant tank modules can be stacked with additional engines mounted to the lower module thrust beam. Two 250,000 pound-thrust engines will be provided for each module. Mass fractions of 0.82 and 0.87 were defined for the single module configuration and three module injection stage configurations respectively.

6

2.0   SUMMARY

The design of the half-size (MLLV) vehicle family is similar to that of the full size (AMLLV) vehicle family, as defined by NASA contract NAS2-4079. The half size (MLLV) vehicle family was sized to have a single-stage-to-orbit payload capability of approximately 500,000 pounds (to a 100 nautical mile circular earth orbit) with additional payload capability approaching 2,000,000 pounds through the use of injection stage modules and/or strap-on stages

The initial study activities, i.e., Design and Performance Trades (as reported in Section 4.1) and Ground and Flight Environment (as reported in Section 4 2) provided the baseline vehicle configuration design concepts and the vehicle environments which established the criteria for the conceptual design of the MLLV vehicle family (as reported in Section 4.3).

2.1   HALF SIZE (MLLV) DESIGN AND PERFORMANCE TRADES

A design and performance trade study resulted in selection of a half-size (MLLV) baseline vehicle family for follow-on study in depth.

2.1.1   Main Stage

The trade studies indicated that a mass fraction of approximately 0.93 to 0.94 could be obtained for the MLLV main stage if the same design concept as previously established for the full size (AMLLV) main stage was followed. (The mass fraction of the main stage of the AMLLV vehicle will be 0.940 to 0.946.)

Trajectory analyses showed that the same trajectory parameters will be required to optimize the trajectory for the half-size (MLLV) vehicle as were required for the full size (AMLLV) vehicle. The optimum thrust-to-weight versus time history selected for the half-size (MLLV) vehicle will, therefore, be the same as that selected for the full size (AMLLV) vehicle. Both single-stage-to-orbit vehicles will require throttling (to 10% engine thrust) of the main stage engines prior to burn out (eighty-nine percent of burn duration) to maximize payload.

The trade studies showed that control requirements (required gimbal angle) will increase slightly as vehicle size is reduced

Optimal design features for the MLLV main stage structures, propulsion systems, pressurization profiles, mixture ratio, etc. proved to be the same as those previously identified for the AMLLV main stage

7

2.1.2   Injection Stage

Trade studies of the injection stage showed that the weight of propellant and thrust values of the injection stage should be equivalent to one-half of those specified for the AMLLV injection stage. The main stage, with or without strap-on stages, will not require throttling when used in conjunction with an injection stage.

Use of an injection stage module(s) will only increase the payload to 100 nautical mile earth orbit by from 6 to 18 percent, dependent on the specific configuration. The major advantages defined for use of the injection stage were the capability of fine control for orbital injection, capability for altitude or plane changes in orbit, and significantly increased payload capabilities for higher energy missions. Use of the injection stage will impose only a minor structural penalty to the main stage in the forward skirt area.

2.1.3   Strap-On Stages

Either 156 and 260 inch solid propellant rocket motors (SRMs) will be acceptable for use as strap-on stages. The 260 inch diameter SRM, however, was selected for the baseline vehicle system to minimize the number of components and to provide comparable SRM's to those of the AMLLV for subsequent cost analyses. Minimum structural penalties will be incurred by attaching these solid strap-on stages to the main stage such that the solid motor thrust is reacted into the forward skirt of the main stage. On the basis of stage height for "optimal" location of the attachment points, eight 260 inch SRM's were selected to augment the main stage for the maximum payload configuration.

The values for total propellant weight and total thrust of the eight solid motors for the MLLV maximum payload configuration will be one-half of those comparable values specified for the twelve motors for the AMLLV maximum payload configuration.

2.2   BASELINE MLLV FAMILY

Illustrated in Figure 2.2.0.0-1 are the main stage, single module injection stage and strap-on solid motor stage used to develop the MLLV family of vehicles.

Four representative configurations of the baseline MLLV family are shown in Figure 2.2.0.0-2. A total of 18 configurations can be developed from the main stage, injection stage modules, and the strap-on stages to provide an incremental range of payloads for the 100 NM mile earth orbit mission of from one-half million pounds to approximately two million pounds, see Figure 2.2.0.0-3. Generally, the design concepts of the vehicle and stage elements are identical to those of the AMLLV family discussed in Section 1.2.

8

DIAMETER 56.67 FEET (17.27 METERS)
LENGTH 15 FEET (4.57 METERS)
WEIGHT 49,955 POUNDS (22,660 KG)
· STRUCTURE 41,380 POUNDS (18,770 KG)
· ENGINES 3,860 POUNDS (1,751 KG)
· SYSTEMS 4,715 POUNDS (2,139 KG)

SINGLE MODULE INJECTION STAGE CONFIGURATION

DIAMETER 260 INCHES (6.60 METERS)
LENGTH 155.17 FEET (47.30 METERS)
WEIGHT 3,221,500 POUNDS (1,461,272 KG)
· PROPELLANT 2,900,000 POUNDS (1,315,440 KG)
· STRUCTURES 321,000 POUNDS (145,606 KG)

STRAP-ON SOLID MOTOR STAGE CONFIGURATION

TOROIDAL MULTICHAMBER/PLUG

DIAMETER 56.67 FEET (17.27 METERS)
LENGTH 137.7 FEET (41.97 METERS)
WEIGHT 357,688 POUNDS (162,247 KG)
· STRUCTURE 218,305 POUNDS (99,023 KG)
· ENGINES 116,613 POUNDS (52,896 KG)
· SYSTEMS 22,770 POUNDS (10,328 KG)

MAIN STAGE CONFIGURATION

FIGURE 2.2.0.0-1 BASELINE MLLV STAGE CONFIGURATIONS, KEY DIMENSIONS AND WEIGHTS

GROSS PAYLOAD~
M/C PLUG 471,000 LBS.
LOW PRESS. TOR 472,000 LBS.
HIGH PRESS. TOR. 492,000 LBS.

LIGHT WEIGHT SKIRT

T_O 8 M LBS
T/W 1.25
W_O 6.4 M LBS.
W_P TOTAL 5.55 M LBS.
λ = .936 M/C PLUG
λ = .943 TOROIDAL(HIGH PRESS)
λ = .945 TOROIDAL (LOW PRESS)
MULTICHAMBER PLUG
PRATT & WHITNEY HIGH
PRESSURE WITH HINGED
MODULES

OR

TOROIDAL/AEROSPIKE

ROCKETDYNE
P_C = 2000 PSI
(HIGH PRESS. TOROIDAL)
P_C = 1200 PSI
(LOW PRESS. TOROIDAL)

82'
220'
138'
680''
LOX
LH₂
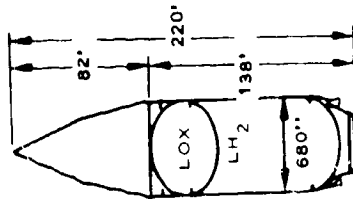
CORE VEHICLE

GROSS PAYLOAD 554,000 LBS

T_O/W_O 1.18
λ CORE .936 (M/C PLUG)
LIGHT WEIGHT SKIRT

INJECTION STAGE

W_{IS} 287,000 LBS
W_P 225,000 LBS.
$\lambda_{I.S.}$ .785
THRUST 250,000 LBS.
(2 ENGINES)

101'
239'
138'
680''
LOX
LH₂

CORE + SINGLE INJECTION
STAGE MODULE

★ ALL PAYLOADS SHOWN FOR ρ 5 LBS FT³ 100 NAUTICAL MILE CIRCULAR ORBIT
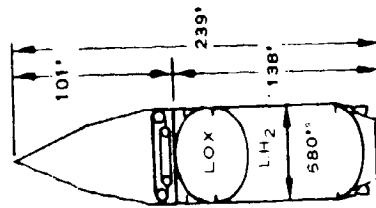
GROSS PAYLOAD 1.76 M LBS
(8 STRAP-ONS)

HEAVY WEIGHT SKIRT
T 8 M LBS
λ CORE = .931

260" STRAP-ONS λ'_S .90
(INCLUDING STAGE
COMPONENTS)

	W_P	T_O	
NO	(M LBS.)	(M LBS.)	T_O/W_O
2	5.8	12.9	1.59[1]
4	11.6	25.8	1.29
6	17.4	38.7	1.44
8	23.2	51.4	1.58

260" MOTOR PERFORMANCE
(EACH)
W_P 2.9 M LBS
F 6.45 M LBS
(1) FOR 2 STRAP-ONS, CORE
IS PARALLEL STAGED

193'
331'
138'
680''
LOX
LH₂
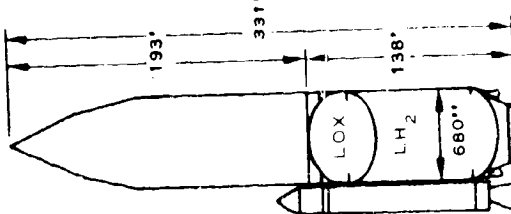
CORE · 8STRAP-ON'S

GROSS PAYLOAD 1.85 M LBS
MULTICHAMBER PLUG
HEAVY WEIGHT SKIRT
T 8.0 M LBS.
λ' CORE = .931

STRAP-ON MOTORS λ's .90
(INCLUDING STAGE)

NO	W_P	T	T_O/W_O
8	23.2	51.4M	1.50

INJECTION STAGE
W_{IS} 805.5K LBS
W_P 675 K LBS
$\lambda'_{I.S.}$ .838
T 750 K LBS
T_O/W_O 0.282

232'
370'
138'
680''
LOX
LH₂
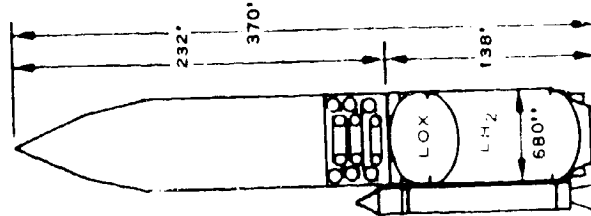
CORE · 8 STRAP-ON'S · 3 INJECTION
STAGE MODULES

FIGURE 2.2.0-2 HALF SIZE (MLLV) BASELINE VEHICLE FAMILY

10
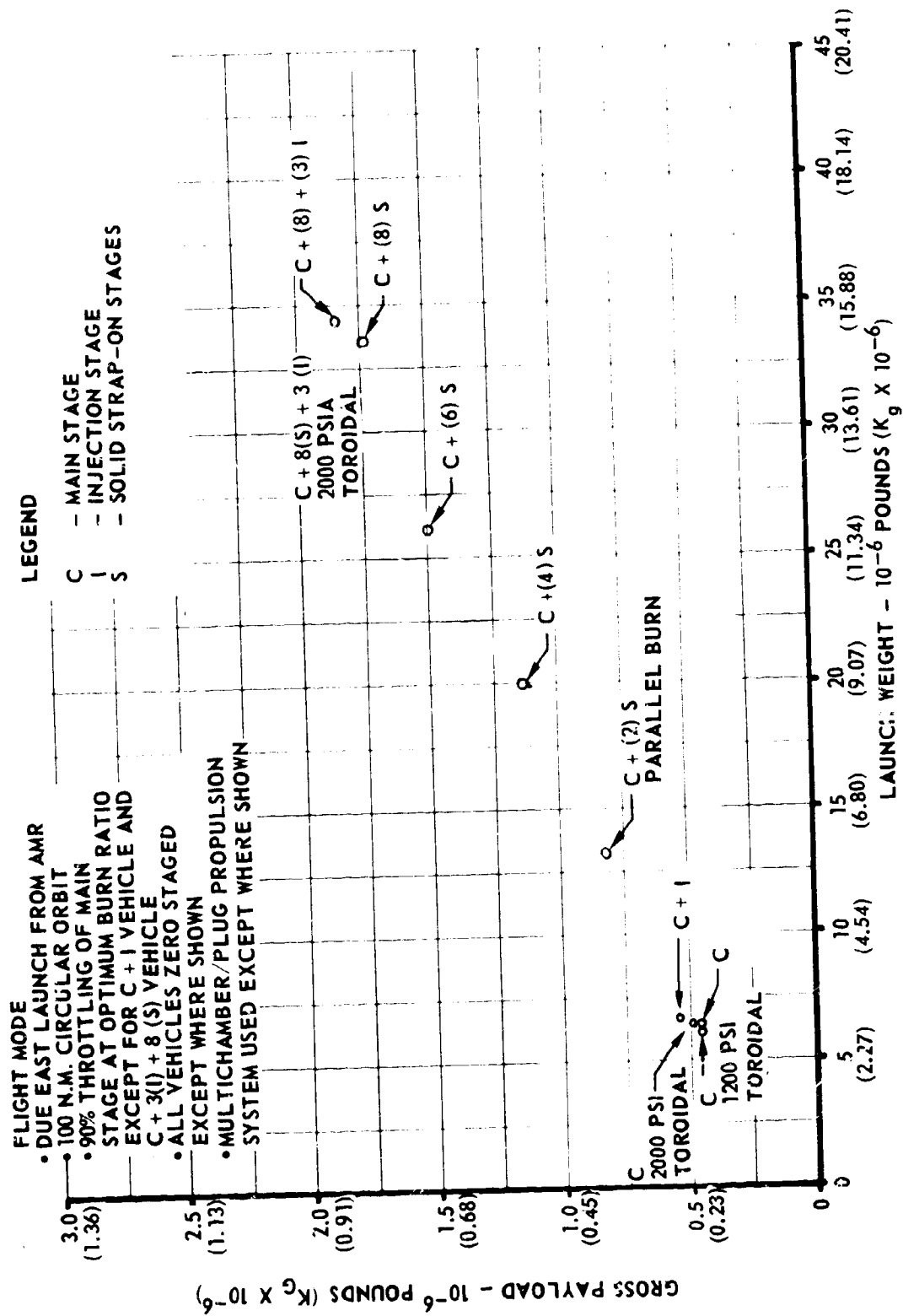
FIGURE 2.2.0.0-3   MLLV PAYLOAD VERSUS LAUNCH WEIGHT

11

2.2.1   Single-Stage-To-Orbit

The single-stage-to-orbit vehicle configuration will consist of a 56.7 foot diameter, 138 foot long main stage employing either the multichamber/plug engine system or a toroidal/aerospike engine system and a payload.

To minimize study program variables, the same instrument unit as used for the Saturn V was specified for the MLLV with the necessary packaging modifications It was assumed that the instrument unit could be packaged into the payload section of the vehicle.

The single-stage-to-orbit vehicle payload capability will be 471,000, 492,000 or 472,000 pounds for the single stage vehicle with the multichamber/plug, the 2000 psia toroidal/aerospike or the 1200 psia toroidal/aerospike propulsion system, respectively. The multichamber/plug engine system weight will be greater than that of the toroidal/aerospike propulsion systems and, therefore, the payload capability will be less than that of the vehicles with the toroidal/aerospike engine systems. The 2000 psia toroidal/aerospike will offer the best combination of engine weight and engine performance and result in the larger payload capability. The 1200 psia toroidal/aerospike will have the lowest weight but its lower specific impulse will reduce the payload capability.

The main stage will use LOX/LH_2 propellants at a mixture ratio of 6:1 by weight, respectively. The total propellant weight will be 5.55 million pounds. The mass fraction for the single-stage-to-orbit main stage with the multichamber/plug engine system will be 0.936 (0.943 for the main stage with the 2000 psia toroidal/aerospike engine system). The sea level liftoff thrust will be 8,000,000 pounds. The mass flow required to provide this thrust will be contained from liftoff until 89% of the main stage propellant had been depleted At this point, the mass flow will be throttled to 10% of the original mass flow and maintained at this rate until orbital injection.

2.2.2   Main Stage Plus Injection Stage

The use of a single injection stage module atop the main stage with the multichamber/ plug engine system will provide an orbital payload capability of 551,000 pounds. Only one module may be used on this configuration because of vehicle lift-off thrust to weight limitations.

This configuration will employ the same main stage, as discussed above This injection stage module will contain 225,000 pounds of LOX/hydrogen propellant at a mixture ratio of 6:1 contained in two concentric toroidal tanks. This module will incorporate two high pressure bell engines with extendible nozzles, each delivering 125,000 pounds of vacuum thrust. The 15 foot tall module will be the same diameter as the main stage. The mass fraction will be 0.785.

12

2.2.3 Main Stage Plus Strap-On Stages

The use of two through eight strap-on stages will provide significant increases in payload capability. The increased payload capability, for the vehicles employing multichamber/plug engine systems, on the main stage, will range from 842,000 pounds (with two strap-on stages) to 1,757,000 pounds (with eight strap-on stages). The trend of payload performance indicates that additional strap-on stages could provide further improvement.

The zero stage flight mode will be the desirable flight mode to maximize the payload of those configurations having the strap-on stages except for the single case where the lift-off thrust of the solid strap-ons will not be sufficient to provide an acceptable lift-off thrust-to-weight. For this case, (i.e., main stage plus two strap-on stages) it will be necessary to launch with a parallel burn (i.e., strap-on stages and main stage propulsion systems ignited simultaneously.

The main stage plus strap-on SRM stage configurations will each have a main stage which is the same as that described for the single-stage-to-orbit vehicle except that it will use a heavier forward skirt. The strap-on stages which will employ 260 inch diameter solid propellant rocket motors, will be attached to the main stage such that the thrust will be reacted into the main stage forward skirt. Each stage will contain 2.9 million pounds of propellant and have a mass fraction of 0.90. The thrust of each stage will be 6.4 million pounds at liftoff. The strap-on stages will employ a 50% regressive trace shape (i.e., the final mass flow will be ore-half the initial mass flow).

2.2.4 Main Stage Plus Strap-On Stage Plus Injection Stage Modules

The maximum payload configuration will consist of a main stage with eight strap-on stages plus a three module injection stage. The payload capability of this vehicle with a multichamber/plug propulsion system on the main stage will be 1,851,000 pounds.

The alternative use of the 2000 psia or 1200 psia toroidal/aerospike engine system on the maximum payload vehicle configuration will provide payload capabilities of 1,859,000 pounds or 1,829,000 pounds, respectively. While the 2000 psia toroidal/ aerospike will provide a significant improvement in the single-stage-to-orbit payload capability (over that of the single stage to orbit vehicle with the multichamber/ plug) the improvement will be insignificant for configurations with strap-on stages.

The three module injection stage for this configuration will consist of an engine module and two fuel modules. The fuel modules will employ the same tankage as the lower engine module. The thrust for the fuel modules will be provided by two additional engines per module mounted on the lower engine module thrust frame. Each of the engines will be identical. Each module will contain 225,000 pounds of propellant. The mass fraction for the combined stack of three injection stage modules will be 0.838.

13

2.3   DESIGN REQUIREMENTS

The "worst condition" design envelope was defined by combining the anticipated loads for the various configurations of the MLLV family. This loads envelope was generally defined by two of the vehicle configurations, i.e., the single-stage-to-orbit configuration, and the configuration consisting of the main stage plus eight strap-on stages plus a three module injection stage. The use of the forward thrust reaction of the strap-on stages will minimize the relative differences in main stage loads for the various configurations.

Increased main stage loads, other than those associated with thrust reaction of the strap-on stages, will primarily be caused by increased tank pressures due to the full tanks at SRM burnout.

The maximum required gimbal angle for the main stage propulsion system will be 3.9° as established by the main stage plus single module injection stage configuration during the maximum dynamic pressure flight regime (max q α). The maximum required gimbal angle for configurations with strap-on stages will also be 3.9° as established by the configuration with the eight strap-on stages plus the three injection stage modules. This gimbal angle must be provided by the strap-on stages as the main stage will be inoperative during the condition of maximum control requirements at max q α (i.e., the vehicles are zero staged).

Relative to the current Saturn V/Apollo abort criteria, all of the vehicles in the half-size vehicle family will be unacceptable with regard to the time to double amplitude during uncontrolled divergence. To allow time for pilot reaction, the minimum allowable time to double amplitude is two seconds. The time to double amplitude of the short L/D "stiff" vehicles in the MLLV vehicle family will range from 0.85 seconds for the single-stage-to-orbit configuration to 1.4 seconds for the maximum payload configuration. This situation can be corrected by the addition of either aft fins or an aft flared skirt to the main stage or by automation of the abort system such that pilot reaction will not be required.

Insulation will be required in the forward skirt area to minimize heating from shock impingement from the nose cones of the SRM stage and to protect the forward skirt from the free stream aerodynamic heating.

The total convective and radiant coincident heat to the main stage base plug during the entire SRM operating time will be 2968 BTU/sq. ft. and 5618 BTU/sq. ft. at the lip and center of the plug, respectively. While ablative cork insulation was specified for the design, an alternative method for protecting the base plug during SRM operation was considered. This method (which would also provide increased reliability through the elimination of the altitude start requirement for the main stage engines) would employ operation of the main stage engines in a throttled condition concurrent with SRM operation. Operation of the main stage engines will circulate liquid hydrogen through the base plug cooling tubes to remove heat in the base region.

2.4   VEHICLE DESIGN FEATURES

A more detailed drawing of the MLLV baseline vehicle elements is shown in Figure
2.4.0.0-1. The main stage LOX and LH_2 tanks will be of 2219-T87 aluminum,
skin-stringer-ring frame construction. The skin panels will consist of weldments
of milled plate with integral longitudinal T-stiffeners. Lateral ring frames will be
mechanically attached to the internal tank cylinder for stability and slosh control.
The common bulkhead will be approximately four inches thick and will be of aluminum
honeycomb construction. Both forward and aft bulkheads will be weldments of
machined gore segments. The common and aft bulkhead designs have a 30° frustum
modification to the theoretical 0.707 eliptical bulkhead to eliminate cramped inter-
sections with the tank walls. Ring frame stiffeners will react the radial forces
caused by the non-tangent bulkhead intersections. Closed cell polyurethane foam
with freon filler will be used to insulate the exterior of the LH_2 tank walls and lower
bulkhead, the LH_2 side of the common bulkhead and the LOX ducts.

The forward and aft skirts will be 7075-T6 aluminum built-up skin-stringer-frame
construction. To eliminate major weight penalties to the main stage, the forward
skirt will be used for core vehicle support at launch.

A heavier weight forward skirt will be provided for use with strap-on stages. The
forward skirt/strap-on stage interface hardware will employ a forward end thrust
takeout spherical ball connection. The aft skirt/strap-on stage interface hardware
will consist of aft end torsion stabilizer tubes and an aft end lateral restraint
incorporating a longitudinal slip joint. Strap-on stage torsion loads and lateral
loads will be reacted at the aft attachment into the main stage thrust structure.
The slip joint will not allow longitudinal loads to be reacted at the aft attachment.
With SRM strap-on stages, the core vehicle will be supported in the launch position
by the SRM stages at the main stage forward skirt.

The baseline main stage vehicle propulsion system will be either a 24 module multi-
chamber/plug engine system or an eight module toroidal/aerospike engine system.
Either system will have a sea level thrust of eight million pounds. Thrust vector
control (TVC) for the vehicle main stage with the multichamber/plug engine system
will be provided by hinging the engine modules by quadrants. TVC for the main stage
with the toroidal/aerospike engine system will be provided by the injection of LOX
fuel through ports in the base plug. Roll control for both systems will be provided
by deflecting the base bleed gases.

A comparison of the relative impacts on the main stage structures of either the
multichamber/plug propulsion system or the toroidal/aerospike system showed
no major differences with the exception of the aft thrust skirt. The thrust skirt
for the vehicle with the multichamber/plug propulsion system will be heavier and
the design will differ due to the method of reacting the thrust.
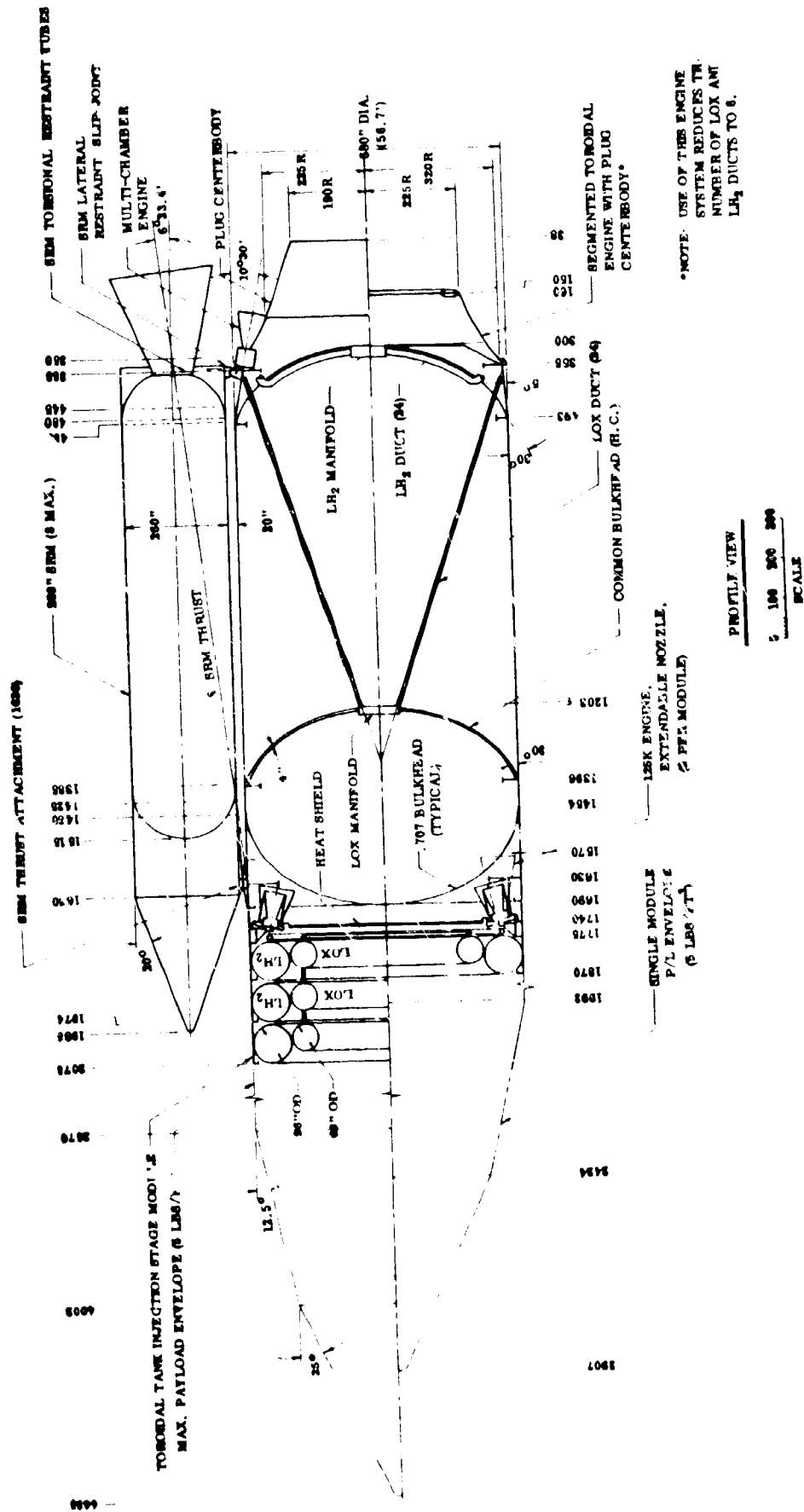
FIGURE 2.4.0.0-1 LINE DRAWING FOR BASELINE MLLV CONFIGURATIONS

2.4   (Continued)

The MLLV injection stage will use a modular tankage arrangement identical in concept to that defined for the AMLLV. Each tank module will have concentric toroidal LOX and LH_2 tanks. The toroidal tanks will be of 2219-T87 aluminum in a semi-monocoque construction and will incorporate honeycomb sandwich web panels inside the tanks (on a 45° spacing) for torsional rigidity and stiffening shear ribs to maintain the corss-section circularity. The inner torus (the oxidizer tank) will hang from a fiberglass cylindrical skirt attached to the outer torus. The outer torus (the LH_2 tank) will be circumferentially shear pin connected with circular bearing fasteners to the outer shell. The skirt for each module will be skin-stringer-frame structure of 7057-T6 aluminum. The thrust structure for the lower injection stage module will consist of two restraining ring frames with six cantilevered thrust posts attached to the skirt. High pressure bell engines, with extendible nozzles will be mounted to the thrust posts. As only two engines will be required for each module, four thrust posts will be vacant for the single module applications. As additional modules are added, additional engines will be added to these remaining thrust posts. Propellant will be provided to the engines from toroidal manifolds which in turn will be fed by the lower module tanks. The engines with the extendible nozzles retracted will be nested into the forward skirt area of the main stage to reduce stage length. The nozzles will be extended and gimballed outward after main stage separation.

The strap-on stages will be complete stages in themselves requiring only command signals from the vehicle instrument unit (i.e., all necessary power, TVC systems, instrumentation, emergency detection systems, destruct systems, etc., will be contained in the strap-on stage). The strap-on stage will incorporate a cylindrical forward skirt (constructed of HY-140 steel) for attachment of the strap-on stage to the main stage and for housing of some of the stage accessories. This forward cylindrical skirt will transmit the loads from the solid motor into a vertical shear post, for subsequent reaction of the loads to the ball fitting in the main stage. Atop this cylindrical skirt will be an aerodynamic nose cone. The stage will also have an HY-140 cylindrical aft skirt which will provide connections for the aft attachment struts and lateral slip joint. The aft skirts will provide the base for supporting the vehicle in the launch position. The aft skirt will house the TVC mechanism and other stage accessories. The SRM will use a monolithic combustion chamber fabricated of 18 percent nickel maraging steel. The SRM will incorporate a polybutadiene, acrylic acid and acriloynitrile (PBAN) propellant grain with a head end ignition motor. TVC will be provided by a flexible seal moveable nozzle system. The nozzle will consist of a maraging steel half shell with an ablative liner.

After burnout, the strap-on stages will be expelled laterally from the main stage through the use of staging rockets mounted in the forward nose cone and the aft cylindrical skirt. Release for separation will be provided by explosive mechanisms located within the attach struts. The separation rockets and the explosive release

2.4   (Continued)

mechanisms will be actuated simultaneously at the time when the main stage
acceleration exceeds the individual acceleration of all of the strap-on stages.

2.5   CONCLUSIONS

The reference AMLLV study defined an attractive launch vehicle design which may
be used to accomplish future manned interplanetary explorations, extended lunar
explorations, and large space station missions. This future vehicle system would
take full advantage of technology advances and large vehicle design experience
that have occurred since the early 1960's especially the advent of altitude compen-
sating aerospike or plug engines.

This half size (MLLV) design activity confirmed that the design concepts were
applicable to a range of vehicle sizes.

The results of these two studies provide a set of considerations to be used in eva-
luating the objectives and achievements of technology development programs.

3.0   STUDY OBJECTIVE, GROUND RULES, GUIDELINES AND
       ASSUMPTIONS

3.1   STUDY OBJECTIVE

This study was directed to define the economic aspects of a future launch vehicle
system.   The work complements the previously completed technological study,
"Advanced Multipurpose Large Launch Vehicles", Contract NAS2-4079. (This
study is herein after referred to as the reference study. The vehicle family
defined by this prior study is hereinafter referred to as the baseline AMLLV
vehicle family.)

The economic aspects defined included:

a.   The non-recurring and recurring costs for implementation and operation
      of the baseline AMLLV vehicle family.

b.   The non-recurring and recurring costs for implementation and operation of
      a half size (MLLV) vehicle family. (Payload capability half that of the base-
      line AMLLV vehicle family.)

c.   Cost effectiveness of program and configuration options.

d.   Cost/size implications and performance/cost implications of selected
      advanced technology applications.

3.2   GROUND RULES, GUIDELINES, AND ASSUMPTIONS

Applicable data from previous and current studies were utilized to the greatest
extent possible. The study, "Advanced Multipurpose Large Launch Vehicles",
NAS2-5079, was used as a basis for this study.

The following ground rules, guidelines, and assumptions were utilized for the
current study activity "Cost Studies of Multipurpose Large Launch Vehicles"
Contract NAS2-5056:

a.   Direct ascent to 100 nautical mile circular earth orbit was the primary mission
      used to size and establish the baseline vehicle design, to establish the trajec-
      tory for heating and control analyses, and as the reference for performance
      comparisons.

b.   The vehicles will be launched due east from AMR.

3.2   (Continued)

c. The basic vehicle configuration employed the following components:

   1. Main (Core) Stage - Sized to provide single stage to orbit payload of
       approximately 500,000 pounds. Propellants were liquid oxygen (LOX)
       and liquid hydrogen (LH_2). Two different engine systems, the multi-
       chamber/plug (Pratt and Whitney) and the toroidal/aerospike (Rocketdyne)
       were considered for the main stage.

   2. Injection Stage - A modular stage for increased payload capability and
       maneuvering. The number of modules was varied from one to three.
       The propulsion system used high pressure bell engines of Pratt and
       Whitney design. The propellants were LOX/LH_2.

   3. Strap-on Stages - Sized to provide a payload to orbit of approximately
       2,000,000 pounds when used to augment the main stage with injection
       stage modules. Solid rocket motors of 156 inch and 260 inch diameters
       were considered.

d. Payload Configurations

   1. The payload, exclusive of the nose cone, had a constant diameter.

   2. Uniform distribution of mass within payload envelope was assumed.

   3. The payload nose cone was the MLV configuration (see Section 4.2.1).

e. Stages and vehicle subsystems were considered expendable.

f. All study vehicles were to be manrated. The design criteria and the necessary
    combination of ground and flight testing were defined based on those established
    for the Saturn IB/Gemini and Saturn V/Apollo systems.

g. Two flight tests were required to qualify the vehicle.

h. A dynamic test vehicle was required.

i. The solid motors required a development program and qualification testing.

j. All propulsion costing, performance, and design data necessary in the evalua-
    tion were compiled from appropriate propulsion contractors (i.e., the contrac-
    tors specifically working on the respective systems).

k. A post 1980 time scale was assumed for implementation.

3.2   (Continued)

l.   The design, test, manufacturing, handling and transportation, facilities and
     launch plans developed under the reference study was used as a basis for
     baseline vehicle family cost definition.

m.   Costs were based on 1968 dollars without an inflationary factor. Funds were
     assumed to be available as required.

n.   Launch and production rates were two vehicles per year.

4.0   HALF SIZE VEHICLE DESIGN

The Phase II activity was divided into two major tasks as follows:

a.   Task 1 - Conceptual design and performance trade studies for selection of a
baseline half size (MLLV) vehicle family for follow-on design, resource
and cost analyses.

b.   Task 2 - Design of the baseline vehicle family and definition of resource
and advanced technology requirements.

The following section (4.1) describes the Task 1 activity, Conceptual Design and
Performance Trades. From this activity, a baseline vehicle was selected for
follow-on study in depth. Section 4.2, Selected Half-Size Vehicle Ground and
Flight Environment, describes the initial portion of the Task 2 activity. Those
studies which were necessary to establish the requirements for design of the
baseline vehicle family are discussed, considering mission requirements and
the anticipated ground and flight environments. Section 4.3, Configuration
Definition, discusses and defines the design of the baseline vehicle family and
its final performance characteristics. Also discussed in this section are the
effects of selected configuration options on the overall performance of the vehicle
family. Volume III, Resource Implications, discusses the resources required
for implementation and operation of the baseline vehicle family. Volume VII,
Advanced Technology Implications, will discuss the technology requirements for
implementation and operation of the baseline vehicle family. Figure 4.0.0.0-1
shows the inter-relationship of these various activities and the input/output for
each.

The design alternatives and their related performance as defined by this design
study were used in the subsequent Phase III activity to (1) evaluate the cost effec-
tiveness of configuration options, and (2) assess the economic value of application
of advanced technologies to further improve the performance of the baseline
vehicle family. These subsequent studies are discussed in Volume VI of the final
report.

4.1   TASK 1 - DESIGN AND PERFORMANCE TRADES

This task, through a logical sequence of design and performance trades, resulted
in selection of a baseline vehicle family for follow-on study in depth. The major
design features for the MLLV vehicle family were determined by these trade
study activities. The initial activity was directed to provide a performance optimized
single stage to orbit vehicle capable of providing approximately 500,000 pounds
of payload to a 100 nautical mile circular earth orbit. Additional trades investi-
gated the desirability of an injection stage. The activity then considered additional
performance (weight) optimized design features for attachment and utilization of
the injection stage module(s) and/or the strap-on stages required to make up the
vehicle family. The final trades investigated the strap-on stage features considering

23

STUDY
GROUND RULES
& GUIDELINES
(SECTION 3.0)

DESIGN AND
PERFORMANCE
TRADES
(SECTION 4.1)

SELECTED
VEHICLE
CHARACTERISTICS
& PERFORMANCE
(SECTION 4.2)

VEHICLE
DESIGN AND
PERFORMANCE
(SECTION 4.3)*

RESOURCE
IMPLICATIONS
(VOLUME III)

TECHNOLOGY
IMPLICATIONS
(VOLUME VII)

TECHNOLOGY
ASSESSMENT
(VOLUME VI)

COST STUDIES
(SECTION 5.0)

(VOLUME V)

● PERFORMANCE
OPTIMIZATION

● MAIN STAGE SIZE
AND CONFIGURATION

● INJECTION STAGE
SIZE AND
CONFIGURATION

● STRAP-ON STAGE
SIZE AND
CONFIGURATION

● PRELIMINARY
PERFORMANCE

● AERODYNAMICS

● PRELIMINARY WEIGHT
AND MASS
CHARACTERISTICS

● STRUCTURAL
CRITERIA & LOADS

● CONTROL
REQUIREMENTS

● HEATING
ENVIRONMENT

● FINAL PERFORMANCE
& EXCHANGE RATIOS

● FINAL WEIGHTS,
STRESS AND
STRUCTURE

● MAIN STAGE
DESIGN

● INJECTION
STAGE DESIGN

● STRAP-ON STAGE
DESIGN

● PERFORMANCE
SENSITIVITIES
TO DESIGN
ALTERNATIVES

● DESIGN PLAN

● DEVELOPMENT AND
TEST

● MANUFACTURING

● TRANSPORTATION

● LAUNCH

● SCHEDULES

● REQUIRED
ADVANCED
TECHNOLOGY
PROGRAM

● RECOMMENDED
ADVANCED
TECHNOLOGY

* SUPPORTING DATA IN VOLUMES VIII AND IX

FIGURE 4.0.0-1 STUDY LOGIC DIAGRAM FOR CONCEPTUAL DESIGN AND RESOURCE
EVALUATION OF HALF-SIZE VEHICLE FAMILY

24

4.1   (Continued)

156 inch and 260 inch diameter solid propellant rocket motors. The results of these trades established the gross dimensions for the vehicle stage elements, their weight targets and their required thrust levels and thrust-time histories. Additionally, these trades established the interface requirements for the various configuration elements and provided the design criteria for design of the interface hardware.

During the course of the previous AMLLV study program, detailed parametric performance and design trade studies were conducted to explore the many options and alternatives offered by the AMLLV concept. These prior studies provided logical considerations from which a reasonable baseline vehicle family was selected. In these prior studies emphasis was placed on investigating the propulsion system interrelationships to the main stage vehicle design and performance, and on the strap-on and injection stage structural impacts on the main stage design that could compromise its single-stage-to-orbit effectiveness.

A review of these previous parametric and design trades showed that many were not size-sensitive and that many of the results could be applied directly to the conceptual design of the half size (MLLV) family. In some cases, additional trade studies were necessary to define the conceptual design of the half size (MLLV) family.

Table 4.1.0.0-I lists the trade studies performed under the reference (AMLLV) contract. Each trade study is described in the table by the fixed conditions, variables or effects investigated, and the selection criteria used. Those trade studies whose results were directly applicable to the half size MLLV family are marked with an "X". Those trade studies which were repeated for the conceptual design of the half size (MLLV) family are marked with an "O". The numbers in parenthesis correspond to the number of the section of this book where that particular trade is discussed in detail as it applied to the half size vehicle. In these discussions, for those instances where the results of the reference contract were used without further analysis, justifications are given.

The effects of scaling the vehicle on both flight performance and design optimization are also discussed as they relate to each of the trade studies. These postulated scaling laws should apply, not only to the two vehicle sizes considered (i.e., AMLLV and half size MLLV vehicles), but also to a spectrum of vehicle sizes, provided that the mission and design concepts are maintained.

The results of the design and performance trades are summarized in the following paragraphs.

25

TRADE STUDY OR ... STUDY	FIXED CONDITIONS	VARIABLE OR FUNCTIONS INVESTIGATED	SELECTION CRITERIA
I. MAIN STAGE (4.1.1) ● SINGLE STAGE TO ORBIT TRAJECTORY OPTIMIZATION (4.1.1.1)	● STAGE MASS FRACTION ● TOTAL PROPELLANT CONSUMPTION ● ENGINE PERFORMANCE ● AERODYNAMIC SHAPE	X THROTTLING X PROPELLANT CONSUMED AT EACH THRUST LEVEL (BURN RATIO)	MAXIMUM PAYLOAD PERFORMANCE
LOX TANK LOCATION (4.1.1.2)	● TOTAL PROPELLANT CONSUMPTION ● TRAJECTORY	X FORWARD OR AFT LOX TANK LOCATION	MINIMUM TANK PRESSURE & CONTROL REQMT
LENGTH TO DIA. RATIO (4.1.1.3)	● LAUNCH CONDITIONS ● FORWARD LOX TANK LOCATION ● AERODYNAMIC SHAPE ● LIFT-OFF THRUST TO WEIGHT = 1.25 ● MIXTURE RATIO 5.5 ● ENGINE P_C ● NUMBER OF ENGINE MODULES (M/C) ● LIFT-OFF THRUST ● PAYLOAD SHAPE AND DENSITY	O ENGINE PERFORMANCE X ENGINE & STRUCTURAL WEIGHTS (AS FUNCTIONS OF L/D) O CONTROL REQUIREMENTS	PAYLOAD PERFORMANCE
MIXTURE RATIO (4.1.1.4)	SAME AS ABOVE EXCEPT STAGE DIA. FIXED MIXTURE RATIO IS A VARIABLE	X ENGINE PERFORMANCE X ENGINE & STRUCTURAL WEIGHTS (AS FUNCTIONS OF MR)	PAYLOAD PERFORMANCE
ULLAGE PRESSURE TRADES (4.1.1.5)	SAME AS ABOVE EXCEPT STAGE DIAMETER FIXED	O STAGE STRUCTURAL WTS. AS FUNCTION OF ULLAGE	STAGE WEIGHT
ENGINE CHAMBER PRESSURE TRADES (4.1.1.6)	SAME AS ABOVE EXCEPT STAGE DIAMETER FIXED ENGINE PRESSURE VARIABLE	O ENG PERFORMANCE & WTS ONLY AS FUNCTION OF P_C	PAYLOAD PERFORMANCE
NUMBER OF MULTI-CHAMBER MODULES TRADE (4.1.1.7)	SAME AS ABOVE WITH STAGE DIA. FIXED AND NO. OF MODULES (VARIABLE)	O ENGINE PERFORMANCE O ENGINE & STRUCTURAL WEIGHTS (AS FUNCTION OF NO. OF MODULES)	PAYLOAD PERFORMANCE
MULTI-CHAMBER HINGED ENGINE TRADE (4.1.1.8)	SAME AS ABOVE EXCEPT TRADE OF HINGE VS. FIXED MODULES	X ENG. PERFORMANCE & WEIGHTS	PAYLOAD PERFORMANCE
II. INJECTION STAGE CONFIGURATIONS (4.1.2) FLIGHT PERFORMANCE (4.1.2.1)	● NOMINAL MAIN STAGE AS USED ABOVE ● REPRESENTATIVE INJECTION STAGE MASS FRACTIONS ● REPRESENTATIVE INJECTION LOX/LH2 PROPULSION SYSTEM	X INJECTION STAGE PROPELLANT X INJECTION STAGE THRUST LEVELS X MAIN STAGE THROTTLING AND BURN-RATIO	PAYLOAD PERFORMANCE WITH PRACTICAL LIFT-OFF THRUST. WEIGHT RATIO
EFFECT ON MAIN STAGE STRUCTURE (4.1.2.2)	● NOMINAL MAIN STAGE ● SELECT INJECTION STG. SIZE AND FLIGHT TRAJ	X MAIN STAGE LOADS	MAIN STAGE WT. PENALTY
III. STRAP-ON CONFIGURATIONS (4.1.3) ● FLIGHT PERFORMANCE AND SOLID MOTOR DESIGN (4.1.3.1)	● NOMINAL MAIN STG. AS ABOVE ● REPRESENTATIVE MTR DESIGNS - WTS, & PERF. SOLIDS - 50% REGRESS THRUST TIME TRACE NOZZLE EXIT AREA - STRAP-ON DIAMETER ● SELECTED INJECTION STG. MODULE FROM ABOVE WITH MASS-FRACTION AS FUNCTION OF NO. OF MODULES	O STRAP-ON DIAMETERS X STRAP-ON THRUST LEVEL O STRAP-ON PROPELLANT WTS. & NUMBER X FLIGHT MODE PARALLEL STAGING ZERO STAGING X MAIN STAGE THROTTLING AND BURN RATIO X INJECTION STAGE SIZE	PAYLOAD PERFORMANCE
EFFECT ON MAIN STAGE STRUCTURE (4.1.3.2)	● NOMINAL MAIN STG. AS ABOVE ● SELECTED STRAP-ON TRAJECTORIES FROM III	O PARALLEL BURN VS. ZERO STAGE X LIQUID VS. SOLID STRAP-ON X FORWARD VS. AFT ATTACHMENT	MINIMUM IMPACT ON MAIN STAGE STRUCTURE WEIGHT

X - DENOTES FAMILY TRADES DIRECTLY APPLICABLE TO HALF SIZE VEHICLE (MLLV)
O - DENOTES TRADES RUN FOR HALF SIZE VEHICLE (MLLV)

26

4.1   (Contined'

Main Stage

The trade studies indicated that a stage mass fraction of approximately 0.93 to
0.94 could be obtained for the half size single-stage-to-orbit vehicle if the same
design concept as previously established for the AMLLV vehicle was followed.
On this basis, the initial MLLV design concept investigated a single-stage-to-orbit vehicle
which was scaled such that the propellant weights and the thrust level were 1/2 of those
specified for the previous AMLLV single-stage-to-orbit vehicle. Trajectory analyses
showed that the optimum thrust-to-weight versus time history for the half-size
MLLV vehicle would be the same as that for the AMLLV vehicle.

Further trade studies investigated the location of the LOX tank. Again, as for the
prior AMLLV studies, forward location of the LOX tank was desirable to minimize
control requirements and the tank pressure requirements.

Trades to optimize the length to diameter ratio (L/D) showed that minimum stage
structural weight would result when the stage diameter was such that a cylindrical
section in the LOX tank was no longer required. Increasing the stage diameter
beyond this point would yield better engine performance which, however, would be
offset by the increased structural weight. The results were the same as those for
the prior AMLLV L/D trades and, therefore, defined the optimum MLLV main stage
as one having the same L/D as the full size AMLLV. Further analyses considered
the effects of vehicle size scaling at a constant L/D on control requirements.

These studies showed that control requirements (required gimbal angle) will increase
as vehicle size is reduced. The anticipated gimbal angle requirements for
the half size main stage, however, will be within the capability of the propulsion
systems considered.

A review of the prior AMLLV mixture ratio investigations showed that a 6:1
mixture ratio, oxygen weight to hydrogen weight, would provide maximum stage
performance considering both payload performance and structural weight. Increased
mixture ratios would minimize the required tank size and decrease the structural
weight while reduced mixture ratios would give improved engine performance.

The ullage pressure trades examined two pressure conditions. The first condition
considered varying the ullage pressure in both the LOX and hydrogen tanks while
maintaining a constant 49 psi differential pressure on the common bulkhead. The
second condition used a fixed ullage pressure of 17.5 psia on the LOX tank (LOX
vapor pressure) and varied the pressure in the LH$_2$ tank. Use of the fixed ullage
pressure in the LOX tank (condition two) increased the core stage structural
efficiency by reducing the weight of the LOX tank and its pressurization system.
The optimum LH$_2$ pressure, as constrained by NPSH requirements, was psia.

27

4.1   (Continued)

Engine chamber pressure trades showed that the engine pressure for the toroidal
engine should be approximately 2000 psia, for optimum performance, while that
of the multichamber/plug engines should be the same as that specified for the
AMLLV (see Volume IX, Appendix A). Pressure below these optimum values
yielded lighter weight engines while pressure above these provided higher
specific impulse.

The study to define the desirable number of engine modules for the half-size (MLLV)
multichamber/plug engine showed that increased performance could be expected
as the number of engine modules increased. Because of geometry constraints, use
of a few propulsion modules required a large expansion ratio for the individual
modules (such that a zero gap condition could be maintained when the nozzles are
used against the center plug). This resulted in an overexpanded condition at sea
level and caused a performance (and weight) penalty. The baseline vehicle for the
reference study employed 24 modules which was optimum for that system. The
half size MLLV vehicle would require approximately 43 modules to be optimum.
Discussions and supporting data from Pratt and Whitney, however, indicated that
the same performance, as obtainable with an optimum number of modules, could
better be provided by equipping the nozzles of the modules with extendible portions.
At some point during the flight trajectory, prior to the time that the nozzles would
be moved in against the plug, these nozzles would be extended to enlarge the expan-
sion ratio. Based on the above, the selected half size vehicle design for the multi-
chamber/plug engine has 24 nozzles such that it is generally comparable with the
baseline AMLLV vehicle. Trades conducted in the latter portion of the study evaluated
the performance gain with the extendible nozzles as a function of cost effectiveness.
This data is reported in volume VI of the final report.

Studies of the proper module positions of the multichamber/plug engine system
during the trajectory showed that improved performance could be obtained by
directing each of the engine modules aft such that the module centerline of thrust
was parallel with the centerline of the vehicle system. At some point (at an
altitude of approximately 48,000 feet) in the trajectory (when the individual expan-
sion cones are running full) the engines will be then tilted in against the plug such
that their individual nozzles contact the plug. The other condition investigated,
i.e., a fixed engine with the individual modules tilted against the plug for the
whole flight regime, showed lower performance. For thrust vector control (TVC),
hinged engines will be required. With this capability, therefore, already provided.
it will be desirable to fly an optimum engine hinge angle profile during the
full flight time trajectory.

Injection Stage

Trade studies of the injection stage showed that the weight of propellant and thrust
values of the injection stage (or stacks of injection stage modules) should be equiva-
lent to 1/2 of those specified for the AMLLV injection stage (under the reference

4.1   (Continued)

contract). The injection stage, therefore, was sized to have 225,000 pounds of propellant and 250,000 pounds of vacuum thrust per module. The main stage without strap-on stages can use only one of these injection stage modules because of the minimum liftoff thrust to weight constraint. Configurations employing the strap-on stages can use stacked multiples of these modules. Three of these modules used with the maximum number of strap-on stages will provide a payload capability of approximately two million pounds to 100 nautical mile earth orbit.

Trajectory studies to evaluate the optimum thrust time histories for the main stage when used in conjunction with the injection stage were conducted under the reference AMLLV study. These trades showed that the main stage would not require throttling when used in conjunction with an injection stage. This was true whether or not the main stage was further augmented by the strap-on stages.

Use of an injection stage module(s) will only increase the payload to 100 nautical mile earth orbit by from 6 to 18 percent dependent on the specific configuration. The major advantages, however, for use of the injection stage are the capability for fine control for orbital injection, capability for altitude or plane changes in orbit, and significantly increased payload capabilities for higher energy missions.

Use of the injection stage with the core vehicle will impose only a minor structural penalty to the main stage. This penalty will occur in the forward skirt area.

Strap-On Stages

Considering both 156 inch and 260 inch solid propellant rocket motors (SRMs), trades were conducted to determine the size and required performance of the strap-on stage propulsion systems. On the basis of the space available about the main stage circumference for attachment of the strap-on stages, and on the basis of best location for attachment points, the 260 inch diameter solid motor was selected for the baseline vehicle system.

Eight motors, each employing 2.9 million pounds of propellant and having an initial thrust of 6.45 million pounds, will be used to augment the main stage for the maximum payload configuration. (The maximum number of 260 inch motors that can go around the main stage is ten.) These rocket motors will have a 50% regressive thrust time history, i.e., the final mass flow will be 1/2 the initial mass flow. In all cases, where there is sufficient thrust for acceptable lift-off the solid motors will be used in a zero mode, i.e., the solid motors will be burned out before the core stage is ignited.

4.1   (Continued)

Minimum structural penalties will be incurred by attaching these solid strap-on stages to the main stage such that the solid motor thrust is reacted into the forward skirt of the main stage. Use of an attachment concept which would react the solid motor thrust at the base of the vehicle will resuit in significant structural penalties. The forward attachment concept can also use an interchangeable forward skirt to maximize payload performance. The heavier weight would be used for those configurations having strap-on stages and the lighter weight forward skirt would be used for those configurations which would not have the strap-on stages.

The combined propellant and combined thrust level of these solid motors for the maximum payload configuration are 1/2 those values specified for the 12 motors for the AMLLV maximum payload configuration.

4.1.1   Main Stage Optimization for Single-Stage-to-Orbit Mission

This activity considered the single-stage-to-orbit mission and defined the gross size and configuration details of the main stage. The effects of scaling the single-stage-to-orbit AMLLV, as defined by the reference contract, were considered. The results of preliminary loads studies indicated that structural efficiency could be maintained while scaling, provided that the length to diameter ratio of the vehicle was maintained constant. These studies further indicated that the optimum trajectory would be insensitive to vehicle size provided that the vehicles in question fly similar missions and that the propellant loading and thrust values are scaled proportionally.

The main stage for the half size vehicle was, therefore, sized by proportionally scaling the propellant loading and the thrust level of the AMLLV main stage by a factor of 1/2. The resulting half-size vehicle main stage preliminary sizing parameters are shown in Table 4.1.1.0-I. These size parameters are compared to those of the full-size vehicle in this table.

Subsequent trajectory studies showed that the initial assumption, i.e., that the optimum trajectory was insensitive to size, was correct. The required thrust-to-weight versus time history for the single-stage-to-orbit operation was found to be identical to that specified for the full-size AMLLV single-stage-to-orbit vehicle.

Subsequent trades defined the configuration details for the optimum main stage configuration. The major elements of this configuration are shown in Figure 4.1.1.0-1. Other studies which considered the impact on the main stage configuration for the attachment of the injection stages and of the strap-on stages are discussed in Sections 4.1.2 and 4.1.3 respectively.

30

PARAMETERS	AMLLV	MLLV
SEA LEVEL THRUST (LBS)	16M	8M
PROPELLANT WEIGHT (LBS)	11.1M	5.55M
DIAMETER (FT)	71.7	56.7
MASS FRACTION (λ')	.936	.933
BURN RATIO (B_2/B_1)	.115	.115
PERCENT THROTTLED %	90	90
NO. OF MODULES	24	24
LIFT OFF THRUST/WEIGHT	1.25	1.25

TABLE 4.1.1.0-I   VEHICLE SIZING PARAMETERS – MAIN STAGE
WITH MULTICHAMBER/PLUG PROPULSION SYSTEM
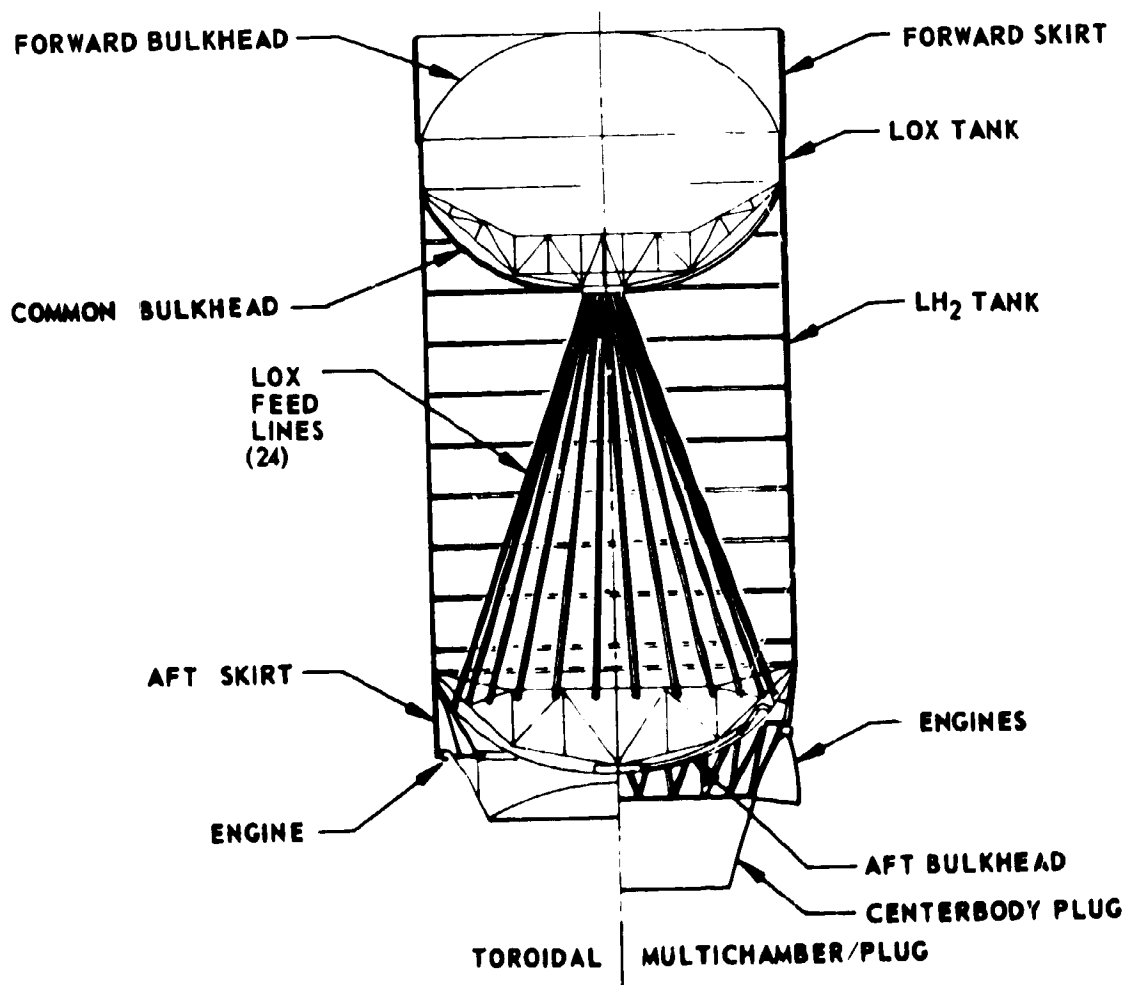
FIGURE 4.1.1.0-1   MAIN STAGE CONFIGURATION ELEMENTS

4.1.1.1 Trajectory Optimization

The first trade study considered trajectory optimization for the single-stage-to-orbit mission to a 100 nautical mile orbit using direct ascent with an easterly launch. This activity defined the optimum flight path (for an initial lift-off thrust to weight at 1.25* with mass flow held constant until engines were throttled), the desired throttling ratio and the time for throttling.

The objective of a trajectory optimization analysis is to maximize the payload capability of a fixed vehicle within prescribed constraints by minimizing the gravity, drag and thrust-vector losses incurred by the vehicle in flight. The relative importance of these losses is dictated primarily by the thrust-to-weight ratio of a vehicle and the number of stages. For the single-stage-to-orbit vehicle, with a lift-off thrust-to-weight ratio of 1.25, drag losses were small such that the problem was reduced to determining the trajectory that minimized the combination of the gravity and thrust-vector losses. This problem was approached in the reference study by employing a gravity-turn/COV computer program, which is a point mass, three dimensional program using a 12 second vertical rise, then a programmed pitch rate from 12 to 35 seconds followed by a gravity turn trajectory through the atmosphere over an oblate earth. Calculus of Variations is then used to determine optimum pitch steering to orbit during the vacuum portion of flight. (Note: Transition from gravity turn to COV occurred at time of main stage throttling to simplify analyses.)

Such trajectory optimization studies for the full size single-stage-to-orbit vehicle (AMLLV main stage, under reference contract) showed that some form of thrust modulation would generally result in a performance increase. Single stage vehicles that directly ascend to orbit and do not employ throttling have relatively short burn times. This results in flying steep trajectories in order to gain the necessary

---

*NOTE: Extensive earlier studies (References 4.1.1.1-1 and -2) of lift-off thrust to weight optimization have shown that for a given lift-off thrust the optimum propellant weight is the maximum that the vehicle can effectively loft (i.e., a minimum lift-off thrust to weight). These studies also showed, however, that to minimize drift (during lift-off) and associated control problems, the lift-off thrust to weight value should not be below approximately 1.25.

4.1.1.1-1 Saturn V Launch Vehicle with 260-Inch Diameter Solid Motors, NASA Contract NAS8-21105, The Boeing Company Document Number D5-13408.

4.1.1.1-2 Minuteman Strap-Ons for Saturn V Vehicles, NASA Contract NAS8-5608 (TOA-36), The Boeing Company Document D5-11424-1 and 2.

4.1.1.1   (Continued)

altitude. Related to this steep trajectory are large thrust-vector losses when the
velocity vector is turned to meet the orbital flight path angle requirements. Compara-
tive plots of flight path angle and altitude versus flight time for the throttled and
unthrottled conditions are shown in Figure 4.1.1.1-1. For the reference study,
core vehicle thrust modulation was accomplished by making a step change in the
thrust. The parameters investigated were the amount of thrust reduction and
the time at which the thrust was reduced.

The results of the core (AMLLV main stage) optimization studies are shown in
Figure 4.1.1.1-2. The percent of throttling is the amount the vacuum thrust is
reduced and the throttling burn ratio is the ratio of the propellants burned during
reduced thrust (B_2) to the propellants burned at full thrust (B_1). The range of
throttling considered was from 60 percent to 95 percent. The largest thrust
reduction considered (95 percent) resulted in the largest payload. (The analyses
considered the I_{sp} penalties associated with throttling). The data showed that an
optimum burn ratio exists for each percent of throttling.

Two additional cases were analyzed for comparative purposes. In one case, the
vehicle was flown to 100 nautical miles with no throttling. This case resulted in
poor payload performance. In the other case, a Hohmann transfer type trajectory
was flown with the vehicle coasting from 50 to 100 nautical miles followed by reig-
nition of the engines and injection into orbit. This latter case resulted in a payload
essentially the same as for the 95 percent throttling case. (No penalty was assumed
for engine reignition.)

Ninety percent throttling was selected for the remainder of the studies
although greater throttling would result in a slight gain in payload.

It was assumed for the half size vehicle trajectory studies that: (1) if the optimum
AMLLV vehicle weights and thrust levels were scaled down proportionally, and
(2) that if the optimum AMLLV thrust-to-weight versus time history was applied;
then an optimum MLLV trajectory and optimum MLLV payload to launch weight
ratio would result. This assumption was based on a conclusion that optimum ratio
of payload weight to vehicle weight should be constant over a range of vehicle
sizes if: (1) the stage mass fraction and the specific impulse of the propulsion
systems are constant, and (2) that drag is proportional to vehicle weight. The flight
trajectory which provides this optimum payload to launch weight ratio should be
the optimum trajectory.
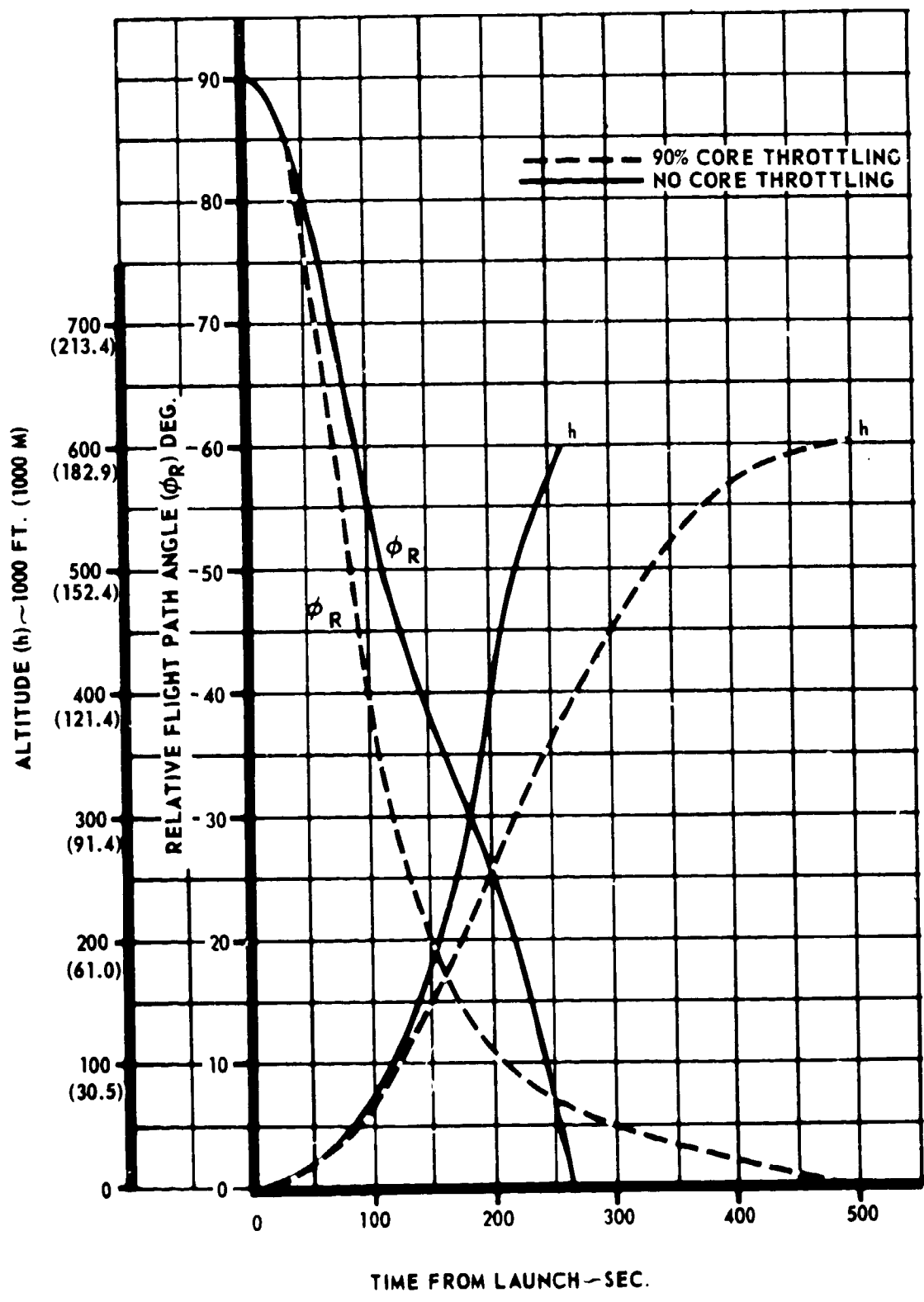
FIGURE 4.1.1.1-1   ALTITUDE AND RELATIVE FLIGHT PATH ANGLE VERSUS
TIME FROM LAUNCH FOR AMLLV (FROM REFERENCE STUDY)

34
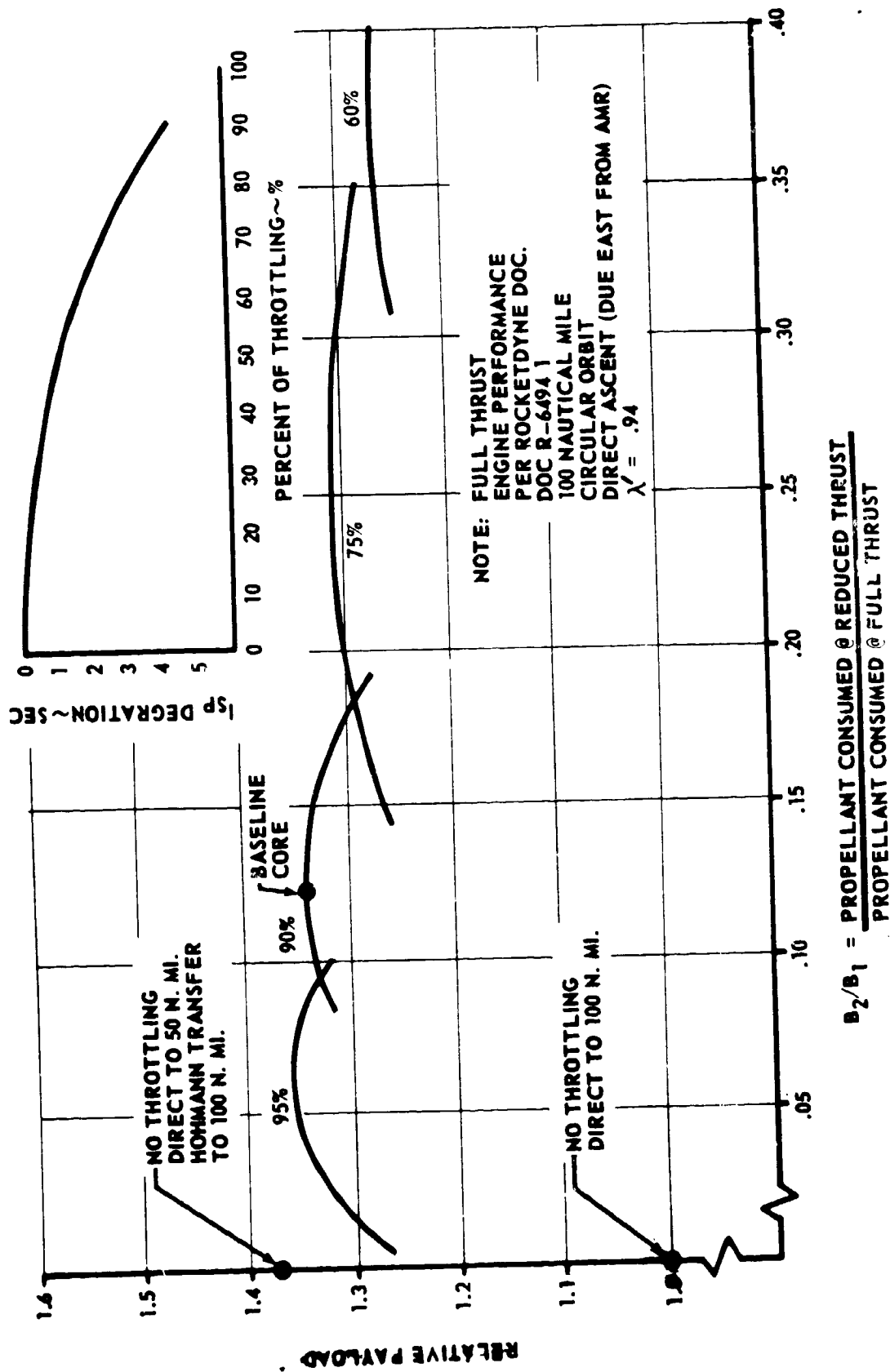
FIGURE 4.1.1.1-2 SINGLE STAGE TO ORBIT VEHICLE TRAJECTORY OPTIMIZATION
(FOR AMLLV FROM REFERENCE STUDY)

$$\frac{B_2}{B_1} = \frac{\text{PROPELLANT CONSUMED @ REDUCED THRUST}}{\text{PROPELLANT CONSUMED @ FULL THRUST}}$$

NOTE: FULL THRUST
ENGINE PERFORMANCE
PER ROCKETDYNE DOC.
DOC R–6494 1
100 NAUTICAL MILE
CIRCULAR ORBIT
DIRECT ASCENT (DUE EAST FROM AMR)
$\lambda' = .94$

35

4.1.1.1 (Continued)

On the basis of the above conclusions and assumptions, the half-size core stage
vehicle was initially sized by proportionally scaling the launch weight and thrust
level of the AMLLV stage by a factor of 1/2. The inputs for the subsequent
trajectory analysis included: (1) 8,000,000 pound lift-off thrust (one half the lift-
off thrust of the AMLLV) with a constant mass flow until 89% of the main stage
propellant had been depleted, (2) a 90% reduction in mass flow at this point (to
10% of original mass flow) and (3) continued operation at this 10% mass flow rate
until propellant depletion. The mass fraction (propellant weight over total stage
weight) for this initial trajectory calculation was established to be 0.940 for the
vehicle with the toroidal engine system, and 0.933 for the vehicle with the multi-
chamber/plug engine system. These inputs provided basically the same thrust-
to-weight versus time history as that for the equivalent full scale AMLLV.

Scaling vehicle weight (and volume) by a factor of 0.5 (at a constant length-to-
diameter ratio) will result in the cross-sectional area being reduced only by a
factor of 0.63. The drag, therefore, is not porportionally scalable. A minor
improvement in engine delivered specific impulse (I_{sp}) will result for the half-size
vehicle, as compared to a full size vehicle with the same length to diameter ratio,
as the expansion ratio will increase as the vehicle size is reduced. (This effect
is discussed in further detail in Section 4.1.1.3.) The propulsion system inputs
for the initial trajectory calculations, included the modified drag and the slight
gain in propulsion efficiency.

The trajectory calculations with these inputs were conducted to prove the initial
assumption that the optimum trajectory is insensitive to size for a specific
thrust-to-weight versus time history.

The resulting trajectory data, assuming 90% throttling and an 0.115 burn ratio,
for the half size single-stage-to-orbit vehicle (see Section 4.2.1 and Volume IX)
were compared to those of the full size (AMLLV) single-stage-to-orbit vehicle.
This comparison showed that the payload achieved for the half size single-stage-
to-orbit was approximately one-half that of the AMLLV. A comparison of the MLLV
flight performance parameters i.e., flight path angle, acceleration, dynamic
pressure, altitude and velocity as illustrated in Figure 4.1.1.1-3 with those of
the AMLLV show that the velocity, altitude and flight path performance very
closely match. The dynamic pressure for the half-size MLLV vehicle is 691 #/ft^2
as compared to 628 #/ft^2 for the AMLLV single-stage-to-orbit. Both vehicles have
their maximum value at 80 seconds. The acceleration of the half-size MLLV is
7.15 versus 6.82 g's for the AMLLV. The maximum value occurs just before the
throttling phase of the core burn for both vehicles. These slight variations in
acceleration and dynamic pressure from the AMLLV values are not significant and
are due to minor variations in the engine performance input data to the computer
for the trajectory run. The close relationships of the comparative parameters were
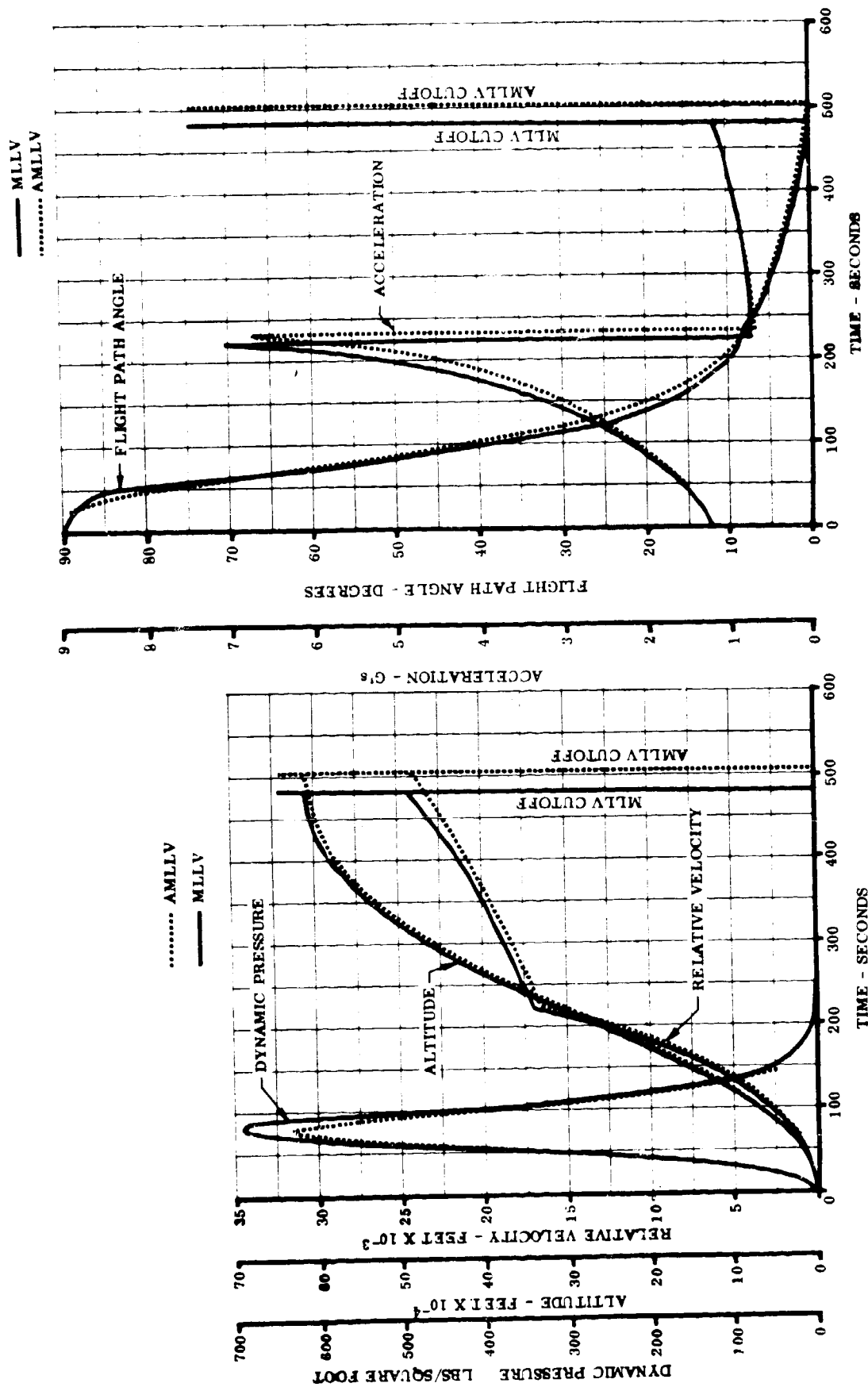
FIGURE 4.1.1.1-3 FLIGHT PATH ANGLE, ACCELERATION, DYNAMIC PRESSURE, ALTITUDE, VELOCITY VERSUS TIME – SINGLE STAGE TO ORBIT (MULTICHAMBER/PLUG)

37

4.1.1.1   (Continued)

indicative that the initial assumption, i.e., trajectory optimization being non-size was valid.

4.1.1.2   LOX Tank Location

During the reference study, an assessment was made primarily considering thrust vector control system requirements, to determine the best location of the LOX tank relative to the liquid hydrogen tank. This assessment showed that location of the LOX tank forward of the hydrogen tank resulted in a reduction in the required gimbal angle by a factor of approximately six relative to configurations with the LOX tank aft of the hydrogen tank (i.e., 3.7 degrees versus 23 degrees). The smaller control requirement for the LOX-tank-forward position was due to the more forward location of the vehicle center of gravity. This resulted in a longer control moment arm and a shorter aerodynamic moment arm (i.e., the center of gravity, CG, of the vehicle was further from the hinge line of the nozzle and closer to the center of pressure, CP, of the vehicle). For the LOX-tank-aft configuration, the vehicle center of gravity was well aft of the center of pressure resulting in a much more aerodynamically unstable vehicle and a smaller correcting moment arm.

The relationships of CP and CG to LOX tank location are basically independent of vehicle size, especially if the length to diameter relationships are maintained between vehicles. For the half size vehicle (MLLV), therefore, the selected configuration has the LOX-tank-forward of the hydrogen tank to minimize the control requirements.

Other factors investigated, to determine the best location for the LOX tank, included tank pressure influences. A review of these factors again showed that the LOX tank forward configuration was desirable.

4.1.1.3   Length-to-Diameter Ratio Trades

The preceeding discussion in Section 4.1.1.1 established the appropriate values for propellant capacity and main stage thrust for the half size vehicle as one-half those of the AMLLV vehicle.

With these values fixed, trades were conducted to define the optimum MLLV main stage diameter (i.e., that diameter which maximizes payload capability). The reference AMLLV study showed that engine performance for a given thrust level improves as the stage base diameter increases (i.e., available expansion ratio increases). As a result for a given main stage thrust and propellant capacity, the total weight to orbit increases as the vehicle diameter (engine base diameter) increases. This data, considering drag effects, are shown in Figure 4.1.1.3-1.

38
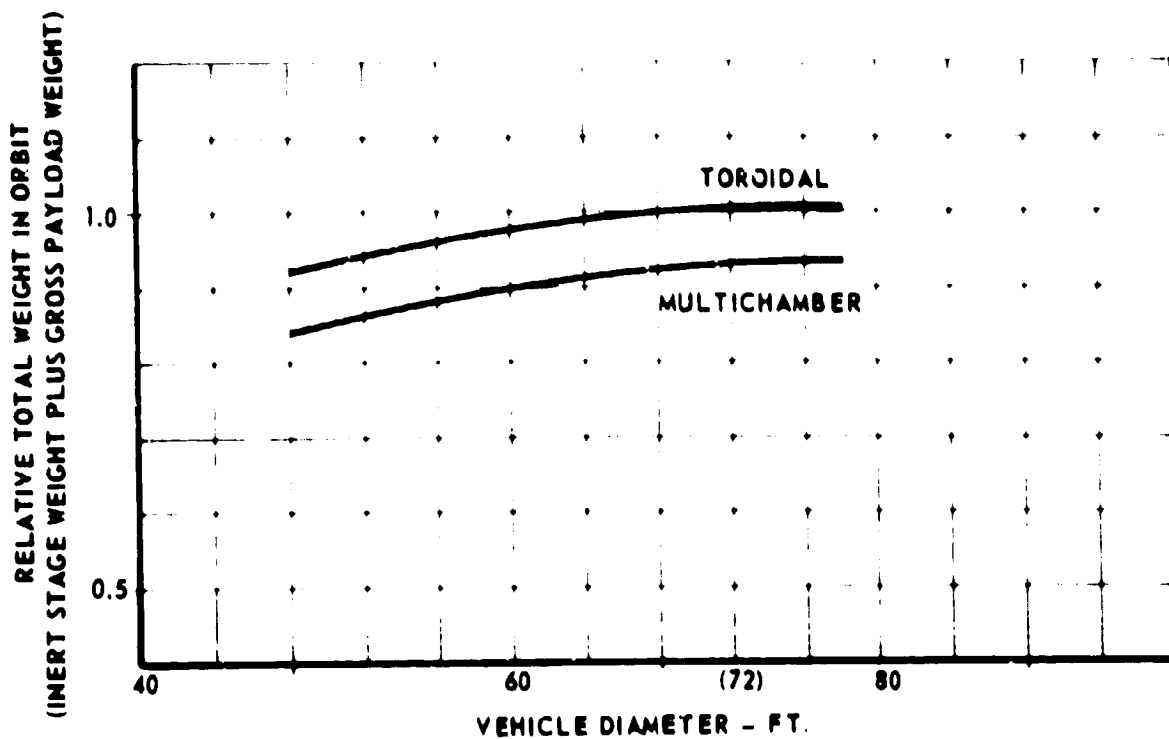
FIGURE 4.1.1.3-1   TOTAL WEIGHT IN ORBIT VERSUS VEHICLE
                    DIAMETER (FOR AMLLV FROM REFERENCE STUDY)
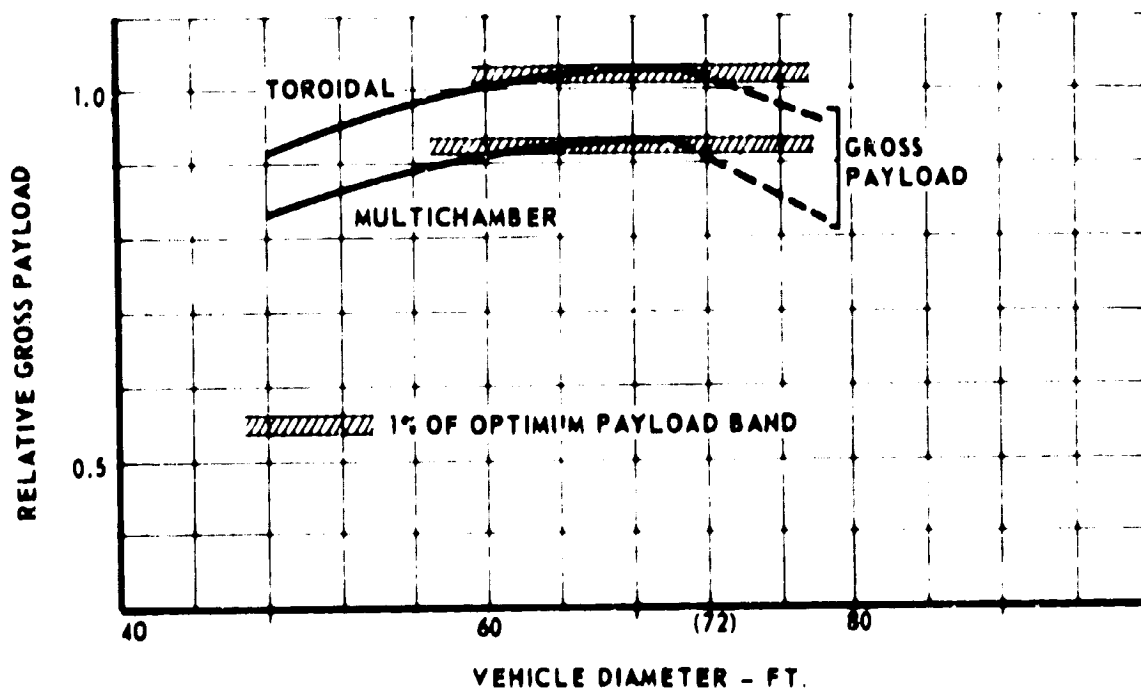
FIGURE 4.1.1.3-2   PAYLOAD WEIGHT VERSUS VEHICLE
                    DIAMETER (FOR AMLLV FROM REFERENCE STUDY)

4.1.1.3   (Continued)

Similarly, the AMLLV trade studies showed that for a fixed propellant loading,
the structural weight will decrease as stage diameter is increased until the
point at which there is no requirement for a cylindrical section in the LOX tank.
For larger diameters than this, the changes required to the LOX tank bulkheads
incur a structural weight increase with increasing diameter.

The combination of these effects in terms of payload to orbit (total weight in orbit
less structural weight and other inert weights) is shown in Figure 4.1.1.3-2.
This figure shows that the optimum diameter is that diameter at which the LOX
tank cylindrical section will not be required.

These results were examined as they relate to the half size vehicle. This review
and subsequent analyses also showed that engine performance will improve as
vehicle diameter is increased. This effect, however, will be offset by the
increased structural weight incurred beyond the diameter where a cylindrical
section of the LOX tank is not required and the LOX bulkheads must be flattened
(below the 0.707 ellipsoid shape). The optimum diameter for the half size vehicle
was, therefore, also found to be that diameter at which there is not a cylindrical
section in the LOX tank.

These analyses indicated that the optimum L/D as specified for the AMLLV is
applicable to a whole range of vehicle sizes of this type. The following scaling
trends were defined:

a.   Engine performance will improve as vehicle size is reduced. (Further dis-
     cussion of this point is included in this section.)

b.   Relative drag (losses) to volume will increase as vehicle size is reduced.

c.   Structural efficiency (usable propellant weight divided by overall stage
     weight, λ') of the primary vehicle structure will be relatively insensitive to
     vehicle size. (See Section 4.3.2.)

d.   For the multichamber/plug engine (in order to have the module nozzles touching
     one another when against the plug), the required expansion ratio of the indivi-
     dual modules increases as the vehicle size is reduced. This geometric effect
     causes a reduction in sea level impulse unless compensated for by staged
     expansion nozzles, reduced overall engine diameter, or other modification
     which will allow for more optimum expansion at sea level while still providing
     zero gap between the nozzles against the plug (optimum condition) at altitude.
     See Section 4.1.1.7.)

4.1.1.3   (Continued)

e.   Required gimbal angle for vehicle control increases as vehicle size is reduced. (See additional discussion in this section.)

Propulsion System Trades

The plug type engine (either the multichamber/plug or the toroidal) has the unique factor in that the effective nozzle exit area of the engine system for vacuum operation is in effect the base area of the engine system. The vacuum expansion ratio (ratio of exit area to throat area, ϵ_V) can be expressed as follows:

$$\epsilon_V = \int \frac{\pi R_E^2}{A_T}$$

Where:

$R_E = f(D) = $ Radius of Effective Plug Nozzle Exit

$A_T = $ Area of Throat

Therefore:

$$\epsilon_V = \int \left(\frac{\pi D^2}{A_T} \right)$$

Toroidal   Multichamber/plug
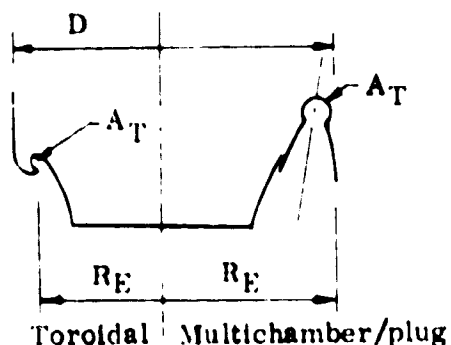
The vacuum expansion area ratio is, therefore, directly proportional to the stage diameter squared.

As shown in Figure 4.1.1.3-3, which was developed in the prior AMLLV study, and as graphically illustrated below, the variations in sea level and vacuum specific impulse with diameter are contrary; that is, as diameter increases, vacuum I_{sp} increases but sea level I_{sp} decreases.
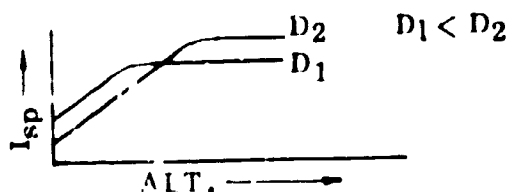
Vacuum performance improves as the stage diameter is increased due to the higher overall vacuum expansion area ratio. The reverse action - that of an I_{sp} loss at sea level - is not as clear. The base pressure on the plug is partially relieved by exhausting the turbopump exhaust through this area.

41

NOTES: (1) $\dfrac{F_{(AMLLV)}}{F_{(MLLV)}} = \dfrac{Wp_{(AMLLV)}}{Wp_{(MLLV)}}$

WHERE: F = THRUST
         W_p = WEIGHT OF PROPELLANT

(2) STAGE LENGTH TO DIAMETER HELD CONSTANT
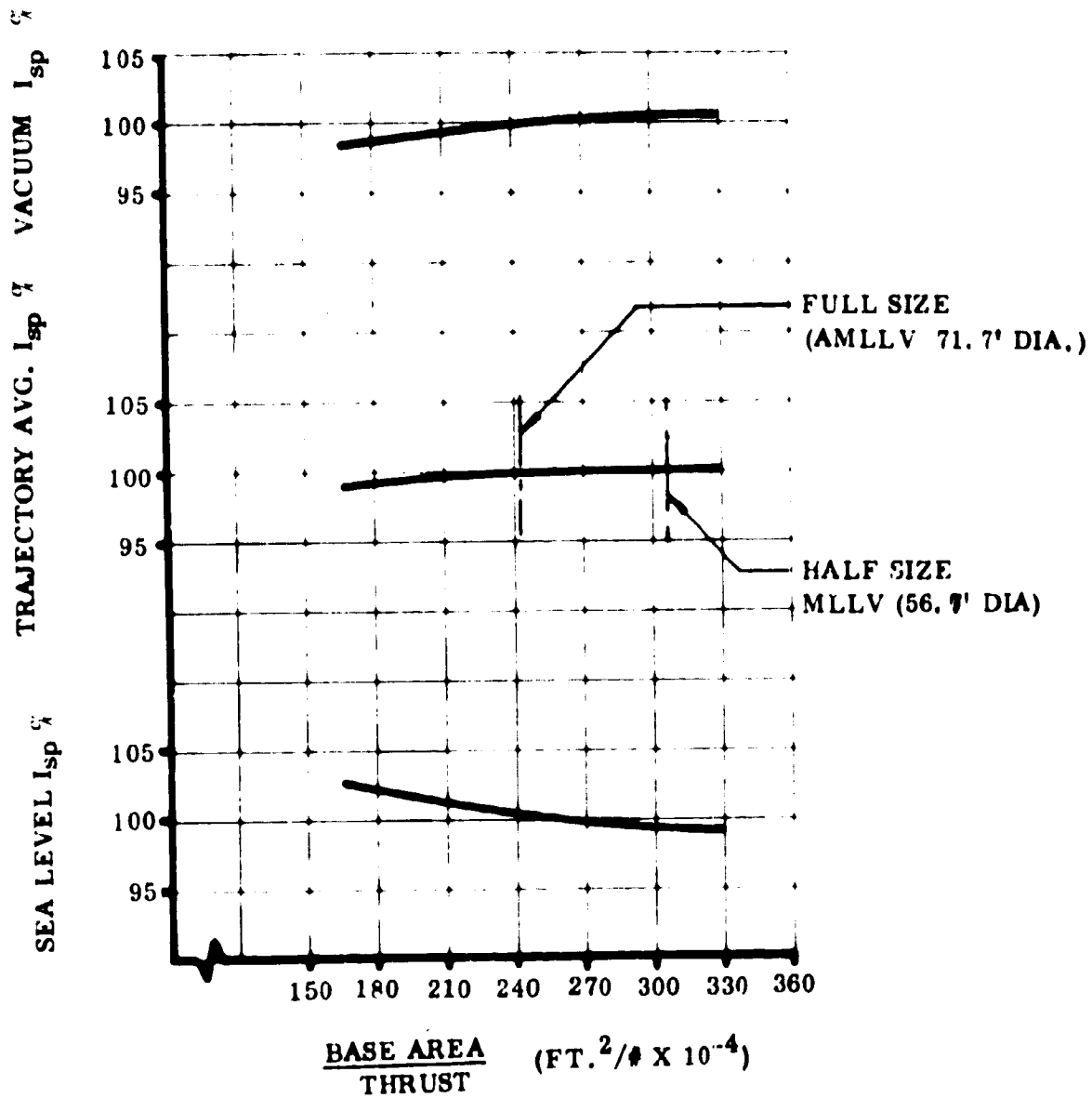
FIGURE 4.1.1.3-3   ENGINE PERFORMANCE VS. RATIO OF BASE AREA TO THRUST
                   AREA

42

4.1.1.3 (Continued)

Increasing the vehicle diameter results in a corresponding increase in base area.
Since, for a given thrust level, the turbopump exhaust flow is unchanged by a
diameter increase, flow per unit area across the base decreases, resulting in
increased base drag and a lower I_{sp} at sea level. Also, the sea level performance
of the toroidal engine is somewhat degraded by the overexpanded exhaust gases at
sea level, in contact with the plug, which pull a negative base pressure. This
degradation increases with plug area.

> NOTE: The latter plug effect is not applicable to the
> multichamber/plug engine system as at sea level the
> individual modules are directed axially and the exhaust
> is not attached to the plug However, for this engine
> system, some additional degradation in sea level performance
> may occur as diameter increases due to a geometry constraint.
> To maintain a "zero gap" condition between adjacent modules,
> when they are against the plug, the required exit diameter
> of the individual modules is a function of number of modules
> and stage diameter. For a given engine pressure level and
> a fixed thrust requirement, this effect may cause overexpansion
> of the individual module nozzles for sea level operation.
> These effects are discussed in more detail in Section 4.1.1.7.

The engine performance data shown in Confidential Appendix (Volume IX) define
these effects. Engine weight changes with diameter are also listed.

To compare relative payload performance, it has been found convenient to define
a "trajectory averaged I_{sp}" as a function of the mean trajectory and the sea level
and vacuum values as shown above in Figure 4.1.1.3-3. The trajectory averaged
I_{sp} of the AMLLV vehicle is indicated on this figure. The trajectory average
I_{sp} associated with a half size vehicle is also shown. Comparing these points,
it is noted that the trend is toward a slightly improved value of I_{sp} with decreasing
overall vehicle size (for a constant L/D and proportional thrust). This can be
understood by the following vacuum expansion ratio (ϵ_v) relationships:

From above:

$$\epsilon_v = f\left(\frac{\pi D^2}{A_T}\right)$$

Where:

$$A_T = \frac{F}{P_c C_f}$$

43

4.1.1.3 (Continued)

F = Thrust (Variable)

P_c = Chamber Pressure (Constant)

C_f = Thrust Coefficient (Constant)

Therefore:

$$\epsilon_v = f\left(\frac{\pi D^2 P_c C_f}{F}\right) \simeq K\ \frac{D^2}{F}$$

And:

$$\frac{\epsilon_{V_1}}{\epsilon_{V_2}} \simeq \left(\frac{D_1}{D_2}\right)^2 \frac{F_2}{F_1}$$

When stage length (L) to diameter (D) is constant:

$L = f(D)$

and volume of tank $(V) = f(D^2 \times L) = f(D^3)$

Therefore: $\dfrac{V_1}{V_2} = \left(\dfrac{D_1}{D_2}\right)^3$

or: $\dfrac{D_1}{D_2} = \left(\dfrac{V_1}{V_2}\right)^{1/3}$

Substituting:

$$\frac{\epsilon_{V_1}}{\epsilon_{V_2}} \simeq \left(\frac{V_1}{V_2}\right)^{2/3} \frac{F_2}{F_1}$$

Therefore if:

$V_1 = 0.5 V_2$ (for half size vehicle)

and:

$F_1 = 0.5 F_2$

Then: $\dfrac{\epsilon_{V_1}}{\epsilon_{V_2}} \simeq (0.5)^{2/3}\ (2) \simeq 1.26$

44

4.1.1.3   (Continued)

I_{sp} is a direct function of the exit velocity of the exhaust gases V_e V_e is a rela-
tively weak function of ϵ . Therefore, I_{sp} is a relatively weak function of ϵ .
As ϵ increases, there is, therefore a nominal increase in I_{sp}. It was concluded
that I_{sp} increases slightly if the stage size is scaled down at a constant L/D and
if thrust is reduced proportionally to the propellant weight decrease.

Structural Trades

The effect of varying vehicle diameter upon the core vehicle weight was assessed
in the reference study by determining the required inert weights for core vehicles
of various diameters. Basic trajectory flight data were used to define the design
loads for the various diameter vehicles. Total propellant weights, ullage volumes
and thrust were held constant for all vehicles, and the requirement for a positive
pressure loading on the common bulkhead was maintained (See Section 4.1.1.5,
Case "a").

The diameter trade study showed that the length of the cylindrical portion of the
LOX tank was reduced as vehicle diameter was increased. A cylindrical section
of the LOX tank was not required for diameters in excess of 72 feet considering
the 0.707 bulkheads. Figure 4.1.1.3-2 shows the results of the diameter trade
structural studies. The preceding required structural weight will decrease with
increasing diameter up to the 72-foot diameter. At this point, the LOX tank
bulkhead shape must be changed to satisfy volume requirements, and a discontinuity
in the slope of the curve occurs in that required structural weight will now increase
with increased diameter beyond this point.

As this data shows, there will be a continued minor improvement in stage mass fraction
as diameter increase (L/D decreases) until such time as the diameter reaches
the point where the LOX tank requires no cylindrical section. Increasing diameter
beyond this point will result in a degradation in mass fraction due to the required
flattening of the LOX tank bulkheads to make the bulkhead diameter coincident with
the stage diameters.

This effect is not size sensitive. It is a geometric constaint typical to all sizes
of vehicles. The half size vehicle, therefore, was sized such that the LOX tank
would have little or no cylindrical section in the LOX tank.

Effects of Vehicle Size Scaling at Constant L/D on Control Requirements

The control studies conducted under the reference contract investigated the gimbal
angle (side thrust) requirements as a function of vehicle thrust, vehicle size and
fineness ratio (L/D).

4.1.1.3   (Continued)

For the prior AMLLV gimbal angle versus L/D - diameter fixed trades, the vehicle length was varied to vary the L/D. As vehicle length was shortened, liftoff weight and, therefore, payload weight was diminished. Thrust to weight was held constant at 1.25 by reducing thrust proportionally. These trades showed that, although the required side force diminished, the gimbal angle requirements increased as the length was shortened. For a minimum required gimbal angle, these trades favored the longer vehicles (those with higher L/D ratios).

For the gimbal angle vs. vehicle size - L/D fixed trades, the overall vehicle size inclusive of payload was varied. Thrust was also varied to maintain a lift-off thrust to weight of 1.25. These studies also showed, that for a constant L/D, the gimbal angle requirements would increase as the overall weight of the vehicle decreased. For a given gimbal angle, the available control moment decreases at a faster rate than the overturning moment as vehicle size is reduced.

For example, considering two vehicles, one of which is one half the size of the other, the following relationships exist:

Assuming for the larger vehicle that the correcting moment (M_{c1}) is equal to the overturning moment (M_{o1})

$$M_{c1} = M_{o1}$$

Where:

M_{c1} = Thrust (F_1) x sine of Gimbal Angle (β_1) x Moment Arm (L_{c1})

and:

M_{o1} is a function of Area (A_1) x moment (L_{o1})

For the half size vehicle, the thrust (F_2) would be $0.5F_1$ similarly

$$\beta_2 = \beta_1$$

$$L_{c2} = \frac{L_{c1}}{\sqrt[3]{2}}$$

$$A_2 = \frac{A_1}{\sqrt[3]{2} \times \sqrt[3]{2}}$$

46

4.1.1.3   (Continued)

and:

$$L_{o2} = \frac{L_{o1}}{\sqrt[3]{2}}$$

Therefore:

$$M_{c2} = \frac{F_1 \sin \beta_1 L_{c1}}{2\sqrt[3]{2}} = \frac{M_{c1}}{2\sqrt[3]{2}}$$

$$M_{o2} = f\left(\frac{A_1 L_{o1}}{\sqrt[3]{2} \times \sqrt[3]{2} \times \sqrt[3]{2}}\right) = f\left(\frac{A_1 L_{o1}}{2}\right)$$

$$\simeq f\left(\frac{M_{o1}}{2}\right)$$

$$\frac{M_{o2}}{M_{c2}} \simeq \frac{2\sqrt[3]{2}\, M_{o1}}{2\, M_{c1}} \simeq 1.26\ \frac{M_{o1}}{M_{c1}}$$

In other words, if the lift-off weight is reduced by a factor of two, the required gimbal angle is increased by a factor of approximately 1.26 (neglecting non-geometric effects such as design tolerances).

The main stage of the AMLLV will require a maximum gimbal angle of approximately 3.6 degrees. A half size vehicle (having the same L/D) therefore should require a gimbal angle of approximately 4.5^o (3.6^o x 1.26).

Considering the above, it is obvious that a more severe control problem will exist for the half size vehicle (MLLV) than for the full size vehicles if the L/D is held constant. The indicated maximum requirement of 4.5 degrees, however, was found to be within the capability of the control systems to be evaluated and was, therefore, judged acceptable. (Note: Final control studies, as discussed in Section 4.2.5, showed a gimbal angle requirement of 3.9 degrees for the half size vehicle configuration. This lower than prognosticated value was due to the use of the root mean square correction for the effect of the scatter terms (variation or tolerances of control parameters) on the MLLV. The AMLLV did not employ the root mean square correction and, therefore, is slightly more conservative in its analysis of the control requirements.

4.1.1.3   (Continued)

The gimbal angle requirement could be reduced by: (1) adding fins or aft flared skirt, (2) by increasing the payload density or (3) by placing the heavier elements of the payload forward.

4.1.1.4   Mixture Ratio Trades

The mixture ratio used in the AMLLV study was six to one by weight (oxygen to hydrogen). This ratio gave the maximum payload vehicle as compared to that provided by other vehicles using mixture ratios of five to one and seven to one. Varying mixture ratio effects both specific impulse and structure. Data from the propulsion contractors showed that a mixture ratio of five to one provided the highest specific impulse. Increasing the ratio to six to one or seven to one resulted in losses in specific impulse of two and seven seconds, respectively. Conversely, the higher overall average propellant density provided by mixture ratios of six or seven to one reduced the tankage volume to contain the propellants. This resulted in reduced weight for the tankage. A secondary effect of the higher density was a further reduction in stage weights due to smaller loads for the shorter vehicles with reduced bending moments.

An analysis of the hydrogen tank showed that, as the mixture ratio was varied from five to one to seven to one, the tank design pressure dropped. The reverse was true for the oxygen tank design pressure where higher mixture ratios resulted in higher design pressure. For both tanks, this variation was between one and two percent for the mixture range studied. An analysis of the combined loads showed that as the mixture ratio increased, the combined compressive load increased and the combined tensile load decreased. The change in mixture ratio only affected the tankage loads. This resulted in a variation of approximately five percent over the mixture ratio range. The smaller tankage required for the increased mixture ratio resulted in stage mass fraction improvement with increased mixture ratio. This improvement was under one half of one percent.

The optimum mixture ratio was, therefore, a combination of the effect of stage mass fraction and specific impulse effect. The drop in specific impulse of six or seven points with the seven to one mixture ratio offset the improvement in stage mass fraction and resulted in payload loss from the optimum payload. At a mixture ratio of five to one, the improved specific impulse was offset slightly by the lower stage mass fraction. Therefore, the mixture ratio of six to one offered the best combination of specific impulse and mass fraction. Approximately one percent increase in payload can be achieved with the six to one mixture ratio over the five to one mixture ratio.

As these variations are not size significant, the recommended mixture ratio for the MLLV was also selected at six to one.

48

4.1.1.5 Ullage Pressure Trades

In the reference study, the structural effect of ullage pressure on stage weight was assessed by considering the effect on design loads and the resulting changes in structural requirements of the nominal, 75 foot diameter stage. The study considered two tank ullage pressure conditions:

a. The ullage pressure in both the LOX and LH_2 tanks was varied to retain a design pressure differential of 49 psi on the common bulkhead. This pressure differential is the minimum required to assure that the bulkhead will always contain a plane tensile stress field.

b. The ullage pressure in the LOX tank was maintained at the LOX vapor pressure (17.5 psia) and the ullage pressure was varied in the LH_2 tank. This condition resulted in a negative (collapsing) differential pressure on the common bulkhead.

The bulkhead used for collapsing load condition was an aluminum honeycomb sandwich designed to meet both strength and stability requirements. This bulkhead was sized by considering both the maximum positive and negative pressure differentials occurring at the apex of the bulkhead. In general, the face sheets were sized for tension loading induced by maximum positive design pressure differentials. In this case, the membrane load was assumed equal in both face sheets. These face sheets were then combined with an aluminum honeycomb core sized for stability requirements for a uniform pressure (equal to the pressure at the apex) on the convex surface of the bulkhead. The method used was to size the core thickness for a hemispherical head with a radius equal to the radius of curvature at the apex of the 0.707 elliptical head.

Results of these prior pressure trades showed that the concept using minimum LOX tank ullage pressure (case number b, common bulkhead compression loads allowed) would result in an increased structural efficiency (minimum weight) for nominal LH_2 tank ullage pressures. This was due to the reduced weights of the LOX tank bulkheads, cylinders, Y-rings, and pressurization system.

On the basis of this prior data, a collapsing differential pressure on the common bulkhead was also assumed for the half-size vehicle design. The ullage pressure in the LOX tank was, therefore, established at the LOX vapor pressure (17.5 psia). Analyses were then conducted to determine the optimum pressure for the liquid hydrogen tank.

The hydrogen tank ullage pressure is a strong contributor to overall structural efficiency as this pressure tends to stabilize the hydrogen tank cylinder to prevent buckling. Sufficient internal pressure can negate the buckling to such a degree that internal stiffeners are not required in the hydrogen tank cylindrical skin. The structure for this pressure condition is a monocoque structure with the wall

4.1.1.5   (Continued)

thickness sized to contain the internal tank pressures in a plane perpendicular to
the vehicle axis. Tensile forces in the planes parallel with the vehicle axis
counterbalance the compressive loads and thereby relieve the buckling stresses.
For a monocoque structure, there is an optimum tank pressure which yields a
minimum weight. For sculptured structure with internal stiffening there are similar
pressure stabilizing effects. Therefore, there is also an optimum pressure for
sculptured structure. The ullage trades considered these effects to define the
optimum LH_2 tank pressure. Figure 4.1.1.5-1 shows the results of these trades.
The data shown for monocoque structure was approximated while the data shown
for the sculptured structure was obtained by detailed quantitative loads and weights
analyses. As this figure shows, the minimum weight structure can be obtained
using a sculptured tank wall and a maximum optimum ullage pressure (vent pressure)
of 24 psia. The optimum pressure for the monocoque tank design is approximately
39 psia. The monocoque tank structure, however, is approximately 10% heavier
than a sculptured structure for equivalent volume tankage.

Ullage pressure must be high enough, however, to maintain the required engine pump
net positive suction head (NPSH) during the overall flight regime. The pressure to
provide the required NPSH for the hydrogen pumps is approximately 24.5 psia.
Normal practice for pressurization system design provides a 1 1/2 psi pressure
band for nominal operation of the system, a 1/2 psi gap between this operating
band and the lower setting for the vent value and a 1 1/2 psi band for nominal
operation of the venting system. These allowances and tolerances for nominal
operation add an additional requirement for ullage pressure of 3.5 psia. Summing
this 3.5 psia to the 24.5 psia gives a minimum vent pressure for NPSH of 28 psia.
The vent pressure of 28 psia is then the minimum allowable design pressure for
sizing the tank wall (24.5 psia is the corresponding design pressure for pressure
stabilization).

With the above limiting case, therefore, the optimum allowable design ullage
pressure is 28 psia. This will be off optimum in terms of structural load alle-
viation as indicated on the figure and will result in a penalty for payload of the
single-stage-to-orbit vehicle of approximately 2500 pounds. Use of a P_{max} of
24 psia would provide an additional 2500 pounds for payload to orbit. Subsequent
investigations in further depth may show that the NPSH requirements can be reduced
or the tolerances for the pressurization system and venting values tightened such
that this optimum design point can be obtained.

The pressurization system, the pressurization schedules, and other considerations
are discussed in detail in Section 4.3.3. The pressurization schedules shown and
discussed in this latter section were used in the loads analyses discussed in
Section 4.2.4.
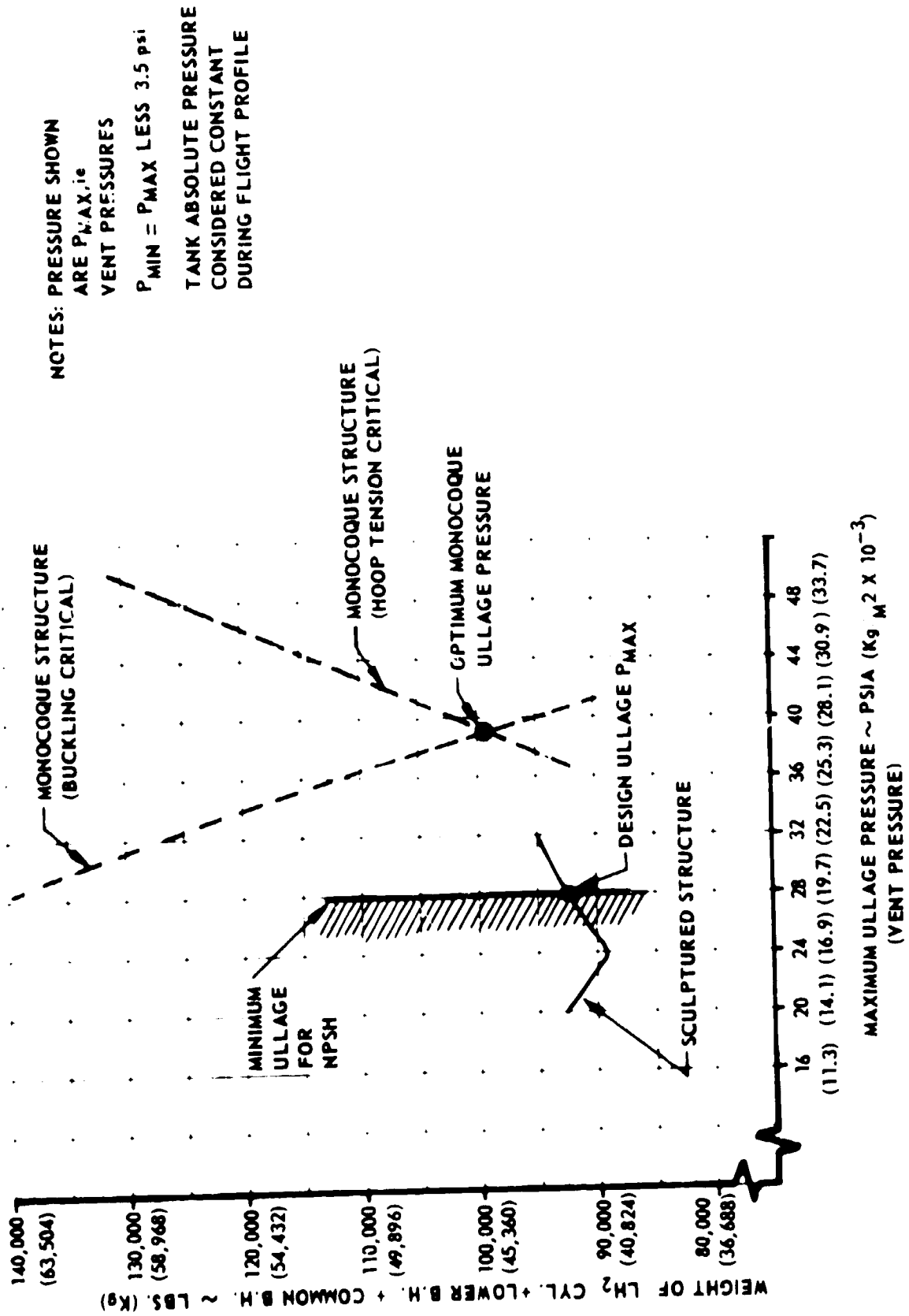
FIGURE 4.1.1.5-1 LH₂ ULLAGE PRESSURE OPTIMIZATION FOR MLLV MAIN STAGE

51

4.1.1.6   Engine Chamber Pressure Trades

In the reference study, trades were conducted to determine the engine chamber
pressure which would optimize the vehicle payload. The results of the study
showed that for either the multichamber/plug or toroidal propulsion systems, the
gross payload was relatively insensitive to chamber pressure. Over the 2000 to
3000 psia pressure range investigated, the payload variation fell within a one
percent of optimum band. Offsetting performance factors included the specific
impulse which increased with pressure and engine weight which also increased
with pressure. The weight of vehicle structure was not effected by the engine
chamber pressure.

Similar trades of toroidal/aerospike chamber pressure versus payload performance
were conducted by Rocketdyne in support of the half size vehicle study. The results
of these trades are shown in Figure 4.1.1.6-1. As these results confirm the
earlier data, the above chamber pressures were also specified for the half size
vehicle family.

Subsequent Rocketdyne data indicated that while reduction in chamber pressure
to 1200 psia would result in an approximate loss of payload of 2%, the adaptability
of existing turbopump machinery to this application could substantially reduce
engine R&D and production costs. This alternative was evaluated in cost/performance
trades (See Volume VI).

4.1.1.7   Number of Propulsion Modules (Multichamber/Plug Engine)

Analyses were conducted, both under the reference AMLLV study and as part of the
half-size MLLV vehicle trade studies, to determine the optimum number of pro-
pulsion modules for the multichamber/plug engine. These analyses indicated that
the mainstage performance was influenced by the number of modules.

Data from Pratt and Whitney has indicated that it is desirable for maximum perfor-
mance that the nozzle exit planes of the propulsion modules be in contact with one
another as they mutually contact the center expansion plug (a zero gap condition -
see discussion at end of this section). For a specified chamber and sea level thrust
condition, the expansion ratio of any single propulsion module, therefore, is a
geometric function of the number of modules and the base diameter of the vehicle.
Dependent upon the base diameter of the vehicle, this geometric effect can result
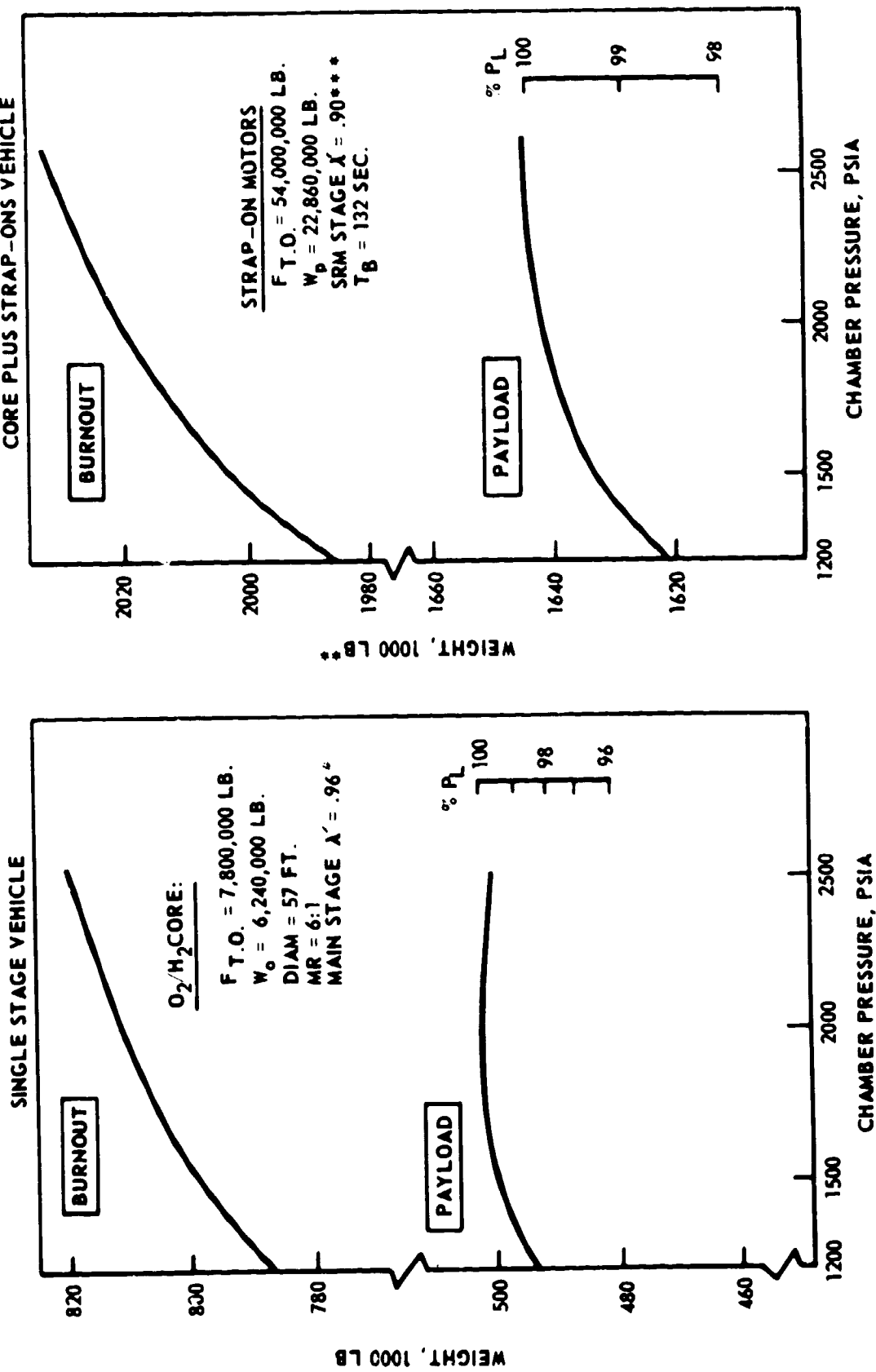
FIGURE 4.1.1.6-1 EFFECT OF CHAMBER PRESSURE ON PAYLOAD (TOROIDAL/ AEROSPIKE ENGINE)

4.1.1.7   (Continued)

in an over-expanded condition for the modules at sea level. For the chamber pressures, the required thrust levels and the vehicle diameters considered in both the reference AMLLV study and in the half-size vehicle study, an over-expanded condition existed for the nozzles at sea level from the use of lesser quantities of modules. As the number of modules increased, the individual module expansion ratio decreased and approached optimum. As the vehicle size was scaled, i.e., from the full size AMLLV to the half-size MLLV, the overexpanded condition was accentuated. In other words, the half-size MLLV vehicle modules had a higher expansion ratio than the full size propulsion modules for configurations having the same number of modules.

The analyses conducted during the reference AMLLV study indicated that the full size AMLLV vehicle required approximately 24 modules to optimize the module expansion ratio and to, therefore, maximize the performance. (These analyses showed, however, that for that size vehicle the performance was relatively insensitive to number of modules in that the payload variation due to number of modules when varied between 12 and 24 was contained within a 1 to 1 1/2% band.)

The half size vehicle analyses considered varying the number of modules from 8 through 32 and investigated the effects of engine diameter and engine pressure on module expansion ratio. This data is shown in Figures 4.1.1.7-1 through 4.1.1.7-3 for engine pressures of 2000 psia, 2500 psia and 3000 psia, respectively. In all cases, the thrust level was fixed at 8 million pounds for sea level conditions. As this data indicates, the geometrically required module expansion ratio will decrease with increasing number of modules and/or decreasing pressure.

Considering the sea level thrust constant, the mass flow that must be produced by the engine system is inversely proportional to the delivered I_{sp}. Therefore, as the number of modules increases, the sea level expansion ratio approaches optimum, the sea level I_{sp} increases, and the required mass flow for lift-off decreases. This decrease in required mass flow thereby reduces the size of the turbo machinery and thrust chambers required to provide the required lift-off thrust. This will result in a decrease in system weight as a function of increased number of modules. This decrease in system weight for the single-stage-to-orbit mission will be directly convertible to a payload increase.

The above effects were reported by Pratt and Whitney for the reference study (see Figure 4.1.1.7-4) and verified for the half-size vehicle study. The Rocketdyne data, however, did not show these same effects. The Rocketdyne data showed an increase in system weight and a resulting payload penalty as the number of modules increased. This anomoly resulted because the Rocketdyne calculations considered mass flow as constant rather than sea level thrust as constant. The Pratt and Whitney assumption more nearly coincides with the actual system requirements.
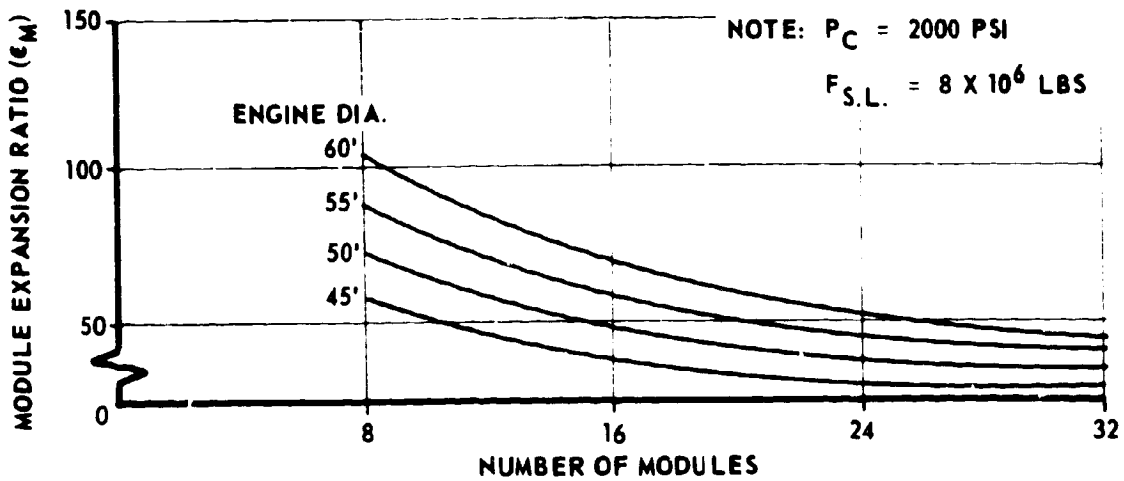
FIGURE 4.1.1.7-1   MODULE EXPANSION RATIO VS. NUMBER OF MODULES
(P_C = 2000 PSI)
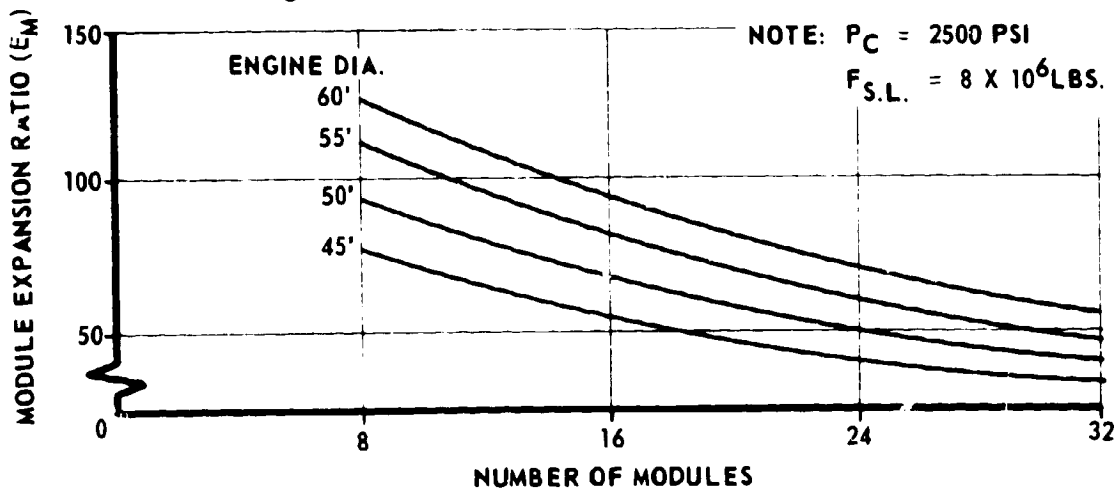
FIGURE 4.1.1.7-2   MODULE EXPANSION RATIO VS. NUMBER OF MODULES
(P_C = 2500 PSI)
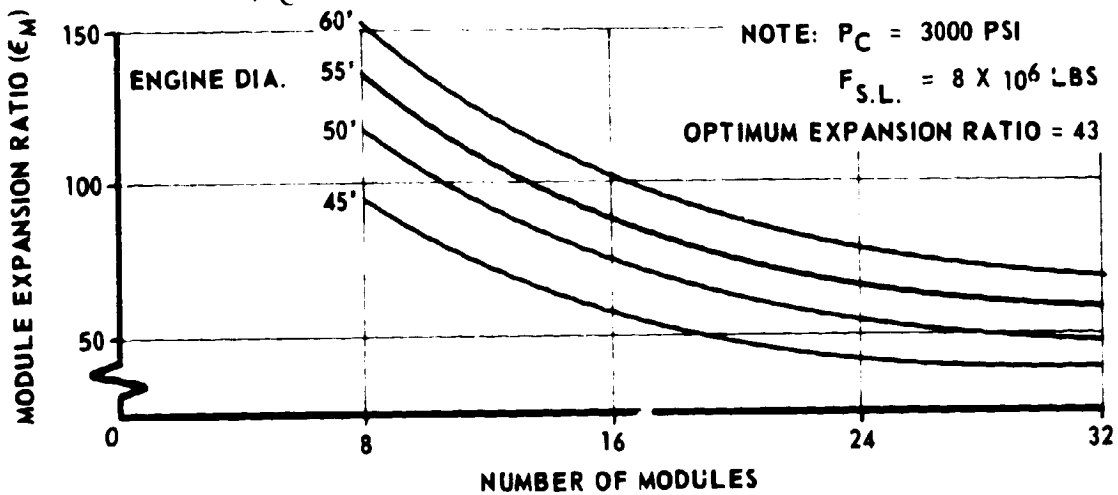
FIGURE 4.1.1.7-3   MODULE EXPANSION RATIO VS. NUMBER OF MODULES
(P_C = 3000 PSI)
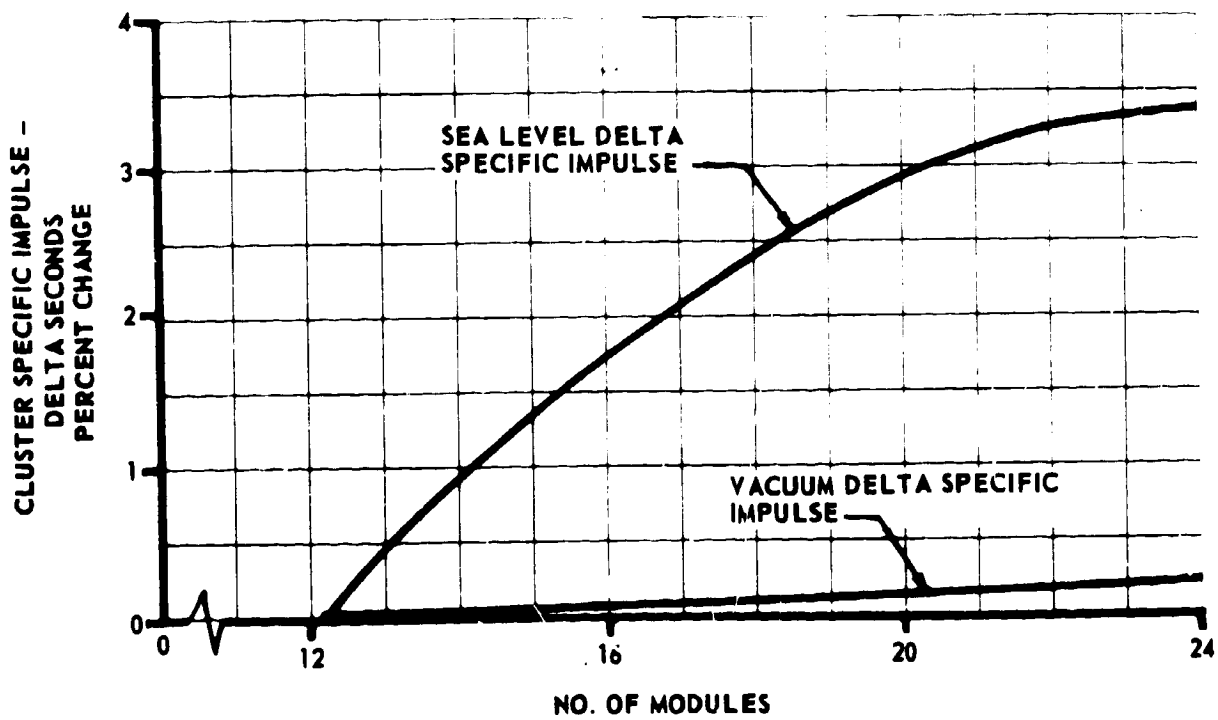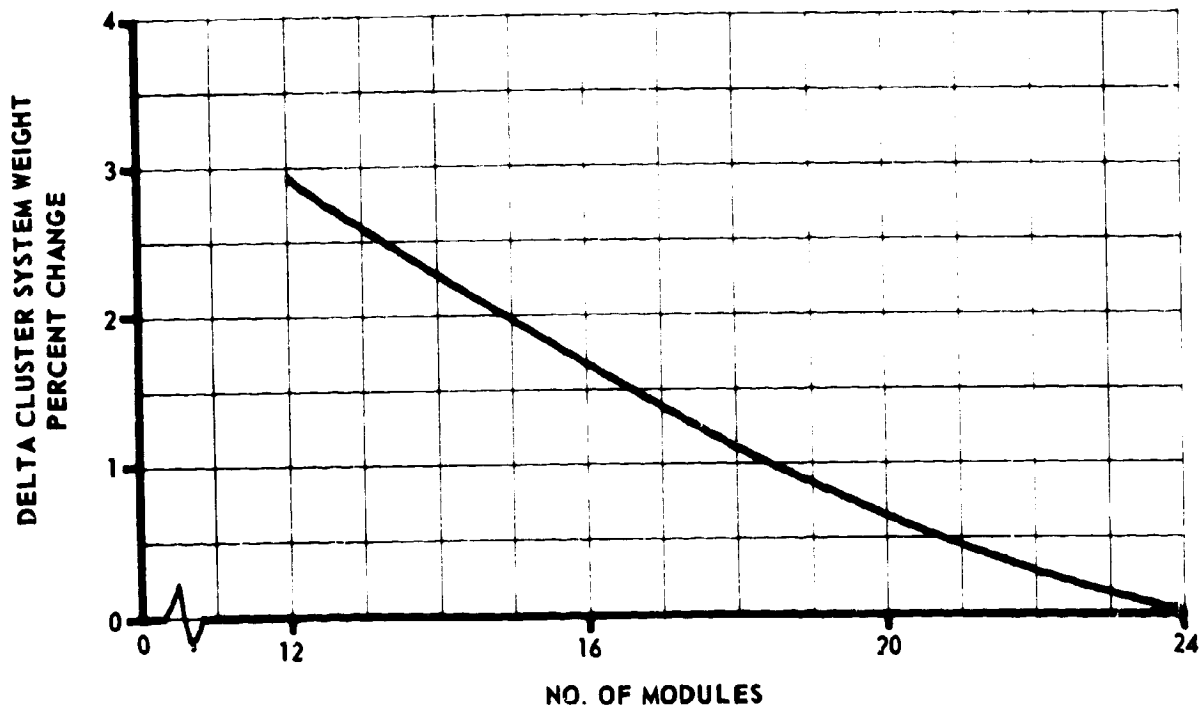
FIGURE 4.1.1.7-4 I_{sp} AND ENGINE WEIGHT AS A FUNCTION OF NUMBER OF MODULES
PRATT AND WHITNEY DATA (FROM AMLLV STUDY)

56

4.1.1.7   (Continued)

The optimum module expansion ratio for the high pressure multichamber/plug propulsion system was defined in the AMLLV study as 43. As indicated by Figure 4.1.1.7-3, more than 32 modules are required to provide this optimum expansion ratio for the half size vehicle modules. Twenty-four modules are not optimum as shown. Corresponding values of delivered specific impulse vs. the number of modules for the 56.7 ft. diameter stage showed that further improvement in sea level of 5.8%, beyond that available with 24 modules, is achievable.

The number of modules for the half size engine system was arbitrarily selected at 24. The basis for this selection primarily was to provide a comparable number of modules for preparation of the cost data for the full size AMLLV vehicle and the half size MLLV vehicle.

Additional data, however, from Pratt and Whitney indicated that improvement in module sea level specific impulse, and the resulting decrease in engine weight, could better be obtained through utilization of a staged expansion cone, i.e., expansion cone with an extendible portion to be extended during the flight time. The extended nozzles would then touch against the plug to provide the zero gap configuration. (Detailed data supporting these recommendations, as provided by Pratt and Whitney, is shown in Volume IX. Discussions showing the advantage of this system and the cost effectiveness are presented in Volume VI.)

Reference report 4.1.1.7-1 showed the results of a trade study made to evaluate the effect of nozzle spacing around the periphery of the plug.

For the initial portion of the MLLV trajectory, the nozzles are aligned axially with the vehicle. The nozzle exhaust is not attached to the plug, and so nozzle spacing has no effect on performance during this stage of flight. During the high altitude portion of the trajectory, the module nozzles are tilted in against the plug. The gap between the modules in the tilted position is given by ℓ/D_E (i.e., in terms of module exit diameters). Cold-flow data reported in Reference 4.1.1.7-1 are indicated in Figure 4.1.1.7-5. These data trends are independent of number of modules, module area ratio, vehicle diameter, and plug length. It is concluded that, without fairings, maximum performance is obtained with zero gap distance. With fairings, data has been extrapolated to show a slight performance increase at gap spacings of about 2. Experimental verification of this latter conclusion has not been made. For this reason and to simplify the plug design, the zero gap configuration without fairings was employed in the MLLV configurations.

Reference 4.1.1.7-1   Pratt and Whitney FR-1415, "Study for Evaluation of
                       Plug Multichamber Configuration," NAS8-11436, Phase
                       I Report
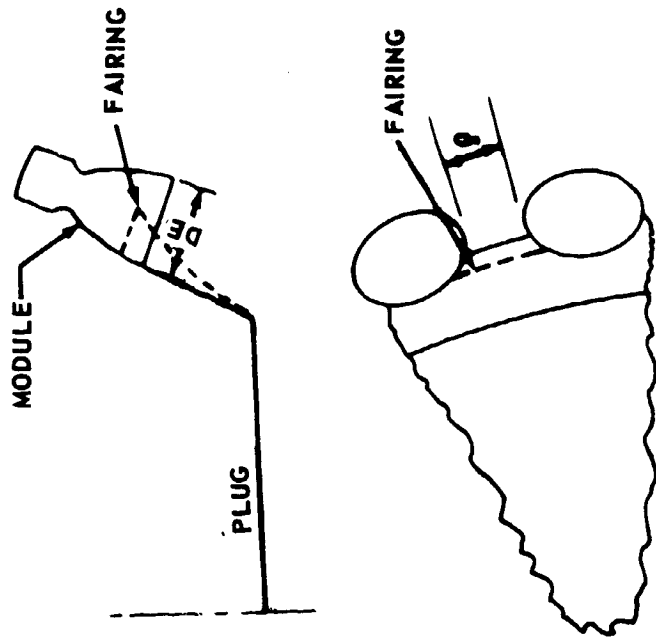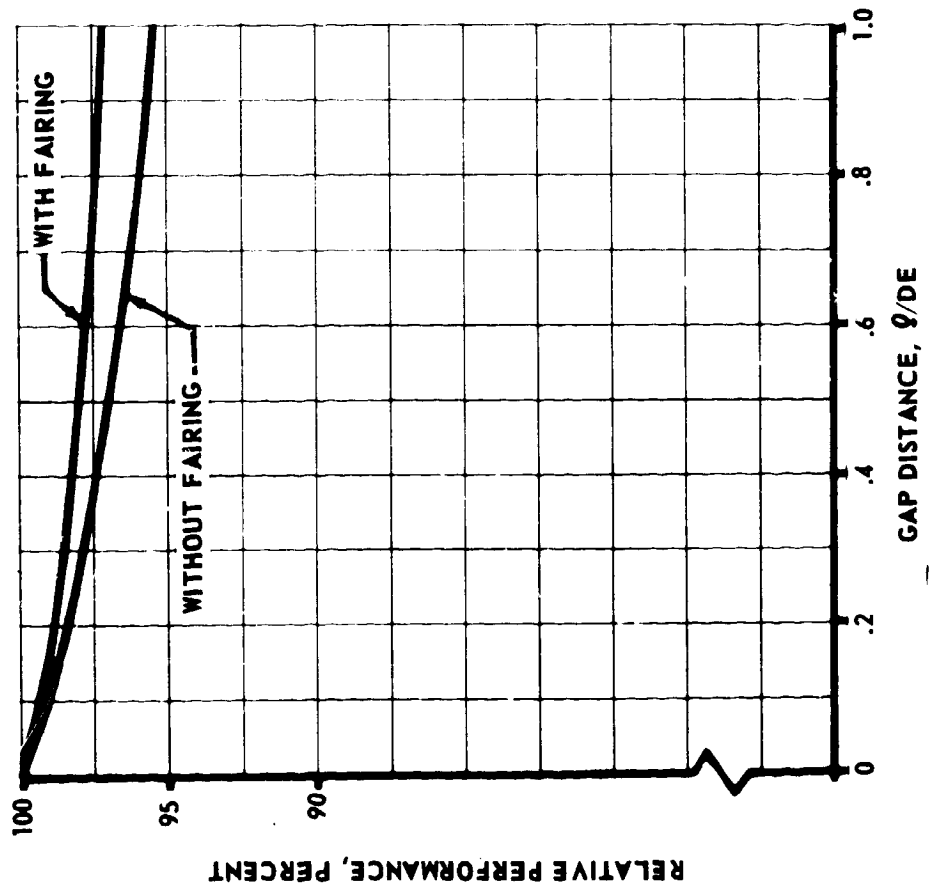
FIGURE 4.1.1.7-5 EFFECT OF MODULE SPACING ON VACUUM PERFORMANCE

4.1.1.8 Multichamber Hinged Engine Trade

In the reference study, performance trades considered the multichamber/plug nozzles with a fixed tilt angle throughout the trajectory versus nozzles with zero tilt angles at lift-off. At altitude, these latter nozzles were tilted inward to take advantage of the plug.

Two engine config.rations were defined for the prior AMLLV trade study, both with 24 million pounds at sea level thrust and a 75-foot basic diameter. The hinged engine system had the engine modules directed straight aft at lift-off and then hinged inward against the plug at 48,000 feet altitude. The other system had the engine modules at the design tilt angle throughout the flight. With axial vehicle thrust identical at sea level for both engine systems, the engine system weight and the altitude thrust were both greater for the fixed tilt angle concept than for the hinged concept. This condition occurred because the tilted engines required a larger lift-off mass flow to compensate for the non-axial thrust (cosine loss).

With the zero tilt at lift-off, axial sea level I_{sp} is greater than that for the fixed tilt angle. The plumes do not interact and the circulation around the nozzle will permit better nozzle efficiency. The fixed tilt angle concept has plume interaction and reduced base pressure. When plug/plume attachment occurs at altitude, the nozzles for both concepts use the plug effectively and, therefore, the specific impulse is identical.

Considering these factors, an approximate 5 percent payload improvement was defined for the hinged nozzle engine system. These prior AMLLV data are shown in Figure 4.1.1.8-1.

These above effects are not size sensitive and will apply directly to the half size vehicle. The hinged nozzle concept was, therefore, selected for the half size vehicle.

The need for a thrust vector control system provides further justification for the selection of the hinged nozzle system over the fixed system.

4.1.2 Injection Stage

The use of an orbital injection stage to increase payload versatility and reduce configuration sensitivities was considered for both core and core-plus-strap-on configurations. A LOX/LH2 stage with toroidal propellant tanks and extendible nozzle high-pressure engine system was selected for the baseline AMLLV injection stage. (See Figure 4.1.2.0-1.) The selected design will provide modular growth capability in that a series of propellant tank modules can be stacked atop the lower (engine) module with additional engines (two engines per module) mounted to a common thrust beam on the lower module. Results of the injection stage trade studies are described in the following sections (4.1.2.1 through 4.1.2.5).
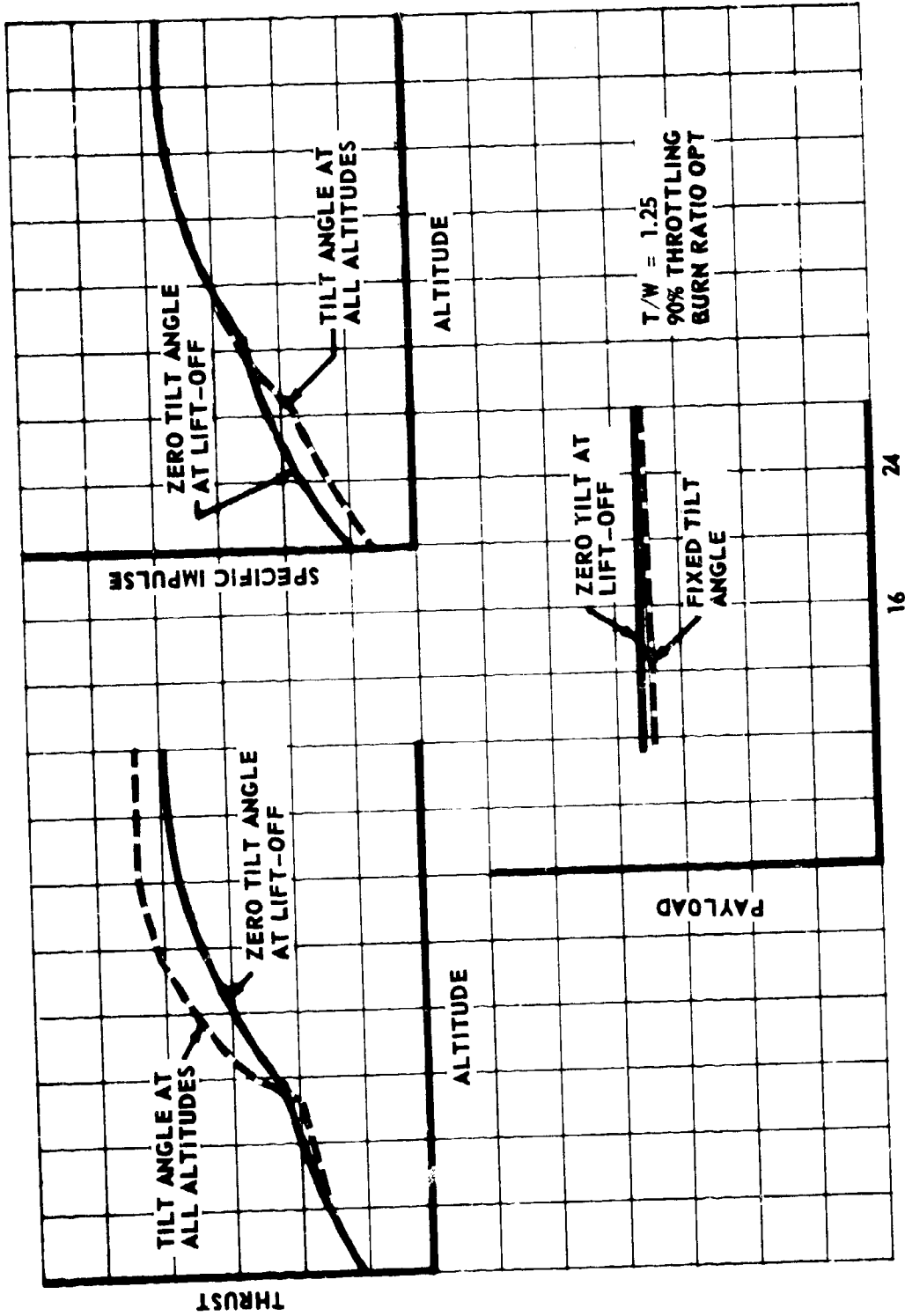
FIGURE 4.1.1.8-1   MULTICHAMBER/PLUG ENGINE - FIXED VS. HINGED MODULED
TRADE (FROM AMLLV STUDY)

HANGER SKIRT
HEAT SHIELD
LOX TANK
LH₂ TANK
ENGINE SUPPORT
TWO RING FRAMES
CYLINDRICAL SKIRT
EXTENDABLE NOZZLE ENGINE
MANIFOLD DUCT
INTERNAL RIB
INJECTION STAGE
FORWARD SKIRT (REF)
CORE VEHICLE (REF)
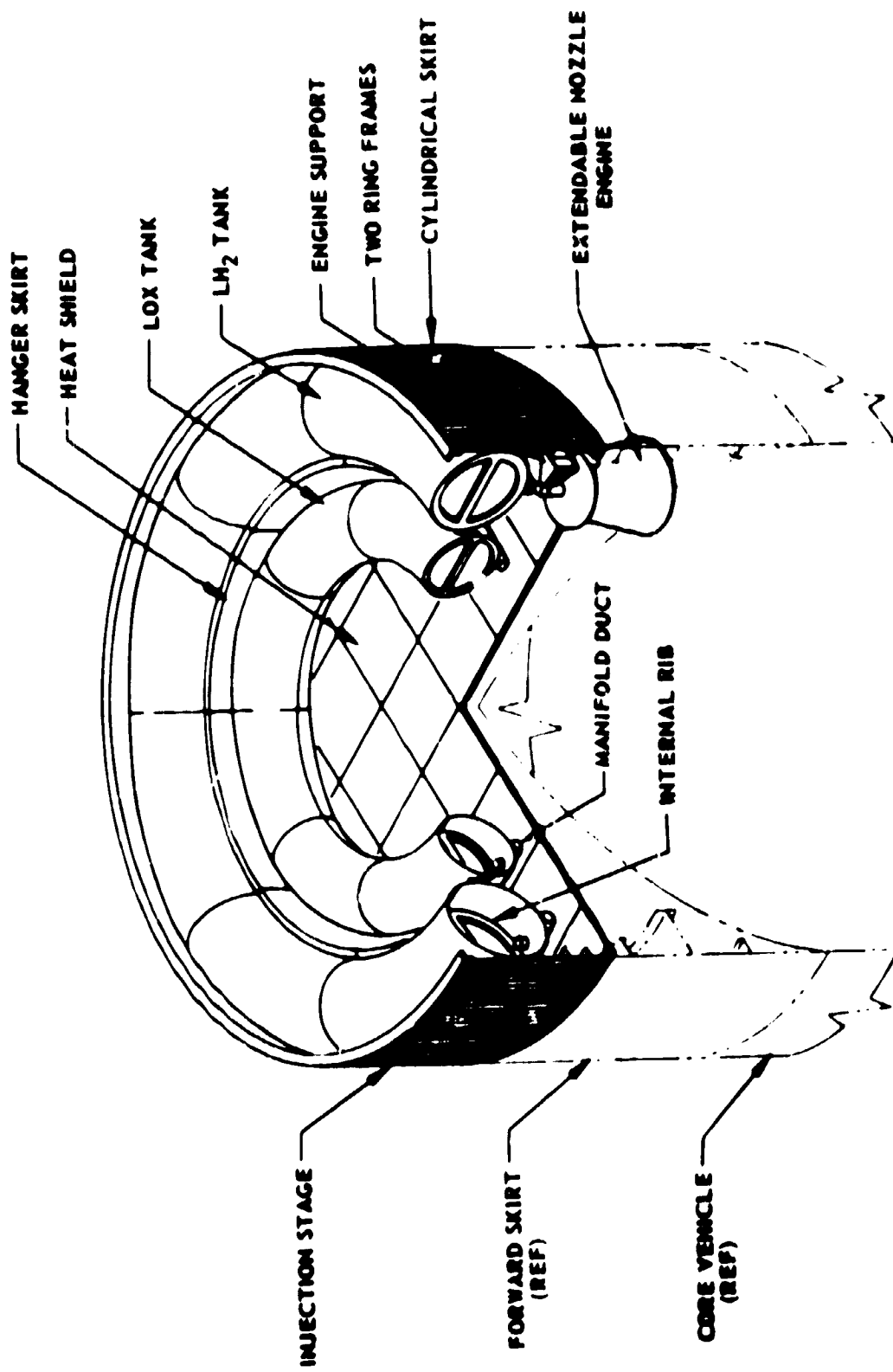
FIGURE 4.1.2.0-1 ORBITAL INJECTION STAGE

4.1.2.1   Structures

For the half size MLLV injection stage, the structural design concepts developed
and verified on the AMLLV program were applied directly. Alternative injection
stage design concepts evaluated in the reference AMLLV study included:

a. Off-loaded tar.'s

b. Full diameter tanks

c. Small tanks or bottles

d. Elliptical tanks

e. Toroidal or semi-toroidal tanks

The prior analyses showed the following: Off-loaded tanks will increase the inert
weight and result in low performance for some missions. Full diameter tanks for
the small quantities of injection stage propellant will necessitate impractical,
heavy tank designs. The use of small bottles or tanks will require special mounting
provisions and will not be adaptable to modular design. Elliptical tanks will require
long skirts and will waste approximately one-third of the enclosed volume. Toroidal
tanks will, however, allow more efficient use of the space and the use of more
efficient structure. The toroidal tank arrangement is also adaptable for modular
stacking to accommodate a range of propellant capacities. For these reasons, the
toroidal tanks design concept was selected for the injection stage.

4.1.2.2   Flight Performance and Sizing

Performance studies were conducted considering a range of injection stage sizes and
main stage throttling modes. For configurations where only the injection stage will
be used with the main stage (i.e., no strap-ons) the injection stage size and subse-
quent payload improvement will be constrained by the practical lower limit for
vehicle lift-off thrust-to-weight (T/W). The main stage was sized for an approximate
lift-off thrust-to-weight of 1.25. An injection stage, plus the additional payload
weight, will reduce this lift-off thrust-to-weight. The lower limit for lift-off T/W
was set at 1.18. The payload increase offered by an appropriately sized injection
stage will be 18 percent for the 100 nautical mile orbit mission. Maximum perfor-
mance for vehicles with injection stages will be obtained from flight modes without
main stage throttling.

Lift-off T/W will not be an influencing factor for configurations where injection
stages are used with the main stage plus strap-on stages. The largest MLLV confi-
guration employing eight strap-on stages will have a lift-off T/W of 1.54 and the
addition of three injection stage modules will reduce this value to only 1.50. For

4.1.2.2   (Continued)

these larger configurations, it was determined that injection stage modules will offer only a relatively small payload performance gain (approximately 5.4% for the 100 nautical mile orbit.

The injection stage optimum size and thrust relationships to main stage size and thrust are not sensitive to vehicle size. Therefore, the half size MLLV injection stage was sized to have approximately half the propellant weight and thrust of the equivalent AMLLV injection stage.

The MLLV injection stage will contain approximately 225,000 pounds of propellant per module. Each engine will produce a vacuum thrust of 125,000 pounds. Two engine 3 will be used per module. The design ullage pressures for the AMLLV injection stage were 24.0 psia and 22.0 psia for the LOX and LH_2 tanks, respectively. Stage size will have little effect on the ullage pressure requirements. These same values will be used for the MLLV injection stages.

The injection stage will provide a practical method for performing a Hohmann transfer type trajectory and will provide a short coupling, high-response control system for accomplishing the final orbital injection maneuver. Single-stage-to-orbit payload capability drops rapidly as higher orbit missions are flown. The injection stage will provide significantly improved capability for higher energy missions (See Figure 4.1.2.2-1).

Other advantages of the injection stage include the capability for orbital altitude changes and/or minor orbital plane changes. Figure 4.1.2.2-2 shows the velocity requirements for making orbit altitude changes, orbit plane changes, and combinations of both maneuvers. The range of ΔV capabilities for the injection stages studied (2000 to 6000 ft/sec) is such that relatively large orbit altitude changes or plane changes may be accomplished.

Small thrust levels are required to provide the fine control necessary in accomplishing precise orbital insertion. This fine control can be obtained using the injection stage after main stage separation. To avoid coupling with the structural bending modes, the rigid body control frequency is usually selected to be approximately one-fourth to one-fifth the first body bending mode frequency. This creates a smooth, though slowly responding, thrust-vector control system. For precise, i.e., fine control, a more responsive system is essential. To accomplish the precise maneuvers required during orbital insertion, the flight control system must be responsive to much smaller error signals. This can be provided by staging to a configuration consisting of an orbital injection stage and the payload, thus greatly increasing body bending frequencies. Staging will minimize the noise entering the flight control system by reducing the vehicle's moment of inertia and flexing due to control deflections. Signal-to-noise ratios will be minimized due to the lower thrust levels required and reduced coupling between the high frequency control system response and higher elastic response of the remaining injection stage and payload.

63

PAYLOAD ~ POUNDS (Kg)

Curve labels:
- CORE ONLY
- CORE PLUS INJECTION STAGE
- CORE PLUS 8 STRAP-ONS
- CORE PLUS 8 STRAP-ONS PLUS 3 INJECTION STAGES

Y-axis values:
- 1M (454K)
- 100K (45.4K)
- 10K (4.54K)
- 1K (454)
- 100 (45.4)

X-axis:
ΔV ~ FEET·SECOND X 10⁻³ (M/SEC X 10⁻³)
- 20 (6.1)
- 30 (9.1)
- 40 (12.2)
- 50 (15.2)
- 60 (18.3)
- 70 (21.3)
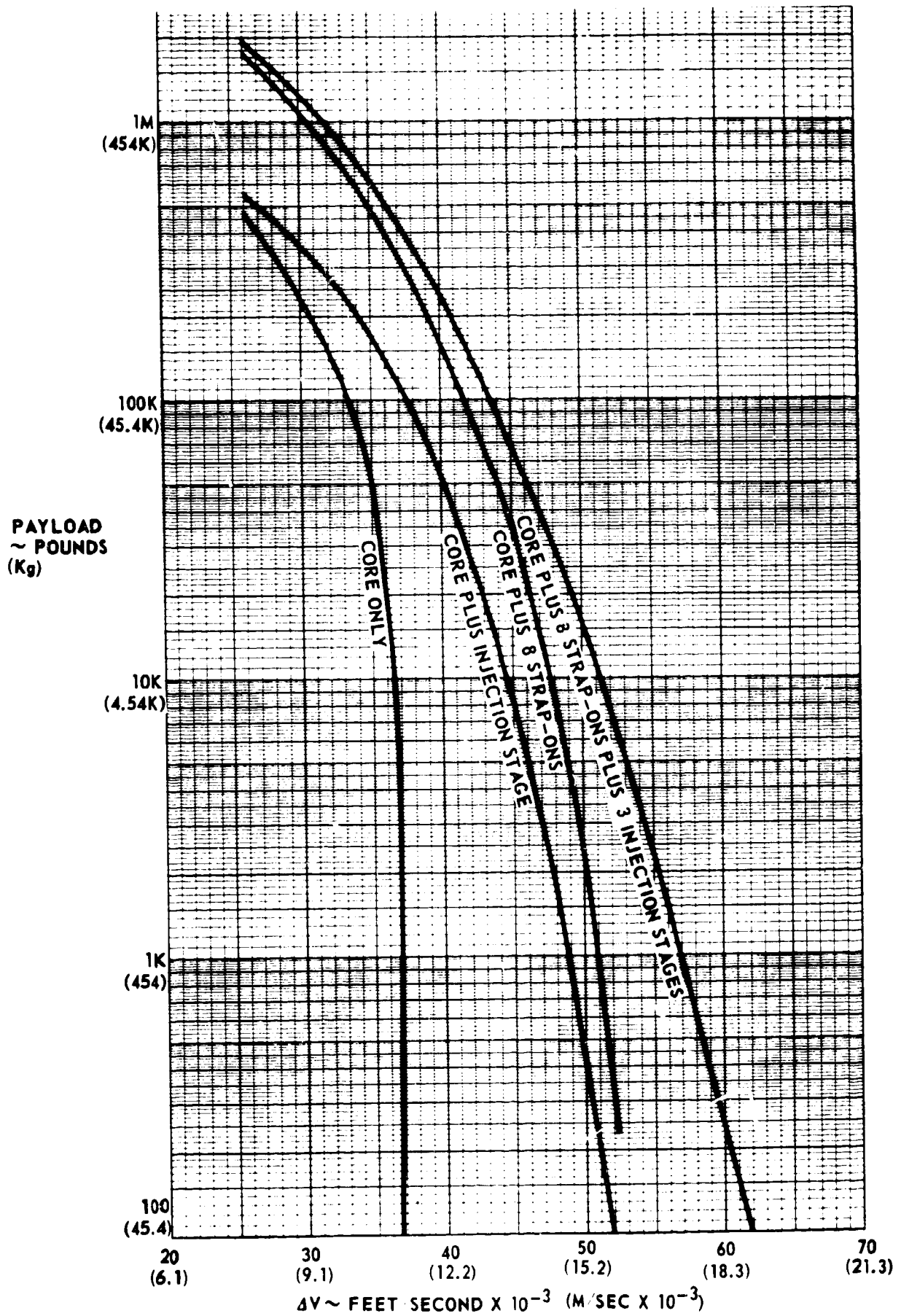
FIGURE 4.1.2.2-1   INJECTION STAGE CAPABILITY FOR HIGH ENERGY MISSIONS
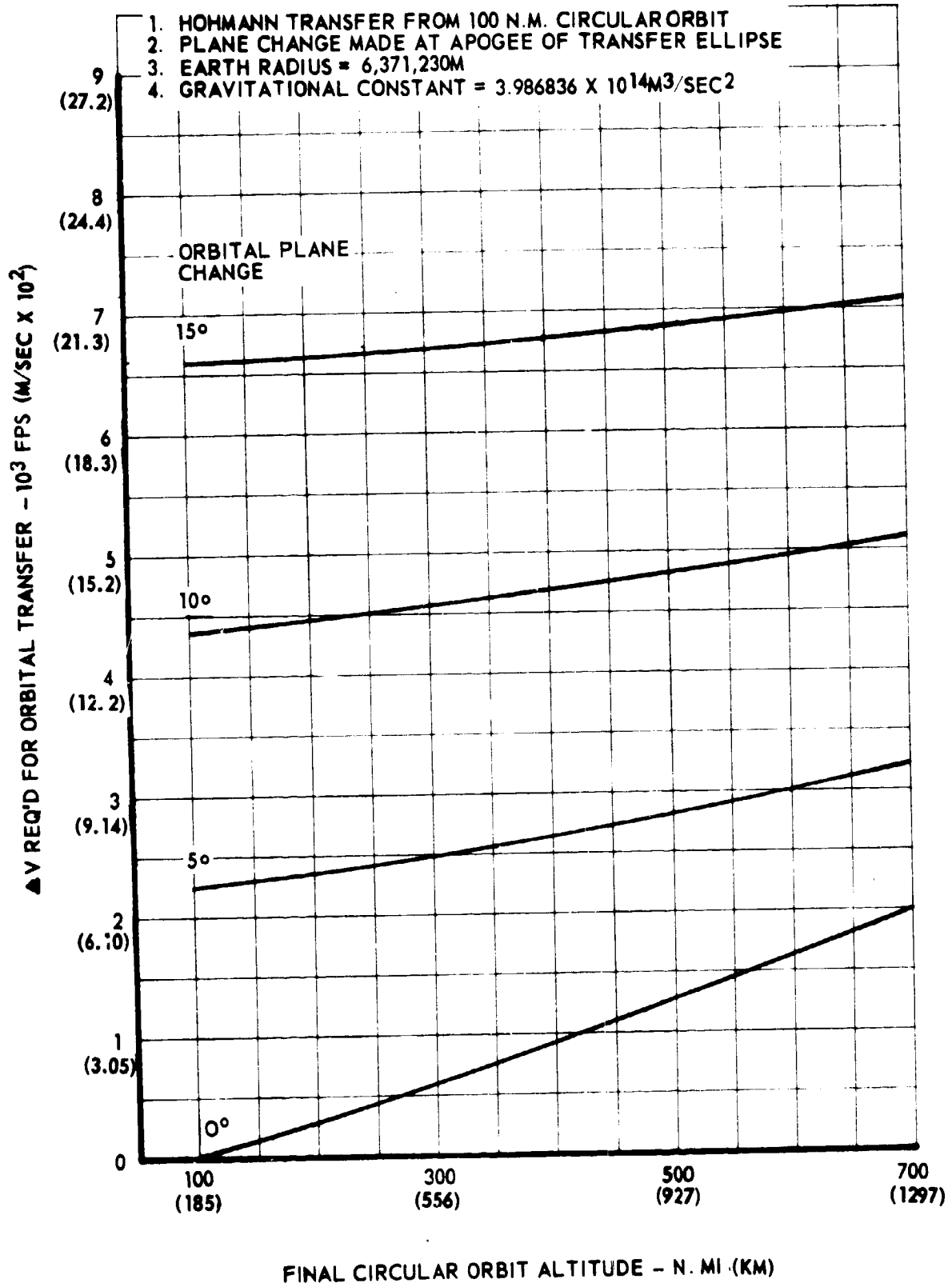
FIGURE 4.1.2.2-2 Δ V REQUIREMENTS FOR ORBITAL ALTITUDE AND PLANE CHANGES

4.1.2.3 Injection Stage Impact on Main Stage Structure

Use of an injection stage will require only minor modifications in the forward skirt and LOX tank area of the main stage structure. Other areas of the single-stage-to-orbit designed main stage will not be adversely affected. These structurel modifications will increase the inert stage weight by only 1.7%.

The injection stage will increase the main stage combined compressive loads principally in the forward skirt and LOX tank areas. These areas would be expected to have increased loads because of the additional weight and length due to the injection stage and the increased payload capability. Conversely, the combined compressive loads for the lower (LH_2 and thrust structure) portion of the vehicle will decrease as the increased payload and injection stage weight will decrease the lift-off thrust-to-weight and result in lower accelerations and dynamic pressure. As the thrust will be reacted at the aft end of the core vehicle on the core plus injection stage vehicle, the injection stage will have little effect on the tension loads.

4.1.2.4 Reduction in Payload Sensitivity to Core Inert Weight

An analysis was conducted to define the reduction of payload sensitivity to core inert weights when the injection stage is used to complement the main stage. Each pound of inert weight increase in the core will decrease the payload in orbit one pound for the core alone configuration. With the addition of an injection stage, approximately 2.2 pounds of core inert weight will result in a one pound payload penalty.

4.1.2.5 Abort Application

Crew abort systems for launch vehicles are designed to have the crew, or crew capsule clear the boosting vehicle by a safe distance before the boost vehicle destruct action is taken. Range safety criteria allow only three seconds delay until the destruct is initiated. A minimum delay period is operationally desirable since it allows the minimum flight path deviation and thereby widens the useable corridor of the flight vehicle.

A crew abort system, therefore, has requirements for a high acceleration and a low propulsive initiation delay. The LOX/LH_2 propulsion system of the injection stage, however, will require approximately 2.7 to 3.0 seconds to attain 90 percent thrust. The location of the injection stage under the overall payload package will provide a thrust-to-weight of less than one. Therefore, the injection stage propulsion system does not have the desired abort system capabilities.

4.1.3 Strap-On Stages

Solid propellant rocket motor (SRM) strap-on stages were selected for the baseline AMLLV family under the reference study. This prior study, however, showed that pressure fed UDMH/N_2O_4 liquid stages could also be used with no significant performance differences. For the half size MLLV studies, only solid propellant rocket motor strap-on stages were considered. Two sizes of SRMs were investigated, 156 and 260 inch diameter motors.

4.1.3.1 Sizing and Performance

The total SRM propellant required for the maximum payload vehicle configuration (to provide approximately 2,000,000 pounds of payload to low earth orbit) was estimated at 23 million pounds. The required sea level thrust at lift-off was estimated to be 54 million pounds. It was determined from geometric constraints that a maximum of sixteen 156 inch SRMs or ten 260 inch SRMs could be used in a single concentric ring. Considering the sixteen 156 inch SRMs, each motor would require the size and performance shown in Table 4.1.3.1-I. The propellant density was assumed to be 0.061 lb_m/in^3 for the calculations.

TABLE 4.1.3.1-I

156 Inch Solid Motor Parameters

Parameters	156" SRM
Initial Sea Level Thrust, lbf	3.4×10^6
Propellant Weight, lb_m	1.44×10^6
Initial Chamber Pressure, psia	1000
Nozzle Area Ratio	7.0
Throat Radius, in	26
Nozzle Length, in	155
Tangent to Tangent Length, in	1350
Total Motor Length, in	1660

These requirements would result in individual 156 inch solid motor with a cylindrical length to diameter ratio of approximately 9 to 1. Four center segments with two end segments would be required per motor. With this high length to diameter ratio, grain erosion will be relatively severe. The length of the 156 inch motor will be such that attachment at the upper end can be in the desired forward skirt location (see Figure 4.1.3.1-1). Separation of these 156 inch solid motors would, however, require a minimum of 32 (two per strap-on) separation motors. The number of strap-on 156 inch stages would require more complex attachment structure and complicate separation dynamics. Use of fewer 156 strap-on stages would increase the required individual stage length and necessitate forward attachment in the payload section.

67
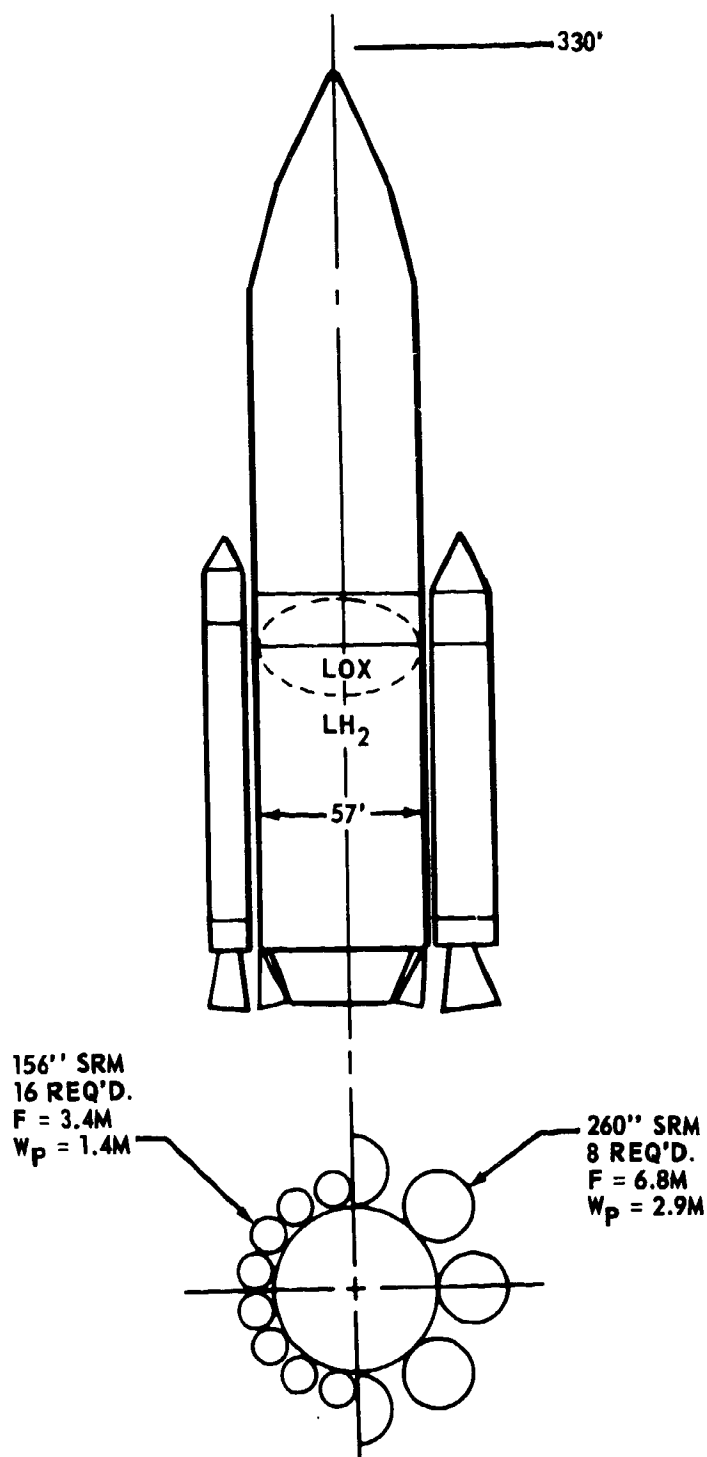
FIGURE 4.1.3.1-1   COMPARISON OF 156" STRAP-ON SRM'S VERSUS 260"
STRAP-ON SRM'S

68

4.1.3.1 (Continued)

As a result of these relatively arbitrary constraints, the use of 156 inch motors was considered only as an alternative for application to the half size vehicle. As the AMLLV baseline family used 260 inch diameter motors, the use of 260 inch motors on this program provided more comparable cost data for the cost/size trade studies.

The use of six, eight and ten 260 inch solid motors was considered for the maximum payload vehicle configuration. The use of six 260 inch motors would allow the use of the same size (thrust and weight) 260 inch motors as were used in the AMLLV study. However, the resulting SRM length would necessitate forward attachment of the 260 inch motors in the payload section of the vehicle. Also, the number of strap-on configurations would be limited to three configurations (2, 4, or 6 strap-ons). The use of eight 260 inch strap-ons will permit attachment in the forward skirt section of the main stage and will permit more vehicle configurations (2, 4, 6 or 8 strap-ons). Use of ten strap-ons would further increase the number of possible configurations. The forward attachment point, however, would be in the propellant tank wall. The selected 260 inch SRM size was, therefore, based on the eight strap-on stage configuration.

Previous studies (References 4.1.1.1-1 and 4.1.3.1-3), which investigated the thrust-time optimization of strap-on booster systems, have shown that a lift-off thrust-to-weight between 1.5 and 1.7 will result in maximum payload. (Thrust-to-weight values in excess of this range generally will tend to impose large structural penalties which will offset any potential payload gain resulting from the higher thrust-to-weight.) These studies have shown that continued strap-on operation at high thrust levels, however, will result in trajectories with both high aerodynamic heating rates and high values for dynamic pressure. These trajectory detriments, however, can be negated by making the SRM thrust-time history regressive, i.e., allowing the SRM thrust to vary optimally through the trajectory. Prior studies have shown that a 50% regressive trace, combined with an initial thrust-to-weight of approximately 1.6, will result in near payload maximization and at the same time acceptable aerodynamic heating rates and dynamic pressures. On the basis of this data and the data from the reference contract, the specified thrust-time history for the SRMs will provide a liftoff thrust-to-weight of 1.6 for the configuration having a main stage plus eight strap-on stages. This will require an initial sea level thrust for each solid motor of approximately 6.8 million pounds. The mass flow history specified was that the mass flow regress at a constant rate during the flight time such that the final mass flow will be 1/2 that required for the initial thrust value (50% regressive). The resulting trajectories, using this data, showed a maximum dynamic pressure during the flight of 1000 pounds per square foot. The anticipated value based on the results of these prior studies for maximum dynamic pressure for this "optimum" burn time history was 950 pounds per square foot.

4.1.3.1-3   Improved Saturn V Vehicles and Intermediate Payload Saturn V Vehicles, NASA Contract NAS8-20266, The Boeing Company Document Number D5-13183-3.

4.1.3.1   (Continued)

The individual SRM design and performance requirements for the eight 260 inch
strap-on overall vehicle confi~uration are shown in Table 4.1.3.1-II.

TABLE 4.1.3.1-II
DESIRED 260 INCH SOLID MOTOR PARAMETERS

Initial Sea Level Thrust, lbs.	6.8×10^6
Propellant Weight, lbs.	2.9×10^6
Initial Chamber Pressure, psia	700
Nozzle Area Ratio	9.0
Throat Radius, in.	47
Nozzle Length, in.	264
Tangent to Tangent Length, in.	922
Total Motor Length, in.	1446
Nozzle Exit Angle (ϵ)	17.5°
Burn Time, Sec.	130

Figures 4.1.3.1-2 and -3 illustrate the required performance for the 260 inch
strap-ons.

For the majority of the various configurations employing strap-on stages, zero
staging will provide the maximum payload. The main stage and strap-ons will be
burned in parallel only in those cases where main stage ignition at launch is required
to achieve a lift-off thrust to weight of not less than 1.18. (A parallel burn mode
with throttled main stage engines may be desirable to reduce thermal effects on
the base plug, eliminate the need for altitude ignition capability of the main stage
engines and improve reliability. Analysis of the effects of throttled main stage
engines at lift-off is a complex analysis and was not a part of this study.)

Throttling of the main stage prior to orbital injection for configurations without
injection stages will provide greater payload capability whether the vehicle is zero
or parallel staged. The AMLLV study demonstrated that with the parallel burn
configurations, a 90 percent main stage throttling at a burn ratio of approximately
0.125 would provide the maximum payload. For the zero staged configurations, 90
percent throttling will increase the time to orbit and thus reduce the flight path
angle. Burn ratio was found not to be a sensitive parameter. The "optimum" thrust-
time relationships are not size sensitive and were applied to the MLLV configurations.

Preliminary trajectory analyses verified the above sizing and performance estimates.
For these studies, the core propellant was fixed at 5.55 million pounds in the main
stage. The drop weight was based on a mass fraction of 0.933. All vehicles were
launched due east from AMR utilizing direct injection to 100-nautical mile circular
orbit. The solid motors were assumed to have a mass fraction of 0.90 (including
attachment structure weight).
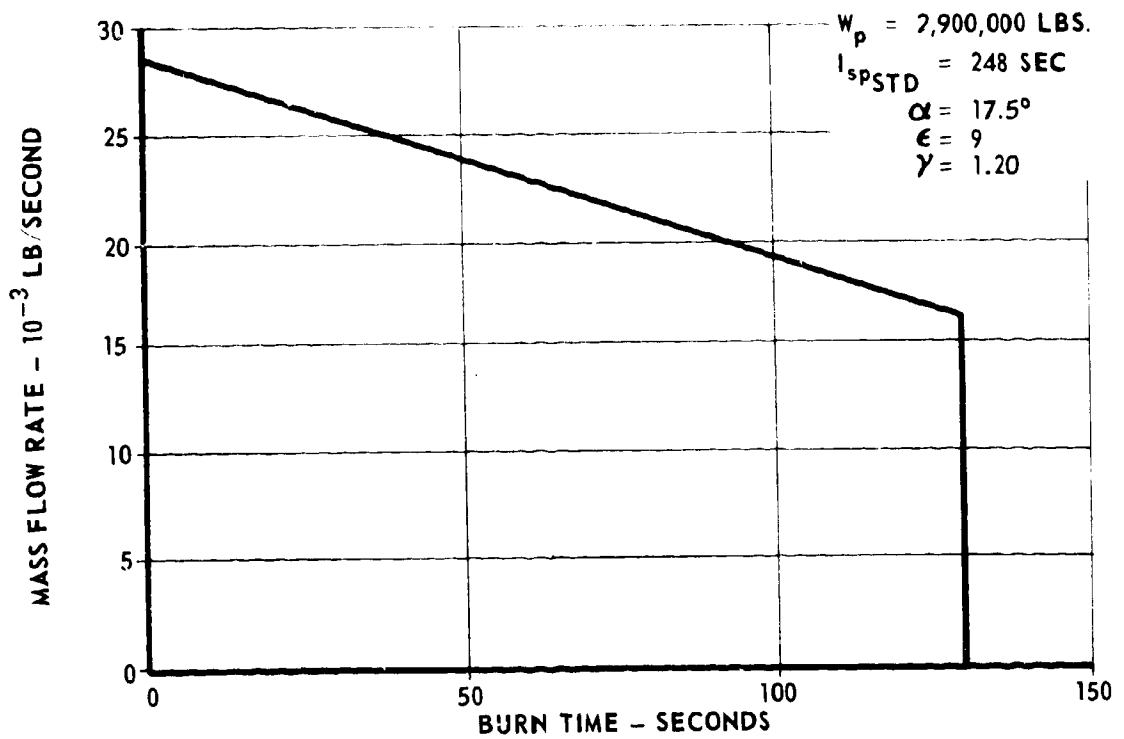
FIGURE 4.1.3.1-2 PRELIMINARY LINEARIZED MASS FLOW VS. TIME
PERFORMANCE OF 260 INCH SOLID ROCKET MOTOR –
MLLV VEHICLE FAMILY
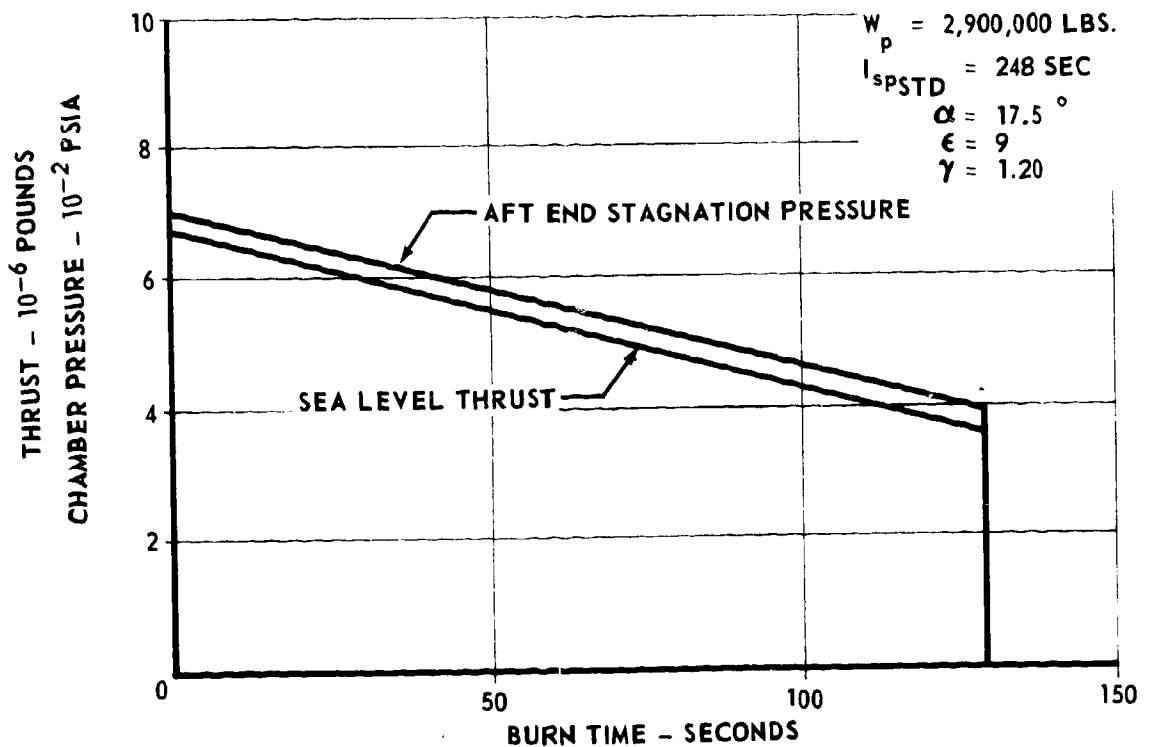
FIGURE 4.1.3.1-3 PRELIMINARY LINEARIZED THRUST AND CHAMBER
PRESSURES VS. TIME PERFORMANCE OF 260 INCH
SOLID ROCKET MOTOR - MLLV VEHICLE FAMILY

71

4.1.3.1   (Continued)

The resulting trajectories were compared with trajectories of similar AMLLV
configurations. These comparisons were done in the same manner as the trajec-
tory comparisons for trajectory optimization of the main stage vehicle (as discussed
in Paragraph 1.1.1.1 above). The close coincidence between the trajectory para-
meters again confirmed that throttling and burn ratio effects are not size sensitive
provided that weight and thrust are scaled proportionally.

4.1.3.2   Strap-On Design Impact on Main Stage Structure

The thrust levels and weights of the strap-on boosters will result in an extremely
large force which must be reacted by the vehicle. The AMLLV main stage was
designed for both forward holddown and forward strap-on thrust reaction to mini-
mize the effects of these large forces on the main stage structure. The main stage
will have the large inertia masses (payload and LOX) located in the upper portions
of the vehicle. The forward thrust plane will allow strap-on thrust load inputs
to the payload and LOX tank through minimum length load paths.

Analyses showed that the SRM strap-on stages will not significantly increase
the required main stage weight (provided that the thrust inputs of the strap-on
stages are reacted at the forward skirt). Vehicle configurations with SRM
strap-ons will, however, require major structural beef-up to the forward skirt
with some minimal additional structure in the aft skirt, tank bulkheads, and the
LOX cylinder. Structural penalties for the single-stage-to-orbit vehicle can be
minimized with interchangeable forward skirts where a heavier skirt is provided
for the strap-on configurations.

Results of the prior AMLLV forward versus aft attachment trades were directly
applicable to the half size vehicle. These results showed the following. For a
single-stage-to-orbit vehicle, the main stage hydrogen tank skin is designed by
the compressive load at maximum $q\alpha$. The compressive loads resulting from aft
attachment of the strap-on stages will be approximately two and one half times the
compressive loads experienced during single-stage-to-orbit vehicle. Therefore,
the aft attachment concept will severely penalize the LH_2 tank structural weight.
When the thrust from the solid motors is introduced in the forward skirt area
(forward attachment concept), the axial loading in the core vehicle LH_2 tank during
strap-on operation is tensile and falls within the tension capability of the core
vehicle as designed for the single stage to orbit mission. The main stage LOX tank
and the LH_2 skin thickness and aft bulkhead are designed by the hoop tension loads
(internal pressure at SRM burnout in zero stage mode). This is independent of
attachment concept.

72

4.1.3.2 (Continued)

The results of the prior AMi LV attachment trade studies were reviewed to obtain
a quantative estimate of the relative structural penalties associated with forward
and aft attachment concepts. For this trade, it was necessary to consider only the
relative weight differences of the LH$_2$ tank walls. This conclusion was arrived
at by qualitatively considering the impact of forward vs. aft attachment on the other
primary structural elements as discusse I below:

a. Bulkheads - the weight of these components will be independent of the
attachment position.

b. Combination of forward skirt and thrust structure - the individual weight of
these two structures will be dependent upon attachment positon; however, it
may be concluded that any variation in the combined weight will be small
as either forward or aft attachment requires the same type of structure.
In one case, forward attachment, it will be necessary to place structure
(post, rings and heavy skin stringer combinations) in the forward skirt.
In the other, aft attachment, it will be necessary to place similar strap-on
provisions in the thrust structure. The thrust structure will be inherently
more stable than the core-alone forward skirt and as such will require fewer
modifications to maintain integrity of the thrust structure for aft attachment.
Aft attachment, however, will require a longer thrust structure to provide
a uniform load distribution at the thrust structure to LH$_2$ tank interface.

c. LOX tank side wall - the weight of the structure will be dependent upon
attachment position; however, for a minimal or zero length side wall, there
will be no significant impact.

d. LH$_2$ tank side wall - the weight of this structure will be dependent upon attach-
ment position. Forward attachment will result in a significant weight reduc-
tion for this structure. The LH$_2$ cylinder was sized twice: First to carry
the N_c (axial compression) loads resulting from aft attachment, and second
to carry the N_c loads from forward attachment. These loads are shown in
Figure 4.1.3.2-1. (This figure is a reproduction of AMLLV data.) Also
shown are the main stage N_c loads for the single-stage-to-orbit mission.
It was determined that internal pressure will be uneffected by attachment
position. Therefore, the changes in the tank wall cross-section for forward
vs. aft attachment will result only from the change in N_c loading with attach-
ment position.

The resulting structural weight estimates for the cylinder as sized for aft
attachment as compared to the structural weight estimates of the cylinder
as sized for forward attachment are shown below:

73
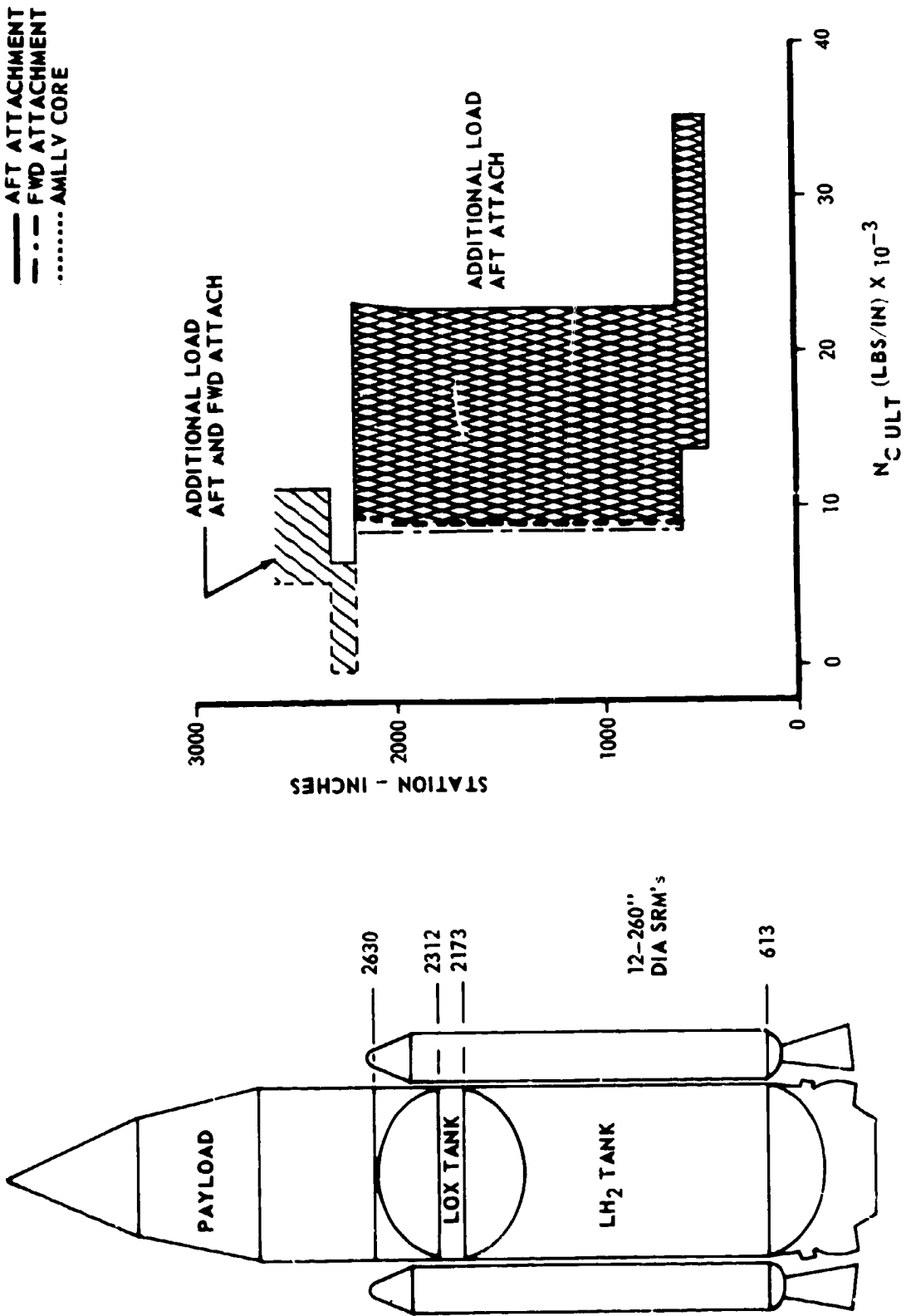
FIGURE 4.1.3.2-1   LOAD COMPARISON - AMLLV - FORWARD VERSUS AFT ATTACHMENT (FOR AMLLV FROM REFERENCE STUDY)

4.1.3.2   (Continued)

	LH$_2$ Tank Cylinder Structural Weight	Main Stage Inert Weight
Fwd Attachment Method	234,864 lbs.	901,527 lbs.
Aft Attachment Method	403,864 lbs.	1,070,527 lbs.

The structural weight data for the forward attachment configuration was obtained from the trade study AMLLV vehicle (Dia. = 75 ft., MR = 6:1 and LH$_2$ Ullage pressure = 28 psia.

The above data indicates that the required stage structural weight for the forward attachment concept will be 85 percent of that required for the aft attachment concept (i.e., a 15% weight saving).

4.2 GROUND AND FLIGHT ENVIRONMENT

As a result of the design and performance trades (as reported in Section 4.1), configurations for the baseline vehicle family were selected for follow-on detailed design and resource studies.

In order to accomplish the structural design and to provide the proper subsystems for the vehicle, it was necessary to investigate the ground and flight environment that the vehicle would experience during its operation. This section of the report describes the ground and flight environment studies that were accomplished, i.e.:

Section Number	Subject
4.2.1	Preliminary Flight Performance and Trajectories
4.2.2	Aerodynamics
4.2.3	Preliminary Vehicle Weight and Mass Characteristics
4.2.4	Loads and Structural Criteria
4.2.5	Control Requirements
4.2.6	Separation Requirements
4.2.7	Heating Environment

The resulting data from these studies established the requirements for the baseline MLLV vehicle design discussed in Section 4.3.

Typical preliminary vehicle configurations, used for the ground and flight environment analyses, and a summary of their anticipated environments are shown in Figures 4.2.0.0-1, 4.2.0.0-2, 4.2.0.0-3 and 4.2.0.0-4.

The mass fraction values shown on these four figures are based on preliminary weight estimates. The payload values shown are the results of the preliminary trajectory runs. Final trajectory runs were accomplished later in the study when the vehicle design had been completed and the final weights were defined. The final weight payload values are reported in the subsequent Section 4.3. The values shown on the figures, however, were those used for the ground and flight environmental studies. Similarly, the trajectory parameters as shown resulted from the preliminary trajectory analyses. These trajectory parameters are compared with the final trajectory parameters in the subsequent Section 4.3.1. As this comparison shows, there were only minor differences between the trajectory parameters for the preliminary trajectory analyses and those of the final trajectory analyses. Comparisons between the preliminary weight estimates and the final weights also showed only minor differences. Because of these close agreements,

77

FIGURE 4.2.0.0-1 GROUND AND FLIGHT ENVIRONMENT SINGLE-STAGE-TO-ORBIT

FLIGHT MODE

- FULL MASS FLOW THRU 89% PROPELLANT DEPLETION THEN

- THROTTLED TO 10% MASS FLOW UNTIL ORBITAL INJECTION

CONTROL

- MAX GIMBAL ANGLE = 3.9°

- TIME TO DOUBLE AMPLITUDE = 0.85 SEC.

NOTE:

HEAVY LINES OR UNDERLINED NUMBERS DENOTE "WORST ENVELOPE" DESIGN CONDITIONS

$W_{PL} \cong 0.50M$ LBS.
$W_{VEH} = 6.4M$ LBS.

MAIN STAGE

MIX RATIO = 6:1
$W_P = 5.55M$ LBS.
$\lambda' = 0.933$
$F_{S.L.} = 8M$ LBS.
LIGHT WEIGHT FORWARD SKIRT

LOADS

MAX q = 691 LBS/FT^2

ACCELERATION (g's)
- LIFT OFF = 1.25
- 89% PROPELLANT DEPLETION = 7.15
- BURNOUT = 0.71

78

FLIGHT MODE

- NO MAIN STAGE THROTTLING

CONTROL

- MAX GIMBAL ANGLE $\simeq 3.9°$
- TIME TO DOUBLE AMPLITUDE < 1.4 SEC.

NOTE:

HEAVY LINES OR UNDERLINED NUMBERS DENOTE "WORST ENVELOPE" DESIGN CONDITIONS

LOADS

MAX q = 617 LBS/FT^2

ACCELERATION (g's)

- LIFTOFF = 1.18
- MAIN STAGE = 8.34 BURN OUT
- INJECTION STAGE IGNITION = 0.30

$W_{PL} \simeq 0.56M$ LBS.

W_{VEH} = 6.8M LBS.

SINGLE MODULE INJECTION STAGE

MIX RATIO = 6:1
W_P = 225K LBS.
λ = 0.80
F_{VAC} = 250K LBS.

MAIN STAGE

MIX RATIO = 6:1
W_P = 5.55M LBS.
λ = 0.933
$F_{S.L.}$ = 8M LBS.
LIGHT WEIGHT FORWARD SKIRT

89'

242'

LOX

LM$_2$

153'

56.7'

N_C (LBS/IN X 10^{-3})

0 1 2 3 4 5 6 7

CUT-OFF

MAX qα

LIFTOFF

CORE IGNITION
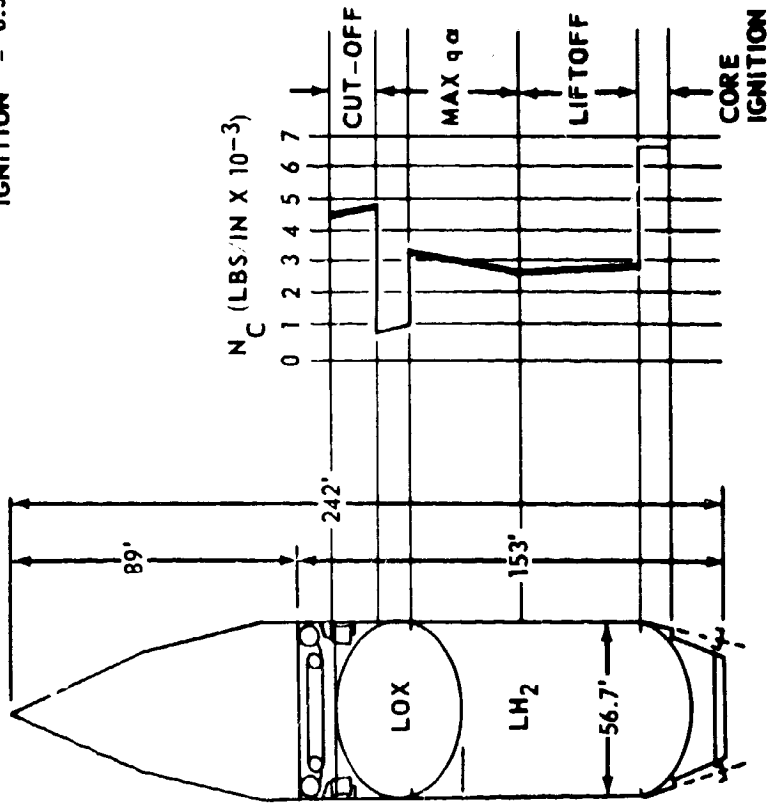
FIGURE 4.2.0.0-2   GROUND AND FLIGHT ENVIRONMENT MAIN STAGE + A SINGLE MODULE INJECTION STAGE

FIGURE 4.2.0.0-3 GROUND AND FLIGHT ENVIRONMENT MAIN STAGE + (8) STRAP-ONS

LOADS

MAX q = 999 LBS/FT^2

ACCELERATION (g's)

- LIFT OFF = 1.62
- SRM BURNOUT = 3.23
- 89% PROPELLANT DEPLETION = 3.66

- MAIN STAGE BURNOUT = 0.47

P_{MAX} (PSIA ULTIMATE)

LOX = 110.0
LH_2 = 50.3

FLIGHT MODE

- ZERO STAGED
- FULL MAIN STAGE MASS FLOW THRU 89% PROPELLANT DEPLETION THEN THROTTLED TO 10% MASS FLOW UNTIL ORBITAL INJECTION

$W_{PL} \cong$ 1.77M LBS.
W_{VEH} = 33.5M LBS.

CONTROL

- MAX SRM GIMBAL ANGLE < 3.9°
- TIME TO DOUBLE AMPLITUDE < 1.4 SEC.

MAIN STAGE

MIX RATIO = 6:1
W_P = 5.55M LBS.
λ' = 0.930
$F_{S.L.}$ = 8M LBS.
HEAVY WEIGHT FORWARD SKIRT

SRM STAGE (8 STRAP-ONS)

W_P = 23.2M LBS.
λ' = 0.90
$F_{S.L.}$ = 54.4M LBS.

NOTE:

HEAVY LINES OR UNDERLINED NUMBERS DENOTE "WORST ENVELOPE" DESIGN CONDITION

80

LOADS

MAX q = 937 LBS/FT^2

ACCELERATION (g's)
- LIFTOFF = 1.59
- SRM BURNOUT = 2.96
- CORE BURNOUT = 3.34
- INJECTION STAGE IGNITION = 0.28

P_{MAX} (PSIA ULTIMATE)

LOX = 103
LH_2 = 50

N_C (LBS IN X 10^{-3})

0 1 2 3 4 5 6 7 8

MAX qα

CORE CUTOFF

CORE IGNITION

362'

192'

170'

56.7'

LOX

LH_2

FLIGHT MODE

- ZERO STAGED
- NO THROTTLING

CONTROL

- MAX SRM GIMBAL ANGLE = 3.9°
- TIME TO DOUBLE AMPLITUDE = 1.4 SEC.

$W_{PL} \simeq$ 1.9M LBS.

W_{VEH} = 34.4M LBS.

THREE MODULE INJECTION STAGE

MIX RATIO = 6:1
W_P = 675K LBS.
λ' = 0.86
F_{VAC} = 750K LBS.

MAIN STAGE

MIX RATIO = 6:1
W_P = 5.55M LBS.
λ' = 0.930
$F_{S.L.}$ = 8M LBS.
HEAVY WEIGHT FORWARD SKIRT

SRM STAGE (8 STRAP-ONS)

W_P = 23.2M LBS.
λ' = 0.90
$F_{S.L.}$ = 54.4M LBS.

NOTE:

HEAVY LINES OR UNDERLINED NUMBERS DENOTE "WORST ENVELOPE" DESIGN CONDITIONS

FIGURE 4.2.0.0-4   GROUND AND FLIGHT ENVIRONMENT MAIN STAGE + 3 MODULE INJECTION + (8) STRAP-ONS

4.2   (Continued)

there were no iterative analyses to refine the ground and flight environmental
data.

The flight modes for each of the four vehicles shown are shown in the upper left-
hand corner of the figures. In general, it was determined that main stage throttling
was desirable for all configurations which did not employ an injection stage. No
main stage throttling was required for configurations employing an injection stage.
The zero stage mode was found to be the desirable flight mode for those configura-
tions having the strap-on stages. The only exception was in the single case where
the lift-off thrust of the solid strap-ons was not sufficient to provide an acceptable
lift-off thrust-to-weight. For this case, (i.e., main stage plus two strap-on
stages) it was necessary to launch with a parallel burn (i.e., strap-on stages
and main stage propulsion systems ignited simultaneously).

The loads studies investigated the "worst condition" design envelope as defined
by a review of the anticipated loads for the many various possible configurations.
It was found that the axial loads envelope was defined by basically two of the
vehicle configurations i.e., the single-stage-to-orbit configuration, and the
configuration consisting of the main stage plus eight strap-on stages plus a three
module injection stage. The use of the forward thrust reaction of the strap-on
stages minimized the relative differences in main stage axial loads for the various
configurations. The major axial loads impact for addition of the strap-on stages
was in the forward skirt region of the vehicle. Four sets of loads data were,
therefore, developed for this area to provide inputs for design of two separate
interchangeable forward skirts, i.e., one for use without strap-on stages and
the other for use with the strap-on stages.

The tank skin thickness will be defined by the maximum internal tank pressure
and the resulting hoop tension. The configuration consisting of a main stage plus
eight strap-on stages established this design condition. The design condition
will occur at SRM cutoff. Only a nominal increase in tank wall thickness, as
designed for the single-stage-to-orbit mission, will be required for this application.

The maximum required gimbal angle for the main stage propulsion system will be
3.9° as established by the main stage plus single module injection stage configura-
tion. This gimbal angle will be required during the maximum dynamic pressure
flight regime (max $q\alpha$). Control requirements other than at the max $q\alpha$
condition will be considerably less than this maximum requirement. The control
requirements for the single-stage-to-orbit vehicle will be approximately the same
as for the main stage plus a single module injection stage vehicle. The maximum
required gimbal angle for the strap-on stages was set by the configuration with
the eight strap-on stages plus the three module injection stage. The required
gimbal angle for this configuration will also be 3.9°. This gimbal angle must be
provided by the solid propellant strap-on stages as the main stage will be

82

4.2   (Continued)

inoperative during the condition of maximum control requirements at the time of
max q α (i.e., the vehicles are zero staged).

Relative to the current Saturn V/Apollo abort criteria, all of the vehicles in the
half-size vehicle family were found to be unacceptable with regard to the time to
double amplitude during uncontrolled divergence. Current Saturn V/Apollo
criteria, to allow time for pilot reaction, specifies that the minimum time to
double amplitude be two seconds. The time to double amplitude of the short L/D
"stiff" vehicles in the MLLV vehicle family ranged from 0.85 seconds for the
single-stage-to-orbit configuration to 1.4 seconds for the maximum payload
configuration. This situation can be corrected by the addition of aft fins or an
aft flared skirt to the main stage or by automation of the abort system, such that
pilot reaction will not be required. This latter approach would reduce the re-
quired response time of the abort system.

The maximum skin temperatures from free stream aerodynamic heating will be
500°F at the forward skirt of the main stage. This temperature will occur with
the configuration employing a main stage and eight strap-on stages. The heating
analyses, however, did not take into account the forward skirt heating that would
result from shock impingement from the nose cones of the strap-on stages.
Insulation will be required in the forward skirt area to account for this shock
impingement. This insulation will, therefore, protect the forward skirt from
the free stream aerodynamic heating.

The requirements for thermal protection of the base plug during the time of SRM
operation were determined. The total convective and radiant heat during the entire
SRM operating time will be 2968 BTU/sq. ft. and 5618 BTU/sq. ft. at the lip
and center of the plug, respectively. The required thickness of the ablative cork
insulation was determined.

An alternative method for protecting the base plug during SRM operation was con-
sidered. This method (which would also provide increased reliability through the
elimination of the altitude start requirement for the main stage engines) would
employ operation of the main stage engines in a throttled condition concurrent
with SRM operation. Operation of the main stage engines will circulate liquid
hydrogen through the regenerative cooling tubes to remove heat in the base region.
Analyses were conducted to define the amount of liquid hydrogen required to cool
the base plug. This value will determine the degree of throttling required during
SRM operation.

Analyses of the impact of various payload densities on the baseline vehicle struc-
tures and control requirements showed that increased densities over the nominal
five pounds per cubic foot would not increase the required structure or the
control requirements. Decreasing the density will, however, increase the
required structure and control requirements.

4.2.1 Preliminary Flight Performance and Trajectories

To provide input data for the subsequent aerodynamics, loads, control, separation, and heating studies, preliminary trajectory analyses were conducted. These studies used preliminary weights as defined during the design and performance trade studies and as extrapolated from the full size AMLLV vehicle studies (reference contract NAS2-4079). The propulsion inputs for these preliminary trajectory analyses were defined during the design and performance trades. Preliminary trajectory analyses were conducted for the following vehicles:

a. Single-stage-to-orbit: 1) with multichamber/plug engines, 2) with toroidal/aerospike engines.

b. Main stage plus a single injection stage module (multichamber/plug on main stage).

c. Main stage plus two 260" solids (multichamber/plug on main stage).

d. Main stage plus four 260" solids (multichamber/plug on main stage).

e. Main stage plus eight 260" solids (multichamber/plug on main stage).

f. Main stage plus three injection stage modules plus eight 260" solids (multichamber/plug on main stage).

Final trajectory data is presented in Section 4.3.1.

The single-stage-to-orbit vehicle analyses indicated no significant differences in the resulting trajectory parameters for either of the two different engine systems under consideration. It was, therefore, concluded that the aerodynamics, loads, control, separation, and heating studies, based on use of either propulsion system, would be applicable to both.

At the completion of the design studies, additional final trajectory analyses were conducted using the final weights and propulsion parameters as developed during the design activities. These final trajectory analyses were compared with the

84

4.2.1   (Continued)

preliminary trajectory analyses to assure that no major differences in trajectory
parameters resulted between the final and preliminary data. These comparisons
are discussed in a subsequent section (Section 4.3.1) of this report. The maximum
variation in designing parameters was less than 2%. Because of this close
agreement, there were no further iterative analyses conducted relative to the
aerodynamics, loads, control, separation and heating studies.

All vehicles were launched due east from AMR and their payloads were inserted
into a 100 NM circular orbit. The weight of main stage usable propellant
(LOX/LH$_2$) was fixed at 5,550,000 pounds at a mixture ratio of 6:1. The initial
main stage propellant mass flow rate for all cases corresponded to that required
to produce 8,000,000 pounds of thrust at sea level. The trajectory analyses were
conducted employing the Plumbline COV computer program which is a point mass,
two dimensional program which assumes a gravity turn trajectory through the
atmosphere and then uses the Calculus of Variations to determine optimum steering
during the latter portion of the flight.

The trajectory mode employed was a 12 second vertical rise followed first by a
25 second optimized tilt maneuver, and then by a gravity turn. For the single-
stage-to-orbit vehicle, the gravity turn was employed until the propulsion system
was throttled. Then COV was used for the remainder of the stage burn time.
For the vehicle consisting of a main stage plus an injection stage module,
no throttling was used and the gravity turn was employed through main stage
burn out. Then COV was initiated with injection stage ignition. The vehicles
employing the strap-on stages used a 12 second rise followed by a gravity turn
during solid motor operation. After the solid motors were staged (i.e., at main
stage ignition), COV was employed. Throttling of the main stage was employed
where the configuration did not have injection stages for final insertion into
orbit. (This technique results in a conservative estimate in payload since more
optimum trajectories could exist.)

The preliminary trajectory analyses were based upon a 680" (56.67 feet) diameter
main stage. The nose cone shape was the same as used in the earlier AMLLV
studies. This nose cone shape is a 25° cone - 12.5° cone frustum combination
(see sketch below) as developed for the Saturn IB vehicle. This particular con-
figuration may be slightly off optimum for the vehicles considered in this study
because of trajectory differences. This shape will, however, provide low values
of vehicle aerodynamic drag and pitching moment, high payload volume, low

4.2.1 (Continued)

pressure differential across the payload shroud (Reference 4.2.1.0-1), and ease of manufacturing. Extensive wind tunnel data is available for this payload shape (Reference 4.2.1.0-2) and it has been flight tested (AS-203 flight, July 5, 1966).
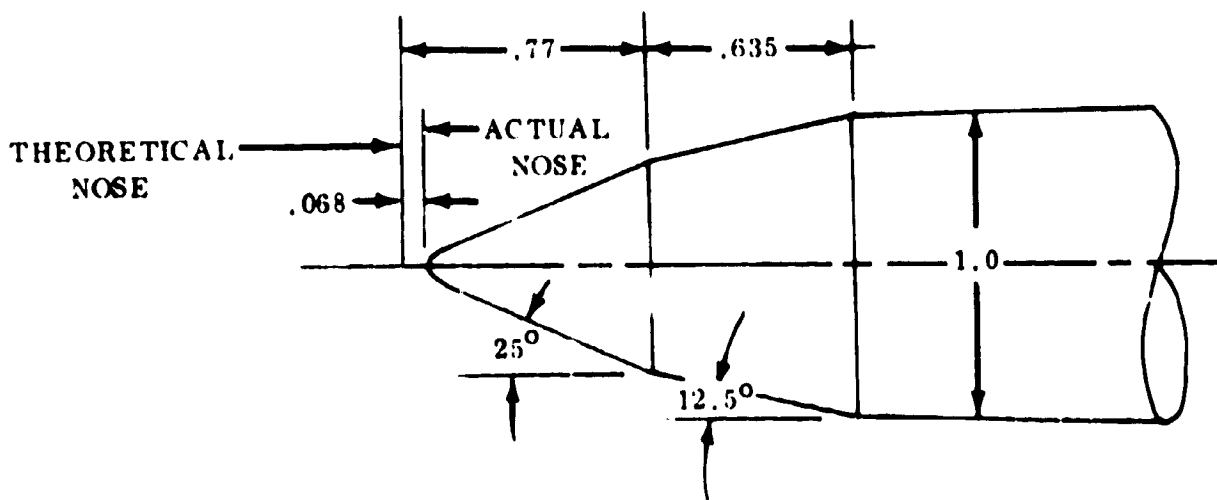
The calculated values for vehicle drag coefficient (C_{DO}) versus mach number for the single-stage-to-orbit vehicle (with this nose cone shape and the 56.67 foot diameter) are shown in Figure 4.2.1.0-1. These same values of C_{DO} versus mach number are applicable to the vehicle consisting of a main stage and one injection stage as the cross sectional area is unchanged. Also shown are the

4.2.1.0-1 "Results of an Experimental Investigation to Determine the Aerodynamic Loadings on Three Saturn Payload Shapes, Technical Note TN-A3-64-16, Chrysler Corporation, Space Division, dated March 1, 1964

4.2.1.0-2 "Results of an Experimental Investigation to Determine the Aerodynamic Loadings on Three Saturn Payload Shapes," Technical Note TN-AE-64-16, (Addendum), Chrysler Corporation, Space Division, dated November 10, 1964

$A_{REF} = 2520 \text{ FT}^2$
$D = 56.67$
$D_{REF} = 17.27 \text{ M}$
$A_{REF} = 234.3 \text{ M}^2$

MAIN STAGE + 8-260 SOLID
STRAP-ON STAGES

SINGLE STAGE TO ORBIT VEHICLE
WITH POWER OFF

SINGLE STAGE TO ORBIT VEHICLE

MACH NUMBER

TOTAL VEHICLE DRAG COEFFICIENT C_{DO}
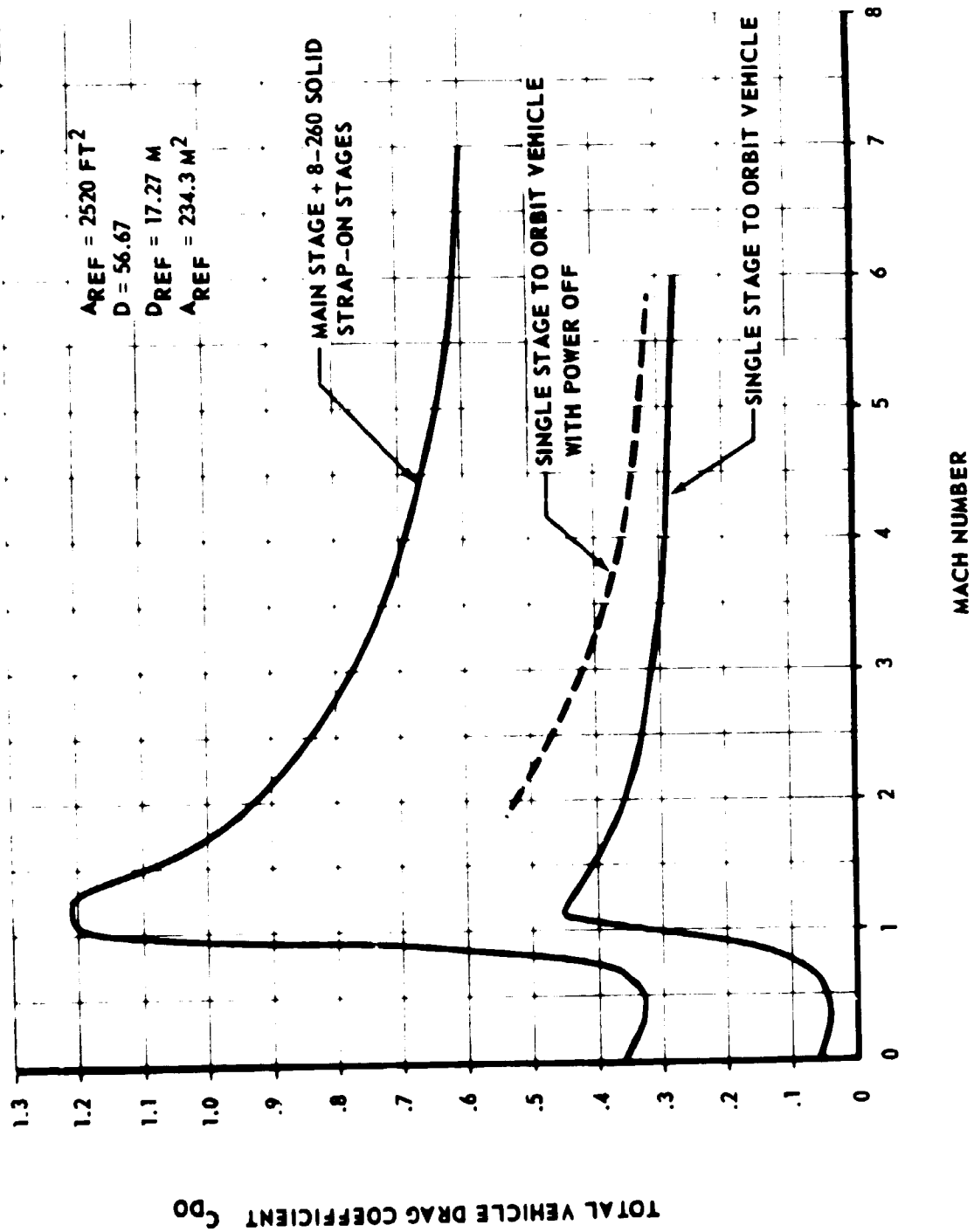
FIGURE 4.2.1.0-1 TOTAL VEHICLE DRAG COEFFICIENT – MLLV VEHICLE

AV-5840-63

87

4.2.1   (Continued)

drag coefficient values for the vehicle with the main stage engines off. This
condition could exist during a coast operation of the vehicle. The remaining
curve on the figure illustrates the drag coefficient versus mach number for the
main stage with eight 260 inch diameter strap-on solid motor stages vehicle. The
large increase in cross sectional area caused by the strap-ons results in a peak
C_{DO} value approximately 2.5 times that of the core alone.

4.2.1.1 Single-Stage-to-Orbit Trajectories

Two separate trajectory analyses were conducted for single-stage-to-orbit, i.e.:

a.   Main stage with multichamber/plug engine system.

b.   Main stage with toroidal/aerospike engine system.

The analyses showed no significant trajectory or payload differences between the
two propulsion systems.

The previous AMLLV performance studies of single-stage-to-orbit vehicles showed
that thrust modulation (throttling) results in a performance increase. Single-
stage-to-orbit vehicles that do not employ throttling have a relatively short burn
time which results in the vehicle flying a steep trajectory in order to gain the
necessary altitude to meet orbital conditions. Relative to this steep trajectory
are large thrust vector angles that result when the velocity vector is turned to
meet the orbital flight path angle requirements. The AMLLV studies also showed
that a single step change in thrust closely approaches the results obtained when
multiple thrust reductions are made   It was assumed for this study, therefore,
that the single-stage-to-orbit vehicle would be throttled by making a single step
change in the thrust.

Therefore, as discussed in Section 4.1.1 above, the engine systems were operated
at full thrust until 89% of the main stage propellant was depleted. At this time,
the mass flow was reduced to 10% of that required for full thrust. Operation at
this reduced level was maintained for the duration of powered flight.

Multichamber/Plug Engine System

For the initial trajectory calculations, a multichamber/plug engine system was
assumed for the main stage. This propulsion system contained 24 propulsion
modules in a zero gap (i.e., no clearance between adjacent modules) configuration.
A fixed mixture ratio of 6:1 was employed.

Engine performance was based on preliminary data supplied by Pratt and Whitney.
The propulsion system data were input to the computer in the form of mass flow

88

4.2.1.1 (Continued)

versus time and a corresponding table of thrust versus altitude. These inputs
accounted for degradation of specific impulse due to operation at the reduced
thrust level after throttling.

The inert weights for the half size vehicle were based on an assumed main stage
λ' (stage mass fraction) of 0.934 (i.e., somewhat less than the value of 0.94
as used for the main stage employing the toroidal engine system because of the
lower inert weight of the toroidal engine).

Table 4.2.1.1-I shows the mission weight history. Significant trajectory para-
meters are plotted in Figures 4.2.1.1-1 and 4.2.1.1-2.

Toroidal/Aerospike Engine System

The main stage inert weight for the single-stage-to-orbit vehicle configuration
with the toroidal engine system was based on a λ' of 0.94. The propulsion data
used was preliminary data provided by Rocketdyne. A chamber pressure of
2,000 psia and a fixed mixture ratio of 6:1 was employed.

The mission weight history is shown in Table 4.2.1.1-II. This data shows that
the payload achieved (480,000 pounds) for the single-stage-to-orbit vehicle was
within 4.0 percent of the target payload of 500,000 pounds. (The λ' used for
the half size vehicle was 0.94 which is slightly less than that achieved for the
AMLLV vehicle with the toroidal engine system of 0.946).

A computation of key flight performance data for the vehicle with the toroidal
propulsion system is listed below:

    a.   Maximum acceleration 6.99 g's at main stage throttling.

    b.   Maximum dynamic pressure 614 lbs./ft.^{2} at 81 seconds.

    c.   Gross payload 480,000 pounds.

These vary slightly from the single-stage-to-orbit vehicle data for the configura-
tion with the multichamber/plug propulsion system of 7.2 g's, 690 lb/ft.^{2} and
476,000 pounds respectively. This data variation is the result of engine per-
formance and engine weight differences. No significant loads, control or
aerodynamic heating occured as a result of these differences. Some design
modifications to the aft skirt are required as a result of the method of reacting
the engine thrust. This is discussed in more detail in Paragraph 4.2.4

TABLE 4.2.1.1-I *PRELIMINARY WEIGHT HISTORY (100 NM ORBIT) SINGLE-STAGE-TO-ORBIT VEHICLE WITH THE MULTICHAMBER/PLUG PROPULSION SYSTEM

IGNITION THRUST (S.L.)	8,000,000 LBS
THROTTLED THRUST (VAC)	1,035,000 LBS
LIFT-OFF WEIGHT	6,418,606 LBS
PROPELLANT CONSUMED	5,550,000 LBS
PROPELLANT BURNED AT FULL THRUST (B1)	4,972,616 LBS
PROPELLANT BURNED AT REDUCED THRUST (B2)	577,384 LBS
BURN RATIO (B2/B1)	0.116
STAGE DROP WEIGHT ($\lambda' = .934$)	392,184 LBS
LAUNCH AZIMUTH	90 DEGS
T/W RATIO AT LIFT-OFF	1.246
GROSS WEIGHT IN ORBIT	868,606 LBS
GROSS PAYLOAD	476,422 LBS

AERODYNAMIC HEATING INDICATOR VALUE = 1,448,560 $\dfrac{K_{gf} - M}{M^2 - DEG}$

MAXIMUM DYNAMIC PRESSURE = 691 LBS/FT^2

*SEE SECTION 4.3.1 FOR FINAL TRAJECTORY
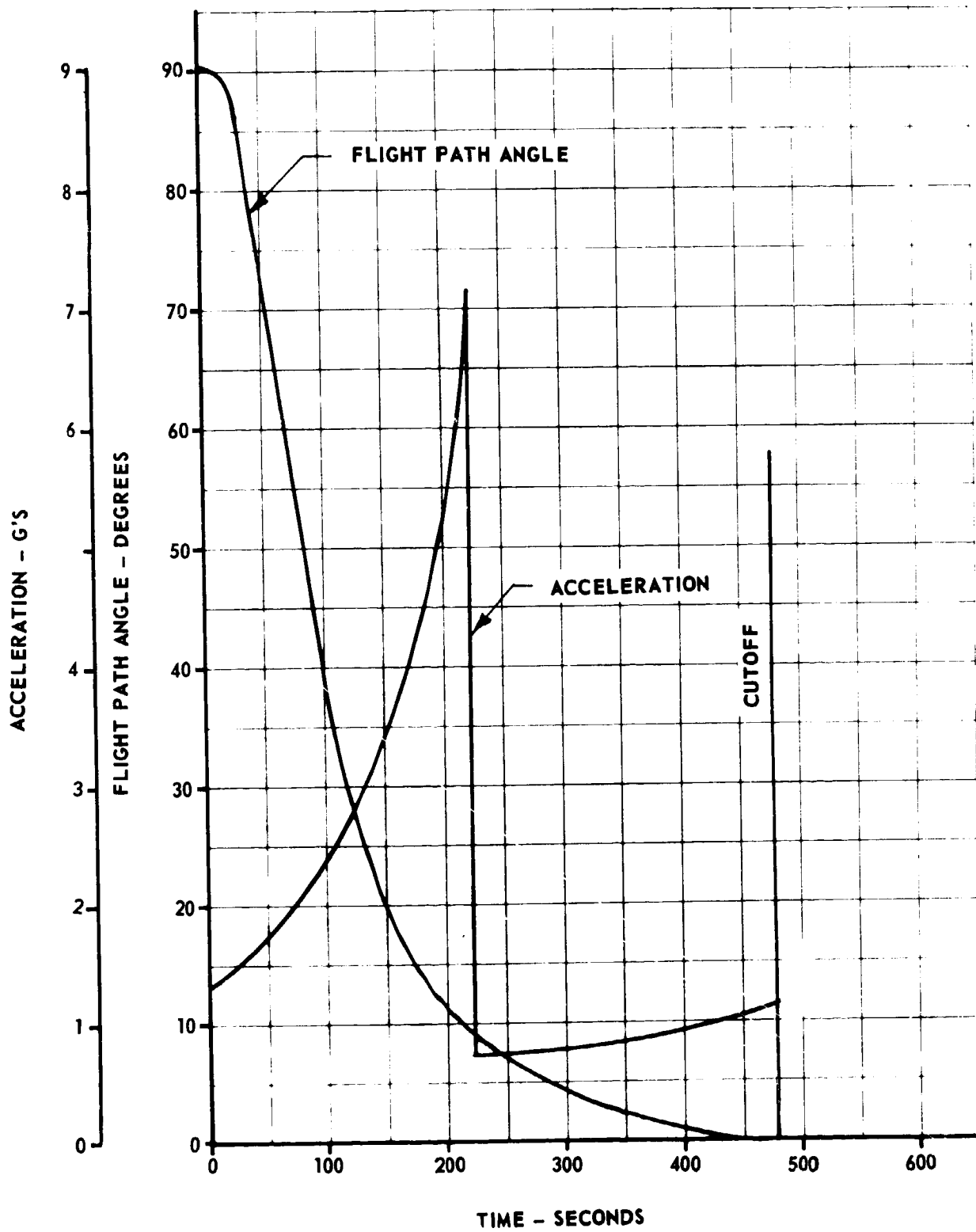
FIGURE 4.2.1.1-1   PRELIMINARY MLLV FLIGHT PATH ANGLE AND ACCELERATION VERSUS
TIME FOR SINGLE STAGE TO ORBIT (MULTICHAMBER/PLUG) VEHICLE
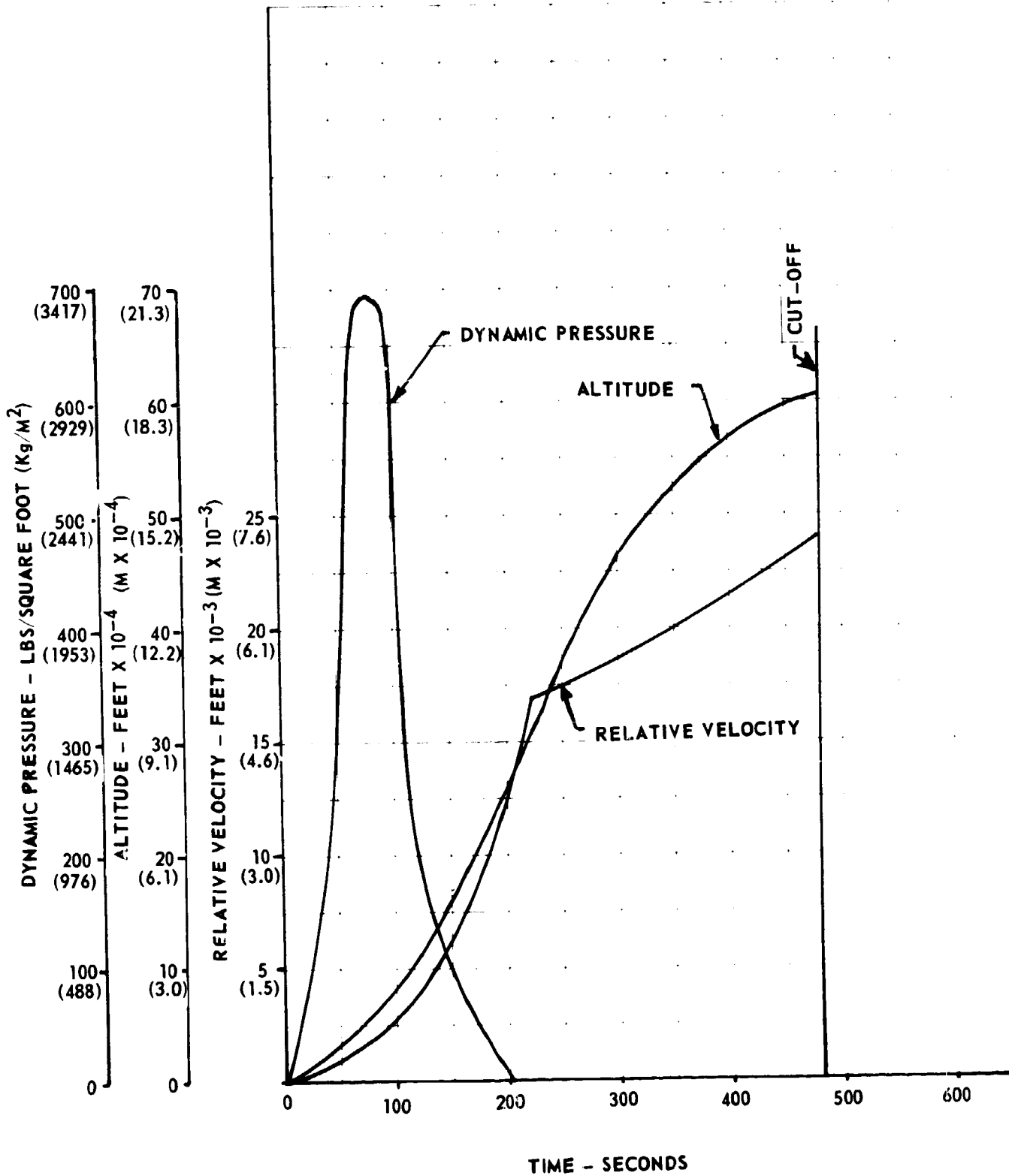
FIGURE 4.2.1.1-2   PRELIMINARY MLLV FLIGHT PATH ANGLE AND ACCELERATION VERSUS
TIME FOR SINGLE STAGE TO ORBIT (MULTICHAMBER/PLUG) VEHICLE

92

TABLE 4.2.1.1-II *PRELIMINARY WEIGHT HISTORY (100 NM ORBIT) SINGLE-STAGE-TO-ORBIT VEHICLE WITH THE 2000 PSIA TOROIDAL PROPULSION SYSTEM

IGNITION THRUST (S.L.)	8,000,000 LBS
THROTTLED THRUST (VAC)	988,740 LBS
LIFT-OFF WEIGHT	6,384,425 LBS
PROPELLANT CONSUMED	5,550,000 LBS
PROPELLANT BURNED AT FULL THRUST (B1)	4,972,620 LBS
PROPELLANT BURNED AT REDUCED THRUST (B2)	577,380 LBS
BURN RATIO (B2/B1)	0.116
STAGE DROP WEIGHT ($\lambda' = .94$)	354,255 LBS
LAUNCH AZIMUTH	90 DEGS
T/W RATIO AT LIFT-OFF	1.253
GROSS WEIGHT IN ORBIT	834,424 LBS
GROSS PAYLOAD	480,169 LBS

AERODYNAMIC HEATING INDICATOR VALUE = 1,239,345 $\dfrac{K_{gf} - M}{M^2 - DEG}$

MAXIMUM DYNAMIC PRESSURE = 614 LBS/FT^2

*SEE SECTION 4.3.1 FOR FINAL TRAJECTORY

4.2.1.2 Main Stage Plus a Single Module Injection Stage Vehicle Trajectory

While the main stage plus injection stage vehicle trajectory mode was similar to that for the single-stage-to-orbit vehicle, the main stage was not throttled. The use of a single module injection stage plus the heavier payload lowered the vehicle thrust-to-weight to 1.178. The main stage employed a multichamber/plug engine system identical to that defined above. (A mass fraction of 0.933 was assumed for the main stage. This slightly lower mass fraction was used to account for the heavier forward skirt.)

The single module injection stage contains two high pressure engines each delivering 125,000 pounds of thrust. The injection stage module mass fraction was assumed to be 0.80. (The single module injection stage for the AMLLV vehicle had a mass fraction of 0.82.) The thrust-to-weight of the injection stage at ignition of 0.297 is within the acceptable levels as determined in the AMLLV study.

The gross payload weight as shown in Table 4.2.1.2-I is approximately half that obtained for the comparable full size AMLLV vehicle, i.e, 560,292 pounds versus 1,180,000 pounds. The maximum acceleration occurs immediately prior to main stage cutoff and is 8.35 g's. This acceleration level can be decreased by minor throttling of the main stage. (Reduction in this acceleration level would reduce the required weight of the lightweight forward skirt used for both this vehicle and the single stage to orbit vehicle.)

4.2.1.3 Main Stage Plus Two Strap-On Stages Vehicle Trajectory

This vehicle employed two strap-on solid motor stages, each containing 2.9 million pounds of propellant, which are burned in a parallel mode with the main stage. A parallel burn mode was necessary since the lift-off thrust of the two SRM's (13.6 million pounds) in a zero stage mode will be insufficient to provide an acceptable lift-off thrust-to-weight ratio (1.02 actual versus 1.18 acceptable minimum). The parallel burn mode provided a total lift-off thrust of 21,600,000 pounds for a lift-off thrust-to-weight of 1.63.

The main stage employed the multichamber/plug engine configuration. The mass fractions used for the main stage and the SRM stages were 0.93 and 0.90 respectively. The lower mass fraction used for this vehicle was the result of a heavier forward skirt used on those configurations employing strap-ons. Ninety percent throttling was employed after consumption of 88.9 percent of the propellant.

Table 4.2.1.3-I shows the mission weight history for this vehicle.

The maximum dynamic pressure for this vehicle, 1213 lb/ft.^{2}, exceeded the arbitrary 950 lb/ft.^{2} limit used for the Saturn V vehicle. It may be desirable to throttle the main stage while in the lower atmosphere to reduce the dynamic

94

TABLE 4.2.1.2-I *PRELIMINARY MISSION WEIGHT HISTORY (100 NM ORBIT)
MAIN STAGE WITH A MULTICHAMBER/PLUG PROPULSION
SYSTEM PLUS A SINGLE MODULE INJECTION STAGE
(UNTHROTTLED MAIN STAGE)

MAIN STAGE

IGNITION THRUST (S.L.)	8,000,000 LBS
LIFT-OFF WEIGHT	6,790,000 LBS
T/W RATIO AT LIFT-OFF	1.178
PROPELLANT CONSUMED	5,550,000 LBS
STAGE DROP WEIGHT ($\lambda' = .933$)	398,458 LBS
LAUNCH AZIMUTH	90 DEGS
MAXIMUM DYNAMIC PRESSURE	617 LBS/FT^2

INJECTION STAGE

IGNITION THRUST (VAC)	250,000 LBS
IGNITION WEIGHT	841,542 LBS
T/W RATIO AT IGNITION	0.297
PROPELLANT CONSUMED	225,000 LBS
STAGE DROP WEIGHT ($\lambda' = .80$)	56,250 LBS
GROSS WEIGHT IN ORBIT	616,542 LBS
GROSS PAYLOAD	560,292 LBS

AERODYNAMIC HEATING INDICATOR VALUE 1,363.878 $\dfrac{K_{gf} - M}{M^2 - DEG}$

*SEE SECTION 4.1.3 FOR FINAL TRAJECTORY

95

TABLE 4.2.1.3-I   PRELIMINARY MISSION WEIGHT HISTORY (100 NM ORBIT)
MAIN STAGE WITH A MULTICHAMBER/PLUG PROPULSION
SYSTEM PLUS 2-260" SRM STAGES (PARALLEL BURN SRM's)

STAGE I (MAIN STAGE PLUS PARALLEL BURN SOLIDS)

LIQUID ENGINE SEA LEVEL THRUST	8,000,000 LBS
SOLID MOTOR SEA LEVEL THRUST	13,600,077 LBS
LIFT-OFF WEIGHT	13,236,684 LBS
PROPELLANT CONSUMED (LIQUID)	5,550,000 LBS
PROPELLANT CONSUMED (SOLID)	5,800,000 LBS
SOLID MOTOR STAGE WEIGHT AT SEPARATION ($\lambda' = .90$)	644,446 LBS
LAUNCH AZIMUTH	90 DEGS
THRUST-TO-WEIGHT RATIO AT LIFT-OFF	1.632
MAXIMUM DYNAMIC PRESSURE	*1213 LBS/FT^2
PROPELLANT BURNED AT FULL THRUST (B_1)	4,933,494 LBS
PROPELLANT BURNED AT REDUCED THRUST (B_2)	616,506 LBS
BURN RATIO (B_2/B_1)	0.1250
THROTTLED THRUST (VAC)	1,035,000 LBS
STAGE DROP WEIGHT ($\lambda' = .93$)	417,742 LBS
GROSS WEIGHT IN ORBIT	1,242,238 LBS
GROSS PAYLOAD	824,496 LBS

*NOTE: This value can be reduced by minor throttling of the core

4.2.1.3 (Continued)

pressure, then the vehicle would be flown unthrottled until a point late in the main stage operation, then fly throttled again until main stage burn out.

The payload capability of this vehicle was 824,496 pounds.

4.2.1.4 Main Stage Plus Four Strap-On Stages Vehicle Trajectory

This vehicle employed four strap-on solid motor stages, each containing 2.9 million pounds of propellant, burned in a zero stage mode. The lift-off thrust of the solid motors of 27.2 million pounds provided a lift-off thrust-to-weight of 1.36. After cut-off of the strap-on stages, the main stage multichamber/plug engine was ignited. The main stage was throttled 90% after consumption of 88.9 percent of the propellant.

The mass fractions used for the main stage and strap-on stages were 0.93 and 0.90 respectively.

Table 4.2.1.4-I lists the mission weight history for this vehicle. The maximum dynamic pressure was 599.9 lb/ft^2. The payload capability of this vehicle was 1,159,481 pounds.

4.2.1.5 Main Stage Plus Eight Strap-On Stages Vehicle Trajectory

This vehicle configuration employed eight 260 inch solid motors, containing 2,900,000 pounds of propellant each. A zero stage mode was flown, i.e, the solid motors were ignited at launch. The 54,400,000 pounds thrust produced by the solid motors (6,800,000 pounds thrust each) resulted in a lift-off thrust-to-weight of 1.623.

After separation of the solid motors, the main stage was ignited and flown in a COV flight mode. Throttling (90%) was used on the main stage after depletion of 89% of main stage propellant. The thrust-to-weight at main stage ignition was 1.336.

The mass fraction of the main stage was assumed to be 0.93 as a result of a heavier forward skirt on the main stage and the use of the multichamber/plug propulsion system. The solid motors were assumed to have a mass fraction of 0.92 without attachment structure. Including the attachment structure, the assumed mass fraction was 0.90.

The gross payload weight as shown in Table 4.2.1.5-I was 1,777,712 pounds which is approximately half the 3,520,000 pounds payload capability of the equivalent AMLLV full size configuration (which consisted of a main stage plus twelve

TABLE 4.2.1.4-1 PRELIMINARY MISSION WEIGHT HISTORY (100 NM ORBIT)
MAIN STAGE WITH MULTICHAMBER/PLUG PROPULSION
SYSTEM PLUS 4-260" SRM STAGES (THROTTLED MAIN
STAGE AND ZERO STAGED SRMS)

SOLID STAGE

IGNITION THRUST (S.L.)	27,200,155 LBS
LIFT-OFF WEIGHT	20,016,114 LBS
T/W RATIO AT LAUNCH	1.359
PROPELLANT CONSUMED	11,600,000 LBS
STAGE DROP WEIGHT ($\lambda' = .90$)	1,288,891 LBS
LAUNCH AZIMUTH	90 DEGS
MAXIMUM DYNAMIC PRESSURE	599.9 LBS/FT^2

MAIN STAGE

IGNITION THRUST (VAC)	10,350,000 LBS
IGNITION WEIGHT	7,127,233 LBS
T/W RATIO AT IGNITION	1.452
PROPELLANT CONSUMED	5,550,000 LBS
PROPELLANT BURNED AT FULL THRUST (B1)	4,931,142 LBS
PROPELLANT BURNED AT REDUCED THRUST (B2)	618,858 LBS
BURN RATIO (B2/B1)	0.1255
THROTTLED THRUST (VAC)	1,035,000 LBS
STAGE DROP WEIGHT ($\lambda' = .93$)	417,742 LBS
GROSS WEIGHT IN ORBIT	1,577,233 LBS
GROSS PAYLOAD	1,159,481 LBS

TABLE 4.2.1.5-I   *PRELIMINARY SRM MISSION WEIGHT HISTORY (100 NM ORBIT)
MAIN STAGE WITH MULTICHAMBER/PLUG PROPULSION
SYSTEM PLUS 8-2 10" SRM STAGES (THROTTLED MAIN STAGE
& ZERO - STAGED SRM)

SOLID STAGE

IGNITION THRUST (S.L.)	54,400,311 LBS
LIFT-OFF WEIGHT	33,523,236 LBS
T/W RATIO AT LAUNCH	1.623
PROPELLANT CONSUMED	23,200,000 LBS
STAGE DROP WEIGHT ($\lambda' = .90$)	2,577,782 LBS
LAUNCH AZIMUTH	90 DEGS
MAXIMUM DYNAMIC PRESSURE	999 LBS/FT^2

MAIN STAGE

IGNITION THRUST (VAC)	10,350,000 LBS
IGNITION WEIGHT	7,745,454 LBS
T/W RATIO AT IGNITION	1.336
PROPELLANT CONSUMED	5,550,000 LBS
PROPELLANT BURNED AT FULL THRUST (B1)	4,931,142 LBS
PROPELLANT BURNED AT REDUCED THRUST (B2)	618,858 LBS
BURN RATIO (B2/B1)	0.1255
THROTTLED THRUST (VAC)	1,035,000 LBS
STAGE DROP WEIGHT ($\lambda' = .93$)	417,742 LBS

GROSS WEIGHT IN ORBIT	2,195,454 LBS
GROSS PAYLOAD	1,777,712 LBS

AERODYNAMIC HEATING INDICATOR VALUE 1,927,201 $\dfrac{K_{gf} - M}{M^2 - DEG}$

*SEE SECTION 4.3.1 FOR FINAL TRAJECTORY

4.2.1.5 (Continued)

strap-on 260 inch motor stages). Two acceleration peaks occurred, one at solid motor separation (130 seconds) and the second just prior to main stage throttling. These peak accelerations were 3.2 g's and 3.67 g's respectively. The maximum dynamic pressure occurred at 61 seconds and was 999 lb/ft^2.

4.2.1.6 Main Stage Plus Eight Strap-On Stages Plus a Three Module Injection Stage Vehicle Trajectory

This configuration consisted of a main stage with a three module injection stage and eight strap-on stages. Each strap-on stage contained 2.9 million pounds of propellant. A zero stage flight mode was utilized. The overall solid motor thrust of 54.4 million pounds provided a lift-off thrust-to-weight of 1.58.

After solid motor burn out, the multichamber/plug engines of the main stage were ignited and burned at full thrust until burn out. No main stage throttling was employed. After main stage burn out, the injection stage engines were ignited and were used to achieve final orbital conditions.

The main stage inert weight was based on a mass fraction of 0.930. The three module injection stage employed a total propellant loading of 675,000 pounds. The total vacuum thrust level was 750,000 lbs. A preliminary mass fraction of 0.86 was assumed for the injection stage inert weight. A mass fraction of 0.90 was assumed for the strap-on stages. This included both the solid motors and the attachment structure necessary to tie the solid motors to the core vehicle.

The mission weight history is shown in Table 4.2.1.6-I. The payload achieved was 1,895,665 pounds. This is 1.4 percent more than the target value of 1,870,000 pounds (half the payload of equivalent AMLLV configuration). The flight performance data, i.e., flight path angle, acceleration dynamic pressure, altitude and velocity are shown in Figures 4.2.1.6-1 and 4.2.1.6-2. The highest acceleration (3.7 g's) occurred at main stage burn out. A slightly lower peak acceleration (2.9 g's) occurred at solid motor burn out. These maximum accelerations are considerably below the 7.15 g's incurred by the single-stage-to-orbit vehicle. A comparison with the comparable AMLLV vehicle consisting of the main stage plus a three module injection stage and twelve solid motor stages showed that the g's for the MLLV 3.37 g's) exceeded those of the AMLLV (3.25 g's). The dynamic pressure was 970 #/sq. ft. for the MLLV versus 932 #/sq. ft. for the AMLLV comparable vehicle. These peaks occurred at approximately the same time during the trajectory flight. These minor variations occurred due to the slight variations in input data used in the computer trajectory.

TABLE 4.2.1.6-I *PRELIMINARY MISSION WEIGHT HISTORY (100 NM ORBIT)
MAIN STAGE WITH MULTICHAMBER/PLUG PROPULSION
SYSTEM PLUS 8-260" SRM PLUS A 3 MODULE INJECTION
STAGE (ZERO STAGED SRM AND UNTHROTTLED MAIN STAGE)

SOLID STAGE

IGNITION THRUST (S.L.)	54,400,000 LBS
LIFT-OFF WEIGHT	34,426,189 LBS
T/W RATIO AT LAUNCH	1.58
PROPELLANT CONSUMED	23,200,000 LBS
STAGE DROP WEIGHT ($\lambda' = .90$)	2,577,782 LBS
LAUNCH AZIMUTH	90 DEGS
MAXIMUM DYNAMIC PRESSURE	970 LBS./FT^2

MAIN STAGE

IGNITION THRUST (VAC)	10,350,000 LBS
IGNITION WEIGHT	8,648,407 LBS
T/W RATIO AT IGNITION	1.20
PROPELLANT CONSUMED	5,550,000 LBS
STAGE DROP ($\lambda' = .93$)	417,742 LBS

INJECTION STAGE (3 MODULES)

IGNITION THRUST (VAC)	750,000 LBS
IGNITION WEIGHT	2,680,665 LBS
T/W RATIO AT IGNITION	0.28
PROPELLANT CONSUMED	675,000 LBS
STAGE DROP WEIGHT ($\lambda' = .86$)	110,000 LBS

GROSS WEIGHT IN ORBIT	2,005,665 LBS
GROSS PAYLOAD	1,895,665 LBS

AERODYNAMIC HEATING INDICATOR VALUE 1,848,814 $\dfrac{K_{gf} - M}{M^2 - DEG}$

*SEE SECTION 4.1.3 FOR FINAL TRAJECTORY
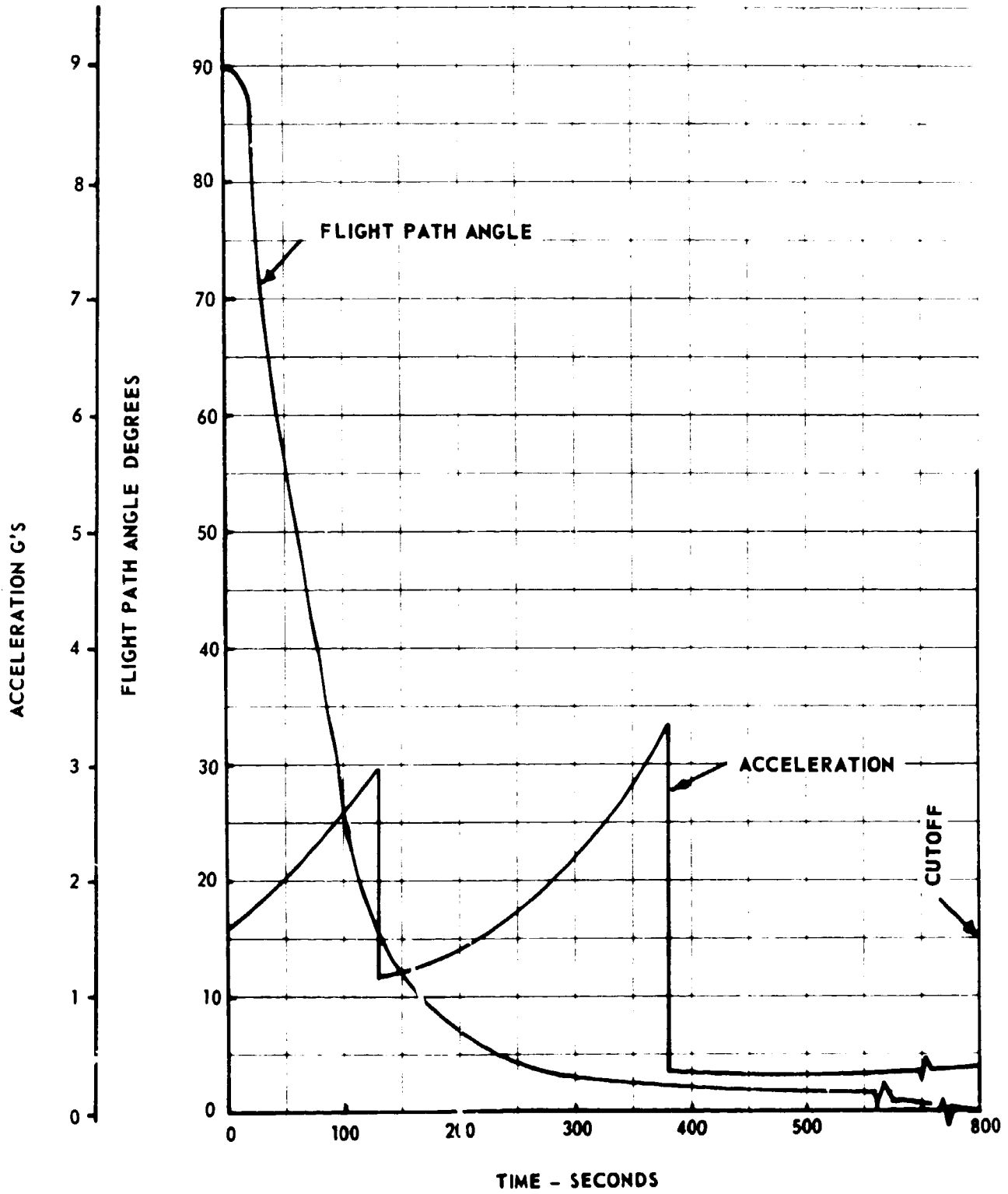
FIGURE 4.2.1.6-1   MLLV FLIGHT PATH ANGLE AND ACCELERATION VERSUS TIME, MAIN STAGE (MULTICHAMBER/PLUG) PLUS A THREE MODULE INJECTION STAGE PLUS EIGHT STRAP-ONS

102
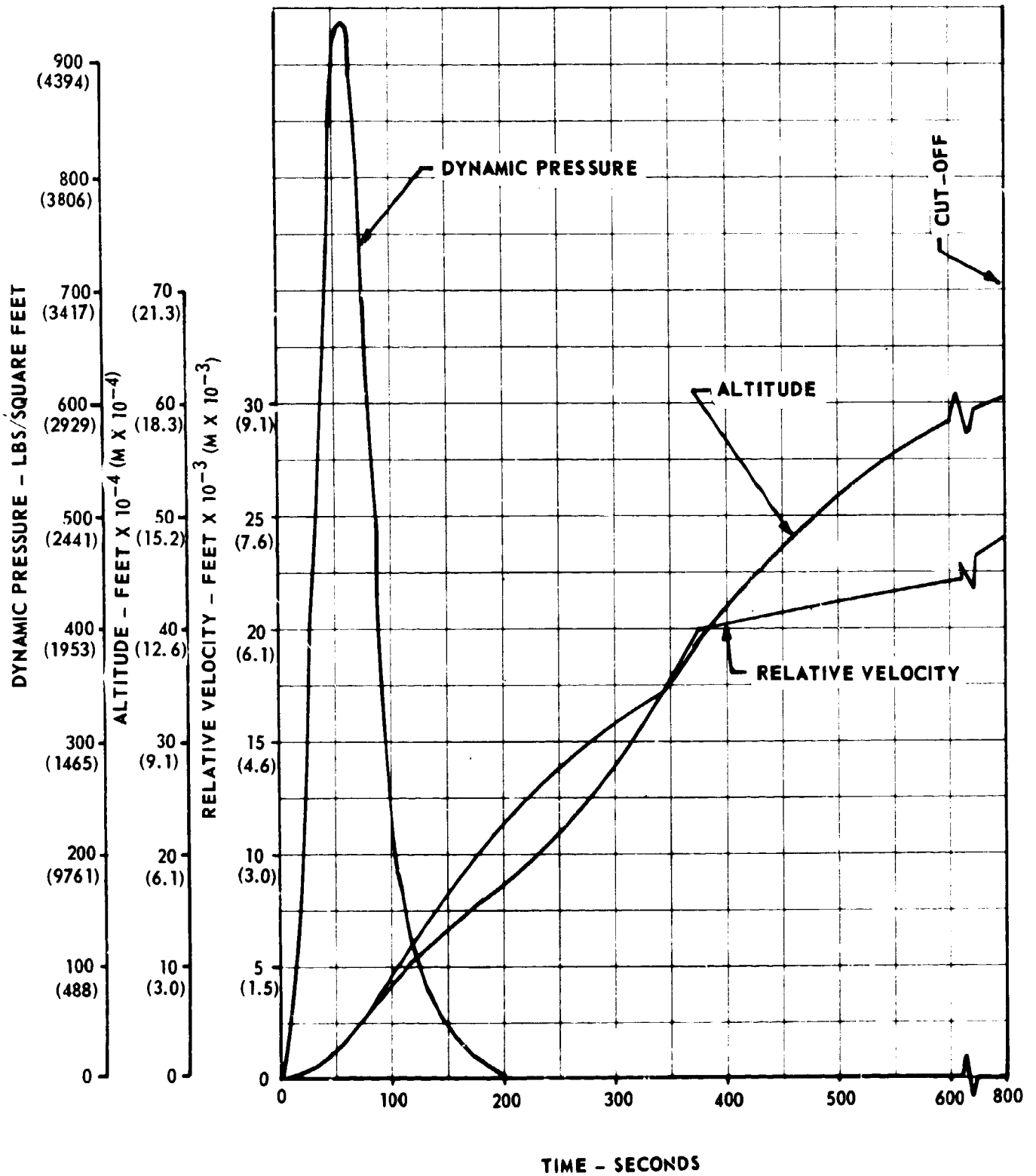
FIGURE 4.2.1.6-2 MLLV FLIGHT PERFORMANCE - DYNAMIC PRESSURE, ALTITUDE, VELOCITY VERSUS TIME, MAIN STAGE (MULTICHAMBER/PLUG) PLUS EIGHT SOLID MOTOR STRAP-ONS PLUS A THREE MODULE INJECTION STAGE

103

4.2.2 Aerodynamics

Aerodynamic analyses were conducted to provide the necessary inputs for the final performance and trajectory calculations, the loads analyses and the control analyses. Static stability data ($C_{Z\alpha}$ and CP/D), drag data (C_{DO}), and local aerodynamic loading distributions for the maximum $q\alpha$ flight regime were calculated for the MLLV single-stage-to-orbit vehicle, and the main stage plus three module injection stage plus eight strap-on stages vehicles.

The location of the vehicle center of pressure and the initial slope of the normal force curve were computed to support the control and structural dynamic analyses. Drag loads on the vehicle during flight were input to the final performance and trajectory analyses. For subsequent loads analyses, the distribution of the aerodynamic forces, both normal to the vehicle center line and parallel to the vehicle center line were determined.

The vehicle reference coordinates are shown below:

$$C_{Z_{TOT}}$$

NORMAL FORCE = C_Z qoS

AXIAL FORCE = CA qo S

S = REF. AREA

qo = .5 V_o^2
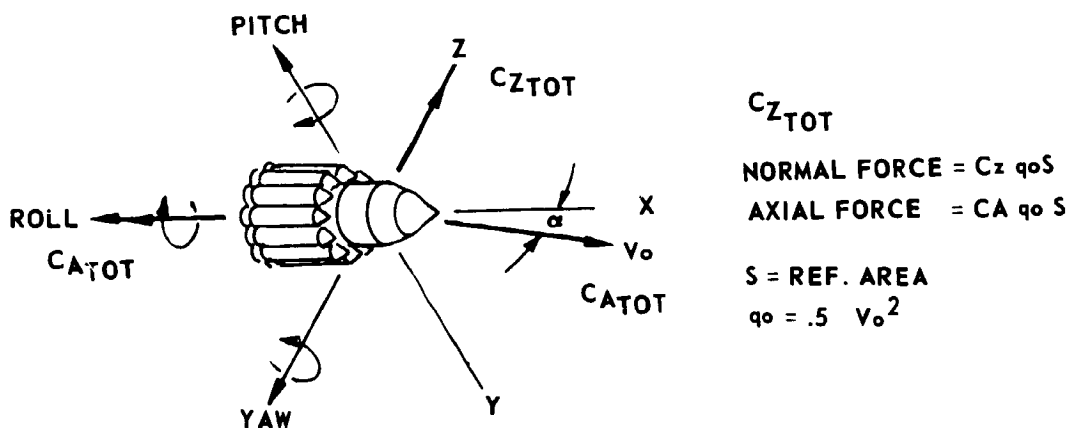
4.2.2.1 Static Stability Data

The initial slope of the normal force curve ($C_{Z\alpha}$) and center of pressure (CP/D) are presented in Figures 4.2.2.1-1 and 4.2.2.1-2 for the core vehicle and for the core vehicle with solid strap-on stages, respectively.

The initial slope of the normal force curve and CP/D for the single-stage-to-orbit vehicle configuration were obtained from the previously mentioned Reference 4.2.1.0-1.

4.2.1.0-1   TM AE-64-16, "Results of an Experimental Investigation to Determine the Aerodynamic Loading on Three Saturn Payloads" Chrysler Report, 1964.

$$A_{REF.} = 2521 \text{ FT.}^2$$

$$D_{REF.} = 56. \_7 \text{ FT.}$$
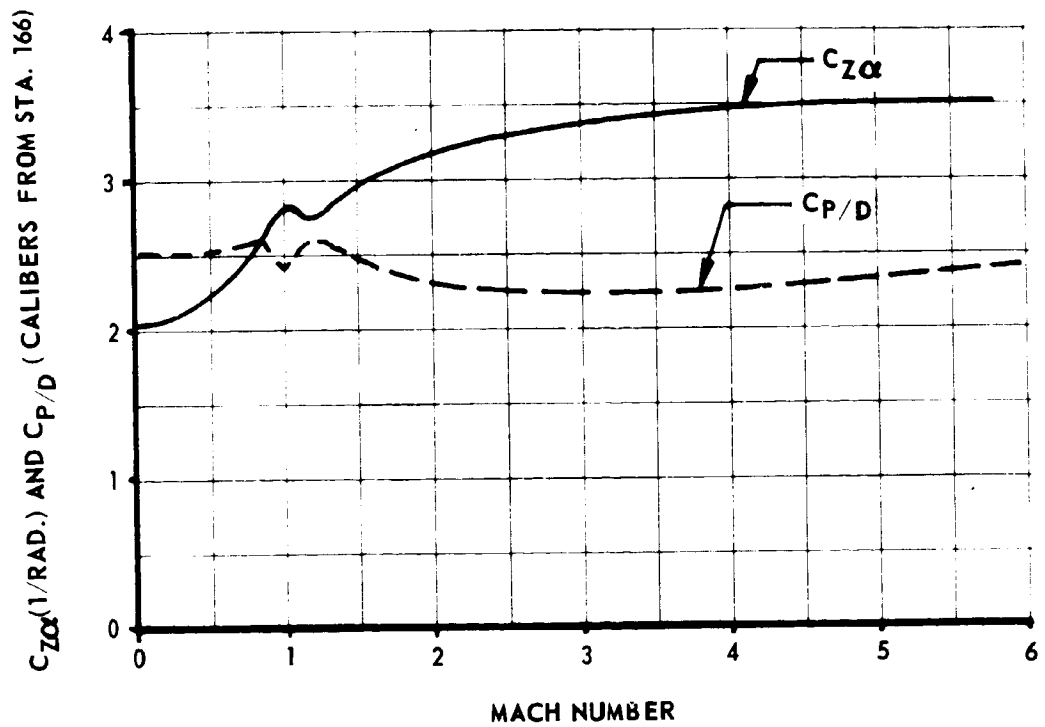
FIGURE 4.2.2.1-1   INITIAL SLOPE OF NORMAL FORCE CURVE AND CENTER OF PRESSURE MLLV CORE
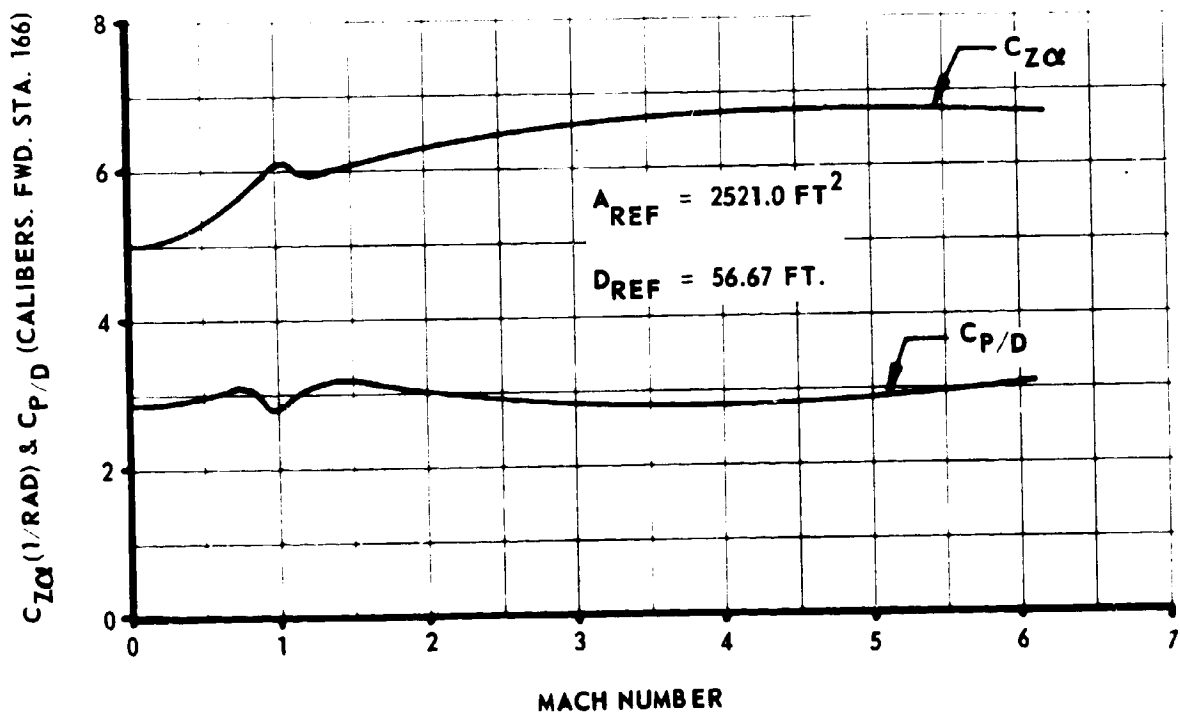
FIGURE 4.2.2.1-2   INITIAL SLOPE OF NORMAL FORCE CURVE AND CENTER OF PRESSURE MLLV VEHICLE WITH 8-260" SOLIDS

4.2.2.1 (Continued)

To determine the $C_{Z\alpha}$ contribution of the solids for the configuration with eight 260 inch solid motors, a curve (Figure 4.2.2.1-2) was generated to show the average normal force contribution of solid strap-on stages to the main stage. The $C_{Z\alpha}$ value, which can be read from this curve for any specific number of strap-ons, is additive to the $C_{Z\alpha}$ of the main stage without strap-ons to define the $C_{Z\alpha}$ of the overall vehicle. This curve was determined by the following procedure: The total normal force slope ($C_{Z\alpha}$) of the core vehicle when fully saturated with strap-on stages (12 strap-ons) was assumed to be equal to the slender body theory value of two with an assumed reference area =

$$\frac{\pi (D\ Core + D\ Solid)^2}{4}.$$

(Note: $C_{Z\alpha} = 3.72$ for Reference Area of 2520 ft.^{2}.) This assumed that the normal force coefficient for the body of revolution is independent of the shape revolved. This is essentially the result obtained by Tsien (Reference 4.2.2.1-1) in proving that the resultant initial slope of the lift curve that Max Munk obtained for an airship hull is the same that would be obtained for a body of revolution in supersonic flow. (Reference 4.2.2.1-1 and 4.2.2.1-2.) Estimates of the contribution of a small number of solids were obtained, using the lift interference techniques developed for wings and reported by Pitts, Neilson and Kaatari in Reference 4.2.2.1-3. The resulting curve is presented in Figure 4.2.2.1-3. This curve cannot be used to obtain the total aerodynamic loading on any individual solids since the loading will vary depending on the solids circumferential location with respect to the plane containing the vehicle axis and the velocity vector.

4.2.2.2 Local Normal Force Distribution

The local normal force distributions for the single-stage-to-orbit vehicle are presented in Figures 4.2.2.2-1 through 4.2.2.2-3. The local normal force distributions for the main stage plus three injection stage modules plus eight solids are presented in Figures 4.2.2.2-4 through 4.2.2.2-7. These curves

---

4.2.2.1-1 Tsien, Hseu - Shen, "Supersonic Flow on an Inclinded Body of Revolution," Journal of the Aeronautical Sciences, Volume 5, pp. 480-483, 1938.

4.2.2.1-2 Munk, M. M., "The Aerodynamic Forces on Airship Hulls," NACA TR No. 184, 1923.

4.2.2.1-3 Pitts, Nielson, and Kaatari, "Lift and Center of Pressure of Wing-Body-Tail Combination at Subsonic, Transonic, and Supersonic Speeds," NACA Report 1307.

REFERENCE AREA = 2521 FT^2

MACH NO. = 1.5 TO 3.0
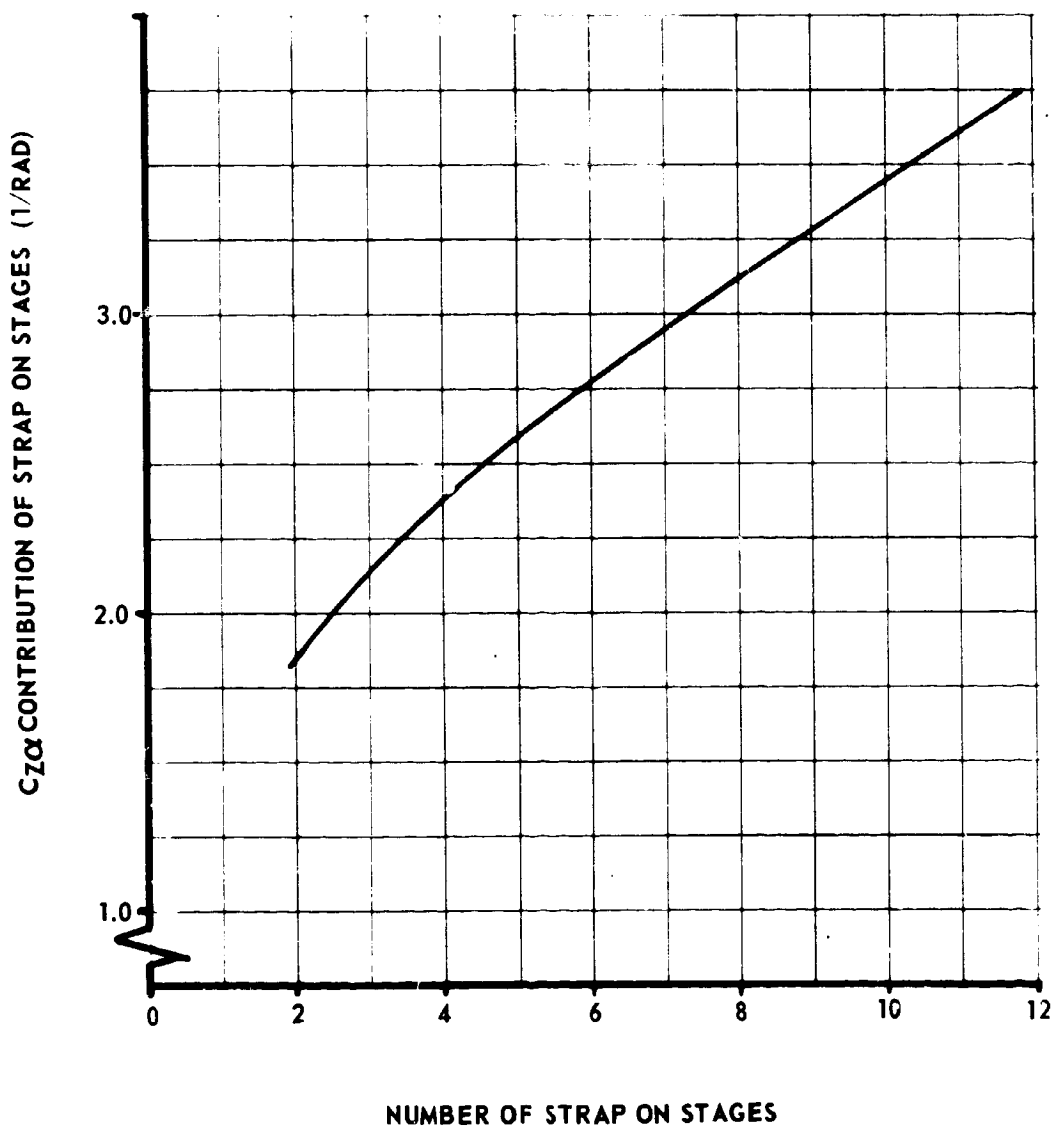
FIGURE 4.2.2.1-3   AVERAGE NORMAL FORCE CONTRIBUTION OF STRAP-ON STAGES
TO CORE VEHICLE

$A_{REF.} = 2521.0 \text{ FT}^2$

$D_{REF.} = 56.67 \text{ FT.}$

$M\infty = 1.12$

FIGURE 4.2.2.2-1   LOCAL NORMAL FORCE DISTRIBUTION MLLV CORE
$M_\infty = 1.12$

$A_{REF.} = 2521.0 \text{ FT}^2$

$D_{REF.} = 56.67 \text{ FT.}$
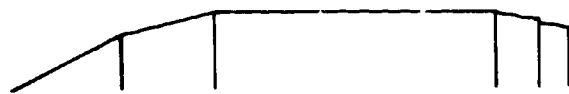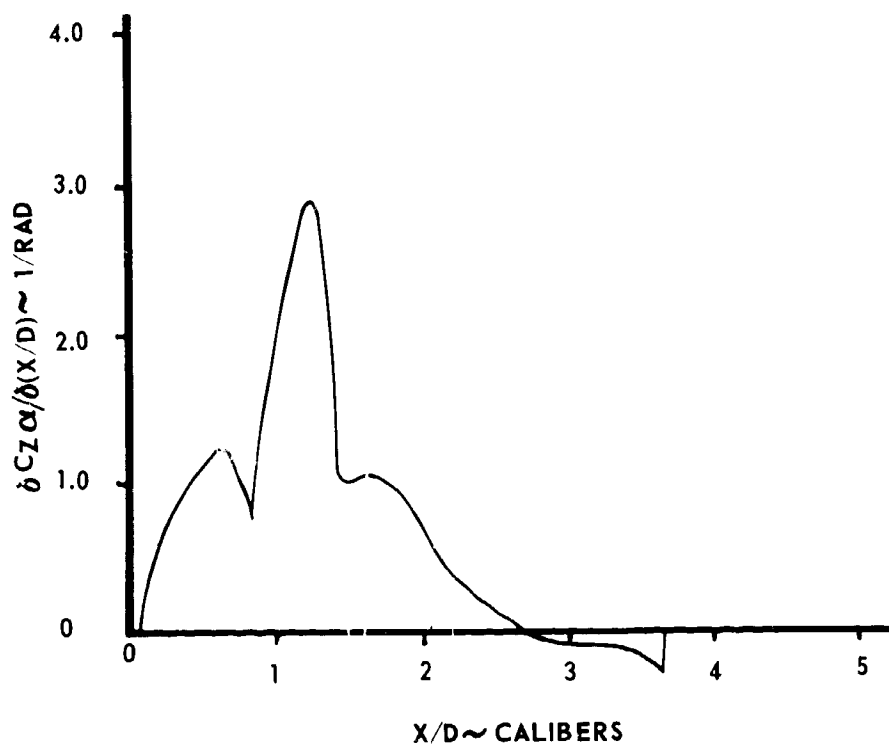
$M\infty = 1.26 \text{ (MAX. q } \alpha \text{)}$

FIGURE 4.2.2.2-2   LOCAL NORMAL FORCE DISTRIBUTION   MLLV CORE
$M\infty = 1.26 \text{ (MAX. q } \alpha \text{)}$

FIGURE 4.2.2.2-3 LOCAL NORMAL FORCE DISTRIBUTION MLLV CORE
$M_\infty = 1.48$
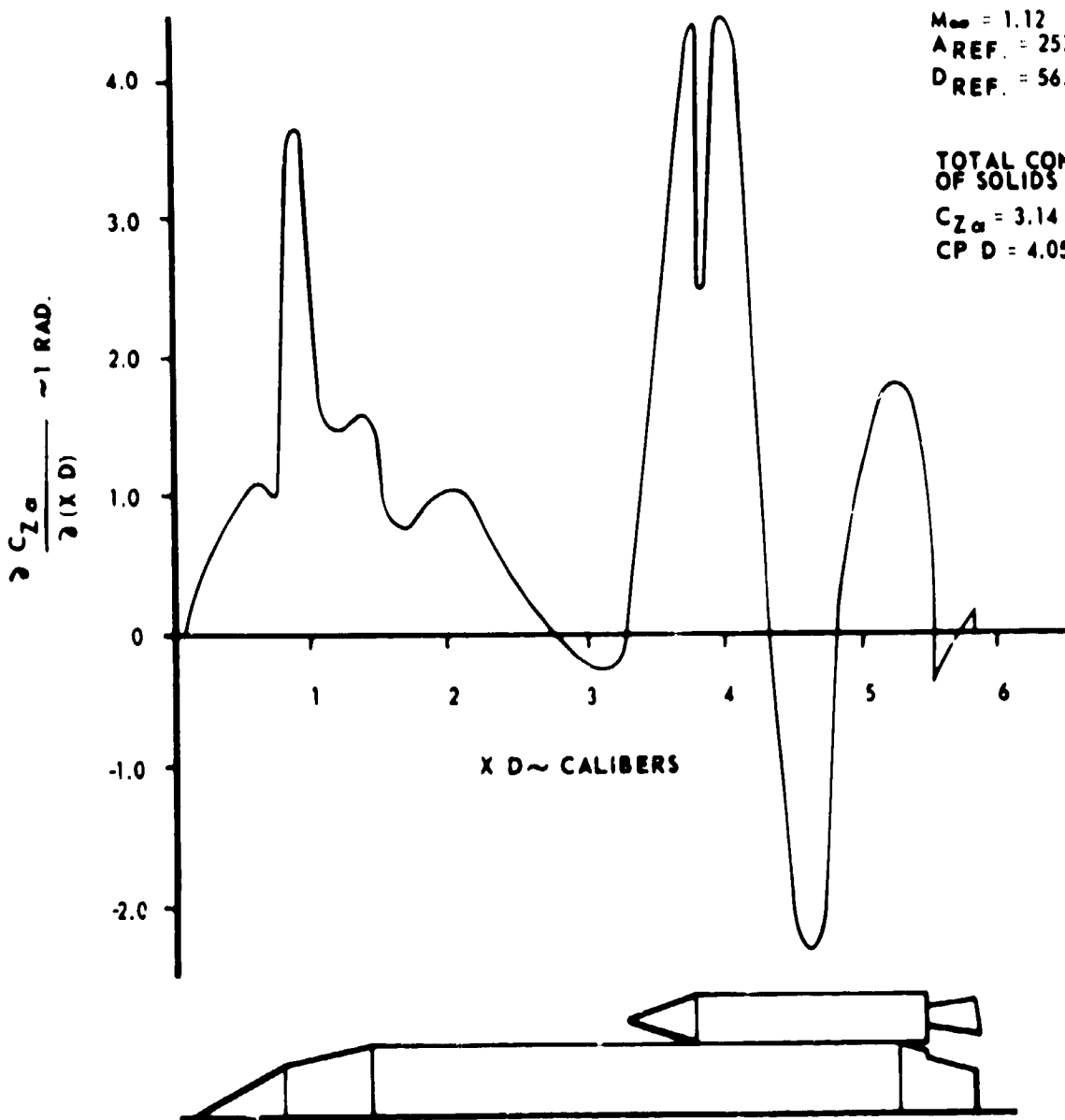
FIGURE 4.2.2.2-4   LOCAL NORMAL FORCE DISTRIBUTION   MLLV WITH 8-260"
SOLIDS $M_\infty = 1.12$

111

$M_\perp = 1.26$
$A_{REF.} = 2521.0 \text{ FT.}^2$
$D_{REF.} = 56.67 \text{ FT.}$

TOTAL CONTRIBUTION OF SOLIDS

$C_{Z_\alpha} = 3.10$
$CP \ D = 4.15$

$\dfrac{\partial C_{Z_\alpha}}{\partial (X \ D)} \sim 1 \text{ RAD.}$

$X \ D \sim \text{CALIBERS}$
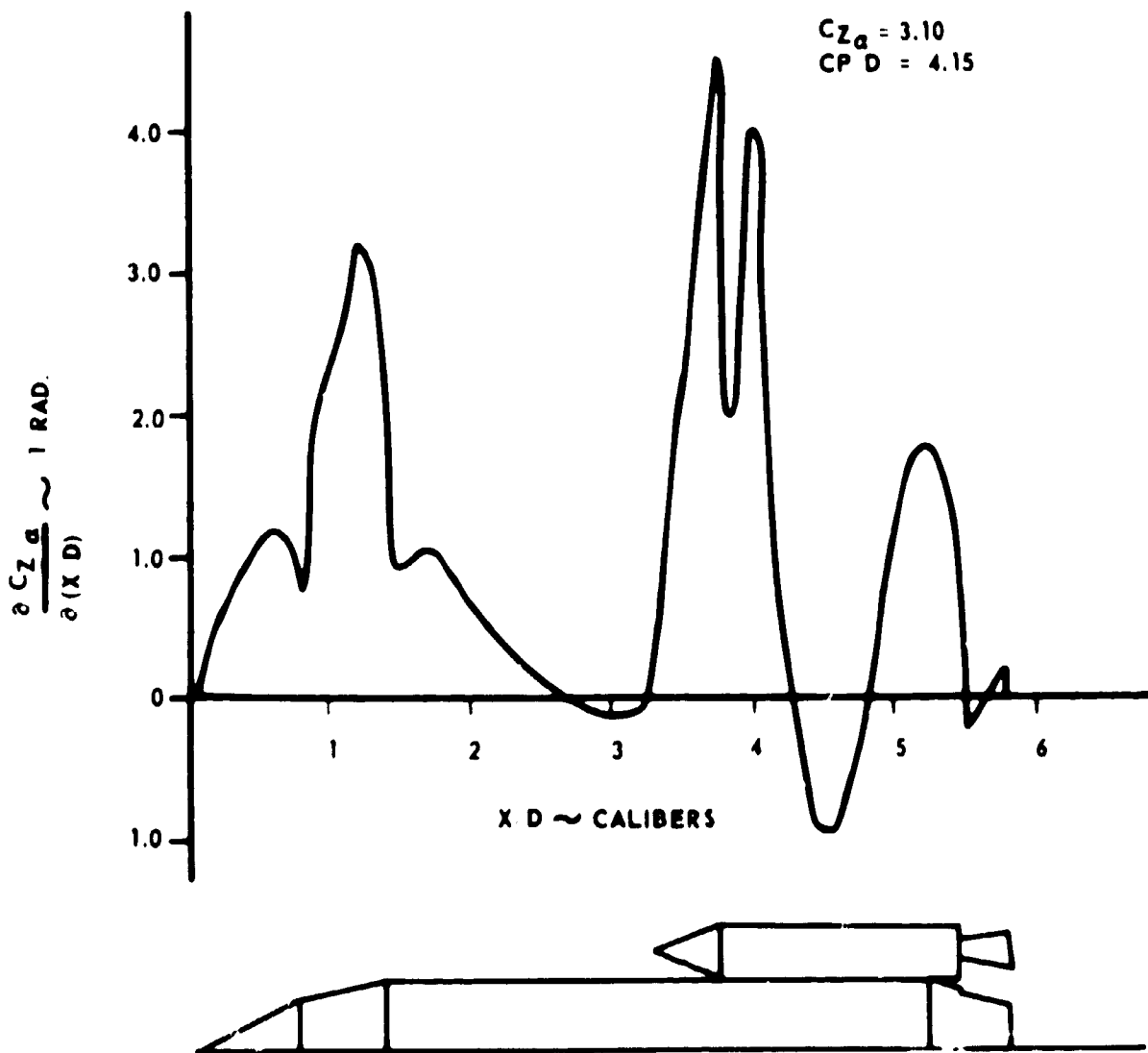
FIGURE 4.2.2.2-5   LOCAL NORMAL FORCE DISTRIBUTION   MLLV WITH 8-260"
SOLIDS $M_\infty = 1.26$ (MAX qα)
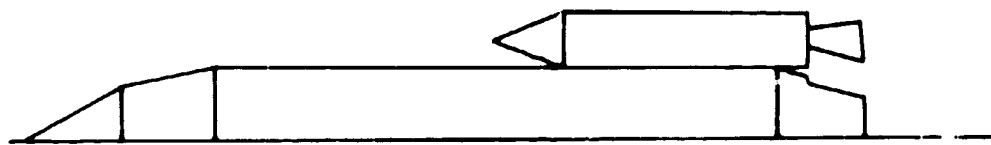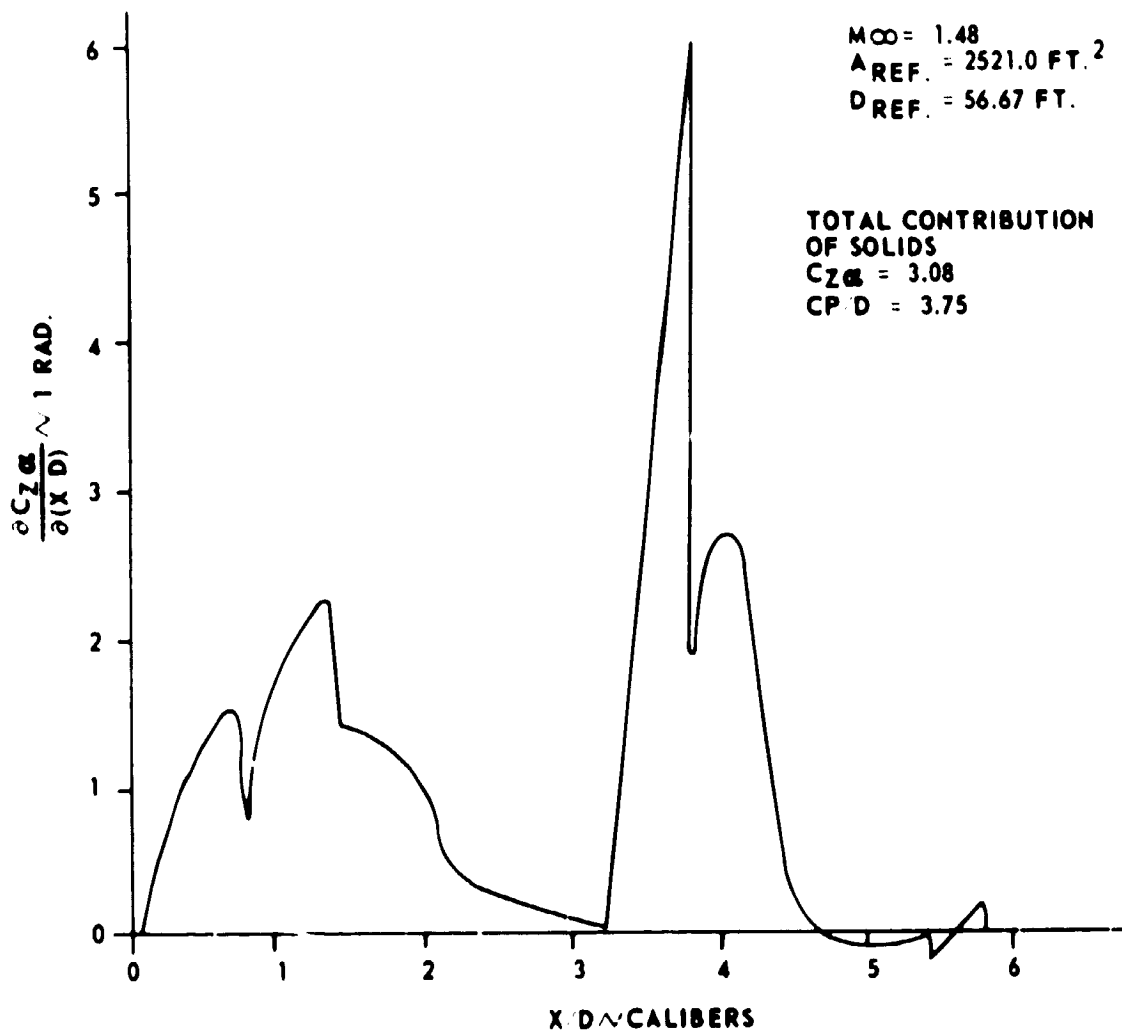
FIGURE 4.2.2.2-6   LOCAL NORMAL FORCE DISTRIBUTION   MLLV WITH 8-260"
SOLIDS M$_\infty$=1.48

113
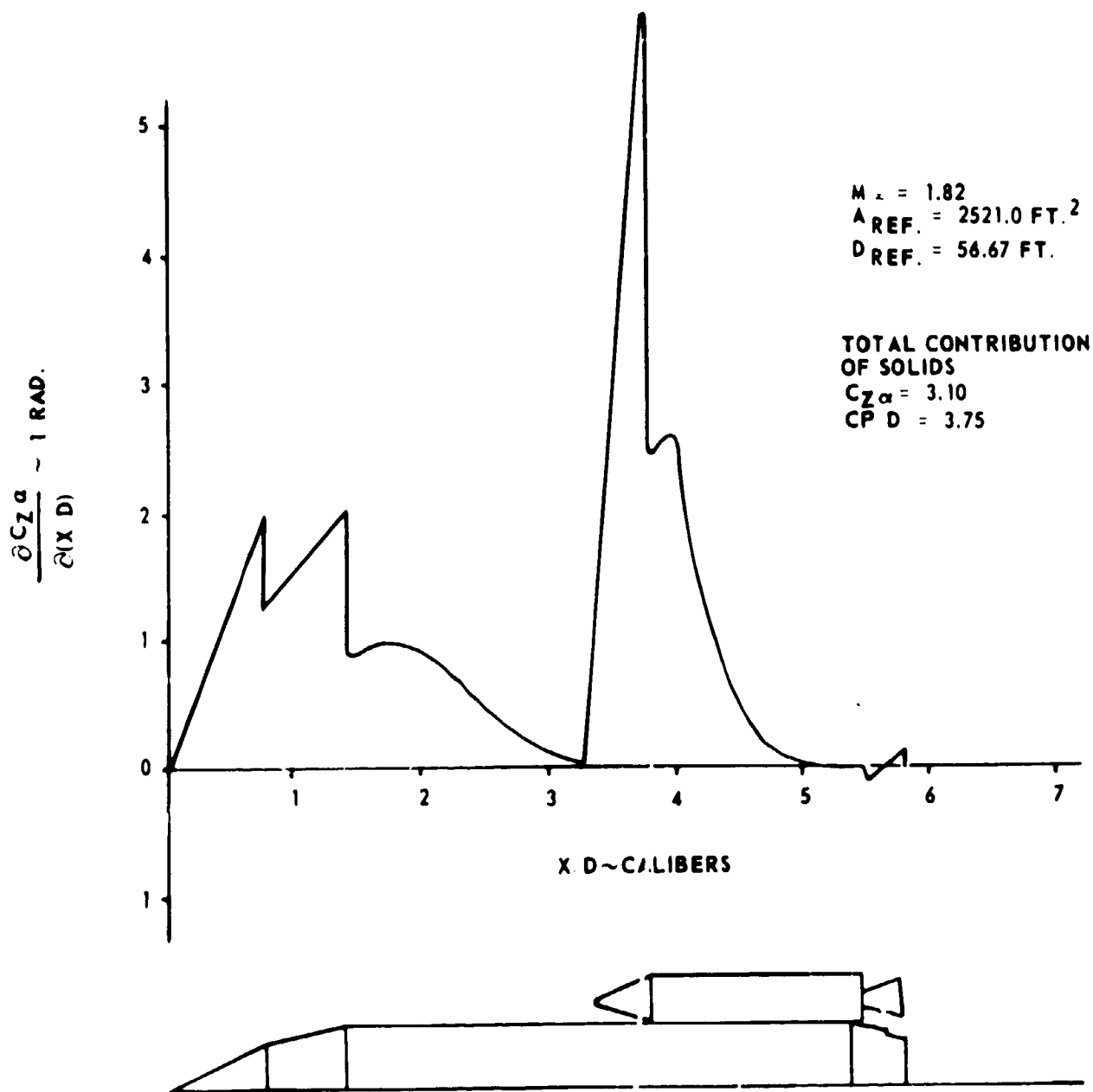
FIGURE 4.2.2.2-7 LOCAL NORMAL FORCE DISTRIBUTION MLLV WITH 8-260"
SOLIDS $M_\infty = 1.82$

4.2.2.2   (Continued)

are applicable to the maximum qα flight regime of both vehicles. The normal force distribution for each of the solid stages assumed to be similar to the local normal force distribution for one solid in a free stream environment.

4.2.2.3   Drag Coefficient

The total vehicle drag coefficients versus mach numbers for the single-stage-to-orbit vehicle and for the main stage plus three injection stage modules plus eight strap-on stage vehicles are shown in Figure 4.2.2.3-1. The drag coefficient at zero angle of attack was assumed to have the following form:

$$C_{DO} = C_{DWAVE} + C_{DBOAT\ TAIL} + C_{DFRICTION} + C_{DSOLIDS} + C_{DPROTUBRANCES} + C_{DBASE}$$

(This equation was also used to analyze the axial force distributions at zero angle of attack since $C_D = C_A$ at zero angle of attack.)

The wave drag was obtained from Reference 4.2.2.0-1. The boattail drag was calcuated by integrating local pressure distributions determined using Prandtl-Meyer analysis of the expanding flow field on the core boattail. The friction drag component ($C_{DFRICTION}$) was obtained from Reference 4.2.2.3-1. The wetted area was assumed to be an adiabatic flat plate since wall temperatures were not available. Compressibility effects were included in the calculation of skin friction drag.

The drag of the solid motor was estimated using wind tunnel data for a clean Saturn V Rift vehicle. These data were obtained from Reference 4.2.2.3-2. The drag of the strap-on stages was modified to account for interference effects due to the stages being in the vicinity of the core vehicle. The interference factor also took into account the estimated drag of the attachment structure. The protuberance area included the strap-on stage support structure and other associated attachment structure.

4.2.2.3-1   Schlichting, Hermann, "Boundary Layer Theory," McGraw Hill Book Company, Inc., 1960

4.2.2.3-2   Morgan, James, R., "Experimental Static Longitudinal Stability and Axial Force Characteristics of the Saturn V Chemical, Rift and Nuclear Vehicles," MSFC Memo M-AERO-E-244-63.
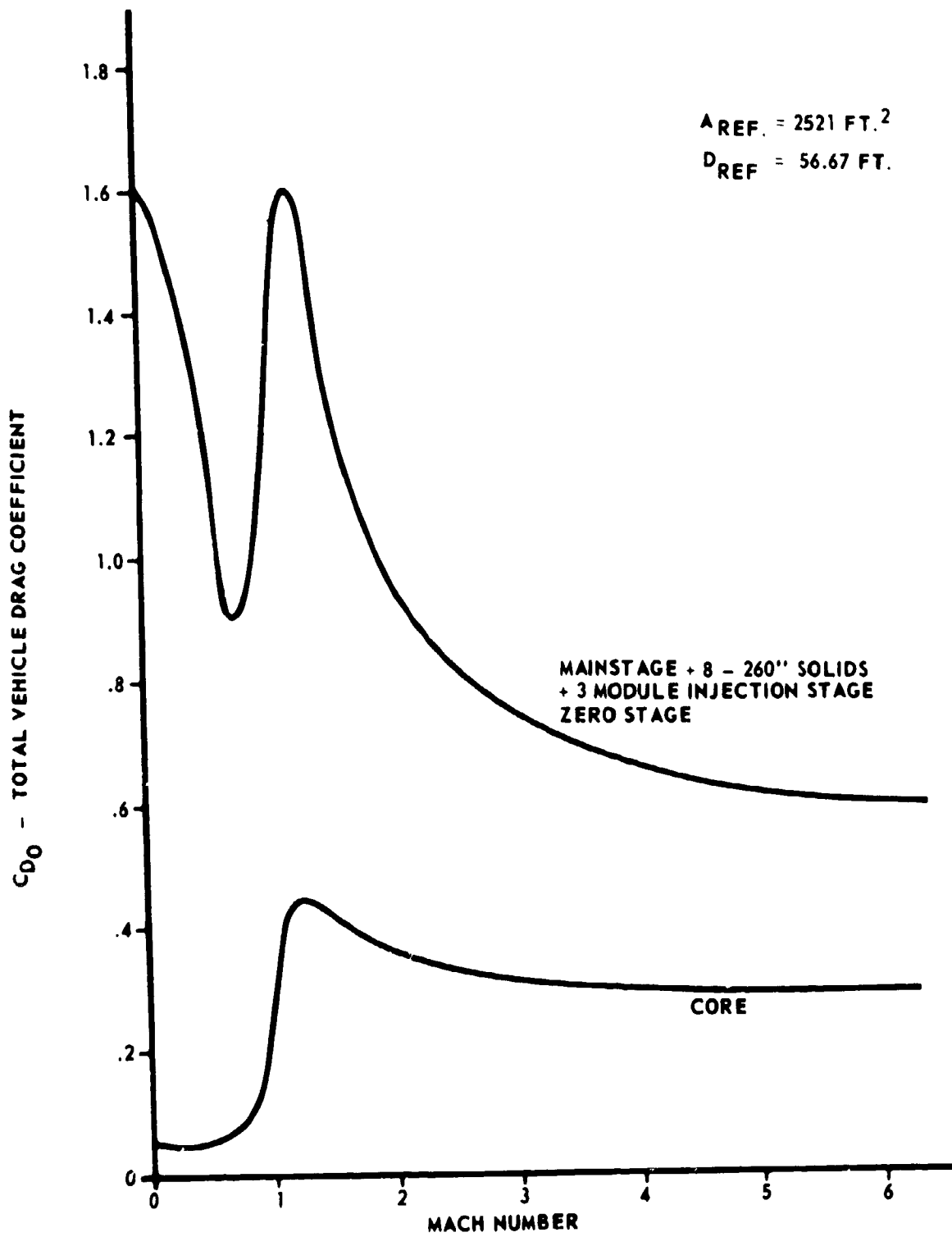
FIGURE 4.2.2.3-1 TOTAL VEHICLE DRAG COEFFICIENT MLLV SINGLE STAGE TO
ORBIT AND MAIN STAGE + INJECTION STAGE + 8-260"
STRAP-ON STAGES VEHICLES

116

4.2.2.3   (Continued)

The base drag of the core vehicle was not included in the drag calculations for the single-stage-to-orbit vehicle since the base pressure was accounted for in the engine performance data. The base drag for the core vehicle was, however, included in the total vehicle drag coefficient for the zero staged vehicle with the eight solid motors.

Base drag for the zero staged MLLV vehicle was calculated using experimental and theoretical techniques presented in References 4.2.2.3-3 and 4.2.2.3-4. Reference 4.2.2.3-5 presents the solid strap-on motor parameters required for this study. Data useful in predicting base pressure on a multichamber/plug engine when the exhaust plumes aspirate the base region are presented in Reference 4.2.2.3-3. The base pressure is presented as a function of engine chamber pressure ratioed to ambient pressure and aspiration vent area ratioed to base area. These data were used to calculate the base pressure curve prior to the time and mach number when the strap-on exhaust plumes would impinge on each other at the vehicle centerline. This impingement time point was assumed to be the time when base drag goes to zero.

The solid rocket motor parameters (Reference 4.2.2.3-5) were used in conjunction with the plume geometry presented in Reference 4.2.2.3-4 to estimate the zero base drag point. The plume geometry is based on nozzle exit plane pressure ratioed to ambient pressure, nozzle exit angle and free stream flow conditions. The plumes for specific trajectory time points were constructed, taking into account adjacent plume impingement, free stream flow characteristics and vehicle geometry.

Analysis of the strap-on exhaust plume geometry just prior to cut-off provided the necessary data point to extrapolate the drag curve into the base reverse flow regime. The plume geometry just prior to strap-on cut-off was determined using Reference 4.2.2.3-4. As the vehicle approaches strap-on stage cut-off, the external plume expansion angle is large, approximately 85°, due to the low ambient

4.2.2.3-3   Report PWA FR 1415, Section VIII, Pratt and Whitney, October 1965.

4.2.2.3-4   NASA TRR-6, "Experimental & Theoretical Studies of Axisymmetric Free Jets," by Eugene S. Love, Carl E. Grigsby, Louise P. Lee, and Mildred S. Woodling, dated 1959.

4.2.2.3-5   Aerojet-General Corporation Letter #SRO-68-5500C-L-98, September 26, 1968 (shown in Volume IX, Appendix C).

4.2.2.3 (Continued)

static pressure. According to Reference 4.2.2.3-4, external flow field has little effect on the exhaust plume because of the low density. Therefore, plume geometry for the rocket exhaust into still air at the required static pressure was used to calculate the base pressure just prior to engine cut-off. To be conservative, base pressure was assumed to be the total pressure obtained when the strap-on nozzle flow shocked down at the vehicle centerline to flow back into the base region. The total pressure behind the internal plume normal shock was calculated using an estimated entrance Mach number calculated from solid motor operating characteristics and estimated plume flow patterns.

The three drag calculations mentioned above provided the necessary data to construct the base drag vs. Mach number curve shown in Figure 4.2.2.3-2.

4.2.2.4 Axial Force Distributions

The axial force distributions are presented in Figures 4.2.2.4-1 through 4.2.2.4-7. These data were generated using wind tunnel test results from Reference 4.2.1.0-2 for the nose cone and Reference 4.2.2.3-5 for the solids. Interference effects as mentioned before were included in the drag contribution of the solids.

4.2.3 Preliminary Vehicle Weight and Mass Characteristics

Preliminary weight and mass characteristics data were prepared to support the performance, control and loads studies of the baseline vehicle family. The preliminary weights prepared to support the performance studies are shown in the mission weight histories for the various vehicle configurations in the preceeding Section 4.2.1. Vehicle distributed weights, as discussed in Section 4.2.3.1, were computed to support the control loads studies. The vehicle mass property data, as discussed in Section 4.2.3.2, was computed to provide inputs for the control analyses. This data included weight, center of gravity and the pitch and roll mass moment of inertia as a function of time.

These weights data were developed from the previous AMLLV study data using the scaling trends indicated by the performance trades reported in Section 4.1. At the conclusion of the design activity, final weights were computed for each of the elements in the baseline vehicle family. These final weights are reported in Section 4.3.2. These final weights were compared to the preliminary weight data shown in this section to assure that there were no significant differences between the final weights and those used for the earlier control and loads analyses. The results of this comparison indicated that this preliminary data was accurate and that the control, flight and ground environments and loads computed from this preliminary data is applicable to the final study results.

118
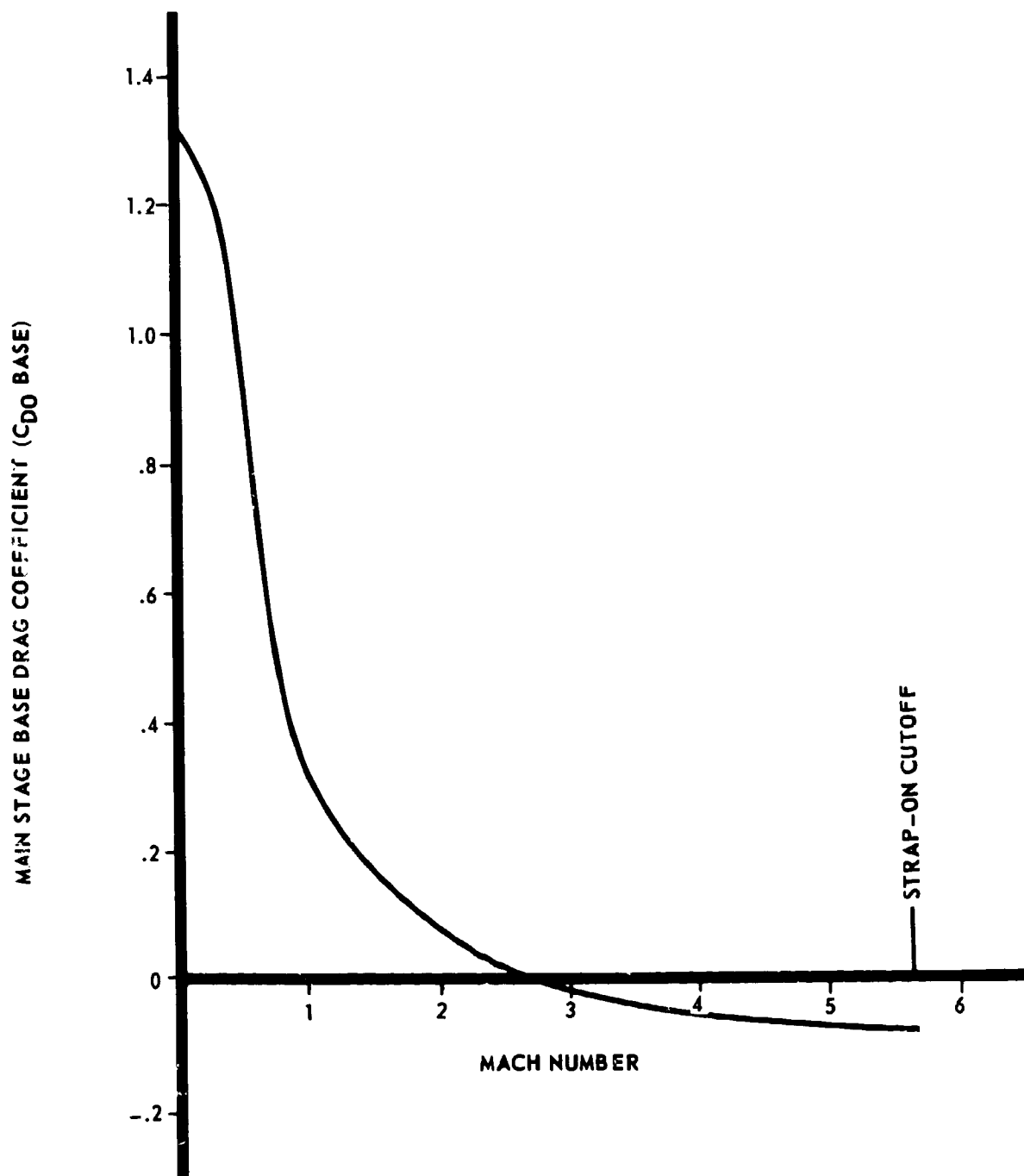
FIGURE 4.2.2.3-2 MAIN STAGE BASE DRAG VS. MACH NO. (EIGHT STRAP-ON STAGES IN A ZERO STAGE MODE)

$A_{REF} = 2521.0 \text{ FT}^2$
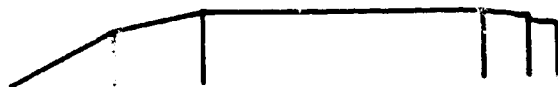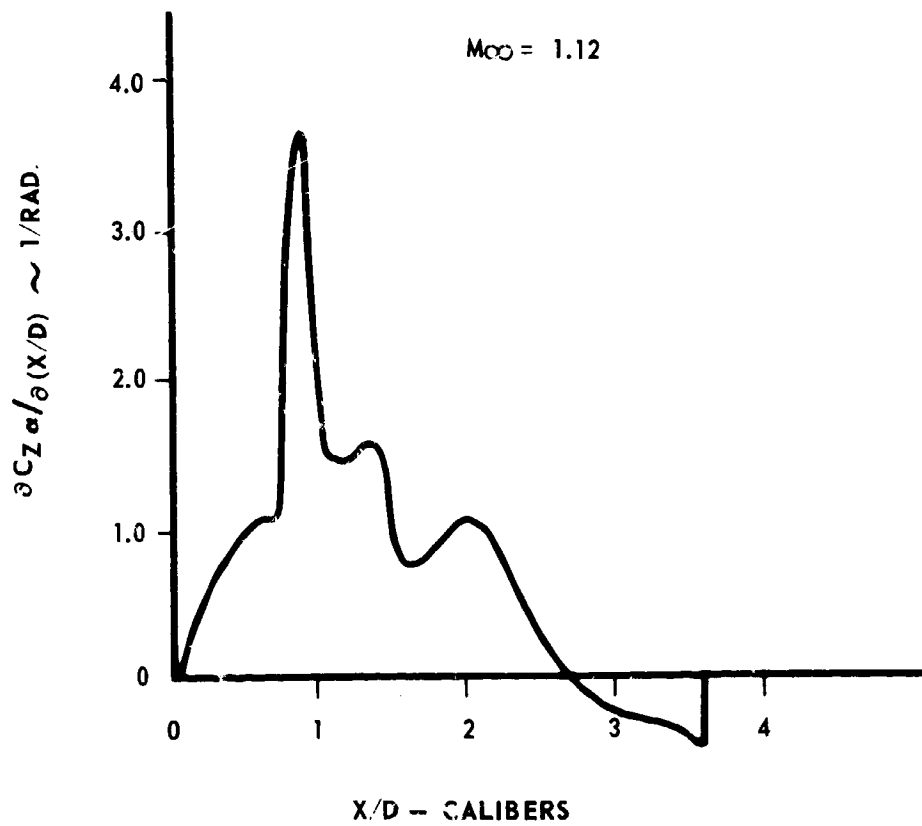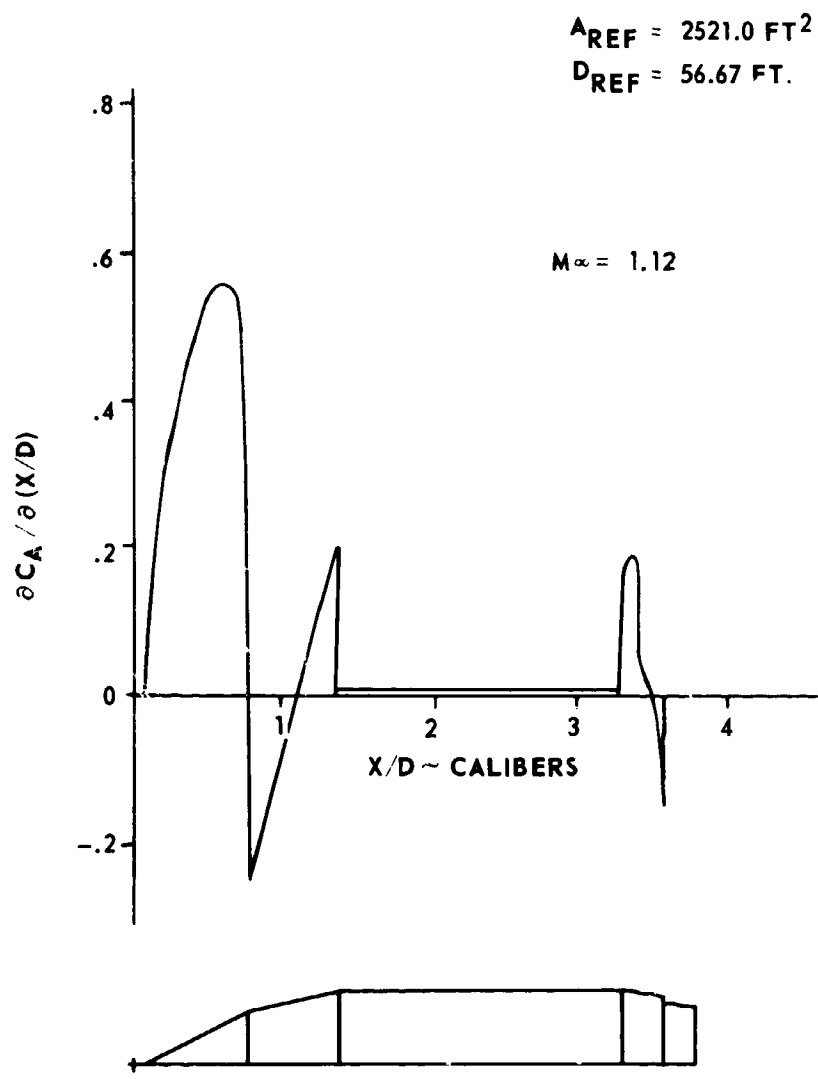
$D_{REF} = 56.67 \text{ FT.}$

$M\alpha = 1.12$

FIGURE 4.2.2.4-1   LOCAL AXIAL FORCE DISTRIBUTION $\sim$ MLLV CORE $M_\infty = 1.12$

$A_{REF.} = 2621.0 \text{ FT}^2$
$D_{REF.} = 56.67 \text{ FT}.$

$M\infty = 1.26$
MAX $q\alpha$

$\partial C_A / \partial (X/D)$

X/D ~ CALIBERS
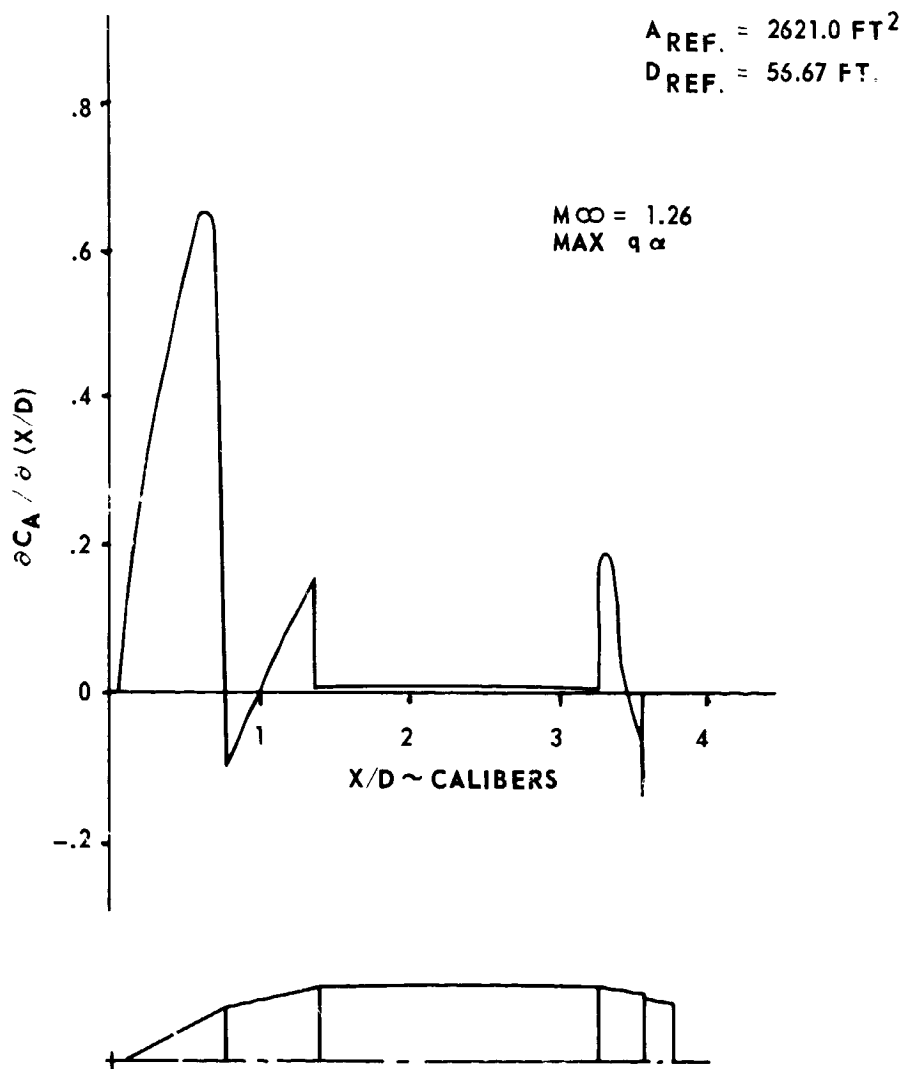
FIGURE 4.2.2.4-2   LOCAL AXIAL FORCE DISTRIVUTION ~ MLLV CORE
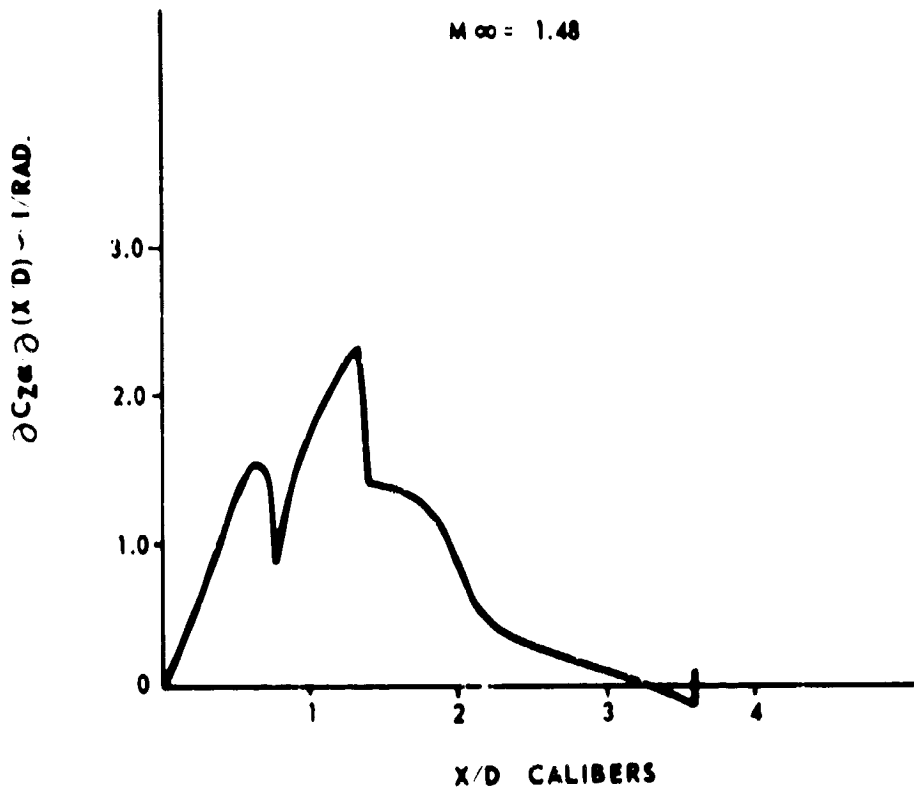$M\infty = 1.26$ (MAX $q\alpha$)

121
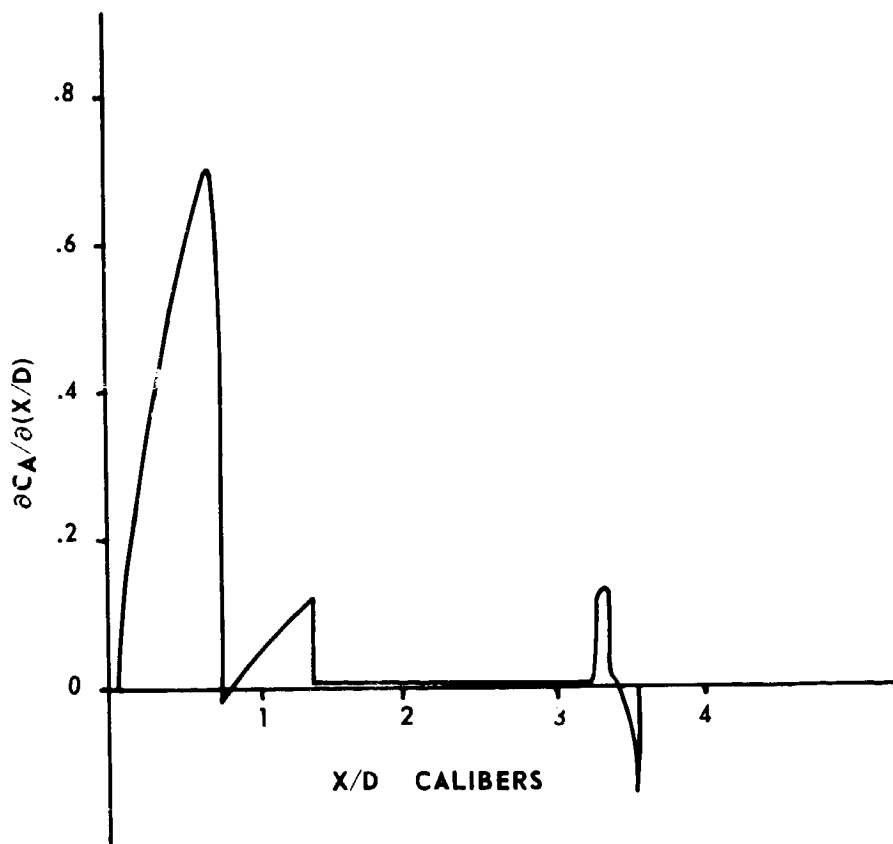
FIGURE 4.2.2.4-3   LOCAL AXIAL FORCE DISTRIBUTION ~ MLLV CORE M_∞ = 1.48
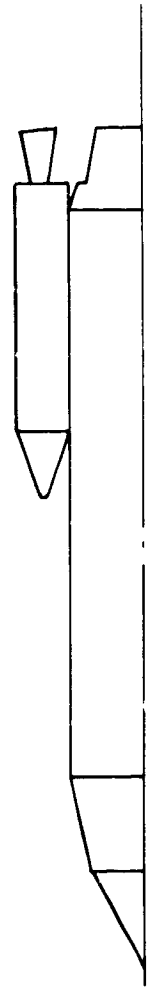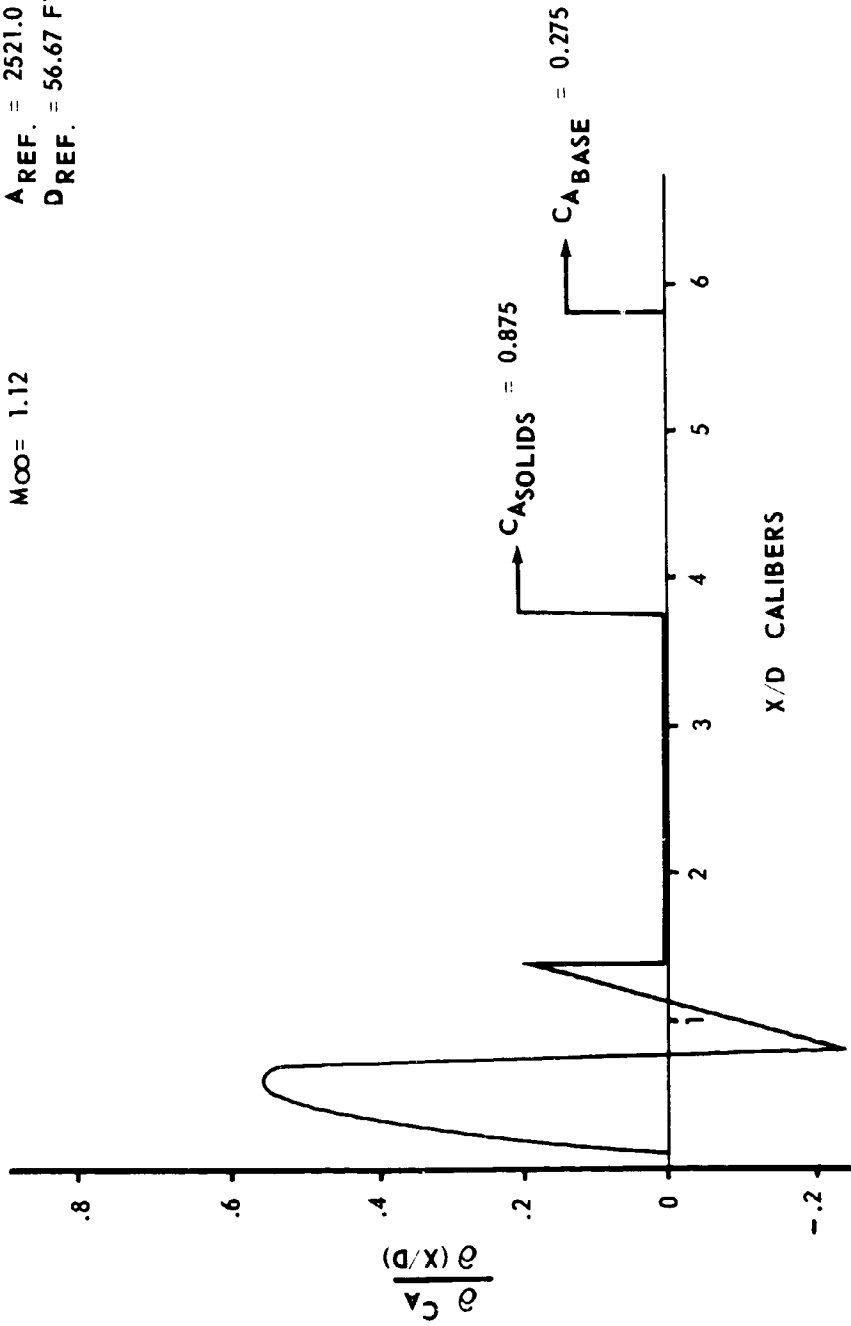
FIGURE 4.2.2.4-4 LOCAL AXIAL FORCE DISTRIBUTION ~ MLLV VEHICLE WITH 8–260"
SOLIDS $M_\infty = 1.12$
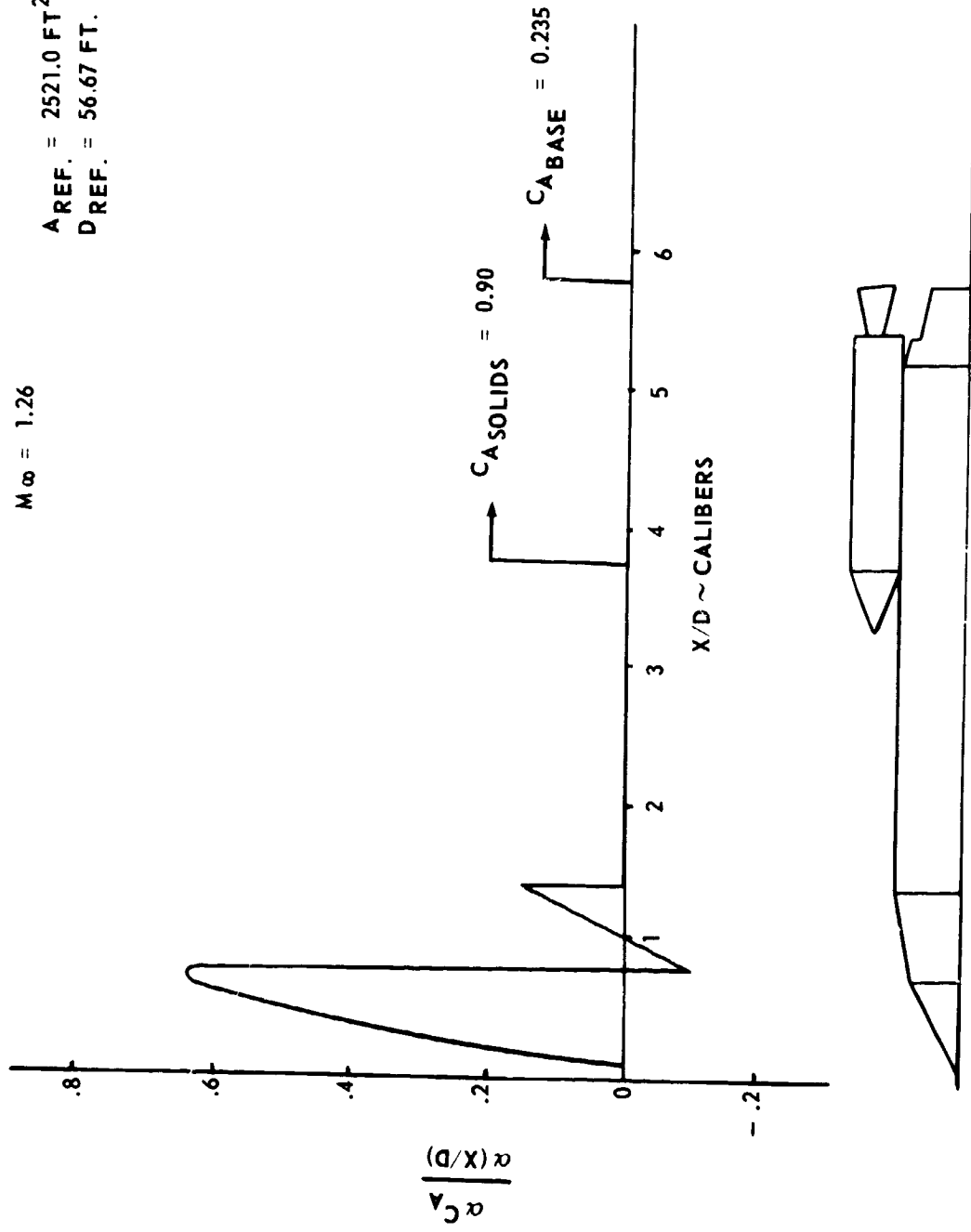
FIGURE 4.2.2.4-5 LOCAL AXIAL FORCE DISTRIBUTION ~ MLLV VEHICLE WITH 8-260"
SOLIDS M_∞ = 1.26
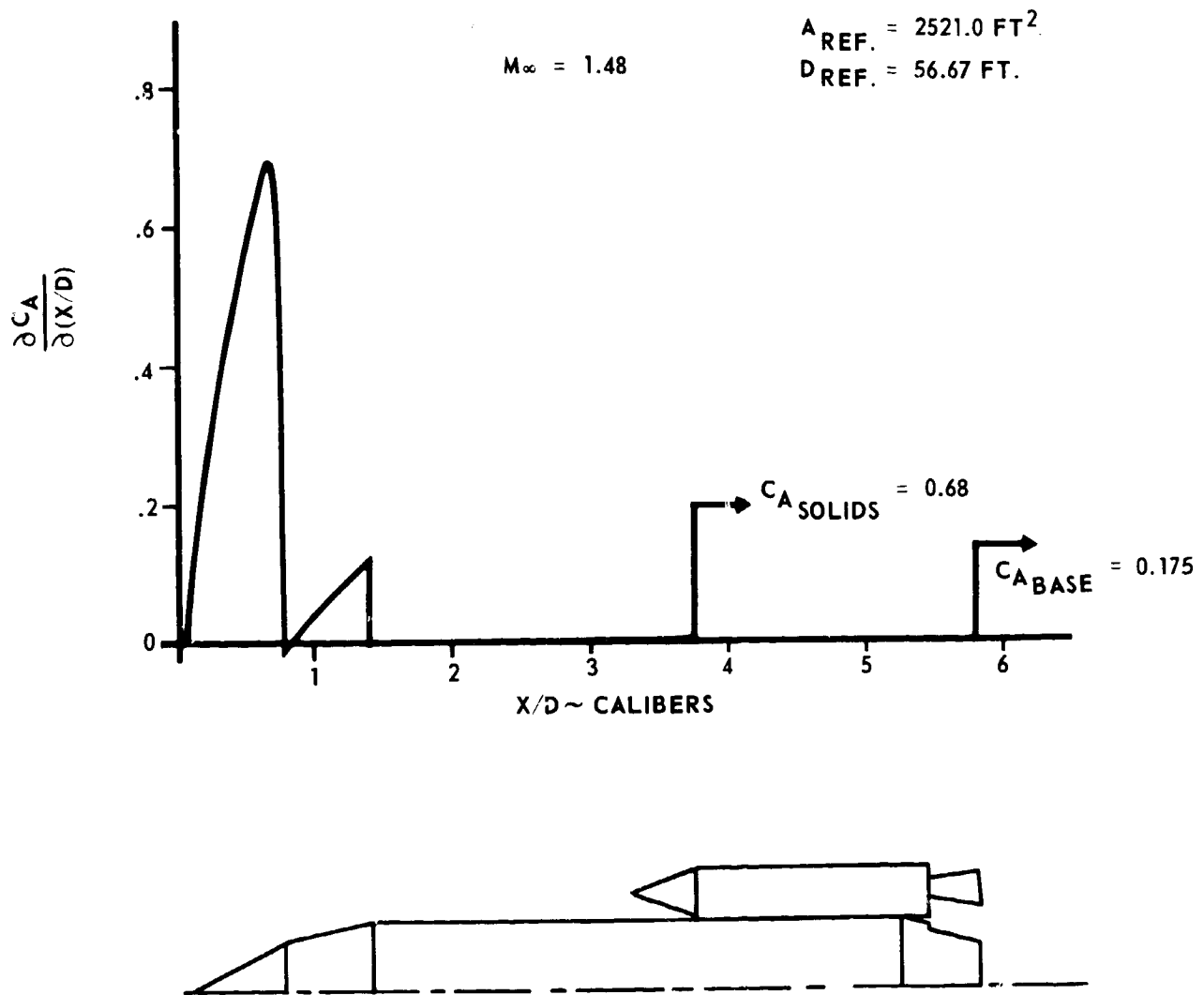
FIGURE 4.2.2.4-6   LOCAL AXIAL FORCE DISTRIBUTION ~ MLLV VEHICLE WITH 8-260"
SOLIDS M_∞ = 1.48

125
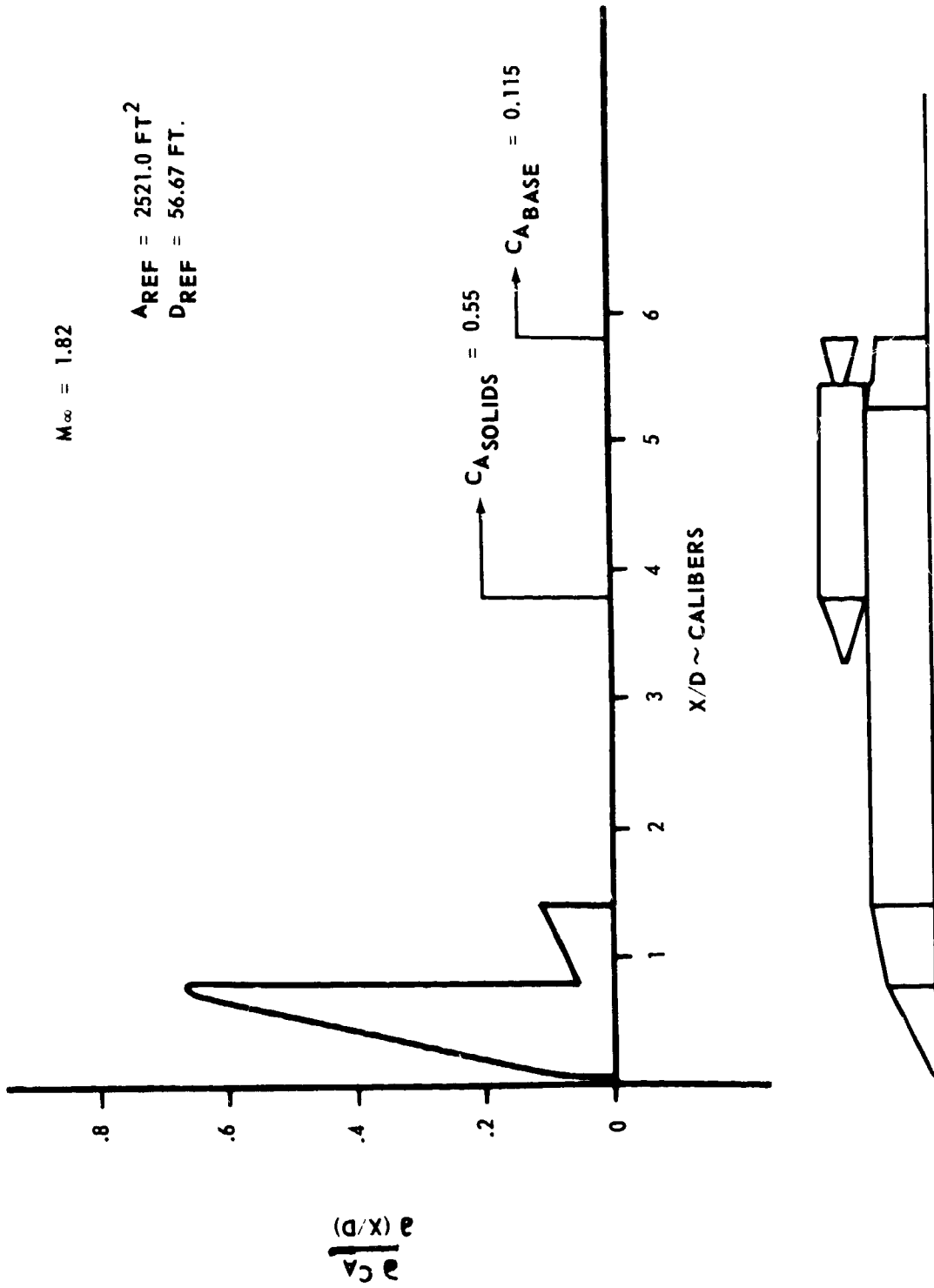
FIGURE 4.2.2.4-7 LOCAL AXIAL FORCE DISTRIBUTION ~ MLLV VEHICLE WITH 8-260"
SOLIDS M_∞ = 1.82

4.2.3.1 Vehicle Weight Distributions

Vehicle weight distributions for the MLLV single-stage-to-orbit vehicle, and for main stage plus the three module injection stage plus eight strap-on stages vehicle, were computed. These weights were based on the structural materials as shown in Table 4.2.3.1-I. Tables 4.2.3.1-II through 4.2.3.1-IV present the weight distributions as a function of the station for the single-stage-to-orbit vehicle. Table 4.2.3.1-II presents the dry weight distributions. The weights shown represent the drop weight of stage (inert weight plus residuals and gases) plus the payload between that station and the next lower station reported. Table 4.2.3.1-III illustrates the weight distribution for the propellant at the time (max $q\alpha$) when the maximum impact on structure occurs due to vehicle weight effects. Table 4.2.3.1-IV lists the weights at key vehicle stations for the time periods at which weights have a significant impact on the loads (on-pad, lift-off, max $q\alpha$ and at 90% throttling) for the single-stage-to-orbit vehicle.

Tables 4.2.3.1-V through 4.2.3.1-VII illustrate the same data for the main stage plus three injection stage modules plus eight strap-on stages vehicle configuration. Table 4.2.3.1-V also identifies the reaction loads at the maximum dynamic pressure condition and the solid motor cut-off condition.

4.2.3.2 Weights Analyses

To conduct the control analyses of the half size vehicle family, the vehicle mass properties were developed. These data included weight, center of gravity and the pitch and roll mass moments of inertia as a function of time.

Figure 4.2.3.2-1 and 4.2.3.2.-2 show these properties for the single-stage-to-orbit vehicle. The abrupt changes in slope of the curves in these two figures result from throttling the main stage engines to ten percent (10%) of their nominal thrust level. The vehicle mass properties for the MLLV main stage plus three injection stage modules plus eight strap-on stages configuration from lift-off through solid motor burn-out are given in Figures 4.2.3.2-3 and 4.2.3.2-4.

4.2.4 Loads and Structural Criteria

Using the aerodynamic inputs, the preliminary weights and the tank pressures as discussed in Section 4.2.2, 4.2.3 and 4.3.3 respectively, analyses were conducted to define the design loads for the various elements in the baseline vehicle family. The loads developed included (1) the loads from ground winds while the vehicle is in the launch position, (2) the in-flight structural loads including the dynamics, and (3) the launch and in-flight acoustical loads. The resulting design loads were subsequently used for stress analysis and design of the main stage and injection stage structures and of the solid motor strap-on stage attachment hardware.

TABLE 4.2.3.1-I   MLLV BASELINE STRUCTURAL DESIGN

STRUCTURAL COMPONENT	STRUCTURAL MATERIALS	CONSTRUCTION
FORWARD SKIRT	7075-T6 ALUMINUM	SKIN, STRINGER, FRAME
FORWARD LOX TANK	2219-T87 ALUMINUM	MONOCOQUE
LOX TANK WALL	2219-T87 ALUMINUM	MONOCOQUE (SHORT CYLINDER BETWEEN Y-RINGS)
COMMON BULKHEAD	2219-T87 ALUMINUM SHEET, 5052 ALUMINUM CORE	HONEYCOMB SANDWICH
LH$_2$ TANK WALL	2219-T87 ALUMINUM	SKIN, STRINGER, FRAME
AFT BULKHEAD	2219-T87 ALUMINUM	MONOCOQUE
THRUST STRUCTURE	7075-T6 ALUMINUM	SKIN, STRINGER, FRAME

TABLE 4.2.3.1-II

VEHICLE DISTRIBUTED WEIGHTS

(STAGE DRY WEIGHT, RESIDUALS, GASES AND PAYLOAD)

MLLV
CORE ALONE
(SINGLE-STAGE-TO-ORBIT VEHICLE)

VEHICLE STATION	WEIGHT (LBS)	
2475.00	17,200	
2338.09	28,050	
2228.88	47,900	
2123.18	64,300	
2015.08	76,940	$W_{PL} = 500,000$ POUNDS
1906.95	90,750	
1798.80	105,650	
1713.00	69,210	
1571.12	26,423	
1462.24	25,841	
1427.54	11,291	INCLUDES
1392.83	77,509	47,400 POUNDS
1336.58	11,545	OF PROPELLANT
1224.08		IN LOX DUCTS
1111.58		
999.08		
886.58		
774.08		
661.58		
549.08	11,545	
492.83	192,111	

TABLE 4.2.3.1-III

PROPELLANT WEIGHT DISTRIBUTION

MLLV
(SINGLE-STAGE-TO-ORBIT VEHICLE)

AT t = 71.94 Sec. (Max, $q\alpha$)

DIA = 680"

	VEHICLE STATION	WEIGHT (LBS)
	492.83	106,110
	549.08	102,913
	661.58	102,913
LH$_2$	774.08	102,913
	886.58	102,913
	968.83	47,498
	1392.83	1,717,950
LOX	1427.54	1,031,500
	1462.24	590,740

TABLE 4.2.3.1-IV
VEHICLE ACCUMULATIVE WEIGHTS
MLLV
(SINGLE-STAGE-TO-ORBIT VEHICLE)

	VEHICLE STATION	ON-PAD (t < 0.00 Sec.)	LIFT-OFF (t = 0.00 Sec.)	MAX qα (t = 71.94 Sec.)	90% THROTTLED
	1680.00	5,928,133 (t)	500,000	500.000	500.000
FWD	1462.24	5,901.710 (t)	526,423	526,423	526,423
AFT	1462.24	5,875,869 (t)	552,264	552.264	552.264
FWD	1392.83	5,864,578 (t)	563,555	563,555	563.555
AFT	1392.83	1,105,799 (t)	5,322,334	3,953,574	1,060.876
FWD	492.83	1,013,438 (t)	5,414,695	4,045,935	1,153,237
AFT	492.83	186,568 (t)	6,241,565	4,644,415	1,268,939
FWD	376.00	170,553 (t)	6,257,580	4,660,430	1,284,953
AFT	376.00	0	6,428,133	4,830,985	1,455,505

NOTES:

(1) (t) denotes tensile loading

(2) All weight in pounds

TABLE 4.2.3.1-V
VEHICLE DISTRIBUTED WEIGHTS
(MAIN STAGE AND INJECTION STAGE DRY WEIGHTS, RESIDUALS, GASES AND PAYLOAD)
MLLV
(MAIN STAGE + (8) STRAP-ON STAGES + (3) MODULE INJECTION STAGE VEHICLE)

	VEHICLE STATION	WEIGHT (LBS)	
	4142.00	17,200	
	4005.09	28,050	
	3895.88	47,900	
	3790.18	64,300	
	3682.08	76,940	
	3573.95	90,750	
	3465.80	105,650	
	3361.00	109,170	
	3257.00		
	3153.00		
	3049.00		
	2945.00		
	2841.00		
	2737.00		
	2633.00		
	2529.00		
	2425.00		
	2321.00		
	2217.00		
	2113.00	109,170	
SOLID MOTOR			SOLID MOTOR
	2013.00	39,700	
ATTACH POINTS			REACTIONS (8) MOTORS
	1909.00	44,300	
	1806.00	77,800	
Sta. 1609 _____			7,852,348 #α Max. qα
	1571.12	52,313	
	1462.24	25,841	1,462,840 #α Motor Cut-off
	1427.54	11,291	
	1392.83	77,506	
	1356.58	11,545	
	1224.08		
	1111.58		
	999.08		
	886.58		
	774.08		
	661.58		
			5,984,920 #α Max qα
	549.08	11,545	
	492.83	197,746	
Sta. 378 _____			1,114,944 #α Motor Cut-off

132

TABLE 4.2.3.1-VI

PROPELLANT WEIGHT DISTRIBUTION

MLLV

(MAIN STAGE + (8) STRAP-ON STAGES + (3) MODULE INJECTION STAGE VEHICLE)

AT t = 56.28 Sec. (Max. $q\alpha$)

	VEHICLE STATION	WEIGHT (LBS)
	492.83	106,110
	549.08	102,913
	661.58	102,913
LH_2 MAIN STAGE	774.08	102,913
	886.58	102,913
	999.08	102,913
	1111.58	102,913
	1207.55	74,262
	1392.83	1,717,950
LOX MAIN STAGE	1427.54	1,031,500
	1462.24	1,959,500
	1806.00	225,000
LH_2 & LOX INJECTION STAGE	1909.00	225,000
	2013.00	225,000

TABLE 4.2.3.1-VII
VEHICLE ACCUMULATIVE WEIGHTS
MILLV
(MAIN STAGE + (8) STRAP-ON STAGES + (3) MODULE INJECTION STAGE VEHICLE)

	VEHICLE STATION	ON-PAD LIFT-OFF MAX. $q\alpha$ SOLID CUT-OFF	CORE IGNITION t=130.31 (Sec.)	CORE CUT-OFF
	2061.00		1,850.000	1,850.000
AFT	2013.00		2,114,700	2,114,700
AFT	1909.09		2,384,000	2,384,000
AFT	1806.00		2,686,000	2,686,000
	1680.00	5,959,658 (t)	2,686,000	2,686,000
FWD	1462.24	5,907,345 (t)	2,738,313	2,738,313
AFT	1462.24	5,881,504 (t)	2,764,154	2,764,154
FWD	1392.83	5,870,213 (t)	2,775,445	2,775,445
AFT	1392.83	1,111,434 (t)	7,534,224	2,825,274
FWD	492.83	1,019,073 (t)	7,626,585	2,917,635
AFT	492.83	192,203 (t)	8,453,455	2,950,855
FWD	376.00	170,553 (t)	8,475,105	2,972,505
AFT	376.00	0	8,645,658	3,143,058

NOTES: (1) (t) denotes tensile loading (2) All weight in pounds

134

NOTE: FIGURE 4.2.3.2-1 OMITTED FROM THIS SPACE IS CLASSIFIED. THIS FIGURE IS PRESENTED IN VOLUME IX (CLASSIFIED APPENDICIES), APPENDIX E.
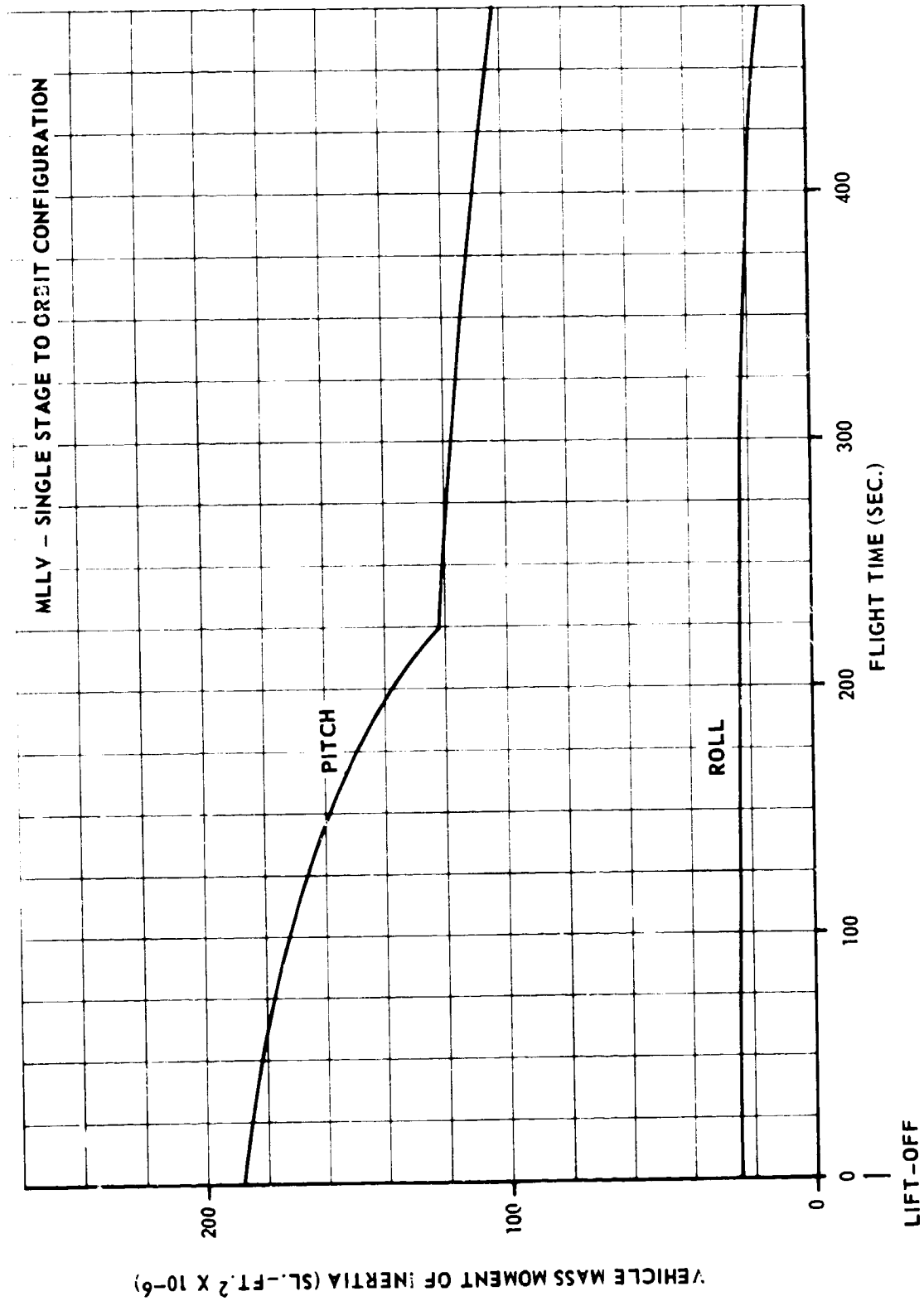
FIGURE 4.2.3.2-2   VEHICLE MASS MOMENT OF INERTIA VS. FLIGHT TIME
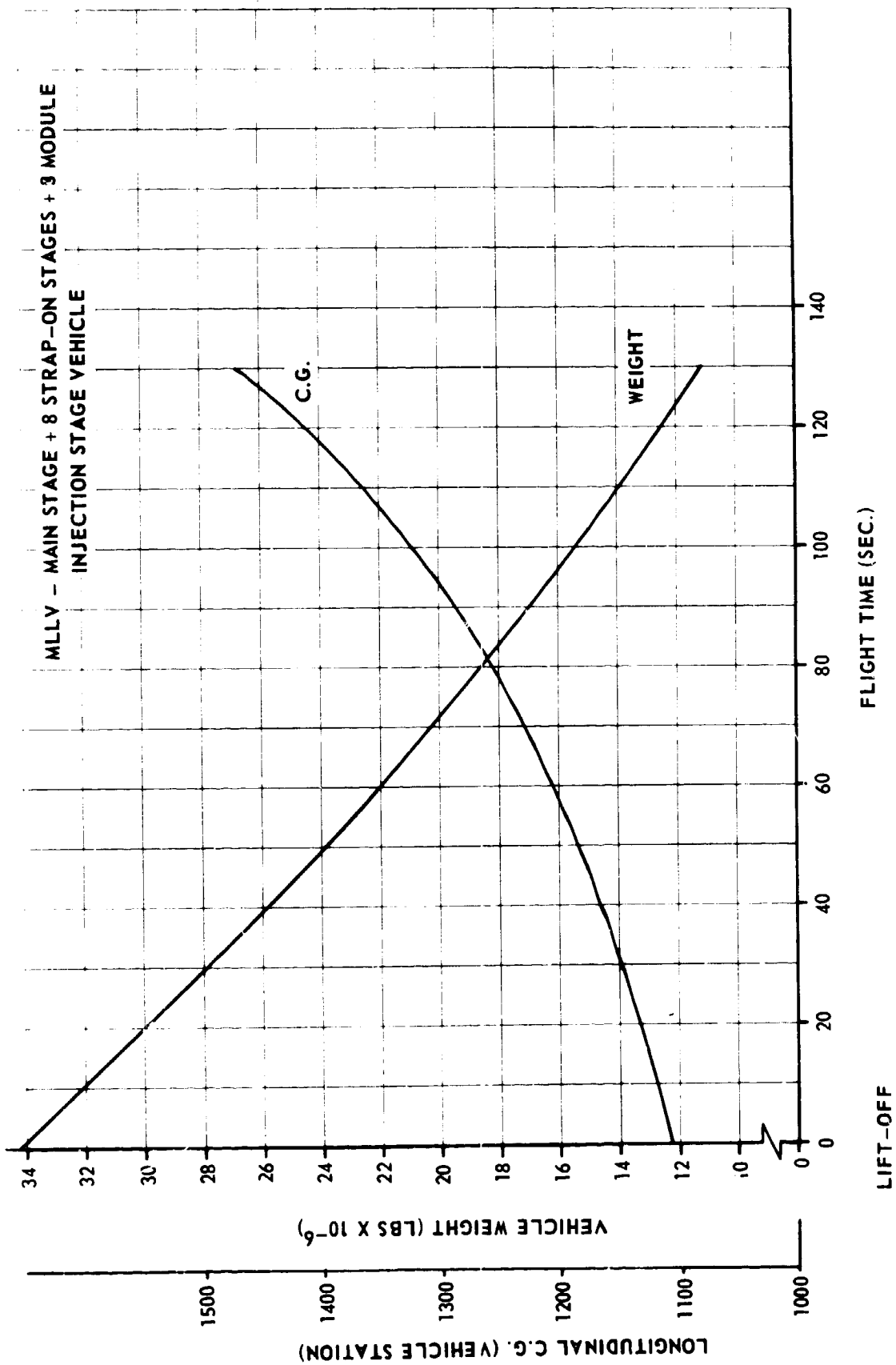
FIGURE 4.2.3.2-3 VEHICLE WEIGHT AND CENTER OF GRAVITY VS. FLIGHT TIME

137
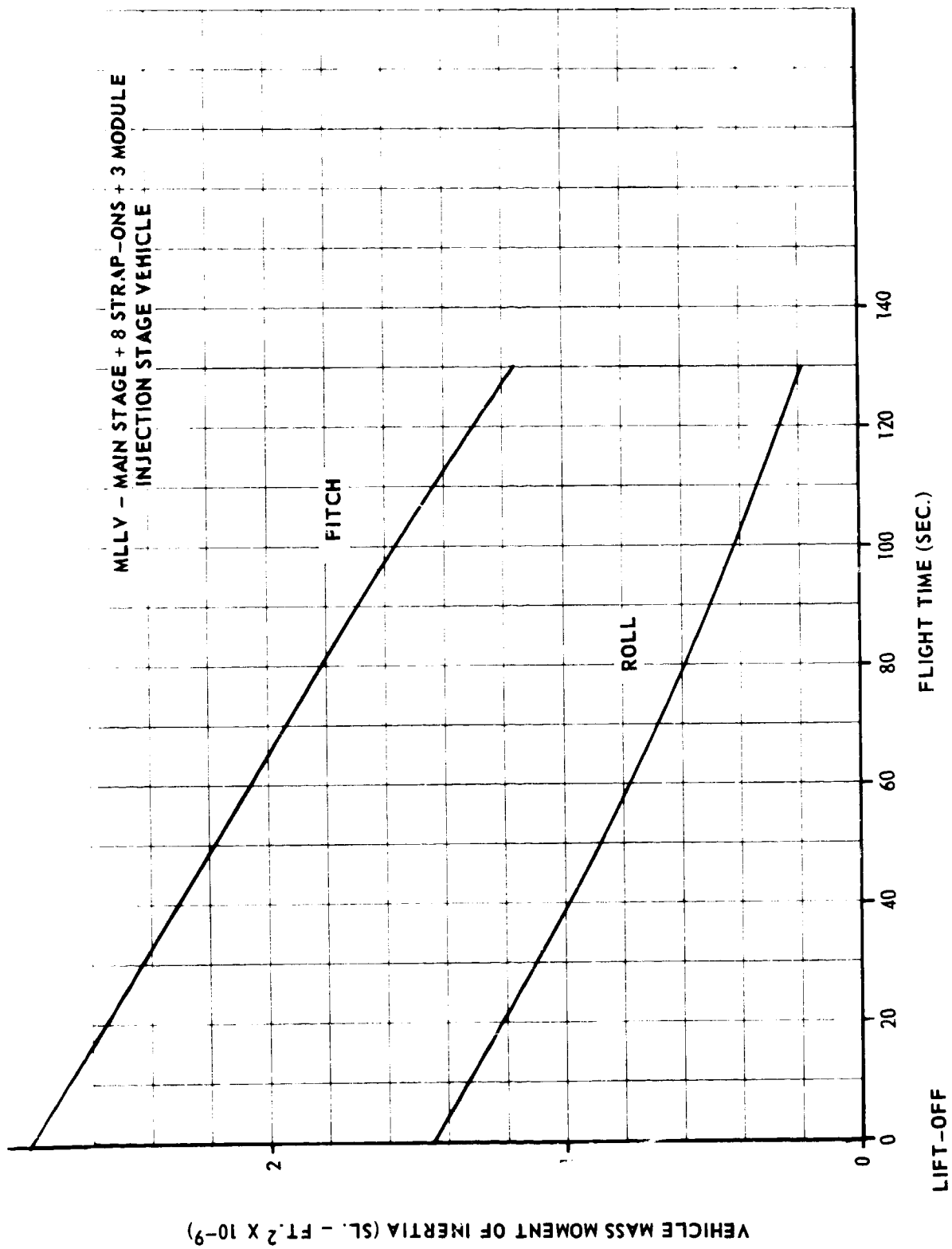
FIGURE 4.2.3.2-4   VEHICLE MASS MOMENT OF INERTIA VS. FLIGHT TIME

138

4.2.4   (Continued)

Considering the multiple utilization of the vehicle stages to make up the various configurations of the baseline vehicle family, this activity was directed to defin the "worst envelope" design loads. This "worst envelope" encompassed the ma mum loads anticipated for all of the possible configuration combinations.

Consideration was also given to the provision of two different forward skirts, i.e.: one for use with configurations without strap-on stages, and one for use with the vehicles employing strap-ons. The "worst condition" design loads for each of these two skirts were defined.

Preliminary loads analyses, combined with a review of the prior AMLLV loads data, defined those specific configurations which generally contributed to the "worst envelope" design loads, i.e.:

a.   Single-stage-to-orbit (M/C) and single-stage-to-orbit with a single injection stage module, M/C + S(I).

b.   Main stage plus eight strap-on stages plus a three module injection stage, M/C + 8(S) + 3S(I).

Detailed loads were developed for these configurations. Some additional loads data were developed for the main stage plus 8 strap-on stages, (M/C + 8S), configuration and for other configurations which could possibly contribute to the worst condition design loads.

The structural criteria used for these loads analyses and a definition of the terms shown in the subsequent discussions is included in Section 4.2.4.9.

4.2.4.1   "Worst Envelope" Design Loads

Figure 4.2.4.1-1 illustrates the combined compressive (N_c) loads for the "worst envelope" main stage design conditions. The LH$_2$ tank section is designed by the single-stage-to-orbit vehicle LH$_2$ tank compressive loads. The aft skirt, LOX tank outer periphery and forward skirt are designed by the compressive loads of the heaviest payload vehicle (i.e.: Main stage plus eight strap-ons plus three module injection stage).

The aft skirt design loads occur at main stage ignition for the largest payload vehicle. The LH$_2$ tank forward section is designed by the max $q\alpha$ loads for the same vehicle. Main stage cut-off for the heaviest payload vehicle designs the short LOX tank cylinder. The lower part of the forward skirt is also designed by the cut-off loads on the heaviest payload vehicle. The upper part of the forward skirt is designed by the max $q\alpha$ of the heaviest payload vehicle.

139

FIGURE 4.2.4. .1   ULTIMATE COMBINED COMPRESSIVE LOAD "WORST ENVELOPE" -
MLLV MAIN STAGE

4.2.4.1   (Continued)

As the forward skirt design loads are highly sensitive to the specific configuration, the variation in the forward skirt loads for the four baseline vehicle configurations studied are also shown on this figure.

Figure 4.2.4.1-2 illustrates the combined tensile (N_t) loads for the "worst envelope" main stage design conditions. The heaviest payload vehicle loads are the "worst envelope" N_t loads for the entire stage except for the upper portion of the forward skirt where the maximum tensile loads occur at rebound of the single-stage-to-orbit vehicle. The tensile loads for the aft skirt, LH_2 tank, LOX tank and lower part of the forward skirt are maximum at the max ($q\alpha$) condition of the heaviest payload vehicle. (The foward skirt tensile loads for each of the four baseline vehicles are shown on the same figure.)

Figures 4.2.4.1-3 and 4.2.4.1-4 show the combined compressive (N_c) and combined tensile (N_t) loads respectively for the main stage of the vehicle consisting of a main stage plus a single module injection stage and the main stage of the vehicle consisting of a main stage plus eight strap-ons. For comparison, the "worst envelope" design loads are also plotted on the figures.

For the compression load envelope, portions of the vehicle designed by the M/C + 8S + 3S(I) are the forward skirt and LOX tank and the aft skirt. The design conditions are max ($q\alpha$), main stage cutoff and main stage ignition respectively as shown on Figure 4.2.4.1-1. On Figure 4.2.4.1-5, max ($q\alpha$) loads for the main stage + 8 SRM vehicle are lower than the corresponding "worst envelope" design loads because the bending moments and longitudinal forces are both lower than those for the main stage + 8 SRM + 3S(I) vehicle. The greater length and increased weight of the main stage + 8 SRM + 3S(I) vehicle are the primary reasons or these differences. Main stage ignition and main stage cut-off compression loads are lower for the M/C + 8(S) vehicle because of the lower weight. The compression load envelope for the LH_2 tank is determined by the max ($q\alpha$) and lift-off conditions for the MLLV main stage as shown on Figure 4.2.4.1-1. On Figure 4.2.4.1-3, loads for the corresponding conditions are shown for the M/C + S(I) vehicle. These loads are essentially the same as the design loads. Slightly higher bending moments on the injection stage configuration are off-set by slightly lower longitudinal forces resulting from lower accelerations at lift-off and max ($q\alpha$).

For the tension load envelope, design loads arise from the max ($q\alpha$) condition for the M/C + 8 SRM + 3S(I) vehicle and the rebound condition for the main stage alone as shown on Figure 4.2.4.1-2. Figure 4.2.4.1-4 shows this "worst envelope" compared with loads for the main stage + S(I) and main stage + 8 SRM vehicles. The rebound condition provides the highest overall tension loads for main stage + S(I) vehicle and these are lower than the design loads at every location. Loads on the forward portion of the forward skirt are only slightly lower than

141
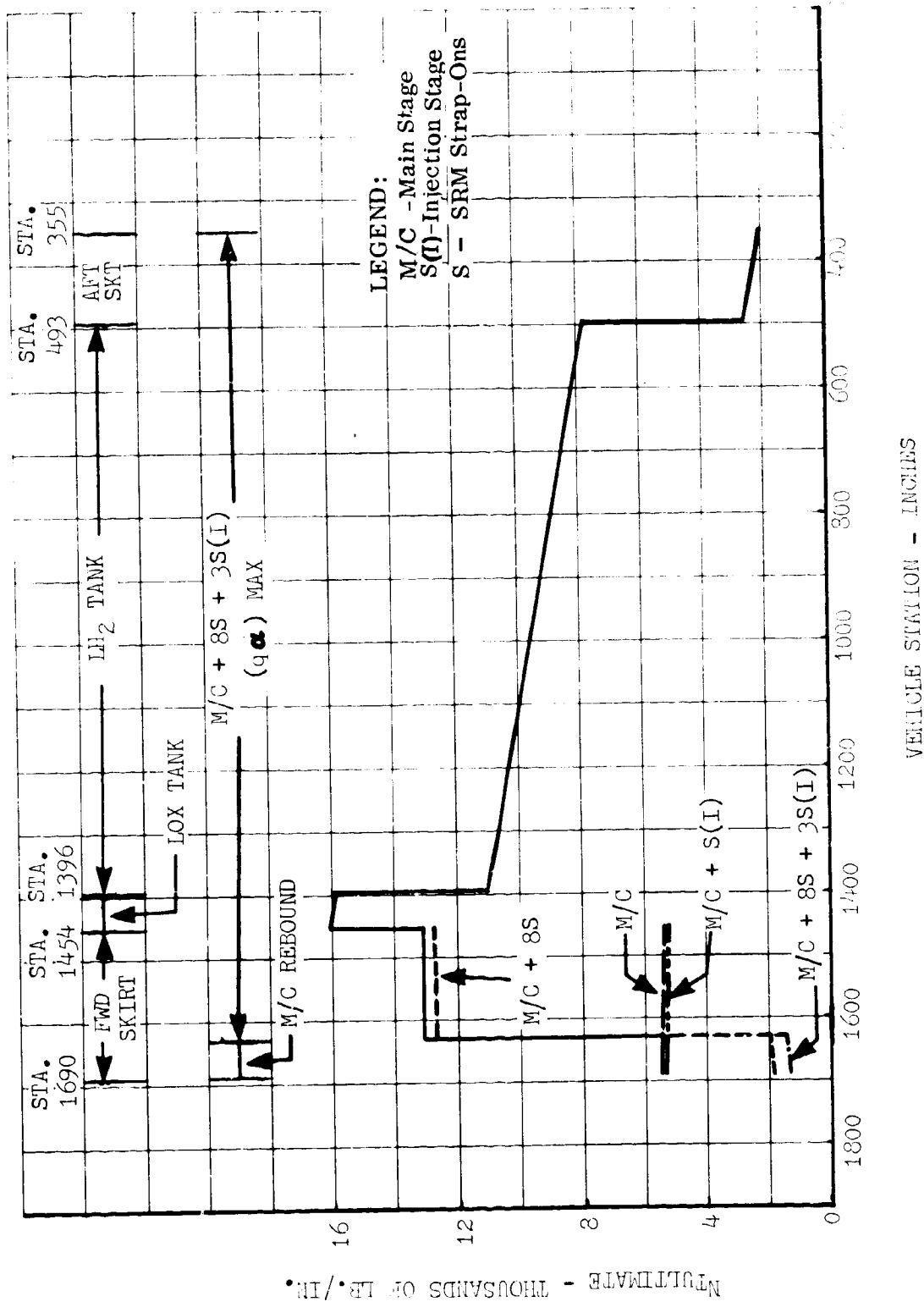
FIGURE 4.2.4.1-2   ULTIMATE COMBINED TENSILE LOAD "WORST ENVELOPE" - MLLV MAIN STAGE

VEHICLE STATION - INCHES

N'ULTIMATE - THOUSANDS OF LB./IN.

142
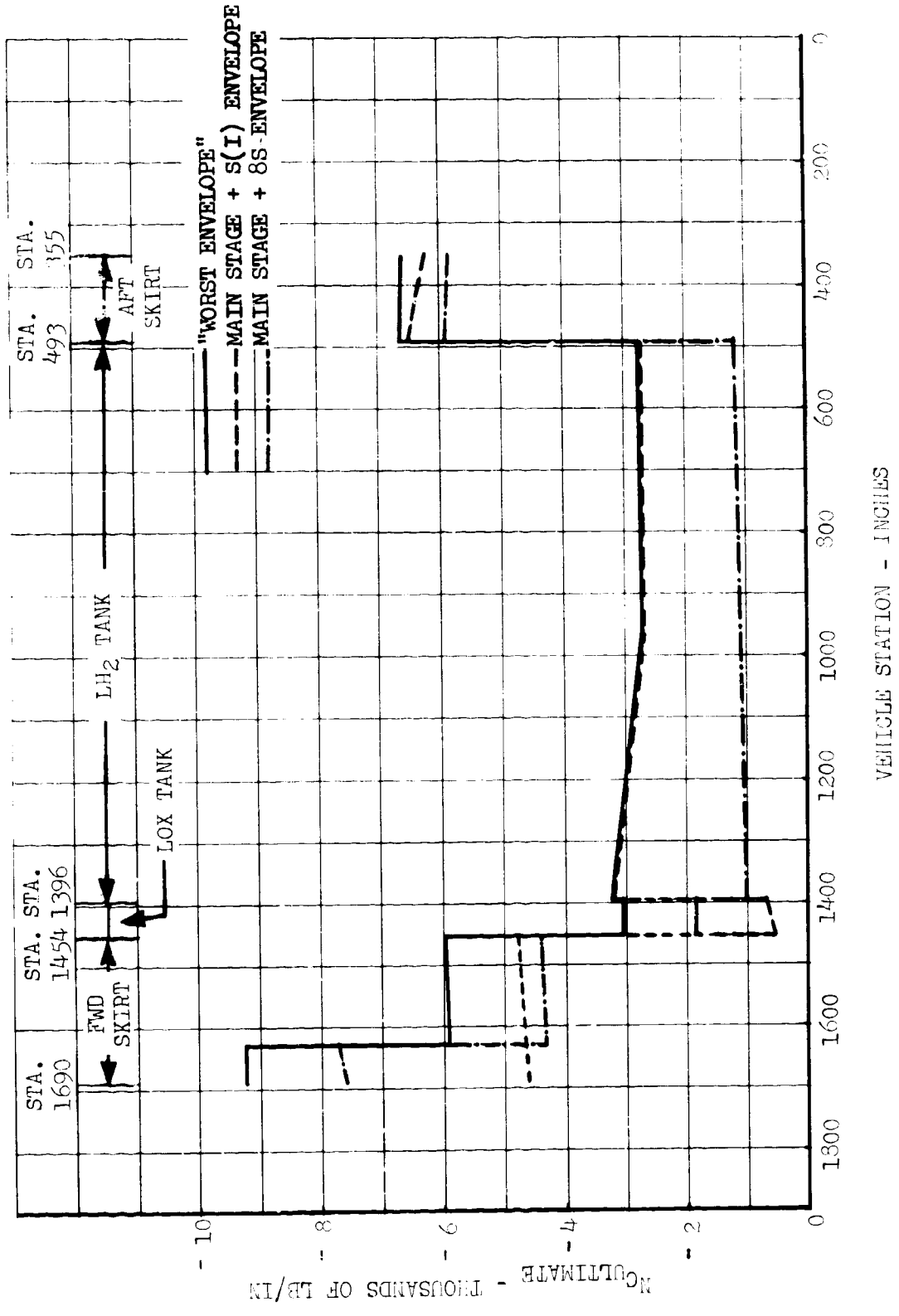
FIGURE 4.2.4.1-3   ULTIMATE COMBINED COMPRESSIVE LOAD ENVELOPES – MLLV
MAIN STAGE PLUS EIGHT STRAP-ON STAGES PLUS A SINGLE MODULE
INJECTION STAGE

143
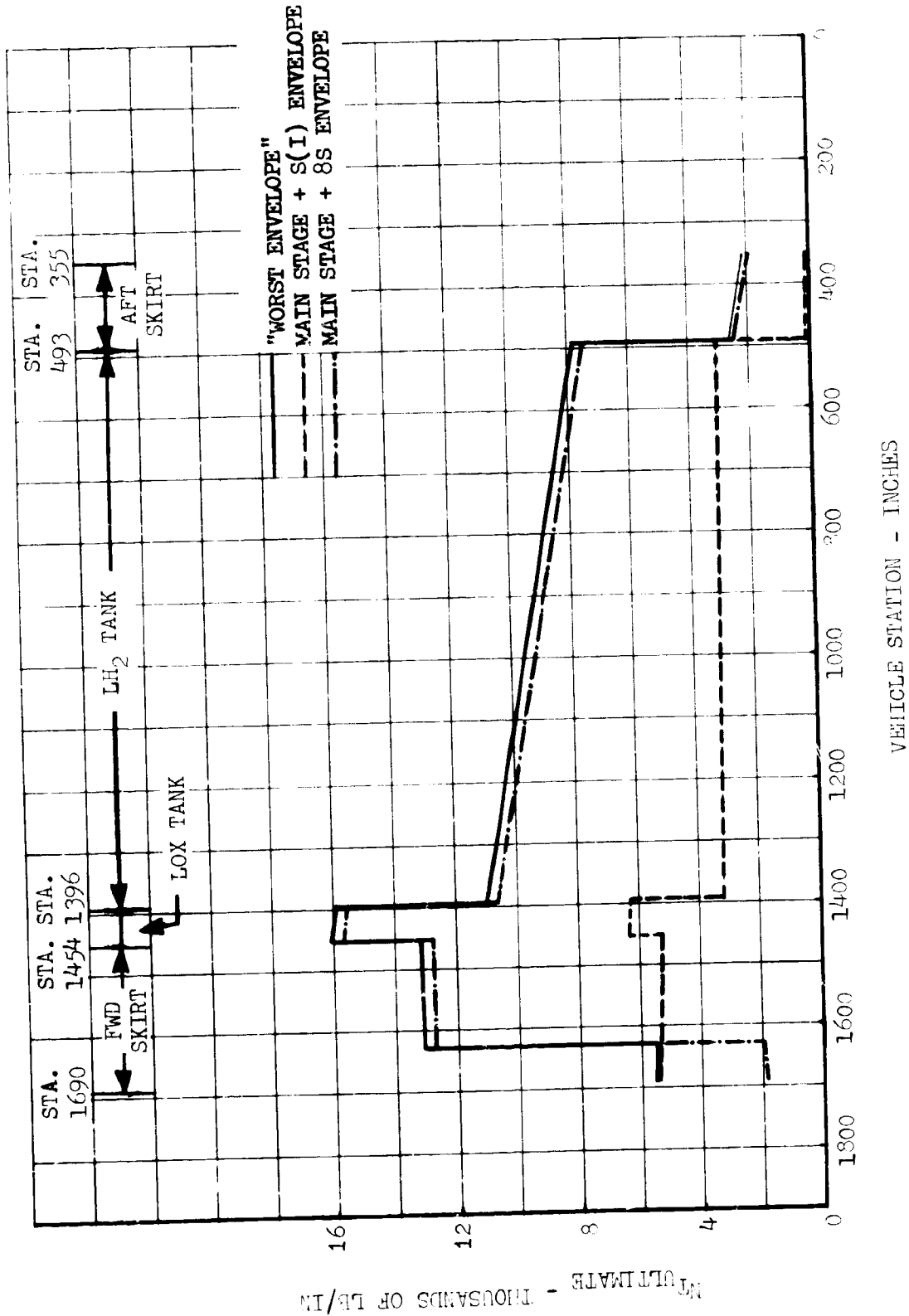
FIGURE 4.2.4.1-4 ULTIMATE COMBINED TENSILE LOAD ENVELOPES - MLLV MAIN STAGE PLUS EIGHT STRAP-ON STAGES PLUS A SINGLE MODULE INJECTION STAGE

144

4.2.4.1   (Continued)

the design values due to the similarity of the two vehicle configurations. The main stage + S(I) vehicle has lower tension loads due to a lower longitudinal tension load factor. The max ($q\alpha$) condition provides the maximum tension loads for the main stage + 8 SRM vehicle and these are lower than the design loads at every location. For that portion of the main stage designed by max ($q\alpha$) for the main stage + 8 SRM + 3S(I) vehicle, corresponding loads for the main stage + 8 SRM vehicle are lower due to lower bending moments. Although the longitudinal tensile loading is greater overall for the main stage + 8 SRM vehicle (due to higher longitudinal acceleration), the higher bending moments on the main stage + 8 SRM + 3S(I) vehicle more than compensate to give higher combined tension loads for this vehicle.

Table 4.2.4.1-I lists the holddown loads in the forward skirt for four of the MLLV configurations. Table 4.2.4.1-II lists the solid motor forward and aft attachment loads for the main stage plus three module injection stage plus eight strap-ons vehicle.

The "worst envelope" design loads for the injection stages were also calculated. The analyses showed that the worst load conditions for the injection stage would occur with the configuration which employs the main stage plus eight strap-on solid motors plus the three module injection stage at the time of max $q\alpha$.

Figure 4.2.4.1-5 shows the N_c ultimate loads versus vehicle stations for the three module injection stage for its worst load condition. As this figure indicates the net compressive load per inch of perimeter will vary from a minimum, at the forward end of the injection stage, of approximately 7300 pounds per inch to a maximum, at the aft end of the injection stage, of 9200 pounds per inch. These injection stage loads were used to size the injection stage structure as discussed in subsequent Section 4.3.4.

4.2.4.2   Loads for Single-Stage-To-Orbit Vehicle and Main Stage Plus A
           Single Module Injection Stage Vehicle

The ground wind shear distributions for a 99.9 percent prelaunch wind and a 99 percent launch wind for the single-stage-to-orbit vehicle are shown in Figure 4.2.4.2-1. The criteria used to develop the shear force assumed a free standing vehicle with a forward holddown concept. Holddown at the forward skirt will result in the maximum shear forces occurring at the forward skirt rather than at the vehicle base.

Figure 4.2.4.2-2 shows the ground wind bending moment distribution for the same wind conditions (for the single-stage-to-orbit vehicle). The low L/D (2.1) ratio will result in a low bending moment compared to the Saturn V which has an L/D ratio of over eight.

TABLE 4.2.4.1-I HOLDDOWN LOADS IN FORWARD SKIRT FOR ALL CONFIGURATIONS

VEHICLE CONFIG. \ LOAD CONDITION	LIGHT WEIGHT FORWARD SKIRT		FORWARD SKIRT FOR STRAP-ON STAGE ATTACHMENT	
	MLLV CORE	MLLV MAIN STAGE + INJECTION STAGE	MAIN STAGE + 8-260" SRM + 3-INJ. STAGES	MAIN STAGE + 3-260" SRM
	F_A – HOLDDOWN LOAD – POUNDS			
ON-PAD, FUELED	1604452.*	1697500.*	1081051.**	968182.**
THRUST BUILD-UP	-39535.*	-30247.*	108105.**	968182.**
REBOUND	2206399.*	2298451.*	N/A	N/A
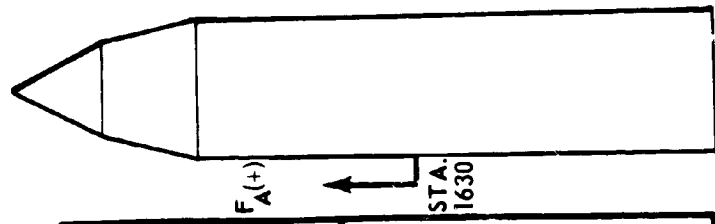
* LOAD OCCURS AT FOUR (4) PLACES
** LOAD OCCURS AT EIGHT (8) PLACES

AV. 5840-57

146

TABLE 4.2.4.1-II SOLID MOTOR ATTACHMENT LOADS

UPPER ATTACHMENT POINT – VEHICLE STATION 1630

LOADING CONDITION	F_A* (LBS)	NORMAL LOAD – (LBS)					TANGENTIAL LOAD – (LBS)				
		①	②	③	④	⑤	①	②	③	④	⑤
ON-PAD FUELED	1,081,051	0	0	0	0	0	0	0	0	0	0
THRUST BUILD-UP	1,081,051	0	0	0	0	0	0	0	0	0	0
LIFT-OFF	1,654,000	165,624	165,624	165,624	165,624	165,624	0	0	0	0	0
Qα MAX.	2,255,421	202,000	370,161	1,105,000	649,801	164,000	0	-421,080	323,000	-654,101	0
SRM CUT-OFF	3,198,006	324,213	324,213	324,213	324,213	324,213	0	0	0	0	0

*FOR ONE (1) SRM

LOWER ATTACHMENT POINT – VEHICLE STATION 355

LOADING CONDITION	F_B (LBS.)	NORMAL LOAD – (LBS.)					TANGENTIAL LOAD – (LBS.)				
		①	②	③	④	⑤	①	②	③	④	⑤
ON-PAD, FUELED	0	0	0	0	0	0	0	0	0	0	0
THRUST BUILD-UP	0	0	0	0	0	0	0	0	0	0	0
LIFT-OFF	0	604,376	604,376	604,376	604,376	604,376	0	0	0	0	0
Qα MAX	0	332,000	706,925	436,000	375,161	540,000	0	165,882	122,000	165,780	0
SRM CUTOFF	0	149,178	149,178	149,178	149,178	149,178	0	0	0	0	0

NOTE: 6.5 DEGREE OUTWARD CANT ON SRM NOZZLES
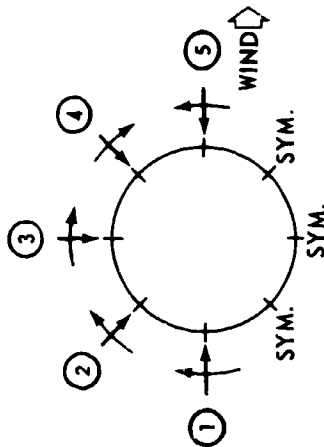
ARROW DIRECTIONS INDICATE ASSUMED POSITIVE DIRECTIONS FOR APPLIED LOADS

F_A = FORWARD AXIAL LOAD
F_B = AFT AXIAL LOAD
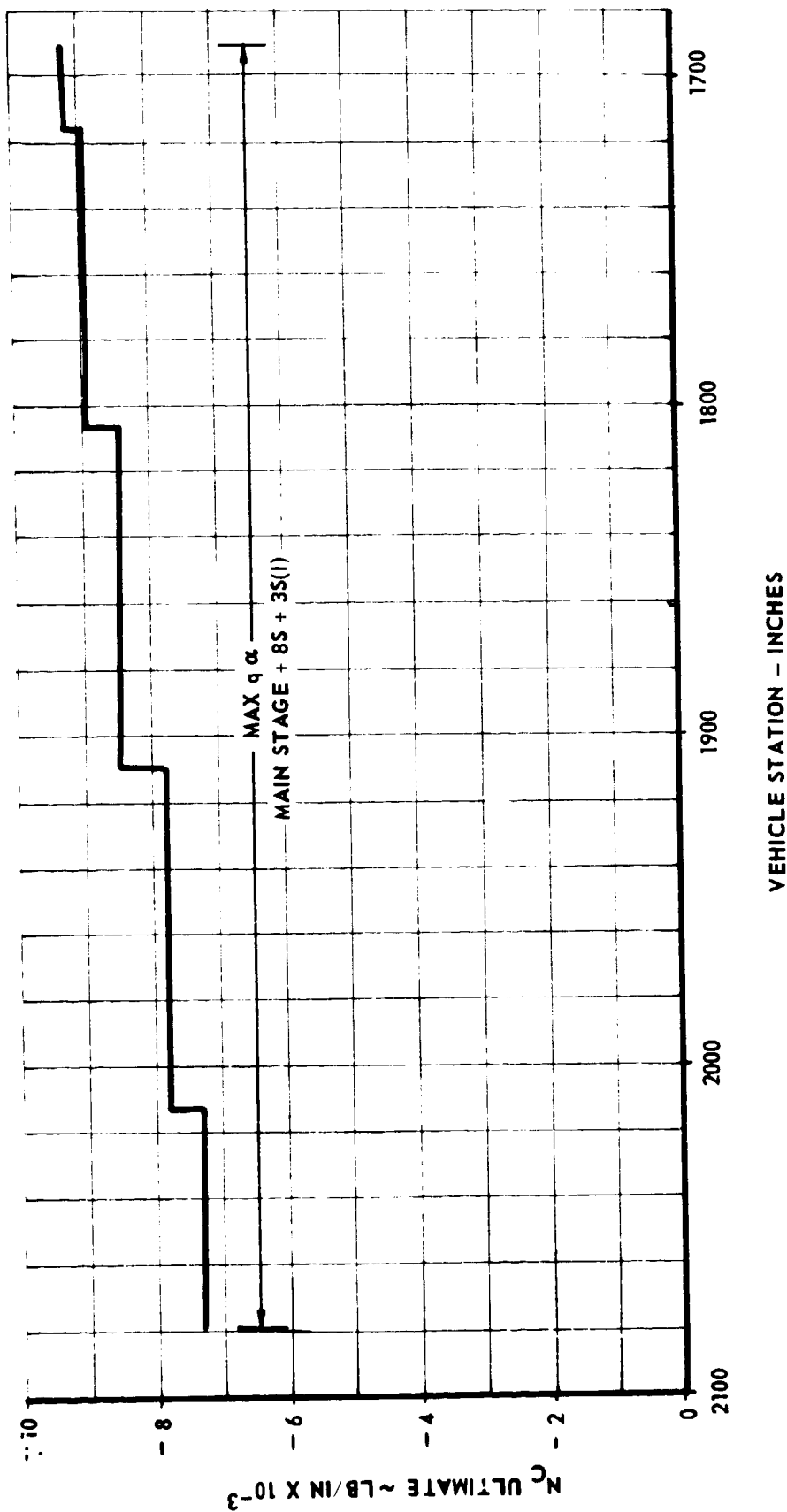
FIGURE 4.2.4.1-5   ULTIMATE COMBINED COMPRESSIVE LOAD ENVELOPE FOR
THREE MODULE INJECTION STAGE
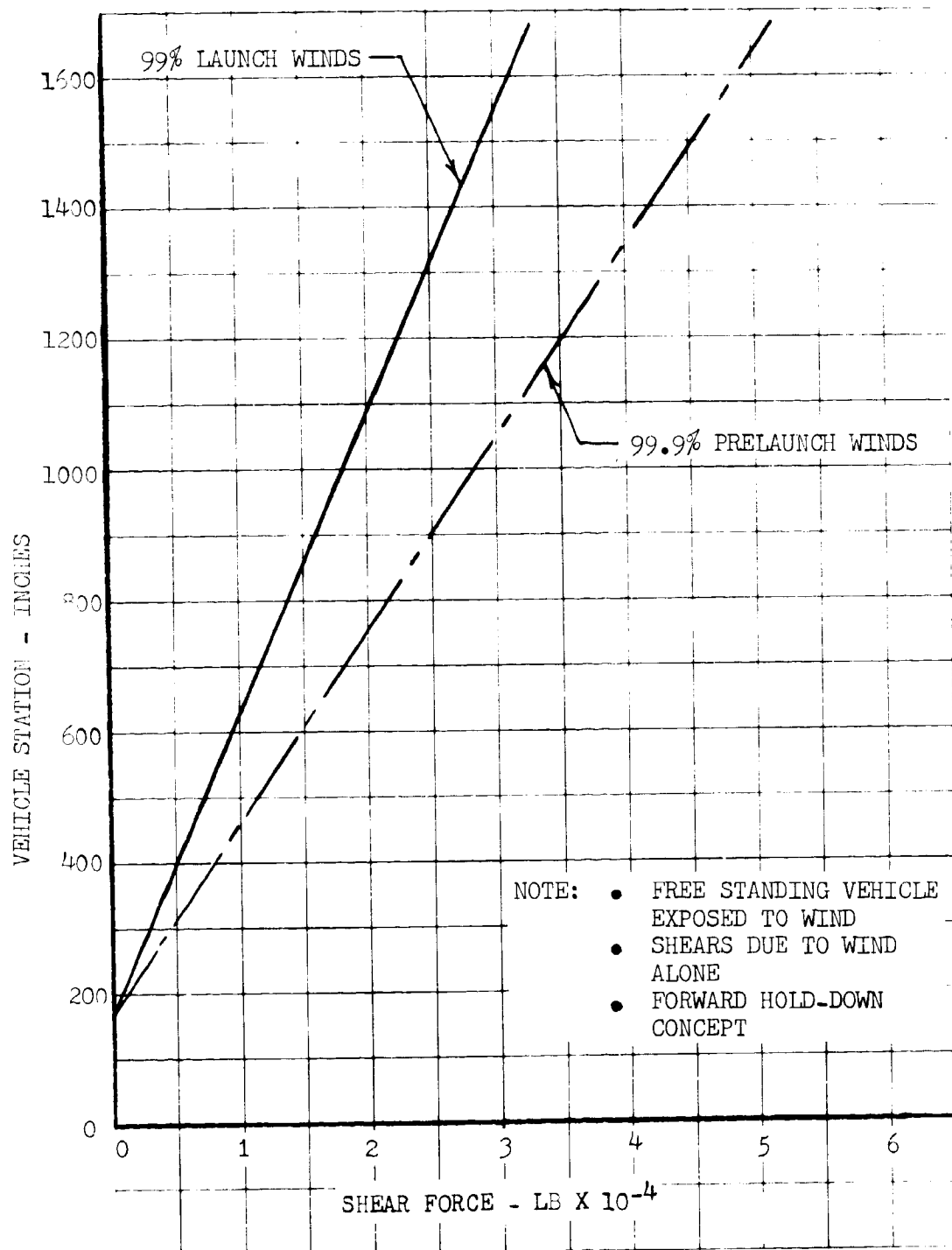
FIGURE 4.2.4.2-1   MLLV SINGLE STAGE TO ORBIT - GROUND WIND SHEAR DISTRIBUTION

149
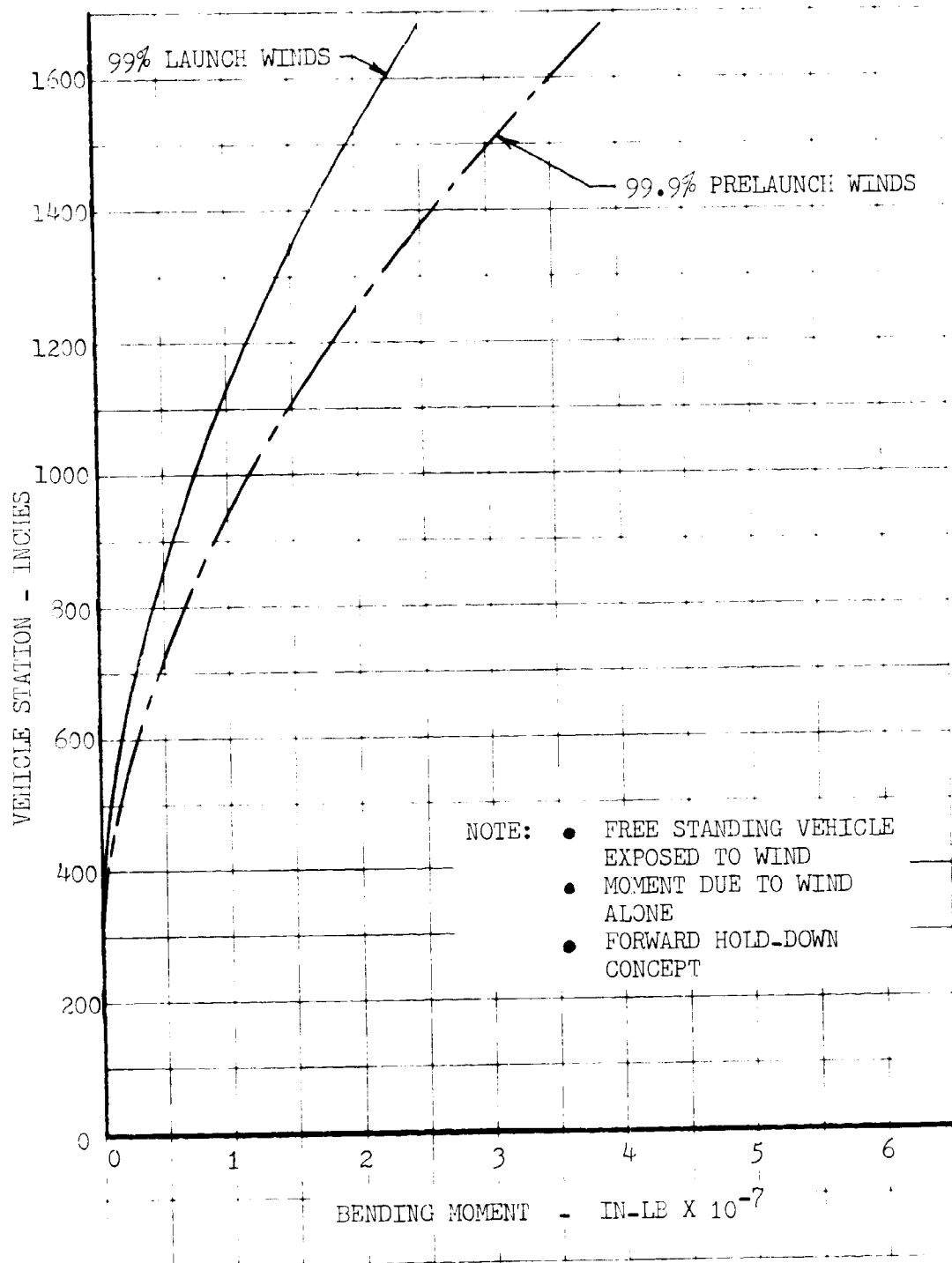
FIGURE 4.2.4.2-2 MLLV SINGLE STAGE TO ORBIT - GROUND WIND BENDING MOMENT
DISTRIBUTION

4.2.4.2 (Continued)

Figures 4.2.4.2-3 through 4.2.4.2-7 depict the longitudinal force distributions for the single-stage-to-orbit vehicle for the on-pad, fueled, unpressurized condition; emergency shutdown condition; lift-off condition; max (qα) condition and at the maximum acceleration condition, respectively. The peak forces from station 355 to 1400 occur at maximum acceleration and are compressive forces. Above station 1400 to station 1690, the peak forces occur at the emergency shutdown condition and are tensile forces. Figure 4.2.4.2-8 represents the longitudinal load factor versus time for the single-stage-to-orbit vehicle.

The inflight bending moment distribution at max qα for the single-stage-to-orbit vehicle is shown in Figure 4.2.4.2-9. The peak value of 440 million inch - pounds occurs at station 1400 (the intersection of the skin and common bulkhead).

Tables 4.2.4.2-I through IV list the detailed load tabulations for the single-stage-to-orbit vehicle at lift-off, rebound, max (qα) and maximum acceleration, respectively. (The symbols shown in these tables are defined in Section 4.2.4.9.)

4.2.4.3 Loads for Light Weight Skirt

Tables 4.2.4.3-I through IV show the light weight forward skirt design loads as defined by the main stage plus a single module injection stage vehicle. Included in the data are the accumulated weights at holddown and flight versus vehicle station, cut-off compressive loads, max (qα) compressive loads, and the rebound tension loads for the forward skirt for single-stage-to-orbit vehicle and the main stage plus a single module injection stage vehicle.

Figure 4.2.4.3-1 illustrates the (N_c) loads for the forward skirts of the single-stage-to-orbit vehicle and for the main stage plus a single module injection stage vehicle. The cut-off condition will design the forward skirt of the latter vehicle while the forward skirt of the former vehicle will be designed by the max (qα) condition at the lower part of the forward skirt and by the cut-off condition on the upper portion of the skirt.

Figure 4.2.4.3-2 illustrates the (N_t) tension loads at rebound for the forward skirt for the above two vehicles. The single-stage-to-orbit vehicle has slightly higher rebound loads due to the lighter weight of vehicle above the attachment points.

4.2.4.4 Loads for Main Stage Plus Eight Strap-On Stages Plus the Three Module Injection Stage Vehicle

The ground wind shear distributions for a 99.9 percent prelaunch wind and a 99 percent launch wind are shown in Figure 4.2.4.4-1. This data was computed assuming a free standing vehicle with the forward holddown concept. The addition of the solid motors increase the shear force over that previously shown for the
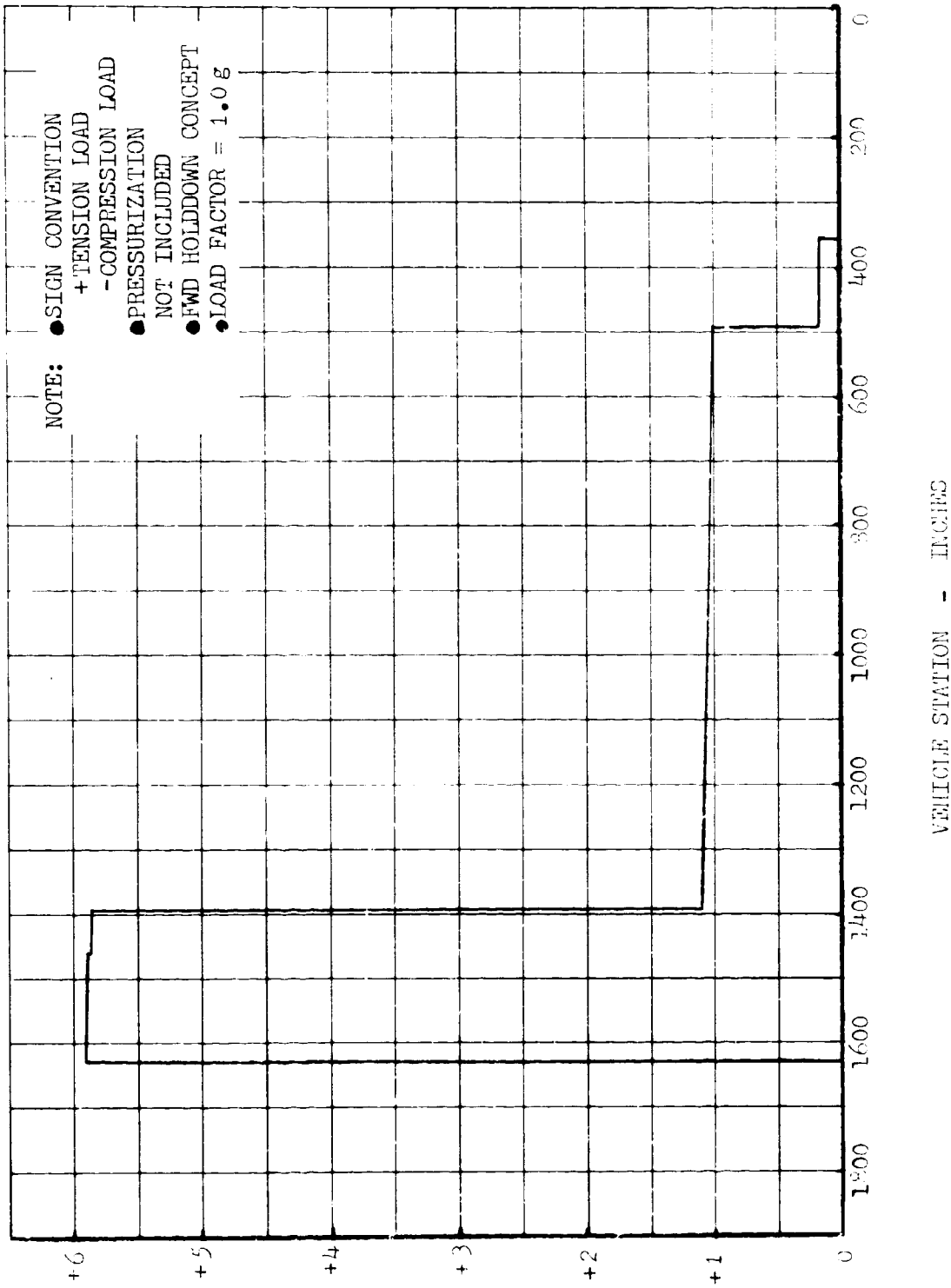
FIGURE 4.2.4.2-3 MLLV SINGLE STAGE TO ORBIT LONGITUDINAL FORCE DISTRIBUTION -
ON PAD FUELED, UNPRESSURIZED CONDITION

152
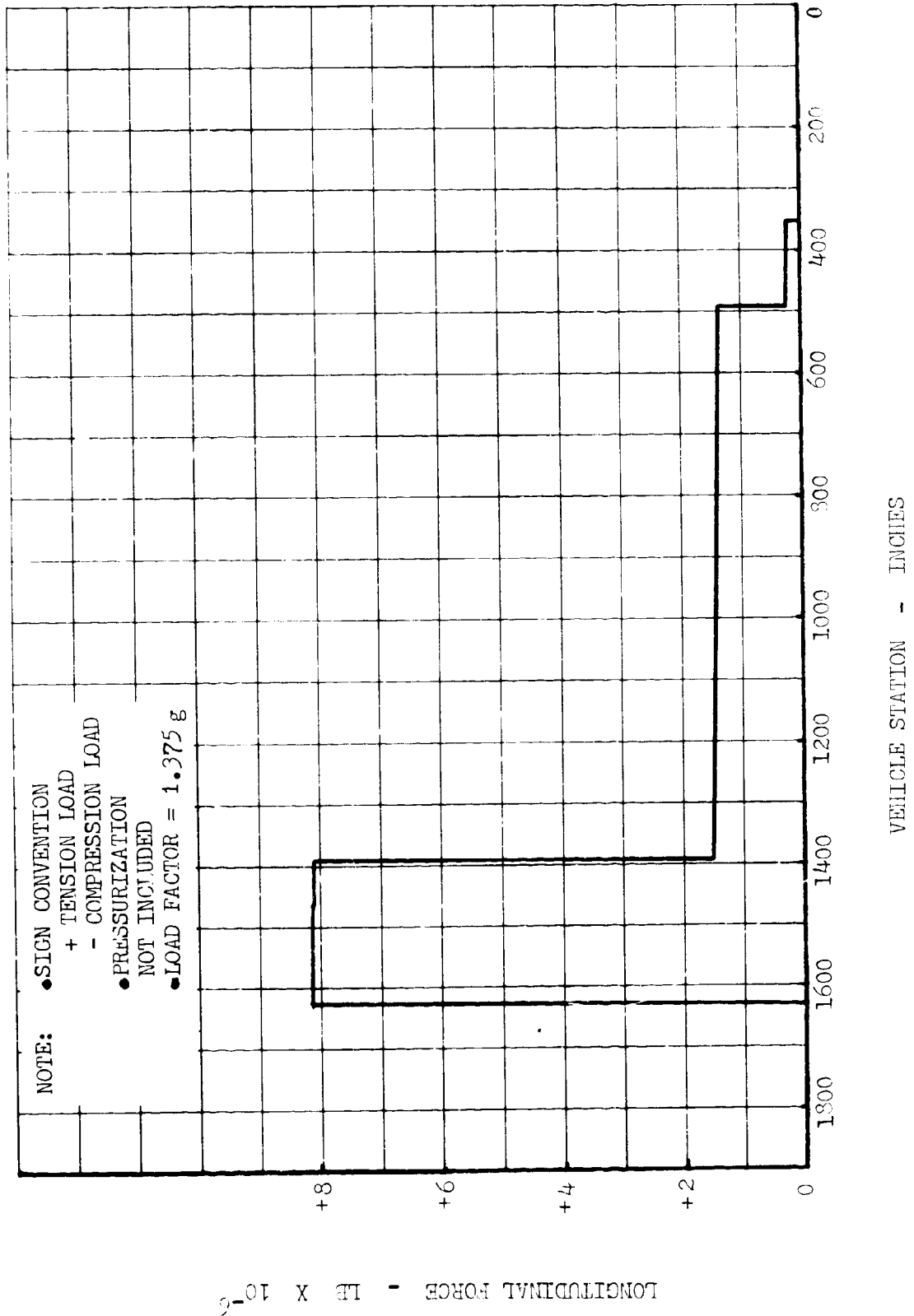
FIGURE 4.2.4.2-4   MLLV SINGLE STAGE TO ORBIT LONGITUDINAL FORCE DISTRIBUTION –
EMERGENCY SHUT-DOWN CONDITION

NOTE: ● SIGN CONVENTION
             + TENSION LOAD
             – COMPRESSION LOAD
           ● PRESSURIZATION
             NOT INCLUDED
           ● LOAD FACTOR = 1.375 g

VEHICLE STATION – INCHES

LONGITUDINAL FORCE – LF X 10⁻⁶

153
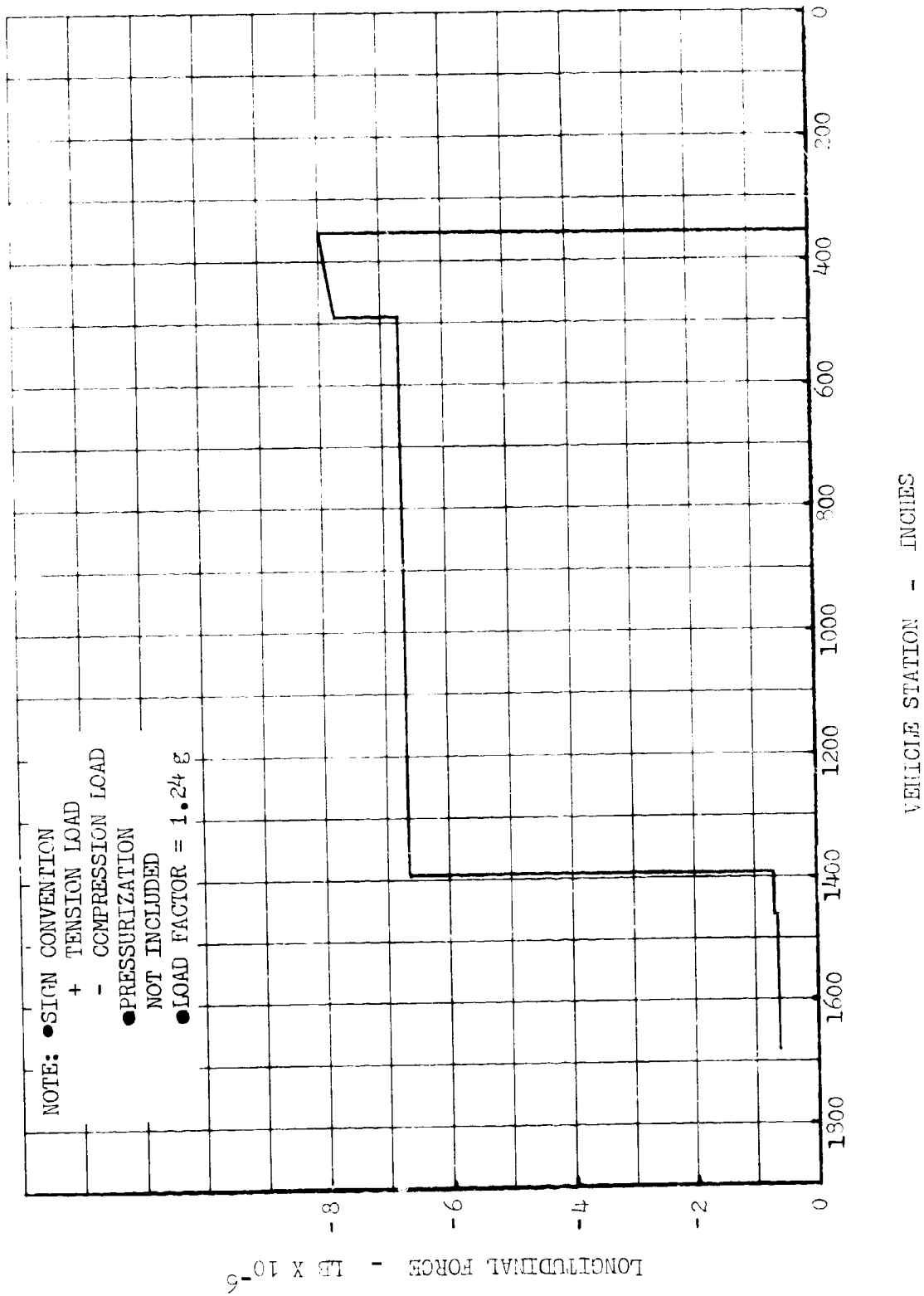
FIGURE 4.2.4.2-5 MLLV SINGLE STAGE TO ORBIT LONGITUDINAL FORCE DISTRIBUTION - LIFT-OFF

154 ·
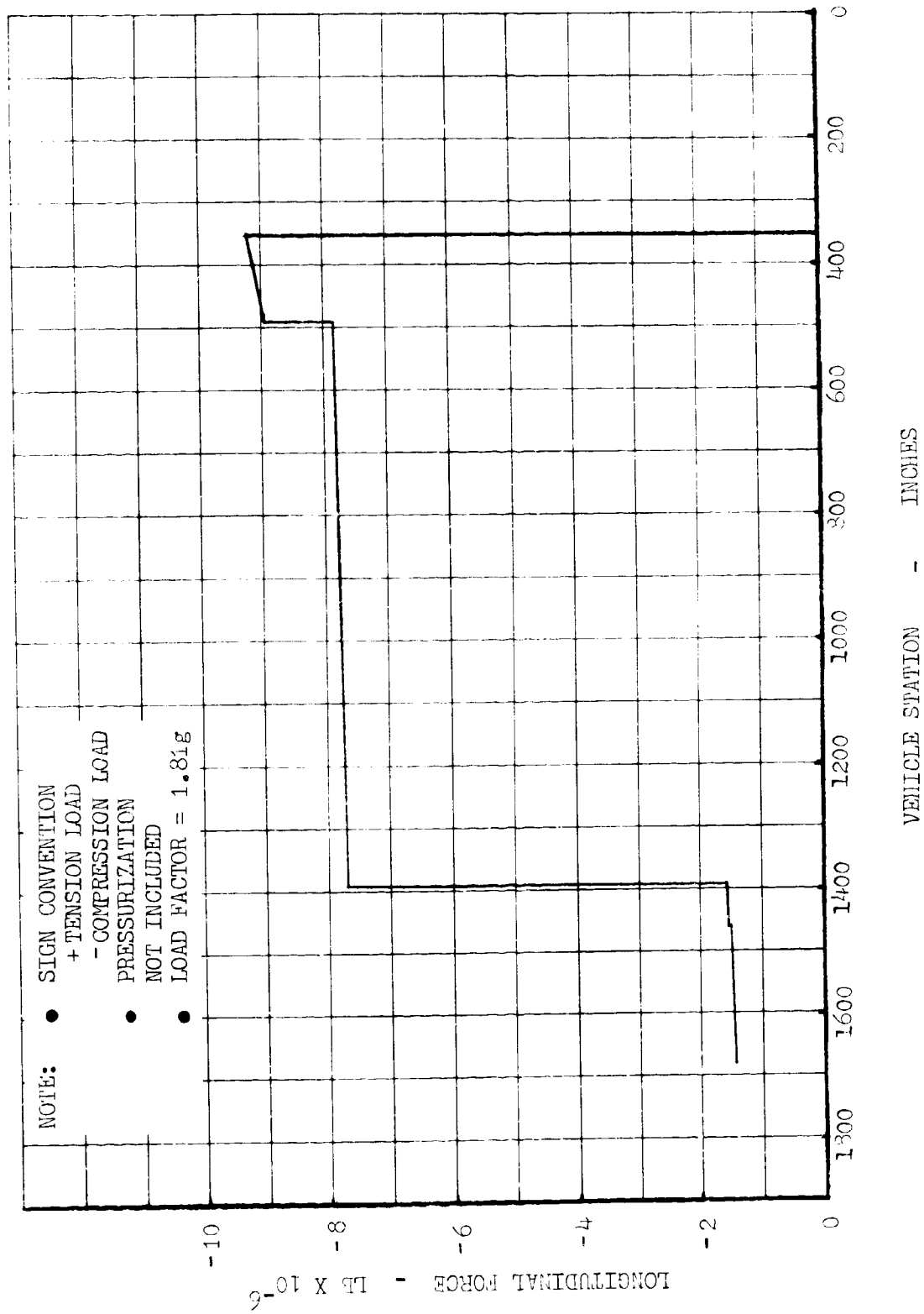
FIGURE 4.2.4.2-6   MLLV SINGLE STAGE TO ORBIT LONGITUDINAL FORCE DISTRIBUTION -
@ MAX (qα)

155
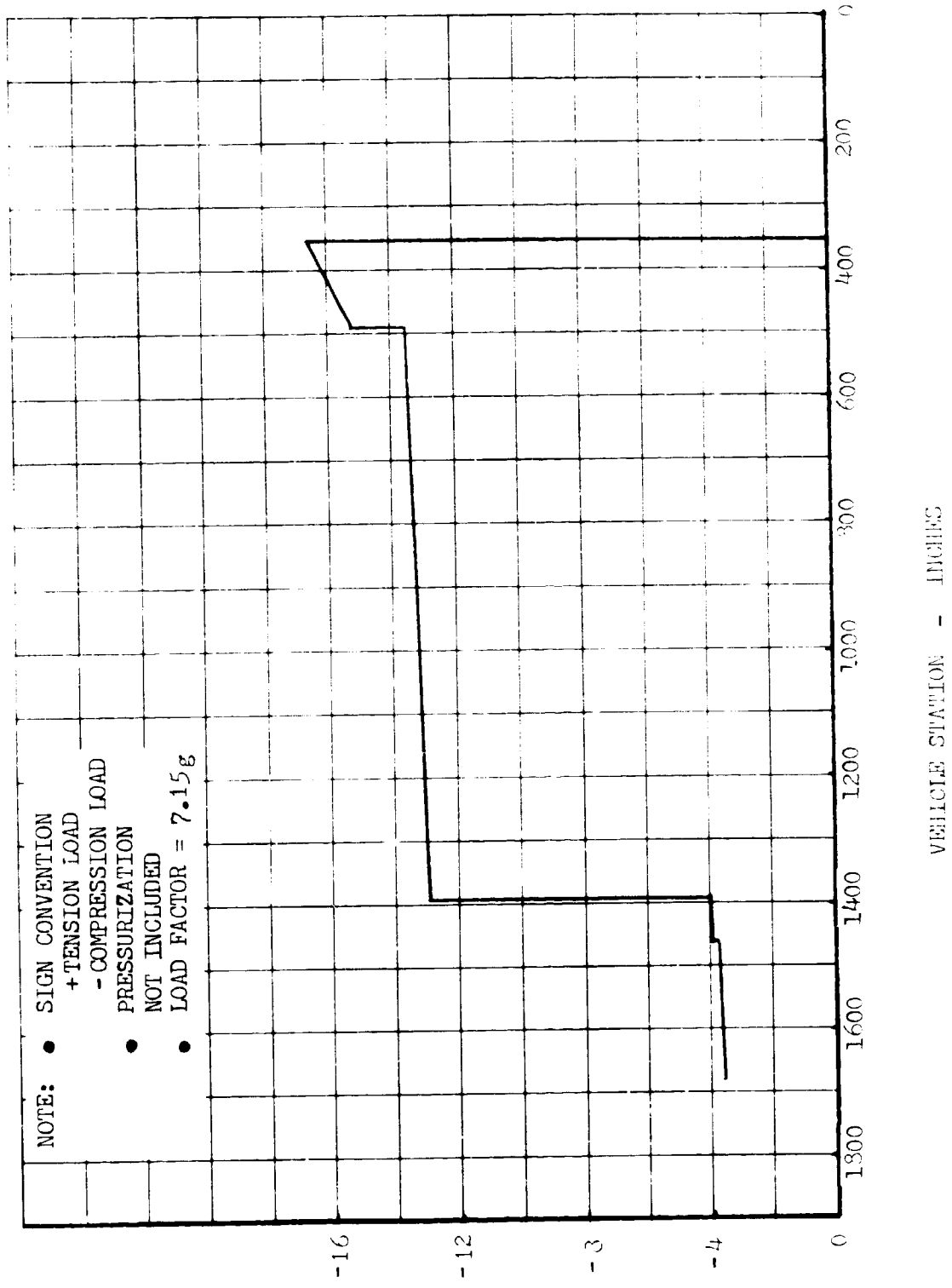
FIGURE 4.2.4.2-7   MLLV SINGLE STAGE TO ORBIT LONGITUDINAL FORCE DISTRIBUTION –
@ MAXIMUM ACCELERATION

156
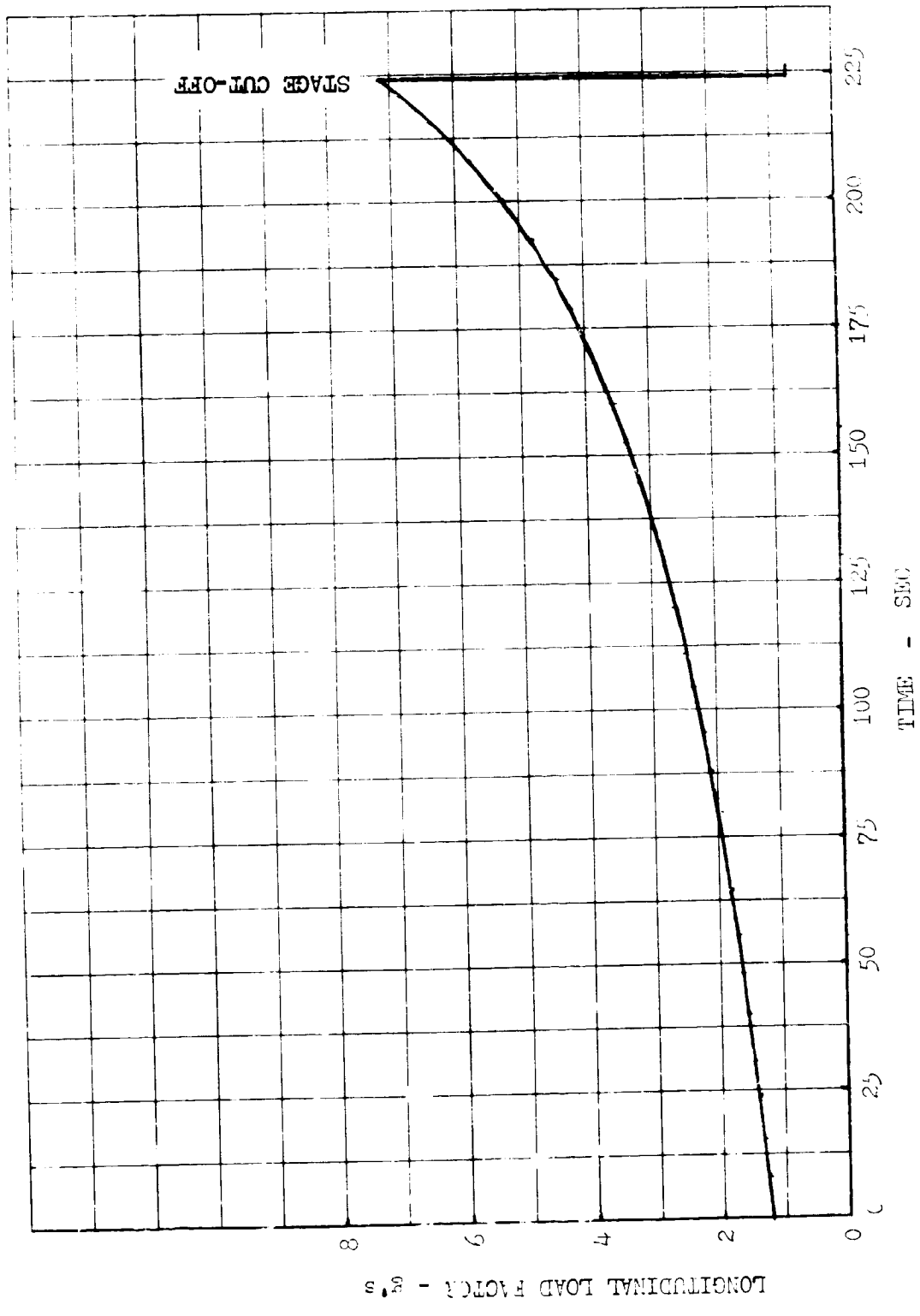
FIGURE 4.2.4.2-8   LONGITUDINAL LOAD FACTOR FOR MLLV – SINGLE STAGE TO ORBIT
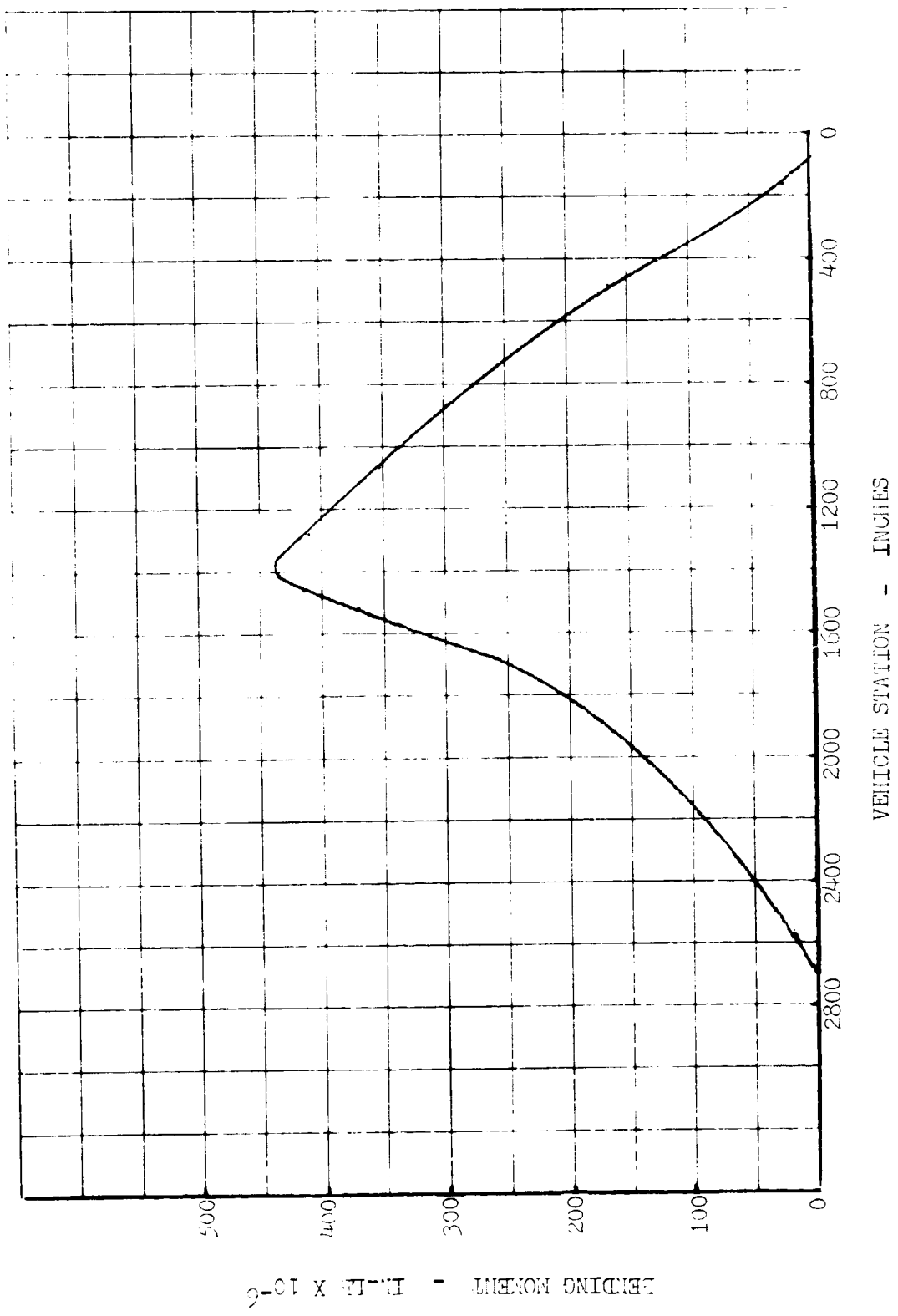
FIGURE 4.2.4.2-9 MLLV SINGLE STAGE TO ORBIT – BENDING MOMENT DISTRIBUTION
@ MAX qα

158

TABLE 4.2.4.2-I   SINGLE-STAGE-TO-ORBIT VEHICLE LIFT-OFF COMPRESSIVE LOADS

VEHICLE STATION	η	W' X 10^{-6} LB	ηW' X 10^{-6} LB	P X 10^{-6} LB	$\dfrac{P}{2\pi R}$ LB/IN	BM X 10^{-6} IN/LB	$\dfrac{BM}{\pi R^2}$ IN/LB	$\dfrac{P_u R\ min}{2}$ LB/IN	$\dfrac{P_u R\ max}{2}$ LB/IN	Nc limit LB/IN	N ultimate LB/IN
355	1.246	6.428	8.009	8.009	3751	0	0			3751	5251
493A		6.421	8.001	8.001	3748	0.8	2			3750	5251
493F		5.415	6.747	6.747	3160	0.8	2	1666	2261	1496	2761
1396A		5.322	6.631	6.631	3160	16.5	45	1666	2261	1485	2745
1396F		.564	.703	.703	329	16.5	45	476	1071		48
1454A		.552	.688	.688	322	18.5	51	476	1071		46
1454F		.526	.655	.655	307	18.5	51			358	501
1690		.500	.623	.623	292	25.0	69			361	505

159

TABLE 4.2.4.2-II SINGLE-STAGE-TO-ORBIT VEHICLE REBOUND LOADS

VEHICLE STATION IN	η	W' x 10^{-6} lb	ηW' x 10^{-6} lb	P x 10^{-6} lb	$\dfrac{P}{2\pi R}$ lb/in	BM x 10^{-6} in-lb	$\dfrac{BM}{\pi R^2}$ lb/in	$\dfrac{P_{umax}R}{2}$ lb/in	N_t limit lb/in	N_t ultimate lb/in
355	1.375	0.171	0.234	0.234	110	0	0		110	154
493A		0.187	0.256	0.256	120	0.8	2		122	171
493F		1.013	1.393	1.393	652	0.8	2	2261	2915	3177
1396A		1.106	1.520	1.520	712	16.5	45	2261	3018	3321
1396F		5.865	8.064	8.064	3775	16.5	45	1071	4891	6419
1454A		5.876	8.079	8.079	3782	18.5	51	1071	4904	6137
1454F		5.902	8.115	8.115	3798	18.5	51		3849	5389
1630A		5.925	8.147	8.147	3816	23.2	64		3850	5432
1630F		(-.503)	(-.692)	(-.692)	(-324)	23.2	64		-	-
1690		(-.500)	(-.688)	(-.688)	(-322)	25	69		-	-

NOTE: COMPRESSIVE LOADS ARE SHOWN AS (-) VALUES

160

TABLE 4.2.4.2-III   SINGLE-STAGE-TO-ORBIT VEHICLE COMBINED LOADS (MAX qα)

STATION IN	η	W' x10⁻⁶ LB	ηW' x10⁻⁶ LB	D x10⁻⁶ LB	P x10⁻⁶ LB	P/2πR LB/IN	BM x10⁻⁶ IN-LB	BM/πR² LB/IN	$\frac{P_{u_{min}}}{2}$ LB/IN	$\frac{P_{u_{max}}}{2}$ LB/IN	N_c limit LB/IN	N_t limit LB/IN	N_c ultimate LB/IN	N_t ultimate LB/IN
355	1.809	-4.660	-8.431	-.548	-8.980	-4,204	100	275	-	-	4,479	-	6,271	-
493A		-4.644	-8.402		-8.951	-4,191	165	455	-	-	4,646	-	6,504	-
493F		-4.046	-7.319		-7.868	-3,684	165	455	3,536	4,131	603	902	2,259	-390
1396A		-3.954	-7.152		-7.701	-3,605	440	1,212	3,536	4,131	1281	1,738	3,208	781
1396F		-.564	-1.019		-1.568	-734	440	1,212	2,346	2,941		3,419	378	3,612
1454A		-.552	-.999		-1.548	-725	415	1,143	2,346	2,941		3,359	769	3,326
1454F		-.526	-.952		-1.501	-703	415	1,143	-	-	1,846	440	2,584	616
1690	1.809	-.500	-.905	-.549	-1.454	-681	255	702	-	-	1,383	21	1,936	29

TABLE 4.2.4.2-IV   SINGLE-STAGE-TO-ORBIT VEHICLE COMBINED LOADS (MAX ACCEL.)

STATION IN	η	W' x10⁻⁶ LB	ηW' x10⁻⁶ LB	D x10⁻⁶ LB	P x10⁻⁶ LB	$\frac{P}{2\pi R}$ LB/IN	BM IN-LB	$\frac{BM}{\pi R^2}$ LB/IN	$\frac{P_{u_{min}}R}{2}$ LB/IN	$\frac{P_{u_{max}}R}{2}$ LB/IN	N_c limit LB/IN	N_t limit LB/IN	N_c ultimate LB/IN	N_t ultimate LB/IN
355	7.151	-1.285	-9.189	0	-9.189	-4304	0	0			4304		6025	
493A		-1.269	-9.075		-9.075	-4250					4250		5950	
493F		-1.153	-8.245		-8.245	-3861			4,165	4,760		899	1240	
1396A		-1.061	-7.587		-7.587	-3553			4,165	4,760		1297	809	
1396F		-.564	-4.030		-4.030	-1,886			2,975	3,570		1684		
1454A		-.552	-3.949		-3.949	-1,849			2,975	3,570		1721		
1454F		-.526	-3.764		-3.764	-1,762					1762		2467	335
1690	7.151	-.500	-3.576	0	-3.576	-1,674	0	0			1674		2344	386

SIGN CONVENTION - COMPRESSIVE LOAD: (-)

161

TABLE 4.2.4.3-I FORWARD SKIRT LONGITUDINAL ACCUMULATIVE WEIGHTS
SINGLE-STAGE-TO-ORBIT VEHICLE AND MAIN STAGE PLUS INJECTION
STAGE VEHICLE

VEHICLE STATION (IN)	ACCUMULATIVE WEIGHT – LBS.			
	ON-PAD (HOLDDOWN) CONDITION*		FLIGHT CONDITION	
	MLLV CORE	MLLV CORE + S(I)	MLLV CORE	MLLV CORE + S(I)
1690	500000 (c)**	841542 (c)	500000 (c)**	841542 (c)
1630 Forward	503300 (c)	844842 (c)	503300 (c)	844842 (c)
1630 Aft	5924833 (t)	5945264 (t)	503300 (c)	844842 (c)
1454 Forward	5901710 (t)	5922141 (t)	526423 (c)	867965 (c)
1454 Aft	5875869 (t)	5896300 (t)	552264 (c)	893806 (c)

* VEHICLE BEING HELD BY FORWARD HOLDDOWN SUPPORTS
** PAYLOAD ASSUMED TO BE 500,000 POUNDS FOR THIS ANALYSIS
NOTE: (c) – COMPRESSIVE LOADING
(t) – TENSILE LOADING

162

TABLE 4.2.4.3–II CUT–OFF COMPRESSION LOADS FOR LIGHT WEIGHT FORWARD SKIRT LOADS

MLLV CONFIG.	VEHICLE STATION (IN)	W' 10^{-6} (LB)	η	$\eta W'$ 10^{-6} (LB)	P 10^{-6} (LB)	$\dfrac{P}{2\pi R}$ (LB/IN)	BM 10^{-6} (IN–LB)	$\dfrac{BM}{\pi R^2}$ (LB/IN)	$P_{u_{min}}$ (PSIG)	$\dfrac{P_{u_{min}} R}{2}$ (LB/IN)	N_c limit (LB/IN)	N_c ultimate (LB/IN)
Core	1690	.500	7.151	3.576	3.576	1675	0 →	0 →	0 →	0 →	1675	2345
	1630	.503300		3.599	3.599	1686					1686	2360
	1454F	.526423		3.764	3.764	1763					1763	2468
	1454A	.552264	→	3.949	3.949	1850			17.5	2975	–	–
Core Plus Injection Stage	1690	.841542	8.339	7.015	7.018	3287	0 →	0 →	0 →	0 →	3287	4602
	1630	.844842		7.045	7.045	3300					3300	4620
	1454F	.867965		7.238	7.238	3390					3390	4746
	1454A	.893806	→	7.453	7.453	3491			17.5	2975	516	1912

163

TABLE 4.2.4.3-III   COMPRESSION LOADS FOR LIGHTWEIGHT FORWARD SKIRT (AT MAX qα)

MLLV CONFIG.	VEHICLE STATION (IN)	W' 10^{-6} (LB)	η	W' 10^{-6} (LB)	D 10^{-6} (LB)	P 10^{-6} (LL)	$\dfrac{P}{2\pi R}$	BM 10^{-6} (LB)	$\dfrac{BM}{\pi R^2}$ (LB/IN)	$\dfrac{P_{u_{min}} R}{2}$ (LB/IN)	N_c limit (LB/IN)	N_c ultimate (LB/IN)
Core	1690	.500	1.81	.905	.549	1.454	681	255	702	0	1383	1936
	1630	.5033	→	.911	→	1.460	684	297	818	→	1502	2103
	1454F	.5264		.953		1.502	703	415	1143		1846	2584
	1454A	.5523		1.000		1.549	725	415	1143	2346	–	269
Core Plus Injection Stage	1690	.8415	1.747	1.470	.487	1.957	-916	245	674	0	1590	2226
	1630	.8448	→	1.476	→	1.963	-919	285	785	→	1704	2386
	1454F	.8680		1.516		2.003	-938	398	1096		2034	2848
	1454A	.8938		1.561		2.048	-959	398	1096	2346	–	531

TABLE 4.2.4.3-IV   REBOUND TENSION LOADS ON LIGHTWEIGHT FORWARD SKIRT

MLLV CONFIG.	VEHICLE STATION (IN)	W' 10^{-6} (LB)	η	$\eta W'$ 10^{-6} (LB)	F 10^{-6} (LB)	$\dfrac{P}{2R}$ (LB/IN)	BM 10^{-6} (IN/LB)	$\dfrac{BM}{\pi R^2}$ (LB/IN)	$P_{u}\ R$ max (PSIG)	$\dfrac{P_{u_{max}}\ R}{2}$ (LB/IN)	N_t limit (LB/IN)	N_t ultimate (LB/IN)
Core	1690	-.500	1.375	-.688	-.688	-322	25.	69	0	0	-	-
	1630F	-.503300		-.692	-.692	-324	23.2	64			-	-
	1630A	5.924833		8.147	8.147	3816	23.2	64			3880	5432
	1454F	5.901710		8.115	8.115	3801	18.5	51			3852	5393
	1454A	5.875869		8.079	8.079	3784	18.5	51	6.3	1071	4906	6440
Core Plus Injection Stage	1690	-.841542	1.353	-1.139	-1.139	-533	25	69	0	0	-	-
	1630F	-.844842		-1.143	-1.143	-535	23.2	64			-	-
	1630A	5.945264		8.043	8.043	3767	23.2	64			3831	5363
	1454F	5.922141		8.013	8.013	3753	18.5	51			3804	5326
	1454A	5.896300		7.978	7.978	3736	18.5	51	6.3	1071	4858	6373

SIGN CONVENTION – COMPRESSIVE LOAD : (–)

165
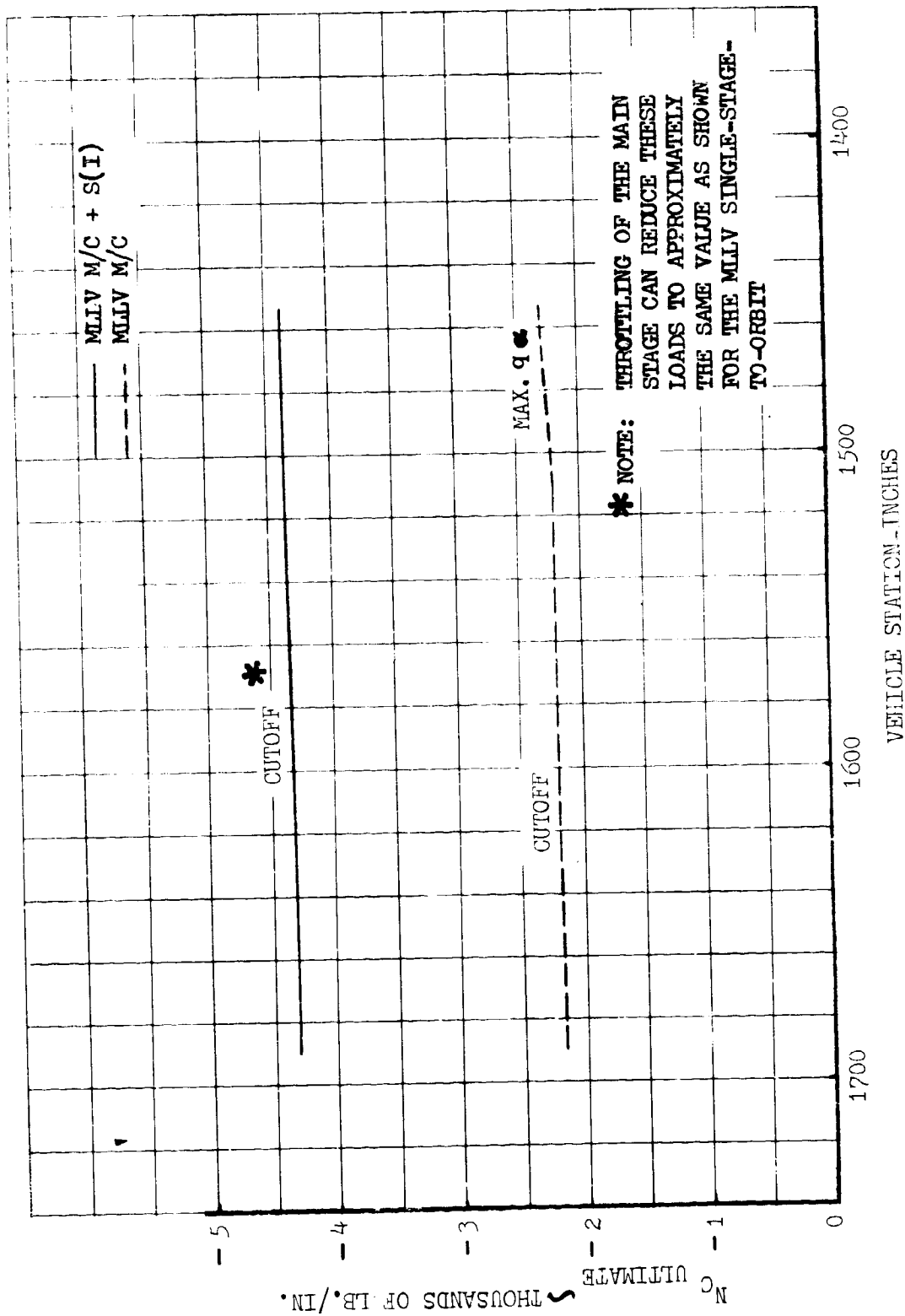
FIGURE 4.2.4.3-1   ULTIMATE COMPRESSIVE LOAD ENVELOPES FOR THE FORWARD SKIRT
FOR THE SINGLE-STAGE-TO-ORBIT VEHICLE AND THE MAIN STAGE
PLUS A SINGLE MODULE INJECTION STAGE VEHICLE

166
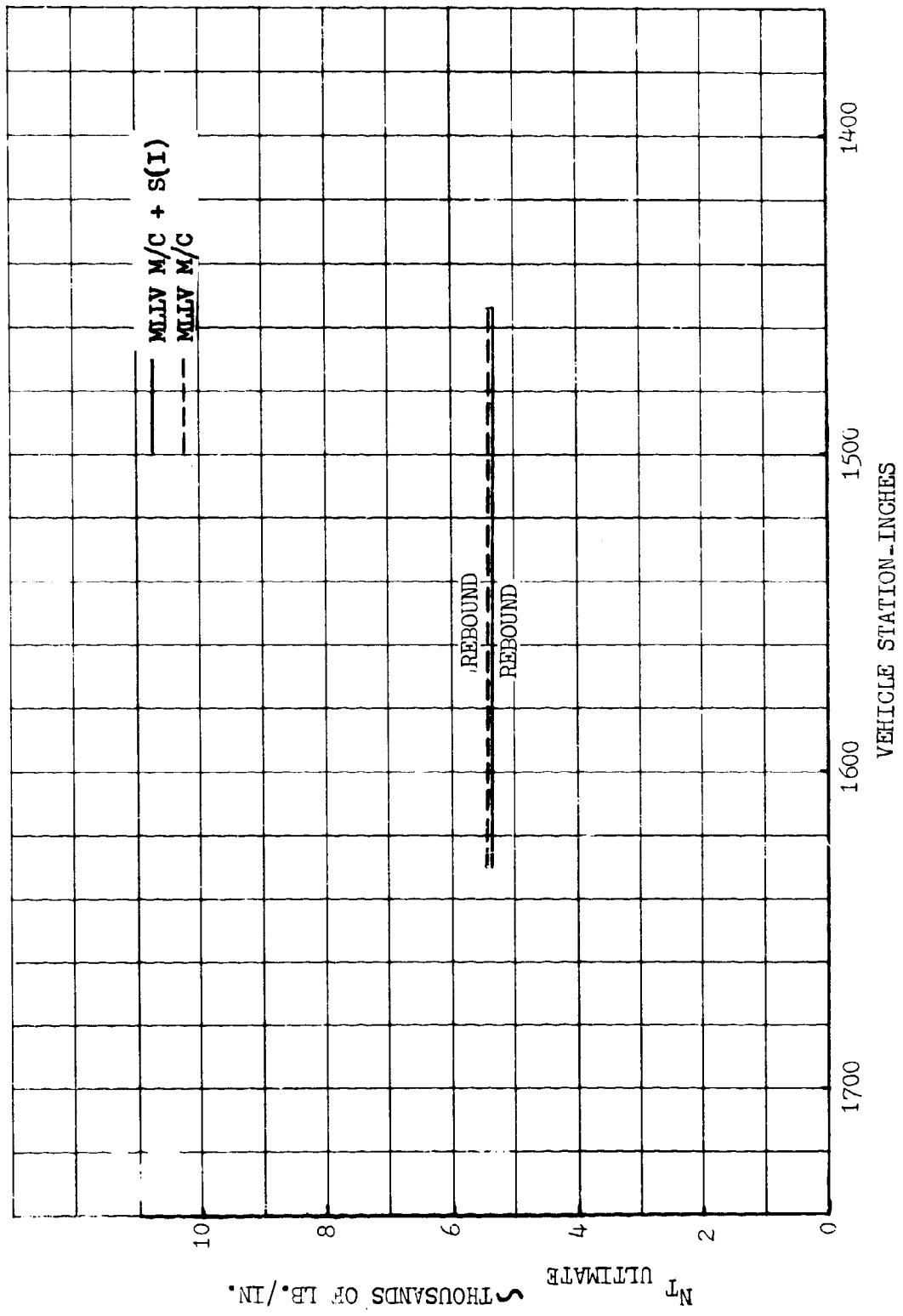
FIGURE 4.2.4.3-2   ULTIMATE TENSION LOAD ENVELOPES FOR THE FORWARD SKIRT FOR
THE SINGLE-STAGE-TO-ORBIT VEHICLE AND THE MAIN STAGE PLUS
A SINGLE MODULE INJECTION STAGE VEHICLE
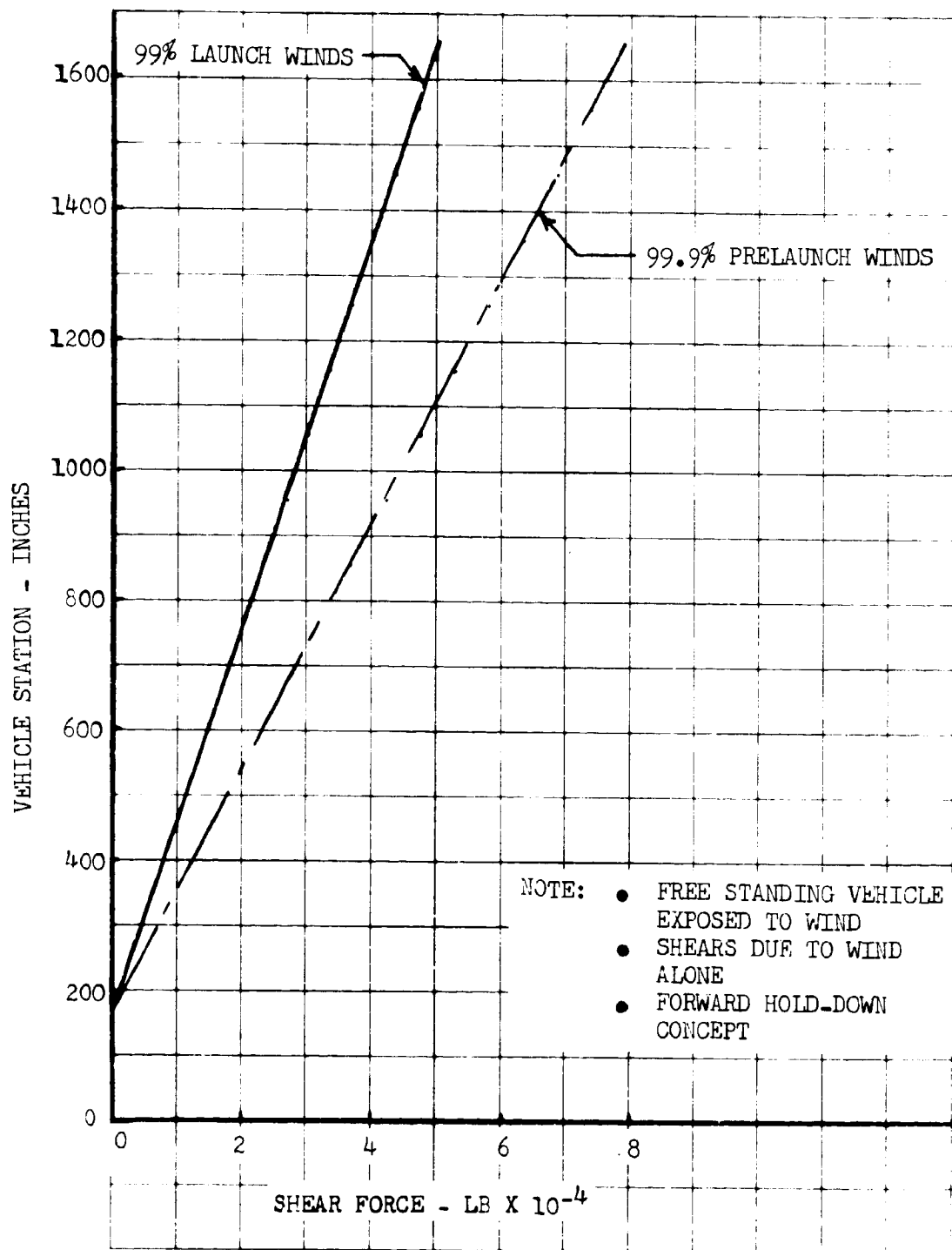
FIGURE 4.2.4.4-1   MLLV M/C + 8 SRM + 3 I(S) GROUND WIND SHEAR DISTRIBUTION

4.2.4.4   (Continued)

single-stage-to-orbit vehicle for equivalent vehicle stations.

Figure 4.2.4.4-2 illustrates the bending moment distribution for the same wind conditions. The addition of the solid motors and injection stage modules increased the bending moment over that previously shown for the single-stage-to-orbit vehicle for equivalent vehicle stations.

Figure 4.2.4.4-3 shows the bending moment for the maximum ($q\alpha$) condition. This is the peak bending moment condition. This bending moment value of 14.4×10^8 in-lb compared to 40.0×10^8 in-lbs for the full size AMLLV equivalent vehicle configuration.

Figures 4.2.4.4-4 through 4.2.4.4-9 show longitudinal force distribution versus vehicle station for the following conditions:

1. On pad fueled, unpressurized
2. Lift-off
3. Maximum $q\alpha$
4. Solid motor cut-off
5. Main stage ignition
6. Main stage maximum acceleration (stage burn out)

The peak longitudinal force (compressive) will occur at main stage ignition for the aft skirt section of the vehicle. For the LH_2 tank section, the peak force (compressive) will occur at main stage cut-off. The LOX tank and the lower portion of the forward skirt will experience maximum longitudinal forces (tension) at solid motor cut-off. The upper portion of the forward skirt will experience its peak load (compressive) at main stage cut-off.

These longitudinal forces coupled with the bending moment and tank pressure conditions will result in the combined compressive loads shown in Figure 4.2.4.4-10 and the combined tension loads shown in Figure 4.2.4.4-11.

Figure 4.2.4.4-12 shows the longitudinal load factor versus time.

The designing conditions for the tank skins due to the tank pressures will occur at the SRM cut-off condition. For the hydrogen tank, the maximum limit pressure will be 28 psig at the top of the tank and 35.3 psig at the bottom of the tank. The LOX tank limit pressure will be 21 psig at the top of the tank and 73.36 psig at the bottom of the tank. Figure 4.2.4.4-13 shows tank pressures versus vehicle station. The design ultimate values are 1.4 times the design limit values.

Tables 4.2.4.4-I through 4.2.4.4-IV list the values used to compute the combined compressive loads and combined tension loads. These are shown for the maximum

169
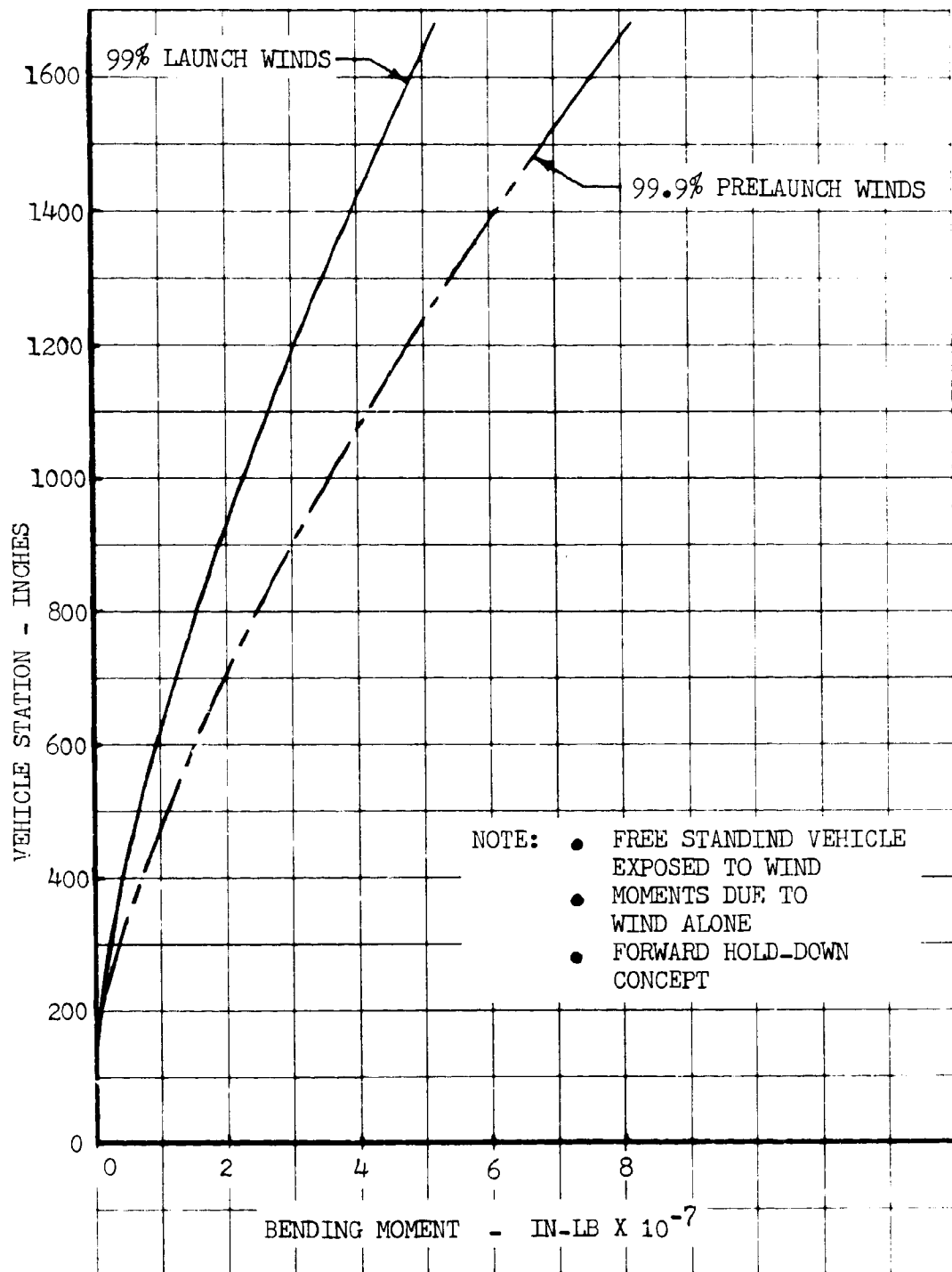
FIGURE 4.2.4.4-2   MLLV M/C + 8 SRM + 3 I(S) GROUND WIND BENDING MOMENT
                    DISTRIBUTION
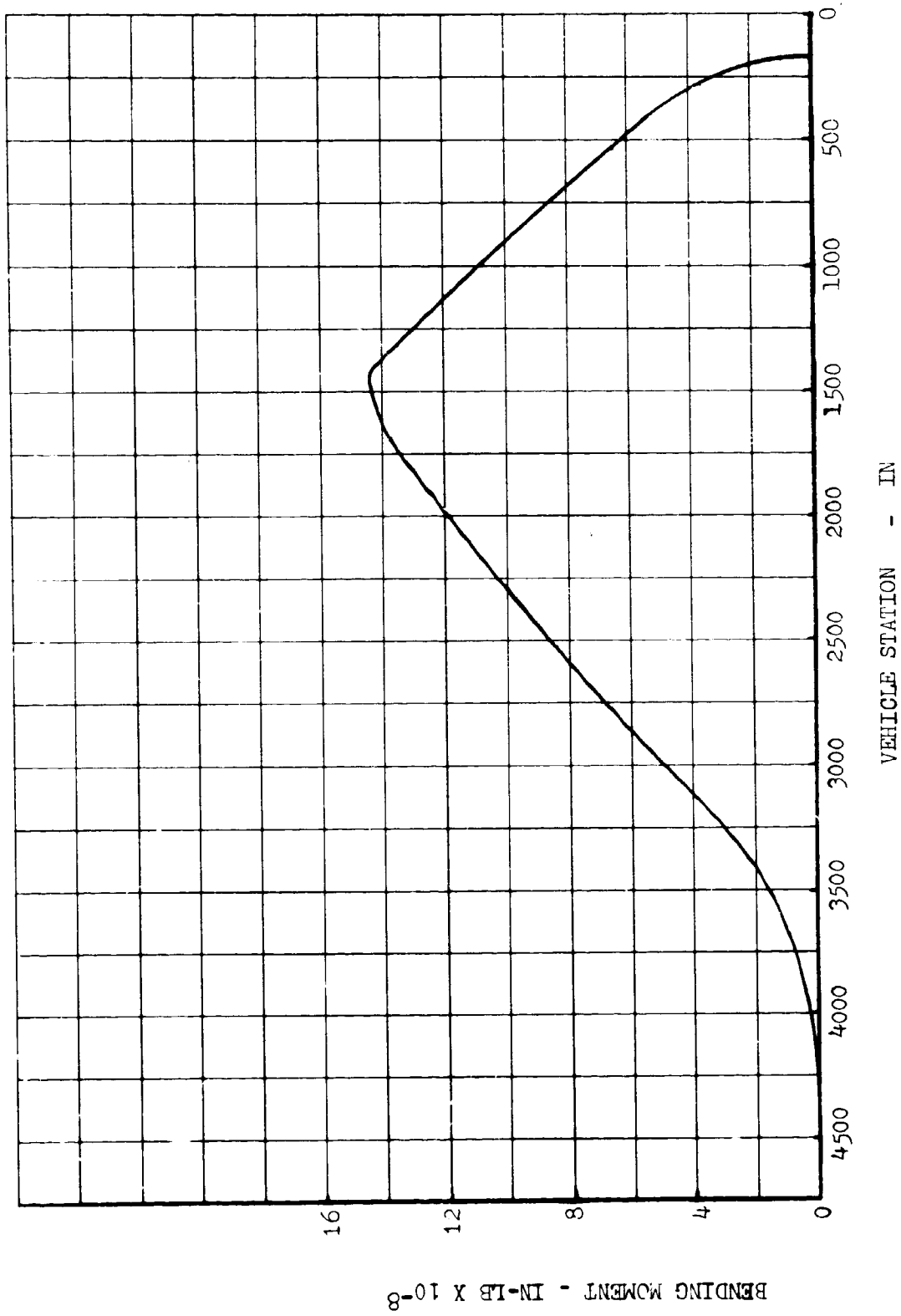
FIGURE 4.2.4.4-3   MLLV M/C + 8 SRM + 3 I(S) BENDING MOMENT DISTRIBUTION - @ MAXIMUM qα

171
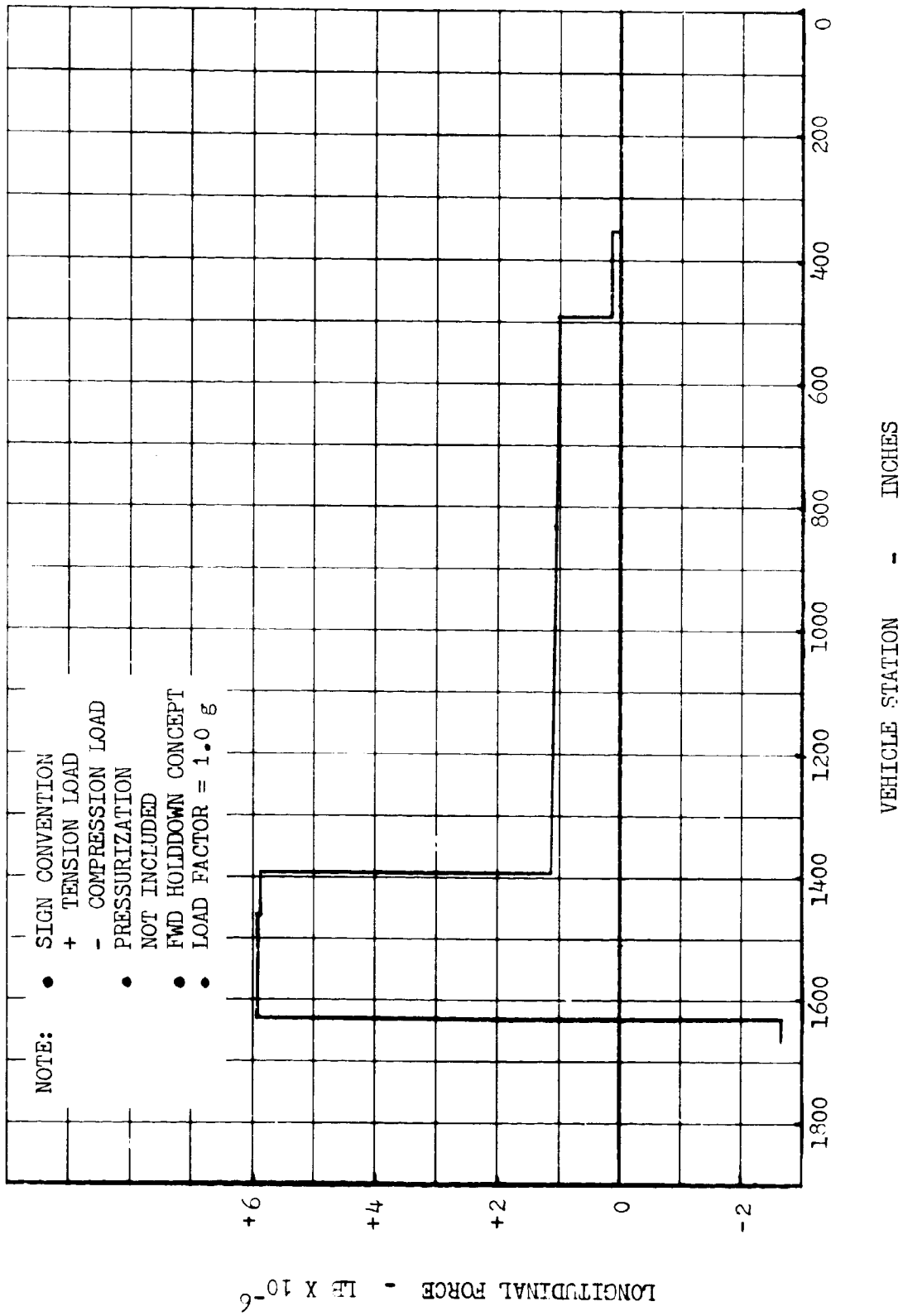
FIGURE 4.2.4.4-4 MLLV M/C + 8 SRM + 3 S(I) LONGITUDINAL FORCE DISTRIBUTION - ON PAD, FUELED, UNPRESSURIZED CONDITION
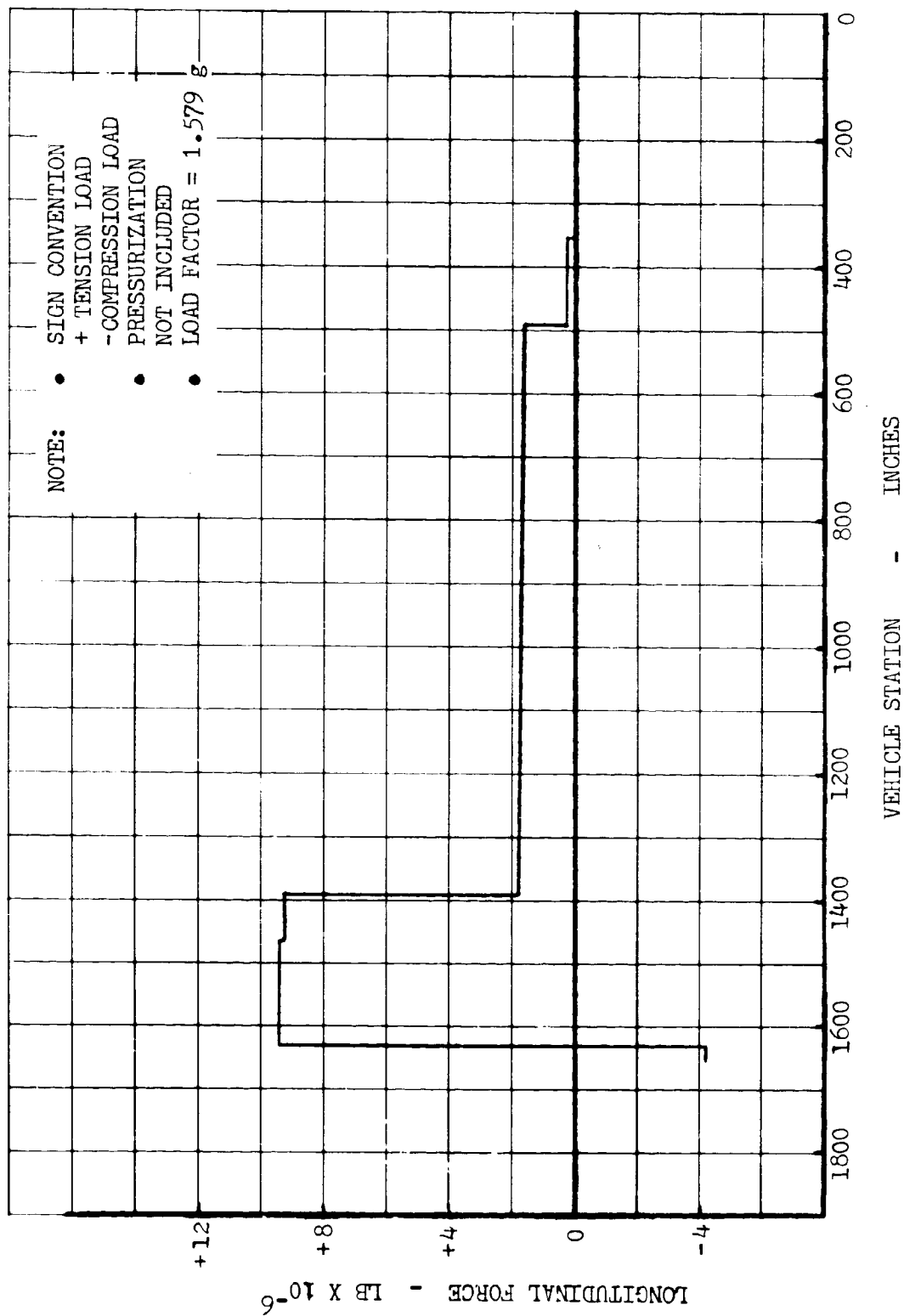
FIGURE 4.2.4.4-5 MLLV M/C + 8 SRM + 3 S(I) LONGITUDINAL FORCE DISTRIBUTION –
LIFT-OFF

173
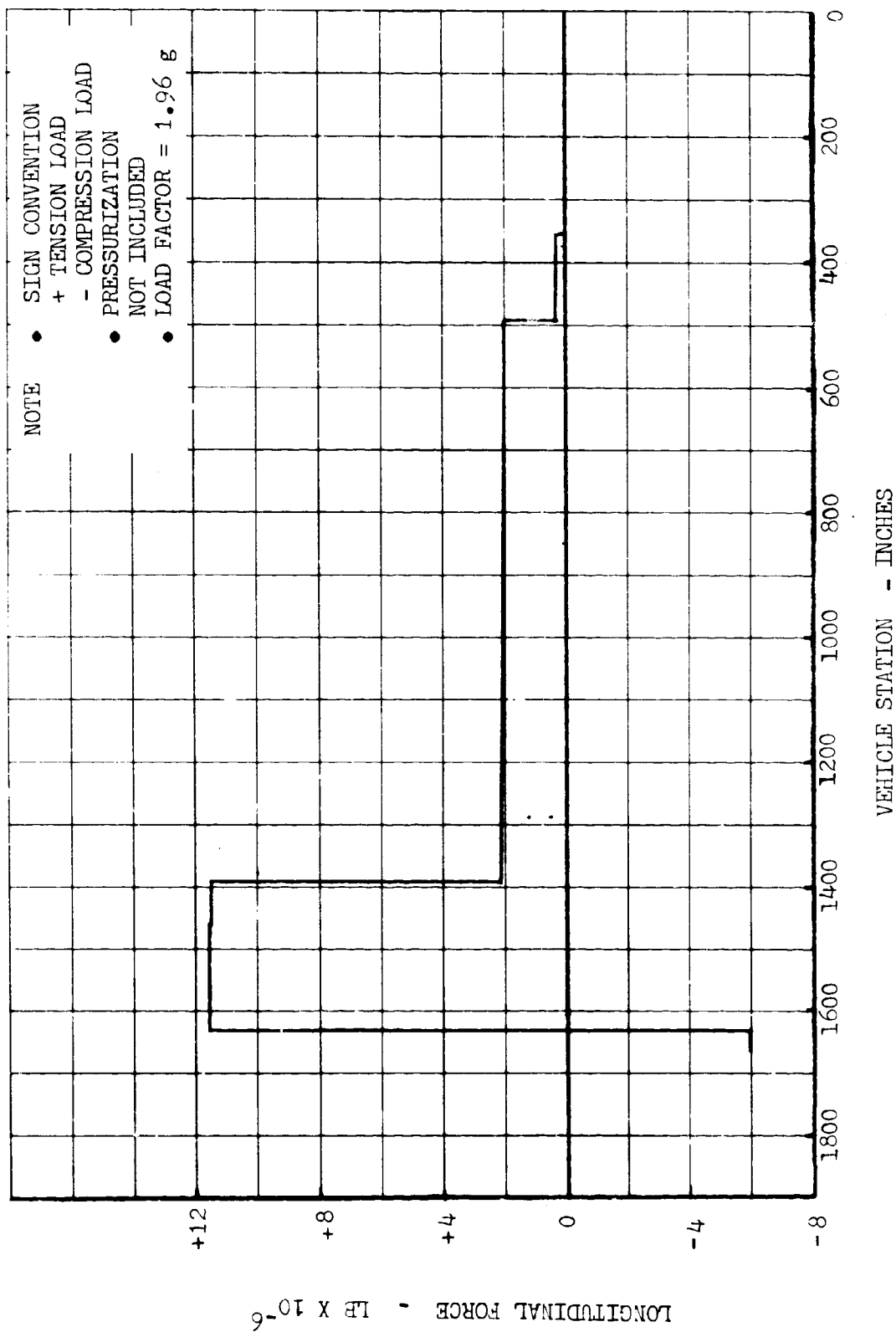
FIGURE 4.2.4.4-6 MLLV M/C + 8 SRM + 3 S(I) LONGITUDINAL FORCE DISTRIBUTION - @ MAX (qα)

174
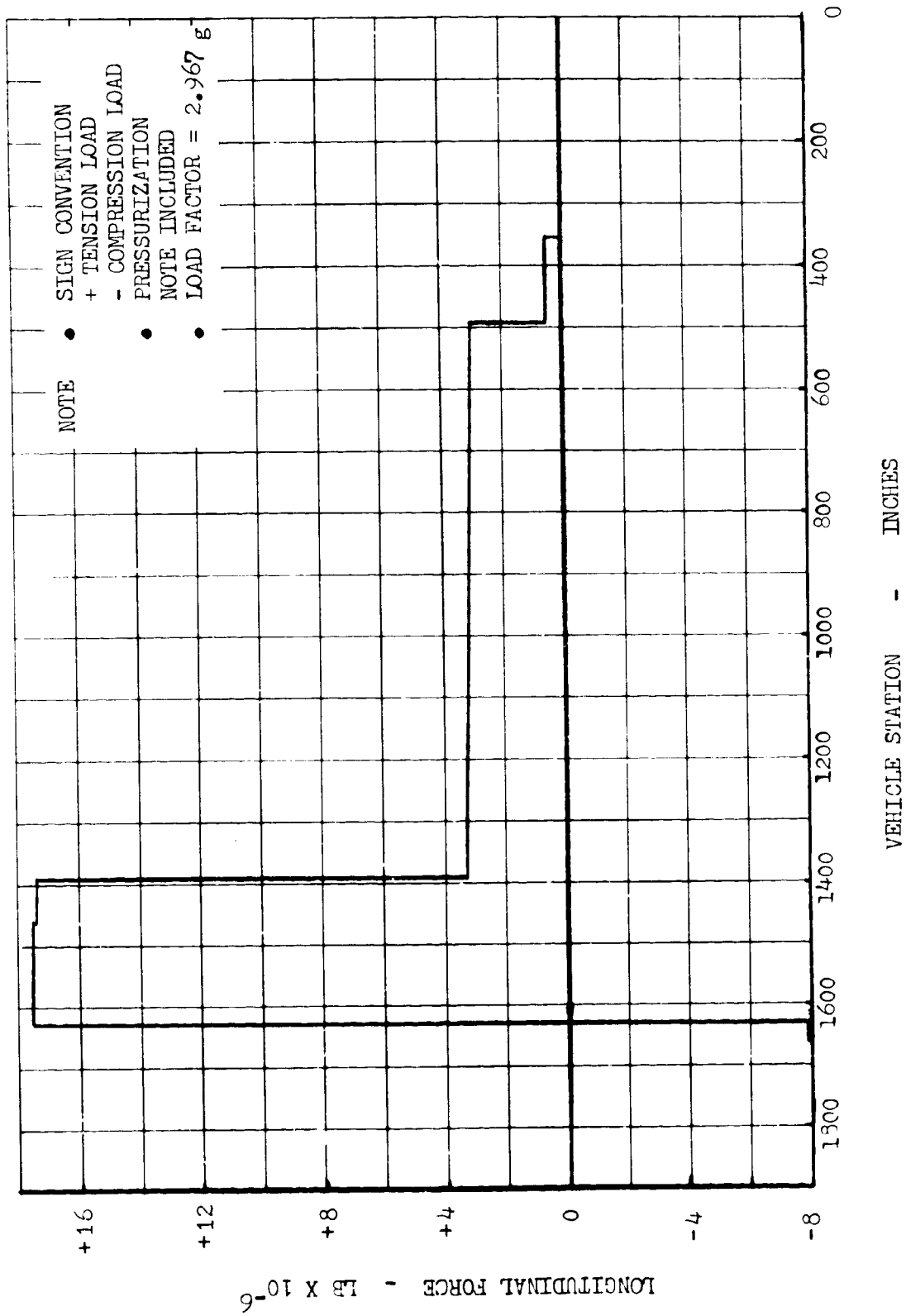
FIGURE 4.2.4.4-7   MLLV M/C + 8 SRM + 3 S(I) LONGITUDINAL FORCE DISTRIBUTION -
@ SRM CUT-OFF

175

FIGURE 4.2.4.4-8 MLLV M/C + 8 SRM + 3 S(I) LONGITUDINAL FORCE DISTRIBUTION -
@ CORE IGNITION

176

NOTE
- SIGN CONVENTION
  + TENSION LOAD
  − COMPRESSION LOAD
- PRESSURIZATION
  NOT INCLUDED
- LOAD FACTOR = 3.338 g

VEHICLE STATION — INCHES

LONGITUDINAL FORCE — LB X 10^{-6}
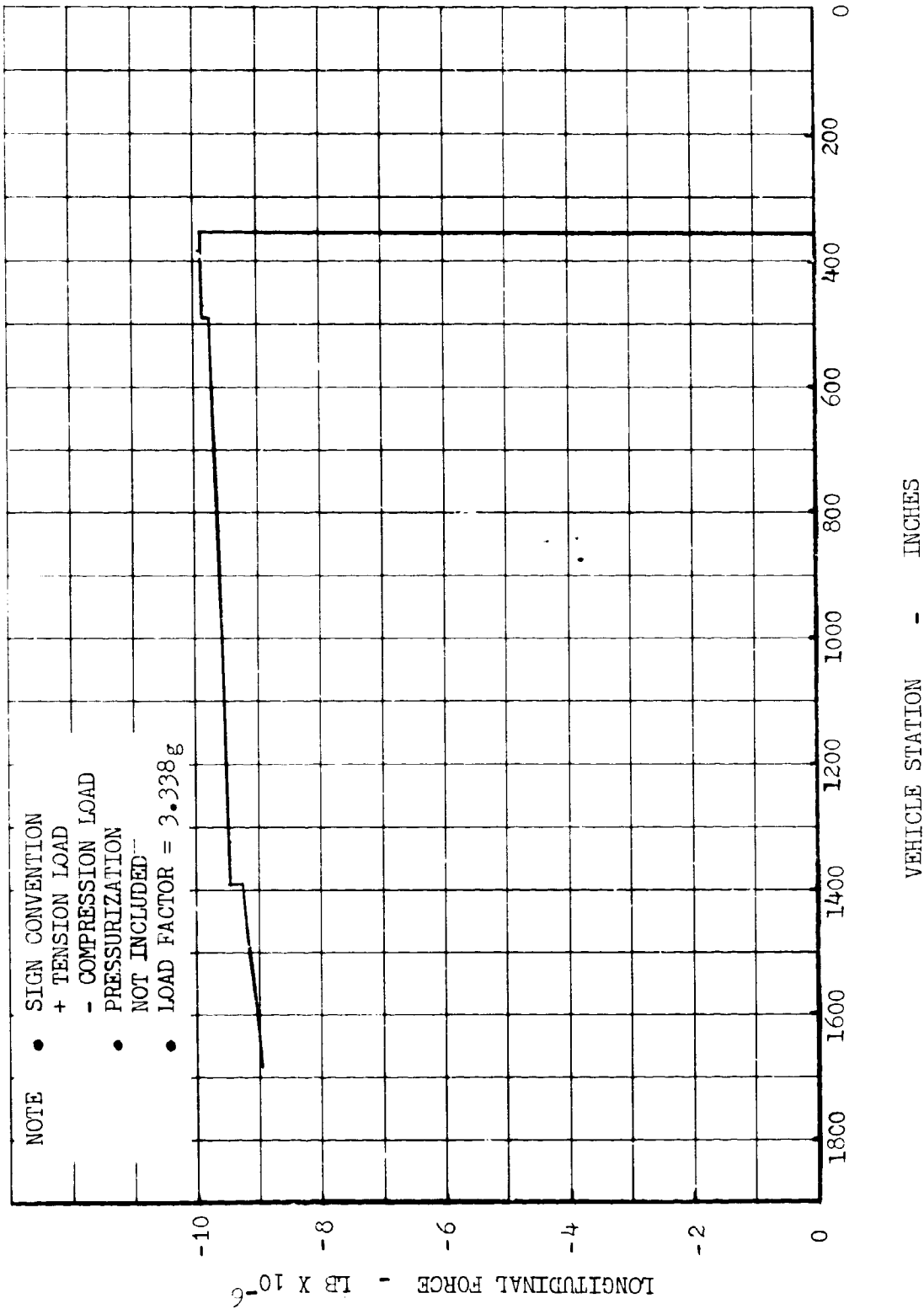
FIGURE 4.2.4.4-9 MLLV M/C + 8 SRM + 3 S(Ⅱ) LONGITUDINAL FORCE DISTRIBUTION –
@ MAX ACCELERATION (CORE BURN OUT)

177
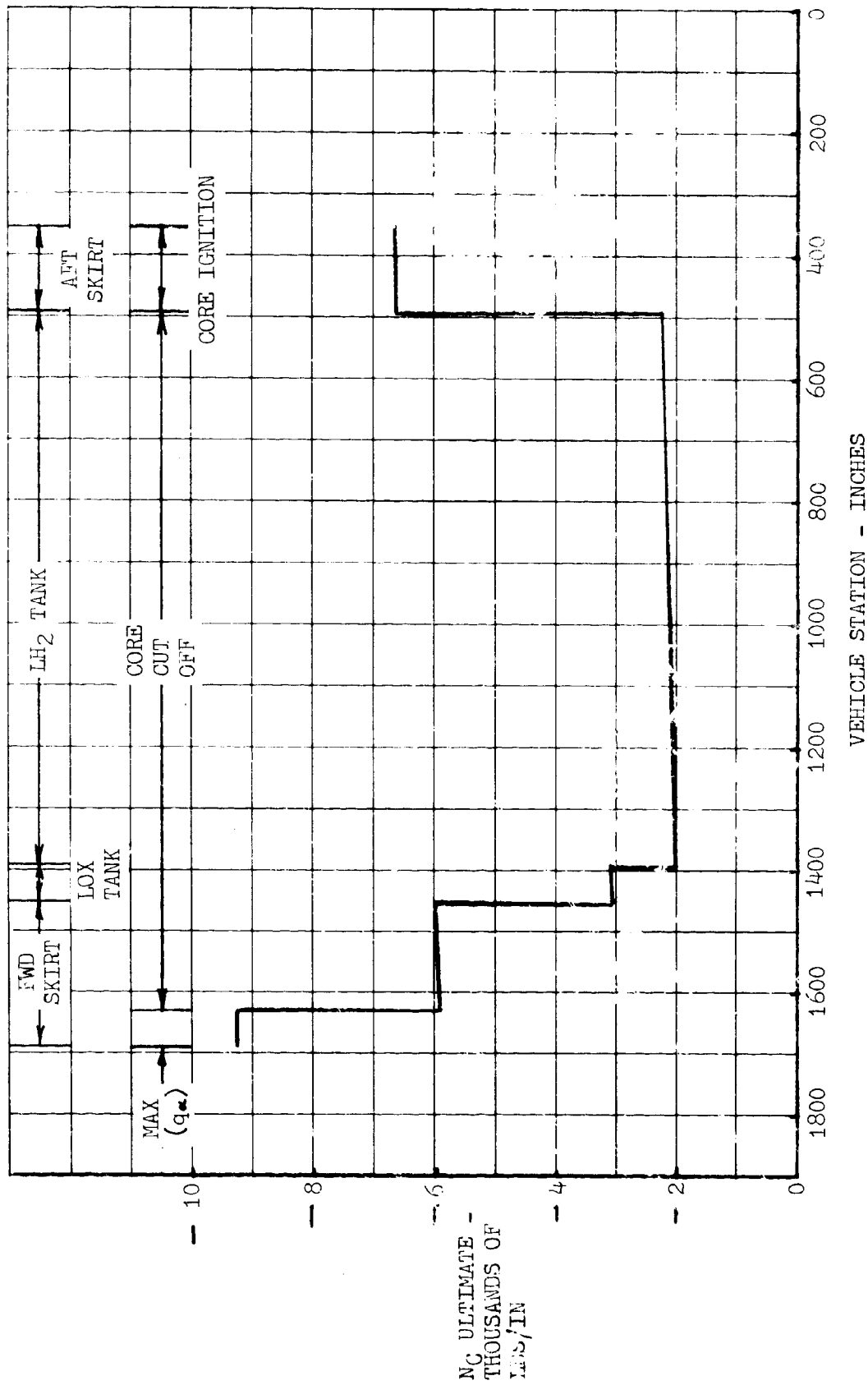
FIGURE 4.2.4.4-10   ULTIMATE COMBINED COMPRESSIVE LOAD ENVELOPE MLLV
M/C + 8 SRM + 3 S(I) FLIGHT
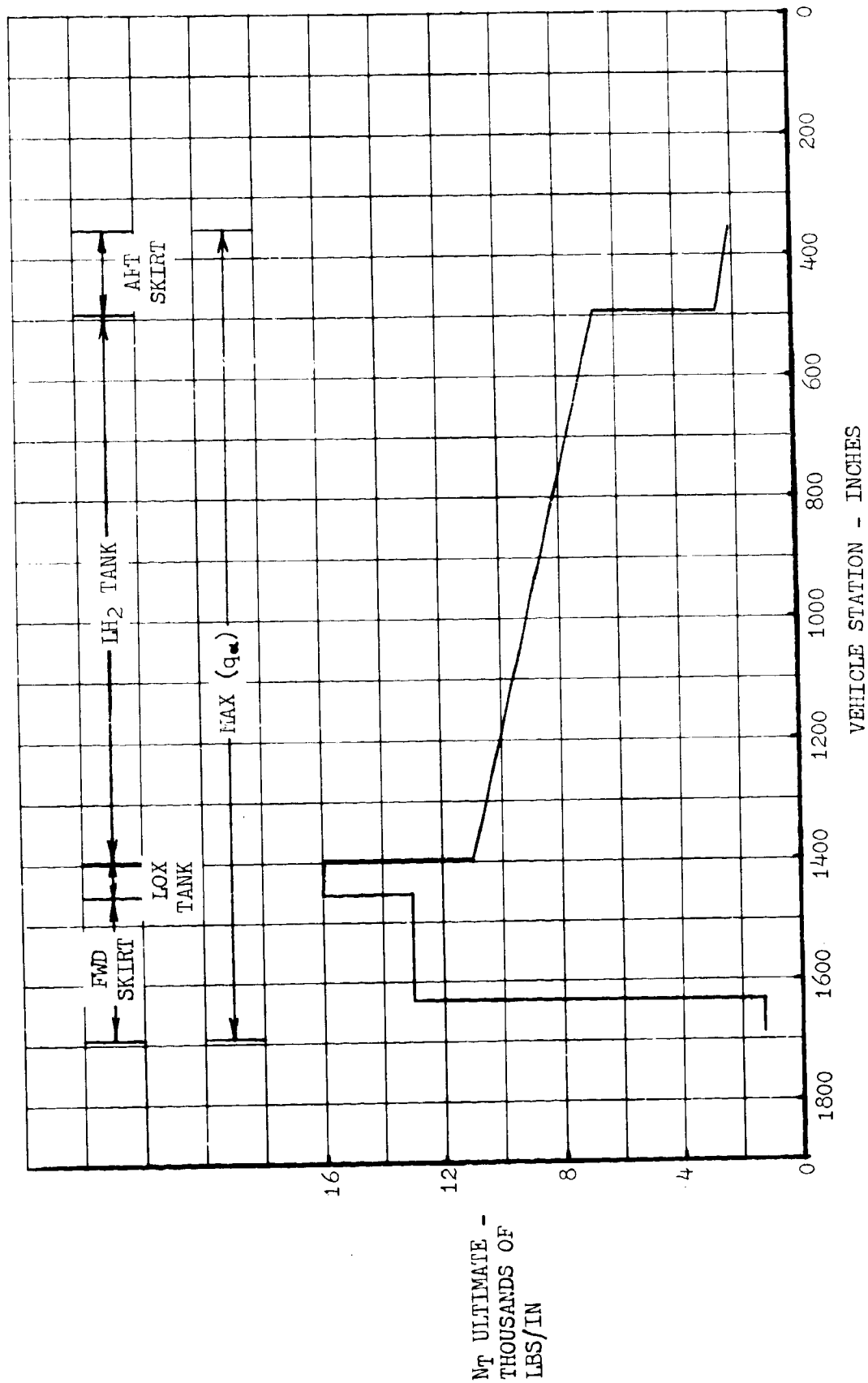
FIGURE 4.2.4.4-11   ULTIMATE COMBINED TENSILE LOAD ENVELOPE MLLV M/C + 8-SRM + 3S(I) FLIGHT

179
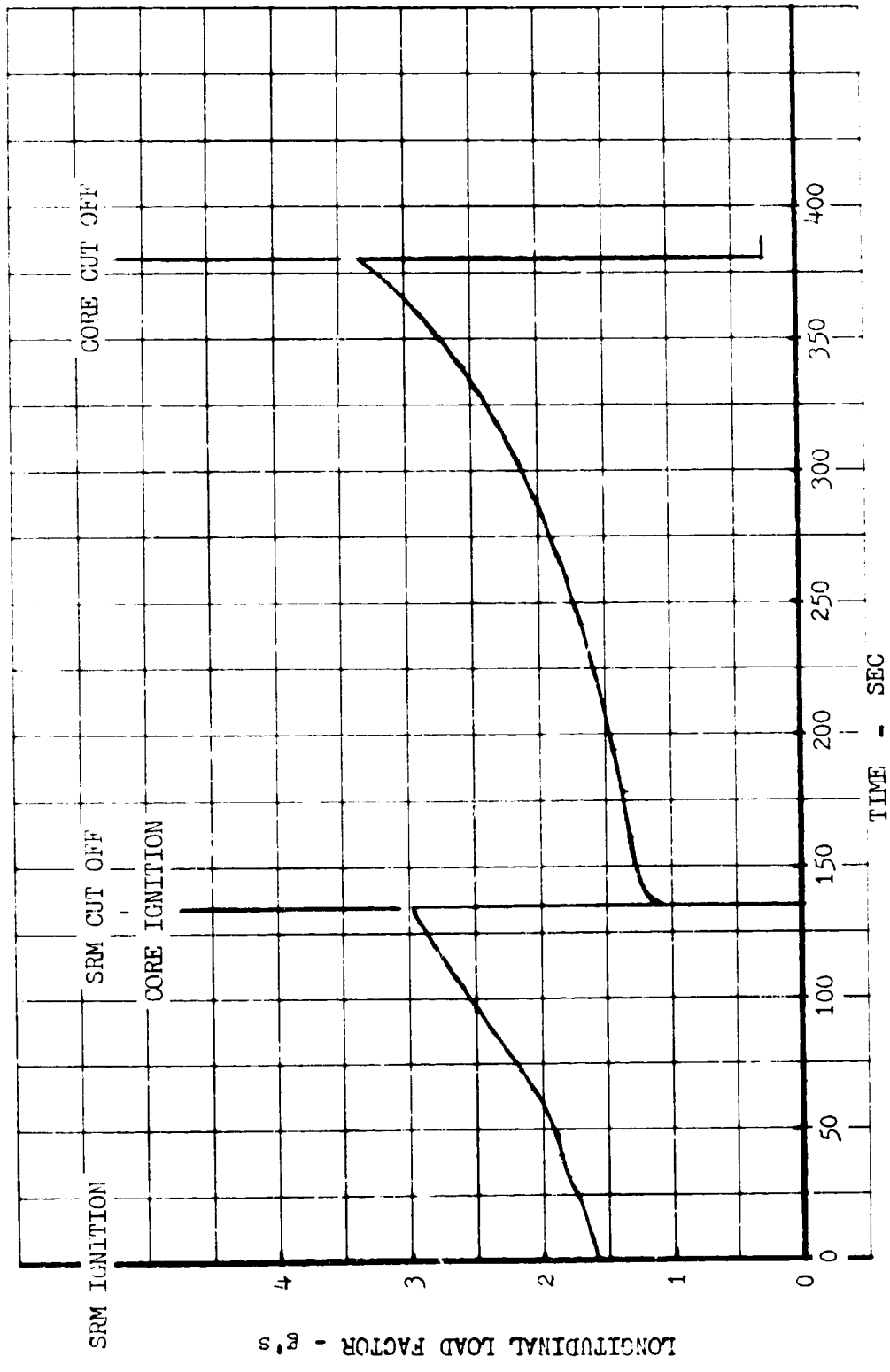
FIGURE 4.2.4.4-12   LONGITUDINAL LOAD FACTOR FOR MLLV M/C + 8 SRM + 3   S(I)

180
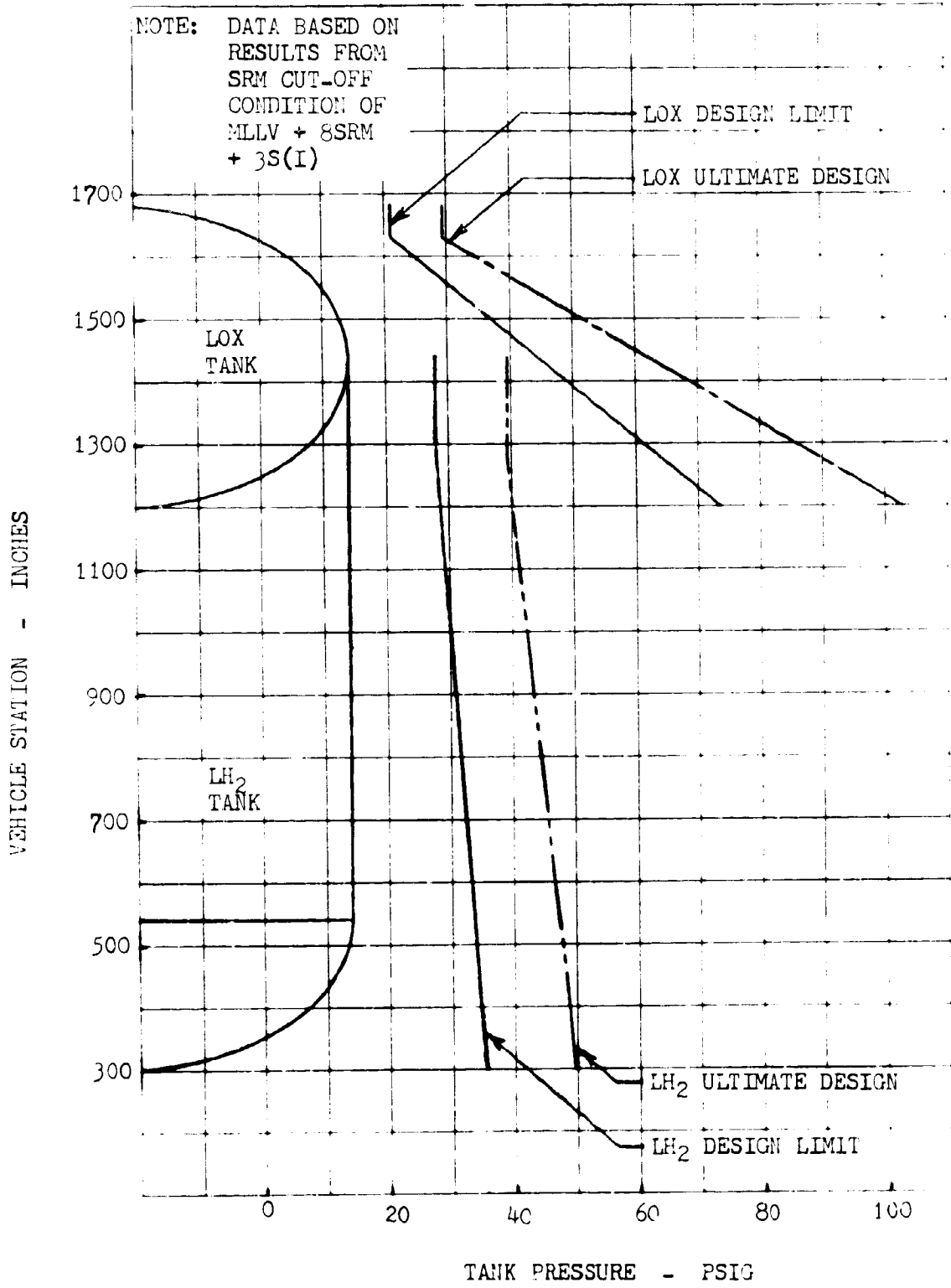
FIGURE 4.2.4.4-13   TANK DESIGN PRESSURES

181

TABLE 4.2.4.4-I   MAIN STAGE PLUS EIGHT SRM STAGES PLUS THREE MODULE INJECTION STAGE VEHICLE COMBINED LOADS MAX (qα)
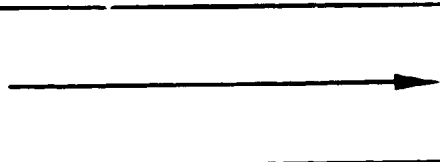
VEHICLE STATION IN	η	W' x10⁻⁶ LB	ηW' x10⁻⁶ LB	D x10⁻⁶ LB	P x10⁻⁶ LB	$\frac{P}{2\pi R}$ LB/IN	BM x10⁻³ IN-LB	$\frac{BM}{\pi R^2}$ LB/IN	$P_u R$ min₁ LB/IN	$P_u R$ max₂ LB/IN	N_c limit LB/IN	N_t limit LB/IN	N_c ultimate LB/IN	N_t ultimate LB/IN
355	1.96	.170	.334	0	.334	.156	490	1350			-1194	1840	-1672	2106
493A		.192	.376		.376	176	614	1692			-1516	1868	-2122	2615
493F		1.019	1.997		1.997	935	614	1692	3511	4106		6733		7764
1396A		1.111	2.178		2.178	1020	1414	3892	3511	4106		9018		10982
1396F		5.870	11.508		11.506	5396	1414	3892	2321	2916		12194		15905
1454A		5.881	11.526		11.528	5396	1438	3959	2321	2916		12271		16013
1454F		5.907	11.578		11.528	5420	1438	3959				9379		23131
1690		-2.686	-5.265	-.742	-6.007	-2812	1375	3786			-6596	974	-9237	1364

TABLE 4.2.4.4-II   MAIN STAGE PLUS EIGHT STRAP-ON SRMs PLUS A THREE MODULE INJECTION STAGE COMBINED LOADS AT SRM CUTOFF

VEHICLE STATION IN	η	W' x10⁻⁶ LB	ηW' x10⁻⁶ LB	P x10⁻⁶ LB	$\frac{P}{2\pi R}$ LB/IN	P_u max R/2 LB/IN	N_c limit LB/IN	N_t limit LB/IN	N_c ultimate LB/IN	N_t ultimate LB/IN
355	2.967	0.170	0.506	0.506	237	4760		237		332
493A		0.192	0.570	0.570	267	4760		267		374
493F		1.019	3.024	3.024	1418	3570		8178		6742
1396A		1.111	3.298	3.298	1544	3570		6304		8922
1396F		5.870	17.417	17.417	8154			11724		14986
1454A		5.881	17.450	17.450	8170			11740		15008
1454F		5.907	17.527	17.527	8206			8206		11488
1690		-2.686	-7.969	-7.969	-3731		-3731		-5223	

SIGN CONVENTION - COMPRESSIVE LOAD: (-)

TABLE 4.2.4.4-II   MAIN STAGE PLUS EIGHT STRAP-ON SRM STAGES PLUS A THREE MODULE INJECTION STAGE VEHICLE
COMBINED LOADS AT MAIN STAGE IGNITION

VEHICLE STATION IN	η	W' $\times 10^{-6}$ lb	ηW' $\times 10^{-6}$ lb	P $\times 10^{-6}$ lb	P/2πR lb/in	$P_u$min R/2 lb/in	$N_c$limit lb/in	$N_c$ultimate lb/in
355	1.196	8.475	10.136	-10.136	-4745		-4745	-6643
493A		8.453	10.110	-10.110	-4733		-4733	-6626
493F		7.627	9.121	-9.121	-4270	4165	-105	-1813
1396A		7.534	9.011	-9.011	-4219	4165	-54	-1742
1396F		2.775	3.319	-3.319	-1554	2975	-	-
1454A		2.764	3.306	-3.306	-1547	2975	-	-
1454F		2.738	3.275	-3.275	-1533		-1533	-2146
1690		2.686	3.212	-3.212	-1504		-1504	-2106

SIGN CONVENTION

- COMPRESSIVE LOAD : (-)

183

TABLE 4.2.4.4-IV MAIN STAGE PLUS EIGHT STRAP-ON SRM STAGES PLUS A THREE MODULE INJECTION STAGE VEHICLE COMBINED LOADS AT MAIN STAGE CUT-OFF

VEHICLE STATION IN	η	W' x10^{-6} lb	ηW' x10^{-6} lb	P x10^{-6} lb	P/2πR lb/in	P$_u$ min R/2 lb/in	N$_c$ limit lb/in	N$_c$ ultimate lb/in
355	3.338	2.973	9.922	-9.922	-4645		-4645	-6503
493A		2.951	9.850	-9.850	-4611		-4611	-6455
493F		2.918	9.739	-9.739	-4569	4165	-404	-2232
1396A		2.825	9.431	-9.431	-4415	4165	-250	-2016
1396F		2.775	9.264	-9.264	-4337	2975	-1362	-3097
1454A		2.764	9.227	-9.227	-4320	2975	-1345	-3073
1454F		2.738	9.140	-9.140	-4279		-4279	-5991
1690		2.686	8.966	-8.966	-4198		-4198	-5877

SIGN CONVENTION

- COMPRESSIVE LOAD : (-)

184

4.2.4.4   (Continued)

$(q\alpha)$ conditions; SRM cut-off, main stage ignition and main stage cut-off condition. The symbols used are defined in Section 4.2.4.9.

Table 4.2.4.4-V is a list of the designing tank pressure conditions at solid motor cut-off. The loads at the SRM attachment points for the main stage plus eight strap-on SRM stages plus a three module injection stage vehicle are shown in Table 4.2.4.4-VI.

4.2.4.5   Loads for Heavy Weight Forward Skirt

Table 4.2.4.5-I through IV show the heavy weight forward skirt loads for the main stage plus eight strap-on stages vehicle and for the main stage plus eight SRM's plus the three module injection stage vehicle. Included in the data are the accumulated weights versus vehicle station at max $(q\alpha)$ and at core cut-off, $q\alpha$ compressive loads, maximum acceleration compressive loads, and tension loads at maximum dynamic pressure.

Figure 4.2.4.5-1 illustrates the ultimate (N_c) loads for the heavy weight forward skirts of above vehicles. The lower portion of the forward skirt is designed by core cut-off and the upper portion of the skirt is designed by max $(q\alpha)$ for both vehicles. The higher (N_c) loads are experienced by the heavier payload vehicle.

Figure 4.2.4.5-2 illustrates the ultimate (N_t) loads for the forward skirts above vehicles. The design loads occur at the max $(q\alpha)$ condition.

4.2.4.6   Structural Dynamics

The structural dynamic characteristics for the MLLV M/C and MLLV M/C + 8-SRM + 3S(I) at max. $(q\alpha)$ are illustrated in Figures 4.2.4.6-1 and 4.2.4.6-2. Figure 4.2.4.6-1 shows the first four mode shapes and frequencies for the MLLV M/C and Figure 4.2.4.6-2 presents the same data for the MLLV M/C + 8 SRM + 3S(I) vehicle. These data were obtained using finite element techniques and the direct stiffness method. Each vehicle was considered to be a series of two-node beam elements having constant stiffness properties. Each beam node had two degrees of freedom (lateral translation and rotation) and had a lumped mass and rotary inertia associated with it. The analysis was performed using the MATMAN Computer Program (Reference 4.2.4.6-1) which is a general purpose matrix manipulation and eigenvalue program. The analysis procedure consisted of first determining the flexibility matrix for the entire vehicle then formulating the free-free dynamic matrix and computing the eigenvalues (frequencies) and eigenvectors

---

4.2.4.6-1   Boeing Document BHA-0235, "General MATRIX Manipulator Program", dated May 14, 1968.

TABLE 4.2.4.4-V

M/C MLLV + 8 SRM + 3S(I)

TANK DESIGN PRESSURES @ SRM CUT-OFF

LH$_2$ TANK

$$h_{Sta.} = 1280$$

$$h_{head} = 980 \text{ in.}$$

$$\rho_{LH_2} = .0025 \text{ \#/in}^3$$

$$\eta = 2.97g$$

$$P_{head} = 7.28 \text{ psig}$$

$$P_{ullage \atop mx} = 28 \text{ psig}$$

$$P_{bottom} = 35.28 \text{ psig}$$

LOX TANK

$$h_{sta.} = 1630$$

$$h_{head} = 430 \text{ in}$$

$$\rho_{LOX} = .041 \text{ \#/in}^3$$

$$\eta = 2.97g$$

$$P_{head} = 52.36 \text{ psig}$$

$$P_{ullage \atop mx} = 21 \text{ psig}$$

$$P_{bottom} = 73.36 \text{ psig}$$

186

TABLE 4.2.4.4-VI   SUMMARY OF 6 VEHICLE APPLIED LOADS AT SRM
ATTACHMENT POINTS. MAIN STAGE + 8 STRAP-ONS + 3
MODULE INJECTION STAGE

LOADING CONDITION	F_A* (LBS.)	F_{1A} (LB.)	F_{2A} (LB.)	F_{3A} (LB.)	F_{1B} (LBS.)	F_{2B} (LB.)	F_{3B} (LB.)
ON-PAD, FUELED	802,327	0	0	0	0	0	0
THRUST BUILD-UP	802,327	0	0	0	0	0	0
LIFT-OFF	1,654,000	165,624	0	-165,624	604,376	0	-604,376
Qα MAX.	2,255,421	588,505	437,715	-1,243,551	540,421	101,095	1,038,505
SRM CUTOFF	3,198,008	324,213	0	-324,213	149,178	0	-149,178

*FOR ONE (1) SRM

187
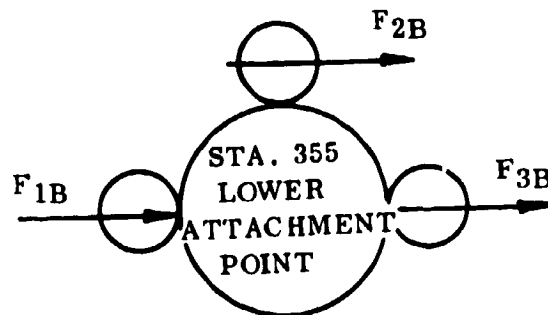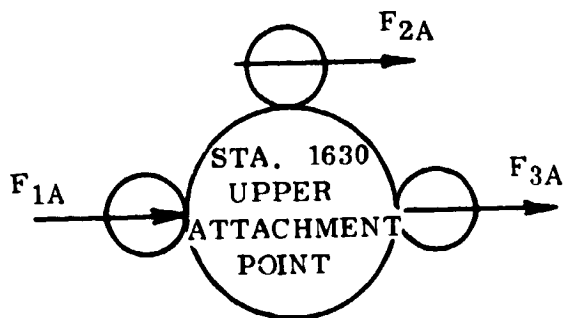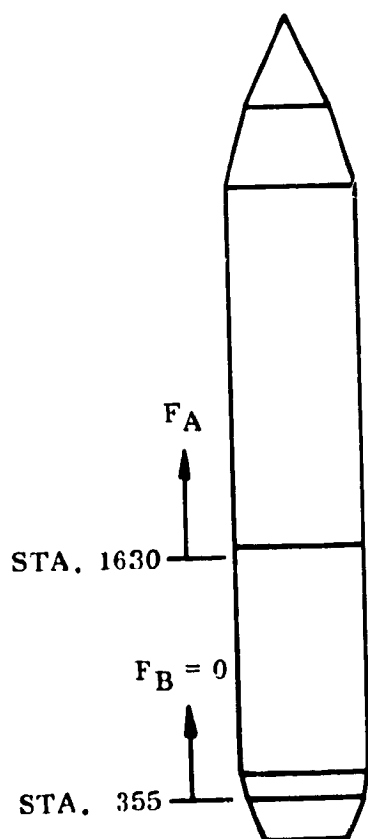
TABLE 4.2.4.5-1   FORWARD SKIRT LONGITUDINAL ACCUMULATIVE WEIGHTS MAIN STAGE PLUS EIGHT STRAP-ONS VEHICLE AND MAIN STAGE PLUS THREE INJECTION MODULES STAGE PLUS EIGHT STRAP-ONS VEHICLE

VEHICLE STATION (IN.)	ACCUMULATIVE WEIGHT - LBS			
	(q_α) MAX CONDITION		CORE CUT-OFF CONDITION	
	CORE + 8-SRM + 3S(I)	CORE + 8-SRM	CORE + 8-SRM + 3 S(I)	CORE + 8-SRM
1690	2686000 (C)	1777712 (C)	2686000 (C)	1777712 (C)
1630F	2697800 (C)	1789512 (C)	2697800 (C)	1789512 (C)
1630A	5947860 (t)	5947860 (t)	2697800 (C)	1789512 (C)
1454F	5907345 (t)	5907345 (t)	2738313 (C)	1830025 (C)
1454A	5881504 (t)	5881504 (t)	2764154 (C)	1855866 (C)

(C) - COMPRESSIVE LOADING

(t) - TENSILE LOADING

188

TABLE 4.2.4.5-II COMPRESSION LOADS ON HEAVY WEIGHT FORWARD SKIRT AT MAX (qα)

MLLV CONFIG.	VEH. STA. (IN.)	W' 10^{-6} (lb)	η	ηW' 10^{-6} (lb)	D 10^{-6} (lb)	P 10^{-6} (lb)	P/2 R (lb/in)	BM 10^{-6} (in/lb)	BM/πR^2 (lb/in)	$\frac{P_u R_{min}}{2}$ (lb/in)	N_c limit (lb/in)	N_c ultimate (lb/in)
Main Stage Plus Eight SRM Stages Plus A Three Module Injection Stage Vehicle	1690	-2.686	1.96	-5.265	-.742	-6.007	-2813	1375	3786	0	-6599	-9239
	1630F	-2.698		-5.288	-.742	-6.030	-2824	1400	3854	-	-6678	-9349
	1630A	5.948		11.658	0	11.658	5460	1400	3854	-	-	-
	1454F	5.907		11.578	0	11.578	5422	1438	3959	-	-	-121
	1454A	5.881		11.527	0	11.527	5399	1438	3959	2321	-	-
Main Stage Plus Eight SRM Stages Vehicle	1690	-1.778	2.023	-3.597	-.791	-4.388	-2055	1229	3384	0	-5439	-7615
	1630F	-1.790		-3.621	-.791	-4.412	-2066	1252	3447	-	-5513	-7718
	1630A	5.948		12.033	0	12.033	5636	1252	3447	-	-	-
	1454F	5.907		11.950	0	11.950	5597	1286	3541	-	-	-
	1454A	5.881		11.897	(	11.897	5572	1286	3541	2321	-	-

SIGN CONVENTION

- COMPRESSIVE LOAD: (-)

189

TABLE 4.2.4.5-III   COMPRESSION LOADS ON HEAVY WEIGHT FORWARD SKIRT AT MAX ACCELERATION

MLLV CONFIG.	VEH. STA. (IN.)	W' 10⁻⁶ (lb)	η (g)	ηW' 10⁻⁶ (lb)	D 10⁻⁶ (lb)	P 10⁻⁶ (lb)	P/2πR (lb/in)	BM 10⁻⁶ (in/lb)	BM/πR² (lb/in)	$\frac{Pu_{min}R}{2}$ (lb/in)	Nc limit (lb/in)	Nc ultimate (lb/in)
Main Stage Plus 8-SRM Plus Three Module Injection Stage Vehicle	1690	-2.686	3.338	-8.966	0	-8.966	-4199	0	0	0	-4199	-5879
	1630	-2.698		-9.006		-9.006	-4218				-4218	-5905
	1454F	-2.738		-9.139		-9.139	-4280				-4280	-5992
	1454A	-2.764		-9.226		-9.226	-4321			2975	-1346	-3074
Main Stage Plus 8-SRM Vehicles	1690	-1.778	3.675	-6.534	0	-6.534	-3060	0	0	0	-3060	-4284
	1630	-1.790		-6.578		-6.578	-3080				-3080	-4312
	1454F	-1.830		-6.725		-6.725	-3149				-3149	-4409
	1454A	-1.856		-6.821		-6.821	-3194			2975	-219	-1497

SIGN CONVENTION

- COMPRESSIVE LOAD : (-)

TABLE 4.2.4.5-IV   TENSION LOADS ON HEAVY WEIGHT FORWARD SKIRT AT MAX (qα)

MLLV CONFIG.	VEHICLE STATION IN	W' 10^{-6} (lb)	η	$\eta W'$ 10^{-6} (lb)	D 10^{-6} (lb)	P 10^{-6} (lb)	$P/2\pi R$ (lb/in)	BM 10^{-6} (in-lb)	$\frac{BM}{\pi R^2}$ (in-lb)	$\frac{P_u R}{2}$ max (in/lb)	N_t limit (in/lb)	N_t ultimate (in/lb)
Main Stage Plus Eight SRM Stages Plus A Three Module Injection Stage Vehicle	1690	-2.686	1.96	-5.265	-.742	-6.007	-2813	1375	3786	0	973	1362
	1630F	-2.698		-5.288	-.742	-6.030	-2824	1400	3854		1030	1442
	1630A	5.948		11.658	0	11.658	5460	1400	3854		9314	13040
	1454F	5.907		11.578	0	11.578	5422	1438	3959		9381	13133
	1454A	5.881		11.527	0	11.527	5397	1438	3959	2916	12274	16017
Main Stage Plus Eight SRM Stage Vehicle	1690	-1.778	2.023	-3.597	-.791	-4.388	-2055	1229	3384	0	1329	1851
	1630F	-1.790		-3.621	-.791	-4.412	-2066	1252	3447		1381	1933
	1630A	5.948		12.033	0	12.033	5636	1252	3447		9083	12716
	1454F	5.907		11.950	0	11.950	5597	1286	3541		9138	12793
	1454A	5.881		11.897	0	11.897	5573	1286	3541	2916	12030	15676

SIGN CONVENTION

- COMPRESSIVE LOAD : (-)

191
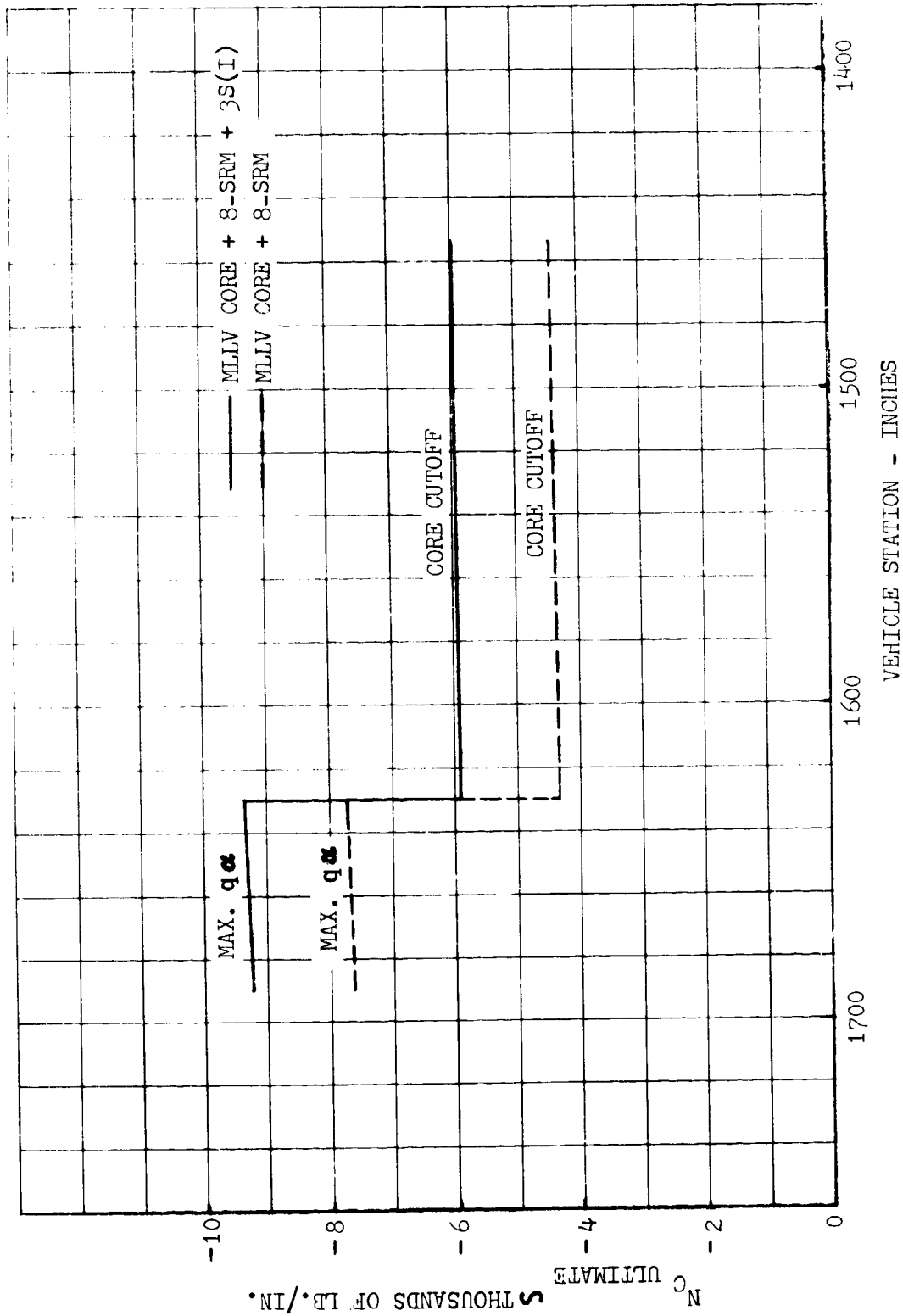
FIGURE 4.2.4.5-1   ULTIMATE COMPRESSIVE LOAD ENVELOPES FOR THE FORWARD SKIRT FOR MAIN STAGE PLUS EIGHT STRAP-ONS VEHICLE AND THE MAIN STAGE PLUS EIGHT STRAP-ONS PLUS THREE INJECTION STAGE MODULES VEHICLE
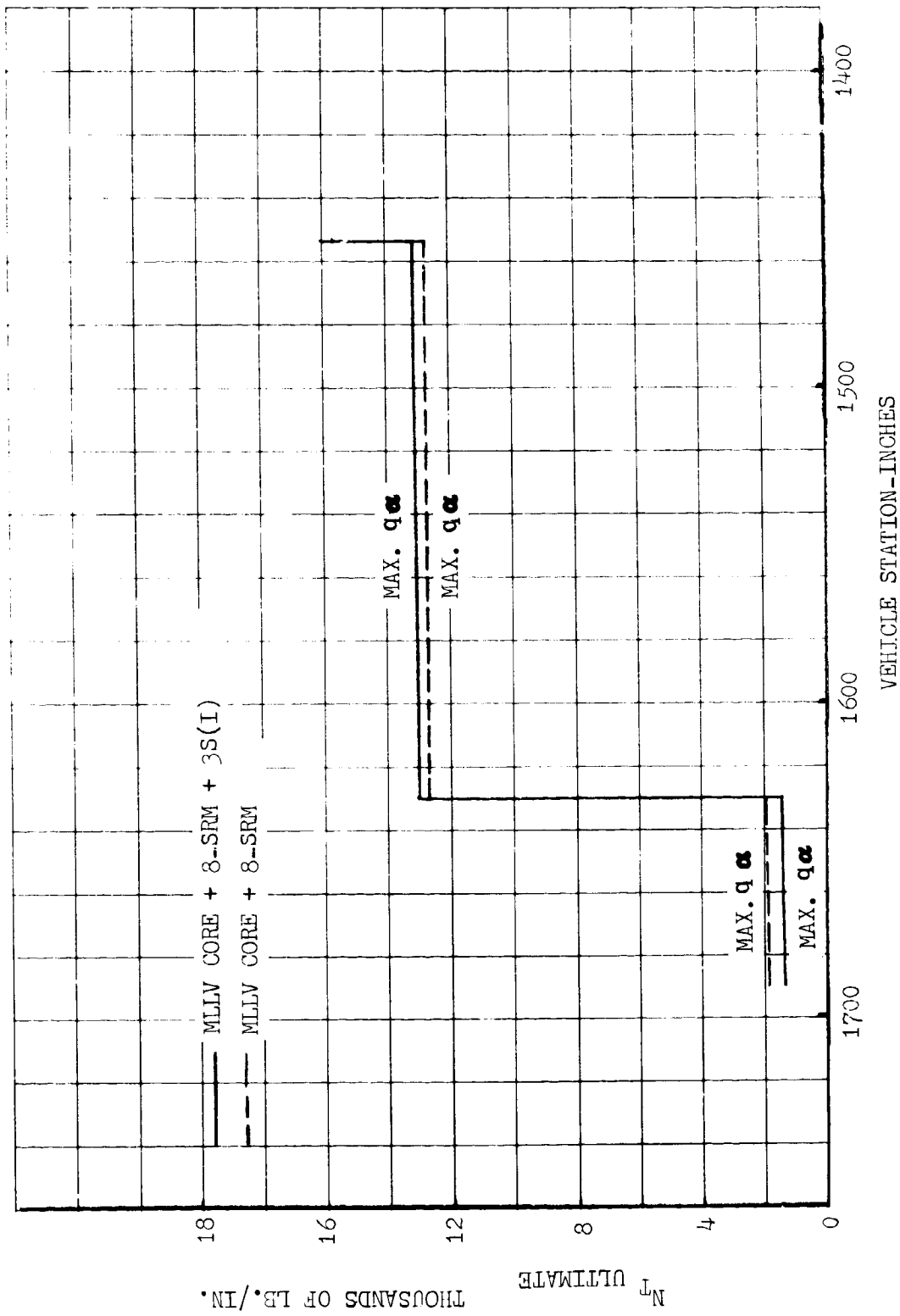
FIGURE 4.2.4.5-2   ULTIMATE TENSION LOAD ENVELOPES FOR THE FORWARD SKIRT
FOR MAIN STAGE PLUS EIGHT STRAP-ONS VEHICLE AND MAIN
STAGE PLUS EIGHT STRAP-ONS PLUS THREE INJECTION STAGE
MODULES VEHICLE

193

RELATIVE
AMPLITUDE
(IN./IN.)

1ST MODE (f_1 = 4.88 cps)

2ND MODE (f_2 = 12.11 cps)

3RD MODE (f_3 = 12.71 cps)

4TH MODE (f_4 = 21.19 cps)

RELATIVE
AMPLITUDE
(IN./IN.)

VEHICLE STATION – INCHES
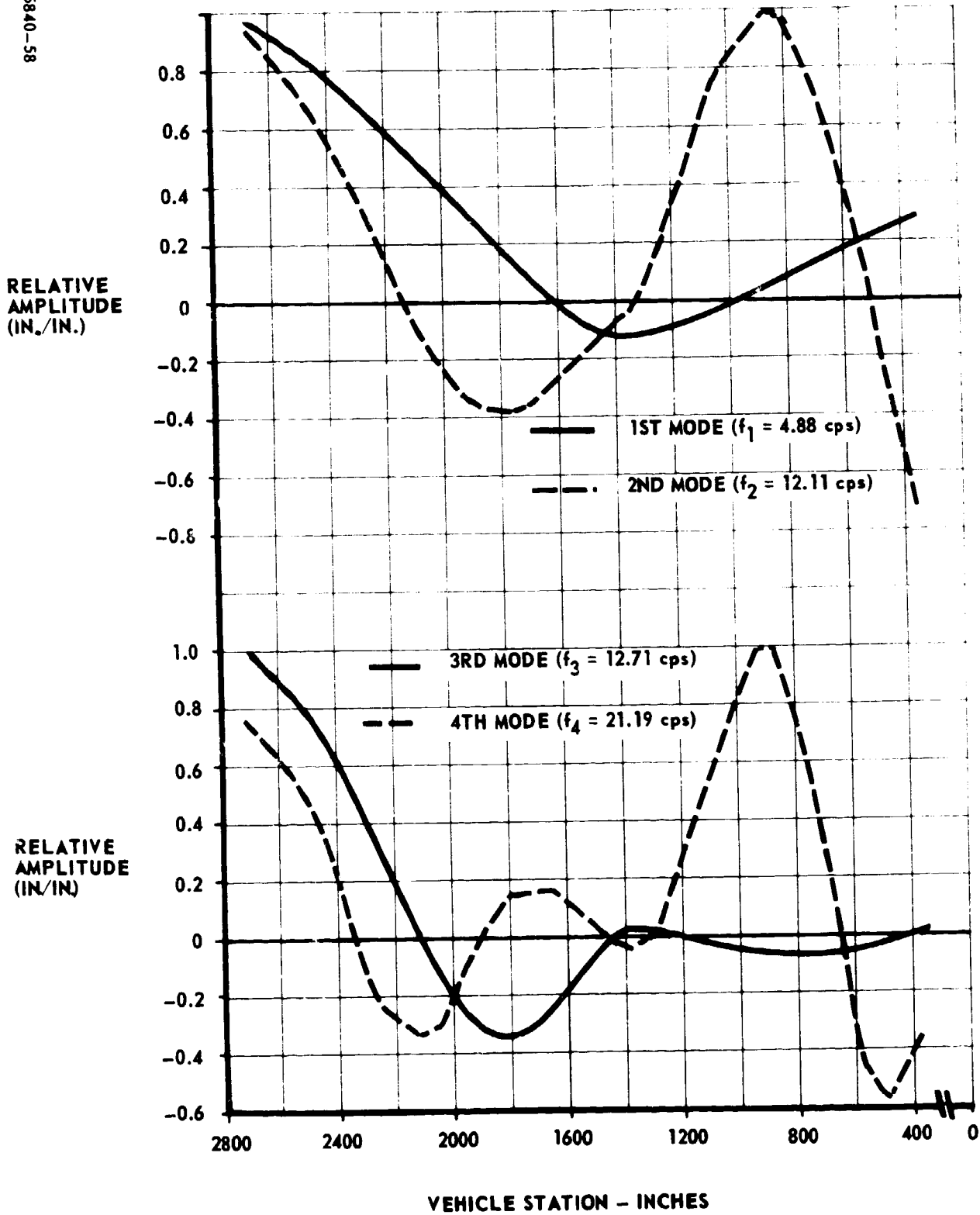
FIGURE 4.2.4.6-1   MODE SHAPES AND FREQUENCIES FOR THE FIRST FOUR LATERAL
BENDING MODES AT MAX (qα) – MLLV SINGLE-STAGE-TO-ORBIT VEHICLE

194
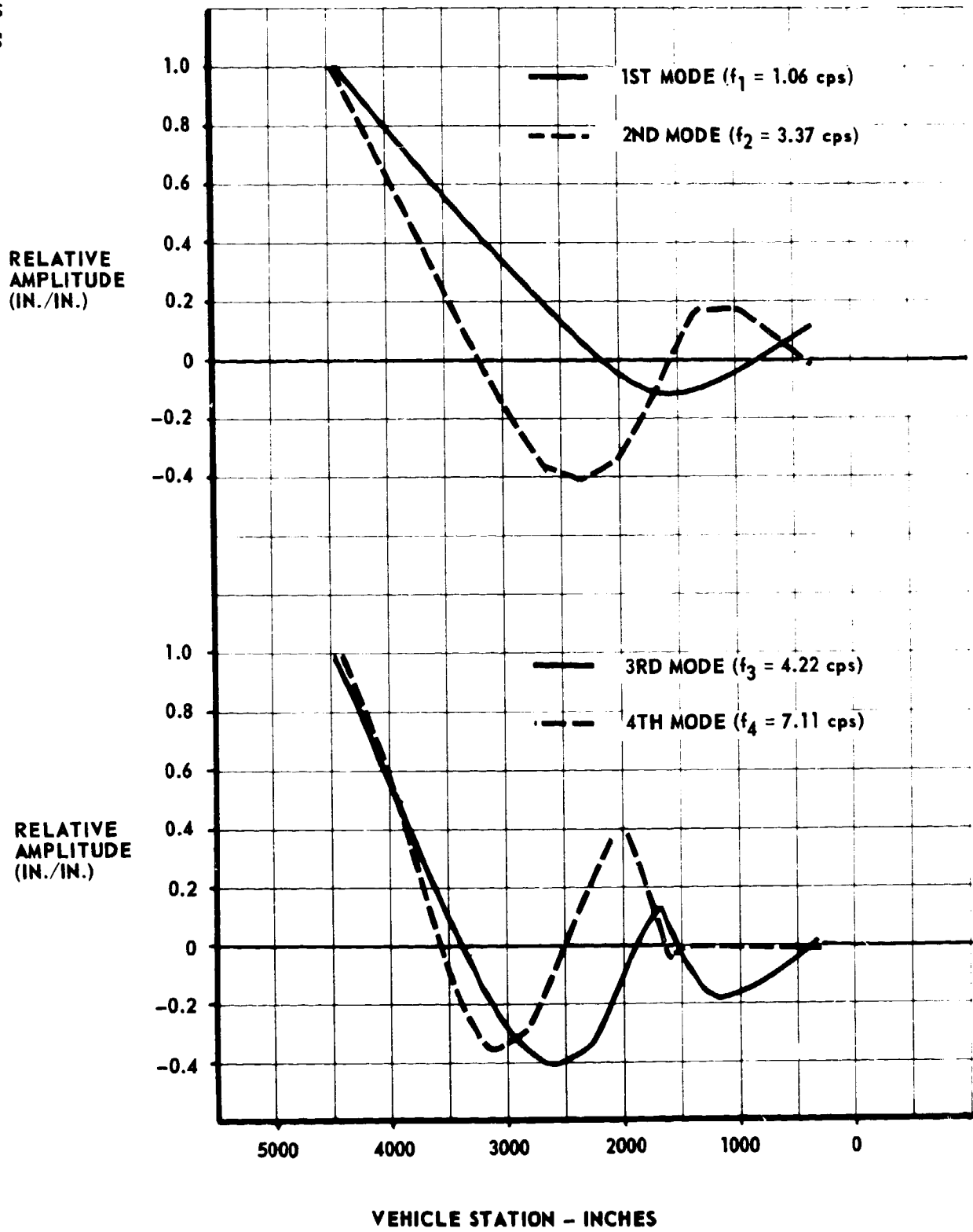
FIGURE 4.2.4.6-2   MODE SHAPES AND FREQUENCIES FOR THE FIRST FOUR LATERAL BENDING
MODES AT MAX (q æ) - MLLV MAIN STAGE PLUS EIGHT STRAP-ON STAGES
PLUS A THREE MODULE INJECTION STAGE VEHICLE

4.2.4.6   (Continued)

(mode shapes). The eigenvalue equation may be stated as follows:

$$\left[\omega_i^2 \, [F][M] - [I]\right]\left[\phi_i\right] = 0 \qquad \text{(Reference 4.2.4.6-2)}$$

Where

$[\omega_i]$ = Modal Frequency

$[\phi_i]$ = Mode Shape Matrix

$[F]$ = Total Vehicle Flexibility Matrix

$[M]$ = Total Vehicle Mass Matrix

$[I]$ = Identity Matrix

The numerical method used to determine the eigenvalues employs the technique of similarity transformations performed on the Upper-Hessenberg representation of the dynamic matrix, $[F][M]$. A detail discussion of this method is contained in Reference 4.2.4.6-1.

The mode shapes and frequencies were compiled for the maximum dynamic pressure region where the control requirements are the most severe. The mode shape for the single-stage-to-orbit vehicle would be less severe due to the dampening effect of the full propellant load by approximately 10-15 percent. The relative amplitude will increase after the maximum dynamic pressure time to approximately 15 to 20 percent greater at propellant depletion. For the largest vehicle, the mode shape and frequency is much lower because of the greater weight of the vehicle. The vehicle would have only a slightly less modal frequency at lift-off then at the maximum dynamic pressure time period. This would increase approximately 20 percent at main stage propellant depletion.

4.2.4.7   Acoustic Environment

The predicted "worst" near field acoustic environment for the single-stage-to-orbit vehicle and for the main stage plus eight strap-on stages plus three injection

---

4.2.4.6-1   Boeing Document BHA-0235, "General MATRIX Manipulator Program," dated 5/14/68.

4.2.4.6-2   Dynamics of Structures, Walter C. Hurty and Moshe F. Rubinstein, Prentice-Hall Inc., 1964.

4.2.4.7   (Continued)

stage modules vehicle are presented below. The worst acoustic condition will occur while the vehicle is at full thrust on the pad. The generated sound at this condition will be amplified through reinforcement due to reflection from the "ground plane."

The "worst" near field acoustic environment for the single-stage-to-orbit vehicle is shown in Figure 4.2.4.7-1. Figure 4.2.4.7-2 presents the "worst" acoustic environment for the MLLV vehicle with three injection stage modules and eight strap-ons. The environment along the length of the vehicle is given in terms of overall sound pressure level (re 0.0002 Dynes/cm^2) versus vehicle station.

The environments were extrapolated from the AMLLV predicted environments. The basic assumptions and method of analysis described in reference 4.2.4.7-1 for the AMLLV also apply to the MLLV acoustic prediction.

The following conditions were assumed:

1.   The vehicle is stationary on the pad.
2.   A single deflection flame bucket and a lumped exhaust stream are assumed.
3.   The sound pressure levels from multi-engine sources are corrected by the square root of the number of engines.

The power of a rocket noise source is determined from engine parameters such as thrust, exhaust gas exit velocity, nozzle exit diameter, flow rate, and number of engines. The acoustic environment is predicted by applying a power value established from the engine parameters to an empirical normalized spectrum function developed from rocket engine static test firings. The acoustic power spectrum function is proportional to the power per unit band width radiated by the source. Emperical corrections are made for near field effects and directional properties of the acoustic source when the exhaust stream is deflected.

The predictions, at the base of the vehicle, are considered conservative because corrections for finite amplitude were not made. Finite amplitude corrections will account for thermal losses in wave propagation of high intensity noise and will reduce the predicted acoustic environment.

4.2.4.7-1   Gruner, W. J., Johnston, G. D., "An Engineering Approach to Prediction of Space Vehicle Acoustic Environments.

197
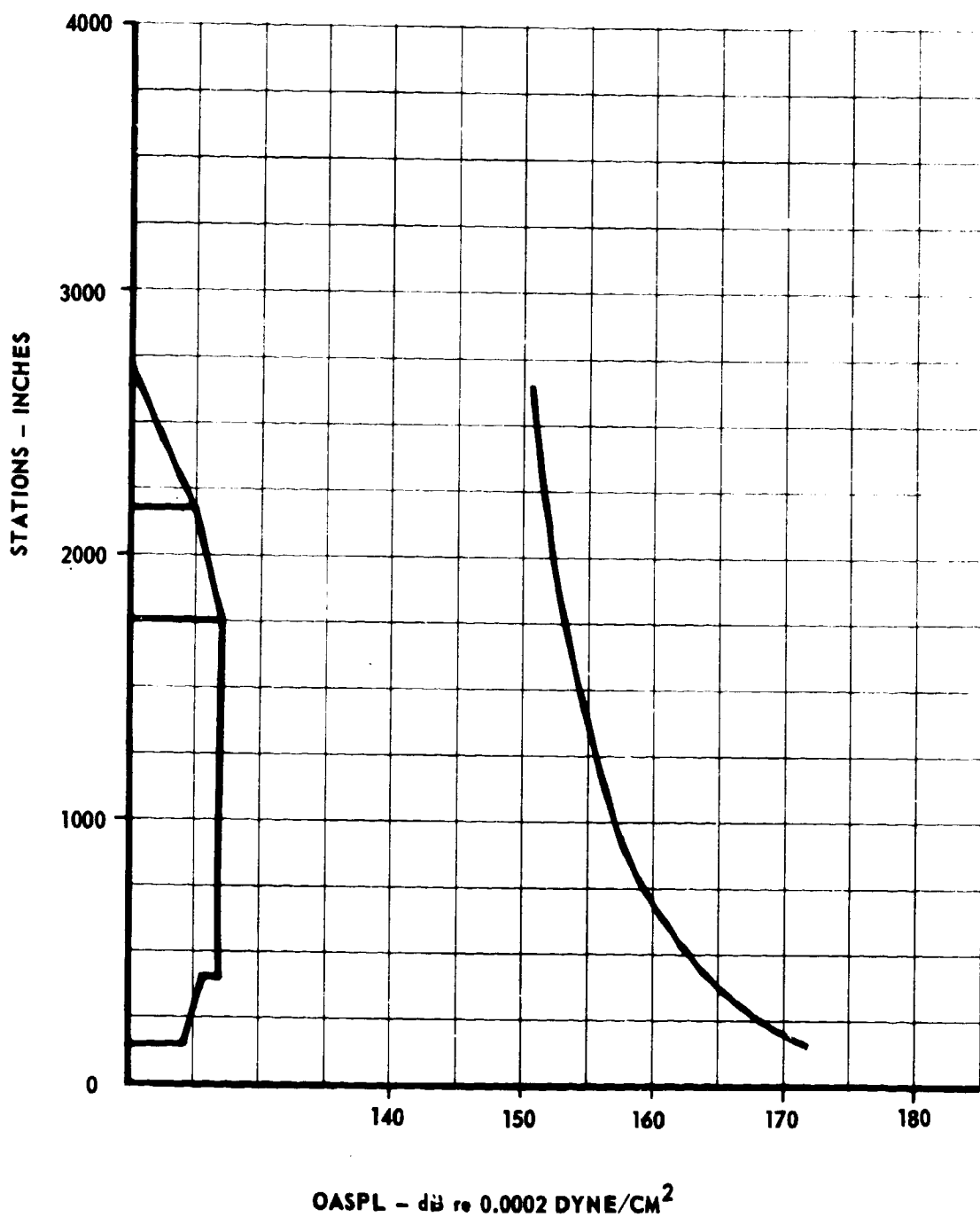
FIGURE 4.2.4.7-1   OVERALL SOUND PRESSURE LEVEL VERSUS STATION, MLLV
SINGLE STAGE TO ORBIT, VEHICLE ON PAD, SINGLE BUCKET
EXHAUST DEFLECTOR

198
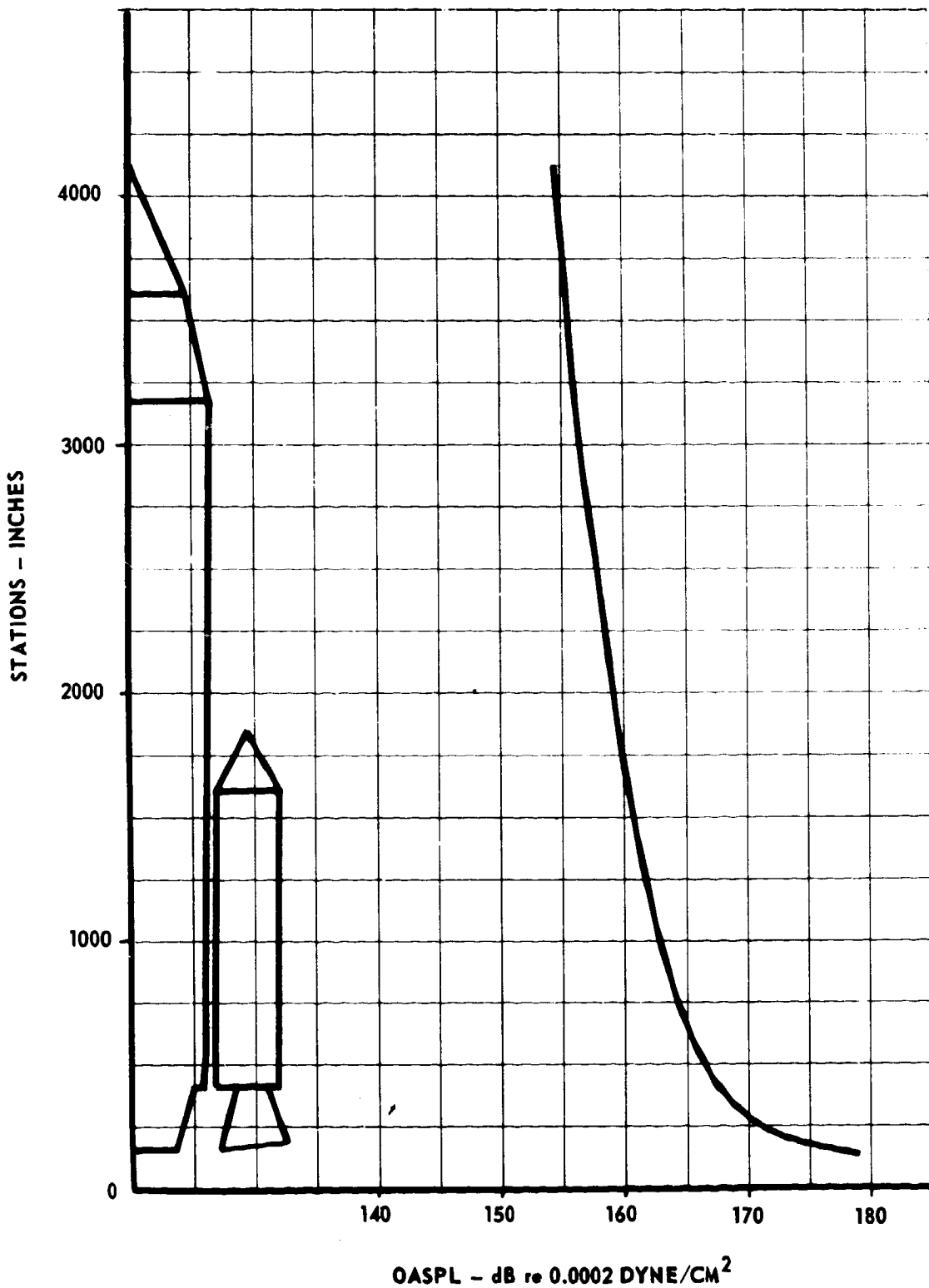
FIGURE 4.2.4.7-2   OVERALL SOUND PRESSURE LEVEL VERSUS STATION MLLV MAIN
STAGE PLUS EIGHT STRAP-ONS, ZERO STAGING, VEHICLE ON PAD,
SINGLE BUCKET EXHAUST DEFLECTOR

199

4.2.4.8   Vibration Environment

The affect of the vibration environment on the major structures of the MLLV
vehicle was investigated. A "worst case" sample, the MLLV zero staged on
the pad with a single bucket exhaust deflector, was used.

The vibration response of a typical panel of the MLLV thrust structure was
predicted by extrapolating acoustic and vibration data from S-IC firings. Panel
response was limited to the first mode assuming no coupling between panels
and no fatigue considerations. The assumptions and prediction techniques used
for the MLLV are the same as those used for the AMLLV vehicle described below:

$$\frac{G_A}{G_S} = \frac{P^2_A \; A_A \; \rho_S \; h_S}{P^2_S \; A_S \; \rho_A \; h_A}$$ (See Reference 4.2.4.8-1)

Where

   G^2 = response power spectral density g^2/cps

   P^2 = acoustic pressure power spectral density $(psi)^2/cps$

   A   = panel area - inch squared

   h   = panel thickness - inches

   ρ = panel material density - lb/in^3

   Subscript A = MLLV (predicted data)

   Subscript S = SATURN V S-IC (test data)

   The equivalent static pressure (Pe) acting on the panel is estimated by:
       $$P_e = G_A h_A \rho_A$$

The three sigma peak equivalent static pressure due to acoustic loading for the
MLLV was more severe than for the AMLLV and was estimated as 4.5 psi. The
three sigma peak equivalent static pressure for the AMLLV was estimated as 3.5 psi.

4.2.4.8-1   Barrett, R. E., "Techniques for Predicting Localized Vibratory
             Environments of Rocket Vehicles." NASA Technical Note D-1836.

4.2.4.8   (Continued)

Extrapolation for the response of the panel was limited to the first mode vibration response assuming no coupling between panels and no fatigue considerations. The acoustic and vibration test data were taken from the exterior skin of the S-1C thrust structure during stage static test firings. These data (transducers BA 5350.1, BA 37, BA 102D) were published in Reference 4.2.4.8-2.

The effects of this equivalent local load on the thrust structure, however, will be small compared to other loads. The affect of vibration on other major structures will also be negligible compared to other applied loads. However, the acoustic and vibration loads on components and secondary structures will be significant. Components and secondary structures must be packaged to reduce the effect of the acoustics and vibration. These items must be acoustically qualified.

4.2.4.9   Structural Criteria, Symbols and Definitions

The structural criteria for this study was the same as that used in the AMLLV (NASA Contract NAS2-4079) study. The Saturn V criteria was in turn the basis for that study. The following criteria, symbols and definitions apply to the preceeding load analyses.

a.   Definitions and Symbols. The following definitions and terms are used for the design of the MLLV to establish uniform nomenclature:

   1.   Factor of Safety, F.S. The factor of safety is the specified factor intended to account for uncertainty in design and manufacture of the vehicle.

   2.   Yield Factor of Safety, Y.F.S. The yield factor of safety is the specified factor intended to preclude detrimental yielding of the structure.

   3.   Ultimate Factor of Safety, U.F.S. The ultimate factor of safety is the specified factor intended to preclude structural failure.

   4.   Detrimental Yielding. Detrimental yielding is that amount of permanent set which would detract from the intended design performance of the structural component in question.

4.2.4.8-2   "Saturn S-1C - 503 Static Test, Vibration Acoustic Data" Boeing Document D5-13644-3.

4.2.4.9 (Continued)

5. **Structural Failure.** A structural failure is one which would preclude the accomplishment of the specified functions of the structural component in question.

6. **Strength Margin, S.M.** The strength margin is the percentage by which the allowable load or stress exceeds the design load or stress.

7. **Limit Load.** The limit load is the maximum load which the structure is expected to encounter during its normal service life.

8. **Design Yield Load.** The design yield load is the limit load multiplied by the specified yield factor of safety.

9. **Design Ultimate Load.** The design ultimate load is the limit load multiplied by the specified ultimate factor of safety.

10. **Limit Pressure.** The limit pressure is the maximum positive (outward) or negative (inward) pressure differential a pressure vessel is expected to encounter during its normal service life, excluding proof testing.

11. **Design Yield Pressure.** Design yield pressure is the limit pressure multiplied by the yield factor of safety.

12. **Design Ultimate Pressure.** Design ultimate pressure is the limit pressure multiplied by the ultimate factor of safety.

13. **Design Proof Pressure.** This is the pressure applied to every pressure vessel prior to its acceptance for service use and is equal to or greater than the limit pressure times the proof pressure factor (1.05).

14. **Design Proof Test Factor.** The design proof test factor is the desired factor intended to assure pressure vessel operational life in terms of any specified number of pressure loading cycles.

15. **Allowable Stress.** The allowable stress is the specified maximum stress to be used for design of the structure. The value used should have a specified exceedance probability associated with it, e.g., 99.0 percent. Derivation of the allowable stress must considered operating temperatures, biaxiability, interaction, fatigue, stability, joint efficiency, etc.

16. **Allowable Yield Stress.** The allowable yield stress is the specified stress which is not to be exceeded when the structure experiences design yield load.

202

4.2.4.9   (Continued)

17. Allowable Ultimate Stress. The allowable ultimate stress is the specified stress which is not to be exceeded when the structure experience design ultimate load.

18. Limit Temperature. The limit temperature is the maximum calculated temperature which will be applied to the structure under the specified conditions of operation.

19. Combined Loads. The combined load (N) is defined as the load per inch of circumference. This combined load includes simultaneous applications of bending moment, axial load, and ullage pressure.

$$N_t \text{ ultimate} = \left(\frac{BM\ (x)}{\pi R^2} + \frac{P\ (x)}{2\pi R} \right) 1.4 + \frac{P_{u\ max}\ (x) R}{2}$$

$$N_c \text{ ultimate} = \left(\frac{BM\ (x)}{\pi R^2} - \frac{P\ (x)}{2\pi R} \right) 1.4 - \frac{P_{u\ min}\ (x)\ R}{2}$$

N_t ultimate = ultimate combined tension load

N_c ultimate = ultimate combined combined compressive load

BM(x)   = bending moment at station x

P(x)   = axial load at station x

P_u min (x)   = minimum ullage pressure at station x

P_u max (x)   = maximum ullage pressure at station x

R   = radius at station x

Sign convention + tension load
                  − compression load

1.4 = factor of safety

The tank pressure at a particular station is defined as:

$\overline{P}$ (t)   = P_u max (t) + N (t) ρ h' (t)

P_u max (t) = maximum ullage pressure at time (t)

N (t)   = Load factor at time (t) − acceleration in g's

h'(t)   = height of the propellant above the station being investigated at time (t)

203

4.2.4.9   (Continued)

$\overline{P}(t)$ = limit pressure at time (t) and the station being investigated

ρ = propellant density

Tank bottom pressures are determined as a function of time. The tank pressure at various stations is determined for various flight times. These are then plotted as vehicle station versus pressure. The maximum envelope of these plots determines the limit design pressure. The ultimate design pressure is:

$$P_{ult} = 1.4 \; (P_{limit})$$

The ultimate design differential pressure (ΔP_{ult} across the common bulkhead) is determined by:

$$\Delta P_{ult} (t) = 1.4 \; (\text{LOX tank bottom pressure} - \text{minimum LH}_2 \text{ ullage} \\ \text{pressure})$$

20. Definitions of symbols used in preceeding tables.

η = Longitudinal load factor - acceleration in g's
W' = Vehicle weight forward of any vehicle station
D = Drag force effective at any vehicle station
P = Longitudinal force (distributed)
BM= Bending moment (distributed)
Pu = Ullage pressure
Nc = Combined compressive load
Nt = Combined tension load

b. Detailed Criteria

1. Structural Design Factors.

a. General Factors of Safety.

Yield   1.10
Ultimate   1.40

Where pressurization contributes to the load bearing capability of structure, a limit and ultimate factor of 1.0 shall be used on the minimum operating pressure for the condition being checked.

203.1

4.2.4.9   (Continued)

    b.   Propellant Containers.

Propellant Tanks	Flight & Propulsion Test Vehicles	
Proof Pressure	C_1 x (limit pressure)	①
Design Yield Pressure	1.10 x (limit pressure)	②
Ultimate Pressure	1.40 x (limit pressure)	②
For the MLLV stage C_1 = 1.05	③	
Flight and propulsion test vehicle negative (collapsing) pressure)		
Ground Handling Condition	2.50 x (limit negative pressure)	
Operating Condition	1.40 x (limit negative pressure)	

① C_1 is the proof test factor and is chosen to ensure pressure vessel service life and is obtained from published test data. The proof pressure envelopes the limit pressure such that the minimum value of proof pressure is equal to or greater than C_1 times limit pressure.

②   Because of room temperature proof testing, the room temperature guaranteed minimum allowable stress is used for structural sizing in the room to cryogenic temperature range.

③   According to the Saturn V test requirements, a proof test factor of 1.05 will guarantee five cycles of limit operation.

Propellant Feedlines   ④

Proof Pressure	1.50 x (max. operating pressure)
Design Yield Pressure	1.10 x (proof pressure)
Ultimate Pressure	2.50 x (max. operating pressure)
Negative (collapsing) pressure	2.50 x (limit negative pressure)

④   The maximum operating pressure shall include such system environmental effects as vehicle acceleration, etc.

2. Design Condition.

    a.   General. The booster will be designed to accept the load and mission requirements of MLLV.

    b.   Ground Handling, Transport, and Storage. Handling and transport loads shall not design primary structure.

4.2.4.9   (Continued)

    c. Design Winds.

        1. Ground Winds.

Structural design of large launch vehicles will assure a free-standing capability for the 99.9 percent probability ground wind during the strongest wind month. Propellant containers may be fueled or unfueled, pressurized or unpressurized

        2. Launch and Flight Winds.

Large launch vehicles will be capable of launch for 95 percent peak winds defined in Reference 4.2.4.9-1 and flight for the 95 percent probability quasi-steady state wind defined in Reference 4.2.4.9-1. Shears and gust values are obtained by reducing the 99 percent probability values by 15 percent. These probability of occurrence values are based on the strongest wind month, currently March. Reduction of shear and gusts values by 15 percent is to account for the simultaneity of these occurrences.

    d. Overpressure.

When the vehicle is on the launch pad and an adjacent vehicle is in an explosive hazard phase of countdown, blast overpressure protection will be accomplished by tank pressurization. The Environmental Protection System for the propellant containers shall be designed such that negative pressure conditions do not exist at any time during assembly, transportation, etc.

    3. Material Properties.

        a. Mechanical Properties.

Material mechanical properties will be in accordance with MIL-HDBK-5, supplemented with data from other approved sources, which will be referenced. Normally, "A" values from MIL-HDBK-5 will be used. The "B" values may be used where multiple load path structure exists if it can be demonstrated that there is an alternate load path which is capable of carrying limit load after the failure of any single element.

4.2.4.9-1 NASA TMX-53328, "Terrestrial Environment Criteria Guidelines for use in Space Vehicle Development," 1966 Revision.

4.2.4.9   (Continued)

       b.   Interaction and Stress Concentration.

         Appropriate interaction formulae will be used to determine
         the margins of safety where combined stresses exist.

       c.   Buckling and Stability.

         Statistical data will be used to establish buckling allowables.
         The 99 percent probability, 95 percent confidence curves will
         be used for preliminary allowables data.

c.   Special Criteria.

   1. Structural Yielding.

     There will be no significant structural yielding or failure, respectively,
     below limit and ultimate load or pressure.

   2. Combination of Internal Pressure and External Loads (Dynamic, Shock,
     Vibration, etc.).

     The stresses resulting from 1.10 x (limit or maximum operating pressure)
     shall be added to these resulting from 1.10 x (limit external loads), and
     this combination of stresses shall not exceed the allowable yield stress
     of the material at the temperature which will exist at the time the stresses
     will be applied.

     The stresses resulting from 1.40 x (limit or maximum operating pressure)
     shall be added to those resulting from 1.40 x (limit external loads), and
     this combination of stresses shall not exceed the allowable ultimate stress
     of the material at the temperature which will exist at the time the stresses
     will be applied.

   3. Stage Separation.

     Following burnout of strap-on or main stage, the expended stage must
     be separated from the remaining stages without damage to them or
     causing a deviation from their intended trajectory. The general factors
     of safety will be used for the separation condition.

4.2.4.9   (Continued)

d.   Structural Interfaces

1. Holddown Provisions.

The MLLV stage shall be designed to withstand the loads resulting from
thrust buildup, full thrust for a total of one second, and release as
in the normal launch sequence. The holddown provisions must also be
capable of withstanding the entire stage operating time with full TVC
deflection (for acceptance static test). Design shall include the resultant
rebound following an engine shutdown with a fully fueled MLLV vehicle.

4.2.5   Control Requirements

Using the aerodynamic, preliminary weight and structural dynamics data, as
reported in Sections 4.2.2, 4.2.3 and 4.2.4, respectively, analyses were
conducted to determine the following :

a.   Flight control system gains
b.   Thrust vector control (TVC) system duty cycle requirements
c.   Uncontrolled divergence rates
d.   Control force requirements during tail-off of strap-on stages
e.   Roll control

Control analyses were conducted on both the single stage to orbit vehicle and
the main stage plus eight strap-on stages plus three injection stage modules
vehicle. The control requirements for these two vehicles are representative of
the control requirements for all of the MLLV configurations. The resulting data
and the supporting calculations are reported in this section and in Volume VIII,
Appendix A.

The control data were used during the subsequent design activity to select and
size the vehicle subsystems and components required for the function of vehicle
control.

These analyses showed that the maximum requirements for main stage TVC will
occur during the time of maximum dynamic pressure of the single-stage-to-orbit
trajectory. Considering scatter terms (as defined below), a maximum effective
gimbal angle of approximately 3.9 degrees will be required.

Prior analyses, during the reference study, showed that the full size AMLLV
vehicle will have marginal uncontrolled divergence rates. Analyses of the half-
size MLLV vehicles showed that scaling down vehicle size will further increase
the uncontrolled divergence rates. The MLLV uncontrolled divergence rates will
be inadequate, as judged by current requirements for man rated vehicles, because
of insufficient time to double amplitude. The current requirements are based on a

207

4.2.5   (Continued)

two second decision and response time for man in the control loop to react to a
vehicle malfunction.At the worst time in the trajectory, the angle of attack will
be approximately 10 degrees. After two seconds, considering the uncontrolled
divergence rates, the MLLV vehicles will have an angle of attack in excess of
20 degrees. (Under previous studies, it was determined that instability exists
with the Apollo nose cone shape at an angle of attack of 17 degrees. Therefore,
with the 20 degree condition existing at the end of two seconds, the MLLV will be
unstable. This assumes that the MLLV nose cone shape and the Apollo nose cone
shape have similar stability characteristics.) When a system malfunction occurs,
the instrument unit will direct the TVC system to place the engines in a null
position; therefore, means of overcoming the instability cannot be achieved with a
TVC system.

Correction of the above problem can be achieved by several methods. These are:

a. The addition of fins or the addition of a flared aft skirt to move the center
   of pressure aft.

b. The use of a computer control system to replace the two second response
   rate of man with a quicker response capability.

c. The use of additional control feedback loops (to supplement attitude/atti-
   tude rate) to reduce the angle cf attack and thus permit greater response
   time.

The use of fins would provide the time to double amplitude required, and would
decrease the TVC requirements for the liquid engine system. The required fin
surface area is approximately 100 square feet each (total of four fins - 400 square
feet). The TVC requirements will be reduced from 3.9 degrees to approximately
three degrees.

Design Winds

First stage boost control requirements are dictated by the magnitude of the wind
that the boost vehicle must pass through. For analyses of flight times other than
launch, the design wind velocity profile was constructed at 95 percent probability
of occurrence. Shear and gust velocity values were obtained by reducing the 99
percent probability of occurrence by 15 percent. These probability of occurrence
velocity values were based on the strongest wind month, March. Reduction of the
shear and gust velocity values by 15 percent accounted for the probability of
simultaneity of these occurrences. Statistical wind data was obtained from NASA
Document TM-X53328 (Reference 4.2.4.9-1).

4.2.5   (Continued)

Design and Construction Tolerances, i.e., "Scatter Terms"

Consideration was given to each of the scatter terms listed below. Simulations
were made of the vehicle response to design wind conditions with the vehicle
described by a set of differential equations having fixed coefficients. These
simulations were made with "scatter terms" applied individually in both the plus
and minus directions. The results of the simulations were combined with each
term taken in the most adverse direction using the root sum squared (RSS)
technique. Several trajectory time points were used to arrive at an envelope of
maximum design points for nozzle deflection, angle of attack, etc.

The single-stage-to-orbit vehicle scatter terms included the following:

a.   Axial center of gravity location $\pm 10"$
b.   Thrust alignment in the nozzle   Combined equivalent of
c.   Nozzle alignment with the vehicle   105 minutes/engine (RSS
     centerline   value for 24 engines =
d.   Thrust vector deflection system   0.309 degrees)
     compliance.
e.   Thrust variance $\pm 1.5\%$
f.   Center of pressure location ± 0.5 Caliber
     (aerodynamic)
g.   Side force coefficient ± 0.2/radian
h.   Lateral center of gravity location $\pm 2"$
i.   Gains $\pm 10\%$

Additional or modified scatter terms for the vehicle configurations with the strap-
on stages included the following solid motor scatter terms:

a.   Thrust variation ($\pm 2\%$)
b.   Burn time variance (± 3 seconds)
c.   Decay time to ten percent nominal thrust at burnout (15 seconds)

4.2.5.1   Single-Stage-To-Orbit Vehicle Control Requirements

Flight Control System Gains

The first body bending mode frequency of the MLLV single-stage-to-orbit launch
vehicle was found to be 4.88 hertz. Rigid control frequency was selected to be
one fourth of this value to avoid control-bending mode coupling. A conventional
damping ratio of 0.7 was used and the flight control system gains calculated. These
data are presented in Figure 4.2.5.1-1.
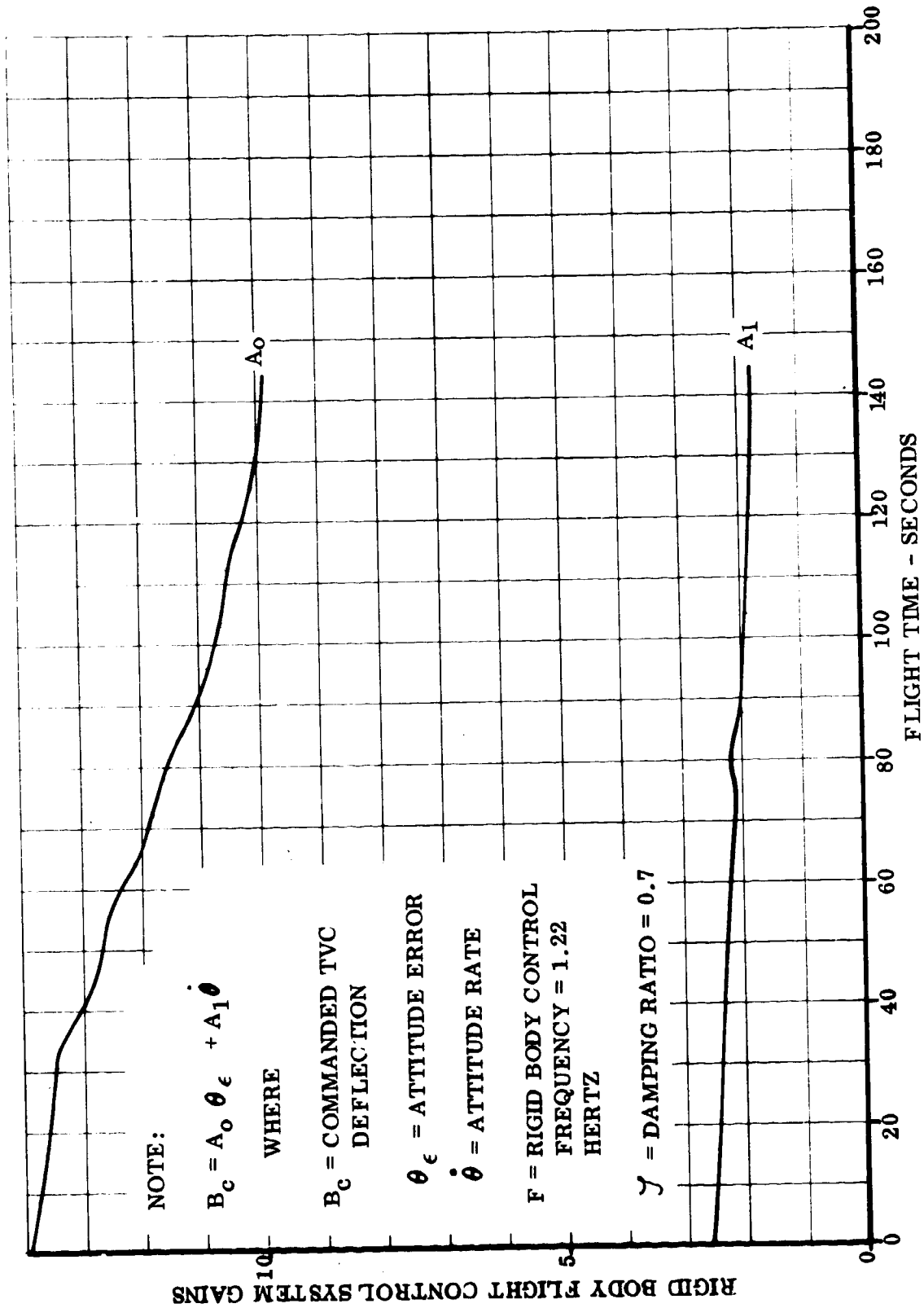
FIGURE 4.2.5.1-1 FLIGHT CONTROL SYSTEM GAINS (SINGLE-STAGE-TO-ORBIT VEHICLE)

NOTE:

$B_c = A_o \theta_\epsilon + A_1 \dot{\theta}$

WHERE

B_c = COMMANDED TVC DEFLECTION

θ_ϵ = ATTITUDE ERROR

$\dot{\theta}$ = ATTITUDE RATE

F = RIGID BODY CONTROL FREQUENCY = 1.22 HERTZ

γ = DAMPING RATIO = 0.7

FLIGHT TIME - SECONDS

RIGID BODY FLIGHT CONTROL SYSTEM GAINS

4.2.5.1   (Continued)

Thrust Deflection Requirements

Selection of the design wind was based on the gust peak occurring at the time maximum dynamic pressure occurred. NASA design wind build-up procedures and post peak behavior, presented in NASA TMX-53328 (Reference 4.2.4.9-1), were followed in completing the construction (see Figure 4.2.5.1-2).

Scatter terms, normally used at max q only on Saturn V design, were applied throughout the MLLV first stage flight in the RSS fashion. Figure 4.2.5.1-3 presents the required thrust deflection envelope for the single-stage-to-orbit vehicle.

Uncontrolled Divergence Rates

The current Saturn V design philosophy requires that time to double amplitude must exceed two seconds to meet man-rating criteria. Figure 4.2.5.1-4 presents time to double amplitude versus flight time for the uncontrolled MLLV single-stage-to-orbit vehicle, both with and without scatter terms considered. In both cases, time to double amplitude was found to be less than for the current minimum specified for man-rating. The addition of fins or a flared skirt could correct this condition (as discussed in Section 4.2.5 above).

4.2.5.2   Main Stage Plus Eight Strap-Ons Plus A Three Module Injection
           Stage Vehicle Control Requirements

Flight Control System Gains

The rigid body flight control frequency was selected to be one fourth of the first body bending mode frequency (1.06 hertz) to avoid a structural-control coupling problem. Figure 4.2.5.2-1 presents the flight control system gains for the pitch (yaw) plane.

Thrust Deflection Requirements

Figure 4.2.5.2-2 shows the design wind used in identifying the maximum duty cycle. It was constructed by the conventional techniques discussed in NASA TMX-53328 (Reference 4.2.4.9-1).

Scatter terms were applied, using the root mean sum squared technique, in those parameters used to describe the launch vehicle for control analyses. The required SRM thrust deflection envelope is shown in Figure 4.2.5.2-3.
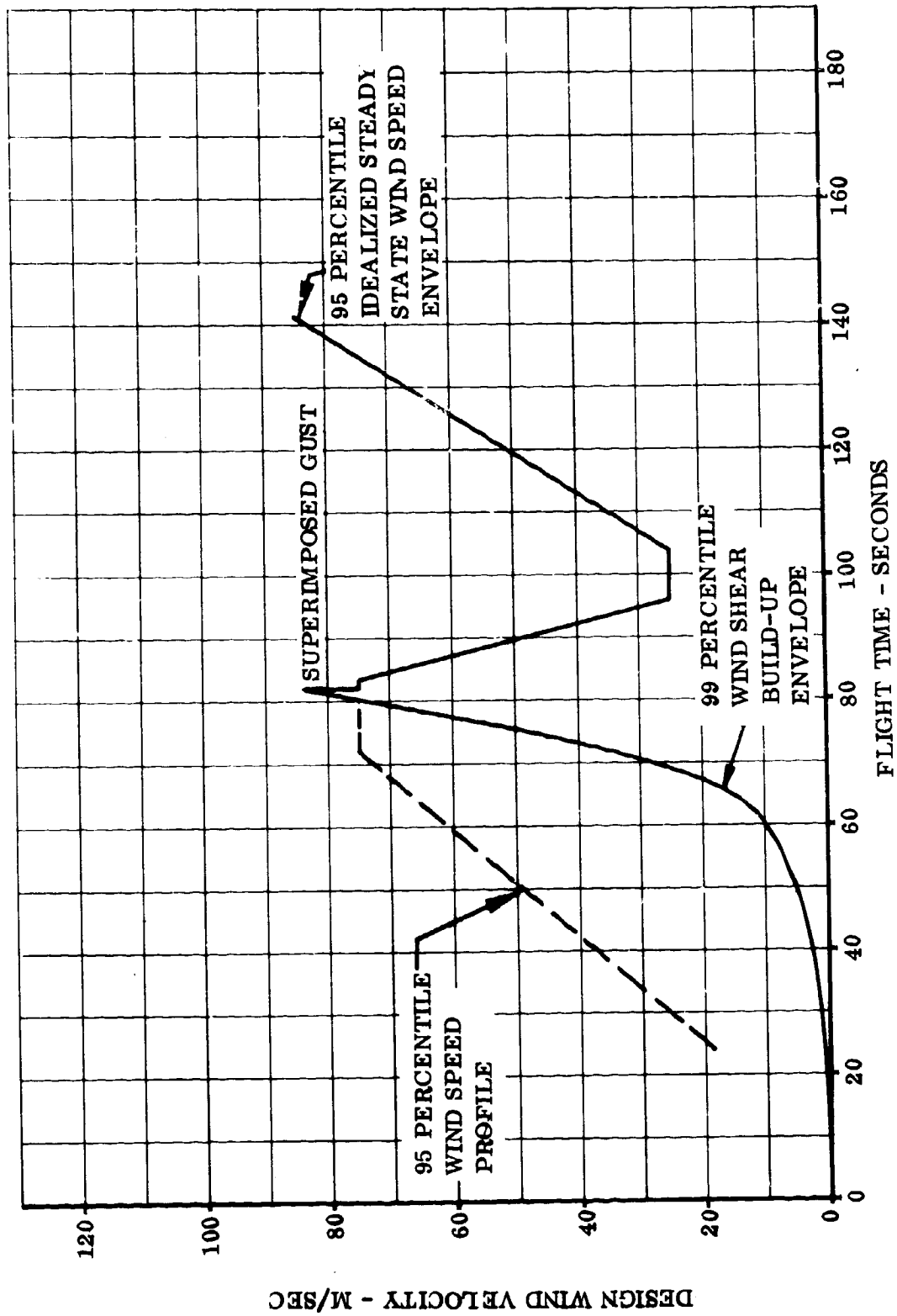
FIGURE 4.2.5.1-2 DESIGN WIND FOR DUTY CYCLE DEFINITION (SINGLE-STAGE-TO-ORBIT VEHICLE)

212

NOTE:

- APPLIED TOLERANCES

  CG $\pm$ 10 INCHES
  lCG $\pm$ 2 INCHES
  $Cz\alpha \pm$ 0.2 1/RADIAN
  CP $\pm$ 340 INCHES
  GAINS $\pm$ 10%
  THRUST $\pm$ 1.5%
  β $\pm$ 0.309 DEGREE

- .95 PERCENTILE DESIGN WIND

WITH SCATTER TERMS

RSS THRUST DEFLECTION - DEG.

FLIGHT TIME - SECONDS
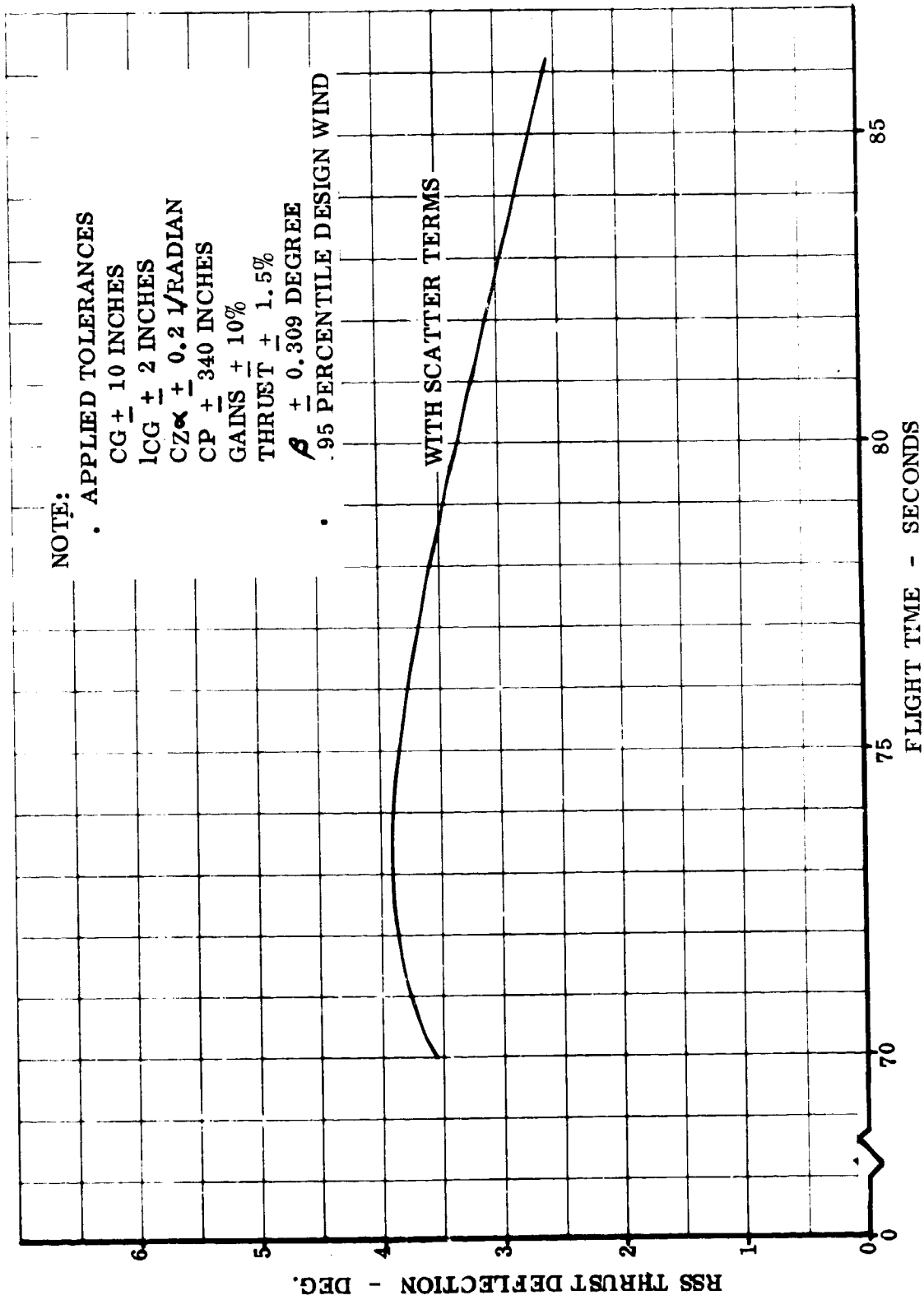
FIGURE 4.2.5.1-3   RSS THRUST DEFLECTION (SINGLE STAGE TO ORBIT VEHICLE)
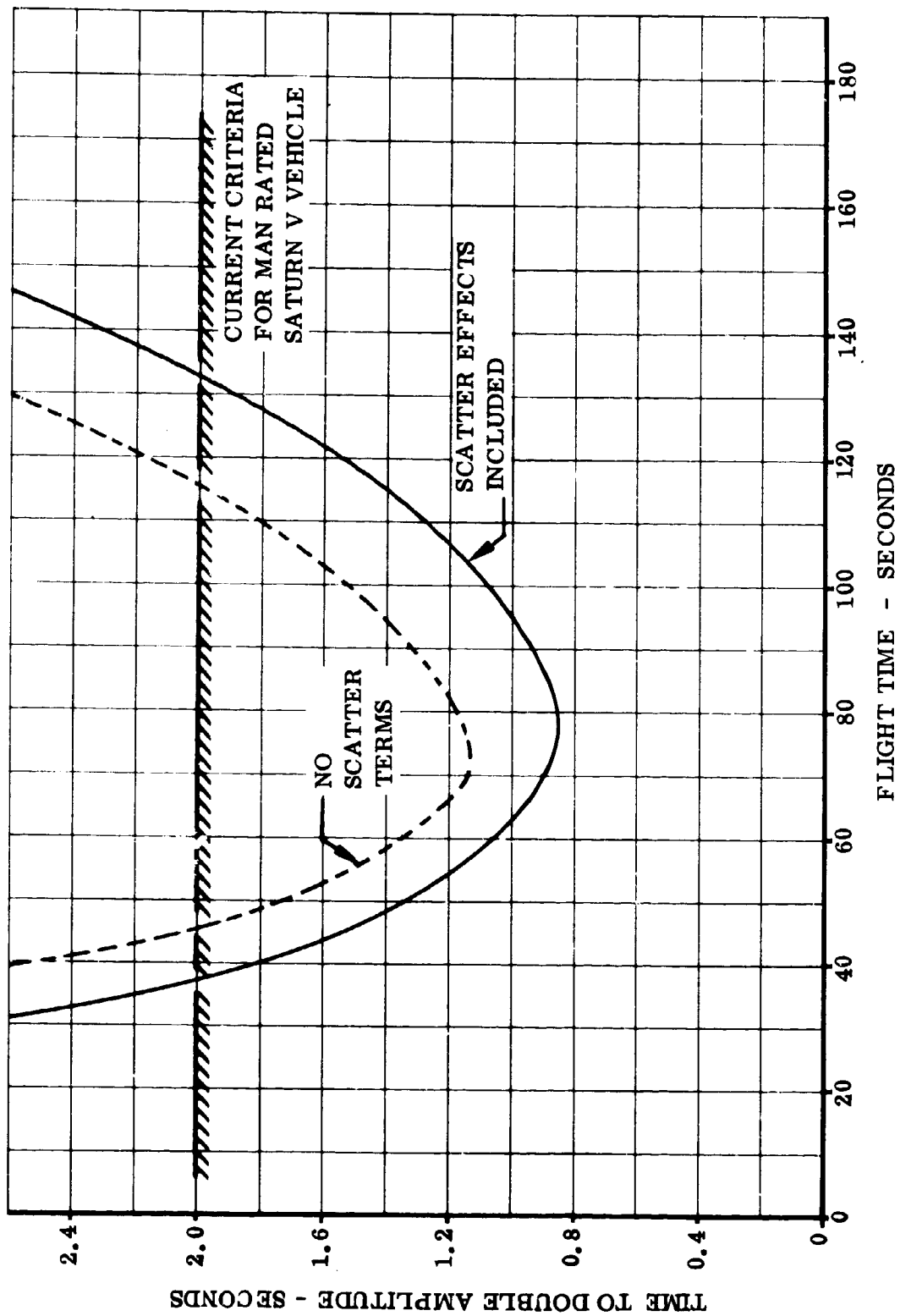
FIGURE 4.2.5.1-4 UNCONTROLLED DIVERGENCE RATE FUNCTION (MLLV SINGLE-STAGE-TO-ORBIT VEHICLE)

NOTE:

$B_c = A_o\theta_\epsilon + A_1\dot{\theta}$

WHERE

B_c = COMMANDED TVC DEFLECTION

θ_ϵ = ATTITUDE ERROR

$\dot{\theta}$ = ATTITUDE RATE

F = RIGID BODY CONTROL FREQUENCY = 0.265 HERTZ

γ = DAMPING RATIO – 0.7

FLIGHT TIME – SECONDS

RIGID BODY FLIGHT CONTROL SYSTEM GAINS
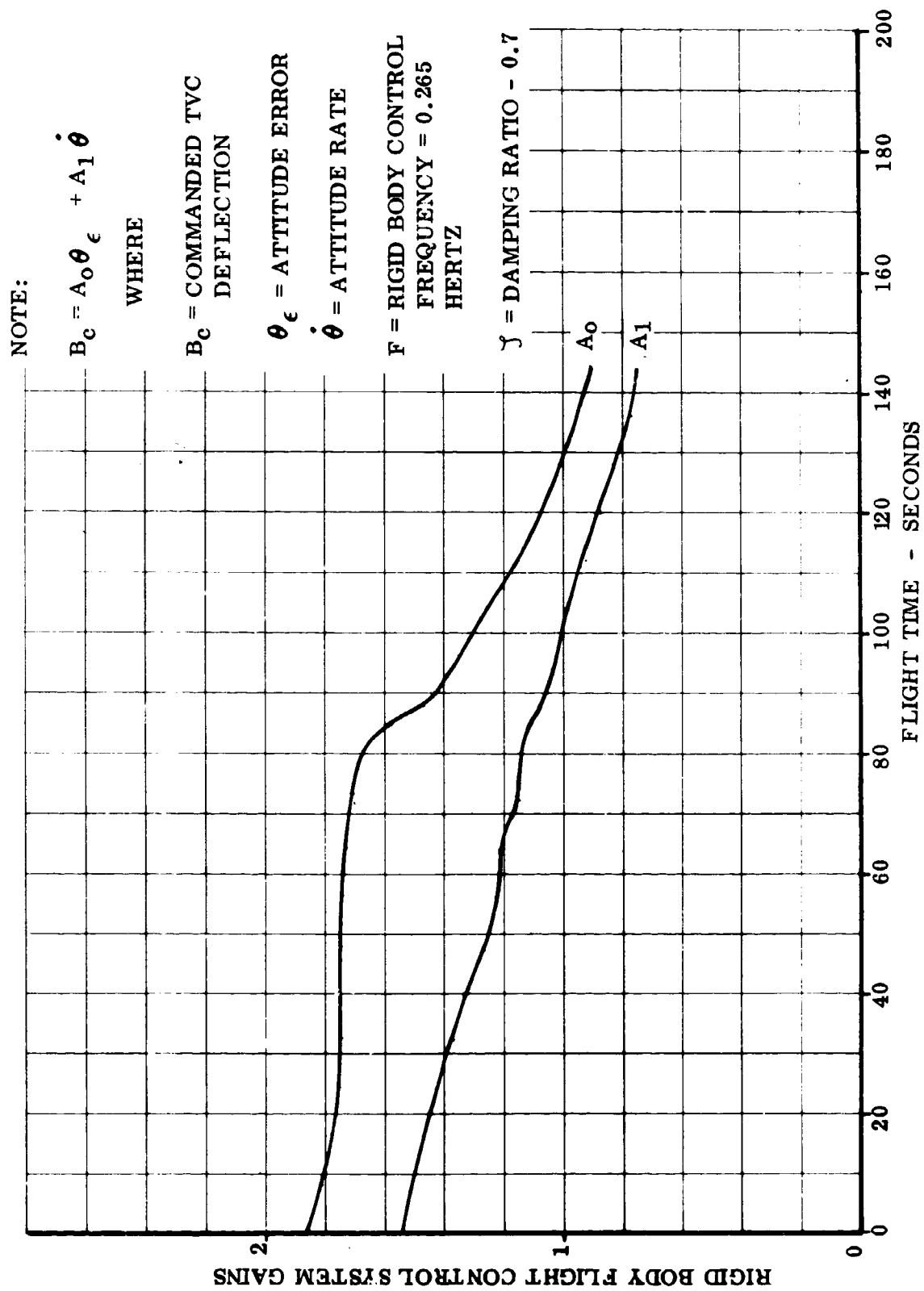
FIGURE 4.2.5.2–1   FLIGHT CONTROL SYSTEM GAINS FOR THE MLLV MULTICHAMBER CORE + 3 MODULE INJECTION STAGE + 8 SRM
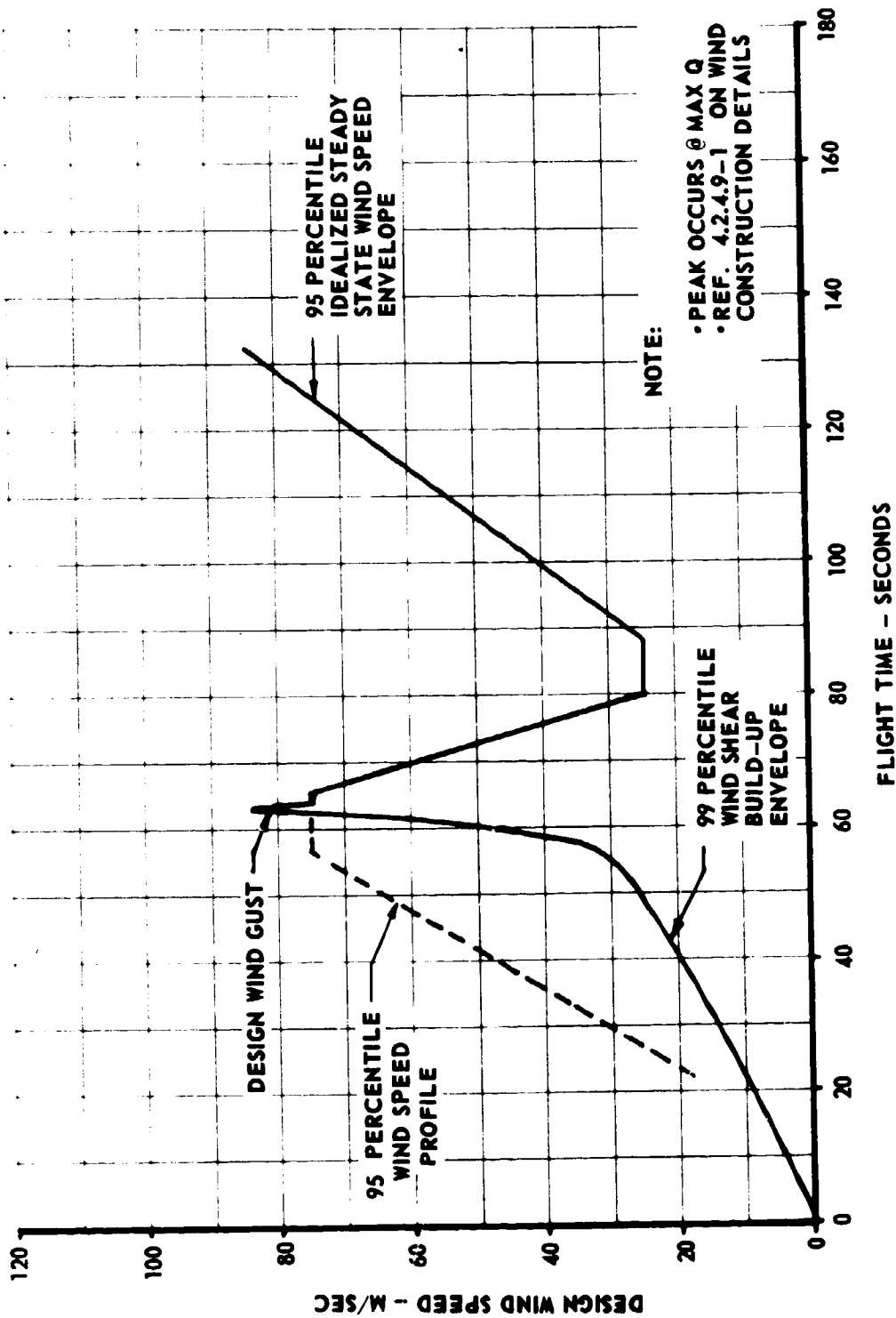
FIGURE 4.2.5.2-2   DESIGN WIND CONDITION MLLV MAIN STAGE PLUS EIGHT
STRAP-ONS

216

NOTE:

APPLIED TOLERANCES

CG $\pm$ 10 INCHES

l_{CG} $\pm$ 2 INCHES

$CZ\alpha$ $\pm$ 0.2 1/RADIAN

CP $\pm$ 340 INCHES

GAINS $\pm$ 10%

THRUST $\pm$ 1.5%

β $\pm$ 0.877 DEGREE

95 PERCENTILE DESIGN WIND

SCATTER TERMS INCLUDED

FLIGHT TIME - SEC.

RSS THRUST DEFLECTION - DEG.
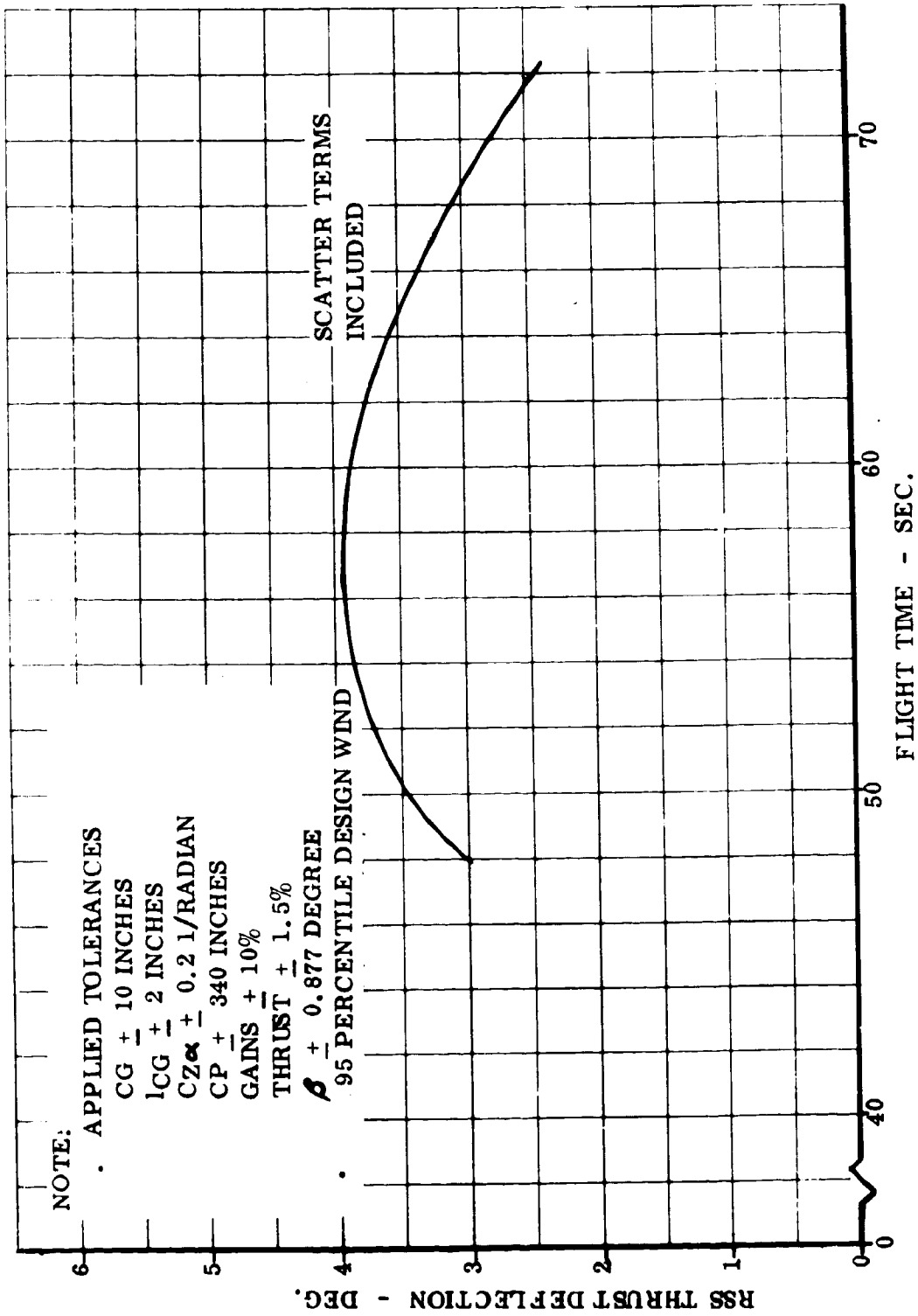
FIGURE 4.2.5.2-3   RSS THRUST DEFLECTIONS FOR THE MLLV MULTICHAMBER CORE + 3 MODULE
INJECTION STAGE + 8 SRM

217

4.2.5.2   (Continued)

Uncontrolled Divergence Rates

Under current man-rating criteria, this vehicle would not be acceptable due to the short times to double amplitude. Time to double amplitude versus flight time, both with and without scatter, are shown in Figure 4.2.5.2-4. These times can only be increased to acceptable levels by reducing the vehicles static instability as previously discussed.

Control Force Requirements During SRM Tail Off

Root summed squared deviations in solid rocket motor burn times were identified and the maximum upsetting moments evaluated. These are compared with the minimum control torques available as shown in Figure 4.2.5.2-5. This figure shows that an excess of control torque is available to offset off-nominal and environmental perturbations. No additional control torque sources are required.

Roll Control

The multichamber/plug propulsion system will utilize liquid hydrogen for base plug cooling. This hydrogen will then be fed to a gas generator (together with LOX) and burned to produce base bleed gases which will reduce base drag. The low deflection requirements for roll control will permit these base bleed gases to be used for roll control.

The toroidal/aerospike propulsion system also uses liquid hydrogen for base plug cooling. This hydrogen can also be diverted for roll control when required by modification to base plug cooling system.

When the vehicle configurations employ strap-on stages, roll control will be provided by the solid motors through the use of the SRM stage thrust vector control system. After separation of the SRM stages from the vehicle, the core stage will obtain roll control as described in the previous paragraph.

4.2.6   Separation and Ullage Impulse Requirements

Analyses were conducted to determine the requirements for separation, retro and/or ullage rockets. The following conditions were evaluated:

a. Main stage and injection stage separation
b. Injection stage ullage
c. Injection stage and payload separation
d. Strap-on stage separation

The data were developed considering the aerodynamic loads and the relative performance of the various vehicle stages as obtained from the preliminary vehicle sizing and trajectory analyses.
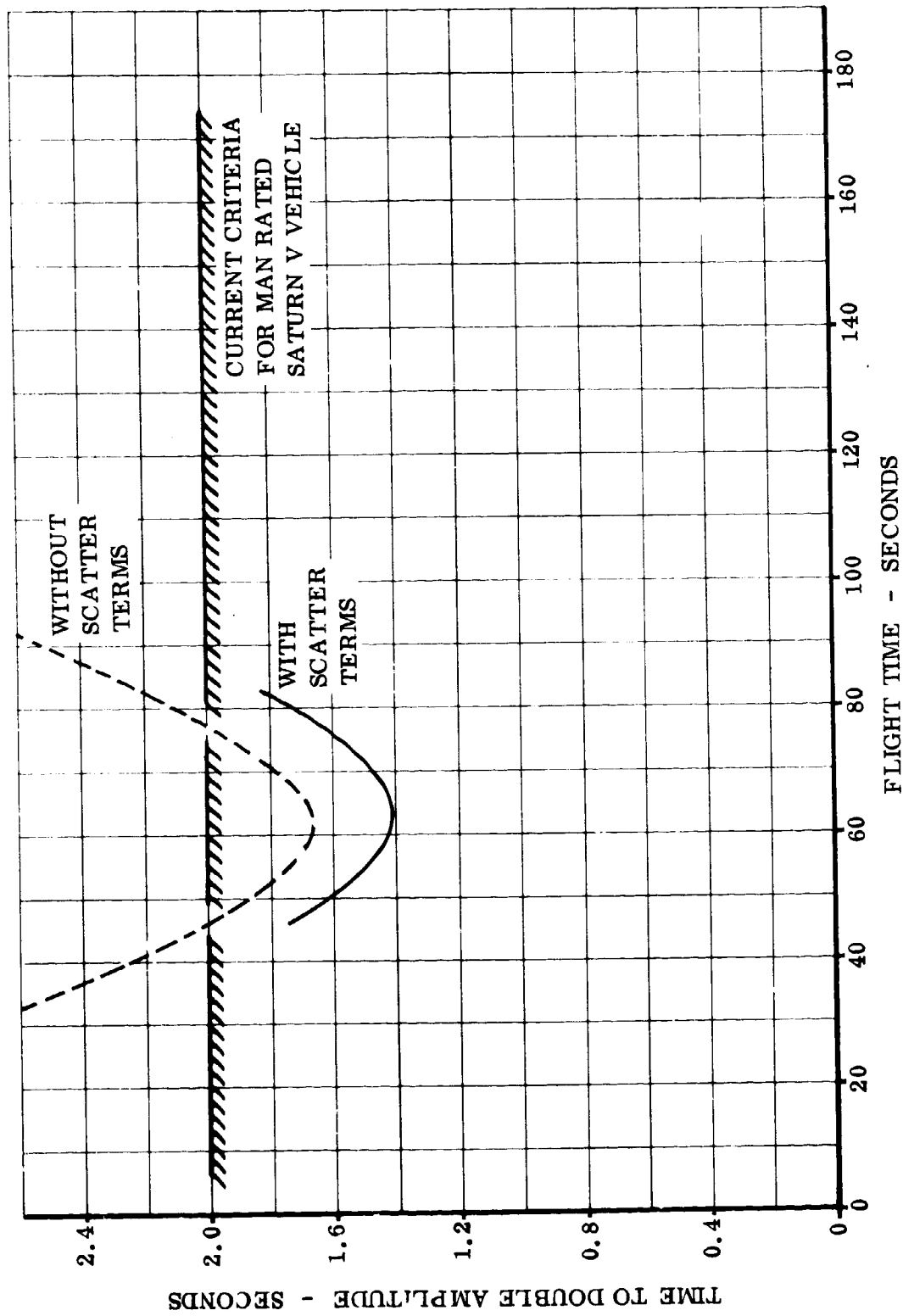
FIGURE 4.2.5.2-4 A MEASURE OF UNCONTROLLED DIVERGENCE RATES
MLLV MAIN STAGE + (8) STRAP-ONS PLUS A THREE
MODULE INJECTION STAGE
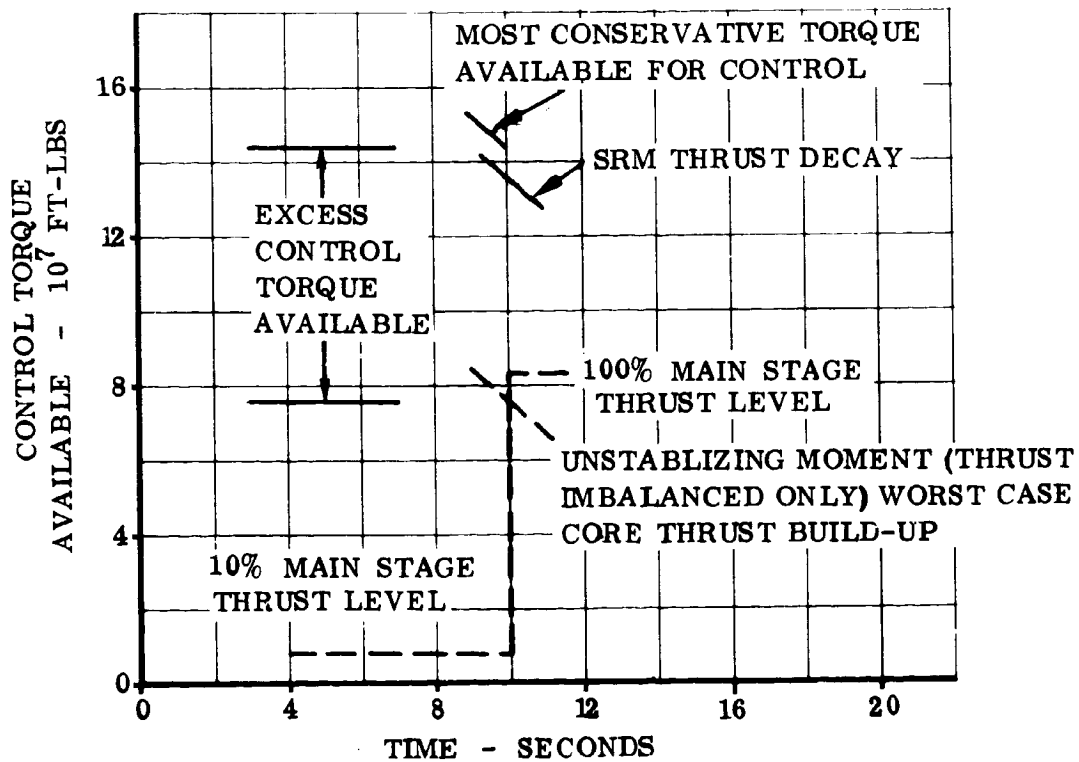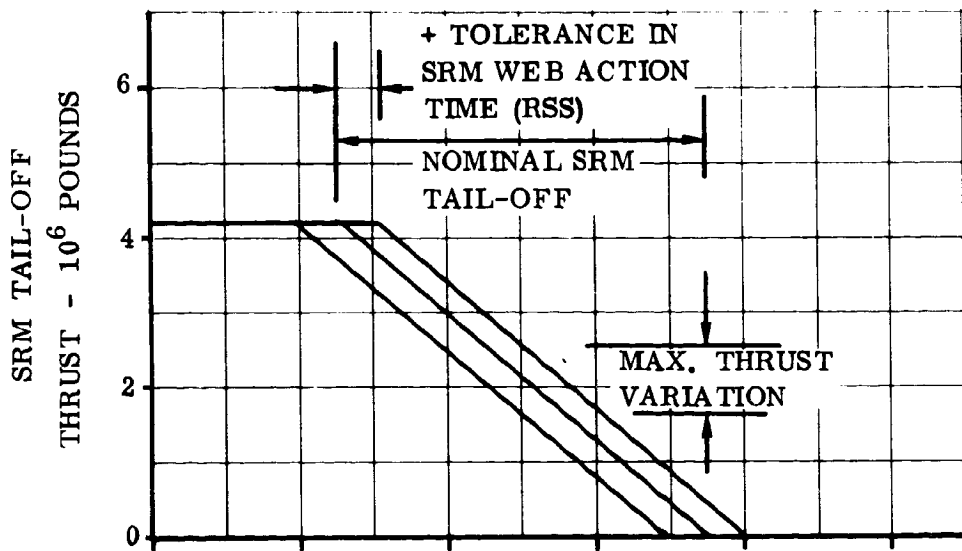
FIGURE 4.2.5.2-5   CONTROL REQUIREMENTS - MLLV MAIN STAGE + (8)
STRAP-ONS PLUS A THREE MODULE INJECTION STAGE

4.2.6   (Continued)

The following criteria were used to establish these thrust requirements:

a. Retrorocket and Ullage Rocket Operations – Separation will be possible when one retrorocket and one ullage rocket are inoperative in the worst possible combination.

b. Dynamics – Separation will be free of collision. Engines on the continuing main stage, during strap-on stage separation, will be operative and the control system acting.

In the absence of other definitive criteria, existing Saturn V criteria were applied.

The results of these analyses were used in subsequent design activity to size the rockets to provide the necessary separation, retro and ullage functions.

4.2.6.1   Main Stage/Injection Stage Separation

Figure 4.2.6.1-1 presents the spent main stage retro acceleration as a function of the time necessary for the injection stage engines to clear the main stage forward skirt. It was assumed that the retro thrust will be applied at a constant level until engine clearance is achieved, then terminated. At any specific clearance time, the associated required retro thrust value can be determined. The product of the time and the associated retro thrust, therefore, is the required separation impulse for that selected time. As clearance time requirements are increased, the necessary separation impulse is reduced as indicated on the figure.

Figure 4.2.6.1-2 shows the effect of the percentage inoperative retro thrust on injection stage engine clearance time and main stage vehicle rotation assuming a "g" separation design condition. It was assumed that all of the inoperative thrust will be on one side of the main stage so that it produces maximum torque. As shown, inoperative retro thrust will have only a minor effect on clearance time, but will have a significant effect on main stage rotation. When 16.61 percent of the retro thrust is inoperative, collision will occur between the main stage and injection stage. This condition applies only for the condition where the full retro thrust will result in a 2 "g" main stage retro acceleration. If the design condition is for a smaller retro acceleration level, a smaller percentage of inoperative retro thrust will then cause similar impact conditions.

Longer burning times for the retro system to provide injection stage engine clearance will result in smaller main stage retro impulse requirements. With smaller retro impulses, however, inoperative retro thrust becomes more critical. The parametric data presented may be used in the selection of motors for injection stage ullage and payload/injection stage separation.

Supporting calculations for this data are shown in Volume VIII, Appendix A.
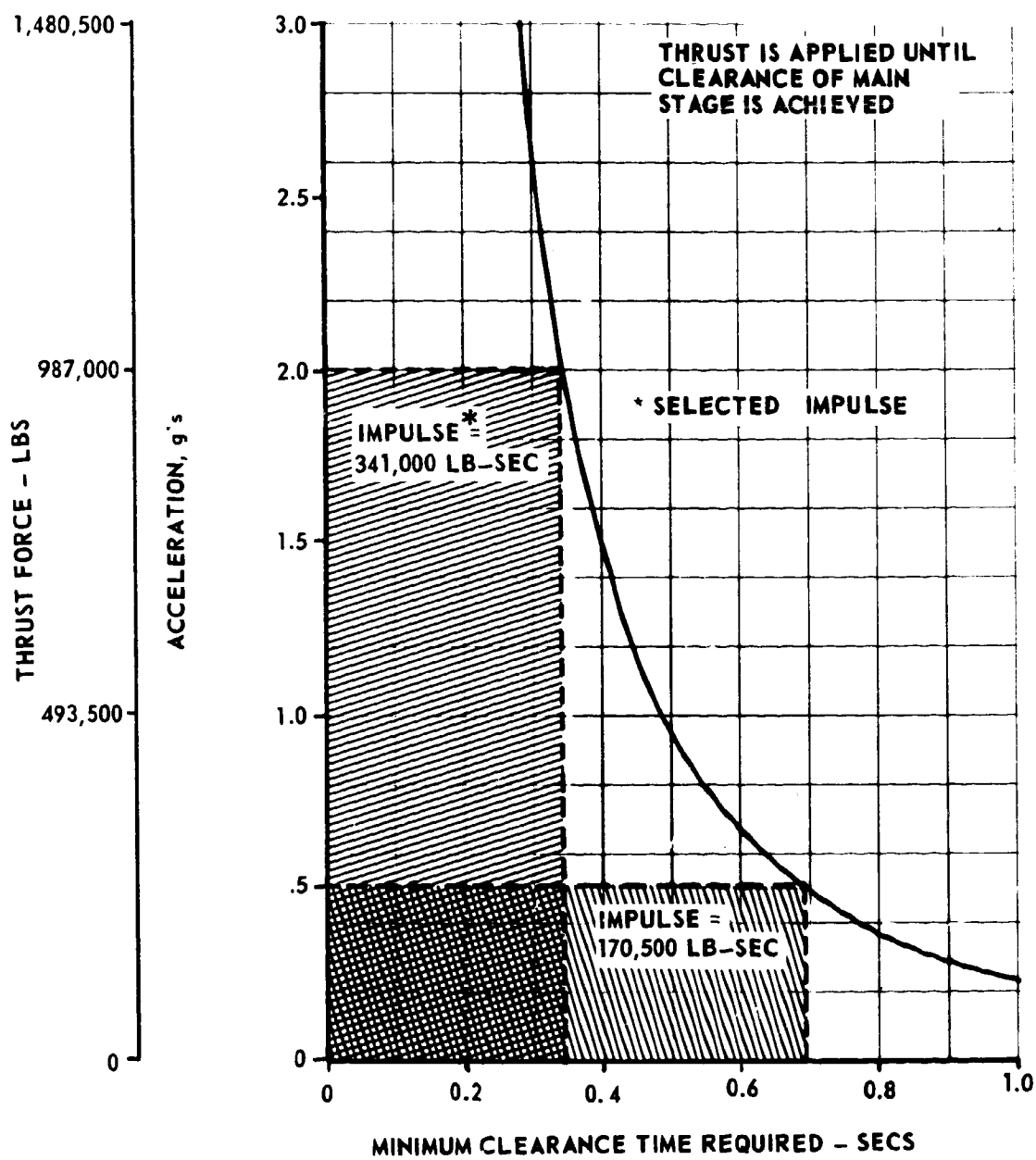
FIGURE 4.2.6.1-1   MAIN STAGE RETRO ACCELERATIONS AND MINIMUM
CLEARANCE TIMES

MAXIMUM ACCELERATION = 2 g's
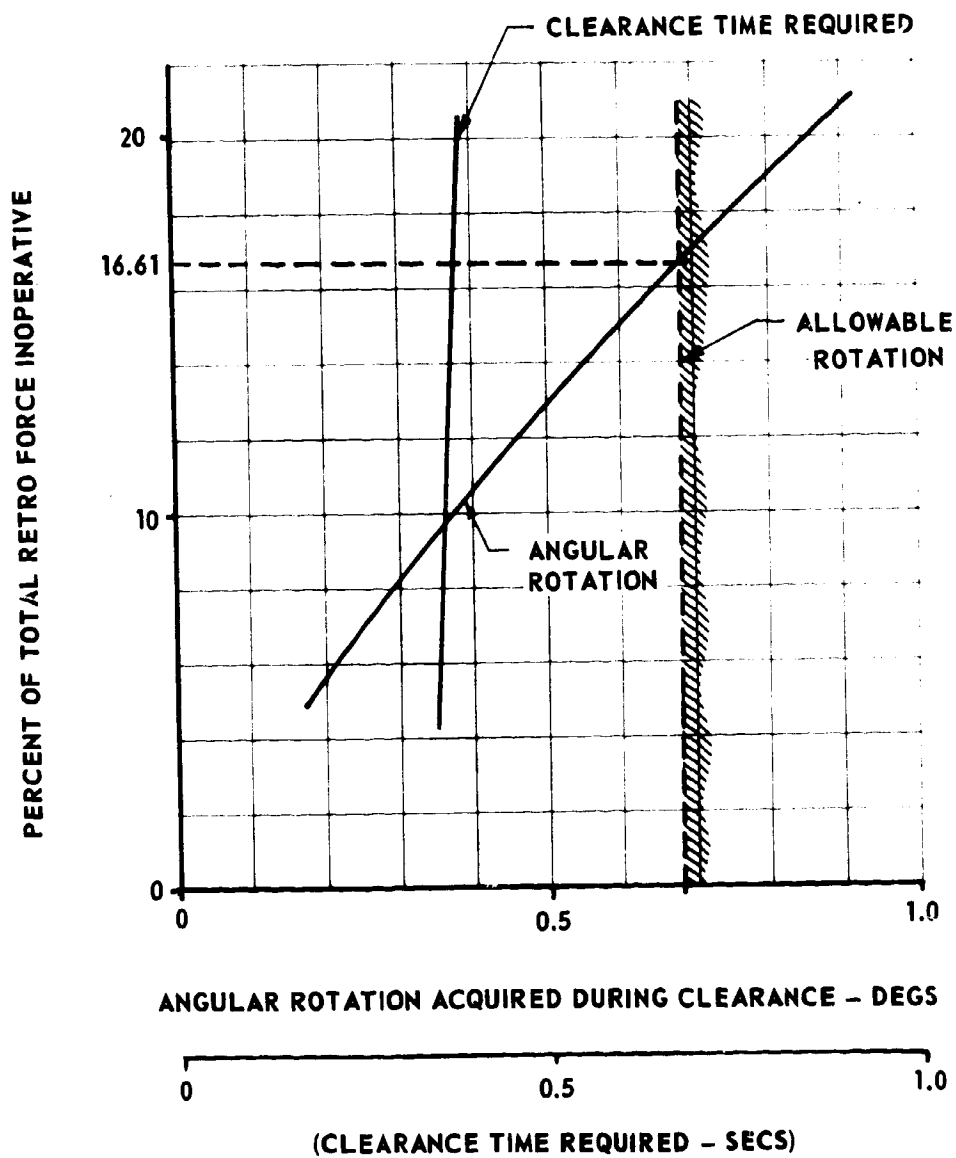
FIGURE 4.2.6.1-2   THE EFFECTS OF INOPERATIVE RETRO THRUST

4.2.6.2 Injection Stage Ullage

Figure 4.2.6.2-1 shows the three module injection stage ullage motor burn time as a function of ullage acceleration for lines of constant impulse.

The selected design point, considering propulsion system requirements (0.02 "g" for 5 seconds) for the MLLV configuration is shown for reference. The design condition requires an ullage impulse of 265,000 lb-sec. If further study should indicate the desirability of a different design point, Figure 4.2.6.2-1 can be used to estimate the required impulse.

4.2.6.3 Injection Stage/Payload Separation

Figure 4.2.6.3-1 shows the required payload/injection stage separation motor burn time for various retro acceleration levels. Impulse lines corresponding to final separation velocities of 5, 10, and 20 ft/sec are shown. For a desired separation velocity, the "g" level and burn time can be selected from this figure.

Supporting calculations for this data are shown in Volume VIII, Appendix A.

4.2.6.4 Strap-On Stage Separation

The shape and size of main stage exhaust plume flow fields affect the separation requirements for the strap-on stages. When the spent strap-on stages enter the main stage exhaust plume, a torque will be applied to the spent stage causing it to tumble. The tumbling stage could collide with the main stage. For this reason, preliminary calculations of the extent of main stage exhaust plume formation were made for the two main stage engine systems currently under consideration for MLLV.

The analysis made use of the NASA/Lewis Thermochemical Equilibrium Program (Reference 4.2.6.4-1) to generate chamber temperature for a given chamber pressure and LOX/LH_2 mixture ratio and to generate values of the ratio of specific heats at various area ratios downstream of the throat.

Reference 4.2.6.4-1 - NASA TN-D-1454, "A General 7090 Computer Program for Computation of Chemical Equilibrium Compositions, Rocket Performance and Chapman-Jouguet Detonations", S. Gordon, October, 1962
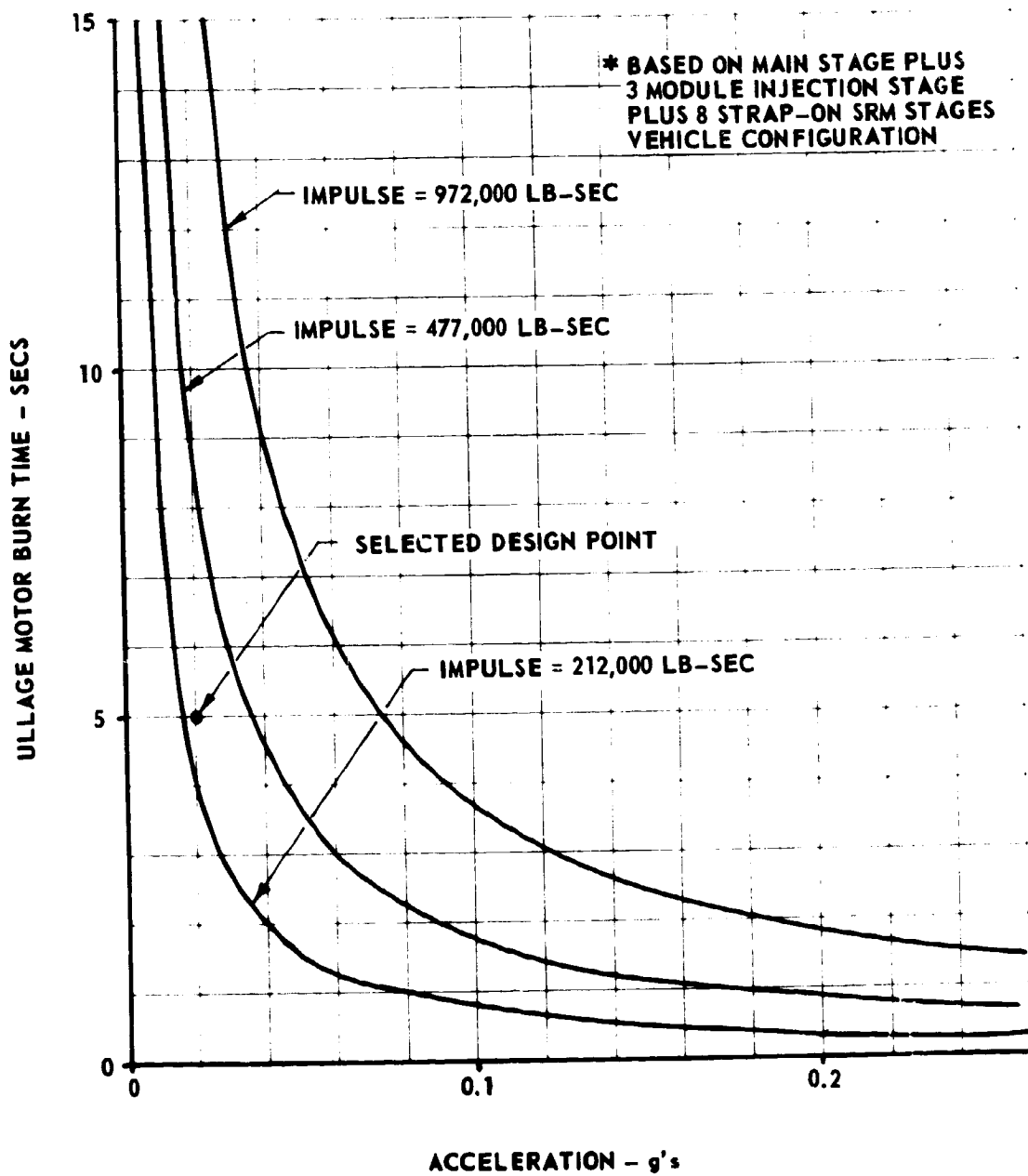
FIGURE 4.2.6.2-1 TOTAL ULLAGE IMPULSE FOR INJECTION STAGE

EMPTY INJECTION STAGE MASS = 3,700 SLUGS (3 MODULE INJECTION STAGE)
THRUST = WEIGHT x g's
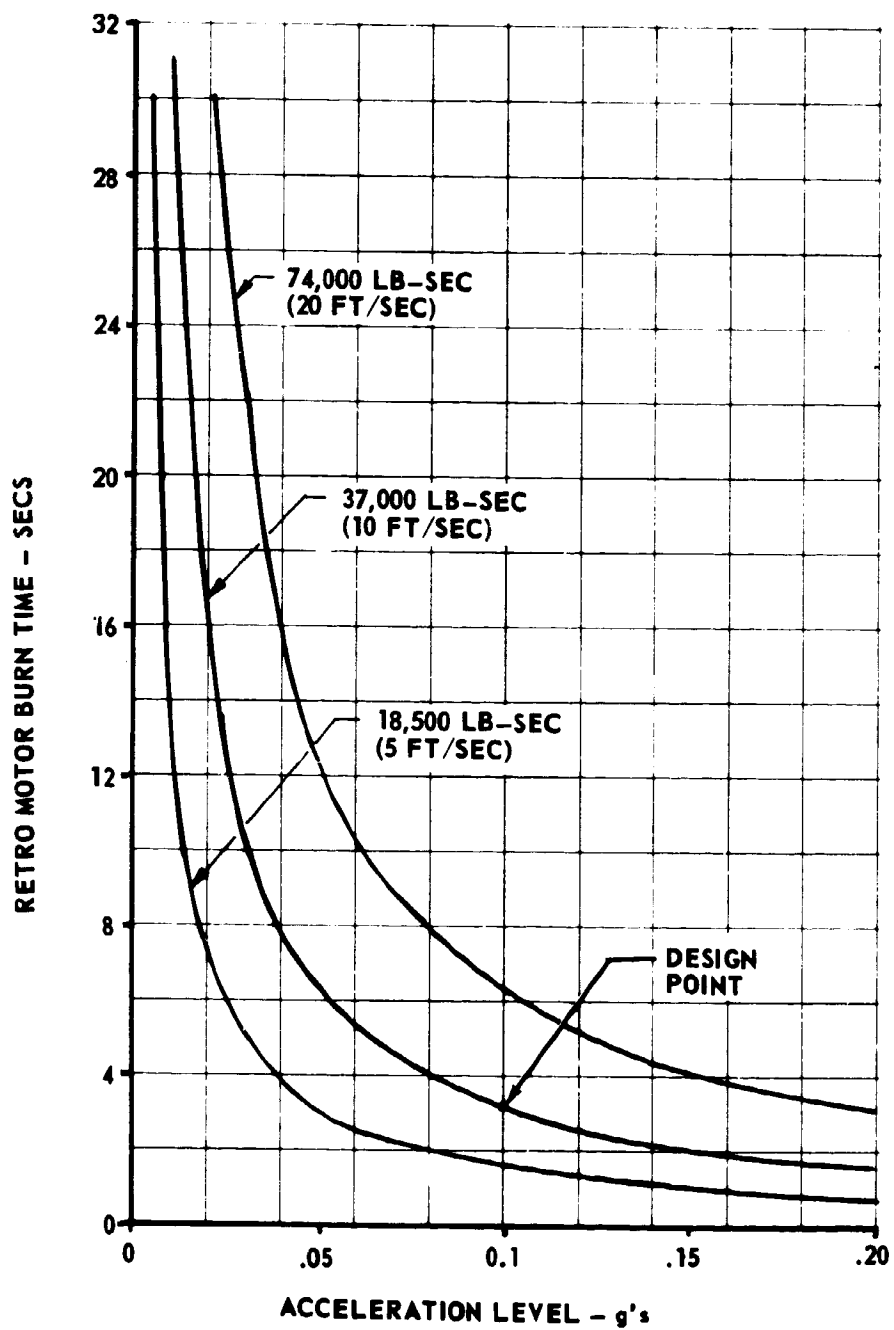
FIGURE 4.2.6.3-1   PAYLOAD/INJECTION STAGE SEPARATION RETRO IMPULSE

4.2.6.4 (Continued)

The "freeze line" is that flow angle for which the temperature of the expanding flow will reach 492°R (the freezing point of water). The maximum flow angle is that flow angle corresponding to an ideal expansion to infinite Mach (M) number. It was assumed: 1) that steam, which will represent a large portion of the exhaust gases, will condense out at or near the freeze line, and 2) that the effects on any body entering the plume outside the freeze line (actually a cone since this is 2D-axisymmetric flow) will be negligible as further expansion of the exhaust beyond this line is insigificant.

The freeze line orientation and maximum flow angle were calculated using an ideal Prandtl-Meyer expansion, represented by changes in the Prandtl-Meyer angle, ν , defined below:

$$\nu = \left(\sqrt{\frac{\gamma+1}{\gamma-1}} \right) \text{TAN}^{-1} \left(\sqrt{\frac{\gamma-1}{\gamma+1}(M^2-1)} \right) - \text{TAN}^{-1} \sqrt{M^2-1}$$

For example, the conditions at the nozzle exit for the multichamber/plug engine (see Figure 4.2.6.4-1), were specified as expansion ratio (ϵ) = 67, Specific Heat Ratio (γ) = 1.20, resulting in a Prandtl-Meyer angle, ν , = 99°. Calculating the Mach number corresponding to an expansion to a temperature of 492°R from:

$$\frac{T_{CHAMBER}}{T} \approx \frac{T_{STAGNATION}}{T} = 1 + \frac{\gamma-1}{2} M^2$$

yields ν = 119° at the freeze line, for a net change in ν of 20°. Since the flow at the exit of the bell nozzle was oriented at 14° from axial, the freeze line will be oriented at 20-14 = 6° from the axial direction.

Similar calculations were made for the toroidal/aerospike engine, assuming axial flow at some point (actually a circular locus of points with the axis at center) in the plane of the base of the plug. For the given area ratio at the plug exit, with an average γ (and applying the NASA/Lewis program) the plane of the throat was axial as shown in Figure 4.2.6.4-2. Several assumptions were made and the analysis was limited as follows:

a. The effects of the external flow field velocity on the exhaust plume were not considered, as the plume size and divergence angle would only be reduced by considering the external flow effects.

b. The engine was assumed to exhaust to vacuum.

c. The NASA/Lewis program uses one-dimensional flow equations, while the engines being considered will have an axisymmetric two-dimensional flow field.
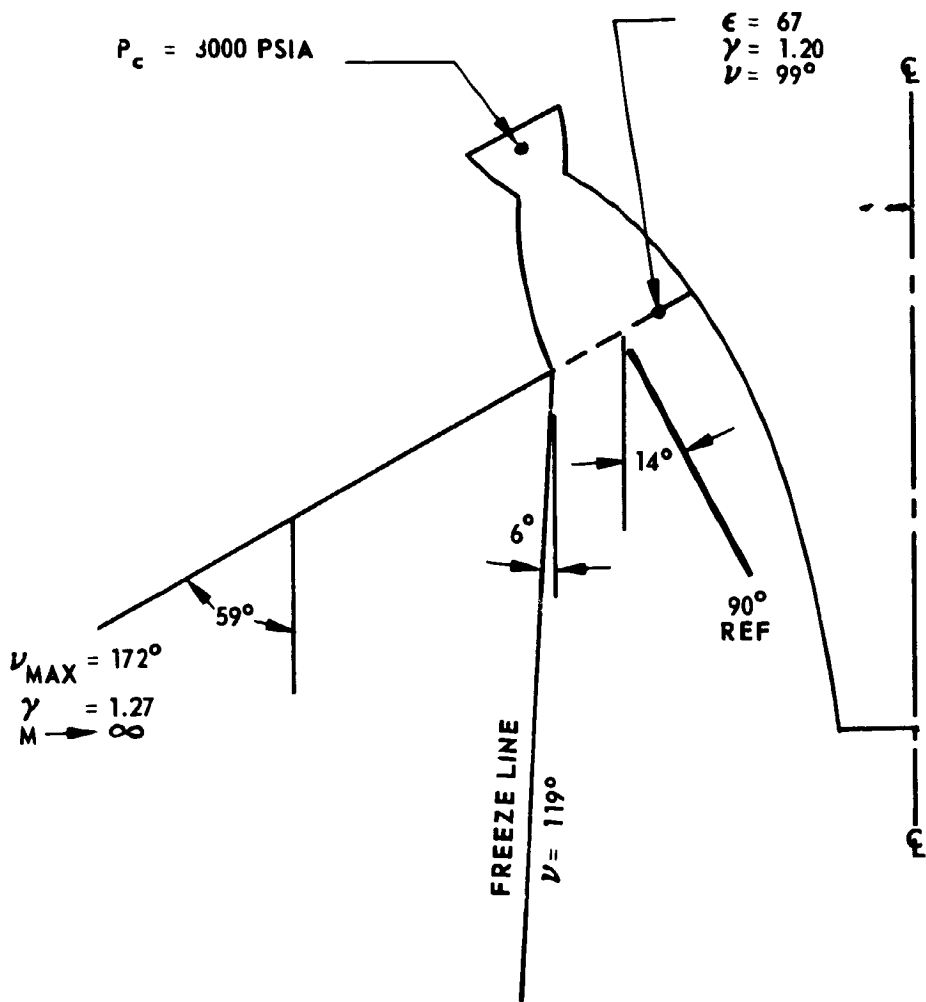
227

FIGURE 4.2.6.4-1 NOZZLE EXIT CONDITIONS - LOX/LH$_2$ MULTICHAMBER PLUG
ENGINE

T_c = 6330° R
P_c = 1200 PSIA

ν_{MAX} = 172°   82°

γ = 1.27

M → ∞

FREEZE LINE

30°

ν = 120°

$\nu \simeq$ 90°
PLUG EXIT
γ = 1.25
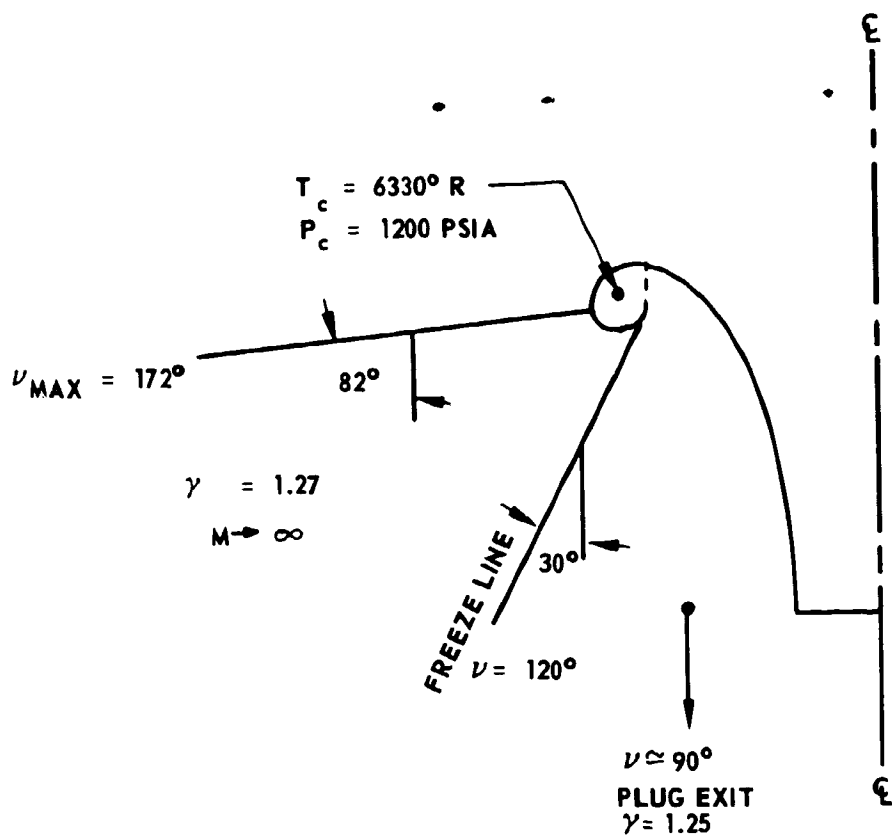
MIXTURE RATIO = 6:1
ν = PRANDTL-MEYER ANGLE
γ = SPECIFIC HEAT RATIO
M = MACH NUMBER

FIGURE 4.2.6.4-2   NOZZLE EXIT CONDITIONS LOX/LH$_2$ AEROSPIKE ENGINE

4.2.6.4   (Continued)

d.   The Prandtl-Meyer angle was calculated using average γ values over the
     given expansion region and refers to two-dimensional flow.

Based on the toroidal/aerospike plume data which provided the widest plume angle,
the strap-on stage lateral thrust and burn time requirements for separation were
calculated.   This data is shown in Figure 4.2.6.4-3.   For a given thrust level, the
required burn time (to prevent the strap-on stage from entering the main stage
exhaust plume prior to the SRM nose cone clearing the aft end of the main stage)
can be determined.

This data shows, for example, that adequate separation motors could have a
combined thrust of 225,700 pounds and a burn time of 2.59 seconds (total impulse
equal to 515,000 pound-seconds).   Larger thrust motors with shorter burn times
are shown to require less total impulse.   Structural considerations will then
dictate acceptable levels.

The maximum lateral aerodynamic force at the time of separation was estimated
to be only 750 pounds.   The axial drag forces at this time were estimated to be
15,000 pounds.   This latter force will be opposed by the tail-off thrust of the solid
motors which also will act to reduce the separation thrust requirements.   None
of these effects were included in the calculations for the data in Figure 4.2.6.4-3.
The data as shown is, therefore, conservative.

Figure 4.2.6.4-4 shows a plot of translational history for various separation
thrust and burn time separation motors.

The solid motor stages along with the forward and aft attachment structure and
fittings will be staged during solid motor burnout.   The staging method will con-
sist of staging rockets mounted in the solid motor nose cone and on the solid motor
aft skirt.   The forward (nose cone) staging rockets will be mounted at an angle to
a line joining the center of the core vehicle and the solid motors.   This will re-
quire more separation motor total impulse, but will reduce the effects of the
forward (nose cone) staging rockets exhaust pressure and temperature on the main
stage.   The exhaust of the aft staging rockets will impact the main stage at the
aft skirt on a region which is not sensitive to the temperature.

4.2.7   Heating Environment

The anticipated aerodynamic and base heating environments were defined for the
baseline vehicle family.   The aerodynamic heating environment was calculated
from the preliminary trajectory parameters as discussed in Section 4.2.1.   The
base plug heating environment was calculated considering the most severe
thermal condition which will occur during operation of the eight SRM strap-on
stages, in a zero stage mode.
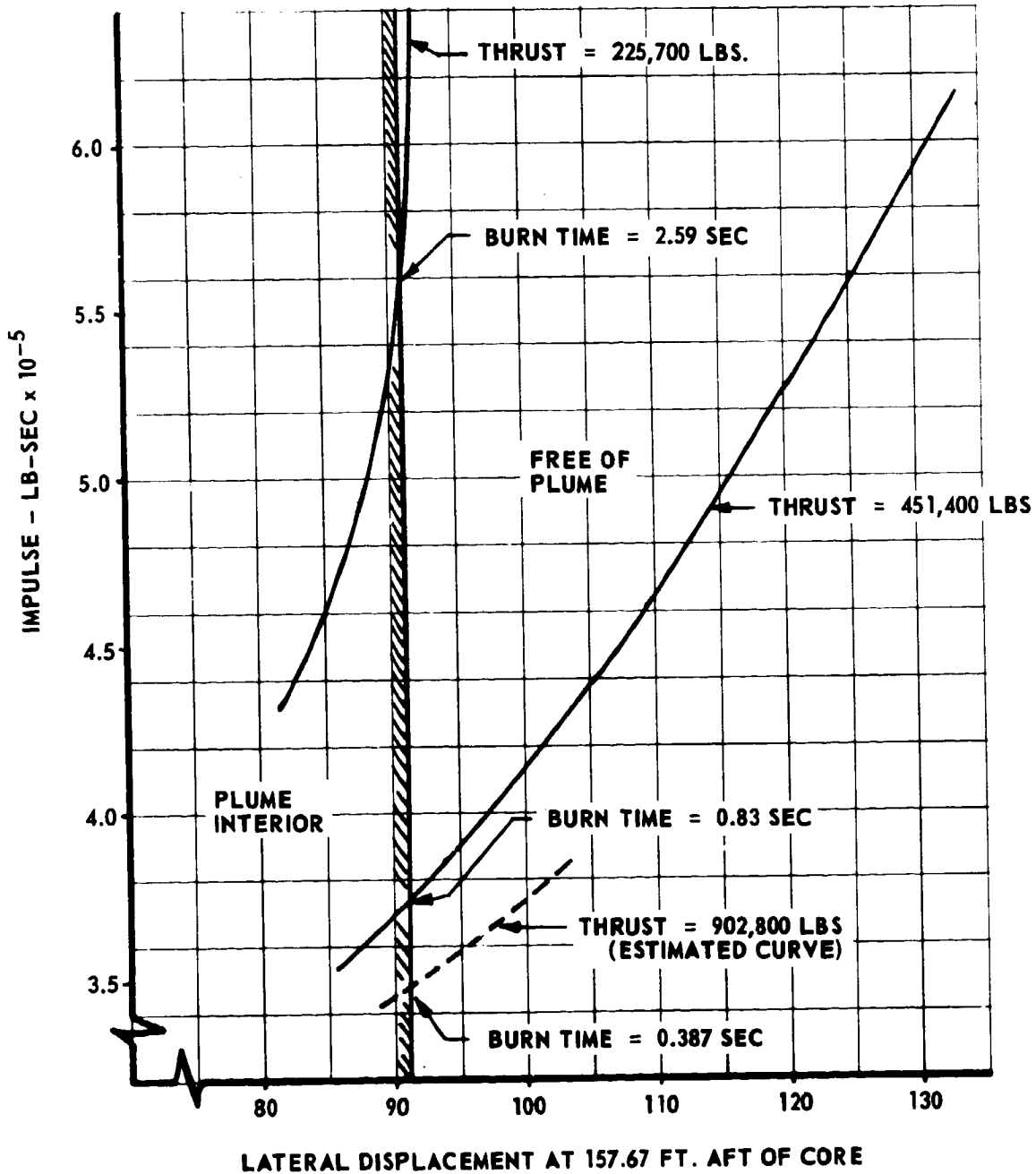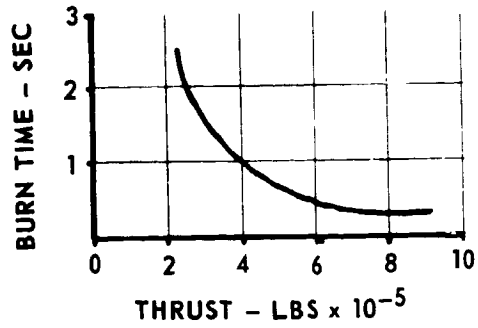
FIGURE 4.2.6.4-3 STRAP-ON STAGE SEPARATION MOTOR REQUIREMENTS FOR
SRM STAGE TO MAIN STAGE SEPARATION

231

	THRUST (LBS)	BURN TIME (SEC)	TOTAL IMPULSE (LB–SEC)
(1)	225,700	2.0	451,400
(2)	225,700	2.41	542,500
(3)	225,700	2.96	645,000
(4)	451,400	0.80	362,000
(5)	451,400	1.60	724,000
(6)	451,400	1.20	542,000
(7)	902,800	0.40	361,120
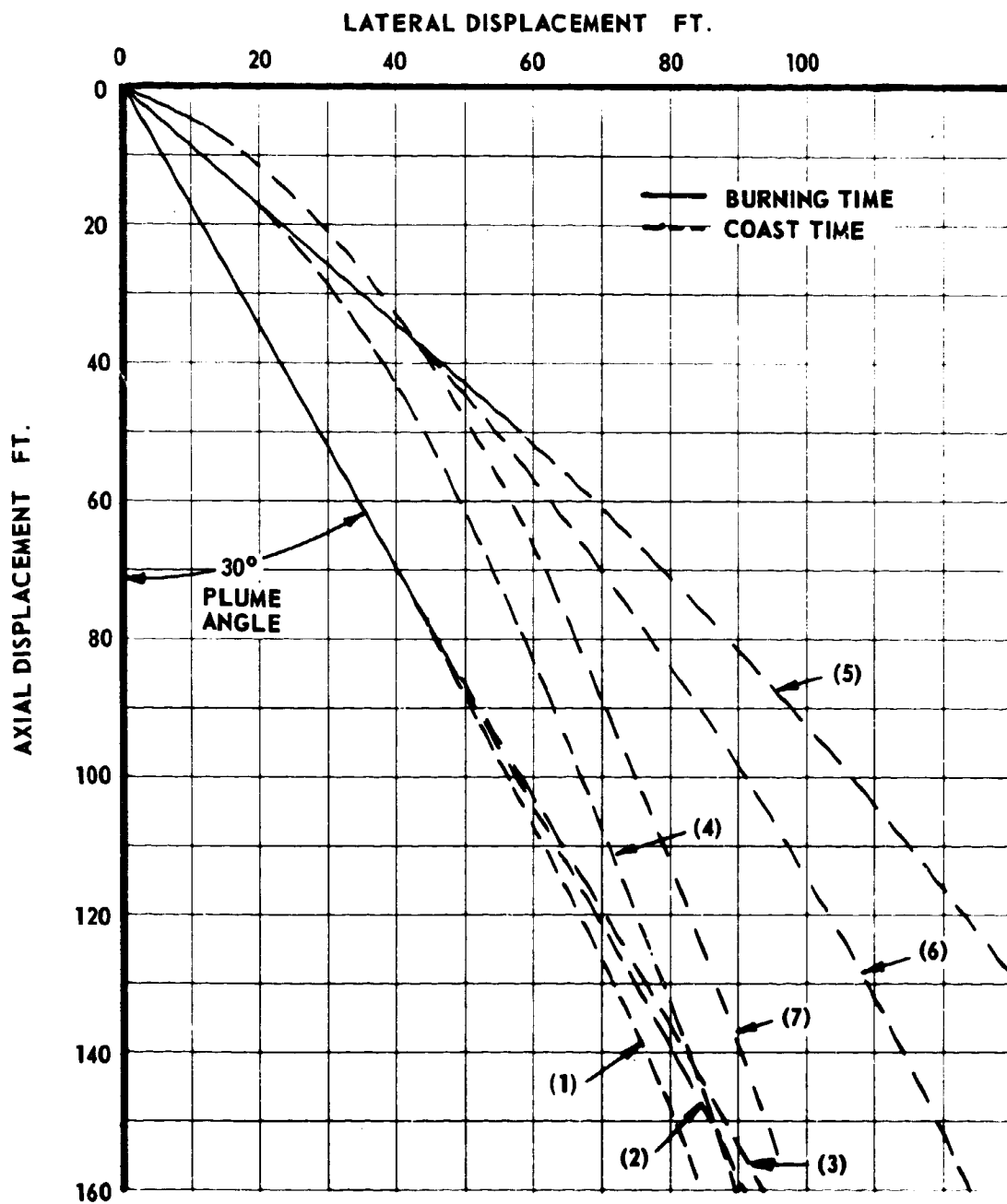
FIGURE 4.2.6.4-4   TRANSLATIONAL DISPLACEMENT FOR VARIOUS THRUST AND BURN TIME SEPARATION MOTORS

4.2.7   (Continued)

This heating analysis also defined the insulation requirements during ground hold for the liquid hydrogen tanks.

The resulting heating environmental data was used for selection and sizing of the insulation materials and for evaluating adequacy of structure in the thermal environment.

4.2.7.1   Aerodynamic Heating

The aerodynamic heating environment was computed for the "worst case" MLLV configuration, i.e.: The main stage plus eight strap-on solid motor stages. Structural temperatures were computed for the forward skirt and the thrust structure. Prior studies (References 4.1.1.1-1, 4.1.1.1-2 and 4.1.3.1-1) have shown the forward skirt to be the zone that reaches the highest temperature. The thrust structure temperature was also computed to illustrate the range of temperatures encountered down the length of the stage.

The clean body aerodynamic heating film coefficients and recovery temperatures for the two locations were determined. One dimensional heat conduction analyses were used to evaluate structural temperature response. The forward skirt was assumed to be 0.15 inch aluminum and the thrust structure was 0.28 inch aluminum. Reradiation was considered. The resulting structural temperatures for the forward skirt and thrust structure are shown in Figure 4.2.7.1-1.

Representative temperatures for the tank skin (0.22 inch aluminum) adjacent the two points considered were extrapolated. These temperatures are included in Figure 4.2.7.1-2.

The structural temperatures shown do not reflect the effect of stiffeners in the structure. A three dimensional heat transfer study to include the effects of stiffeners would show reduced temperatures.

The temperatures shown will exceed the normal design limit (250°F) for aluminum. Temperatures above this limit will reduce the strength of the structures. Therefore, it will be necessary to insulate the main stage to keep within the 250°F temperature limit. A film of polyurethane foam will be sprayed into the main stage skin to maintain the temperature below 250°F. Approximately 2300 pounds of foam insulation will be required for the main stage forward skirt and cylindrical section of the LOX tank. The 5000 pounds of foam insulation provided for the LH_2 tank skin for ground hold conditions (see Section 4.2.7.3) will adequately insulate this region during flight.
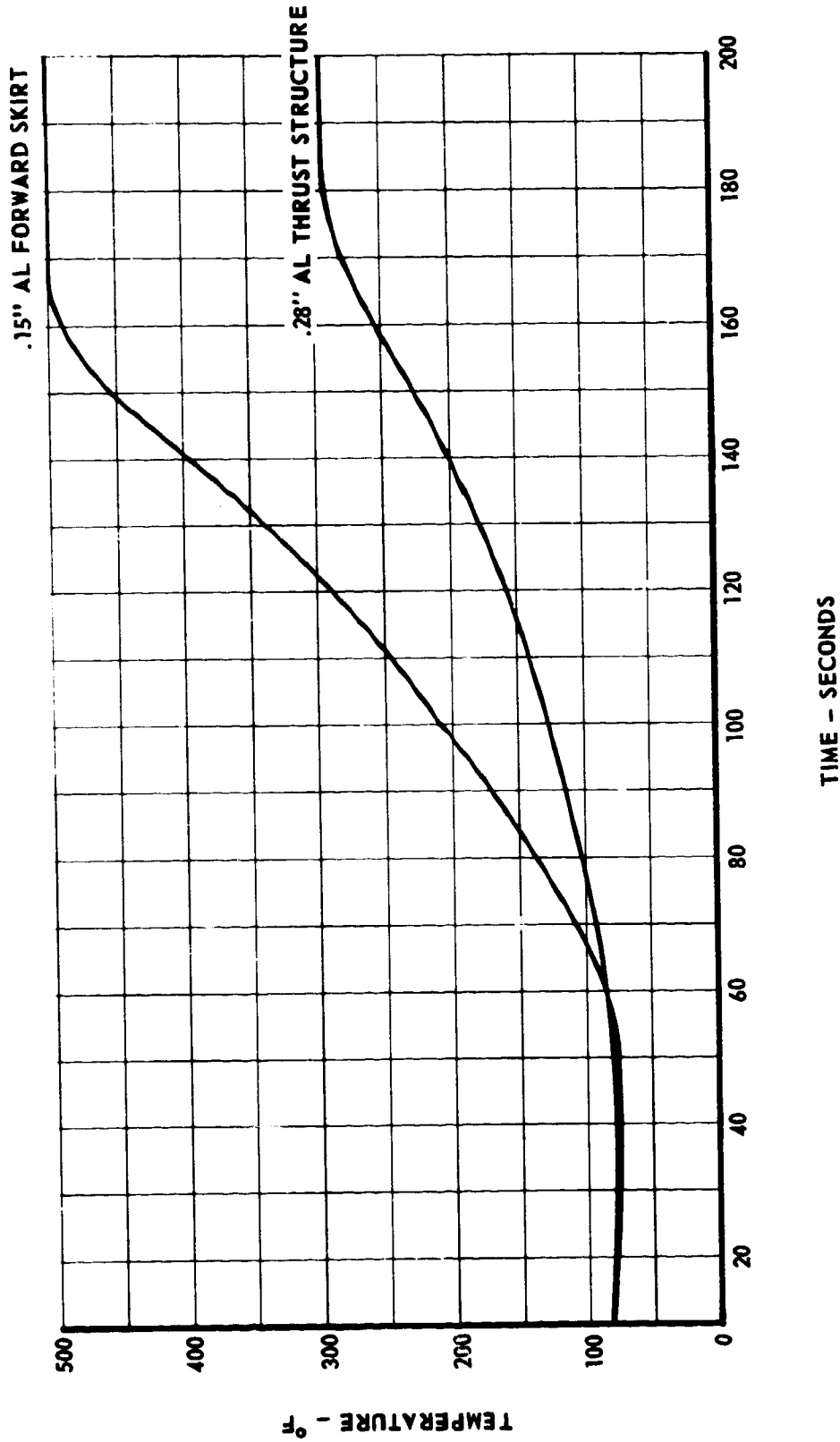
FIGURE 4.2.7.1-1   SKIN SURFACE HISTORY MLLV MAIN STAGE PLUS 8
STRAP-ON STAGES

FORWARD SKIRT
0. 15'' AL

TANK SKIN
0.22'' AL

THRUST STRUCTURE
0.28'' AL

* EXTRAPOLATED DATA

500°F

370°F *

235°F *

280°F
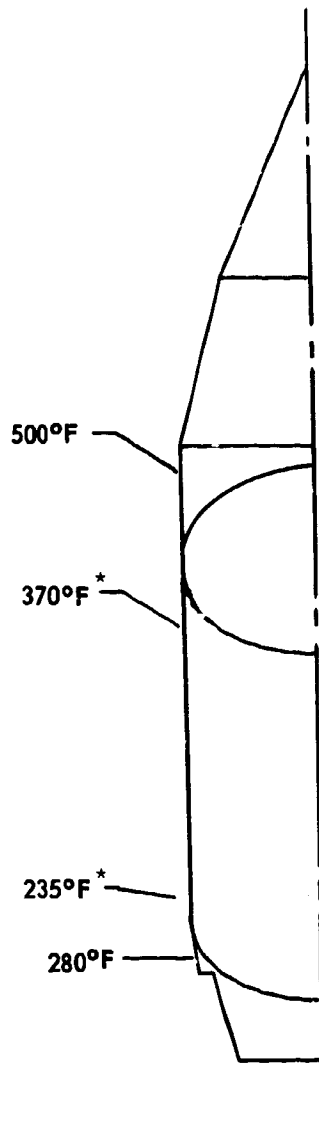
FIGURE 4.2.7.1-2   SKIN SURFACE TEMPERATURES - MAIN STAGE + EIGHT 260
                   INCH SRM

235

4.2.7.2   Base Heating

The convective and radiation heating parameters for the base region of the zero stage strap-on MLLV configuration were determined. The convective heating flux as a function of skin temperature for the zero stage configurations with eight strap-on stages was evaluated by a "Blitz" computerized heat transfer analysis which predicts the recirculated gas flow field of the SRM strap-on stages. The radiation flux from a single SRM plume was determined in the AMLLV study and is presented in Figure 4.2.7.2-1. The radiation view factors (fraction of one plume surface area seen from a fixed location) and plume emittance, and consequently the incident radiation heat flux, was assumed to be basically identical for both the AMLLV and the MLLV solid motors. To confirm this assumption, the radiative heating environment was determined for two points on the MLLV base plug as shown in Figure 4.2.7.2-2.

The radiation heating environment from the 260" SRM to the base plug will vary from sea level to high altitude. The sea level plume was assumed to be cylindrical with an emissivity of 1.0. The altitude plume was assumed to be a cone with a half angle equal to half angle of nozzle (17.5^0) and an emissivity of 0.3. The plume radiosity with these assumptions of a single MLLV 260" SRM is 60 BTU/ft^2-sec at sea level and 18 BTU/ft^2-sec at high altitude. The plume radiosity was assumed constant over the plume length and is a conservative assumption. (Heat losses which occur to air outside of plume are neglected thus indicated slightly higher heat input.)

The incident radiation heat flux at a point on the plug was determined by the relation

$$q_R \text{ (BTU/ft}^2\text{-sec)} = F_V F_B B$$

where the view factor (F_V) from a differential area to the plume surface), the blockage factor (F_B) and the plume radiosity (B) are known (see Table 4.2.7.2-I). The view factors from a differential area to a cylinder are readily available in reference 4.2.7.2-1. The view factors from a differential area to a cone were determined by a Blitz computerized program using the technique described in reference 4.2.7.2-2. The blockage factor, F_B, reflects the number of plumes visible to the differential area and was determined geometrically. The center of the plug will see all eight plumes while a point on the plug side wall will see approximately 2.5 of the plumes.

Reference 4.2.7.2-1 – Radiation Heat Transfer, E. M. Sparrow and R. D. Cess, Brooks Cole Publishing Company, Belmont, California, 1966.
Reference 4.2.7.2-2 – A New and Simpler Formulation for Radiative Angle Factors, E. M. Sparrow, Journal of Heat Transfer, Volume 85, Ser. C, No. 2, pp. 81-88, 1963.
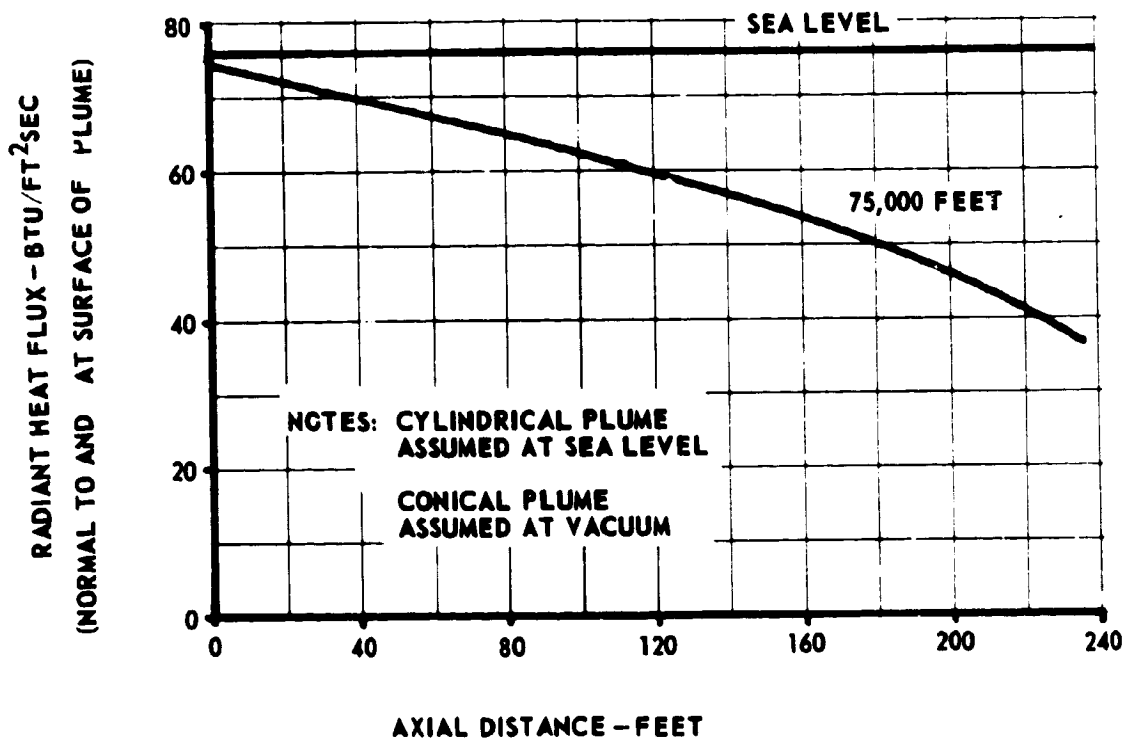
FIGURE 4.2.7.2-1 260 INCH SRM PLUME EMITTANCE AS A FUNCTION OF
AXIAL POSITION FROM EXIT CONE OF SRM

SRM NOZZLE HALF ANGLE β = 17.5°
RADIUS OF SRM NOZZLE EXIT R_e = 130"
APEX OF SRM NOZZLE CONE Y_1 = 413"
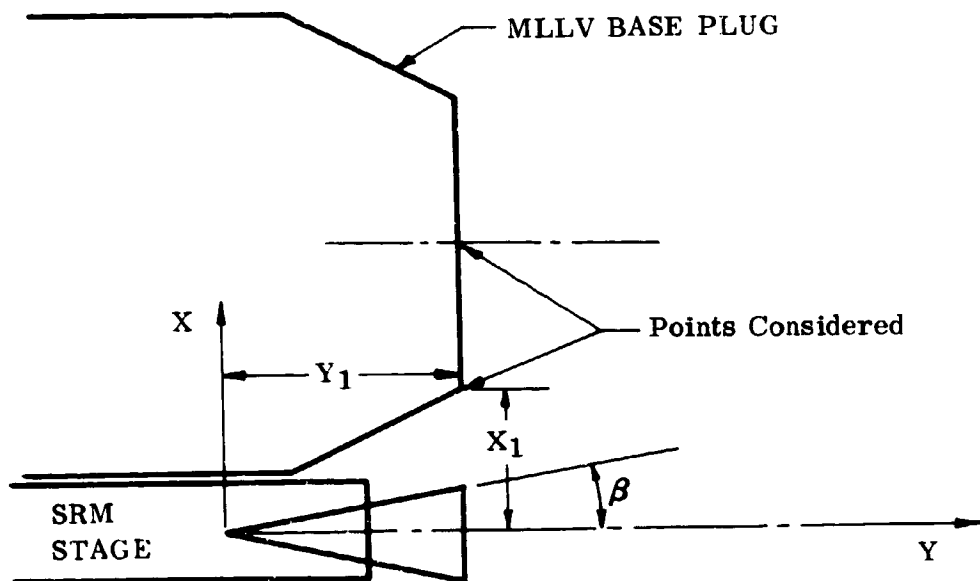
FIGURE 4.2.7.2-2 GEOMETRY FOR VIEW FACTOR FROM DIFFERENTIAL
AREA TO A CONE

TABLE 4.2.7.2-I   VIEW FACTORS FROM DIFFERENTIAL
AREA TO PLUME SURFACE

	DISTANCE (IN)	F_V SEA LEVEL	F_V ALTITUDE	F_B
WALL	250	0.176	0.354	2.50
CENTER	470	0.090	0.277	8.0

NOTE: DISTANCES TO WALL EQUAL X_1
DISTANCE TO CENTER EQUAL X
AS SHOWN IN FIGURE 4.2.7.2-2

TABLE 4.2.7.2-II   THERMAL PROTECTION REQUIREMENTS

	Q_R BTU/FT^2	Q_C BTU/FT^2	Q_T BTU/FT^2	t IN	LH_2 LB/FT^2
WALL	2750	218	2968	0.544	15.6
CENTER	5400	218	5618	1.03	29.6

NOTE: t = THICKNESS OF CORK ESTIMATED TO BE
REQUIRED AT WALL (X_1) AND CENTERBODY
PLUG CENTER (X) AS SHOWN IN
FIGURE 4.2.7.2-2

LH_2 = QUANTITY OF LH_2 REQUIRED AT SAME
LOCATIONS

4.2.7.2   (Continued)

The convective heating flux predicted for the half size MLLV plug with various wall temperatures is shown in Figure 4.2.7.2-3. An aspirated flow region will exist for the first 10-15 seconds, providing cooling of components heated by plume radiation. Recirculation will begin at about 10 seconds and choked reverse flow will occur at about 75 seconds. It was assumed that the convective heating will be constant after choking occurs.

The total incident heat (Q_T) given in Table 4.2.7.2-II is the sum of the convective heat (Q_C) and radiant heat (Q_R) applied to the two locations on the plug over the 130 second SRM burn time. The radiant heating was determined by averaging the sea level and attitude heating rates over the burn time.

Using the values for total incident heat, additional analyses were conducted to define the required thickness of ablative cork to adequately insulate the base plug.

An alternative method for protecting the base plug during SRM operation was also considered. This method (which would also provide increased reliability through the elimination of the altitude start requirement for the main stage engines) would employ operation of the main stage engines in a throttled condition concurrent with SRM operation. Operation of the main stage engines will circulate liquid hydrogen through the regenerative cooling tubes to remove heat in the base region. Analyses were conducted to define the amount of liquid hydrogen required to cool the base plug. This value will determine the degree of throttling required during SRM operation.

The cork ablator and hydrogen coolant requirements as determined using the properties indicated below are presented at the right of Table 4.2.7.2-II. These requirements include a factor of safety of 1.2.

<u>Cork (BMS-8-70)</u>

Density	30 lb/ft^3
Specific Heat	0.47 BTU/lb-$^\circ$R
Heat of Ablation	2200 BTU/lb
Ablation Temperature	1000°F

<u>Hydrogen</u>

Heat of Vaporization	190 BTU/lb*

* This value may be used for preliminary design purposes for any
  moderate pressure cooling system, although heat of vaporization will
  decrease with increasing pressure.

240
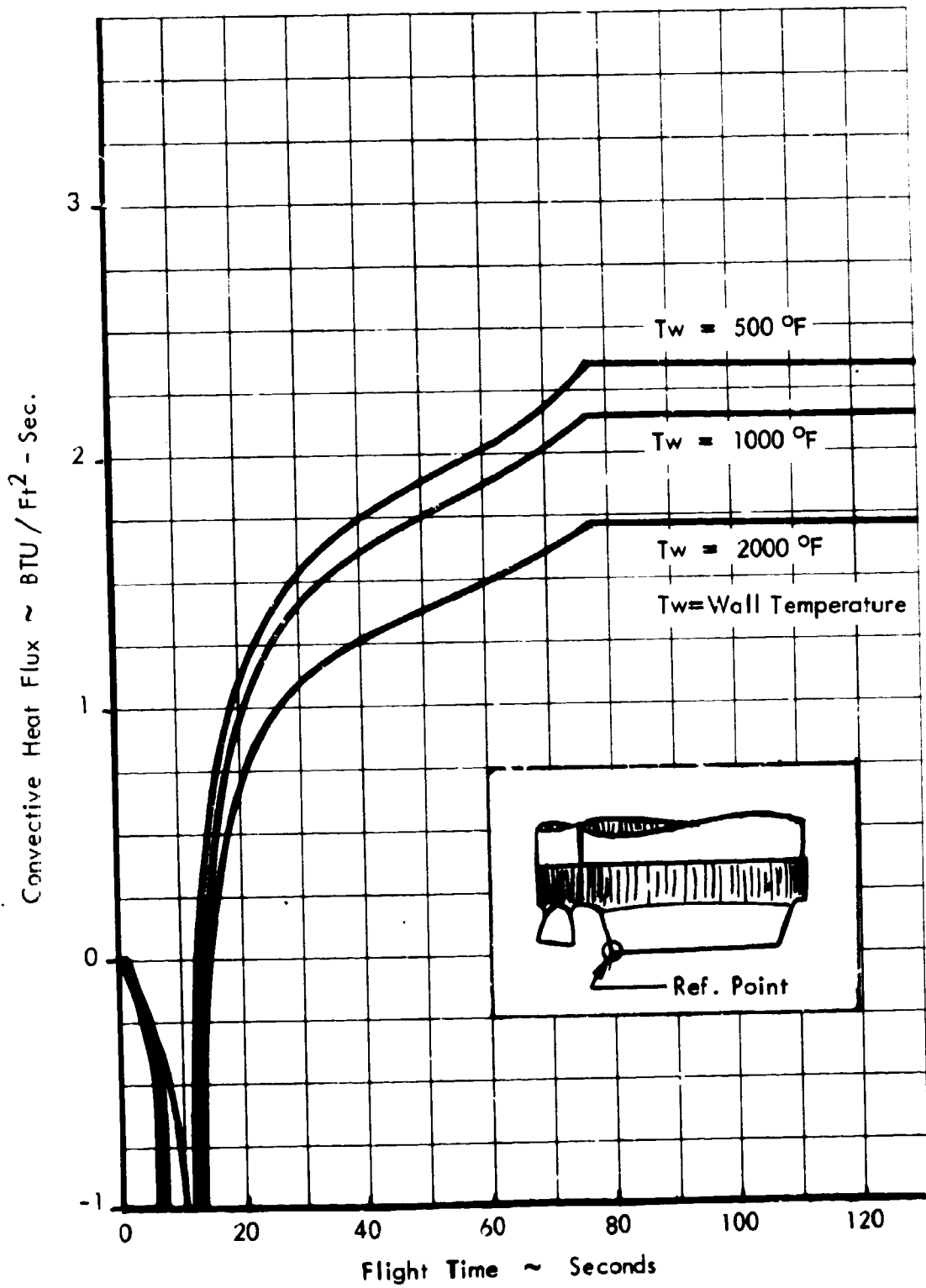
FIGURE 4.2.7.2-3   BASE REGION CONVECTIVE HEATING RATE AS A FUNCTION
OF FLIGHT TIME AND SKIN TEMPERATURE (MLLV MAIN
STAGE + 8 STRAP-ONS)

241

4.2.7.2   (Continued)

It was assumed that no re-radiation will occur for either protection system. This
is justified by considering that any base surface will blacken up quickly and act
as a black surface, similar to the cork. The convective heat loads were based on
a surface temperature of $1000^{\circ}F$, the ablative temperature of the cork. While
the surface may be at a different temperature if hydrogen cooling is employed,
the convective flux will be negligible compared to the radiative flux such that the
total flux may be assumed independent of the cooling technique employed.

A thickness of 0.544 inches of cork will be required at the lip of the plug and 1.03
inches of cork at the center of the plug to protect the plug during SRM operation.
With these thicknesses almost all of the ablator will be gone by the time of main
stage ignition (7,280 pounds of cork).

The total hydrogen coolant requirements for the 130 second period are 15.6
pounds per square foot at the lip of the plug and 29.6 pounds per square foot at
the center of the plug (82,800 pounds of liquid hydrogen).

4.2.7.3   LH$_2$ Tank Insulation

The data on the internal insulation requirements for the AMLLV LH$_2$ tank during
ground hold is directly applicable to the half size MLLV. The variables
affecting the heat transfer on the half size tank are identical to those on the
full size tank. The insulation considered was a polyurethane sprayed
foam, closed cell with freon filler. The following insulation requirements
were defined for the MLLV.

Hydrogen Side of Common Bulkhead	1220 pounds
Outside of LH$_2$ Lower Bulkhead	1380 pounds
Skin of LH$_2$ Tank	5000 pounds

The density of the foamed insulation is approximately two pounds per cubic
foot. The thermal conductivity is approximately 1.25 times 10^{-2} $\dfrac{BTU}{Hr, \ R^{\circ}, \ Ft^2}$.

4.3   CONCEPTUAL DESIGN AND PERFORMANCE

The previous two sections, Design and Performance Trades (Section 4.1) and
Ground and Flight Environment (Section 4.2) provided the baseline vehicle confi-
guration design concepts and the vehicle environments which established the design
criteria of the MLLV vehicle family. This section, Configuration Definition,
describes (1) the final flight performance and weights; (2) the individual stages
(main stage, injection stage and solid motor strap-on stages); (3) the on-board
test and checkout system, and (4) the effect of different payload densities and
different propulsion systems structures, control and payload performance.

The configurations that comprise the MLLV vehicle family will provide a range of
payloads from approximately 470,000 pounds to approximately 1,850,000 pounds
through the use of various quantities of strap-on stages and injection stage modules
with the main stage. Figure 4.3.0.0-1 shows payload performance versus liftoff
weight for representative configurations of the vehicle family. The vehicles shown
incorporate a main stage with the multichamber/plug engine system. Also shown
for reference is the performance of the single-stage-to-orbit vehicle with the
toroidal/aerospike engine system.

As the data on this figure indicates, the use of the injection stage modules will provide
only nominal increases in payload capability for the 100 n. mi. earth orbital
mission. Use of the injection stage modules, however, will provide major increases
in payload capability for higher energy missions beyond the 100 n. mi. earth
orbit (see Section 4.1.2). Other advantages defined for use of the injection stage
include the capability for orbital plane or altitude changes.

The performance analyses indicated that "optimum" trajectories, for those confi-
gurations which do not incorporate injection stage modules, will require main stage
throttling. Those configurations which do incorporate the injection stage modules,
however, will not require main stage throttling "optimization". In some cases,
however, it will be desirable to throttle the main stage to minimize the burnout
g's of the main stage and thereby reduce vehicle loads and increase passenger com-
forts (i.e., for the main stage plus a single module injection stage vehicle
configuration).

The trajectory analyses also showed that the "optimum" trajectories for the vehicles
incorporating the strap-on stages will require a zero stage mode (where only the
strap-on stages are ignited at liftoff with main stage ignition after strap-on burnout).
The only exception to this case will be the configuration employing two strap-on
stages. For this configuration the liftoff thrust provided by the two strap-on stages
will be insufficient to provide an acceptable liftoff thrust-to-weight and thereby
will require a parallel burn flight mode wherein the two strap-on stages and the
main stage are ignited simultaneously at liftoff.
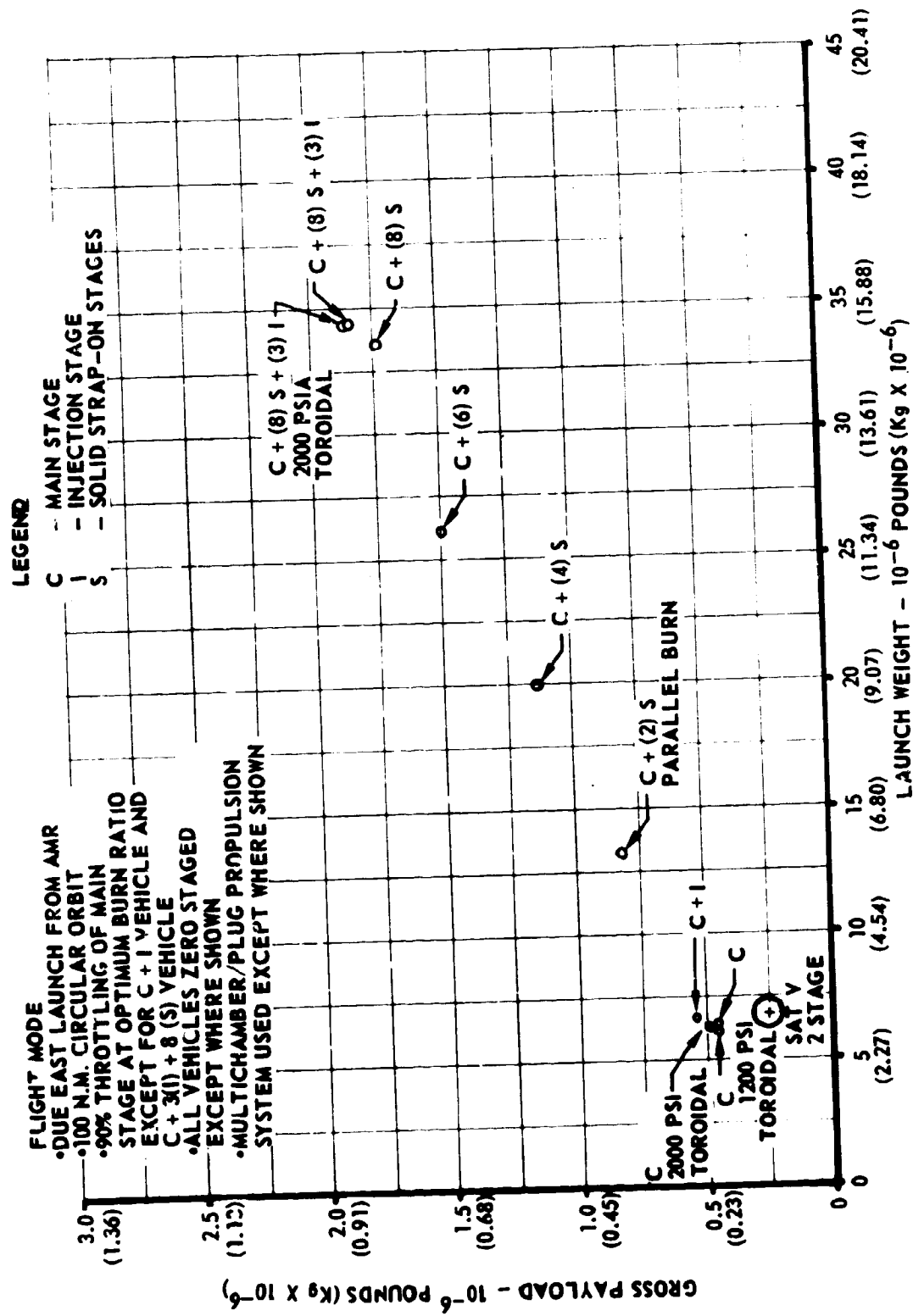
FIGURE 4.3.0.0-1 MLLV PAYLOAD VERSUS LAUNCH WEIGHT

244

4.3   (Continued)

As Figure 4.3.0.0-1 indicates, the higher performance vehicles, in terms of payload weight to launch weight ratio, are those which do not incorporate the strap-on stages. Increased quantities of strap-on stages will reduce the vehicle efficiency as measured by the payload weight to liftoff weight ratio

The final weight estimates are discussed in detail in Section 4.3.2.

The MLLV baseline vehicle will be similar to the AMLLV baseline vehicle. A drawing of the MLLV baseline vehicle is shown in Figure 4.3.0.0-2. The diameter of the main stage will be 680 inches (56.7 ft.) as compared to 860 inches (71.7 ft.) for the AMLLV main stage. This diameter will provide for a true 0.707 spheroid for the LOX tank and, therefore, the elimination of a cylindrical section in the LOX tank. The design will, however, include a small cylindrical section as shown due to the addition of a 30° conical frustum to the exterior periphery of the common bulkhead for ease of manufacture.

LOX feed lines will feed from the bottom of the LOX tank to the individual multi-chamber/plug engines or toroidal/aerospike segments so that fluid flow loads can be reacted by the thrust ring on the thrust structure. Both the LOX and LH_2 tanks will be 2219-T87 aluminum, skin-stringer-frame construction. The common bulkhead will be an aluminum honeycomb approximately four inches thick. Both forward and aft bulkheads will be machined and welded gore bulkheads. The common and aft bulkhead designs will have a 30° frustum modification to the theoretical 0.707 elliptical bulkhead to eliminate cramped intersections with the tank walls. Ring frame stiffeners will react the radial forces caused by the non-tangent bulkhead intersections.

The forward and aft skirts will be 7075-T6 aluminum built-up skin-stringer-frame construction with holddown or SRM thrust posts located in the forward skirt to eliminate major weight penalties to the main stage.

The strap-on stage center lines of thrust will be through the core attachment ring and skin line intersection to eliminate any moments to the main stage from the SRM thrust. The strap-on stage attachment hardware will employ a spherical ball connection at the forward end for thrust take-out and aft end torsion stabilizer tubes and an aft end lateral restraint incorporating a longitudinal slip-joint. Strap-on stage torsion loads and lateral loads will be reacted into the engine attachment thrust ring. The slip joint will not allow longitudinal loads to be reacted at the aft attachment. The relatively long main stage forward skirt will evenly distribute the loads to adjacent structure. SRM stages can be added in pairs to a maximum of eight strap-ons. With SRM strap-on stages, the core vehicle will be supported and held down by the SRM's.

245

SRM THRUST ATTACHMENT (1630)

260" SRM (8 MAX.)

4485 4002 3570 2078 1988 1974 1660 1515 1460 1425 1385 485 480 445 355 350

TOROIDAL TANK INJECTION STAGE MODULE
MAX. PAYLOAD ENVELOPE (5 LBS/FT^3)

20°

260"

¢ SRM THRUST

12.5°

25°

96"OD

69" OD

LH$_2$

LH$_2$

LOX

LOX

1"

20"

HEAT SHIELD

LOX MANIFOLD

LH$_2$ MANIFOLD

LH$_2$ DUCT (24)

.707 BULKHEAD
(TYPICAL)

30°

30°

5°

2907 2424 1992 1870 1775 1740 1690 1630 1570 1454 1396 1203 493 355 300 160

LOX DUCT (24)

COMMON BULKHEAD (H.C.)

SINGLE MODULE
P/L ENVELOPE
(5 LBS/FT^3)

125K ENGINE,
EXTENDABLE NOZZLE,
(2 PER MODULE)

PROFILE VIEW

0   100   200   300

SCALE

SRM TORSIONAL RESTRAINT TUBES

355
350

SRM LATERAL
RESTRAINT SLIP-JOINT

MULTI-CHAMBER
ENGINE
$6°33.4'$

PLUG CENTERBODY
$10°30'$

225 R

190 R

680" DIA.
(56.7')

225 R

320 R

35.5
300

160
150

38

DUCT (24)

SEGMENTED TOROIDAL
ENGINE WITH PLUG
CENTERBODY*

*NOTE: USE OF THIS ENGINE
SYSTEM REDUCES THE
NUMBER OF LOX AND
LH_2 DUCTS TO 8.

PLUG NOZZLE
(GIMBALLED-
INWARD POSITION)
MULTI-CHAMBER
PLUG ENGINE SYS.

260" SRM

SRM TORSIONAL RESTRAINT TUBES

SRM THRUST ATTACHMENT (FWD)
AND LATERAL RESTRAINT (AFT)

TOROIDAL ENGINE
SYSTEM

REAR VIEW

FIGURE 4.3.0.0-2   LINE DRAWING FOR BASELINE MLLV CONFIGURATIONS

247/248

FOLDOUT FRAME 2

4.3 (Continued)

The main stage propulsion system will be a 24 multichamber/plug engine system (or a 28 or 8 segment toroidal/aerospike engine system) with a combined sea level thrust of 8 million pounds.

A thrust ring will be located at the top of the main stage thrust chambers to receive the SRM aft attachment loads. The AMLLV thrust ring was located at the thrust centroid to reduce bending loads and engine deflection. A similar approach for the MLLV main stage would have resulted in the requirement for a second thrust ring for the SRM attachment. Combining the rings will increase the centerbody plug weight to maintain engine rigidity, but will eliminate this requirement for a second thrust ring in the aft skirt.

The MLLV injection stage will use a modular tankage arrangement identical in concept to that defined for the AMLLV. Each tank module will have concentric toroidal LOX and LH_2 tanks. Two high pressure bell engines with extendible nozzles will be used with each tankage module to provide a combined vacuum thrust of 250,000 pounds. Additional thrust will be provided by attaching another pair of engines per each additional module. These engines will be attached to the lower module.

The injection stage toroidal tanks will be of semi-monocoque construction and will incorporate honeycomb sandwich web panels inside the tanks (on a 45° spacing) for torsional rigidity and stiffening shear ribs to maintain the cross-section circularity. The inner torus (the oxidizer tank) will hang from a fiberglass cylindrical skirt attached to the outer torus. The outer torus (the LH_2 tank) will be circumferentially shear pin connected with circular bearing fasteners to the outer shell. The tanks for each module will carry 225,000 pounds of propellant. The skirt for each module will be a skin stringer frame structure of 7075-T6 aluminum. The thrust structure for the lower injection stage module will consist of two restraining ring frames and six vertical thrust posts attached to the skirt. Two high pressure bell engines, with a vacuum thrust of 125,000 pounds each, will be provided for each module. The engines will be mounted on cantilevered trusses from the ring frames at the thrust posts. As only two engines will be required for each module four thrust posts will be vacant for the single module applications. As additional modules are added, additional engines will be added to these remaining thrust posts. Propellant will be provided to the engines from toroidal manifolds fed by the lower module tankage. Upper module propellants will flow through the lower module tankage to these manifolds. The engines with the extendible nozzles retracted will be nested into the forward skirt area of the main stage to reduce stage length. They will extend their nozzles and gimbal outward after main stage separation.

249

4.3   (Continued)

The strap-on stages will incorporate 260 inch diameter solid propellant rocket
motors, each containing 2.9 million pounds of propellant and having an initial
thrust of 6.45 million pounds. The strap-on stages will be complete stages in
themselves requiring only command signals from the vehicle instrument unit (i.e.,
all necessary power, emergency detection systems, destruct systems, etc., will
be contained in the strap-on stage). The strap-on stage will incorporate a cylindri-
cal forward skirt for attachment of the strap-on stage to the main stage and for
housing of some of the stage accessories. This forward cylindrical skirt will
transmit the loads from the solid motor into a vertical shear post for subsequent
reaction of the loads to the ball fitting in the main stage. Atop this cylindrical
skirt will be an aerodynamic nose cone. The stage will also have an aft skirt
which will provide connections for the aft attachment struts and lateral slip joint.
This aft skirt will provide the base for supporting the vehicle in the launch position.
(The main stage support point will be at the forward strap-on stage attachment
plane). The aft skirt will house the TVC mechanism and other stage accessories.

After burnout of the strap-on stages, the expended stages will be expelled laterally
from the main stage through the use of staging rockets in the forward nose cone
and aft cylindrical skirt. Release for separation will be provided by explosive
mechanisms in the attach struts. The separation rockets and explosive release
mechanisms will be actuated simultaneously at the time when the main stage accel-
eration exceeds the acceleration of the individual acceleration on all of the strap-on
stages.

An on-board test and checkout system will be used to provide checkout capability
during test and operational use of the equipment. The decentralized checkout system
will be used, i.e., each stage will have a self-evaluating capability designed and
manufactured into its individual subsystems. Each stage checkout system can be
operated by a ground-based computer system or by the instrument unit on the vehicle.
With this system, launch operational times will be decreased.

Analyses of the impact of various payload densities on the baseline vehicle structures
and control requirements were conducted. These analyses showed that increased
densities over the nominal five pounds per cubic foot (payload density used for the
baseline vehicle) would not increase the required structure. The analysis did show,
however, that decreasing the density would increase the required structure. The
combined compressive (N_c) loads will exceed the design loads for all of the main
stage structure aft of the forward skirt. The combined tension (N_t) loads will be
less than the design loads except in the area of the forward skirt. Here the loads
will slightly exceed the design loads. An additional ring in the LH_2 tank will meet
the new loads requirements for a payload density of two pounds per cubic foot.

4.3   (Continued)

The control requirements will be reduced by a higher density payload. The center of pressure will be located further aft, thus reducing the aerodynamic moment arm which will decrease the TVC requirements. The time to double amplitude will increase. With the lower density payload, the TVC requirements will increase (approximately 5.1 degrees at a density of two pounds per cubic foot) and the time to double amplitude will be reduced.

A comparison was conducted relative to the single-stage-to-orbit vehicle to determine the relative impacts of the engine systems under consideration, i.e., the multichamber/plug propulsion system vs. the toroidal/aerospike system. These trades showed that no major differences would exist in the primary main stage structures for use of either of these systems with the exception of the aft thrust skirts.

No significant differences were defined for the control requirements of either engine system. Use of the toroidal/aerospike propulsion system will provide a larger vacuum exhaust plume cone than the multichamber/plug systems. The separation requirements for the strap-on stages (to prevent the stages from falling into the plume) will therefore be increased.

The trajectory averaged specific impulse for the multichamber/plug system will be slightly higher than that of the toroidal/aerospike system. The combined effects of the weight and specific impulse differences will result in higher payload performance for the single-stage-to-orbit vehicle with the toroidal/aerospike system.

Note: The above engine comparisons are based on data as provided by Rocketdyne for the toroidal/aerospike and by Pratt and Whitney for the multichamber/plug respectively. It is not certain whether the data as provided was developed on exactly the same basis. Therefore, any comparisons are of a general nature and are not necessarily indicative of actual system differences.

4.3.1 Final MLLV Flight Trajectories and Performance

This section presents the final flight performance and trajectories for the MLLV configurations. The trajectory programs used, assumptions, results and analyses of the results are discussed. The final trajectory parameters are compared to those of the preliminary trajectory analyses (see Section 4.2.1) and of the equivalent AMLLV configurations.

4.3.1.1 Flight Performance and Trajectories

The final trajectory analyses considered ten MLLV configurations and used the final weight estimates (see Section 4.3.2), aerodynamics (see Section 4.2.2) and the

4.3.1.1   (Continued)

final propulsion system performance data (see Section 4.3.1 and Volume IX).
Trajectories were flown for:

a.   The single-stage-to-orbit vehicle - multichamber/plug propulsion
     system (single position nozzle).

b.   Single-stage-to-orbit vehicle - 1200 psia toroidal/aerospike propulsion system.

c.   Single-stage-to-orbit vehicle - 2000 psia toroidal/aerospike propulsion system.

d.   Single-stage-to-orbit vehicle - multichamber/plug propulsion
     system. (two position nozzle.)

e.   Main stage plus a single module injection stage vehicle - multichamber/
     plug propulsion system. (Single position nozzle).

f.   Main stage plus eight strap-on solid motor stages vehicle - multi-
     chamber/plug propulsion system. (Single position nozzle).

g.   Main stage plus eight strap-on stages plus a three module injection stage
     vehicle - multichamber/plug propulsion system. (Single position
     nozzle).

h.   Main stage plus eight strap-on stages plus a three module injection stage
     vehicle - multichamber/plug propulsion system (Two position nozzle).

i.   Main stage plus eight strap-on stages plus a three module injection stage
     vehicle - 1200 psia toroidal/aerospike propulsion system.

j.   Main stage plus eight strap-on stages plus a three module injection stage
     vehicle - 2000 psia toroidal/aerospike propulsion system.

The computer printouts of these trajectories are shown in the Appendix D, Volume IX.
A discussion of the trajectory mode is presented in the previous Section 4.2.1.

Two trajectories flown during the trade studies, which are indicative of the performance
of other configurations in the MLLV family, are also shown in Appendix D, Volume IX,
i.e.:

a.   Main stage plus two strap-on stages vehicle - multichamber/plug
     propulsion system (Single position nozzle).

b.   Main stage plus four strap-on stages vehicle - multichamber/plug
     (Single position nozzle).

252

4.3.1.1 (Continued)

Each of the final baseline MLLV trajectories are discussed below and are compared to the results of the preliminary trajectories and to the similar AMLLV type vehicle configurations.

Single-Stage-To-Orbit Vehicles

The single-stage-to-orbit vehicles were sized to orbit a payload of approximately 500,000 pounds to 100 nautical mile orbit. Configurations employing four different engine systems were analyzed. Table 4.3.1.1-I shows the mission weight history data for these configurations. For each trajectory, the liftoff thrust was held constant at 8,000,000 pounds. The variations in thrust-to-weight ratio, therefore, were due to the minor variations in vehicle launch weight. Except for a minor increase in the aft skirt weight for the single-stage-to-orbit vehicle with the multichamber/plug, all of the inert weight differences of the main stage were due to the variations in the propulsion system. These variations in the aft skirt and propulsion system weights resulted in mass fractions of 0.936, 0.937, 0.943, and 0.945 for the multichamber/plug single position nozzle, multichamber/plug two position nozzle, 2000 psia toroidal and the 1200 psia toroidal propulsion system, respectively. The estimated propulsion system weights as supplied by the engine manufacturer were 116,613; 108,213; 75,050; and 60,240 pounds respectively.

The single-stage-to-orbit vehicles with the multichamber/plug engine systems will be capable of placing a larger weight (stage plus payload) in orbit because of the higher delivered specific impulse. However, the heavier weight of the multichamber/plug propulsion system will result in less payload, as the gross payload is the total weight to orbit less the weight of the main stage (including its engine system). A comparison of the payload capabilities of the vehicle with the multichamber/plug and the vehicle with the 2000 psia toroidal/aerospike thus shows that the single-stage-to-orbit vehicle with the toroidal/aerospike engine system will have a higher payload capability as a result of the lower engine weight. The vehicle with the 1200 psia toroidal/aerospike system will have the best mass fraction because of its lowest engine weight. The lower performance (specific impulse) due to the lower operating pressure, however, will offset the effect of the improved mass fraction and will result in a payload capability considerably lower (8%) than that of the vehicle with the 2000 pressure toroidal/aerospike system(comparable to that of the multichamber/plug system).

Table 4.3.1.1-II shows the comparative performance data for the single-stage-to-orbit MLLV vehicles. Shown on this table are the final trajectory data, the preliminary trajectory data, and the comparable data for the single-stage-to-orbit vehicles of the AMLLV family. The liftoff weight and thrust values between the MLLV final trajectory data and the preliminary trajectory data did not vary significantly. The main differences were due to re used inert weights for the

TABLE 4.3.1.1-I   MISSION WEIGHT HISTORY - SINGLE STAGE TO ORBIT VEHICLE

PARAMETER		HIGH PRESSURE MULTICHAMPER/ PLUG (SINGLE POSITION NOZZLE)	HIGH PRESSURE (2000 PSIA) TOROIDAL/ AEROSPIKE	LOW PRESSURE (1200 PSIA) TOROIDAL/ AEROSPIKE	HIGH PRESSURE MULTICHAMBER/ PLUG (TWO POSITION NOZZLE)
Ignition Thrust (S.L.)	lbs	8,000,000	8,000,000	8,000,000	8,000,000
Throttled Thrust (VAC)	lbs	1,007,085	983,000	997,000	960,000
Lift-Off Weight	lbs	6,402,820	6,378,363	6,344,696	6,396,977
T/W Ratio at Lift-Off		1.249	1.254	1.261	1.250
Launch Azimuth	degs	90	90	90	90
Propellant Consumed	lbs	5,550,000	5,550,000	5,550,000	5,550,000
Full Thrust Propellant (B1)	lbs	4,972,620	4,972,519	4,972,620	4,972,600
Throttled Propellant (B2)	lbs	577,380	577,381	577,380	577,400
Burn Ratio (B2/B1)		0.116	0.116	0.116	0.116
Stage Drop Weight	lbs	381,166	337,306	322,496	372,766
Stage Mass Fraction (λ)		0.936	0.943	0.945	0.937
Gross Weight in Orbit	lbs	852,815	828,360	794,696	846,971
Gross Payload	lbs	471,649	491,054	472,200	474,205

TABLE 4.3.1.1-II   COMPARATIVE PERFORMANCE DATA – SINGLE-STAGE-TO-ORBIT VEHICLES

	PARAMETER	SINGLE STAGE TO ORBIT VEHICLE WITH MULTICHAMBER/PLUG (SINGLE POSITION NOZZLE)	SINGLE STAGE TO ORBIT VEHICLE WITH MULTICHAMBER/PLUG (TWO POSITION NOZZLE)	SINGLE STAGE TO ORBIT VEHICLE WITH 2000 PSIA TOROIDAL/AEROSPIKE	SINGLE STAGE TO ORBIT VEHICLE WITH 1200 PSIA TOROIDAL/AEROSPIKE
FINAL TRAJECTORY	LIFT OFF WEIGHT (LBS)	6,402,820 *	6,344,977 *	6,378,363	6,344,696
	LIFT OFF THRUST (LBS)	8,000,000	8,000,000	8,000,000	8,000,000
	ACC. PRIOR TO COV (FT/SEC^2)	*	*	*	*
	ACC. AT CUTOFF (FT/SEC^2)	*	*		
	DYNAMIC PRESSURE (#/FT^2)	651 AT 80 SEC	563 AT 81 SEC	601 AT 83 SEC	638 AT 81 SEC
	MASS FLOW UNTHROTTLED (#/SEC)	*	*	*	*
	MASS FLOW THROTTLED (#/SEC)	*	*	*	*
	GROSS PAYLOAD (LBS)	471,649	474,205	491,054	472,200
PRELIMINARY TRAJECTORY	LIFT OFF WEIGHT (LBS)	6,418,606 *		6,384,400	
	LIFT OFF THRUST (LBS)	8,000,000		8,000,000	
	ACC. PRIOR TO COV (FT/SEC^2)	*		*	
	ACC. AT CUTOFF (FT/SEC^2)	*		*	
	DYNAMIC PRESSURE (#/FT^2)	692 AT 80 SEC		614 AT 81 SEC	
	MASS FLOW UNTHROTTLED (#/SEC)	*		*	
	MASS FLOW THROTTLED (#/SEC)	*		*	
	GROSS PAYLOAD (LBS)	476,422		480,169	
AMLLV	LIFT OFF WEIGHT (LBS)	12,800,000	N/A	12,800,000	N/A
	LIFT OFF THRUST (LBS)	16,000,000		16,000,000	
	ACC. PRIOR TO COV (FT/SEC^2)	*		*	
	ACC. AT CUTOFF (FT/SEC^2)	*		*	
	DYNAMIC PRESSURE (#/FT^2)	628 AT 80 SEC		635 AT 81 SEC	
	MASS FLOW UNTHROTTLED (#/SEC)	*		*	
	MASS FLOW THROTTLED (#/SEC)	*		*	
	GROSS PAYLOAD (LBS)	1,028,887		980,652	

*THE DATA OMITTED FROM THIS TABLE IS CLASSIFIED. THIS TABLE, WITH THE CLASSIFIED DATA INCLUDED, IS SHOWN IN VOLUME IX, (CLASSIFIED APPENDIX), APPENDIX E.

4.3.1.1   (Continued)

propulsion systems. These revised weights showed a heavier weight for the multi-chamber/plug propulsion system trajectory analysis and a lighter weight for the toroidal propulsion system than was used in the preliminary trajectory analyses. The maximum acceleration just prior to throttling, and the secondary peak acceleration at main stage cut-off for the final trajectories closely approximate those values obtained from the preliminary trajectories and are also approximately the same as those obtained from the AMLLV vehicle trajectories. A more significant variation was noted in the dynamic pressure. Considering the single-stage-to-orbit vehicle with the multichamber/plug propulsion system, the maximum dynamic pressure (max q) obtained during the preliminary trajectories was considerably higher than that obtained from the final trajectory or from the previous AMLLV trajectory.

The increase in dynamic pressure was the result of revised engine performance input data from that estimated for the preliminary trajectories (which were based on AMLLV engine data). The final data indicated that a lower mass flow would give the necessary liftoff thrust. This lower mass flow, coupled with the smaller increase in I_{sp} as the vehicle approached altitude, resulted in a slightly lower energy input to the vehicle up to the time of maximum dynamic pressure. This lower energy resulted in a lower dynamic pressure. The AMLLV single-stage-to-orbit vehicle with the multichamber/plug had the lowest dynamic pressure. This lower value was also the results of less energy expended prior to maximum dynamic pressure. The AMLLV variation was the result of the base diameter effect which resulted in a lower average I_{sp} up to the time of maximum dynamic pressure.

The use of two position nozzles in lieu of fixed nozzles on the modules of the multi-chamber/plug engine resulted in a more near optimum nozzle expansion ratio at liftoff. As a result the mass flow to achieve the desired 8 million pounds of sea level thrust was lower. This in turn resulted in a longer first stage burn time of 515 seconds.

The maximum dynamic pressure values for the vehicles with the 2000 psia toroidal/aerospike system are approximately the same as those for the single-stage-to-orbit vehicle with the multichamber/plug system. The higher value obtained for the final trajectory was the result of the propulsion contractor supplied finalized propulsion input which indicated a higher specific impulse for the engine then had been estimated for the preliminary trajectory propulsion input. As a result, greater energy was applied to the vehicle prior to maximum dynamic pressure which resulted in the higher maximum dynamic pressure obtained for the final trajectory.

For the single-stage-to-orbit vehicle with the 1200 psia toroidal/aerospike engine, the maximum dynamic pressure was lower than that of either the multichamber/plug or the 2000 psia toroidal/aerospike system. Operating the engine at the lower pressure, reduced the specific impulse and resulted in a lower energy input to the

4.3.1.1   (Continued)

vehicle prior to maximum dynamic pressure. All of the values of maximum
dynamic pressures are considerably lower than the nominal 950 pounds per square
foot used as a design criteria on the Saturn V program.

Main Stage Plus Single Injection Stage Vehicle

The main stage plus single injection stage vehicle will utilize the same main stage
as will be used for the single-stage-to-orbit vehicle. Therefore, the inert weight
and propellant loadings used in the trajectory analyses were identical. The confi-
guration analyzed had the multichamber/plug propulsion system with a single
position nozzle on the main stage.

Table 4.3.1.1-III presents the mission weight history. The liftoff thrust-to-weight
was 1.18. An arbitrary restriction on liftoff thrust-to-weight minimum value of
1.18 precluded the addition of further injection stage module to the core plus
injection stage family. The thrust-to-weight of the injection stage on ignition was
0.298. As shown in the previous AMLLV studies, a low injection stage thrust-to-
weight (maximizing the propellant capacity) results in greater payload capability.

The final inert weight for the injection stage was higher than estimated in the
preliminary trajectory studies. The injection stage mass fraction was 0.785 as
compared to the 0.80 mass fraction utilized for the preliminary trajectory studies.
(The AMLLV single module injection stage had a mass fraction of 0.82.) As a
result of this lower mass fraction, the payload to orbit was lower than that estimated
in the preliminary studies. The gross payload was 553,593 pounds as compared to
the 560,292 pounds obtained in the preliminary trajectory analysis.

As shown in Table 4.3.1.1-IV, the performance parameters for this vehicle confi-
guration showed no significant variation between the final trajectory values and
the preliminary trajectory values. Comparison with the AMLLV performance para-
meters showed no significant differences. The dynamic pressure for the AMLLV
was 587 pounds per square foot as compared to 579 per square foot for the final
trajectory of the half-size vehicle. This difference is attributed to the difference
in propulsion parameters utilized for the half-size vehicle and the lower stage mass
fraction.

Main Stage Plus Eight Strap-On Stages Vehicle

The main stage plus eight strap-on stages vehicle will utilize the main stage deve-
loped for the single-stage-to-orbit vehicle with a heavy weight forward skirt and
the addition of fittings to the lower thrust ring for SRM attachment. The eight solid
motor strap-on stages will provide a liftoff (sea level) thrust, for the zero stage
flight mode, of 51,680,311 pounds. (See Table 4.3.1.1-V.) This value is lower
than the 54,400,000 pounds utilized in the preliminary vehicle performance trades.

TABLE 4.3.1.1-III   MISSION WEIGHT HISTORY - MAIN STAGE PLUS A SINGLE INJECTION MODULE
(MAIN STAGE EMPLOYED A MULTICHAMBER/PLUG PROPULSION SYSTEM WITH
A SINGLE POSITION NOZZLE)

MAIN STAGE	
IGNITION THRUST (S.L.)	8,000,000 LBS.
LIFT-OFF WEIGHT	6,771,401 LBS.
T/W RATIO AT LIFT-OFF	1.181
PROPELLANT CONSUMED	5,550,000 LBS.
STAGE DROP WEIGHT ($\lambda' = .936$)	381,166 LBS.
LAUNCH AZIMUTH	90 DEGS.
DYNAMIC PRESSURE	579 LBS./FT^2
INJECTION STAGE	
IGNITION THRUST (VAC)	250,000 LBS.
IGNITION WEIGHT	840,228 LBS.
T/W RATIO AT IGNITION	.298
PROPELLANT CONSUMED	225,000 LBS.
STAGE DROP WEIGHT ($\lambda' = .785$)	61,635 LBS.
GROSS WEIGHT IN ORBIT	615,228 LBS.
GROSS PAYLOAD	553,593 LBS.

TABLE 4.3.1.1-IV COMPARATIVE PERFORMANCE DATA – MAIN STAGE PLUS A SINGLE INJECTION STAGE VEHICLE (MAIN STAGE EMPLOYED A MULTI-CHAMBER/PLUG PROPULSION SYSTEM WITH A SINGLE POSITION NOZZLE)

PARAMETER		
FINAL TRAJECTORY	LIFT OFF WEIGHT (LBS)	6,771,401
	LIFT OFF THRUST (LBS)	8,000,000
	ACC. AT MAIN STAGE CUT OFF (FT/SEC^2)	*
	ACC. AT INJ. STAGE CUT OFF (FT/SEC^2)	*
	DYNAMIC PRESSURE (#/FT^2)	578 AT 88 SEC
	MAIN STAGE MASS FLOW (#/SEC)	*
	INJ. STAGE MASS FLOW (#/SEC)	*
	GROSS PAYLOAD (LBS)	553,593
PRELIMINARY TRAJECTORY	LIFT OFF WEIGHT (LBS)	6,790,000
	LIFT OFF THRUST (LBS)	8,000,000
	ACC. AT MAIN STAGE CUT OFF (FT/SEC^2)	*
	ACC. AT INJ. STAGE CUT OFF (FT/SEC^2)	*
	DYNAMIC PRESSURE (#/FT^2)	617 AT 88 SEC
	MAIN STAGE MASS FLOW (#/SEC)	*
	INJ. STAGE MASS FLOW (#/SEC)	—
	GROSS PAYLOAD (LBS)	560,292
AMLLV TRAJECTORY	LIFT OFF WEIGHT (LBS)	13,535,173
	LIFT OFF THRUST (LBS)	16,000,000
	ACC. AT MAIN STAGE CUT OFF (FT/SEC^2)	*
	ACC. AT INJ. STAGE CUT OFF (FT/SEC^2)	*
	DYNAMIC PRESSURE (#/FT^2)	587 AT 90 SEC
	MAIN STAGE MASS FLOW (#/SEC)	*
	INJ. STAGE MASS FLOW (#/SEC)	*
	GROSS PAYLOAD (LBS)	1,178,356

*THE DATA OMITTED FROM THIS TABLE IS CLASSIFIED. THIS TABLE, WITH THE CLASSIFIED DATA INCLUDED, IS SHOWN IN VOLUME IX, (CLASSIFIED APPENDIX), APPENDIX E.

TABLE 4.3.1.1-V   MISSION WEIGHT HISTORY - MAIN STAGE PLUS EIGHT STRAP-ON STAGE VEHICLE   (MAIN STAGE PROPULSION SYSTEM EMPLOYED A MULTICHAMBER/PLUG WITH A SINGLE POSITION NOZZLE)

FLIGHT MODE - ZERO STAGED SRM'S WITH THROTTLED CORE

SOLID STAGE

IGNITION THRUST (S.L.)	51,680,311 LBS.
LIFT-OFF WEIGHT	33,488,881 LBS.
T/W RATIO AT LAUNCH	1.543
PROPELLANT CAPACITY	23,200,000 LBS.
PROPELLANT CONSUMED	23,196,023 LBS.
STAGE DROP WEIGHT	2,577,782 LBS.
LAUNCH AZIMUTH	90 DEG.
MASS FRACTION (λ')	0.902

MAIN STAGE

IGNITION THRUST (VAC)	10,070,845 LBS.
IGNITION WEIGHT	7,715,076 LBS.
T/W RATIO AT IGNITION	1.305
PROPELLANT CAPACITY	5,550,000 LBS.
PROPELLANT CONSUMED AT FULL THRUST (B1)	*
PROPELLANT CONSUMED AT REDUCED THRUST (B2)	*
BURN RATIO (B2/B1)	.1255
THROTTLED THRUST (VAC)	1,007,085 LBS.
STAGE DROP WEIGHT	408,207 LBS.
MASS FRACTION (λ')	0.932

GROSS WEIGHT IN ORBIT	2,165,076 LBS.
GROSS PAYLOAD	1,756,869 LBS.

*THE DATA OMITTED FROM THIS TABLE IS CLASSIFIED.   THIS TABLE, WITH THE CLASSIFIED DATA INCLUDED, IS SHOWN IN VOLUME IX, (CLASSIFIED APPENDIX), APPENDIX E.

260

4.3.1.1   (Continued)

This difference is attributable to the revised shaping of the solid motor thrust-time history as requested by the propulsion contractor. (See section 4.3.5.1 for further discussion.)

The solid motor manufacturer recommended that the initial thrust level be decreased to reduce the high pressure required for the higher initial thrust level. This pressure decrease will decrease the inert weight of the SRM case and improve the mass fraction. The SRM stage mass fraction very closely approximated that used in the preliminary trajectories for this vehicle. The final strap-on stage mass fraction was 0.902 and that used in the preliminary trajectories was 0.90.

As a result, the liftoff thrust-to-weight ratio was reduced to 1.543 for the final trajectory as compared to 1.623 in the preliminary trajectory. The mass fraction used in the final trajectory for the strap-on stages was 0.902 which closely matched the approximate value of 0.90 used in the preliminary trades. The main stage mass fraction also very closely approximated that used in the preliminary trajectories (0.931 vs. 0.930). The gross payload obtained in the final trajectory was 1,757,000 pounds vs. 1,778,000 pounds obtained in the preliminary trajectory. This slight reduction in payload can be attributed to the propulsion contractor lower propulsion performance estimates (specific impulse) for the single nozzle position multichamber/plug propulsion system utilized in the final trajectory than the estimated performance values utilized in the preliminary trajectory.

Table 4.3.1.1-VI shows the comparative performance data for the main stage plus eight strap-on stages vehicle. This data compares the final trajectory performance, the preliminary trajectory performance, and the AMLLV trajectory for the comparable vehicle. The parameters of liftoff weight, acceleration prior to SRM cutoff, acceleration prior to throttling, and acceleration prior to core cutoff were matched very closely for all three configurations. The maximum dynamic pressure (999 #/ Sq. ft.) of the preliminary trajectory for this vehicle was 50 pounds per square foot higher than the final trajectory (949 #/sq. ft.). This can be attributed to the higher energy input into the vehicle due to the higher solid motor impulse applied to the vehicle prior to the time maximum dynamic pressure occurred (the mid-portion solid motor thrust-time history). The trace shaping of the solid motor reduced the energy input for the final trajectory. The AMLLV maximum dynamic pressure is close to that obtained for the preliminary trajectory. The AMLLV solid motor trace shape was not modified to reduce the initial thrust peak and, therefore, the AMLLV main stage plus eight strap-on vehicle has a maximum dynamic pressure similar to that obtained for the preliminary trajectory.

TABLE 4.3.1.1-VI COMPARATIVE PERFORMANCE DATA - MAIN STAGE PLUS EIGHT STRAP-ON STAGE VEHICLE (MAIN STAGE PROPULSION SYSTEM EMPLOYED A MULTICHAMBER/PLUG PROPULSION SYSTEM WITH A SINGLE POSITION NOZZLE)

*THE DATA OMITTED FROM THIS TABLE, THIS TABLE IS CLASSIFIED. CLASSIFIED DATA INCLUDED, IS SHOWN IN VOLUME IX, (CLASSIFIED APPENDIX), APPENDIX E.

	PARAMETER	
FINAL TRAJECTORY	LIFT OFF WEIGHT (LBS)	33,488,881
	LIFT OFF THRUST (LBS)	51,680,311
	MAX ACC PRIOR TO SRM CUT OFF (FT/SEC^2)	104 AT 120 SEC
	MAX ACC PRIOR TO THROTTLING (FT/SEC^2)	*
	MAX ACC AT MAIN STAGE CUT OFF (FT/SEC^2)	*
	DYNAMIC PRESSURE (#/FT^2)	949 AT 61 SEC
	INITIAL SRM MASS FLOW (#/SEC)	218,400
	FINAL SRM MASS FLOW (#/SEC)	110,080
	MAIN STAGE MASS FLOW (#/SEC)	*
	GROSS PAYLOAD (LBS)	1,756,869
PRELIMINARY TRAJECTORY	LIFT OFF WEIGHT (LBS)	33,523,300
	LIFT OFF THRUST (LBS)	54,400,300
	MAX ACC PRIOR TO SRM CUT OFF (FT/SEC^2)	103 AT 130 SEC
	MAX ACC PRIOR TO THROTTLING (FT/SEC^2)	*
	MAX ACC AT MAIN STAGE CUT OFF (FT/SEC^2)	*
	DYNAMIC PRESSURE (#/FT^2)	999 AT 61 SEC
	INITIAL SRM MASS FLOW (#/SEC)	228,900
	FINAL SRM MASS FLOW (#/SEC)	127,200
	MAIN STAGE MASS FLOW (#/SEC)	*
	GROSS PAYLOAD (LBS)	1,777,712
AMLLV TRAJECTORY	LIFT OFF WEIGHT (LBS)	66,132,000
	LIFT OFF THRUST (LBS)	108,000,500
	MAX ACC PRIOR TO SRM CUT OFF (FT/SEC^2)	100 AT 31 SEC
	MAX ACC PRIOR TO THROTTLING (FT/SEC^2)	*
	MAX ACC AT MAIN STAGE CUT OFF (FT/SEC^2)	*
	DYNAMIC PRESSURE (#/FT^2)	997 AT 60 SEC
	INITIAL SRM MASS FLOW (#/SEC)	452,400
	FINAL SRM MASS FLOW (#/SEC)	242,400
	MAIN STAGE MASS FLOW (#/SEC)	*
	GROSS PAYLOAD (LBS)	3,472,000

4.3.1.1   (Continued)

Main Stage Plus Eight Strap-Ons Plus a Tree Module Injection Stage Vehicle

The vehicles consisting of a main stage plus eight strap-on stages plus a three module injection stage were sized to provide an approximate payload of 1/2 of that obtained for the maximum payload vehicle of the AMLLV program. The gross payload obtained for the MLLV configurations ranged from 1,829,000 pounds to 1,859,000 pounds depending on the propulsion system employed on the main stage.

For these configurations, the vehicles were zero staged, i.e., the eight strap-on solid motor stages were ignited at liftoff. The main stage was not ignited until the strap-on stages were expended. With the ignition of the main stage, a COV trajectory was flown. The main stage for these vehicle configurations were flown without a throttled mode. A three module injection stage provided the final impulse and orbital injection of the payload.

Table 4.3.1.1-VII presents the mission weight histories for the maximum payload vehicles. These vehicles are the same except for the propulsion system employed on the main stage. The liftoff thrust was that of the eight strap-on stages, i.e., 51.6 million pounds (6.45 million pounds per SRM). The resulting liftoff thrust to weight was 1.50 as compared to the preliminary trajectory liftoff thrust to weight of 1.58 (vehicle with multichamber/plug propulsion system on main stage). The larger preliminary value was the result of the higher SRM thrust at liftoff (54.4 million pounds).

The mass fraction of the main stage (with the multichamber/plug propulsion system) used in the final trajectory very closely approximated the estimated mass fraction used in the preliminary trajectory. The final stage mass fraction calculated was 0.931 versus the preliminary estimate of C.930. The most significant variation in stage mass fraction occurred with the injection stage. The mass fraction obtained in the final weight analyses was 0.838. The mass fraction utilized in the preliminary flight trajectory was 0.860. As a result, the final injection stage drop weight was approximately 20,000 pounds heavier than the estimated injection stage weight used in the preliminary trajectories. The gross payload obtained in the final trajectory was 1,851,000 pounds as compared to 1,896,000 pounds for the preliminary trajectory.

For the final performance analysis, the maximum payload vehicle (main stage plus three module injection stage plus eight strap-on stages vehicle), three additional configurations were flown. These configurations used the same stage except for the following change to the main stage propulsion system:

a.   Multichamber/plug propulsion system on the main stage with a two position nozzle.

263

TABLE 4.3.1.1-VII   MISSION WEIGHT HISTORY - MAIN STAGE PLUS EIGHT STRAP-ONS PLUS THREE MODULE INJECTION STAGE VEHICLE

PARAMETER / VEHICLE	HIGH PRESSURE MULTICHAMBER/ PLUG (SINGLE POSITION NOZZLE) *	HIGH PRESSURE 2000 PSIA TOROIDAL/ AEROSPIKE	LOW PRESSURE 1200 PSIA TOROIDAL/ AEROSPIKE	HIGH PRESSURE MULTICHAMBER/PLUG (TWO POSITION NOZZLE) *
SRM STAGE				
IGNITION THRUST (S.L.)	51,680,311 LBS.	51,680,311 LBS.	51,680,311 LBS.	51,680,311 LBS.
LIFT-OFF WEIGHT	34,388,973 LBS.	34,353,183 LBS.	34,307,940 LBS.	34,367,100 LBS.
T/W RATIO AT LAUNCH	1.503	1.504	1.506	1.504
SRM PROPELLANT CAPACITY	23,200,000 LBS.	23,200,000 LBS.	23,200,000 LBS.	23,200,000 LES.
SRM PROPELLANT CONSUMED	23,196,023 LBS.	23,196,024 LBS.	23,196,024 LBS.	23,196,024 LBS.
STAGE DROP WEIGHT	2,577,782 LBS.	2,577,782 LBS.	2,577,782 LBS.	2,577,782 LBS.
LAUNCH AZIMUTH	90 DEG.	90 DEG.	90 DEG.	90 DEG.
STAGE MASS FRACTION	0.902	0.902	0.902	0.902
MAIN STAGE				
IGNITION THRUST (VAC)	10,070,845 LBS.	9,830,000 LBS.	9,970,000 LBS.	9,600,000 LBS.
IGNITION WEIGHT	8,615,168 LBS.	8,579,377 LBS.	8,534,134 LBS.	8,593,294 LBS.
T/W RATIO AT IGNITION	1.169	1.146	1.168	1.117
PROPELLANT CONSUMED	5,550,000 LBS.	5,550,000 LBS.	5,550,000 LBS.	5,550,000 LBS.
STAGE DROP WEIGHT	408,208 LBS.	364,347 LBS.	349,537 LBS.	399,807 LBS.
STAGE MASS FRACTION	0.932	0.938	0.941	0.933
INJECTION STAGE				
IGNITION THRUST (VAC)	750,000 LBS.	750,000 LBS.	750,000 LBS.	750,000 LBS.
IGNITION WEIGHT	2,656,960 LBS.	2,665,030 LBS.	2,634,597 LBS.	2,643,487 LBS.
T/W RATIO AT IGNITION	0.282	0.281	0.285	0.284
PROPELLANT CONSUMED	675,000 LBS.	675,000 LBS.	675,000 LBS.	675,000 LBS.
STAGE DROP WEIGHT	130,520 LBS.	130,520 LBS.	130,520 LBS.	130,520 LBS.
STAGE MASS FRACTION	0.838	0.838	0.838	0.838
GROSS WEIGHT IN ORBIT	1,981,961 LBS.	1,990,030 LBS.	1,959,597 LBS.	1,968,487 LBS.
GROSS PAYLOAD	1,851,441 LBS.	1,859,510 LBS.	1,829,077 LBS.	1,837,967 LBS.

*THE DATA OMITTED FROM THIS TABLE IS CLASSIFIED. THIS TABLE, WITH THE CLASSIFIED DATA INCLUDED, IS SHOWN IN VOLUME IX, (CLASSIFIED APPENDIX), APPENDIX E.

4.3.1.1   (Continued)

b.   2000 psia toroidal/aerospike propulsion system on the main stage.

c.   1200 psia toroidal/aerospike propulsion system in the main stage.

While the changes in propulsion system on the main stage had a significant effect on the payload capability of the single-stage-to-orbit vehicle, (see Table 4.3.1.1-I) its effect was less significant for the maximum payload vehicle because of the strap-on stages and the injection stage. The 2000 psia toroidal/aerospike propulsion system vehicle puts the most gross weight into orbit and also the most payload. The multichamber/plug system with the single position nozzle puts up almost the same gross weight and payload. The 1200 psia toroidal/aerospike and the multi-chamber/plug with the two position nozzle put up a lesser gross weight and payload. The 1200 psia toroidal system puts up 1,829,000 pounds payload as compared to 1,859,000 pounds for the 2000 psia toroidal and 1,851,000 pounds and 1,838,000 pounds for the multichamber/plug single position nozzle vehicle and multichamber/plug two position nozzle, respectively.

A comparison of the final performance shows that the different propulsion systems on the main stage will have little effect in the vehicle accelerations and dynamic pressure. The injection stage and the strap-on solid motor stages overrode the main stage propulsion system differences. The single position multichamber/plug propulsion system vehicle and the 2000 psia toroidal/aerospike system provided the maximum payloads. These vehicles were more nearly optimized in burn ratio and mass flow rates. Some improvement in payload could be obtained if these parameters were optimized for the multichamber/plug two position nozzle and the 1200 psia toroidal/aerospike vehicle. Table 4.3.1.1-VIII shows comparative final performance data for vehicles with four different main stage propulsion systems. For the vehicle configuration with the multichamber/plug and the single position nozzle, comparative data with the preliminary trajectory results and the AMLLV trajectory results are also shown.

The lower liftoff thrust for the final trajectory of the single position multichamber/plug vehicle was the result of the SRM trace shape. The effect of this trace shape was also observed in the maximum acceleration prior to solid motor cut-off. This value decreased from 96 to 86 feet per second squared. The maximum acceleration prior to main stage cut-off and at injection stage cut-off were similar for the trajectories. The maximum dynamic pressure decreased from 939 pounds per square foot to 887 pounds per square foot as a result the lower energy input to the vehicle resulting from the reduced initial SRM thrust level. Maximum dynamic pressure for the AMLLV trajectory more closely approximated the dynamic pressure obtained with the preliminary trajectory. (For the AMLLV vehicle, the solid motor trace shape was not modified to reduce the initial thrust pressure level.)

TABLE 4.3.1.1-VIII   COMPARATIVE PERFORMANCE DATA – MAIN STAGE PLUS EIGHT STRAP-ON SRM STAGES PLUS A THREE MODULE INJECTION STAGE VEHICLES

PARAMETER	MAIN STAGE WITH ** MULTI-CHAMBER/PLUG SINGLE POS NOZZLE	MAIN STAGE WITH 2000 PSIA TOROIDAL/AEROSPIKE	MAIN STAGE WITH 1200 PSIA TOROIDAL/AEROSPIKE	MAIN STAGE WITH ** MULTI-CHAMBER/PLUG TWO POSITION NOZZLE
FINAL TRAJECTORY				
LIFT OFF WEIGHT (LBS)	34,388,973	34,353,183	34,307,940	34,367,100
LIFT OFF THRUST (LBS)	51,680,311	51,680,311	51,680,311	51,680,311
MAX ACC PRIOR TO SRM CUTOFF (FT/SEC^2)	96 AT 120 SEC	97 AT 120	97 AT 120 SEC	97 AT 120 SEC
MAX ACC PRIOR TO MAIN STAGE CUTOFF (FT/SEC^2)	**	**	**	**
MAX ACC AT INJECTION CUTOFF (FT/SEC^2)	**	**	**	**
DYNAMIC PRESSURE (#/FT^2)	888 AT 63 SEC	889 AT 62 SEC	897 AT 67 SEC	882 AT 63 SEC
INITIAL SRM MASS FLOW (#/SEC)	218,400	218,400	218,400	218,400
FINAL SRM MASS FLOW (#/SEC)	110,080	110,080	110,080	110,080
MAIN STAGE MASS FLOW (#/SEC)	**	**	**	**
INJECTION MASS FLOW (#/SEC)	**	**	**	**
GROSS PAYLOAD (LBS)	1,851,440	1,859,510	1,829,077	1,837,967
PREM TRAJECTORY				
LIFT OFF WEIGHT (LBS)	34,426,000	N/A *	N/A *	N/A *
LIFT OFF THRUST (LBS)	54,400,000			
MAX ACC PRIOR TO SRM CUTOFF (FT/SEC^2)	96 AT 130 SEC			
MAX ACC PRIOR TO MAIN STAGE CUTOFF (FT/SEC^2)	**			
MAX ACC PRIOR TO INJECTION CUTOFF (FT/SEC^2)	**			
DYNAMIC PRESSURE (#/FT^2)	939 AT 63 SEC			
INITIAL SRM MASS FLOW (E/SEC)	228,900			
FINAL SRM MASS FLOW (#/SEC)	127,200			
MAIN STAGE MASS FLOW (#/SEC)	**			
INJECTION MASS FLOW (#/SEC)	**			
GROSS PAYLOAD (LBS)	1,895,605			
ANLLY TRAJECTORY				
LIFT OFF WEIGHT (LBS)	67,896,000	N/A *		N/A *
LIFT OFF THRUST (LBS)	108,000,000			
MAX ACC PRIOR TO SRM CUTOFF (FT/SEC^2)	92 AT 132 SEC			
MAX ACC PRIOR TO MAIN STAGE CUTOFF (FT/SEC^2)	**			
MAX ACC PRIOR TO INJECTION CUTOFF (FT/SEC^2)	**			
DYNAMIC PRESSURE (#/FT^2)	938 AT 62 SEC			
INITIAL SRM MASS FLOW (#/SEC)	452,400			
FINAL SRM MASS FLOW (#/SEC)	242,400			
MAIN STAGE MASS FLOW (#/SEC)	**			
INJECTION STAGE MASS FLOW (#/SEC)	**	* NOT AVAILABLE		
GROSS PAYLOAD (LBS)	3,740,000			

*THE DATA OMITTED FROM THIS TABLE IS CLASSIFIED. THIS TABLE, WITH THE CLASSIFIED DATA INCLUDED, IS SHOWN IN VOLUME IX, (CLASSIFIED APPENDIX), APPENDIX E.

* NOT AVAILABLE

4.3.1.1   (Continued)

The initial and final values for SRM mass flow rate on the final trajectory were
lower than those of the preliminary trajectory as a result of the modified SRM
trace shape. The mass flow values for the main and the injection stage were
approximately the same for the final and preliminary trajectories. Those of the
AMLLV were approximately double those of the half size vehicle as would be expected.

Final Trajectory Summary

Figure 4.3.0.0-1 above shows a summary of the gross payloads to 100 NM orbit
versus launch weight for the MLLV configurations studied. A range of payload
capability between one-half million pounds up to two million pounds can be achieved
with various combinations of the main stage, injection stage modules, and strap-
on solid stages. A second conclusion that can be derived from this summary is that
the main stage with strap-ons vehicle configurations have not achieved the maximum
possible payload and that the addition of more solid propellants will continue to
provide further payload improvements. The injection stage itself does not appear
to significantly increase the payload capability for the 100 N M mission. As stated
in previous paragraphs, its main advantages are to provide orbital maneuvering
and increased payload capability for higher energy missions.

4.3.1.2   Vehicle Exchange Ratios

Using the payloads indicated for the baseline configurations as constants, curves
were prepared to show launch weight sensitivities, of the various MLLV configura-
tions, to stage mass fraction and to specific impulse. Curves were also prepared
to show the relationship of stage mass fraction to propellant density. This data
was prepared for use in the Phase III, Task III activity for evaluation of the cost/
performance potential of advanced technologies. The resulting data application
of this data to those particular analyses is shown and discussed in Volume VI
of this final report.

4.3.2   Final Weights

This section contains the final weights defined for the main stage, injection stage
modules and the solid motor strap-on stages. The sources of weight data, the
assumptions used and the results are presented.

The structural weights were obtained from stress analyses of the main and injection
stages. The design data used are reported in Sections 4.3.3 and 4.3.4 below. The
main stage propulsion system weights were selected from parametric weights data
provided by Pratt and Whitney and Rocketdyne for the multichamber/plug and toroidal/
aerospike propulsion systems, respectively. The plug support structure weight
was developed from a design and stress analysis considering the main stage to
propulsion system interface. The propulsion/mechanical system weights were

4.3.2   (Continued)

developed for the MLLV based on the same concepts as used for the AMLLV system. Sections 4.3.3 and 4.3.4 describe in detail the engines and their supporting propulsion/mechanical systems and provide detailed weight breakdowns. The electrical/electronic equipment and instrumentation weights were based on using micro-electronics and state-of-the-art improvements in power systems.

Separation system weights were based on the separation rocket motor impulse requirements considering the criteria that successful separation will be attained even though one separation motor fails to operate. The main stage/injection stage separation requirements were based on giving the spent main stage having the same separation deceleration as the current S-IC stage.

Residual propellants were assumed to consist of one tenth of one percent (0.1%) of the (LOX) and one percent (1.0%) of the LH_2 (same as was used in the AMLLV study). The injection stage weights considered the modular stacking concept to arrive at the weights for combination of one, two, and three injection stage modules. The structural weights were obtained from stress analyses of the injection stage as presented in paragraph 4.3.4. Injection stage engine weights data were obtained from parametric weights data provided by Pratt and Whitney.

Two engines weighing 1930 pounds each were included for the first injection stage module. Each additional module required two additional engines. These engines will be added to the thrust ring frame of the first injection stage module. The injection stage residual propellants were three percent (3%) of the usable propellant weight for the lower module of the injection stage with 1,000 pounds added for each additional module. The electrical/electronic equipment and instrumentation weights were based on the use of microelectronics and state-of-the-art improvements in power systems. The weight of the injection stage ullage rockets were estimated by determining total impulse requirements and using representative separation rocket motor weights to meet these impulse requirements.

Table 4.3.2.0-I presents the MLLV main stage weight for the single-stage-to-orbit vehicle with either the multichamber/plug propulsion system, the 2,000 psi toroidal/aerospike propulsion system or the 1200 psig toroidal/aerospike. The resulting mass fractions were 0.936 for the multichamber/plug vehicle and 0.943 and 0.945 for the toroidal/aerospike propulsion system vehicles. Corresponding vehicles from the AMLLV study had mass fractions of 0.940 for the multichamber/ plug vehicle and 0.946 for the 2000 psia toroidal/aerospike vehicle. The slightly lower mass fraction obtained for the half size MLLV was the result of weights of components on the main stage which were not directly scalable such as engines, the electrical/electronic equipment, instrumentation, and stage insulation. The preliminary trajectory analyses used mass fractions of 0.933 and 0.936 for the multichamber/plug and 2000 toroidal/aerospike systems, respectively. (The 1200

TABLE 4.3.2.0-I   MAIN STAGE - SINGLE-STAGE-TO-ORBIT VEHICLES

	MAIN STAGE WITH MULTICHAMBER/PLUG PROPULSION SYSTEM		MAIN STAGE WITH 2000 PSIA TOROIDAL/AEROSPIKE PROPULSION SYSTEM		MAIN STAGE WITH 1200 PSIA TOROIDAL/AEROSPIKE PROPULSION SYSTEM	
	MAJOR COMPONENTS	DETAIL BREAKDOWN	MAJOR COMPONENTS	DETAIL BREAKDOWN	MAJOR COMPONENTS	DETAIL BREAKDOWN
Stage Structure	210,840		208,652		208,652	
Forward Skirt		(28,560)		(28,560)		(28,560)
Holddown Post		2,500		2,500		2,500
Cylindrical Skirt		23,760		23,760		23,760
Insulation		2,300		2,300		2,300
Propellant Containers		(165,513)		(165,513)		(165,513)
Upper Bulkhead		14,525		14,525		14,525
Common Bulkhead		35,055		35,055		35,055
Common Bulkhead		1,220		1,220		1,220
Insulation		25,030		25,030		25,030
Lower Bulkhead		1,380		1,380		1,380
Lower Bulkhead						
Insulation		8,000		8,000		8,000
Oxidizer Cylinder		65,167		65,167		65,167
Fuel Cylinder		5,000		5,000		5,000
Fuel Cylinder						
Insulation		10,136		10,136		10,136
Propellant Delivery System						
Thrust Structure		(16,767)		(14,579)		(14,579)
Cylindrical Skirt		10,080		10,389		10,389
Thrust Posts		2,677		-		-
Lower Thrust Ring		4,010		4,190		4,190
Propulsion System	116,613		75,050		60,240	
Pressurization System	14,532		14,532		14,532	
Equipment & Instrumentation	2,500		2,500		2,500	
Separation System	5,738		5,738		5,738	
Contingency	7,465		7,356		7,356	
Total Dry Weight	357,688		313,828		299,018	
Residual Propellants	12,638		12,638		12,638	
Pressurization Gases	7,840		7,840		7,840	
Propellant Trapped in Eng.	3,000		3,000		2,490	
Stage Weight at Separation	381,166		337,306		321,986	
Mainstage Propellant	5,550,000		5,550,000		5,550,000	
Stage at Lift-Off	5,931,166		5,887,306		5,871,986	
Stage Mass Fraction (λ)	0.936		0.943		0.945	

NOTE: ALL WEIGHT IN POUNDS.

4.3.2   (Continued)

psia toroidal/aerospike was not studied during the trade phase of this study.)
As the preliminary and final weights were in close agreement, the conclusions based
on the preliminary weight data were valid such that no iterative loads or control
analyses were required.

Table 4.3.2.0-II lists the MLLV main stage weights for the vehicle consisting
of a main stage plus a single injection stage module. The forward skirt for this
vehicle and that for the single stage to orbit vehicle will be identical and were sized
for the more severe loads which will occur for the main stage plus the single
module injection stage vehicle. A minor weight penalty, therefore, was imposed on
the single stage to orbit vehicle. (Minor throttling of the main stage for this latter
vehicle could reduce the skirt weight.) The mass fraction obtained for this main
stage was 0.936 as compared to the 0.939 value obtained for the corresponding
main stage of the AMLLV. As stated previously, the reason for the slightly
different mass fraction were the components which were not directly scalable.
For this weight analysis, the propulsion system assumed was the multichamber/
plug propulsion system. The data obtained from the preliminary analyses are
valid since the final mass fraction varied only slightly from that used for the
preliminary analyses.

Table 4.3.2.0-III lists the weight breakdown for the main stage of the configura-
tions which will incorporate strap-on stages. For all strap-on vehicle configura-
tions, the same "heavy" weight forward skirt will be utilized. This skirt will be
designed by the most severe loads condition (max. payload vehicle) and thus
will, therefore, be slightly oversized for the other configurations. The main stage
mass fraction obtained was 0.931. This value corresponds to the 0.936 mass
fraction obtained for the equivalent AMLLV main stage. It was assumed for this
weight analysis that the multichamber/plug propulsion system will be utilized.
The data from the flight environmental analyses are valid since the preliminary
weights resulted in a mass fraction of 0.930 which was only 0.001 lower than that
mass fraction based on the final weights.

Table 4.3.2.0-IV lists the injection stage weight for one, two and three module
combinations. The mass fractions obtained were 0.785, 0.825, 0.838 respectively.

These values correspond to mass fractions of 0.82, 0.84, and 0.87 for the equivalent
AMLLV injection stage module combinations. As with the main stage, the injection
stage module mass fractions were below those of the prior AMLLV study due to the
non-scalable stages components. The preliminary injection stage module weights
gave mass fractions of 0.80, 0.83 and 0.86 for the one, two and three module
injection stage, respectively.

TABLE 4.3.2.0-II   MAIN STAGE – MAIN STAGE PLUS SINGLE INJECTION STAGE
VEHICLE (Multichamber/Plug Engine System)

	MAJOR COMPONENTS	DETAIL BREAKDOWN
Stage Structure	210,840	
Forward Skirt		(28,560)
Holddown Post		2,500
Cylindrical Skirt		23,760
Insulation		2,300
Propellant Containers		(165,513)
Upper Bulkhead		14,525
Common Bulkhead		35,055
Common Bulkhead Insulation		1,220
Lower Bulkhead		25,030
Lower Bulkhead Insulation		1,380
Oxidizer Cylinder		8,000
Fuel Cylinder		65,167
Fuel Cylinder Insulation		5,000
Propellant Delivery System		10,136
Thrust Structure		(16,767)
Cylindrical Skirt		10,080
Thrust Posts		2,677
Lower Thrust Ring		4,010
Propulsion System	116,613	
Pressurization System	14,532	
Equipment and Instrumentation	2,500	
Separation System	5,738	
Contingency	7,465	
Total Dry Weight	357,688	
Residual Propellants	12,638	
Pressurization Gases	7,840	
Propellant Trapped in Engines	3,000	
Stage Weight at Separation	381,166	
Mainstage Propellant	5,550,000	
Stage at Lift-Off	5,931,166	
Stage Mass Fraction (λ)	0.936	

NOTE: ALL WEIGHT IN POUNDS

TABLE 4.3.2.0-III MAIN STAGE WEIGHT - MAIN STAGE FOR STRAP-ON
CONFIGURATIONS (MULTICHAMBER/PLUG ENGINE
SYSTEM

	MAJOR COMPONENTS	DETAIL BREAKDOWN
Stage Structure	237,148	
Forward Skirt		(48,284)
Thrust Post		10,567
Cylindrical Skirt		35,41?
Insulation		2,300
Propellant Containers		(165,513)
Upper Bulkhead		14,525
Common Bulkhead		35,055
Command Bulkhead Insulation		1,220
Lower Bulkhead		25,030
Lower Bulkhead Insulation		1,380
Oxidizer Cylinder		8,000
Fuel Cylinder		65,167
Fuel Cylinder Insulation		5,000
Propellant Delivery System		10,136
Thrust Structure		(23,351)
Cylindrical Skirt		10,080
Thrust Post		2,677
Lower Thrust Ring		10,594
Propulsion System	116,613	
Pressurization System	14,532	
Equipment and Instrumentation	2,500	
Separation System	5,738	
Contingency	8,198	
Total Dry Weight	384,729	
Residual Propellants	12,638	
Pressurization Gases	7,840	
Propellant Trapped in Engines	3,000	
Stage Weight at Separation	408,207	
Mainstage Propellant	5,550,000	
Stage at Lift-Off	5,958,207	
Stage Mass Fraction (λ)	0.931	
NOTE: All Weight in Pounds		

TABLE 4.3.2.0-IV   MLLV INJECTION STAGE WEIGHTS

COMPONENT	1 MODULE	2 MODULES	3 MODULES
Stage Structure	(41,380)	(67,055)	(93,820)
Cylindrical Skirt	12,575	21,370	31,260
LH$_2$ Tank	11,815	23,630	35,445
Hanger Skirt	100	200	300
LOX Tank	3,710	7,420	11,130
Thrust Structure	9,340	9,435	9,525
Base Heat Protection	2,680	2,680	2,680
Ullage Rockets	1,160	2,320	3,480
Propulsion System	(3,860)	(7,720)	(11,580)
Propellant Feed System	(875)	(1,830)	(2,780)
Pressurization System	(570)	(1,140)	(1,710)
Equipment & Instrumentation	(1,200)	(1,300)	(1,400)
Contingency (5% of Structure)	(2,070)	(3,350)	(4,690)
Total Dry Weight	49,955	82,395	115,980
Residual Propellants	11,250	12,250	13,250
Pressurization Gases	430	860	1,290
Stage Inert Weight (Total)	61,635	95,505	130,520
Usable Propellant	225,000	450,000	675,000
Stage Mass Fraction (λ')	0.785	0.825	0.838

4.3.2   (Continued)

Table 4.3.2.0-V lists the weight breakdown for a single strap-on stage. The mass fractions determined were 0.915 and 0.902 for the SRM and the complete stage, respectively. These values were the same as used for the AMLLV and in the preliminary performance analyses.

Preliminary weight data, referred to above, are reported in the preceeding Section 4.2.3.

4.3.3   Main Stage

This section presents the detailed design data for the main stage of the Multipurpose Large Launch Vehicle including the stage and subsystems, description, design concept, materials and performance. The design and performance data are presented for both the multichamber/plug and the toroidal/aerospike main stage configurations. Comparisons of the vehicle design and performance parameters with the different propulsion systems are shown in subsequent Section 4.3.7.2.

The main stage, sized to orbit one half million pounds payload to low Earth orbit will contain 5.55 million pounds of LOX/LH$_2$ propellant and have 8.0 million pounds of liftoff thrust. The inert weight (stage drop weight) of 337,300 pounds will result in a stage mass fraction of approximately 0.943 (numbers quoted are for the toroidal/aerospike main stage). For comparison, the MLLV single-stage-to-orbit vehicle will have approximately twice the payload capability of the S-IC/S-II Saturn V derivative with only a nine percent increase in inert weight. Physically, the MLLV main stage is over 1.7 times the diameter of the S-IC/S-II but is approximately 80 feet shorter.

A comparison of the MLLV main stage to the AMLLV main stage shows the MLLV has half the payload capability with slightly more than half the inert weight. Physically the MLLV is approximately 80 percent of the diameter of the AMLLV main stage and will be approximately 18 feet shorter (AMLLV dimensions divided by the cube root of two).

4.3.3.1   Structural Design

The structural design of the main stage was based on the application of proven (S-IC) fabrication techniques and materials. Design details are as shown in Figure 4.3.3.1-1. The optimum arrangement of components were defined in the conceptual design section 4.2.

The structure will be principally conventional skin-stringer-frame construction using 2219-T87 aluminum for the propellant tanks and 7075-T6 aluminum for the forward skirt and thrust structure. The design will have a forward LOX tank to

274

TABLE 4.3.2.0-V   MLLV SOLID MOTOR STRAP-ON STAGE WEIGHT

	MAJOR COMPONENTS	DETAIL BREAKDOWN
Steel Chamber	181,190	
Forward Head and Skirt		18,360
Cylinder		146,560
Aft Head and Skirt		16,270
Insulation	17,559	
Liner	1,537	
Nozzle Assembly	40,710	
Steel Support		4,025
Steel Closure		8,400
Flexseal Assembly		16,820
Carbon Cloth Phenolic		3,730
Silica Cloth Phenolic		2,775
Insulation		4,960
Forward Exit Cone Assembly	10,825	
Steel Shell		4,635
Carbon Cloth Phenolic		4,030
Silica Cloth Phenolic		2,160
Aft Exit Cone Assembly	14,115	
Honeycomb Structure		3,435
Silica Cloth Phenolic		10,680
TVC Actuation System	2,145	
Igniter Assembly	1,579	
Motor Inert Weight	269,660	
Motor Propellant Weight	2,900,000	
Total Motor Weight	3,169,660	
Stage Component Weights	46,060	
Attachment Structure		39,215
Aft Separation Motors		1,785
Nose Cone Structure Plus Insulation		2,680
Nose Cone Separation Motors		2,380
Total Strap-On Stage Weight	3,215,720	
Motor Mass Fraction (χ)		0.915
Stage Mass Fraction (χ')		0.902

NOTE: ALL WEIGHTS IN POUNDS
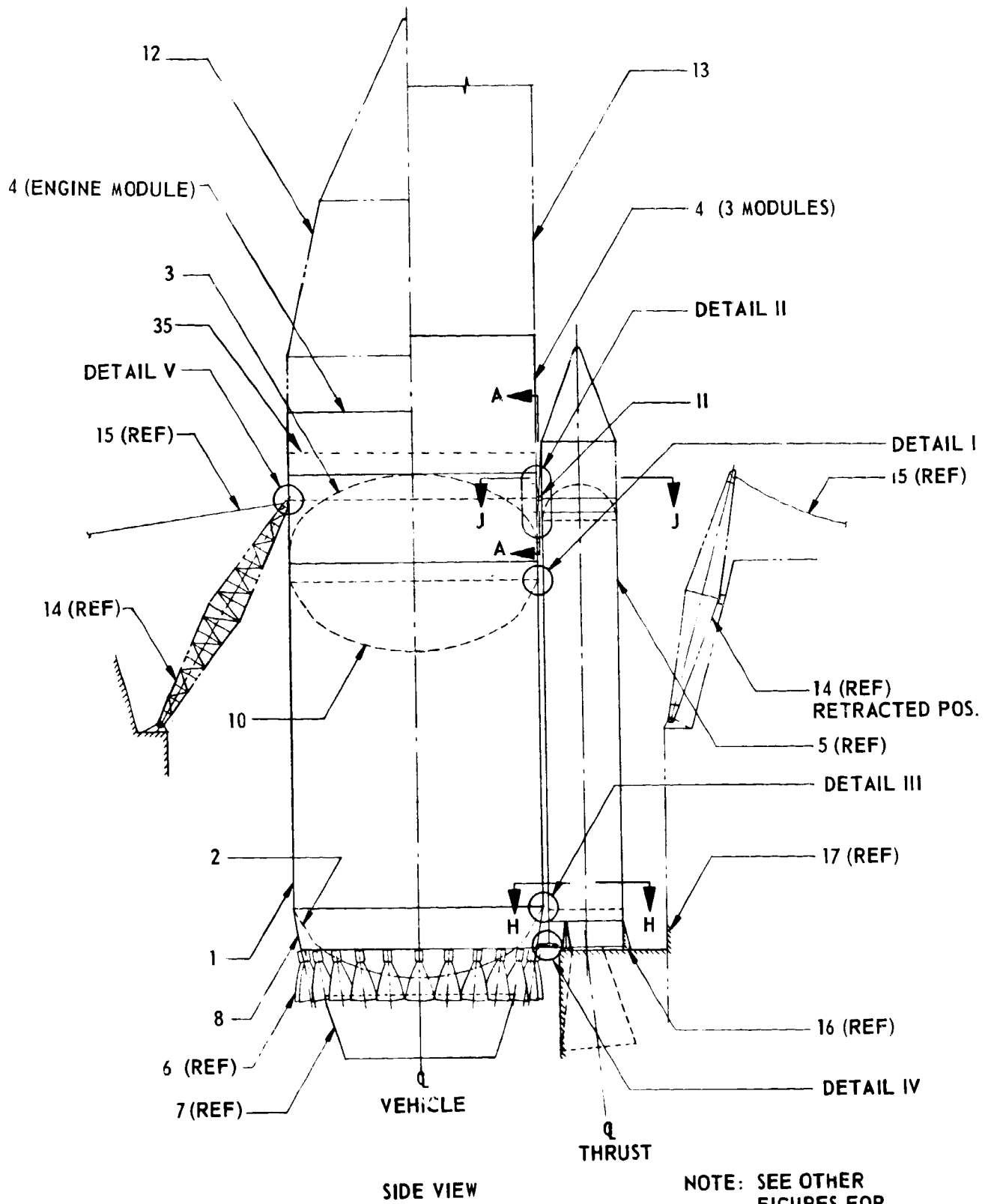
1.
2.
3.
4.
5.

6.
7.
8.

9.

10.
11.

12.

13.

14.
15.
16.
17.
18.
19.

20.

21.
22.

23.

24.
25.
26.

27.

28.

29.

30.
31.
32.

33.
34.
35.

36.

37.
38.

NOTE: SEE OTHER
FIGURES FOR
DETAILS I THRU V

SIDE VIEW

FIGURE 4.3.3.1-1   MLLV STRUCTURAL DESIGN

MLLV CORE STAGE
LOWER BULKHEAD CORE STAGE
UPPER BULKHEAD CORE STAGE
INJECTION STAGE
SOLID ROCKET MOTOR (SRM) STRAP-ON -260"
DIAMETER MOTOR (REF)
ENGINE (REF)
CENTERBODY PLUG (REF)
AFT SKIRT 7075-T6 AL SKIN-STRINGER-FRAME
CONSTRUCTION
FORWARD SKIRT 7075- T6
FRAME CONSTRUCTION (DETAIL II)
COMMON BULKHEAD CORE STAGE
SRM THRUST ATTACHMENT STRUCTURE, PIN
JOINT
PAYLOAD ENVELOPE SINGLE MODULE INJECTION
STAGE
PAYLOAD ENVELOPE TRIPLE MODULE INJECTION
STAGE
BOOM CORE HOLDDOWN SCHEMATIC ONLY (REF)
BOOM GUY WIRES (REF)
SRM BASE SUPPORT (REF)
LAUNCH FACILITY (REF) SCHEMATIC ONL
INSULATION FOAM (DETAIL III EXTERNAL)
T-STRINGER, LH$_2$ TANK 2219-T87 AL EXTRUSION
WELDED OR RIVETED (OPT) TO SKIN DETAIL III
LH$_2$ TANK SKIN MILLED 2219-T87 RING WELDED
RIVETS ALUMINUM (DETAIL I)
COMMON FITTING MACHINED 2219-T87 RING
WELDED BETWEEN COMMON BULKHEAD LOX
CYLINDER AND LH$_2$ CYLINDER
LOX CYLINDER INTEGRALLY STIFFENED
MACHINED 2219-T87 PLATE
BLIND FASTENER
SHIM LAMINATED
UPPER FACING HONEYCOMB COMMON BULKHEAD
CHEM MILLED 2219-T87 PLATE
LOWER FACING HONEYCOMB COMMON BULKHEAD
CHEM MILLED 2219-T87 PLATE
HONEYCOMB CORE 5052 AL FLEX-CORE BRAZED
OR ADHESIVELY BONDED
Y-RING COMMON BULKHEAD 2219-T87 AL
ALUMINUM EXTRUSTION
JUNCTION RING FRAME COMMON BULKHEAD
STIFFENER ANGLE 2219-T87 AL EXTRUSION
STRINGER FORWARD SKIRT FORMED 7075-
T6 AL SHEET
SKIN FORWARD SKIRT 7075-T6 AL SHEET
RING ANGLE 7075-T6 AL EXTRUSION
HEAT SHIELD INJECTION STAGE (REF)
HONEYCOMB WITH REFRASIL FACING
RING FRAME FIELD SPLICE BUILT-UP
CONSTRUCTION 7075-T6 AL
AFT SKIRT, INJECTION STAGE OR PAYLOAD (REF)
SHEAR BOLT PATTERN SPLICE JOINT

39. Y-RING UPPER BULKHEAD MACHINED 2219-T87 RING WITH INTEGRAL STIFFENERS
40. SPLICE PLATE 2219-T87 AL SHEET
41. INTERMEDIATE RING LH$_2$ TANK ALUMINUM HONEYCOMB CONSTRUCTION ADHESIVELY BONDED
42. JUNCTION RING FRAME LOWER BULKHEAD ALUMINUM HONEYCOMB CONSTRUCTION BRAZED OR BONDED
43. JUNCTION RING FRAME LOWER BULKHEAD
44. STRINGER AFT SKIRT FORMED 7075-T6 AL SHEET
45. SKIN AFT SKIRT 7075-T6 AL SHEET
46. SPLICE PLATE INNER 7075 - T6
47.
48. } SPLICE PLATES OUTER 7075 - T6
49.
50. SRM THRUST POST 7075-T6 AL DIE FORGING
51. SHEAR PIN, SRM THRUST 4340 STEEL HT. 270 KSI
52. EXPLOSIVE NUT SRM STAGING RELEASE
53. RETAINER BOLT STEEL
54. RETAINER WASHER FITTING STEEL
55. SPECIAL SPHERICAL BEARING BEARING FITTING 4340 STEEL (FOR SRM CONFIGURATION ONLY)
56. SRM ATTACHMENT STRUCTURE (REF)
57. BOLT RETAINER FITTING 7075-T6 AL DIE FORGING
58. BACKUP FITTING SRM FORWARD ATTACHMENT 7075-T6 AL DIE FORGING
59. DEEP RING FRAME ASSEMBLY (SRM CONFIGURATION ONLY)
60. INTERMEDIATE RING FRAME AL HONEYCOMB CONSTRUCTION
61. SRM SIDE LOAD FITTING AFT ATTACHMENT WITH SPHERICAL BEARING (REF)
62. SLIP JOINT FITTING AFT SRM ATTACHMENT 7075-T6 AL DIE FORGING
63. TUBULAR STRUT AFT SRM ATTACHMENT
64. ATTACHMENT FITTING AFT SRM TUBULAR STRUT 7075-T6 AL DIE FORGING
65. SPHERICAL BEARING ATTACHMENT
66. TENSION BOLT AFT SRM STRUT STEEL
67. HOLDDOWN POST 7075-T6 AL DIE FORGING
68. SPHERICAL BEARING ASSEMBLY 4340 STEEL (FOR CORE ONLY HOLDDOWN)
69. EXPLOSIVE NUT HOLDDOWN RELEASE (REF)
70. SHEAR PIN RETAINER FITTING 7075-T6 AL DIE FORGING
71. DEEP RING FRAME ASSEMBLY (CORE ALONE CONFIGURATION ONLY)
72. BACKUP FITTING CORE HOLDDOWN ATTACHMENT 7075-T6 AL DIE FORGING
73. BACKUP FITTING SRM AFT ATTACHMENT 7075-T6 AL DIE FORGING
74. EXPLOSIVE NUT TUBULAR SRM STRUT RELEASE
75. FITTING TUBULAR AFT SRM ATTACHMENT (REF)
76. SHEAR PIN 4340 STEEL HT. 270 KSI SLEEVE (CORE ALONE HOLDDOWN ONLY)
77. TENSION BOLT 220 KSI STEEL

4.3.3.1 (Continued)

minimize control requirements. Both the aerospike and plug engine systems favor a low length/diameter (L/D) stage design which will allow efficient structural design of the propellant tanks.

The common bulkhead will be a sandwich structure designed to take buckling loads that occur near propellant depletion. This construction was determined to be more efficient than increasing the LOX tank pressure to maintain the bulkhead in tension. The bulkheads and tank skins will be designed for loads encountered during the zero stage operation of the M/C + 8(S) + 3S(I) vehicle. Flight conditions for the single-stage-to-orbit vehicle will result in the maximum compressive loads for the LH_2 tank shell and thrust structure. Since the forward skirt will be subjected to a wide range of combined compressive loads from 4,600 pounds to 9,300 pounds per square inch the design of two different forward skirts is provided to minimize the weight penalties.

The use of the forward skirt for vehicle support and solid motor thrust takeout will minimize ground wind and emergency rebound main stage loads and in-flight bending moments for the core plus strap-on configurations. The forward skirt reaction point will provide a short load path between the support or thrust take-out connections of the large inertia payload and LOX tank elements.

The thrust structure was the only major element of the stage whose design was influenced by the engine systems. For the multichamber/plug engine system, a thrust post will be required for each engine module to react the concentrated thrust load. By comparison, the thrust structure for the same thrust level toroidal/aerospike engine system will be 2,188 pounds lighter.

In the reference AMLLV study, a representative thrust structure skin panel was analyzed to determine its reaction to the acoustical loading encountered in the twelve 260-inch solid motor AMLLV configuration. The three sigma peak static pressure for the AMLLV was computed to be 3.5 psi which will result in an estimated maximum cyclic stress of 3,000 pounds per square inch. This stress is well within the fatigue life of 7075-T6 aluminum plate. (The overall sound pressure level was estimated to vary from 179 db at the base of the plug to 160 db at the forward slange of the forward skirt.) No problems are anticipated for the MLLV despite the three sigma peak static pressure of 4.5 psi as the acoustic loads (see Section 4.2.4.8) are not significant compared to other loads in the high acoustic (thrust structure) region of the vehicle.

Main stage control requirements of 3.9 degrees total thrust vector deflection were determined based on design wind and accounting for center of pressure, center of gravity, and thrust vector variations. This requirement is within the hinging capability of a multichamber engine module and the LOX or liquid injection system vectoring capability of the toroidal/aerospike engine system (per engine contractors letters, Volume IX Appendices A and B).

279

4.3.3.1   (Continued)

Primary structure "requirements" were determined based upon the design load envelope as defined for two vehicle configurations (see previous section 4.2.4).

The two configurations were:

a.   Single-stage-to-orbit vehicle.

b.   Main stage plus three injection stage modules with eight 260 inch diameter solid motor strap-on stages vehicle.

The propellant tanks were sized for the highest loads and internal pressures associated with the above vehicles. The forward and aft skirts were designed to meet propulsion system and strap-on solid motor stage "requirements". This approach resulted in one tank configuration for all vehicles and two sets of forward and aft skirts. The two aft skirt designs meet the "requirements" of the two engine configurations: (1) One aft skirt design is for the multichamber/plug propulsion system and (2) the other aft skirt design is for the segmented toroidal/aerospike system. Both aft skirts will be adequate for the above listed two vehicle configurations with the provision for a heavier aft thrust ring section to support the solid strap-on attachment loads. The design of the MLLV is similar to the Saturn V/S-IC in that the tankage is a welded integrally stiffened structure and the skirts are mechanically fastened hat-stiffened structures. The MLLV propellants are LOX-LH$_2$ which will require the tankage material to perform satisfactorily at cryogenic temperature. The "requirement" of cryogenic properties of material, compatibility with LOX and liquid hydrogen and other considerations narrowed the selection of baseline material to aluminum alloys. 2219-T87 Aluminum alloy was selected for the tankage construction because of its excellent fusion weldability and other qualities particularly in the fracture toughness area. Aluminum alloy 7075-T6 was chosen over 7178-T7 for the skirts primarily because of corrosion resistance even though the 7178-T6 has a slightly higher strength-to-weight ratio. The choice of 7075-T6 alloy is also supported by previous successful applications on the S-IC and numerous aircraft structures. Table 4.3.3.1-I lists the structural materials used for the various structural components of the core stage. Materials and method of construction are also identified in this table.

Included herein is a summary of the design conditions/restrictions and analyses methods/techniques for sizing main stage major structural elements. The back-up stress calculations are shown in Volume VIII, Appendix B.

Propellant Tanks and Lines

The tanks and bulkheads will be 2219-T87 aluminum. Either brazed aluminum or built-up aluminum ring frames will be bolted to the integral skin-stringer tank walls. Insulation (5000 pounds of insulation) will be bonded to the outside of the

TABLE 4.3.3.1-I MLLV BASELINE STRUCTURAL DESIGN

STRUCTURAL COMPONENT	STAGE LOCATION		STRUCTURAL MATERIALS	CONSTRUCTION
	FROM STA.	TO STA.		
FORWARD SKIRT	1450	1690	7075–T6 ALUMINUM	SKIN, STRINGER, FRAME
FORWARD LOX TANK BULKHEAD	1450	1690	2219–T87 ALUMINUM	MONOCOQUE
LOX TANK WALL	1396	1450	2219–T87 ALUMINUM	MONOCOQUE (SHORT CYLINDER BETWEEN Y–RINGS)
COMMON BULKHEAD	1203	1396	2219–T87 ALUMINUM FACINGS, 5052 ALUMINUM CORE	HONEYCOMB SANDWICH
LH$_2$ TANK WALL	493	1396	2219–T87 ALUMINUM	SKIN, STRINGER, FRAME
AFT BULKHEAD	300	493	2219–T87 ALUMINUM	MONOCOQUE
THRUST STRUCTURE	355	493	7075–T6 ALUMINUM	SKIN, STRINGER, FRAME

4.3.3.1   (Continued)

entire LH$_2$ tankage to (1) prevent formation of liquid air on the tank wall exterior,
(2) minimize boiloff at ground hold, and (3) maintain the tank wall structure below
-50°F. Propellant topping will be used to compensate for LH$_2$ boiloff during ground
hold. The LOX duct and common bulkhead (1220 pounds of insulation) also will have
an insulation coating to prevent LOX freezing and differential thermal stresses in
the honeycomb facings. The lower (LH$_2$) bulkhead will be insulated with 1380 pounds
of polyurethane foam insulation.

Semi-elliptical 0.707 bulkheads with peripheral conical frustums will be used for
both the common and LH$_2$ bulkheads. The semi-elliptical bulkheads will be tangent
to the truncated cone which intersects the cylindrical sidewalls at a 30 degree angle.
A true 0.707 ellipse will be used for the upper LOX bulkhead. The forward LOX and
aft LH$_2$ bulkheads are monocoque shells which were designed for the non-uniform
internal pressure applied to the bulkheads for the strap-on configuration. The
analysis considered the meridional membrane stresses for determining required
skin thickness at various points on the shell. The common bulkhead is a sandwich
construction sized for non-uniform internal pressure for the strap-on vehicle
configuration and for a uniform external pressure applied near LOX depletion for
the core vehicle. The internal pressures designed the face sheet thickness required
for bulkhead strength, and the external pressure loading due to differences in ullage
pressures in the two tanks dictated honeycomb core requirements for bulkhead
stability.

The common bulkhead as shown in Detail I, of Figure 4.3.3.1-2 will be brazed
or adhesively bonded honeycomb structure. Preformed and welded 2219-T87
aluminum facings will be welded to the -29 and -22 "Y" ring fittings before being
brazed or bonded to the aluminum flex-core (5052) so that inspection of the welds
can be made from both sides. Final bulkhead joining will be made with shims and
blind fasteners. The LOX tank will be welded to the -22 common fitting after the
-30 junction rings is bolted on. This junction ring will take the radial component
of the common bulkhead load.

Detail III of Figure 4.3.3.1-2 shows the 30 degree intersection of the lower LH$_2$
bulkhead with the sidewall. Besides facilitating welding, the 30 degree semi-
elliptical bulkhead will decrease the thrust skirt length. Detail II shows the true
0.707 elliptical upper LOX bulkhead intersecting the integral tee stringers in the
LOX cylinder. Both upper and lower bulkheads will be monocoque 2219-T87
aluminum with weld lands but no waffle patterns.

The side wall configuration of the propellant tanks was sized for the maximum loading
conditions for all modes of operation. The tank skin thickness was determined by the
circumferential membrane stresses induced by internal pressure. The pressures
in the LOX tank were high enough to require a tank wall skin thickness capable of
carrying the design axial compressive loading in that region. An elastic stability

DETAIL III
AFT SKIRT AND LH$_2$ TANK CONNECTION

VIEW F-F
AFT SKIRT

VIEW E-E
AFT SKIRT SPLICE CONNECTION

VIEW D-D
INTEGRAL STIFFENER

FORWARD SKIRT

STA493

FWD

RAD
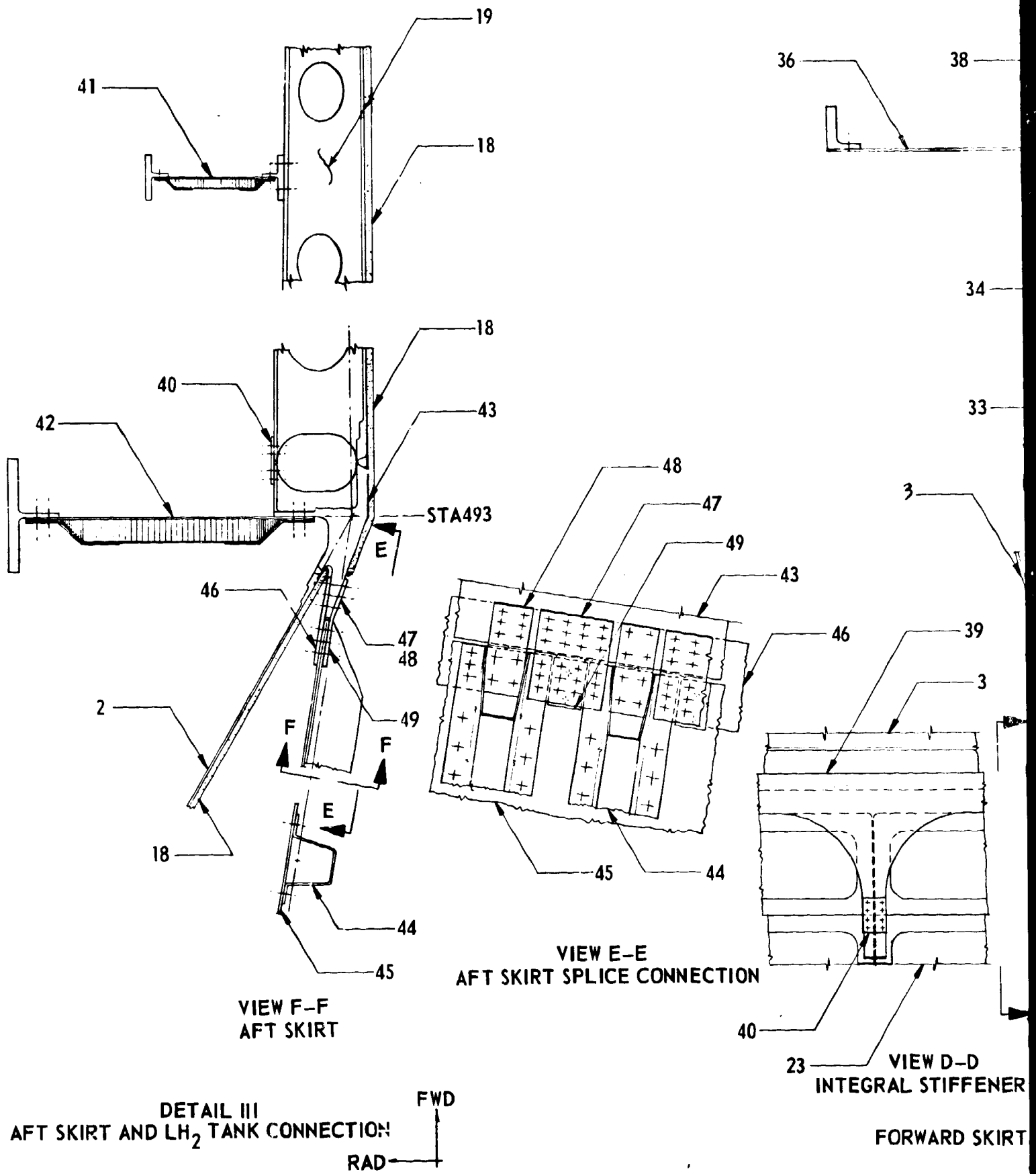
FIGURE 4.3.3.1-2   MLLV STRUCTURAL D

37

38

STA 1690

34

9

33

32

39

39

3

D

40

18

23

D

D-D
FFENER SPLICE

DETAIL II
RD SKIRT AND LOX TANK JUNCTION

FWD

RAD

31

SECT C-C

22

22

25

C

C

STA 1396

24

29

FINAL
WELD

19

18

23

22

26

25

B

B

20

19

29

WELD

18

28

27

SECTION B-B
T-STRINGER ATTACHMENT

30

ASSEMBLY DETAIL
COMMON BULKHEAD

18

19

21

20

SECTION B-B (OPTIONAL)
T-STRINGER ATTACHMENT

DETAIL I
COMMON BULKHEAD JUNCTION

WD

RAD

URAL DESIGN DETAILS

4.3.3.1　　(Continued)

analysis was performed to size integral tee stiffeners for compressive loading in the LH_2 tank. The design analysis evaluated general and local instability modes in accordance with reference 4.3.3.1-1. The longitudinal stiffeners were sized and spaced so that the entire skin was effective in carrying the axial compressive load. Stiffener spacing was determined by the Von Karman effective width formula.

Figure 4.3.3.1-3 presents the structural sizes for the LOX and LH_2 tanks. The number and size of propellant feed lines will be dependent on the engine system used. The multichamber/plug system, with its 24 modules, will have 24 LOX and 24 LH₂ lines. The toroidal/aerospike system will require only eight of each line to feed its eight modules.

Individual propellant lines were chosen over a single LOX duct in the center to allow penetration of the aft LH_2 bulkhead in areas of low stress level and to direct the dynamic head loads at the ring frame to skirt junction. Propellant conditioning will also be much easier with individual straight lines than the circuitous path from a center duct system feeding a spider duct system to the individual turbopumps. The ducts could be either thin walled aluminum or aluminum honeycomb. Aluminum honeycomb was selected for greater rigidity. The LOX ducts will be tied together and braced with high strength tension rods attached to collars surrounding each duct. The collars, held rigidly in place by the tension rods, will act as radial dampers. These collars will act as coulomb impact dampers to prevent lateral excitation from inducing destructive resonant lateral modes of vibration in the LOX ducts (experience has shown such lateral modes constitute a serious problem). A bellows at the bottom of each duct will provide for unrestrained bulkhead movement, or impact loads, at duct penetrations. A fine wire mesh will be wrapped around the duct tepee assembly to act as an LH_2 slosh damper and to give more support to the ducts.

Antivortex baffles will be provided for both tanks. These baffles will consist of a tubular truss with a fine wire mesh sail.

Individual LH_2 ducts will be installed inside the bulkhead, going from the center of the aft LH_2 bulkhead up to their exit penetrations, to eliminate external insulated high pressure feed lines and for bulkhead penetration in a low stress level area. Clamp and bellows will tie the lines to the bulkhead and to allow relative movement of the bulkhead.

The LOX ducts inside the LH_2 tank were sized for possible negative pressure requirements only. The lateral support system for LOX ducts was not considered for this preliminary design study.

Low propellants residuals will be achieved through the use of a propellant utilization (P.U.) system consisting of a series of liquid-level sensors in both propellant tanks.

4.3.3.1-1　　D5-13272, "Analysis of Stability Critical Orthotropic Cylinders Subjected to Axial Compression", 1966.

COMMON BULKHEAD

AVERAGE THICKNESS OF SANDWICH FACE SHEET t_f = 0.155"

SECTION 1-1

BULKHEAD AVERAGE THICKNESS 0.126"

MONOCOQUE TANK WALL THICKNESS 0.75"

LOX TANK

LH$_2$ TANK

BULKHEAD AVERAGE THICKNESS 0.225"

STA 1690
STA 1450
STA 1396
STA 1203
STA 493
STA 300
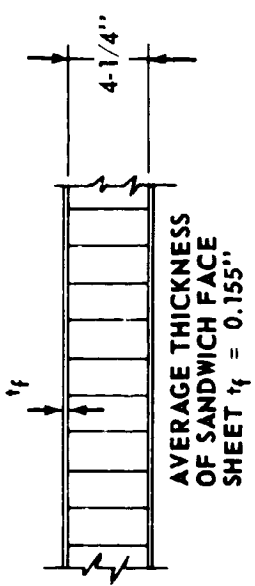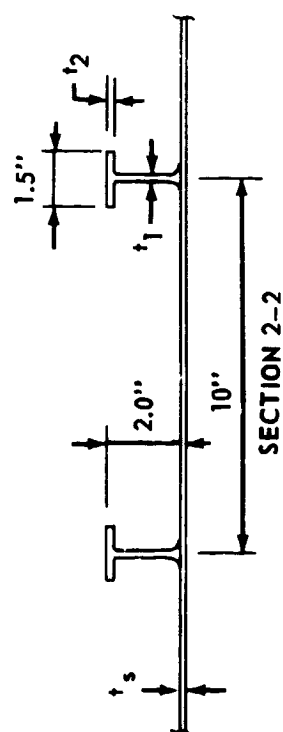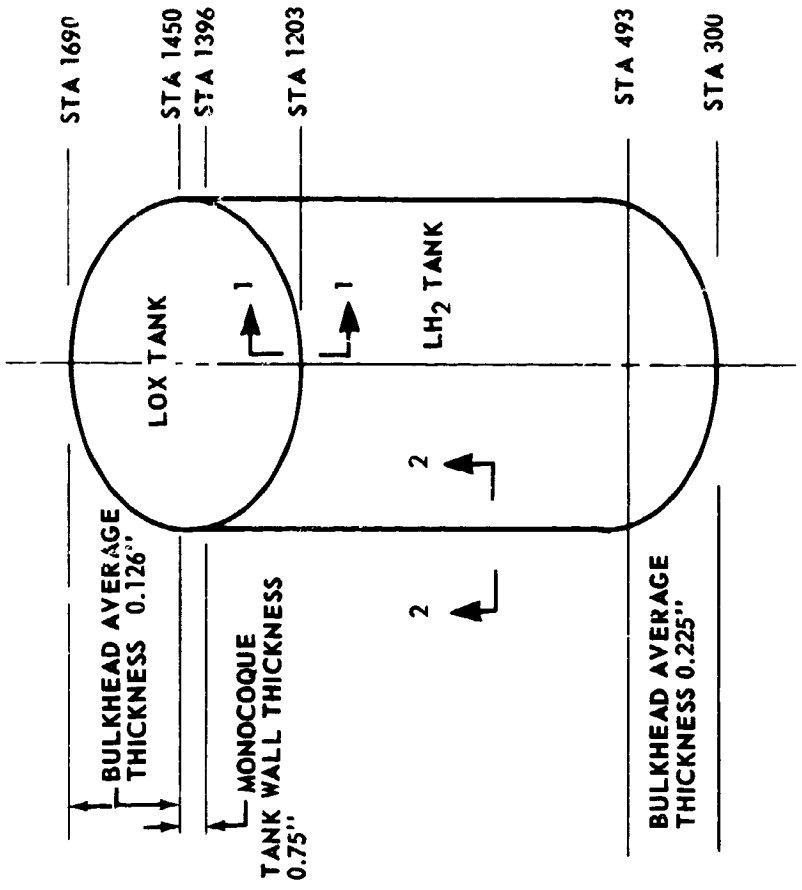
NOTE: WELD LAND THICKNESS, ETC., NOT INCLUDED

SECTION 2-2

LH$_2$ TANK SIDEWALL

LOCATION	t_s(IN)	t_1 (IN)	t_2 (IN)	LH$_2$ TANK INTER. RINGS
				AREA 2.5 IN^2/RING SPACING 64.5"
STA 503	0.26	0.10	0.15	
STA 1381	0.22	0.10	0.20	

FIGURE 4.3.3.1-3   MLLV MAIN STAGE PROPELLANT TANK STRUCTURE

286

4.3.3.1   (Continued)

The liquid levels wiil be sensed at close-time intervals near cutoff. The signals
will be fed to a computer to determine the necessary flow corrections to assure LOX
depletion and minimum hydrogen residuals, while maintaining reasonable mixture
ratios.

Forward Skirt

The forward skirt will be of 7075-T6 aluminum skin-stringer-frame construction
as shown in Detail II, of Figure 4.3.3.1-2. The field splice to the payload or injection
stage will be a circumferential bolt pattern to accommodate manufacturing tolerances.
A deep ring in the skirt (Station 1630) will take the radial component of the holddown
(Detail V, Figure 4.3.3.1-5) or strap-on stage loads (Sections A-A and G-G of
Figure 4.3.3.1-4). Two interchangeable forward skirts will be provided. One, light
weight skirt, will be designed for those configurations without strap-on stages.
A heavy weight skirt will be designed for configurations having strap-on stages.
The latter will have a larger deep ring and heavier gage skins and stringers.

The mainstage/holddown and/or SRM thrust fittings will be bolted to the forward
skirt for connection to the holddown arms or SRM forward skirt fitting with a pin
and spherical bearing. The radial components of load will be taken by the deep ring.

The forward skirt, which is subjected to concentrated axial and radial loads as well
as uniformly distributed loading, was sized using the same approach as that used
for the multichamber/plug engine thrust structure. A combination of concentrated
load and uniformly distributed loading will occur during holddown, single stage
rebound, and solid motor strap-on operation. A shear lag analysis was used
to size the posts and adjacent skin for concentrated axial loads on the posts in order
to assure a uniform axial load distribution at the LOX tank upper Y-ring. Shell
stability requirements were satisfied by sizing the longitudinal skin stiffeners and
intermediate rings for uniform axial compressive loading. Strength requirements
dictated the size of the thrust ring located to react radial concentrated loading.

Table 4.3.3.1-II lists the forward skirt structural sizes. Both the light weight
skirt (upper portion of the table) and the heavy weight (lower portion of the table)
are identified. (This table was based on uniform distribution of the combined
compressive load. For this analysis it was assumed that tapered spice thrust post
extending to Station 1775 (injection stage or payload). A later analysis was
conducted assuming the forward skirt as a one way shear path. This latter approach
was used for this program.)

36

STA 1690

STA 1690

5 (REF)

51

55

57

52

58

STA 1630   STA 1630

59

54

56 (REF)

53

3

50

60

℄ SRM THRUST

STA 1570   STA 1570

32
9

SECTION G–G
SRM THRUST TAKEOUT

FWD

DETAIL VIII

RAD
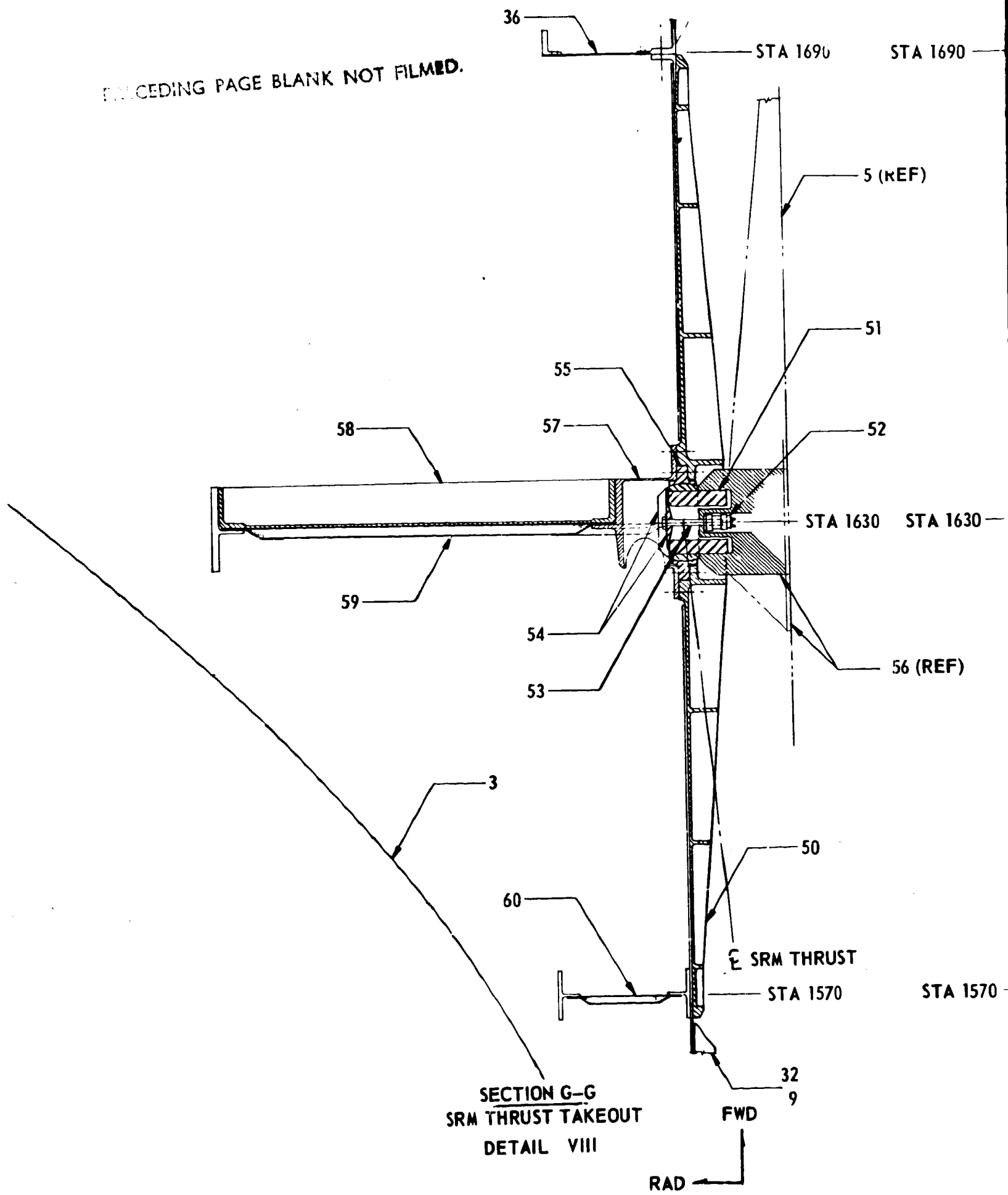
FIGURE 4.3.3.1-4   MLLV FORWARD SKIRT STRUCTURAL DESIGN DETAILS

STA 1690

FIELD SPLICE

5 (REF)

32

51

51

50

52

59

30 STA 1630

56 (REF)

60

STA 1570

33

G
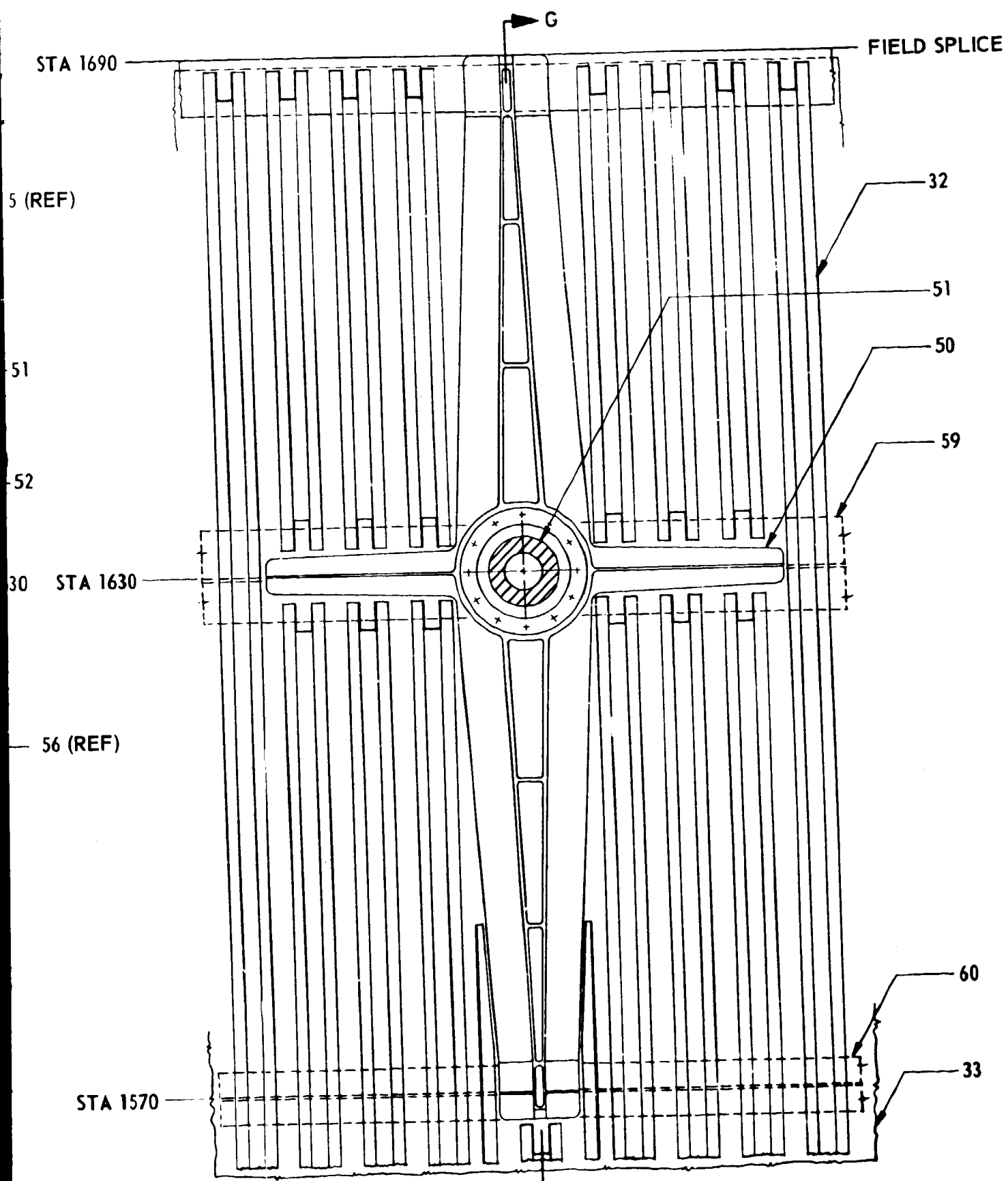
VIEW A-A
SRM THRUST POST FITTING

DETAIL IX

DESIGN DETAILS

67

59

33

68

69

72   70

STA 1630

14 (REF)

71

77

76

58

57

42
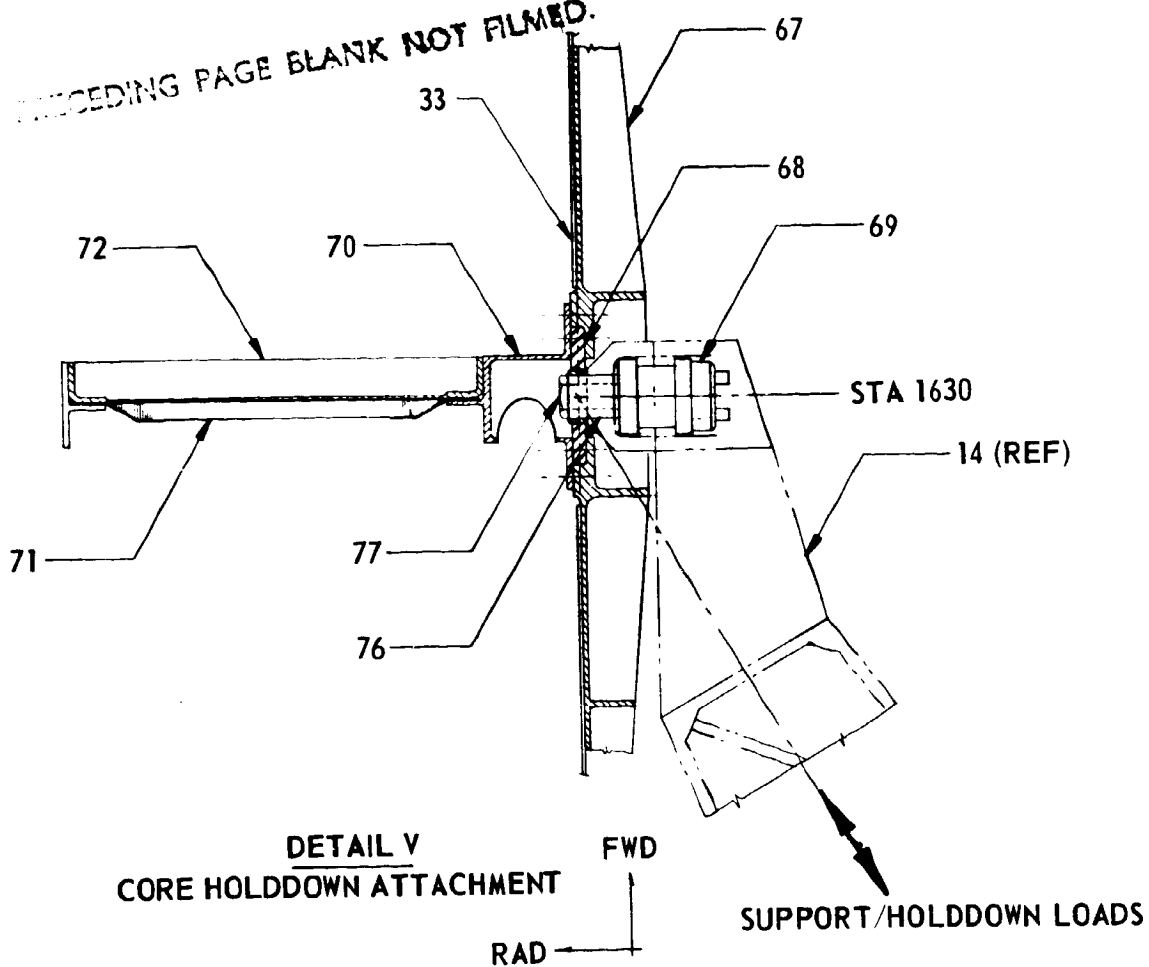
DETAIL V
CORE HOLDDOWN ATTACHMENT

FWD

RAD

SUPPORT/HOLDDOWN LOADS

73

8

65

74

73

66

STA 355

42

64

SEE DET

FWD
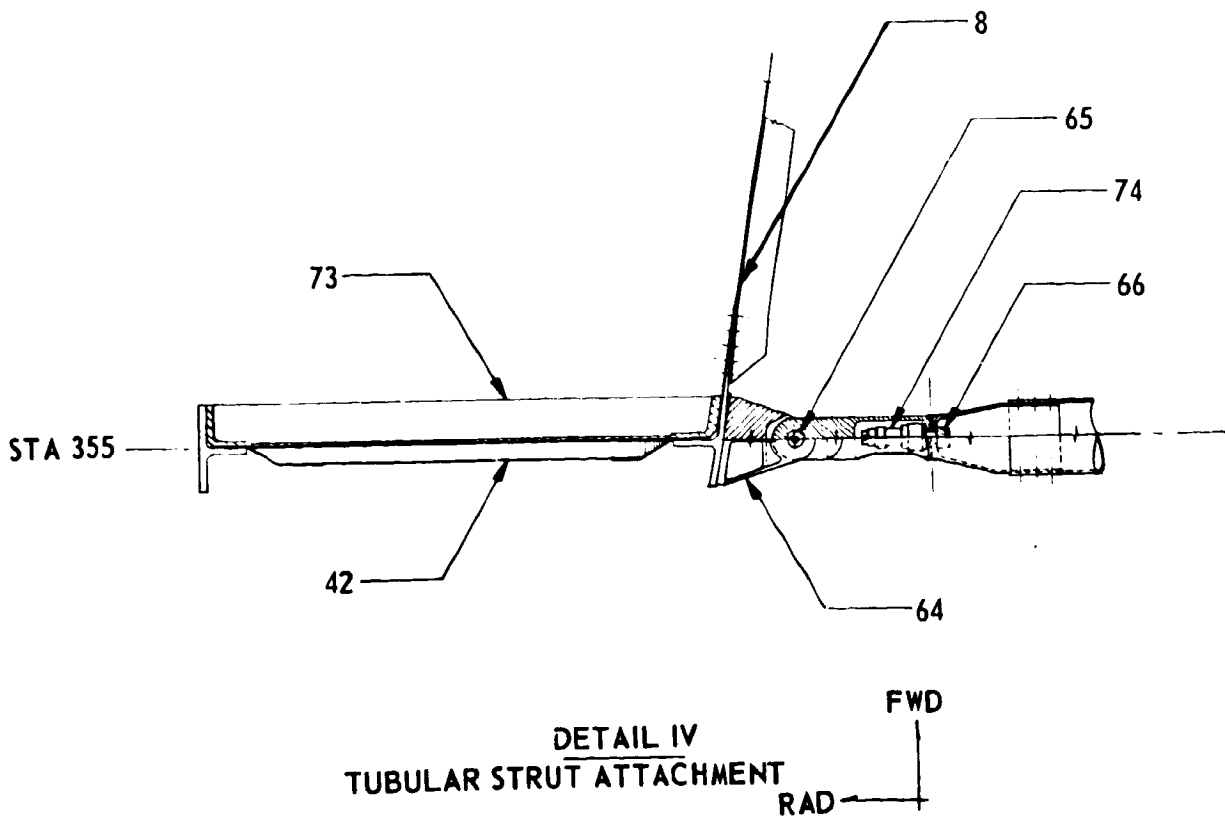
DETAIL IV
TUBULAR STRUT ATTACHMENT

RAD

FIGURE 4.3.3.1-5   MLLV FORWARD AND AFT ATTACHMENT DESIGN DE

59
56 (REF)
5 (REF)
58

(1)
TANGENTIAL

(2)
RADIAL

(3)
VERTICAL

57

50
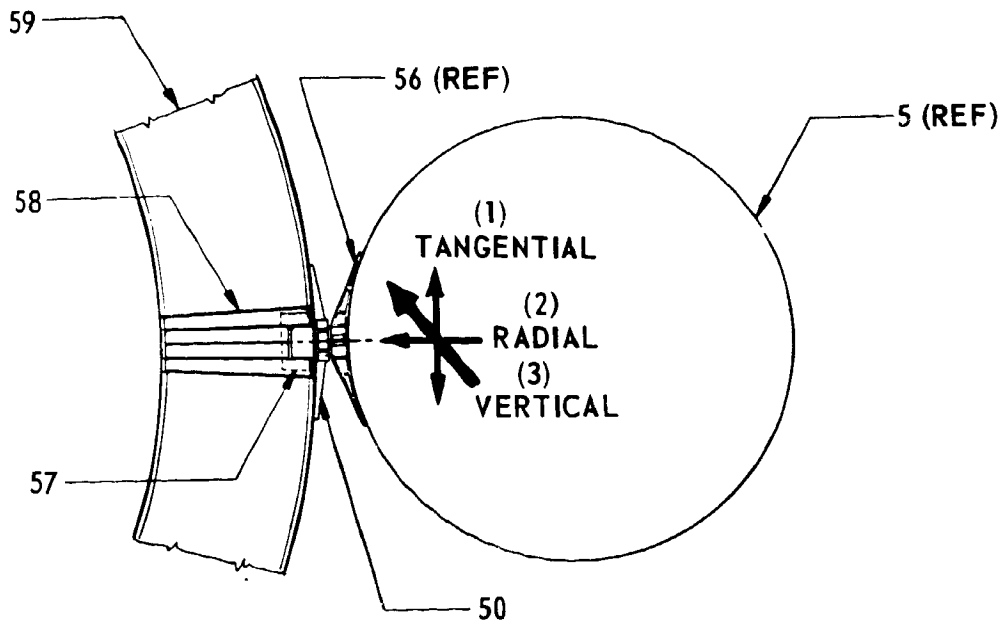
VIEW J–J
SRM FORWARD ATTACHMENT
DETAIL VI

5 (REF)

42

73

(5)
**AXIAL
ROLL**
5 (REF)

61

62

(4)
**TANGENTIAL
(LATERAL)**

64

73
SEE DETAIL IV

(6)
AXIAL (ROLL)

5 (REF)

63

75 (REF)
VIEW H–H
SRM AFT ATTACHMENT
DETAIL VII
RAD

ESIGN DETAILS
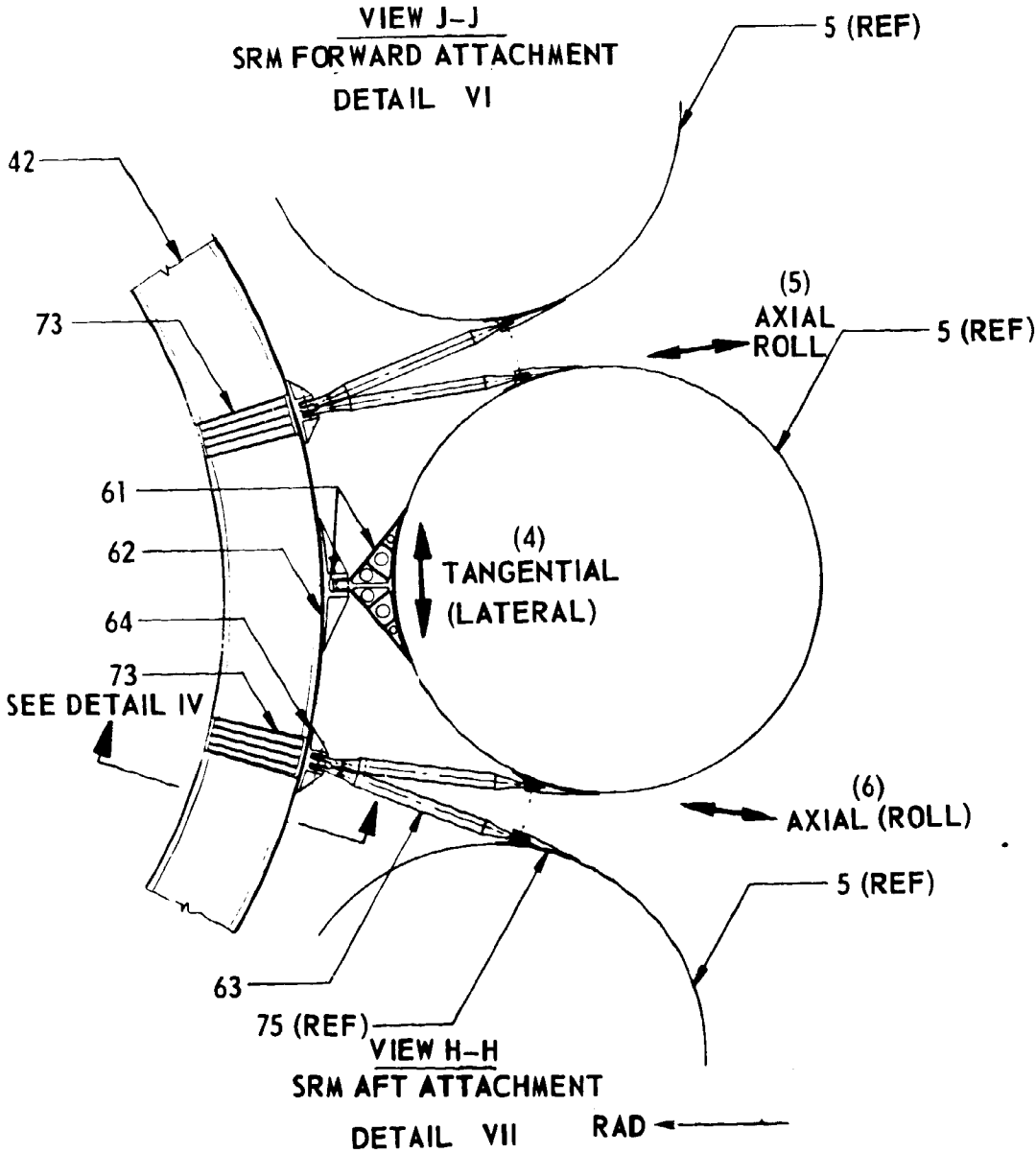
TABLE 4.3.3.1-II MLLV FORWARD SKIRT STRUCTURAL SIZES

VEHICLE OPERATIONAL MODE	LOCATION (STATION)	RING AREA (IN.²)	THRUST POST (IN.²)	SKIN–STRINGER (IN.)					
				t_1	t_2	t_3	t_4	a	b
SINGLE STAGE (CORE + INJECTION STAGE)	1455	—	10	0.11	0.072	0.072	0.10	3.20	2.50
	1515	6	[1]	←→	←→	←→	←→	←→	←→
	1572	6		←→	←→	←→	←→	←→	←→
	1630	66.75	50	←→	←→	←→	←→	←→	←→
	1690	12.0	5	0.11	0.072	0.072	0.10	3.20	2.50
CORE + SRM + INJECTION STAGE	1455	—	14	0.125	0.075	0.075	0.10	3.40	2.75
	1515	8	[1]	←→	←→	←→	←→	←→	←→
	1572	8		←→	←→	←→	←→	←→	←→
	1630	87.7	98	0.125	0.075	0.075	0.10	3.40	2.75
	1690	8	[1]	←→	←→	←→	←→	←→	[1]
	1733	8		[1]	[1]	[1]	[1]	[1]	
	1775	[2]	14	0.135	0.10	0.10	0.135	3.40	3.50
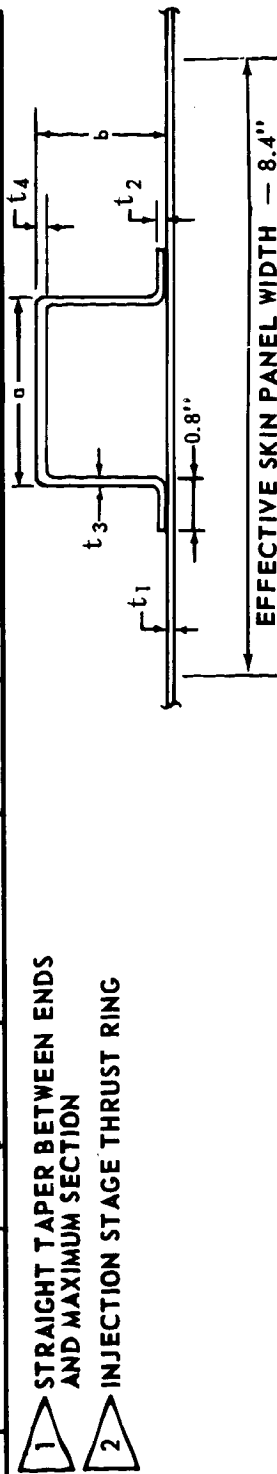
[1] STRAIGHT TAPER BETWEEN ENDS AND MAXIMUM SECTION

[2] INJECTION STAGE THRUST RING

EFFECTIVE SKIN PANEL WIDTH — 8.4"

293

4.3.3.1   (Continued)

Aft Skirt

The aft skirt will also be a 7075-T6 aluminum skin-stringer-frame built-up contruc-tion as shown in Detail III of Figure 4.3.3.1-2. The inward skirt taper will allow an optimal load path with enclosure of the engine system within the vehicle outer perimeter. A deep thrust ring at the bottom and an internal junction ring at the top will take the radial components of the engine and the strap-on stage aft attachment loads.

Preliminary design sizing of the multichamber/plug thrust skirt structural elements required the evaluation of shear lag effect, reference 4.3.3.1-2, caused by the concentrated thrust loads. This approach was used to size the thrust posts and stiffened shell to obtain a uniform axial load distribution at the juncture of the LH_2 tank and the thrust structure. General and local instability failure modes of the stiffened shell were evaluated in the upper region of the thrust structure where the axial compressive load distribution was assumed to be uniform. General instability, as applied to axially compressed cylinders, is defined as the failure mode in which the intermediate rings and the stringer-shell elements buckle together. Local insta-bility considers (1) the buckling of individual panels between stiffeners, (2) the skin-stiffener panel buckling between two rings, (3) the crippling of stiffener elements, and (4) local yielding of individual element at end attachments where secondary stresses may represent a sizable portion of the total stress (Reference 4.3.3.1-1).

The approximate optimum design approach for achieving the simultaneous failure modes of both general and local instability as advanced in reference 4.3.3.1-1 was used as a guide to size the intermediate rings. Timoshenko's criterion of sizing rings and Shanley's criterion for ring stiffness (Reference 4.3.3.1-3) were also evaluated for comparison.

The lower thrust ring was sized for strength requirements dictated by the calculated internal load distribution (Reference 4.3.3.1-4) induced in the ring by the radial thrust load component at the engine-skin interface. The upper thrust ring was combined with the LH_2 tank Y-ring. The Y-ring, therefore, was sized for the distributed radial load at the forward end of the thrust skirt and for the discontinuity forces induced by the maximum internal tank pressure in the vicinity of the LH_2 cylinder-bulkhead juncture. The Y-ring also will serve as a stabilizing ring for the LH_2 tank and thrust structure.

4.3.3.1-2   Kuhn, Paul, "Stress in Aircraft and Shell Structures", McGraw-Hill Book Company, Incorporated, New York, 1956.

4.3.3.1-3   Shanley, F. R., "Weight Strength Analysis of Aircraft Structures", Dover Publications Incorporated, New York, 1960.

4.3.3.1-4   NASA-MSFC Astronautic Structures Manual.

4.3.3.1   (Continued)

The toroidal/aerospike engine thrust structure was analyzed as a stiffened cylinder subjected to a uniformly distributed loading at the engine-skirt interface. The method of stability analysis (Reference 4.3.3.1-1) was the same as that used for the multi-chamber/plug thrust structure. The interface between the engine and thrust structure was assumed to be a pinned connection with the result that no bending moment was applied to the skirt at the engine attachment. Table 4.3.3.1-III identifies the dimensions of the aft skirt structure. Since the propulsion system affects the aft skirt structural sizes, both the multichamber/plug and toroidal/aerospike propulsion systems were determined.

Thrust Structure

The thrust structures for the two engine systems will be essentially the same except for the thrust posts required for the multichamber/plug engine and the air shroud for the toroidal/aerospike engine. The thrust structure for either system will consist of a 7075-T6 aluminum skin-stringer-frame-skirt tapered down and inward to a deep ring frame, to the engine system interface.

A deep frame in the thrust structure (directly forward of engine thrust fittings) will act as a mounting frame for strap-on aft attachments.

Helium pressurant bottles (at 37° Rankine and 3,000 pounds per square inch), will be located in the aft skirt area. The helium will be passed through an engine heat exchanger before being fed into the LOX tank. LH_2 for pressurization will be tapped off the LH_2 inlet pump and directed to an engine heat exchanger, before being fed into the LH_2 tank. Both pressurization feed lines will be enclosed in an external tunnel attached to the tank walls.

Holddown and Strap-On Stage (SRM) Attachment

The forward holddown and support concept was adopted to reduce ground wind, emergency rebound, and strap-on thrust reaction loads on the main stage structure. Holddown and support points in the forward skirt will reduce load path length for support of the LOX tank and will reduce vehicle loads due to ground winds by minimizing the free standing height. The fueled stage will be subjected to tension loads rather than compression loads in the skin structures. Impact of strap-on motors on the core vehicle will also be minimized by reacting strap-on thrust into the forward skirt which will induce axial tension loads in the main stage rather than imposing increased compressive loads as through use of an aft thrust reaction.

295

TABLE 4.3.3.1-III MLLV AFT SKIRT STRUCTURAL SIZES

PROPULSION SYSTEM	LOCATION (STATION)	RING AREA (IN.²)	THRUST POST AREA (IN.²)	SKIN – STRINGER (IN.)				
				a	t_1	t_2	t_3	t_4
MULTI-CHAMBER ENGINE	355	50.5 *	12.4	3.0	0.125	0.063	0.063	0.10
	355	18.9 *				STRAIGHT TAPER	STRAIGHT TAPER	STRAIGHT TAPER
	401	8.0						
	447	8.0						
	493	9.4	3.5	3.0	0.125	0.08	0.08	0.125
TOROIDAL ENGINE	355	50.5 *	NO THRUST POSTS	3.0	0.125	0.08	0.08	0.125
	355	18.9 *						
	401	10.0						
	447	10.0						
	493	9.4		3.0	0.125	0.08	0.08	0.125
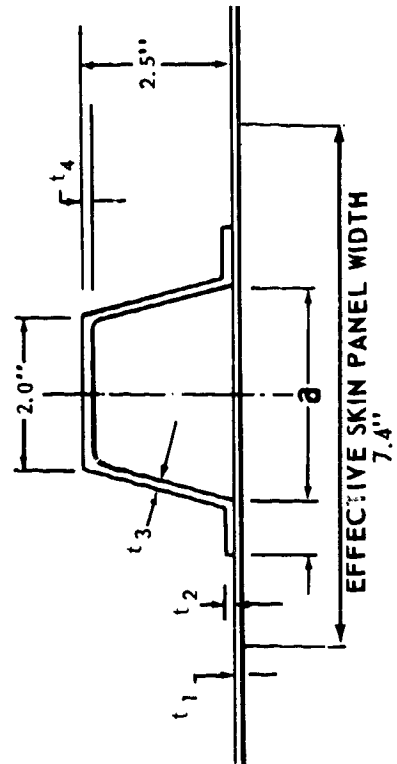
* THE LARGER RING SECTION IS USED ON SOLID ROCKET MOTOR STRAP–ON VEHICLE

2.5"

2.0"

EFFECTIVE SKIN PANEL WIDTH
7.4"

4.3.3.1   (Continued)

Large shear post forgings will be bolted into the forward skirt to take the holddown
and strap-on thrust loads as shown in Figures 4 3.3.1-2 and 4 3 3 1-4. A 230
ksi heat treated 4340 hollow steel pin in the forward skirt shear post will react
the strap-on stage thrust load at the skin line so that bending is not introduced
into the forward skirt. Backup fittings (Section G-G of Figure 4.3 3 1-5) will
locally strengthen the deep ring for the radial thrust component.

The spherical bearing fitting will allow mating freedom and relieve binding at
strap-on staging. The fitting will be a press fit into the shear post. All three
axis reactions will be taken by this ball joint. Lateral loads will be minimized as
the SRM thrust axis is through this joint. The other strap-on restraints will
be supplied by the tubular struts (torsion loads) and a longitudinal slip joint
(lateral loads) at the aft end as shown in Section H-H. The aft attachment, because
of the slip joint, will not react axial loads. The canted SRM thrust axis will negate
the aft later aload. A solid spherical bearing in the SRM stage side load fitting
will provide the necessary mating freedom. Separation will be achieved by explosive
nuts in the forward ball joint (Section G-G) and both aft tubular struts (Detail IV).
Solid rocket staging motors located in the strap-on stage nose cone and on the
aft skirt will propel the strap-on stage sideways after release.

A nominal clearance of 20" between the core vehicle and the strap-on stages will
be provided for access to permit installation and inspection.

The vehicle will be supported through the strap-on stages when they are used. These
strap-on stages will be supported by their aft skirts while in the launch position.
No holddown is assumed to be necessary. In the case of two strap-on stages, no
holddown is required as the launch weight exceeds the main stage thrust by
approximately 50 percent. It may be desirable to use the holddown structure to
prevent vibrational motion, i.e., swaying of the vehicle prior to SRM ignition.

The launch support and holddown concept shown on Figure 4.3.3.1-1 schematically
depicts the vehicle without strap-ons supported by booms that will pull back upon
vehicle release. Boom attachment to the vehicle is shown in Detail V of Figure
4.3.3.1-5. Vehicle release will be accomplished by releasing and driving a
tension/shear pin inward.

4.3.3.2   Propulsion System for the MLLV Main Stage

Three different propulsion systems were analyzed for potential application to the
MLLV main stage. These systems were a high pressure multichamber/plug
propulsion system and a 2000 psia and a 1200 psia toroidal/aerospike propulsion
system. Each of these systems are discussed briefly below. The requirements for
the propulsion systems were provided by The Boeing Company, to the propulsion

4.3.3.2   (Continued)

system contractors. Pratt and Whitney provided propulsion data for the multi-chamber/plug propulsion system. Rocketdyne provided propulsion data for both the multichamber/plug and the toroidal/aerospike propulsion systems. As a portion of the performance data is classified, the classified data is presented in the Confidential Volume IX, Appendices A and B.

Multichamber/Plug Engine System

The multichamber/plug engine system will consist of a series of bell engine modules clustered around a centerbody plug as shown in Volume IX, Appendix A, pages A.1-60 and A.1-61. The engine module thrust will be directed axially at liftoff and will swing back in against the plug for operation at altitude. The honeycombed structure sealing bulkhead will keep engine exhaust from recirculating as well as increasing the plug area for the aerospike effect. The plug will be LH_2 cooled. The plug will be supported by a tubular truss, either 6AL-4V titanium or filament type construction. Spherical bearings at the tube ends will provide for mating tolerances and will ensure proper alignment for the pinned connections.

The multichamber/plug engines will be attached to thrust fittings at the aft section of the thrust posts. The engine manufacturer will furnish the plug centerbody and engine system. The interface with the vehicle contractor would be the engine thrust fittings and the aft truss fittings. The vehicle contractor will furnish the truss structure.

Key design and performance parameters for the multichamber/plug propulsion system are shown in Table 4.3.3.2-I. Volume IX, Appendix A contains the Pratt and Whitney parametric propulsion data (Confidential Document PDS-2957, Reference 4.3.3.2-1, is included in Volume IX, Appendix A.) Included in the report are parametric performance, weights and size data. Confidential Drawing L-218069 (page A.1-59) in Volume IX, Appendix A depicts the installed engine system.

A breakdown of the estimated weight of the multichamber/plug engine system as provided by Pratt and Whitney is presented in Table 4.3.3.2-II. Part of the plug support structure as shown by the asterisk has been attributed to the main stage structure. This reduced the multichamber/plug weight by 1,487 pounds to the 116,613 pounds shown in the main stage weight summaries, Tables 4.3.2.0-I and II.

4.3.3.2-1   "MLLV Plug Cluster Rocket Engine Performance", Pratt and Whitney Report No. PDS-2957, September 13, 1968.

TABLE 4.3.3.2-I MULTICHAMBER/PLUG BASELINE PROPULSION SYSTEM

Vehicle base diameter - 56.67 ft.

Plug - 10% of isentropic length

Number of modules - 24

O_2/H_2 at MR - 6:1

Single position nozzles for individual modules

Sea level thrust - 8×10^6 lbf

Throttled operation to 10% vacuum thrust

Operational mode - Thrust parallel to vehicle centerline at lift-off. Modules hinge into plug at optimum transition altitude unless gimbal capability is still required for TVC.

Minimum effective gimbal angle for TVC - 3.9°

Gap between adjacent nozzles - zero

Gas generator exhaust products used for plug base pressurization

Module expansion ratio - 67

Module exit diameter - 78 inches

Module length, gimbal axis to exit plane - 140 inches

Module power package clearance diameter - 85 inches

Plug cluster length, gimbal plane to plug end - 312 inches

4.3.3.2   (Continued)

TABLE 4.3.3.2-II

PLUG CLUSTER ENGINE WEIGHT BREAKDOWN

Modules	100,800 lbs.
Plug	8,500 lbs.
Plug Support Structure	3,000 lbs.*
TVC	5,100 lbs.
Plumbing and Miscellaneous	700 lbs.
	118,100 lbs.*

* Includes weight of items which may be
common to vehicle structure

The engine design will provide the equivalent of an effective gimbal angle of 3.9
degrees by hinging opposing quadrants of engines (6 engines per quadrant) radially
about the plug. (Each hinged engine must therefore be vectored in excess of
seven degrees.) Based on a sensitivity study conducted by Pratt and Whitney,
a slightly larger effective gimbal angle could be provided, if necessary, (with
essentially no performance degradation) by increasing the design tilt angle for
operation against the plug. If still further side force is required, differential
throttling could be used, as throttling capability is already incorporated in the
engine design. Performance of the TVC system is the same as reported previously
(Reference 4.3.3.2-4). Location of the TVC actuator attachment points on the
engine is shown on Pratt and Whitney Layout drawing L-218069. Final definition
of these actuator points, however, will require additional coordination between the
engine and vehicle contractors.

A Pratt and Whitney study of a hydrogen system for plug base pressurization was
completed. It was concluded that there would be insufficient heat transferred to the
hydrogen used for cooling the plug side-wall to raise its temperature to a satis-
factory level for base pressurization. Thus, the originally selected gas generator
base pressurization system as defined for the AMLLV was also specified for the
MLLV configuration. This method is shown on Pratt and Whitney Drawing L-218069.

Toroidal/Aerospike Engine System

The 2000 psia toroidal/aerospike engine system will be an eight segment, open
chamber engine system as shown in Volume IX, Appendix B, pages B.1-65 and B.1-66.

4.3.3.2-4   "Thrust Vector Control - Plug Cluster", Pratt and Whitney Report
SRM FR-2325 dated 1966.

4.3.3.2 (Continued)

Page B.1-49 shows an alternative 1200 psia toroidal/aerospike engine system evaluated in subsequent cost/performance trades.) The combustion chamber will be LH_2 cooled. The engine will interface with the vehicle at the vehicle thrust structure frame, located at Station 355, and the oxidizer and fuel pump inlet flanges. The helium and hydrogen gas pressurant lines will interface at the ports located on each hydrogen turbopump exhaust duct. Each engine segment will attach to the vehicle thrust structure through bolted flange connections at the interface frame. The bolts will be loaded in tension and support the dry engine weight. While the engine is operating, the thrust will be transmitted to the vehicle through the structural attach frame. Normal firing will produce no moment to the aft thrust ring, only vertical thrust loads and radial components into the deep ring frame.

The engine will utilize one fuel and one oxidizer pump inlet supply duct for each segment. The turbopump locations as shown were selected to provide the easiest method for mounting the turbopump to the centerbody.

A mylar/phenolic/aluminum aerodynamic fairing will protect the overhanging thrust chamber from wind loads.

The design and performance parameters for the 1200 psia and 2000 psia toroidal/ aerospike propulsion systems are shown in Table 4.3.3.2-III.

TABLE 4.3.3.2-III

TOROIDAL/AEROSPIKE BASELINE PROPULSION SYSTEM

a.	Chamber Pressure (PSIA)	1,200	2,000
b.	Nominal Sea Level Thrust (lbs)	8,000,000	8,000,000
c.	Propellants	LOX/LH_2	LOX/LH_2
d.	Mixture Ratio	6:1	6:1
e.	System Diameter (feet)	56.7	56.7
f.	Nozzle Length (% of 15° Cone) (feet)	10	10
g.	Area Ratio	80	139
h.	Number of Modules	8	8
i.	Engine Length (feet)	11	11
j.	Effective Gimbal Angle (degs)	3.9	3.9
l.	Overall Length Mount Flange to Plug End (inches)	130	133
m.	Base Plug Diameter (inches)	478	474

4.3.3.2   (Continued)

The variation of specific impulse with altitude and engine weight was obtained from the propulsion contractor. This data is reported in Reference 4.3.3.2-3 which is contained in Volume IX, Appendix B.

The Rocketdyne parametric data was supplied for the 2000 psia toroidal/aerospike propulsion system in References 4.3.3.2-2 and 4.3.3.2-3. The data also included alternative engine system data based on an operating pressure of 1200 psia. (The initial AMLLV study used a 2000 psia operating pressure.) The 1200 psia chamber pressure was recommended by Rocketdyne because existing turbo machinery designs and technology could be used. The parametric propulsion data covers a range of one million to 24 million pounds thrust over a propulsion system diameter of 25 to 82 feet. Area ratios, engine length, specific impulse (sea level to vacuum) versus altitude and thrust versus altitude were presented.

The toroidal/aerospike engine will be of a segmented, modular construction (Figure 4.3.3.2-1) in which the engine is directly integrated with the aft end of the stages. Thrust vector control will be provided by fluid injection of LOX and differential throttling of the modules.

4.3.3.3   Fluid Systems Requirements for the Main Stage

Fluid systems requirements for the MLLV main stage were examined considering the prior AMLLV vehicle studies. Many of the AMLLV concept and data were applied to the smaller MLLV vehicle as indicated below:

a. Pressurization Technique - The AMLLV pressurization approach as shown in Figure 4.3.3.3-1 will be used. Hydrogen will be bled back from the primary LH$_2$ pump, heated to 350°R in a turbine exhaust duct heat exchanger, and used to pressurize the LH$_2$ tank. The LOX tank will be pressurized with helium • heated to 500°R in a turbine exhaust heat exchanger. The helium will initially be stored in insulated 3000 psia titanium pressure vessels located in the vehicle base area. The helium will be held at approximately 37°R prior to liftoff by circulation of GSE LH$_2$ through an internal heat exchanger. During pressurization system operation, a small fraction of the heated helium will be by-passed through the helium bottle internal heat exchanger to heat the remaining gas and reduce residuals. Approximately 120 BTU/sec will be required to hold bottle temperature at 37°R during bottle blowdown.

4.3.3.2-2   "Parametric Data for Advanced O$_2$H$_2$ Aerospike and Multichamber Plug Nozzle Engines", Enclosure 2 to Rocketdyne Letter No. 68RC12017, dated September 13, 1968.

4.3.3.2-3   "Advanced O$_2$H$_2$ Engine Data for an 8,000,000 Pound Thrust Multipurpose Large Launch Vehicle (MLLV)", Enclosure 2 to Rocketdyne Letter No. 68RC15283, dated December 20, 1968.
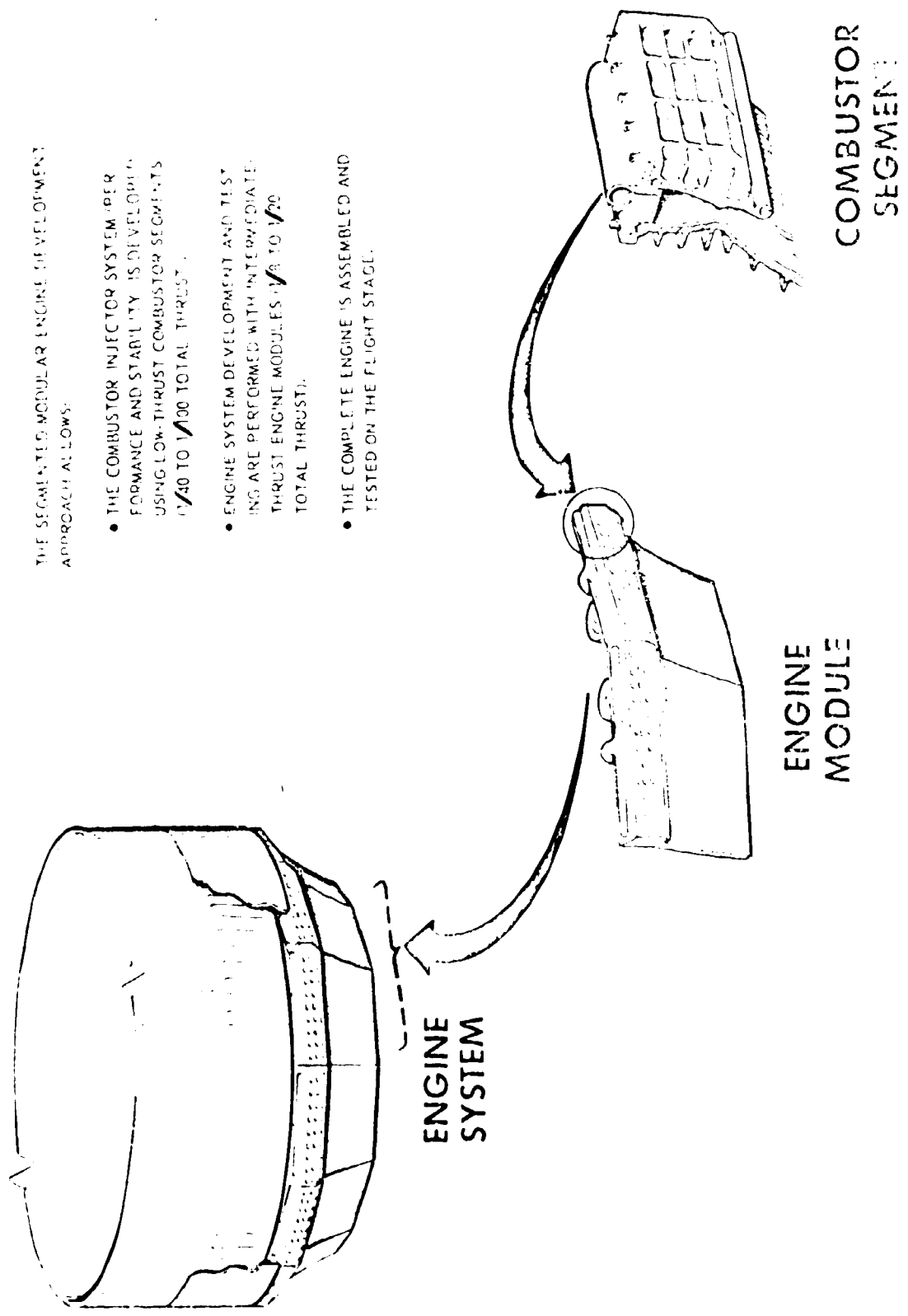
THE SEGMENTED MODULAR ENGINE DEVELOPMENT APPROACH ALLOWS:

- THE COMBUSTOR INJECTOR SYSTEM PERFORMANCE AND STABILITY IS DEVELOPED USING LOW-THRUST COMBUSTOR SEGMENTS (1/40 TO 1/100 TOTAL THRUST).

- ENGINE SYSTEM DEVELOPMENT AND TESTING ARE PERFORMED WITH INTERMEDIATE THRUST ENGINE MODULES (1/8 TO 1/20 TOTAL THRUST).

- THE COMPLETE ENGINE IS ASSEMBLED AND TESTED ON THE FLIGHT STAGE.

COMBUSTOR SEGMENT

ENGINE MODULE

ENGINE SYSTEM

FIGURE 4.3.3.2-1   TOROIDAL/AEROSPIKE SEGMENTED MODULAR ENGINE
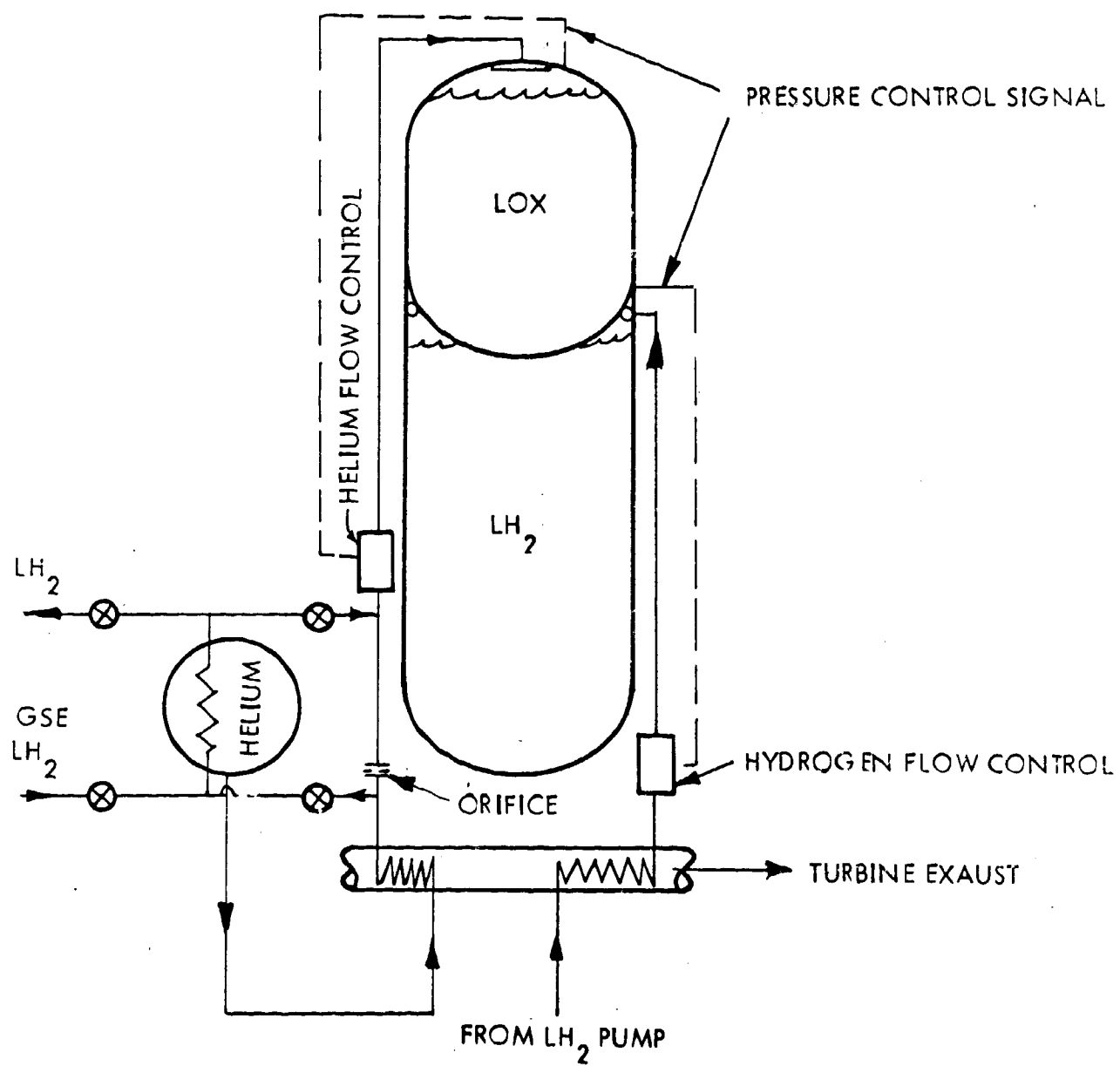
FIGURE 4.3.3.3-1 PRESSURIZATION SYSTEM SCHEMATIC - EXTERNAL
            HELIUM TANKS

304

4.3.3.3   (Continued)

b.   Fluid Systems Weights and Sizes - MLLV fluid systems weights were ratioed
     from the AMLLV stage and are shown in Table 4.3.3.3-I.   Line sizes and
     miscellaneous pressurization system information are shown in Table 4.3.3.3-II.

c.   Ullage Pressure Schedules - The ullage pressure schedules used for the AMLLV
     main stage (Figure 4.3.3.3-2) may also be used for MLLV main stage due
     to the following considerations:

     1.   Engine NPSH requirements will be identical.

     2.   LOX tank ullage pressure is determined only by the maximum vapor
          pressure expected for the LOX.

     3. LH_2 tank ullage pressure determined for AMLLV will be high enough to
          be independent of acceleration head effects.   (Note: LH_2 ullage pressure
          trades for the MLLV, as reported in Section 4.1.1.5, established that
          the optimum pressure, as constrained by NPSH requirements, will be
          the same as specified for the AMLLV.)

     4.   Losses in the LH_2 feed system will remain the same since feedline
          diameter will be reduced to maintain constant flow velocity.

d.   LOX Depletion Considerations - The data for LOX depletion cutoff generated
     for AMLLV are shown in Figure 4.3.3.3-3.   This data will also apply to the
     MLLV since the trajectories are identical.   The figure shows the acceleration
     head required to maintain NPSH for the LOX system versus the LOX head above
     the pump inlet.   The lines of constant g's show the change in acceleration head
     required as LOX is depleted under a constant vehicle acceleration.   The required
     acceleration head to prevent cavitation at 100 percent thrust is shown as the
     upper dashed line.   When the engine is operating at ten percent thrust, the
     line losses will be significantly reduced and the required acceleration head
     will be reduced to the level shown by the lower dashed line.   The data points
     plotted on the figure show AMLLV and MLLV acceleration head at full thrust
     and ten percent thrust.   These data indicate pump cavitation will begin when
     the LOX level in the feedlines is approximately 18 feet above the pump inlet for
     the worst case.   The maximum cavitation period is 0.5 seconds.   The ullage
     pressure required to prevent cavitation until LOX depletion would be approximately
     15 psia.

e.   Zero-Staging Considerations - The propellant pressure and temperature require-
     ments established by Pratt and Whitney for AMLLV engine start-up (Figures
     4.3.3.3-4 and 4.3.3.3-5) also apply to MLLV.   As before, the LH_2 tank ullage
     pressure will meet these requirements but some acceleration head will be
     required to bring LOX pump inlet pressure into the start region.   As seen in

305

TABLE 4.3.3.3-I   MLLV MAIN STAGE FLUID SYSTEM WEIGHT

SYSTEM		LH$_2$ TANK (LBS)	LOX TANK (LBS)	TOTAL (LBS)
A.	Fill and Drain	318	226	544
B.	Vent and Relief	1,050	500	1,550
C.	Propellant Utilization			930
D.	Pneumatic Control System			
	1. Hardware			707
	2. Helium			160
E.	Chilldown	2,120	1,270	3,390
F.	Pressurization			
	1. Helium			
	Prepressurization	1,415	85	1,500
	Pressurization		2,220	2,220
	2. Hydrogen			
	Pressurization	3,960		3,960
	3. Helium Tanks		2,660	2,660
	4. Helium Tank Insulation		400	400
	5. Heat Exchangers	707	354	1,061
	6. Ducting and Miscellaneous	2,180	1,110	3,290
G.	Total Fluid Systems	11,750	8,825	22,372

TABLE 4. 3. 3. 3-II MLLV MAIN STAGE FLUID SYSTEMS DATA SUMMARY
(Multichamber/ Plug Engine System)

System	LH$_2$ Tank	LOX Tank
Pressurization		
1. Pressurant	Vaporized Hydrogen	Helium
2. Pressurant Inlet Temperature	350°R	500°R
3. Pressurant Heating Source	Turbine Exhaust Heat Exchanger	Turbine Exhaust Heat Exchanger
4. Pressurant Flow Rate @ Full Thrust	15. 8 lb/sec	7. 1 lb/sec
5. Helium Bottle Heat Required for Isothermal Blowdown		120 BTU/sec
6. Helium Bottles Required		4 - 60" Titanium Tanks (Minimum)
7. Helium Storage Conditions		3000 psia @ 37°R
8. Pressurant Duct Size	9"	9"
Vent and Relief		
1. Valve and Line Size	12" (Two Valves)	12" (Two Valves)
Fill and Drain		
1. Valve and Line Size	12" (2 Lines, 2 Valves)	12" (2 Lines, 2 Valves)
Feed System		
1. Feed Line Diameter	9. 5" (24 Lines)	8" (24 Lines)
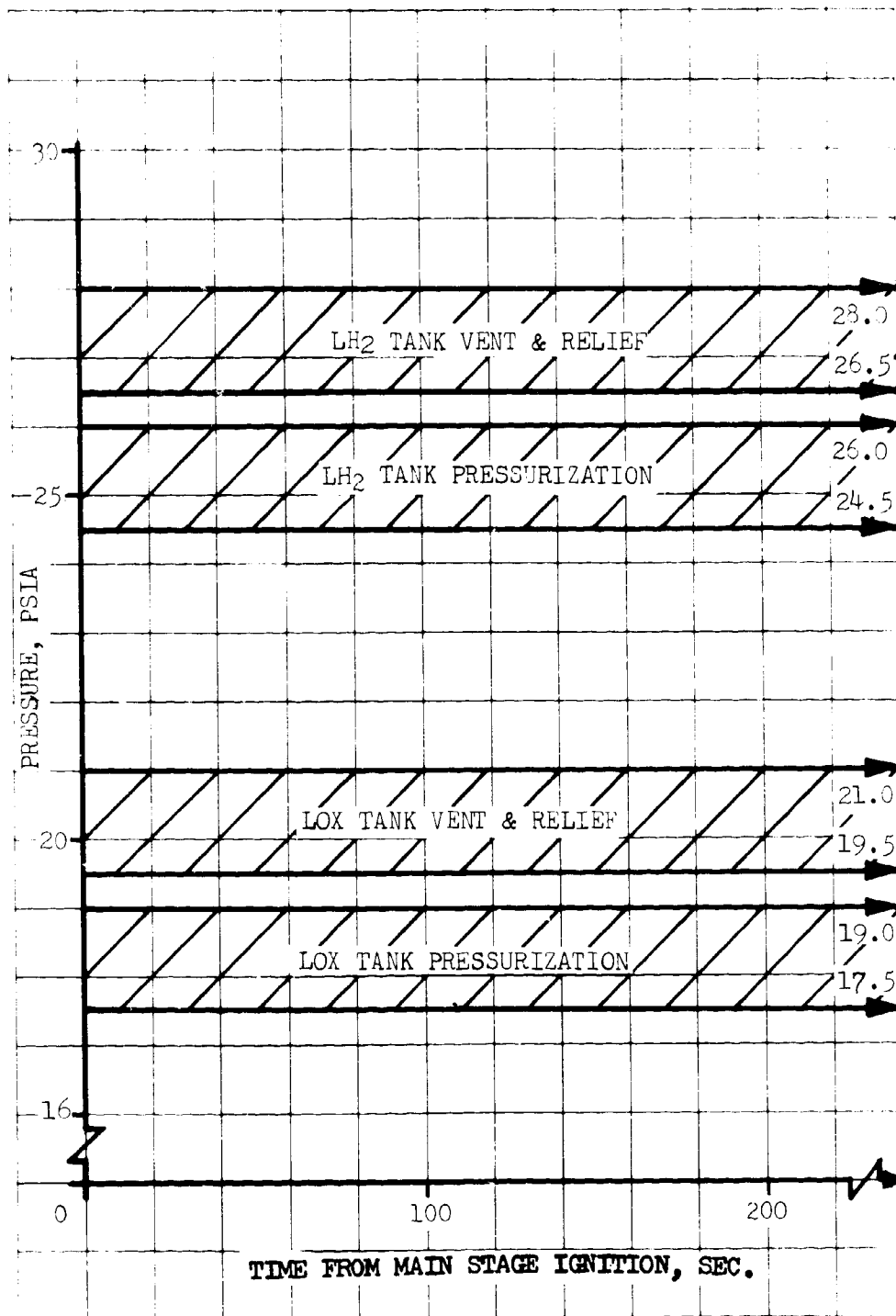
FIGURE 4.3.3.3-2   MLLV MAIN STAGE PRESSURIZATION SCHEDULES

NOTE: FIGURE 4.3.3.3-3 OMITTED FROM THIS SPACE IS
CLASSIFIED. THIS FIGURE IS PRESENTED IN VOLUME IX
(CLASSIFIED APPENDIX), APPENDIX E.

NOTE: FIGURE 4.3.3.3-4 OMITTED FROM THIS SPACE IS CLASSIFIED. THIS FIGURE IS PRESENTED IN VOLUME IX (CLASSIFIED APPENDIX), APPENDIX E.

NOTE: FIGURE 4.3.3.3-5 OMITTED FROM THIS SPACE IS
CLASSIFIED. THIS FIGURE IS PRESENTED IN VOLUME IX
(CLASSIFIED APPENDIX), APPENDIX E.

4.3.3.3   (Continued)

   Figure 4.3.3.3-6, the stage acceleration required for MLLV core ignition will
   be very close to that for AMLLV.

The fluid systems requirements will apply to both the multichamber and toroidal/
aerospike engine systems. The following factors will permit the use of identical
systems:

a.   NPSH requirements of the toroidal/aerospike and multichamber engines will be
     identical.

b.   The hardware forward of the engines will be basically the same, and will
     therefore produce similar flow losses.

c.   Trajectories of the two vehicles will be similar and will result in approximately
     the same fluid acceleration head at the engine inlets.

d.   Maximum propellant vapor pressure will be the same for both configurations.

4.3.3.4   Separation

The main stage will be separated from the injection stage just above the main
stage/injection stage field splice ring. The release will be provided by a linear
shaped pyrotechnic charge. The main stage retro rockets will be ignited simul-
taneous with the firing of the linear shaped pyrotechnic charge (after main stage
cut-off). The retro thrust will apply until the injection stage engines clear the
main stage forward skirt. Assuming a two g separation acceleration, a total
impulse of 341,000 pound-seconds will be required. The separation motors must
burn for a minimum of 0.34 seconds and have a thrust of approximately one
million pounds. Although a longer burning time will result in less impulse required,
the two g retro acceleration was selected because in the event of 16.6 percent of
the retro motors being inoperative, separation can still be successfully achieved.
Section 4.2.6.1 defined the main stage/injection stage separation requirements.

Ten retro motors burning for 0.35 seconds and having a total thrust of 975,000
pounds (97,500 pounds thrust each motor) will produce the total impulse required.
Thus a successful separation can be achieved with one retro rocket out. Two
retro rockets out would prevent separation.

4.3.4   Injection Stage Design

This section presents the detailed design data for the injection stage of the MLLV
including the stage and subsystem description, design, concept, materials and
performance. The injection stage for the MLLV was sized from the AMLLV confi-
guration injection stage. The engine and weight of propellant per module were
reduced to one-half that of an AMLLV injection stage module. The design concepts,

312

NOTE: FIGURE 4.3.3.3-6 OMITTED FROM THIS SPACE IS CLASSIFIED. THIS FIGURE IS PRESENTED IN VOLUME IX (CLASSIFIED APPENDIX), APPENDIX E.

4.3.4   (Continued)

materials and performance were held constant whenever possible to reduce the study program variables.

Figure 4.3.4.0-1 illustrates the injection stage design concept. The diameter of the injection stage was fixed at the diameter of the main stage. The design will permit the stacking of additional modules above the engine module. Each module will consist of a LOX/LH$_2$ propellant system with toroidal propellant tanks and two high pressure (3000 psia) bell engines with extendible nozzles. As additional modules are stacked above the lower injection stage modules, additional engines (two per module) will be mounted to the thrust beam of the lower injection stage module.

4.3.4.1   Injection Stage Structures

The injection stage "worst envelope" design loads will result from the vehicle configuration consisting of a main stage plus a three module injection stage and eight 260 strap-on stages. Using these "worst envelope" design loads, the major structural components of the injection stage were sized.

Subsequent Figures 4.3.4.1-1 through 4.3.4.1-3 illustrate the structural details of the injection stage. Table 4.3.4.1-I lists the structural components, structural materials and the method of construction. Backup stress notes and calculations are shown in Volume VIII, Appendix B.

Propellant Tanks

The monocoque, torus shaped propellant tanks were sized for combined maximum internal pressure and bending loads (for the three module injection stage). Either vertical aluminum honeycomb sandwich web panel assemblies or 2219-T87 stiffener assemblies will be provided inside the tanks at 45° spacing for torsional rigidity (cross-section circularity). The inner (LOX) tank will hang from a fiberglass cylindrical skirt attached to the outer (LH$_2$) tank. The outer torus, LH$_2$ tank, will be circumferentially shear pin connected to the skirt with spherical bearing fasteners. (See Figures 4.3.4.1-1 and 4.3.4.1-2).

2219-T87 aluminum alloy was chosen for the propellant tanks because of its excellent fusion weldability and other desirable qualities particularly in the fracture toughness area.

The tanks will be connected by a stainless steel convolute bolted into the aluminum tanks (Figure 4.3.4.1-3, Detail III). A teflon outer convolute will act as an insulator for the inner convolute and will be coated with a spray-on polyurethane. Propellants will drain from the upper tanks into the lower tanks during injection stage operation; residuals in the upper tanks will, therefore, be negligible by thrust termination.

HANGER SKIRT

HEAT SHIELD

LOX TANK

LH$_2$ TANK

ENGINE SUPPORT

CYLINDRICAL SKIRT

EXTENDABLE NOZZLE
ENGINE (1930 LB. EA.)

MANIFOLD DUCT

INTERNAL RIB

HEIGHT 15'
DIAMETER 56.7'

SINGLE MODULE
INJECTION STAGE

FORWARD SKIRT
(REF)

CORE VEHICLE
(REF)

STRUCTURE	41,380 LBS.
ENGINES (2)	3,860
SYSTEMS	4,715
DRY WEIGHT	49,955 LBS.
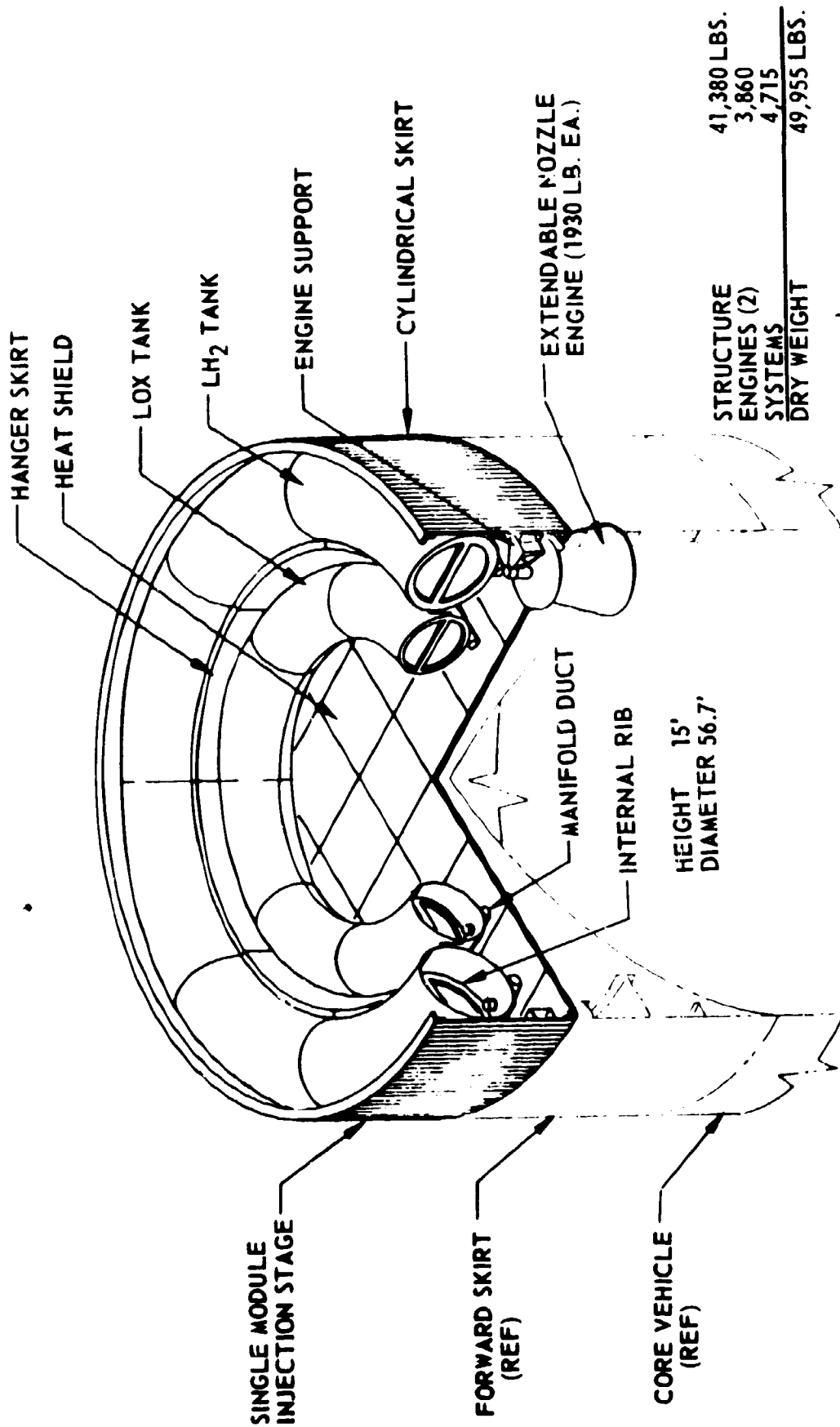
FIGURE 4.3.4.0-1   INJECTION STAGE ENGINE MODULE DESIGN

315

3

SEE DETAIL II

SINGLE MODULE
CONFIGURATION

SEE DETAIL I

2

1

SECTION A–A

17

2

19

23

22

20

18

61.0R

22

23

20

19

STA 1822

STA. 1804

WELDED JOINT (TYP)
34.5 R

1

DETAIL I
INNER TORUS SUSPENSION

FWD

RAD

26

7

8

6

5

DETAIL I

DETAIL IV

DETAIL II

A

STAGING STA 1730

SINGLE MODULE
CONFIGURATION

16

9

11

15

MLLV CORE

VEHICLE

PROFILE VIEW

FWD
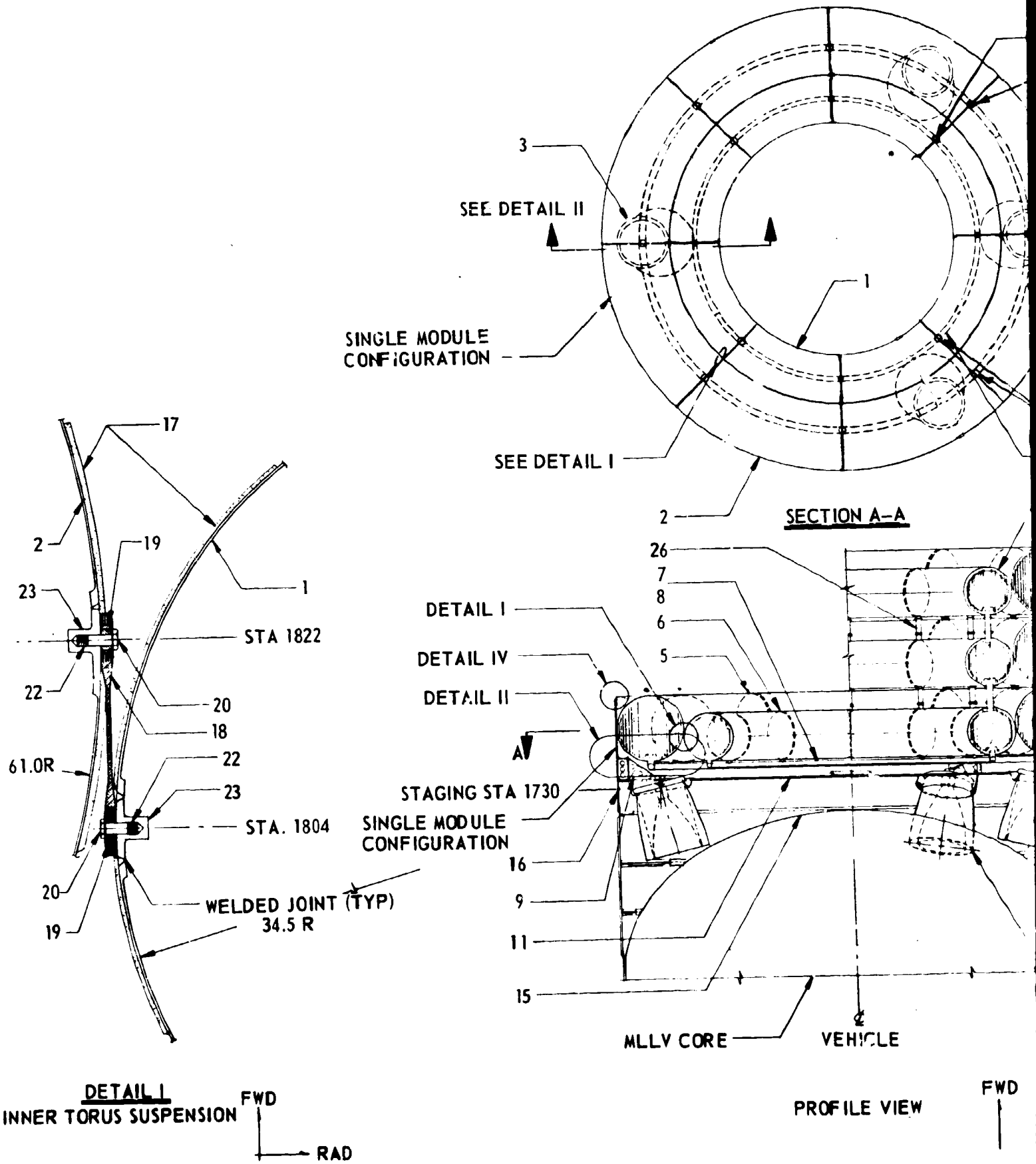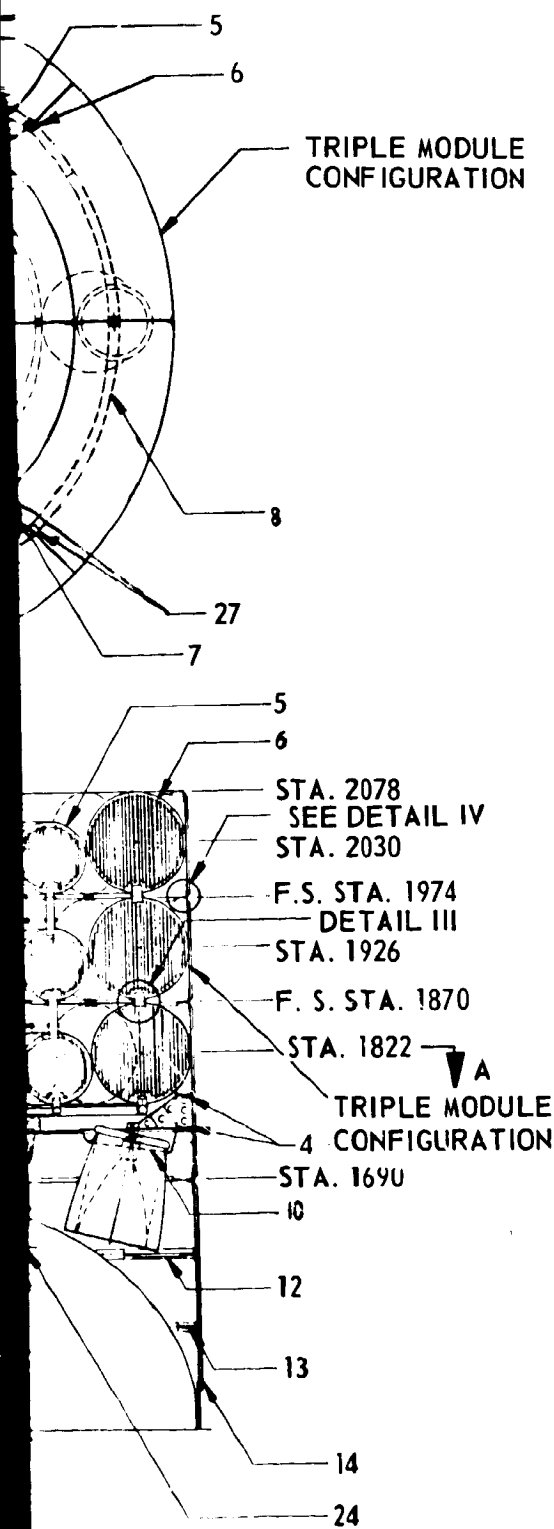
1.	LOX TANK 2219-T87 AL ALLOY, WELDED TORUS TANK
2.	LH$_2$ TANK 2219-T87 AL ALLOY, WELDED TORUS TANK
3.	ENGINE 125K THRUST, EXTENDIBLE NOZZLE, GIMBALING TYPE
4.	THRUST RING FRAME 7075-T6
5.	SHEAR RIB, LOX TORUS 2219-T87 AL ALLOY (8 PLACES)
6.	SHEAR RIB, LH$_2$ TORUS 2219-T87 AL ALLOY (8 PLACES)
7.	LOX FEED LINE MANIFOLD 2219-T87 AL ALLOY
8.	LH$_2$ FEED LINE MANIFOLD 2219-T87 AL ALLOY
9.	ENGINE MOUNT FORGING 7075-T6 AL ALLOY
10	FLEXIBLE HEAT SHIELD
11.	HEAT SHIELD HONEYCOMB WITH REFRASIL FACING
12.	DEEP RING FRAME CORE FORWARD SKIRT (REF)
13.	INTERMEDIATE RING FRAME CORE FWD SKIRT (REF)
14.	CORE FORWARD SKIRT (REF)
15.	FORWARD DOME MAIN STAGE LOX TANK (REF)
16.	SEPARATION JOINT-LINEAR SHAPED CHARGE
17.	INSULATION BONDED POLYURETHANE FOAM
18.	HANGER SKIRT CROSS-PLY FIBERGLASS/EPOXY LAMINATE CYLINDRICAL SKIRT ASSEMBLY WITH EDGE INSERTS
19.	SPHERICAL BEARING
20.	SHEAR BOLT AND WASHER
21.	SHEAR BOLT AND NUTPLATE
22.	HELI-CORE INSERT STEEL
23.	CIRCUMFERENTIAL ATTACHMENT FITTING 2219-T87 EXTRUSION WELDED INTO TORUS
24.	EXTENDIBLE NOZZLE SECTION
25.	EXHAUST PLUME
26.	INTERCONNECT FEED LINE WAFER DRAINAGE LINE WITH BELLOWS JOINT
27.	FLOAT VALVE WITH SOLENOID ACTUATOR
28.	LIQUID LEVEL SENSOR FOR FLOAT VALVE
29.	WEB STIFFENERS FORMED 2219-T87 AL ALLOY
30.	WEB, SHEAR RIB 2219-T87 AL ALLOY SHEET
31.	TEE RING 2219-T87 AL EXTRUSION WELDED INTO TORUS
32.	CONVOLUTE, STAINLESS STEEL
33.	INSULATOR TEFLON CONVOLUTE
34.	DOUBLER
35.	BOLTING RING PLATE CONVOLUTE ATTACHMENT 2219-T87 AL ALLOY
36.	ATTACHMENT BOLT RING PATTERN
37.	SKIN CYLINDRICAL SKIRT INJECTION STAGE 7075-T6 AL ALLOY
38.	STIFFENER EXTERNAL STRINGER FORMED 7075-T6 AL HAT SECTION
39.	RING FRAME INTERMEDIATE 7075-T6 AL BUILTUP CONSTRUCTION
40.	SHEAR PIN FIELD SPLICE ATTACHMENT

FIGURE 4.3.4.1-1 INJECTION STAGE DESIGN

STATION 1822

30 (FIXED)

20
19
22

21

29

30 (REMOVABLE)

34

SECTION D
FLOAT VALVE

30
31
21
17

SECTION E-E
RIB ATTACH

38

37

38
37

SECT. C-C
SKIN STIFFENER ATTACH

C   C

E

17

E

34

D

4

STA 1775

B

9

28

B   DETAIL
OUTER TORUS SUS

27

28

29

CTION D-D
VALVE ATTACH

30

29

D

28

27

17

8

DETAIL II
ORUS SUSPENSION

FWD

RADIAL

19

18

30 (FIXED)

23

STA 1804

30

30 REMOVABLE

31

17

31

17

2

1
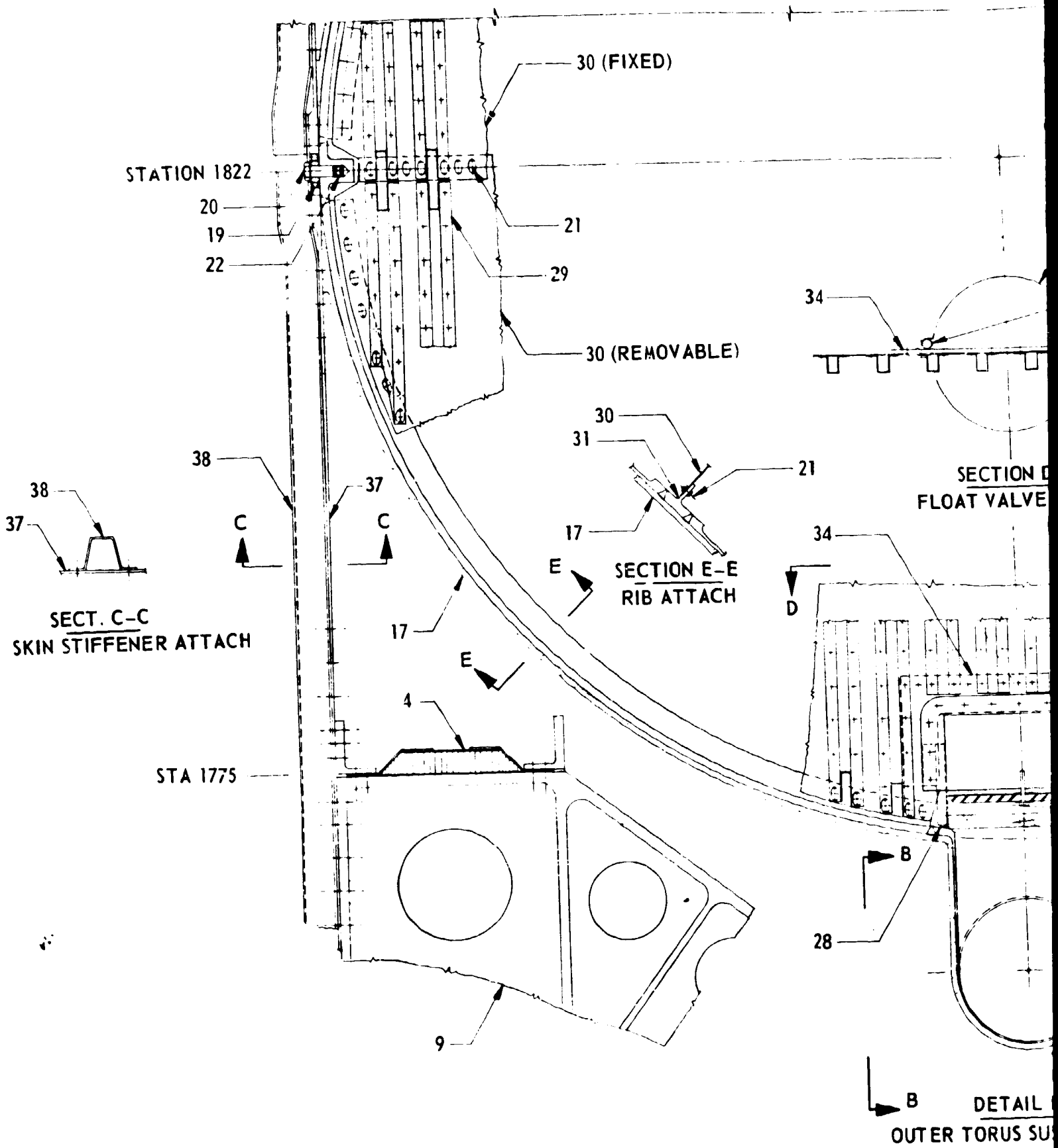
FIGURE 4.3.4.1-2   INJECTION STAGE DESIGN

FOLDOUT FRAME 2   319/320

37

38

40

39

FIELD SPLICE

(TYPICAL)
STATIONS 2078
1974
1870

38

37
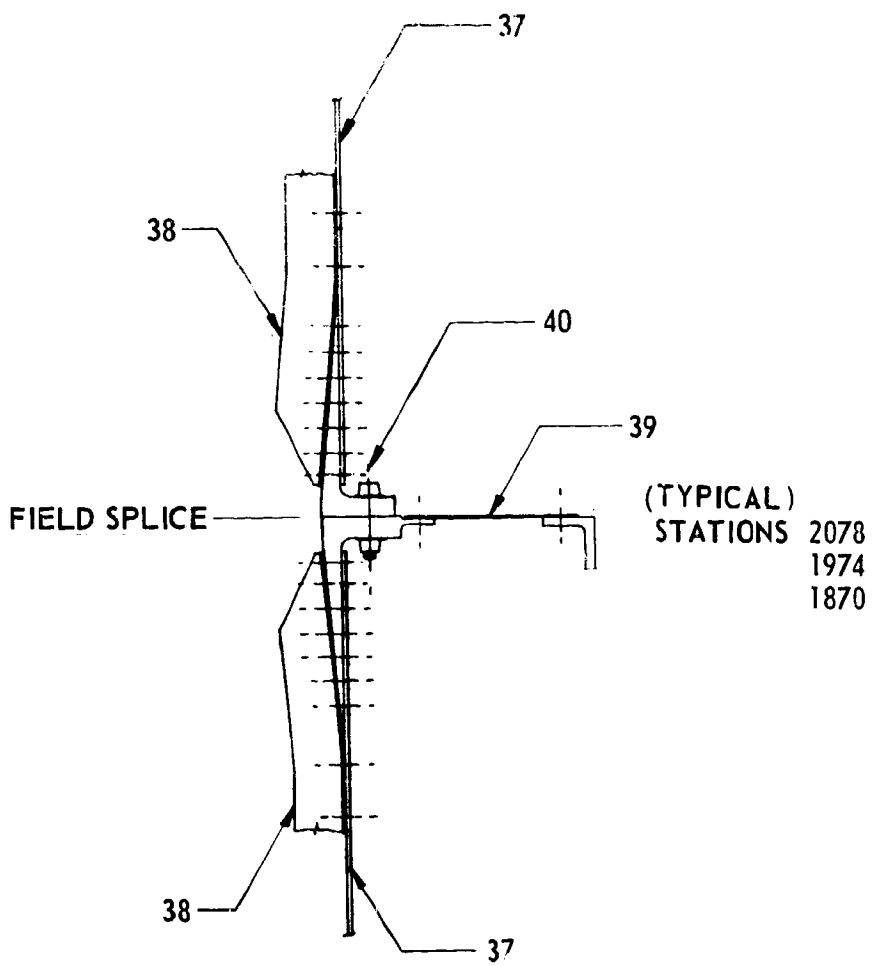
DETAIL IV
TYPICAL MODULE CONNECTION

FWD.

RADIAL

DETAIL III
TANK INTERCONNECT JOINT

FWD

RADIAL

VIEW B-B
MANIFOLD ATTACHMENT

FWD.

CIRCUM.

TO ENGINE
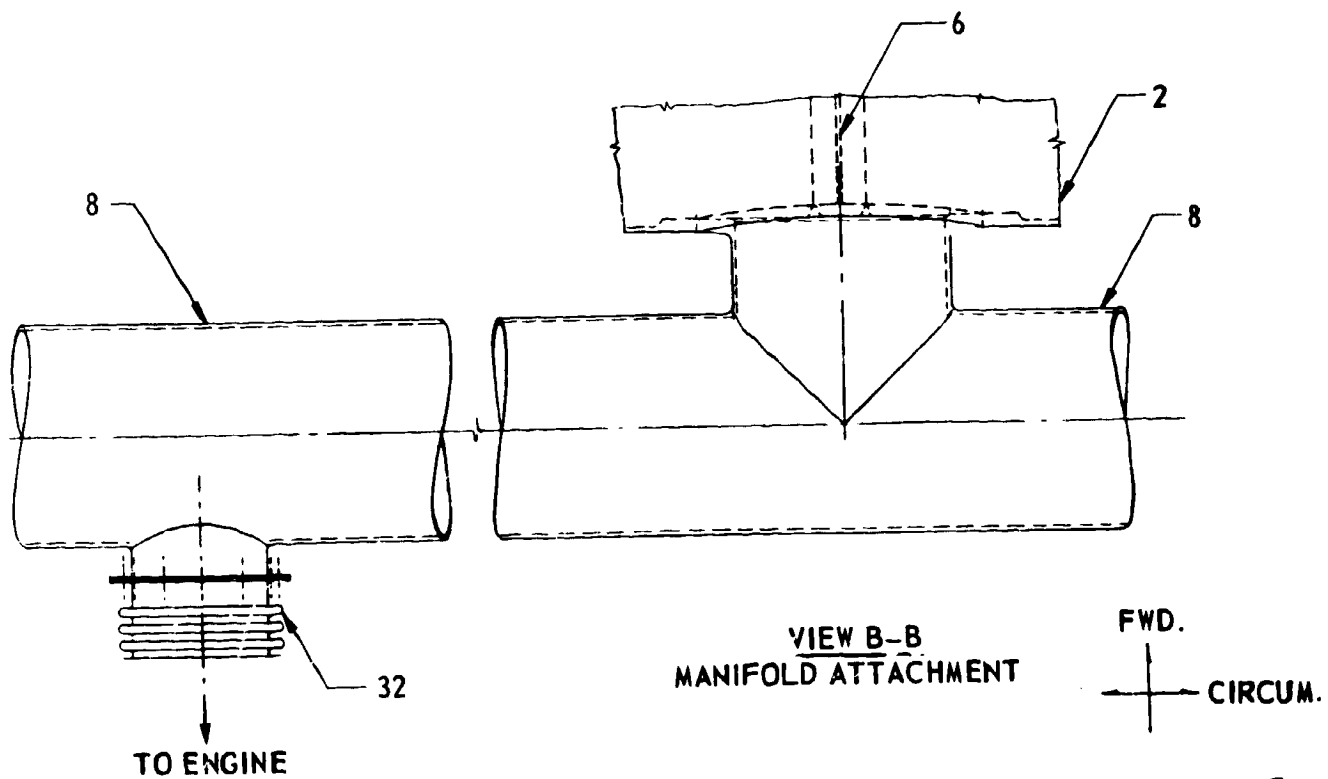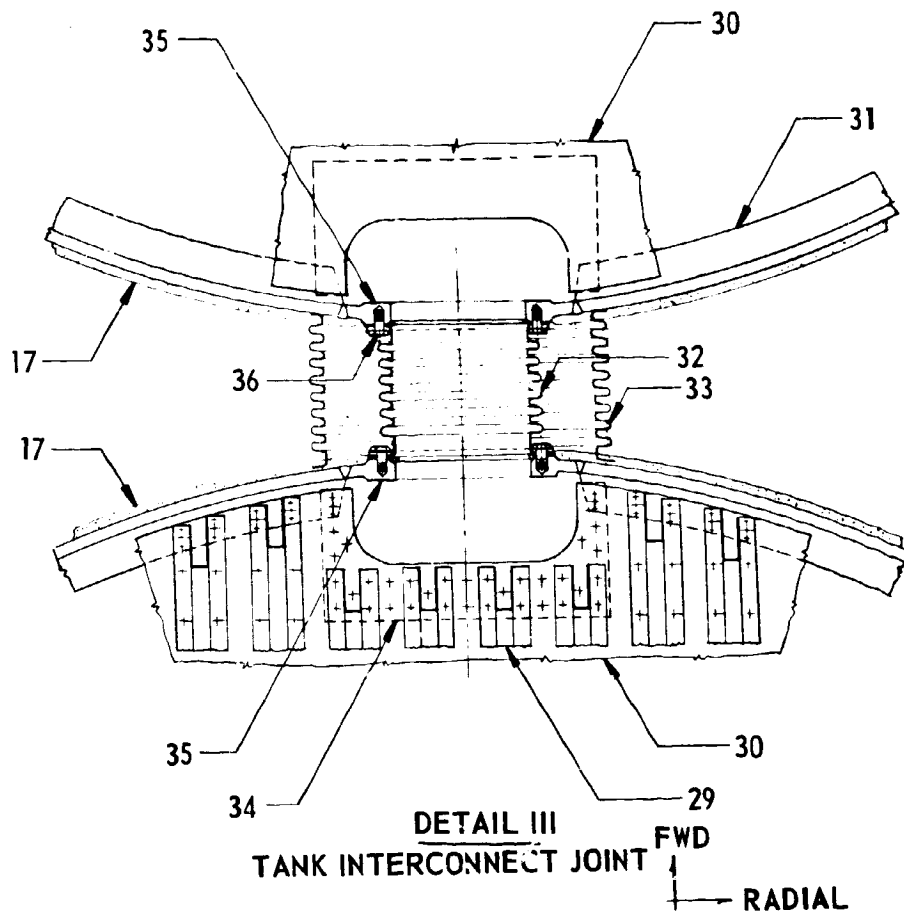
FIGURE 4.3.4.1-3 INJECTION STAGE DESIGN

TABLE 4.3.4.1-I MLLV BASELINE INJECTION STAGE DESIGN

STRUCTURAL COMPONENT	STRUCTURAL MATERIALS	CONSTRUCTION
CYLINDRICAL SKIRT	7075-T6 ALUMINUM	SKIN, STRINGER, FRAME
LOX TORUS TANK	2219-T87 ALUMINUM	SEMI-MONOCOQUE
HANGER SKIRT	CROSS-PLY FIBER-GLASS/EPOXY LAMINATE	FIBERGLASS LAMINATE
LH$_2$ TORUS TANK THRUST RING FRAMES	2219-T87 ALUMINUM	SEMI-MONOCOQUE
LOX & LH$_2$ RIBS	2219-T87 ALUMINUM FACINGS WITH 5052 ALUMINUM CORE	HONEYCOMB
MANIFOLDS	2219-T87 ALUMINUM	MONOCOQUE
ENGINE ATTACHMENT THRUST STRUCTURE	7075-T6 ALUMINUM ALLOY	DIE FORGING

4.3.4.1   (Continued)

Toroidal manifolds attached to the lower module will effectively drain the aft tanks.
Float valves will insure manifold suction of liquids and not gases no matter what
position the tank assumes. All the engines will be flex-joint connected to the
manifolds, which will be sized to feed all size engines with only one float valve
open in each manifold. The design concept of the feed line system is shown in
Figure 4.3 4.1-3.

Cylindrical Skirts and Thrust Structure

Each module will have a 7075-T6 aluminum cylindrical skirt of skin-stringer-frame
construction. These module skirts will be joined by a circumferential bolt pattern,
as shown in Detail IV, of Figure 4.3.4.1-3.

The skirts enclosing the three module injection stage propellant tanks were sized
for the stability critical N_c load induced at max q for the main stage with eight
strap-ons plus a three module injection stage vehicle. The thrust structure in the
lower injection stage module will consist of two thrust rings and six engine mount
forgings (thrust posts). Each engine mount will transmit the vertical thrust compon-
ent to the reinforced skirt. The external skirt reinforcing will shear the engine
thrust load into the skirt skin. The two thrust rings will react the coupling loads
which result from the cantilevered engine mounting plus engine gimbaling. The
engine mounts will be pin connected at the ends to the engines.

Aluminum alloy 7075-T6 was chosen for the injection stages skirt and thrust structure
because of its good strength to weight ratio and corrosion resistance.

4.3.4.2   Propulsion Systems

The engines will be mounted on cantilever forgings from two (moment-restraining)
ring frames. Additional engines will be added as additional modules are added.
The extendible nozzle engines will be nested into the forward skirt area of the main
stage to save stage length. They will extend their nozzle and gimbal outward after
main stage and injection stage separation.

The engine design used in evaluating the injection stage performance was the high
chamber pressure translating nozzle concept as defined by Pratt and Whitney. This
engine will utilize liquid hydrogen and liquid oxygen propellants. The translating
nozzle will provide a means of minimizing the engine installation envelope. The
major portion of the nozzle will be dumped cooled. The engine will use a preburner
cycle. This engine will have the capability to operate at various mixture ratios for
better propellant utilization. Major engine parameters are shown below:

4.3.4.2   (Continued)

Propellants	LOX/LH$_2$
Vacuum thrust	125,000 lbs (Single Engine)
Area ratio	300
Specific Impulse	Classified (See Volume IX, Appendix A)
Weight	1,930 lbs
No. of engines	Two per module
Exit Diameter	125 inches
Stowed Length	120 inches

The ullage pressures will be the same as used for the AMLLV injection stage as stage size will have only a slight effect on the ullage pressure requirements. The ullage pressure for LOX tanks will be 24 psia and 22 psia for the LH$_2$ tank.

4.3.4.3   Separation and Ullage

Main stage/injection stage separation will be similar to that of the S-IC/S-II. The main stage will separate just above the injection stage field splice ring (Station 1690) at the separation station (1730). The ring will then be staged from around the engines. The engines will be gimballed inward immediately upon main stage separation and prior to ring separation to provide additional separation clearance. After ring separation the engines will then be gimballed outward and the nozzles extended. Injection stage release will be provided by a linear shaped pyrotechnic charge. Main stage retro rockets and injection stage ullage rockets will be ignited simultaneous to firing of the shaped charge and initiation of the injection stage ignition sequence. Four motors with 23,000 pounds thrust each operating for 3.7 seconds will provide the required ullage impulse of 265,000 pound seconds. (See Section 4.2.6.2 for additional separation data.)

4.3.5   Strap-On Stage

The 260" diameter solid propellant rocket motors (SRMs) for the MLLV strap-on stages will consist of (1) a combustion chamber, (2) a canted nozzle, (3) the thrust vector control system, (4) the solid propellant fuel, (5) the ignition system, and (6) the destruct system. The SRM data presented in this section was provided by the Aerojet General Corporation.

4.3.5   (Continued)

Each SRM will be converted into a strap-on stage by the addition of on-board power sources, on board test and checkout system, flight instrumentation, aft skirt, heat shield, forward thrust attachment structure, nose cone and a solid motor separation system. Figure 4.3.5.0-1 illustrates the major motor and stage components.

The eight strap-on stages will be mounted equidistant about the main stage on a 980-inch diameter circle. The motors will be mounted parallel to the stage centerline. All of the motors will contain thrust vector control provisions. Configurations with less than eight strap-ons will employ the same attach points with the stages arranged symetrically about the main stage.

The solid motors will be ignited simultaneously at liftoff, and will be staged simultaneously after the net acceleration of each and all of the strap-on stages is less than that of the core vehicle. (This applies for all launches employing strap-ons except where only two strap-ons are used in which case a parallel launch mode will be used. These SRM stages will be separated when both SRM's operating pressure drops to ten percent of maximum pressure.)

Some development tests have been conducted on the 260-inch diameter solid motors. These motors did not contain the quantity of solid propellant as required by this program nor did they provide a thrust level as high as that defined for the MLLV application. A four motor development and six motor qualification program will be required to qualify the SRM for operational use.

4.3.5.1   Solid Rocket Motor Performance and Variability

a.   Nominal Motor Performance - The solid rocket motor will contain 2.9 million pounds of a polybutadiene (PBAN) propellant and will produce 665 million pound-seconds of total impulse. The nominal sea level axial thrust will rise from 6.45 to 6.75 million pounds during the initial 7.5 seconds of operation and will gradually decrease at a uniform rate to approximately 3.7 million pounds (sea level thrust) at the end of web action time. The web action time will be 129 seconds. An additional 4 seconds tail off time will be required to reduce the pressure to approximately 10 percent of the initial pressure. The initial pressure will be 667 psia. At web action time, the chamber pressure will be reduced to 400 psia. The nozzle expansion ratio will be 8.06 as limited by the restraint on the nozzle exit cone diameter. This arbitrary restraint limits the exit cone diameter to the case diameter, i.e., 260 inches.

Table 4.3.5.1-I illustrates the major ballistic performance parameters of the SRM at 80° F. The regressive design of the motor will result in decreasing thrust, pressure and mass flow with motor burn time as shown in Figures 4.3.5.1-1, -2 and -3. To insure the maximum dynamic pressure did not

FIGURE 4.3.5.0-1 SOLID ROCKET MOTOR STRAP-ON STAGE

NOSE CONE

FORWARD
ATTACHMENT
STRUCTURE

IGNITER

IGNITER SAFETY &
ARMING DEVICE

FORWARD STAGING ROCKETS (4)
TWO FACING LEFT 35°
TWO FACING RIGHT 35°

NOZZLE

NOZZLE ACTUATOR

MOTOR CASE

DESTRUCT
RACEWAY

AFT ATTACHMENT
STRUCTURE

AFT STAGING ROCKETS (3)

SUPPORT STRUTS

HEAT SHIELD
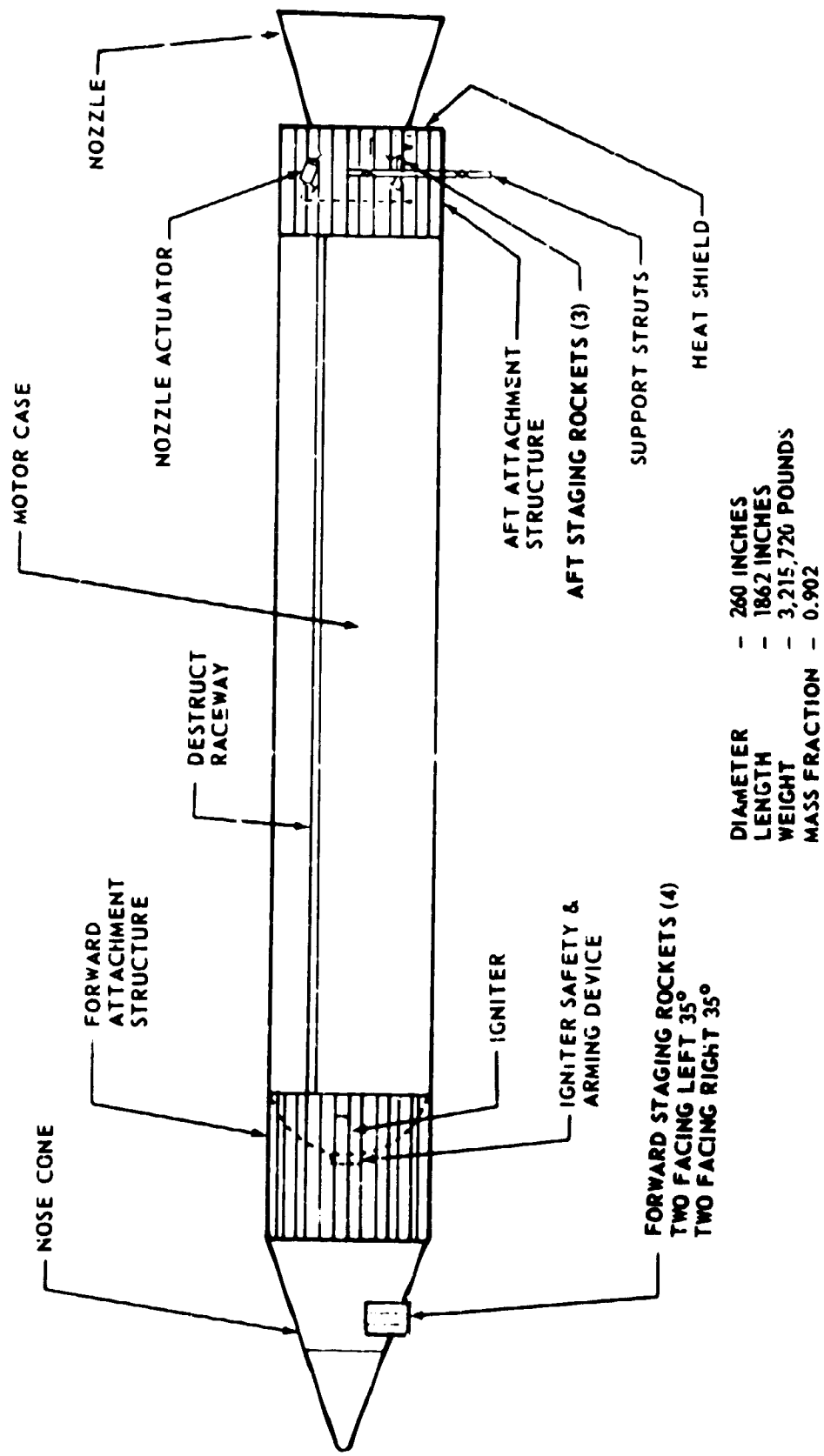
DIAMETER   —   260 INCHES
LENGTH   —   1862 INCHES
WEIGHT   —   3,215,726 POUNDS
MASS FRACTION —   0.902

327

TABLE 4.3.5.1-I BALLISTIC PERFORMANCE SUMMARY - 260-INCH DIAMETER MOTOR

	Boeing Specified Target	Aerojet-General Design
Propellant Weight, lbm	2,900,000	2,900,000
Total Impulse @ Sea Level, lbf-sec		665,000,000
Initial Axial Thrust, lbf	6,800,000	6,450,000
Average Thrust, lbf		5,120,000
Maximum Thrust @ Sea Level, lbf		6,750,000
Specific Impulse Standard, lbf-sec/lbm	248	248
Specific Impulse, Delivered @ Sea Level, lbf-sec/lbm		229.3
Maximum Expected Operating Pressure, psia		800
Maximum Nominal Pressure, psia		755
Initial Stagnation Pressure, psia	700	667
Average Stagnation Pressure, psia		533
Propellant Burn Rate @ 600 psia, in/sec		0.625
Burn Rate Pressure Exponent		0.4
Propellant Density, lbm/in^3	0.063	0.063
Port-to-Throat Area Ratio		1.30
Nozzle Throat Diameter, Initial, Final, in		91.61 - 93.17
Nozzle Exit Diameter, in	260	260
Nozzle Expansion Ratio		8.06
Nozzle Exit Half-Angle, Degrees	17.5	17.5
Web Action Time, sec	130	129
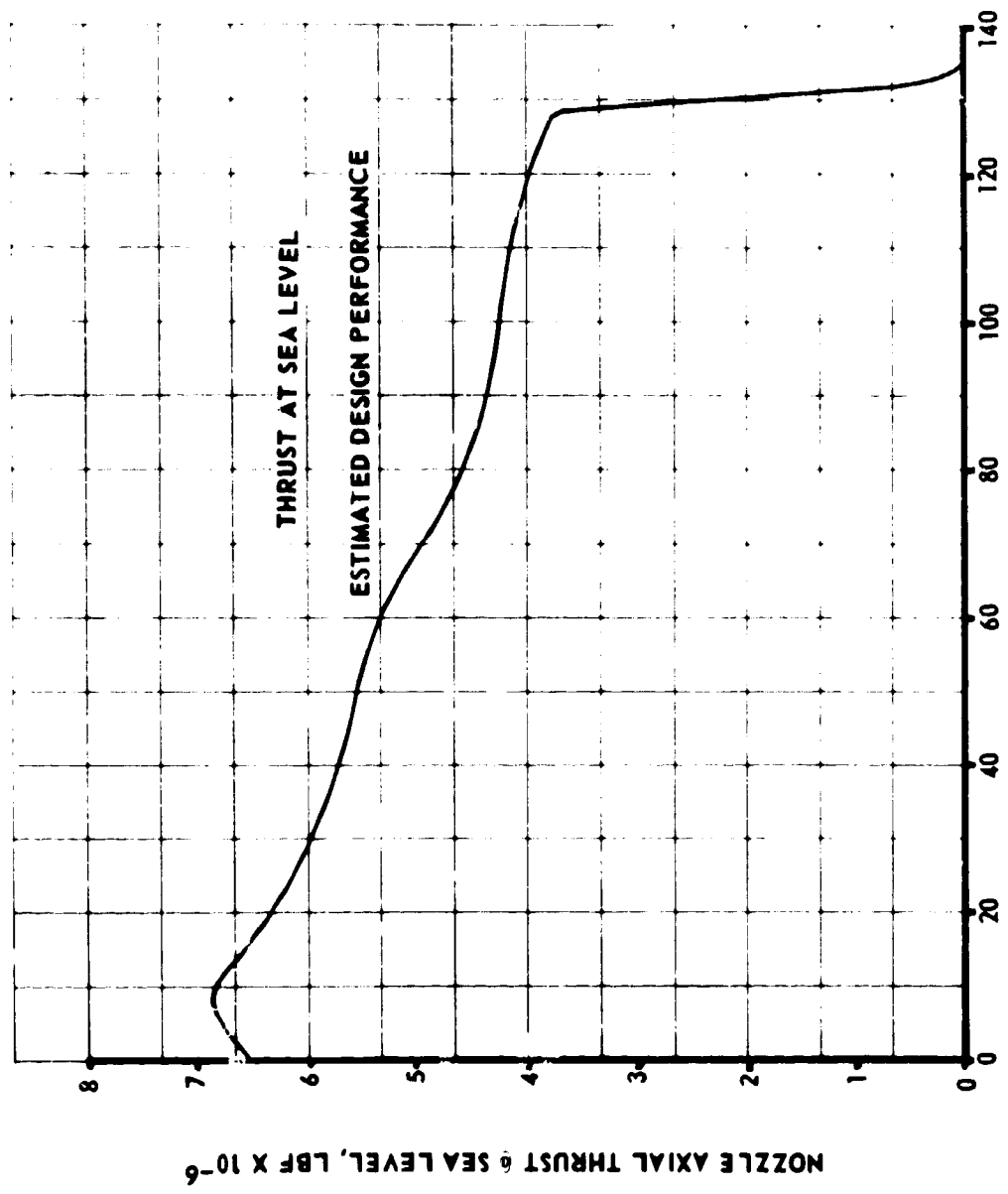
FIGURE 4.3.5.1-1   260 INCH SRM BALLISTIC PARAMETERS - THRUST VS. TIME
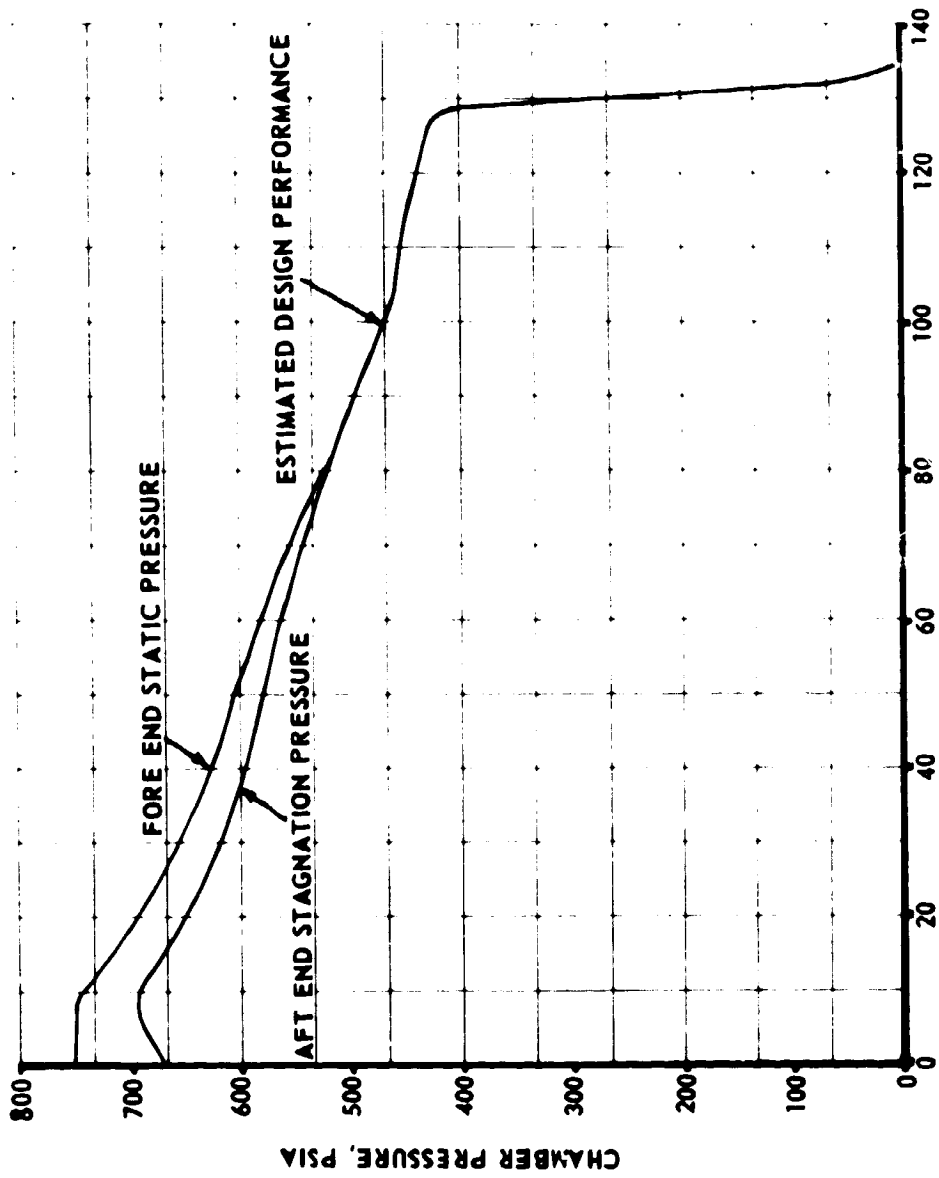
FIGURE 4.3.5.1-2 260 INCH SRM BALLISTIC PARAMETERS – CHAMBER PRESSURE VS. TIME
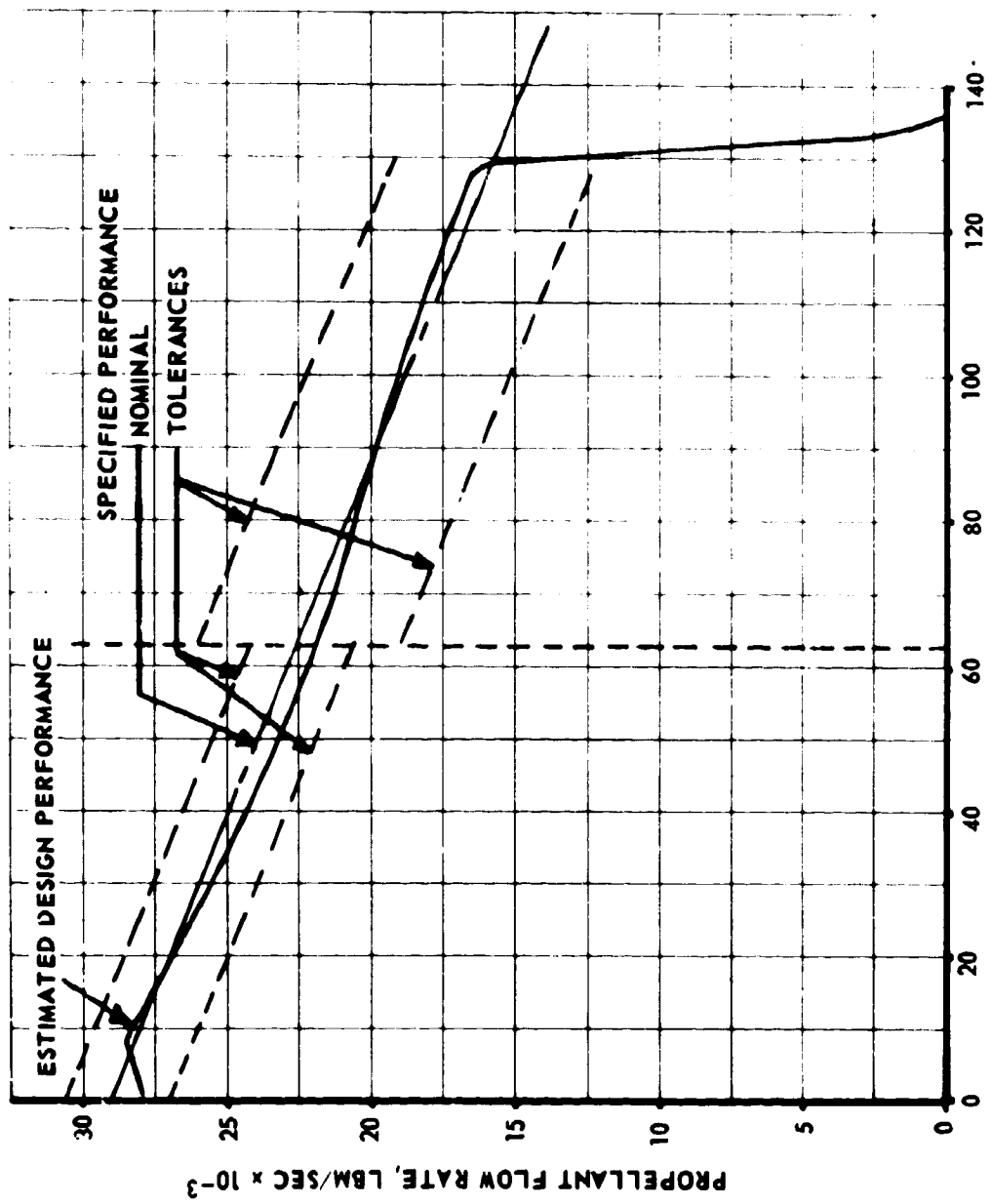
FIGURE 4.3.5.1-3   260 INCH SRM BALLISTIC PARAMETERS – PROPELLANT FLOW
RATE VS. TIME

4.3.5.1   (Continued)

become excessive, the mass flow as shown in Figure 4.3.5.1-3 was specified
to the restricted tolerances shown for the first 63 seconds. A more liberal
tolerance was permitted after maximum dynamic pressure.

b.   Solid Motor Performance Variability - The estimated variability of 260-inch
diameter SRM performance characteristics are shown in Table 4.3.5.1-II.
These performance variations are based on actual variance data generated in
current and past solid rocket programs, such as Minuteman and Polaris.
However, each parameter was individually studied for application to 260-inch
diameter SRM's. Consequently, the percentage variation values represent
the propulsion contractor's (Aerojet General) best engineering estimates of the
motor-to-motor variances to be expected for the MLLV applications. (The
ignition interval variance provides an example of such data extrapolation.
This variance will range from 20 to 45 percent on current motors. However,
the three 260-inch diameter motor test firings to data indicate a much smaller
value; the $3\sigma/\bar{X}$, as calculated from the observed range of 0.336 to 0.342
seconds (3.13 percent). This low value is considered somewhat fortuitous and is
not expected to be typical. It is estimated that the $3\sigma/\bar{X}$ value will be in the
10 to 20 percent range.

4.3.5.2   SRM Design Safety Margins

Ideally, design safety margins for SRM components would be fixed by determining
analytically the values which would result in the desired probability of success
in the intended application. Unfortunately, this analytical capability is still in the
process of development. It was thus necessary to establish design safety margins,
in large degree, on the basis of engineering judgment together with prior experience
in obtaining the desired levels of reliability.

The recommended design factors of safety for various components of the 260 inch
diameter motors are shown below. The motor case and general structure factors
of safety are based on the NASA/MSFC vehicle safety factor requirements.

Component	Factor of Safety
Motor Case	1.20 (Yield Strength)
Nozzle	
Structure	1.30 (Yield Strength)
Ablative Thickness	1.50

TABLE 4.3.5.1-II   SRM PERFORMANCE VARIABILITY

Parameter	$3\sigma/\bar{X}$ (%)
Propellant Weight	0.30
Specific Impulse	0.12
Total Impulse	0.32
Propellant Burning Rate	1.65
Web Burning Time	2.3
Axial Thrust	2.3
Chamber Pressure	2.5
Nozzle Throat Area	0.33
Motor Inert Weight	1.34
Ignition Variance	*

* Refer to discussion in Section 4.3.5.1, subparagraph b.

4.3.5.2   (Continued)

Component	Factor of Safety
Chamber Insulation Thickness	1.50
Propellant Grain Structure	1.50 (Ultimate Strength)
Ignition System Structure	1.25 (Yield Strength)
General Structure	1.40 (Ultimate Strength)

4.3.5.3   Motor Configuration

The motor design is based on component designs which have been demonstrated in static test firings of 260-inch diameter, short length motors (nominal 1,700,000 pounds propellant weight) of the 260-inch diameter Motor Feasibility Demonstration Program, conducted by Aerojet-General Corporation. Figure 4.3.5.0-1 above identifies major motor components and Figure 4.3.5.3-1 shows overall dimensions.

a.   Motor Case - Dimensions for the complete motor assembly including nozzle are shown in Figure 4.3.5.3-1. The motor will use a monolithic combustion chamber fabricated of 18 percent nickel maraging steel having a minimum yield strength of 200,000 psia @ 0.2 percent offset. The motor case will consist of a cylinderical section 916 inches long with a nominal diameter of 260-inches and two hemispherical heads. The membrane components were assumed to be forged or shear-spun, eliminating the need for longitudinal welds. Forged Y-rings will be used to join the cylindrical section to the respective forward and aft heads and skirts. The forward head will have a 28-inch diameter igniter boss for the installation of the ignition motor. The aft head will have a large port with a 180-inch diameter bolt circle for attachment of the nozzle. Forged flange rings will be used for the igniter attachment flange in the forward head and the nozzle attachment flange in the aft head. Nominal wall thicknesses for the cylindrical section will be 0.678 inches and 0.402 inches for the forward and aft heads.

The solid motor skirts will consist of a cylindrical section welded to the end of the Y-rings. The forward and aft skirts will be drilled to allow for mating with the attachment structure. The attachment structure will be joined to the solid motor skirts with pins.

The buckling capacity of the motor skirts has been analyzed using the 90 percent probability of Reference 4.3.5.3-1. This analysis results in a

---

4.3.5.3-1   J. G. Schumacher and B. Lincoln, Development of Design Curves for the Stability of Thin Pressurized and Unpressurized Circular Cylinders. General Dynamics Corporation, Report AZD-27-275, dated 8 May 1959.

334
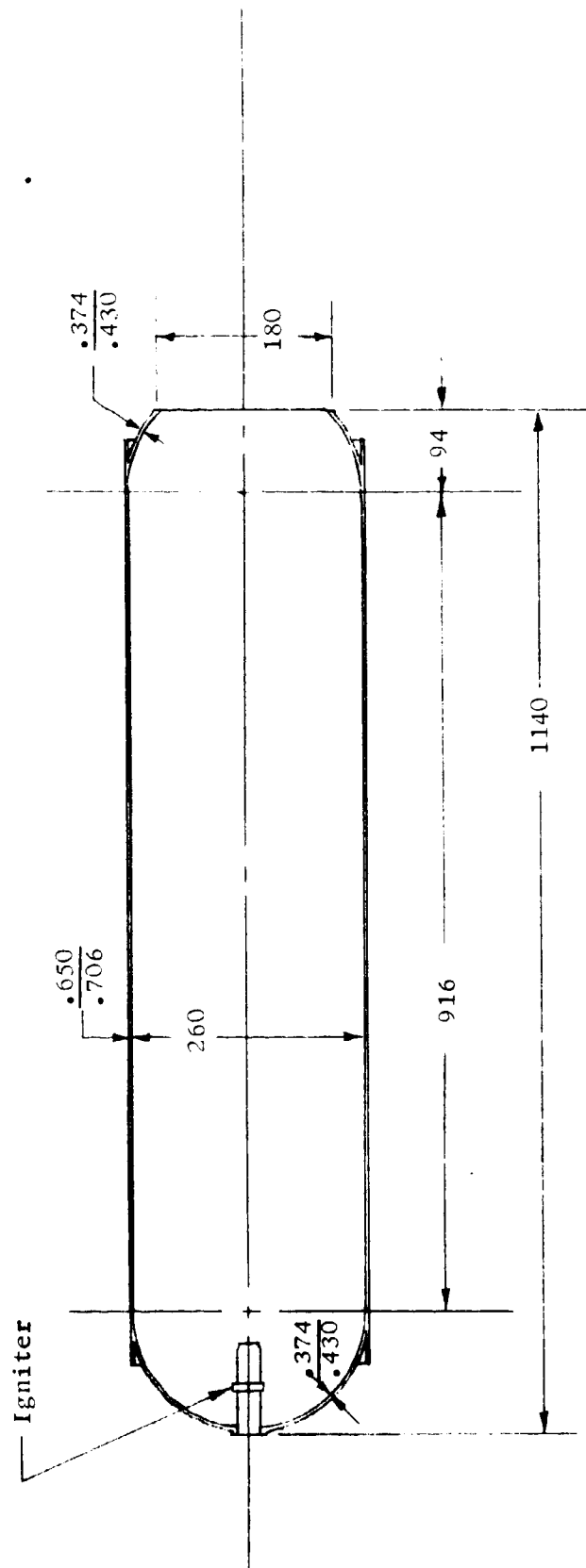
FIGURE 4.3.5.3-1 CHAMBER CONFIGURATION 260 INCH-DIA STRAP-ON MOTOR
FOR HALF-SIZE MLLV

335

4.3.5.3   (Continued)

critical load of 49 x 10^6 pounds for pure axial compression and 4 x 10^9 in-pounds for pure bending. It should be noted that an interaction of axial compression and bending loads will reduce the individual critical loads given above. The analysis is applicable to either forward or aft skirt, and is based on the following skirt parameters:

Skirt length = 60 inches

Skirt minimum thickness = 0.80 inch

Skirt diameter = 260 inches

Modulus of elasticity (E) = 27 x 10^6 psi

b.   The nozzle design for the 260-inch strap-on stage is shown in Figure 4.3.5.3-2. This flexible seal type nozzle will be capable of five degrees of jet thrust deflection. The nozzle will have a submerged entrance section configuration similar to the 260-SL-3 design. The nozzle divergence section contour will be 17.5 degree half angle extending to 8.06 expansion ratio. The initial nozzle throat diameter and the initial exit cone diameter will be 91.61 and 260 inches, respectively. The nozzle will be submerged to provide for incorporation of the flexible seal design.

MATERIAL

① CARBON CLOTH PHENOLIC
② SILICA CLOTH PHENOLIC
③ 18 PERCENT MARAGING STEEL
④ ALUMINUM HONEYCOMB CORE
⑤ FIBERGLASS CLOTH
⑥ 4130 STEEL
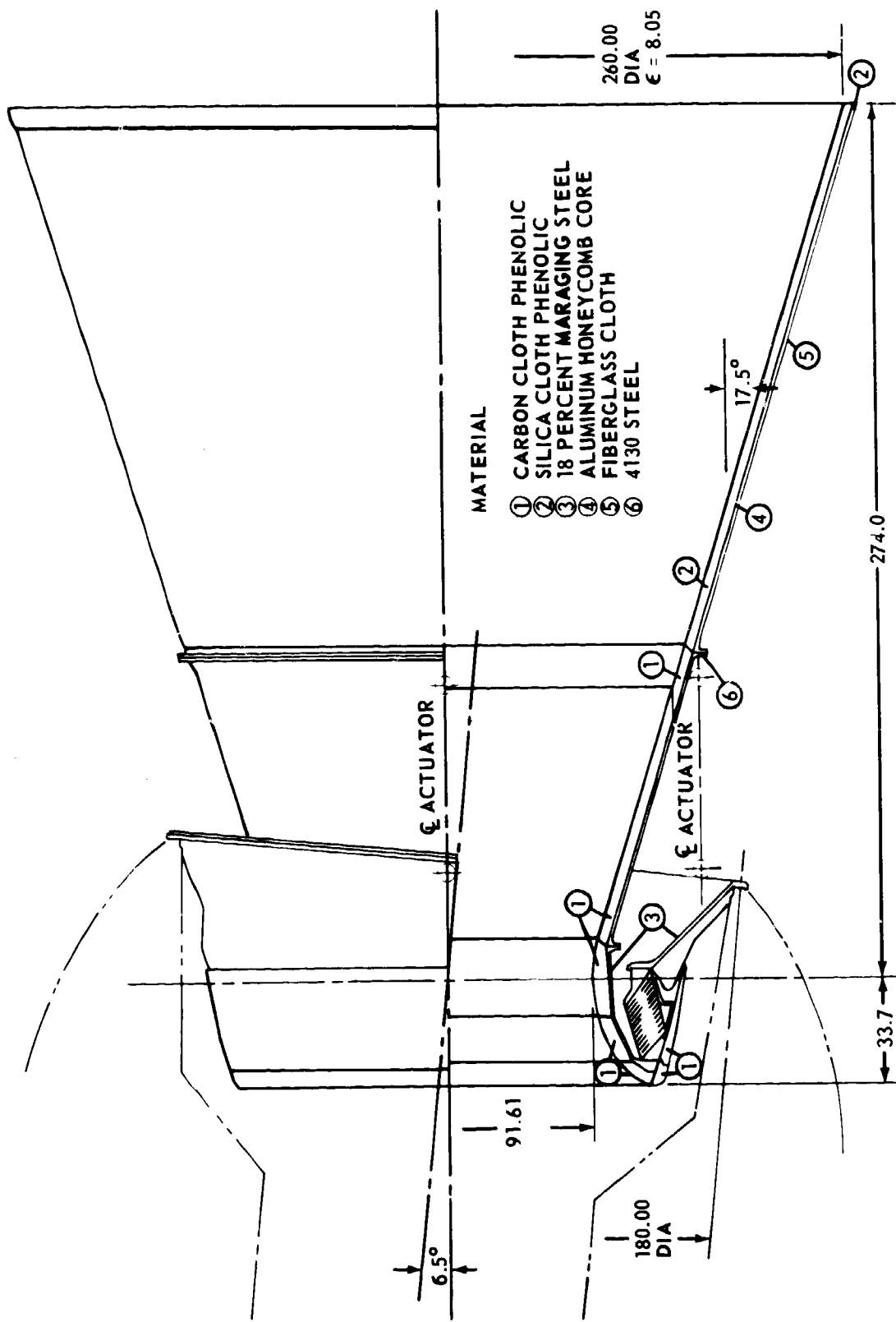
FIGURE 4.3.5.3-2   NOZZLE ASSEMBLY 260-INCH MOTOR

4.3.5.3 (Continued)

The nozzle will use materials that have been demonstrated on the 260-inch motor program. Carbon cloth phenolic and silica cloth phenolic will be used on the ablation surface at low and high area ratios, respectively. Eighteen percent nickel maraging steel will be used for the forward nozzle support structure and the nozzle mounting closure. The nozzle forward exit cone support structure will be 4130 steel. A honeycomb structure consisting of aluminum core and fiberglass facing will be used for structural support of the exit cone assembly.

The flexible seal design will have alternate layers of elastomer and steel and will be supported by steel end flanges. The thickness and width of the layers will be sized to meet the structural requirement due to axial load, rotational force, and elastic stability. The deflection torque for the flexible seal is 1.26×10^6 ft-lb and the system design torque is 1.6×10^6 ft-lb.

c. Thrust Vector Control System - The solid rocket motor (SRM) thrust vector control (TVC) system selected for the vehicle will be a flexible seal movable nozzle system. Each SRM will have system consisting of (1) a flexible seal which is an integral part of the nozzle, (2) two servo-actuators (one for the pitch and one for the yaw positions), (3) a hydraulic power system, (4) hydraulic and electrical circuitry systems. The hydraulic power system will consist of a gas generator, turbine, pump, accumulator, regulator and relief system, and a reservoir. Either a pressurized nitrogen tank or a solid propellant motor can provide the gas generation system. With either system, an electric motor with an auxiliary pump can provide the power for actuation during ground checkout.

The fluid supply system will provide hydraulic power for the solid motor flexible nozzle thrust vector control system. During flight, the system will operate on MIL-H 5056 or MIL-R-25576B hydraulic fuel. The on-pad checkout will utilize ground source hydraulic fuel.

Two servoactuators will be used for each motor with one on each of the pitch and yaw planes. The type of servoactuators will be similar to those currently used on the F-1 engine of the Saturn V/S-IC stage. The force output per actuator will be 244,000 pounds based on an area of 122 square inches and 2000 psi minimum operating pressure. The stroke of the actuator will be 16.6 inches.

Control of the double acting actuator will be effected by a hydraulic servovalve, with electrical signal input from the guidance system. The servovalve will have a flow capacity of 200 gpm at 1000 psia pressure drop. A mechanical feedback mechanism will be included in the servoactuator.

338

4.3.5.3 (Continued)

A circulating hydraulic system will be used consisting of a variable delivery, constant pressure pump that is driven by a turbine. The turbine will be powered by a hot gas generator. Two power supply units will be used per nozzle, and the units will be cross-linked for redundancy so that each pump can provide hydraulic pressure to both actuators in the event one pump fails. Minimum pressure supplied by the power unit to the servoactuator will be 2500 psi. The minimum pump flow rate capacity for both actuators is 200 gpm.

During operation, the hydraulic fluid will flow from the hydraulic reservoir to the servo-valve into the servo-actuator, and return to the reservoir. The pressurization system will be initiated just prior to SRM ignition. Sufficient hydraulic fluid will be provided to allow for servo leakage through the SRM operation.

The signal to start the TVC system will be sent by the MLLV Instrument Unit (see section 4.3.7) while the vehicle is on the launch pad. The solid motor TVC system will be required throughout the operation of the solid motors. The maximum capability will be required in the maximum dynamic pressure regime. When TVC is required, the Instrument Unit will supply a control signal to the pitch and yaw servo-valves. The servo-valves will then activate the hydraulic actuator.

The thrust vector control system is capable of vectoring the flexible seal type movable nozzle to a 5-degree deflection angle with a thrust deflection rate capability of 3 degrees per second.

d. Propellant Grain - A detailed grain design study was performed by the Aerojet-General Corporation to establish the configuration which could best meet the SRM performance requirements specified. The thrust and chamber pressure vs. time curves for the resulting design are shown in the proceeding Figures 4.3.5.1-1, -2, and -3.

The selected grain configuration is shown in Figure 4.3.5.3-3. The forward portion of the grain will have a six point-star cross-section. This will provide the high surface area needed to meet the initial thrust requirements, and will burn out rapidly to provide the desired regressive performance. The aft section of the grain will be circular in cross-section. This type of grain configuration will be adaptable to nearly any ballistic curve shape requirement, and will be geometrically sliverless. The star points will be unequally spaced to achieve curve linearity. The nominal propellant burn ratio will be 0.625 in/sec at 600 psia. The propellant properties required for this grain design can be readily obtained with a composite propellant formulation based on a terpolymer of polybutadiene, acrylic acid and acrilonitrile with ammonium perchloride oxidizer, powdered aluminum and burning rate additions. Key ballistic properties include:
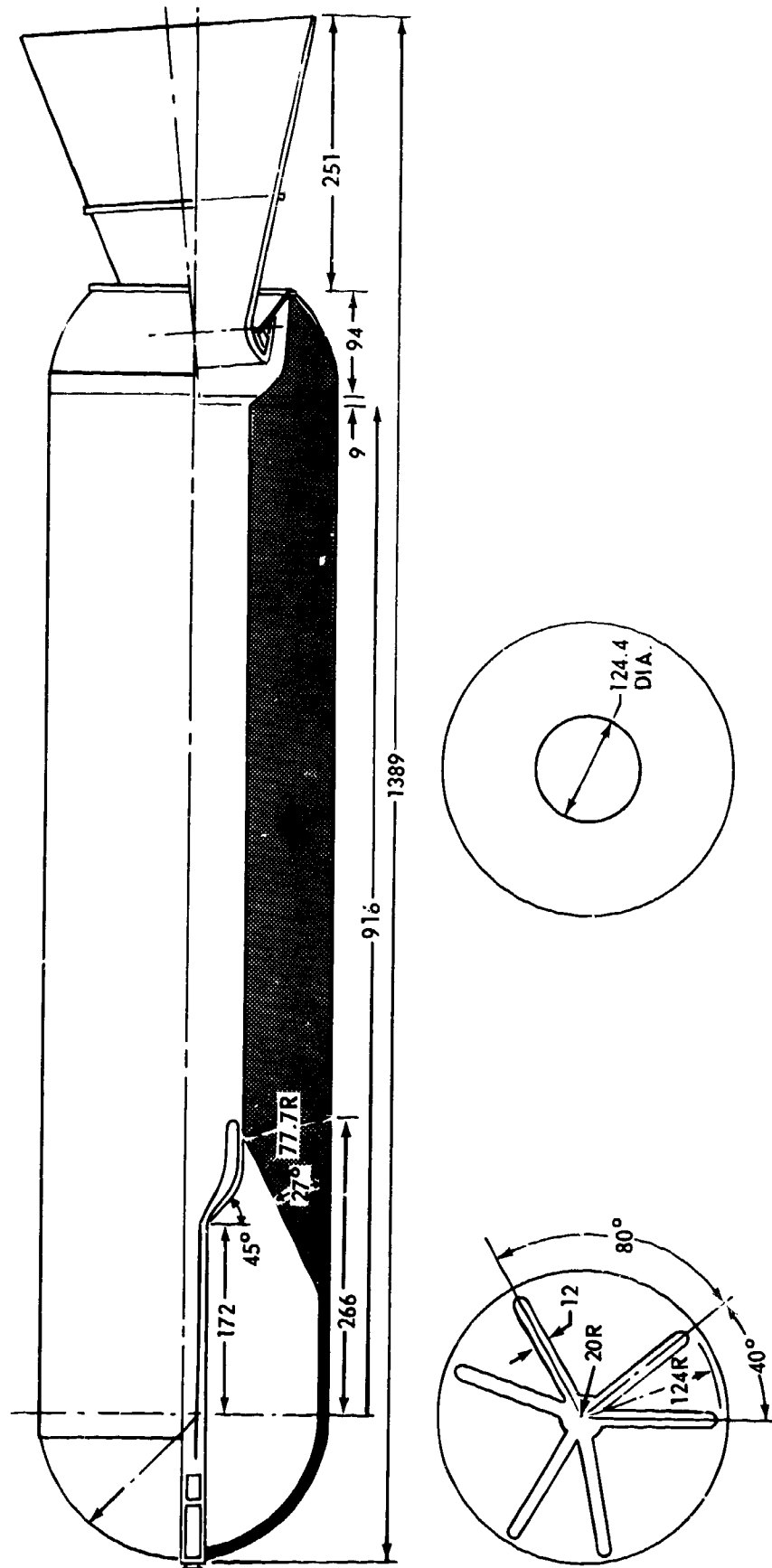
FIGURE 4.3.5.3-3 PROPELLANT GRAIN AND MOTOR ASSEMBLY

4.3.5.3   (Continued)

.   Burning rate - 0.625 at 600 psia in/sec

.   Specific Impulse - 244.6 sec (1,000 psia chamber pressure, opt.
                                    expansion at sea level, 15° nozzle half angle)

.   Density - 0.063 lb/in^3

The motor was sized to contain the specified 2,900,000 lb. of propellant with
a port-to-throat area ratio of 1.30. The submerged entrance of the nozzle
will require an enlarged port at the end of the grain.

e.   Ignition System - The 260 inch diameter SRM head-end ignition motor assembly
     design configuration as shown in Figure 4.3.5.3-4 will consist of three assemblies:
     the ignition motor (or main igniter charge); ignition motor booster; and the
     booster initiator.

     1.   Ignition Motor - The ignition motor will consist of 595 pounds of propellant
           contained in a high-strength steel chamber. The 28-inch diameter ignition
           motor chamber will be fabricated from Ladish D6aC rolled-ring steel forgings,
           heat-treated to 185,000 psi minimum yield strength. A lock-strip will be
           incorporated to facilitate propellant insulation and final assembly. The
           internal and external surfaces of the ignition motor will be insulated with
           vulcanized Gen-Gard V-44 rubber to prevent burn through and possible
           ejection of the chamber during motor operation. Combustion gases will
           be exhausted through four nozzles in the aft head of the chamber. The
           nozzle ports will be canted 55 degrees from the motor centerline to effect
           jet impingement on the propellant surface, thereby increasing the delivered
           heat flux. Silican cloth phenolic inserts will be used to maintain nozzle
           integrity during itnition motor operation.

           The ignition motor propellant will be AND-3254, an polybutadiene (PBAN)
           formulation with a burning rate of 0.87 in/sec at 1000 psia. The grain design
           will be a 35-tooth internal gear configuration, with a nominal web thickness
           of 0.32 inch.

           Installation of the ignition motor will be accomplished from the aft end
           through the motor bore, and the forward head of the igniter chamber forms
           the igniter boss closure in the motor forward head. This method of instal-
           lation will permit the use of a smaller access boss diameter, eliminating
           the necessity of separate igniter mounting adapter, and simplifying the design
           of the igniter boss in the chamber forward head.

341

FIGURE 4.3.5.3-4   IGNITION MOTOR

4.3.5.3 (Continued)

2. Ignition Motor Booster - The ignition motor booster will be a lengthened version of the Minuteman Wing VI Second Stage Mod C-2 igniter, containing 9.6 pounds of ANB-3254 propellant.

3. Booster Initiator - The booster initiator will be 100 grams of 2A-size boron-potassium nitrate ignition pellets, contained in a small chamber mounted at the forward end of the booster chamber.

4. Ignition Motor Assembly System - A schematic diagram of the ignition motor assembly actuation system is presented in Figure 4.3.5.3-5. There will be two completely independent systems, each capable of delivering the actuation stimulus to each SRM. In each system, two AGX-2010 Explosive Bridge Wire (EBW) electric detonators will be mounted into a simple electromechanical safety-and-arming device. The S/A unit will provide a positive mechanical barrier between the EBW detonators and the down-stream confined detonation fuse (CDF) detonators. The device will include both a visual and an electrically remote indication of position. A manual safety-lock will be incorporated to prevent inadvertent movement of the mechanical barrier during pre-launch operations.

The actuation stimulus will be directed through the downstream detonators and confined detonating fuses into a junction block. At the junction block, the detonation stimulus will be transferred to separate fuses going to each of the SRMs. At each motor disconnect, another junction block will provide a crossover between the fuses from each system. From the disconnect and crossover, the actuation stimulus will be carried through confined detonating fuses to the two detonators installed in the ignition motor booster initiator. One initiator detonator will be capable of igniting the boron-potassium nitrate pellets.

5. Ignition System Performance - The preliminary ignition motor performance curve, presented in Figure 4.3.5.3-6, includes estimated 3-sigma limits based on propellant temperature sensitivity and expected grain configuration dimensional variations. An estimated SRM ignition transient envelope, shown in Figure 4.3.4.3-7, is based on an initial motor fore-end steady-state operating pressure of 700 psia.

6. Ignition System Operational Sequence - The ignition motor will be installed in the SRM at the motor manufacturer's processing facility; the booster initiator can be installed either at the processing facility or during pre-launch operations. The CDF, electric EBW detonators, safety-and-arming device and EBW firing units will be checked out during pre-launch assembly. At approximately T-30 seconds, the EBW firing unit capacitors will be charged. The S/A units will be armed at approximately T-10 seconds.

TO SRM 1
TO SRM 2
JUNCTION BLOCK

TO SRM 3
TO SRM 4
TO SRM 3
TO SRM 4
TO SRM 1
TO SRM 2

CDF

S/A DEVICE

AGX-2010
DETONATOR
ELECTRIC WIRE

ELECTRIC WIRE

AGX-4403
DETONATOR

GSE

ACTUATION
SYSTEM 1

ACTUATION
SYSTEM 2

CROSSOVER
BLOCK
SRM DISCONNECT
CDF
CDF
FROM ACTUATION
SYSTEM 1
FROM ACTUATION
SYSTEM 2
SRM ENVELOPE
TO IGNITION
MOTOR BOOSTER
INITIATOR DETONATORS

TO JUNCTION
ELECTRIC
MOTOR
CDF
MECHANICAL
BARRIER

'ARM'

AGX-2010
EBW
DETONATORS

TYPICAL S/A DEVICE

NOTE:

CDF = CONFINED DETONATING FUZE
EBW = EXPLOSIVE BRIDGE WIRE

FIGURE 4.3.5.3-5   IGNITION ACTUATION SYSTEM

344
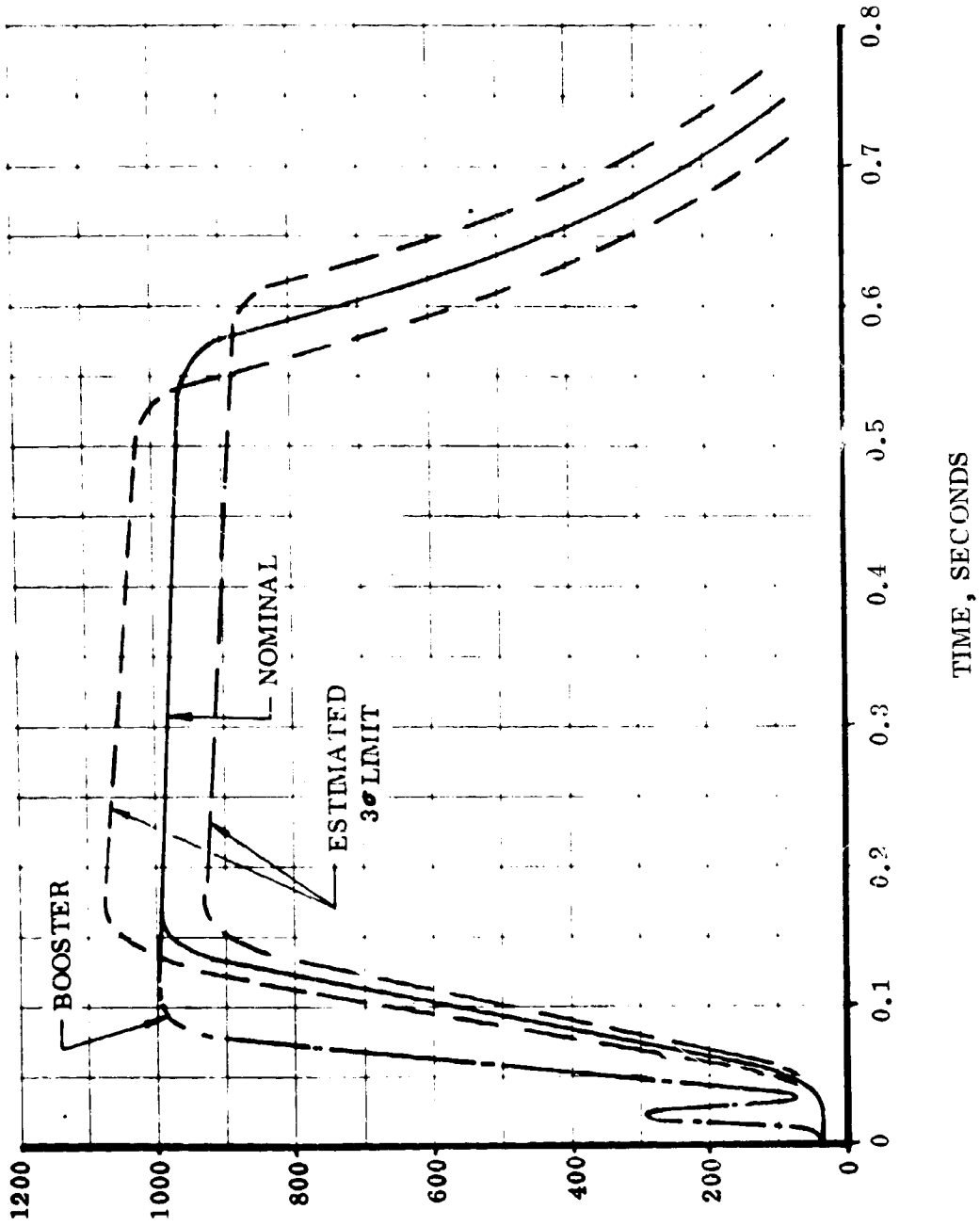
FIGURE 4.3.5.3-6   PRELIMINARY IGNITION MOTOR PERFORMANCE
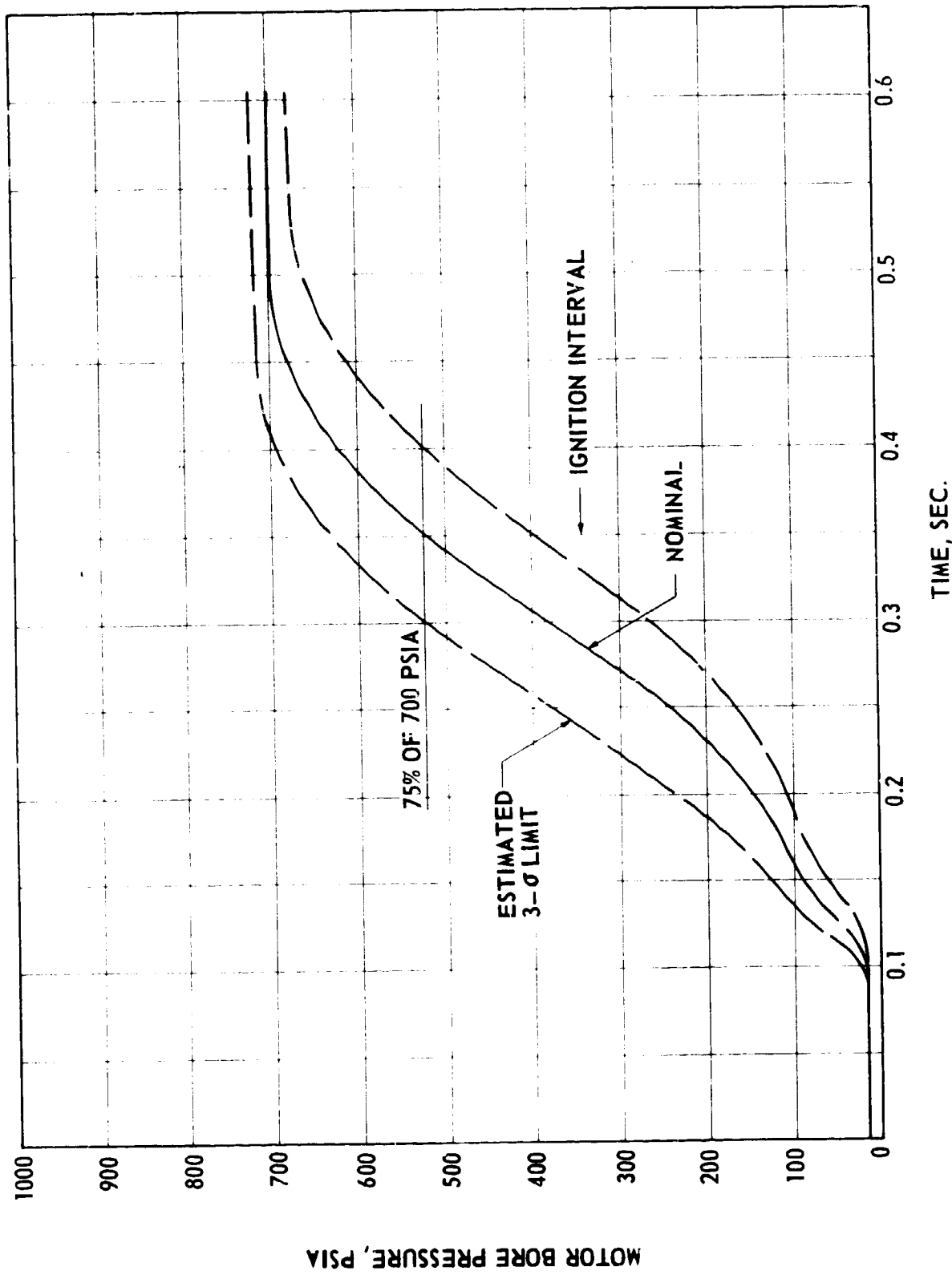
FIGURE 4.3.5.3-7 ESTIMATED SRM IGNITION TRANSIENT

4.3.5.3 (Continued)

f. SRM Destruct System – Range safety considerations require that each SRM carry a destruct system capable of rendering the SRM nonpropulsive upon receipt of a command signal or upon inadvertent separation of the SRM from the core vehicle. The recommended destruct equipment, therefore, will consist of a command destruct system (CDS) and an inadvertent separation destruct system (ISDS).

The CDS will consist of a safety-and-arming (S/A) device, confined detonating fuses, and redundant linear-shaped charges (LSC). The S/A device will be mounted either in the nose section, or in the SRM aft skirt. Confined detonating fuses will be used to transfer the explosive stimulus from redundant detonators in the S/A device to the LSC mounted in the SRM raceway, as shown in Figure 4.3.5.3-8.

The SRM ISDS will be a "hot wire" system. The ISDS will be activated by the breaking of redundant hot wires and safety ground wires in the core vehicle/ SRM connecting cables. The primary function of the ISDS will be to activate destruct in the event that command link is lost from the core vehicle due to premature separation of the SRM. The ISDS will also monitor the S/A device fire command circuits for hazardous voltage while the vehicle is in the prelaunch conditions. On command from the core vehicle, the ISDS will be disabled prior to staging.

Module	
Enable/Disable	1. In "Enable" condition, ISDS destruct command signal will be cleared to the separation detector module.
Enable/Disable	2. In "Disable" condition, signal cannot reach separation detector module.
Separation Detector	Will permit destruct signal to each timer module and destruct firing module, provided there is no input from the umbilical "hot wires."
Timer	Will provide a manual switching function delay in the destruct signal for manned flights for crew escape.
Destruct Firing	Last logic control for destruct channels; for actuation, the following will be required: 1. ISDS power applied. 2. Destruct fire command "Disable" removed. 3. Output signal received from timer module.

347

CABLES

DESTRUCT SYSTEM
SHAPED CHARGE

SRM CASE WALL
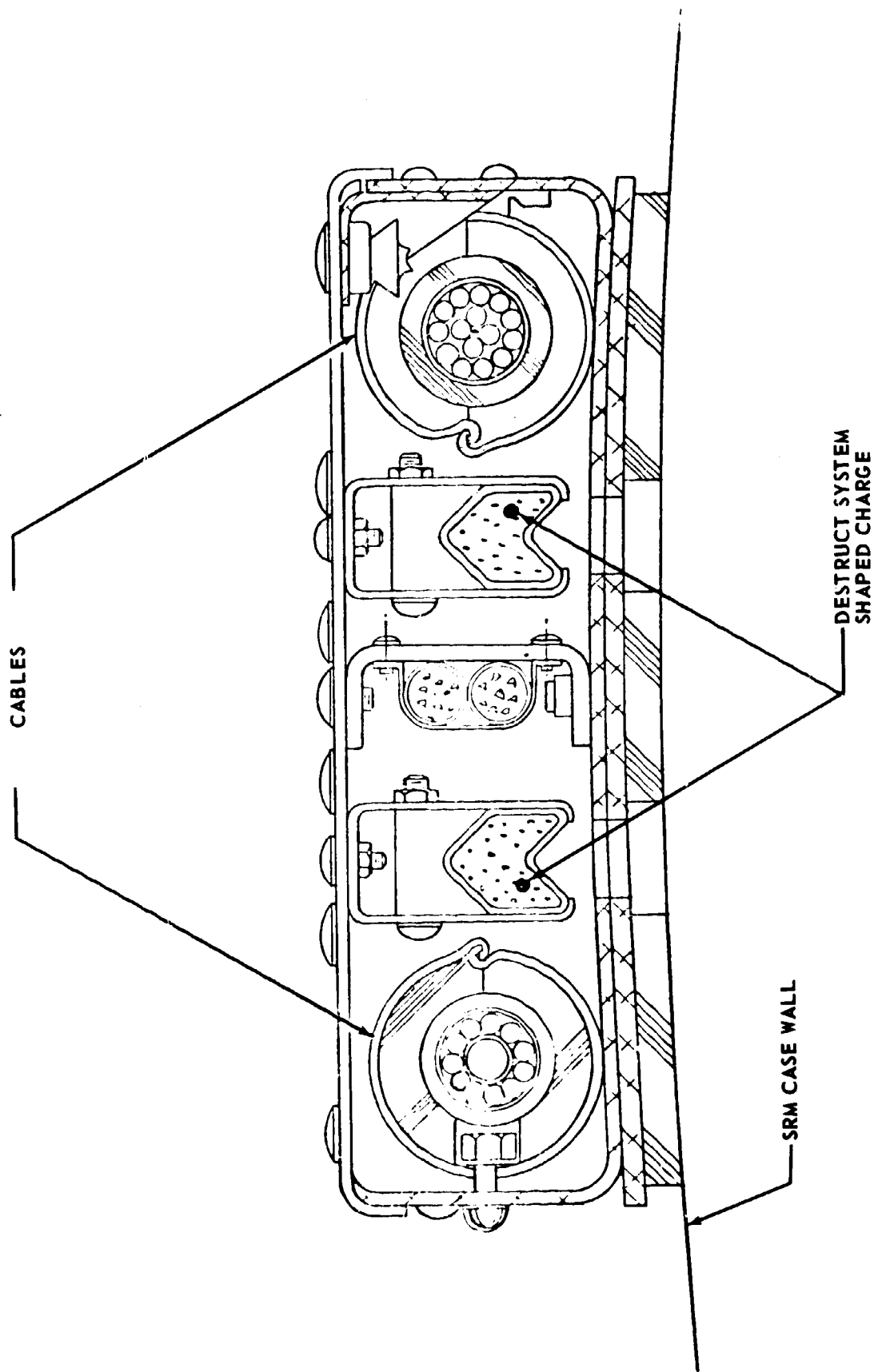
FIGURE 4.3.5.3-8   DESTRUCT SYSTEM INSTALLATION

4.3.5.3   (Continued)

Voltage Regulator

Will provide pre-launch checkout function to maintain the required regulation of raw power for stray voltage detector module.

Stray Voltage Detector

Will provide a monitor function during pre-launch checkout to detect and indicate hazardous voltage in circuit prior to making connections to electric pyrotechnic initiators.

Battery

Will provide required power for ISDS.

A schematic diagram of the ISDS electronic logic is presented in Figure 4.3.5.3-9.

The ISDS destruct actuation signal will be transmitted from detonators contained in a safety-and-arming device, through confined detonating fuse, and into a junction block at the head-end of the CDS linear-shaped charge.

The ISDS will be armed prior to flight by applying 28 volts d.c. to the "Enable" input of the Enable/Disable and Separation Detector Modules. Prior to arming and throughout normal flight, 28 volts d.c. will be applied to the separation detector module input from the core vehicle power system. Should premature SRM separation occur before normal staging, the 28-volt input to the separation detector will be lost and a signal will be applied to the destruct firing command module, resulting in a SRM destruct command. In normal flight, the issuance of a destruct command at staging will be prevented by applying 28 volts to the "disable" input of the Enable/Disable Module and by returning both the CDS and ISDS safety-and-arming devices to the "safe" condition.

4.3.5.4   Associated Strap-On Stage Hardware Elements

This section defines the major hardware elements, other than the 260-inch solid propellant rocket motor, required to complete the strap-on stage. These components include a nose cone, a forward attachment structure, an aft attachment structure, and aft support fittings.

a.   Nose Cone - The nose cone assembly is shown in Figure 4.3.5.4-1. The nose cone assembly will provide an aerodynamic fairing for the strap-on stage and a mounting structure for the staging motors, instrumentation components, electrical and ordnance cabling, and core umbilical connections.

The assembly will basically consist of a semimonocoque shell of aluminum skins stiffened with aluminum longerons and rings fastened with bolts and rivets. The nose cone assembly will have a 40 degree included angle. The staging rocket

349

NOTE:

ISDS = INADVERTENT SEPARATION DESTRUCT SYSTEM

DFC = DETONATING FUSE – CONFINED

SVD = STRAY VOLTAGE DETECTOR
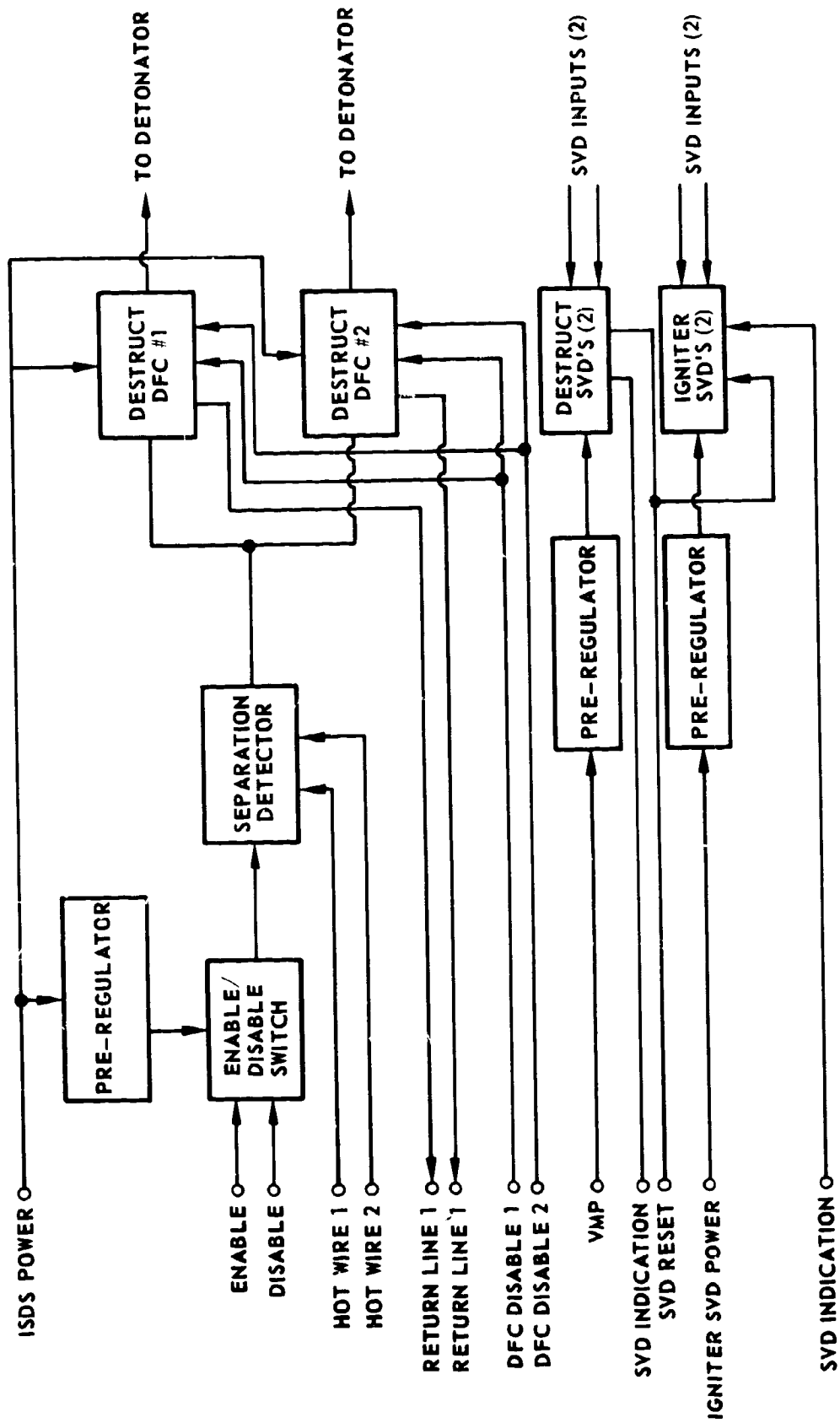
FIGURE 4.3.5.3-9   SCHEMATIC OF ISDS ELECTRONIC LOGIC FUNCTION

STAGING ROCKETS (2)
(2 PLACES)

NOSE FAIRING ASSEMBLY

NOSE SECTION ASSEMBLY

STAGING ROCKET FAIRING
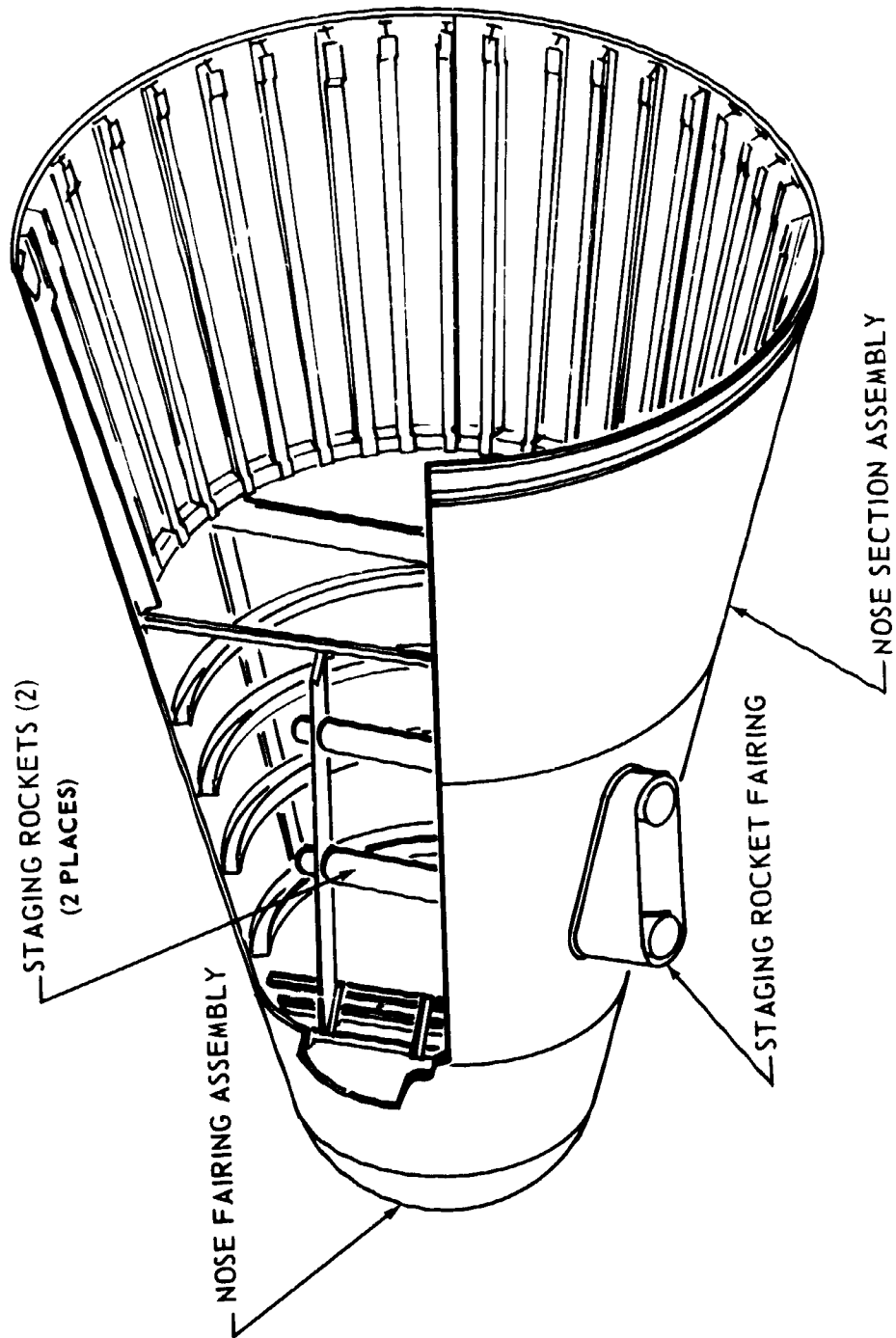
2,680 LBS. – NOSE CONE STRUCTURAL WEIGHT
2,380 LBS. – STAGING ROCKET (4) WEIGHT
5,060 LBS. TOTAL

FIGURE 4.3.5.4-1   SRM NOSE SECTION ASSEMBLY

4.3.5.4   (Continued)

nozzles will extend through the shell and will be protected from aerodynamic loads by fairings riveted in place. The nose section will be attached to the forward SRM attach structure by removable shear bolts.

b. Attachment Structures - The solid motors will be attached to the core vehicle by a forward and aft attachment structure. The forward attachment plane will be located at Station 1630 and the aft attachment plane will be located at Station 355.

The attachment structure is designed so that the aft attachment structure will react lateral and torsional loads, and the forward attachment will react longitudinal and lateral loads.

1. Aft Attachment Structure - The aft attachment structure for each solid motor will consist of an aft skin-frame-stiffener SRM skirt with fittings, and two support struts as shown in Figure 4.3.5.4-2. The skirt will be a one-piece weldment of formed sections, external stiffeners, and rolled plate. The design takes advantage of the high yield strength properties and good producibility characteristics of the HY-140 steel. The attachment fitting will be attached to the solid motor at the motor's aft skirt by a row of pins. The attachment fitting will mate to the core vehicle with a solid motor side fitting containing a spherical bearing. This SRM fitting will mate with a die forged longitudinal slip joint fitting on the core vehicle. This core fitting will be located at Station 355 at the thrust frame lower bulkhead. Aft attachment details are shown in the previous Figure 4.3.3.1-5.

The two tubular struts will react torsional loads. These struts will be pinned at both the SRM attachment point and the core attachment point with spherical bearing attachments. The attachment at the core side will mate with a die forged 7075-T6AL die forged fitting.

2. Forward Attachment Structure - The forward attachment structure will be attached to the solid motor skirt at Station 1460 and extend to Station 1660 where it will attach to the SRM nose cone. The structure will be a skin-frame-stiffener welded cylinder fabricated from HY-140 steel with a thrust post for transmittal of the solid motor thrust into the main stage as shown in Figure 4.3.5.4-3. The thrust will be reacted at Station 1630 through a bushing mounted on the SRM attachment structure to a mating bushing mounted on the main stage. The bushing will be press fit into a spherical bearing fitting. The thrust will be transmitted from the attachment fitting into the main stage thrust post. The previous Figures 4.3.3.1-4 and 4.3.3.1-5 illustrate the forward attachment concept.

INTERMEDIATE RINGS
OF STRETCHED-FORMED AND
MECHANICALLY FASTENED
I BEAM QUADRANTS STRAIGHT
SECTION ACROSS FLAT

CONICAL SKIN RING
COMPOSED OF ROLLED
AND WELDED SKIN PANELS.
RIB STIFFENERS ARE WELDED
TO CYLINDER AFTER
FORWARD AND BASE RINGS
ARE WELDED AND INTERMEDIATE
RINGS ARE ATTACHED.

AFT ATTACHMENT STRUCTURE
DIMENSIONS

DIAMETER – 260 INCHES
HEIGHT – 60 INCHES
WEIGHT – 9050 LBS

FORWARD INTERFACE RING
A CYLINDRICALLY ROLLED
AND WELDED I-BEAM WITH
ONE ELONGATED ATTACH
FLANGE

ATTACH RING SIMILAR
TO BUT LARGER THAN
INTERMEDIATE RINGS

VEHICLE
SUPPORT POSTS–
WELDMENTS OF
TWO FORGINGS
EACH (3 REQ'D)

SUPPORT STRUT
ATTACH LUGS
(3 PLACES EQUIDISTANCE)

STABILIZATION
SUPPORT
STRUTS
OF TITANIUM

3 STAGING
ROCKETS
(CANTED)

SRM SIDE
LOAD FITTING

BASE RING
BUTT WELDED
TO AFT FLARE
SIMILAR TO
INTERMEDIATE
RINGS

FIGURE 4.3.5.4.2 SOLID MOTOR AFT ATTACHMENT STRUCTURE

353

INTERMEDIATE RINGS
OF ROLLED AND
MECHANICALLY FASTENED
I-BEAM QUADRANTS

FORWARD SKIN RING
COMPOSED OF 14 ROLLED
AND WELDED SKIN PANELS.
LONGITUDINAL STIFFENERS
ARE WELDED TO RING AFTER
FORWARD AND AFT THRUST
RINGS ARE WELDED AND
INTERMEDIATE RINGS ARE
ATTACHED

FORWARD ATTACHMENT STRUCTURE
DIMENSIONS

DIAMETER — 260 INCHES
HEIGHT — 200 INCHES
WEIGHT — 30,165 LBS

AFT SKIN
RING

AFT THRUST RING
SIMILAR TO FORWARD
THRUST RING

FORWARD THRUST RING
CONSISTS OF FOUR
QUADRANTS BUILT UP
FROM TEE SECTION
CHORDS AND Z SECTION
STIFFENED WEBS
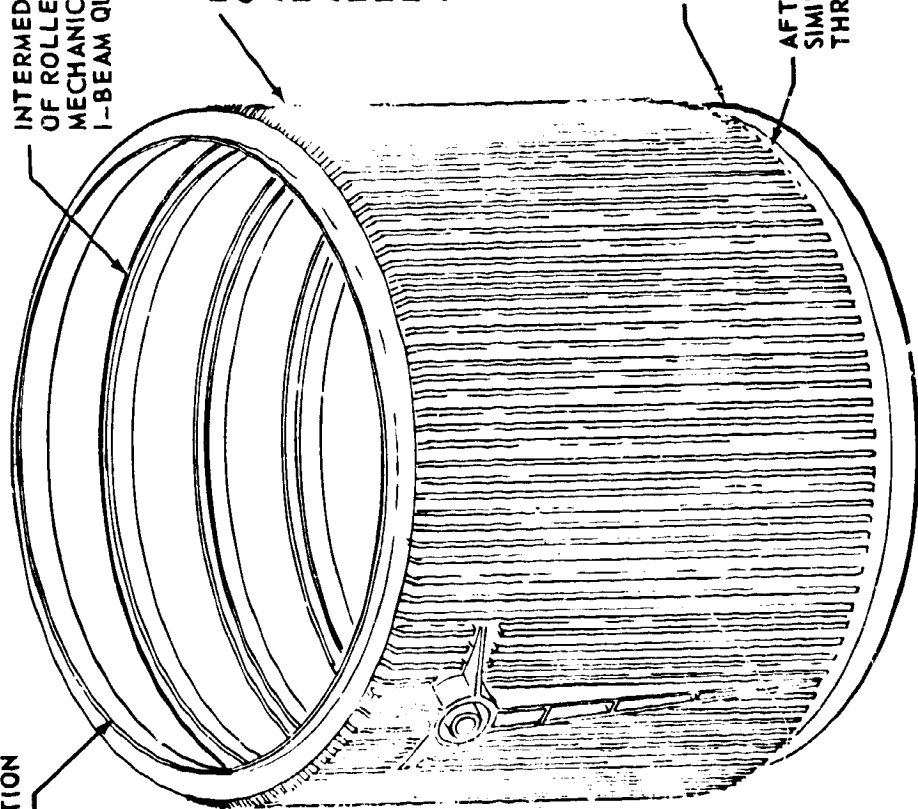
FIGURE 4.3.5.4-3   SRM FORWARD ATTACHMENT STRUCTURE

354

4.3.5.4 (Continued)

3. Holddown and Solid Motor (SRM) Attachment - The innovation of the forward holddown and support concept was adopted to reduce ground wind, emergency rebound, and strap-on thrust reaction loads on the main stage structure. Providing holddown and support points in the forward skirt will reduce load path length for supporting the LOX tank and will reduce vehicle loads due to ground winds as compared to a base supported, free-standing stage design. Impact of strap-on motors on the main stage will be minimized by reacting strap-on thrust into the main stage forward skirt which will reduce axial compressive loads in the main stage, rather than imposing increased loads by use of an aft attachment.

Large shear post forgings will be bolted into both the SRM forward attachment structure and the main stage forward skirt to take the holddown and strap-on thrust loads.

A 230 ksi heat treated 4340 hollow steel pin in the main stage shear post will react the SRM thrust load at the skin line so that bending is not introduced into the main stage forward skirt. Backup fittings will locally strengthen the deep ring in the main stage forward skirt for the radial thrust component. (See Figure 4.3.3.1-4.)

The spherical bearing fitting will allow mating freedom and relieve binding at solid motor staging. The fitting will be a press fit into the shear post. All three axis reactions will be taken by this ball joint. The other restraints will be supplied by the tubular struts (roll) and slip joint(side) at the aft end. A solid spherical bearing in the fitting will provide the necessary mating freedom.

d. Solid Motor Staging System - The staging system for each SRM stage will consist of four staging rockets located in the nose cone and three staging rockets located on the aft skirt. Separation will be achieved by activation of explosive nuts located in the forward ball joint and in both aft tubular struts. The staging rockets in the forward and aft skirt will propel the SRM stage sideways after release.

A nominal 20 inch clearance between the core vehicle and the strap-on stages will provide access for installation and inspection requirements.

The forward (nose cone) staging rockets will be mounted at approximately a 40 degree angle to a line joining the center of the core vehicle and the SRM stages. This will reduce the impact of the staging rockets exhaust products and the exhaust temperature on the core vehicle at the forward skirt/injection stage intersection. The exhaust products and temperature of the aft staging rockets will not impact the core vehicle significantly. Off-the-shelf staging rockets can be used.

355

4.3.5.5 Separation Motors

Performance data for solid rocket motors which have been qualified and have been, or currently are in production by Aerojet, were reviewed to select the rockets best suited for usage as separation rockets. Requirements specified by Boeing for the total thrust and impulse were as shown below:

Staging rockets thrust, min.	257,000 lbf
Total impulse, min.	514,000 lb-sec
Burn time (approximate)	2 Seconds

These requirements can best be met utilizing seven of the Aerojet-General Corporation Genie MD-1 motors. Figure 4.3.5.5-1 shows the basic configuration and performance data for these separation motors. Separation of the solid motor stage from the main stage is discussed in Section 4.2.6.

4.3.6 On-Board Test and Checkout System

The purpose of vehicle testing is to determine the present status of that vehicle and its subsystems, and, where possible, to predict their future integrity. Testing is generally conducted in a sequential, one-step-at-a-time fashion, verifying in order each testable parameter of vehicle performance. These parameters are simulated, measured, and compared against limits.

An on-board checkout system will be an integral part of the MLLV prime flight equipment to provide checkout capability during all the major phases of the test and service life of that prime equipment. A generalized diagram of the MLLV on-board checkout and data management system concept is present in Figure 4.3.6.0-1.

Present checkout methods for space vehicle utilize extensive ground support equipment to determine the vehicle "ready" condition, with access through numerous umbilical connections and telemetry links. The equipment used varies in type and configuration between the various test locations, making test data correlation difficult. With the advances being made in electronics functional density, size, and reduced power consumption, it is feasible to perform this testing on the MLLV configurations with a large share of the equipment located on board each stage.

With the checkout equipment on board, checkout system/stage system interconnects will be permanently established at the factory. This will minimize the chance of human error at checkout and launch sites. Confidence levels and test depths will be increased over present methods. Requirements for ground checkout complexes will be reduced and systems will be less costly and more flexible.

Igniter

A

A

AMP-3248

17.27
Dia

66.35

Insulation

Genie MD I Motor Case

15.00
Dia

A-A
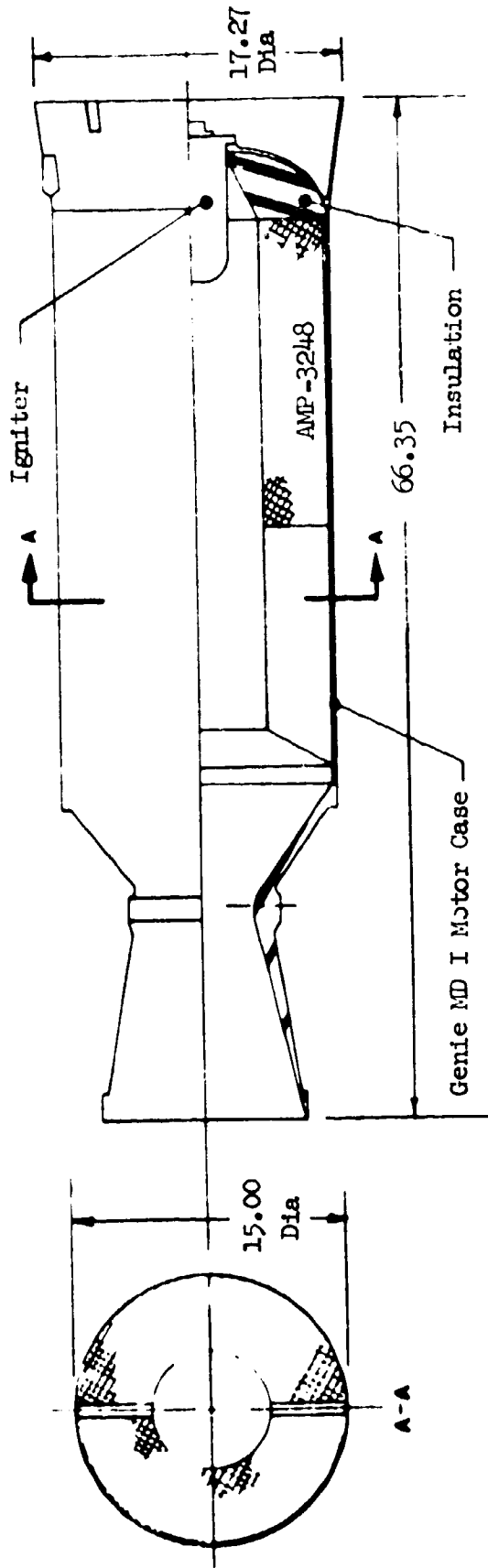
Performance Summary

Firing Duration , Seconds	2.0
Total Impulse , lb/sec	82,000
Average Thrust , lb	41,000
Ave. Chamber pressure, psi	1500

I_{sp}	244.0
Burning Rate In/sec	2.20
Burning Rate Exponent	.47
Density lb/cu. in.	.066
Propellant weight, lb	304

FIGURE 4.3.5.5-1 SEPARATION MOTORS

TYPICAL SUBSYSTEMS

POWER

PROPULSION

FLIGHT CONTROL

UNIQUE TEST CIRCUITRY

TRANSLATOR AND DATA RETRIEVAL

CREW CONTROL AND DISPLAY (MANNED) OR ON-BOARD COMPUTER EVALUATION (UNMANNED)

TRANSMITTER AND RECEIVER

TRANSLATOR DATA RETRIEVAL TREND ANALYSIS PREDICTION
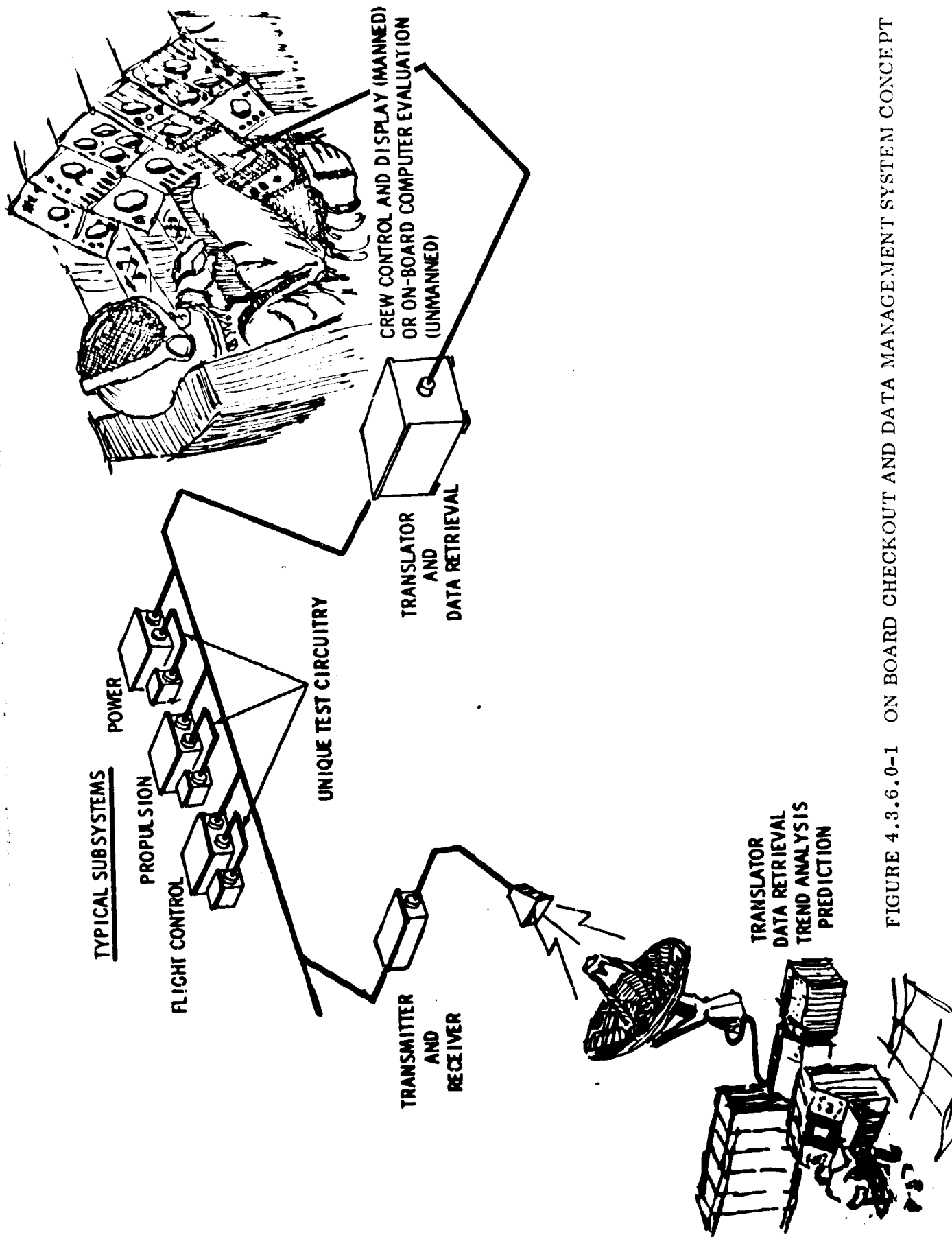
FIGURE 4.3.6.0-1   ON BOARD CHECKOUT AND DATA MANAGEMENT SYSTEM CONCEPT

4.3.6 (Continued)

The preceding discussion was primarily concerned with testing during the mission or flight phase. Testing during other phases, such as manufacturing, post-manufacturing, and pre-flight, must recognize and utilize the capability of an incorporated on-board test system. The types of testing to conducted during these phases is tabulated below:

Manufacturing

Individual Subsystem

Subsystem Post Installation

Integrated Subsystem (Composite Vehicle)

Post Manufacturing

Individual Subsystem

Propulsion System

Integrated Subsystem

Preflight

Integrated Subsystem

Simulated Flight

Examination of these various test phases reveals that as far as individual tests are concerned, there will not be a great deal of difference relative to the various test phases. The order of conduct for the test, the detail level and perhaps tolerance may, however, vary from location to location or phase to phase. Adequate flexibility in the test system, as regards test sequencing and tolerances, can readily accommodate these variations.

There were two basic systems considered for the MLLV on-board checkout, i.e., a centralized and a decentralized system.

For the centralized system, a central test set will contain switching and measurement capability, comparators, programming capability and ability to make logical decisions based upon measurement evaluation. This approach will have a minimal impact on the subsystems and will be relatively easy to test, install, and check out.

4.3.6   (Continued)

A major disadvantage to this centralized system, however, is that test and checkout capability will not exist until the vehicle (or stage) assembly is complete. In-process subsystem tests will require different test gear and procedures to accomplish those tests that will ultimately be accomplished by the on-board system. This disadvantage can be overcome in either of two ways:

a.   A test and checkout system (which duplicates the on-board system) at each of several test stations.

b.   Use of a decentralized system approach.

Another major disadvantage for this system is the large amount of wiring that will be required. Each sensor, which must be continuously monitored, must have a minimum of two wires connecting it with the central test set. Use of decentralized multiplexers and power sources for other than continuous monitoring will reduce the amount of wiring. Use of a totally decentralized approach, however, will even further reduce the wiring requirements.

For the decentralized system approach, each functional vehicle subsystem will have a local self-evaluating capability through designed-in features and/or adjacent test sets. The test functions will be supervised by a centrally located controller that can initiate the evaluation and collect the generated data for distribution to ground stations and to the flight crew. This type of system leads to a reduction in logistics requirements, an improvement in maintenance efforts, and a reduced error possibility between test sites in control and documentation.

The system defined for the MLLV vehicle family is the decentralized system. Each vehicle stage checkout system will be independent of other stages and will have the capability of talking to a ground-based computer by either a "hard line" or transmitting through the I.U. or spacecraft computer. (A large share of checkout equipment will be on board, but still a limited amount of ground support equipment will need to be used.)

4.3.6.1   General Test System Requirements

The following requirements for the MLLV on board test and checkout system were established:

a.   The test set will be capable of operating under local control or in conjunction with an external computer, with the computer being any distance from the test set.

4.3.6.1 (Continued)

b. The test set will be capable of operating in automatic, or full manual modes.

c. Stimuli will not be included in the test set. However, provisions for programming and routing of stimuli would be included.

d. Maximum utilization will be made of self check features that provide test system confidence.

e. The system will incorporate capability for vehicle malfunction detection, and programming for automatic repair of within system malfunctions.

f. Design will be such that loss of the flight computer will not cause loss of critical malfunction monitoring capability.

g. The programming for the control computer will permit the operator to communicate with the test set in normal engineering English, with the computer acting as translator.

h. The translator will be such that the operator need have no detailed knowledge of the test set or programming language.

4.3.6.2 System Description

Figure 4.3.6.2-1 shows the system block diagram for the decentralized system of the MLLV vehicle family. The selector, sequence and command set will:

a. Accept data instructions, either from the MLLV on board computer or directly from the ground computer, for transfer to the applicable test set.

b. Transfer results from the test set to the computer.

Control of the test set will be based on a universal memory concept, that is, all equipment to be controlled will have a small memory associated with it. Instructions will be routed to, and stored in these memories, for decoding upon an execute command. This concept will provide for unlimited expansion for stimuli or switching matrices.

Measurement and evaluation of test results will be performed in digital format to benefit from the higher occurrances attainable. Analysis will be converted to frequency by a highly stable voltage to frequency converter.

The data link, between the test set and the computer, will be two-way. Instructions can be transferred to the test set while responses are transferred to the computer.
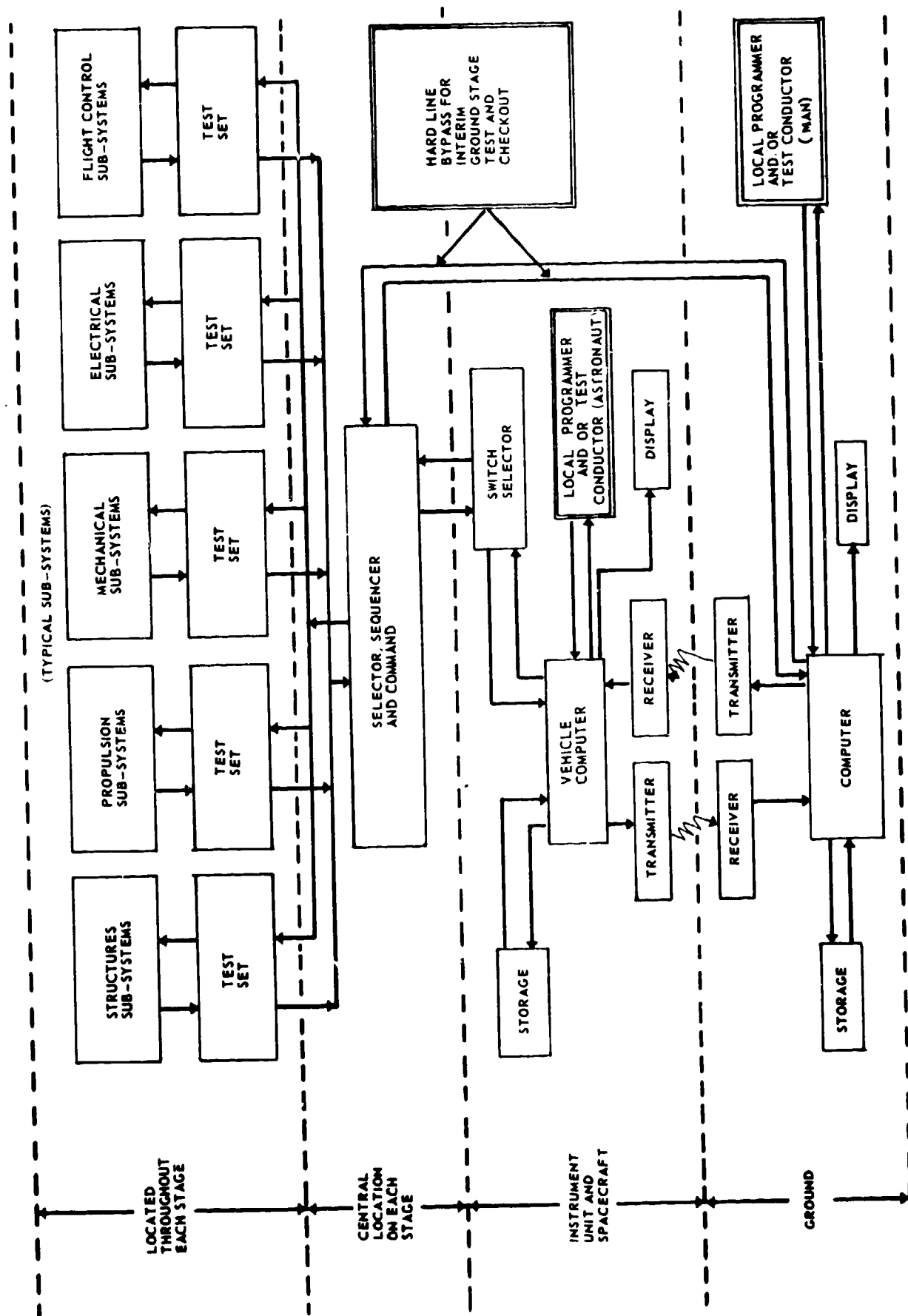
FIGURE 4.3.6.2-1 SYSTEM BLOCK DIAGRAM

4.3.6.2   (Continued)

The data link will report status of message processing at the computer complex also. The purpose of the data link will be to provide the means of achieving remote control of the test set. The data link will have the added function of providing verification and status indications of significant events.

In order to obtain the flexibility and versatility necessary for real time operation, the test set will operate in any one of three principal modes; automatic, single step, and new test. In addition, a self-check mode will be provided to verify the functional integrity of the test set, and a repetitive single step mode for continuous evaluation of a selected test measurement.

In each of the modes, the computer will serve as a translator between the test set and the test conductor.

Table 4.3.6.2-I describes the system in each of its three principal modes, identifying the roles of the test conductor and the test set. (Recognize the continuing role of the computer as the language translator between these two system elements.)

TABLE 4.3.6.2-I OPERATIONAL MODES

Test Conductor	Test Set
Automatic Mode	
Will request a block of tests for a particular system.	Will provide detailed programming (including fault isolation) for all test steps within the requested block. Will implement the testing and proceeds to the end of the block or until a sequence hold is obtained.
Single-Step Mode	
Will request conduct of a single-test measurement within a system.	Will provide programming necessary to establish the proper conditions for obtaining the requested measurement, will make and present the value of the measurement.
New Test Mode	
Will request tests to be conducted by providing detailed setup and measurement instructions to the test set.	Will present available test set capability options, will perform each requested step and report back status of setup and measured results.

363

4.3.6.2 (Continued)

The primary mode of operation for the system will be the automatic mode. Use of this mode will relieve the computer memory of the thousands of detailed instructions that can be predetermined by the design specialists and test system engineers, and will permit the computer to perform time sharing functions, data reduction, and data formating for display.

The test will be developed to conform to the building block principal. Functional elements may be added or deleted to an individual test set to accommodate a specific application.

The functional building blocks to be used in the development model will include signal conditioners, evaluators, switching matrices, memories, logic control and response elements.

Operation of the test set will be initiated by a twenty-four bit command word from the computer. This command word will be decoded by the test set. Based upon the decoded word, the test set will either switch its main gate to its local programmer (for the automatic and the single-step mode) or will keep its main gate latched awaiting further instructions from the computer (new test mode).

Functionally, the test set will be divided into two sections: the control section and the response section. The control section will perform the programming and test sequencing functions while the response section will include the measuring and evaluation functions.

The prime function of the control section will be to route and verify the data flow into the control, or universal, memories. These memories will be on etched cards. The source of data, computer or local programmer, to be loaded in each universal memory will be determined by a special word from the computer, which will establish the control mode. Each of the words will be checked for parity and loaded into the memory with the corresponding address. At this point, the memory data will be checked for agreement with the input data.

The response section will be a flexible digital voltmeter and digital frequency meter. Arithmetic capability will be limited to summing. Ratio analog measurement can be stored for future use in comparison of time variant signals.

The performance specifications for the control and response section of the test set are shown in Table 4.3.6.2-II.

Each memory will consist of a single etched card which is addressable by the test set but which may be physically located external to the test set with its associated stimulus equipment or other building blocks. When the necessary memories have been

364

TABLE 4.3.6.2-II ON BOARD TEST SET SPECIFICATIONS

PARAMETER	SPECIFICATION
Input Word Rate, Computer to Test Set	75KC maximum
Input Bit Rate, Test Set to Universal Memory	1.2 megabits/second
Memory Cycle Time	13 microseconds
Number Base	Binary
Word Length	24 bits
Checking	24 bits parity, 16 bits equality
Output	Test result or test number Go, No-Go High Limit, No-Go Low Limit Polarity Test Set Address Parity
Evaluation Modes	Frequency AC-DC Peak or Average Voltage Time Interval Period Count (EPUT) Ratio Difference Sum

Accuracies		
Frequency	$<$10KC	1 cps
	$>$10KC	$\pm$ 0.01%
Voltage	DC	$\pm$ 0.1%
	AC	$\pm$ 0.5% 20 cps - 100KC $\pm$ 1.0% 10 cps - 200KC
Period	100 sec.	$\pm$ 1 count
Input Impedance	$>$0.1V - 100Kohm $<$1 megohm	

365

4.3.6.2 (Continued)

loaded and the loaded words checked for agreement with the command words. the execute bit of the last command word will instruct the response section of the test set that a measurement is to begin. This will cause the memories to begin an evaluation delay, switch stimulus and respond matrices, program the stimulus generator, set up the signal conditions and program the counters and tolerance comparator. The measurement itself will take place after the programmed evaluation delay.

The measured value will then compare to programmed limits, and the result used to initiate the next test step, to drop into a fault isolation sub-routine, to reevaluate, or simply to notify the computer of the measured value, depending upon the selected operating mode and the test results.

The test set, then, will be able to perform the necessary functions of programming. test point connection, stimuli activation, measurement and reporting. These functions will be placed into a small, light weight packages that can be placed throughout the MLLV vehicle stages and spacecraft or payload. These test sets will be under the general supervisory control of the computer.

The minor weight penalty incurred by installation of the test sets onto the MLLV vehicle will be partially offset by a reduction in many of the umbilical connectors which fly with current vehicles.

Test sets in accordance with the broad requirements discussed above have been developed. The developed hardware can be "tailored" to the MLLV vehicle or spacecraft. Figure 4.3.6.2-2 is a cut-away view of such a test set. It utilizes solid state input switching and contains 1,000 microcircuit networks. It is 676 cubic inches in volume, weighs 25 pounds, and draws 50 watts of power. The microcircuits in the test set are mounted on six-layer, clearance hole type, etched circuit boards. Each of the 35, 2.25 by 4.85 inch boards in the set can mount up to 48 microcircuit devices - 24 on each side in a three by eight arrangement. Two of the six layers of each board will be used for power distribution and for heat transfer. Simple conductive cooling to a standard thermal panel will provide adequate environmental control for the test set.

A test language for the control of the space packaged automatic checkout system has been developed. The checkout equipment can be connected to an IBM 7044 computer, which will serve as a language translator between the test equipment and the human operator. The language translator will guide the test operator by asking questions, by listing all available alternatives for selection by the operator, or by requesting numerical information. All communications are in English and are structured in normal sentences with a minimum of coding. Figure 4.3.6.2-3 shows a typical exchange with the computer; entries proceeded by the time (hours/minutes/seconds) and the operator response preceeded by (H).

366

SPACE PACKAGED AUTOMATIC CHECKOUT EQUIPMENT
THAT PROVIDES VEHICLE TEST DATA DURING THE
MISSION AS WELL AS DURING PRE-LAUNCH

- 1000 BTL MICROCIRCUIT NETWORKS
- 676 CUBIC IN., 25 POUNDS, 50 W POWER

SOLID STATE INPUT SWITCHING
- 0.1% MEASUREMENT ACCURACY

FIGURE 4.3.6.2-2   ON BOARD TEST AND CHECKOUT SET

FIGURE 4.3.6.2-3 TYPICAL COMPUTER PRINT-OUT

14/44/03 FOR A DESCRIPTION OF THE TEST SET TYPE THE NUMBER 1
14/44/08 FOR A GLOSSARY OF TERMS TYPE THE NUMBER 2
14/44/12 FOR A DEMONSTRATION OF THE TEST SET TYPE THE NUMBER 3
14/44/17 FOR THE AUTOMATIC MODE TYPE THE NUMBER 4
14/44/22 FOR THE SINGLE STEP MODE TYPE THE NUMBER 5
14/44/26 FOR THE REPETITIVE SINGLE STEP MODE TYPE THE NUMBER 6
14/44/31 FOR THE NEW TEST MODE TYPE THE NUMBER 7
14/44/35 FOR THE SELF TEST MODE TYPE THE NUMBER 8

M,7
14/45/55 SELECT THE DESIRED MEASUREMENT MODE
14/45/59 FOR DC VOLTAGE TYPE THE NUMBER 1
14/46/02 FOR AC VOLTAGE TYPE THE NUMBER 2
14/46/06 FOR EPUT TYPE THE NUMBER 3
14/46/09 FOR TIME TYPE THE NUMBER 4
14/46/12 FOR COUNT TYPE THE NUMBER 5
14/46/15 FOR INTEGRAL TYPE THE NUMBER 6
14/46/18 FOR AVERAGE TYPE THE NUMBER 7
14/46/21 FOR SYNCHRONIZED SAMPLE TYPE THE NUMBER 8
14/46/25 FOR PEAK TYPE THE NUMBER 9

M,6
14/49/51 SELECT THE POLARITY OF THE HALF CYCLE TO BE INTEGRATED
14/49/56 FOR THE POSITIVE HALF CYCLE TYPE THE NUMBER 1
14/50/01 FOR THE NEGATIVE HALF CYCLE TYPE THE NUMBER 2

M,2
14/50/08 SELECT THE VOLTAGE RANGE WHICH THE MAXIMUM SIGNAL VOLTAGE WILL NOT
          EXCEED
14/50/14 FOR A MAXIMUM OF 0.1 VOLTS TYPE THE NUMBER 1
14/50/16 FOR A MAXIMUM OF 1.0 VOLTS TYPE THE NUMBER 2
14/50/21 FOR A MAXIMUM OF 10 VOLTS TYPE THE NUMBER 3
14/50/26 FOR A MAXIMUM OF 100 VOLTS TYPE THE NUMBER 4
14/50/30 FOR A MAXIMUM OF 300 VOLTS TYPE THE NUMBER 5
14/50/35

M,3
14/50/49 SELECT THE TIME RANGE WITHIN WHICH THE PERIOD OF THE HALF CYCLE
          TO BE MEASURED WILL FALL
14/50/55 FOR A MAXIMUM PERIOD OF 0.1 SECONDS TYPE THE NUMBER 1
14/50/59 FOR A MAXIMUM PERIOD OF 1 SECONDS TYPE THE NUMBER 2
14/51/07 FOR A MAXIMUM PERIOD OF 10 SECONDS TYPE THE NUMBER 3
14/51/14 FOR A MAXIMUM PERIOD OF 100 SECONDS TYPE THE NUMBER 4
14/51/19 FOR A MAXIMUM PERIOD OF 1000 SECONDS TYPE THE NUMBER 5

M,2
14/51/37 TYPE THE VALUE OF THE MORE POSITIVE LIMIT FOR THIS TEST.
14/51/43 IF THE VALUE IS TO BE NEGATIVE, PRECEDE IT WITH A .

M,5.14
14/52/17 TYPE THE VALUE OF THE MORE NEGATIVE LIMIT FOR THIS TEST.
14/52/23 IF THE VALUE IS TO BE NEGATIVE, PRECEDE IT WITH A .

M,3.14
14/52/38 TYPE THE VALUE OF THE DESIRED EVALUATION DELAY, ENTER THE VALUE
14/52/50 TO THE NEAREST 0.1 SECOND OR TO THE NEAREST 0.1 MILLISECOND
14/52/57 IF THE VALUE IS TO BE IN MILLISECONDS PRECEDE THE VALUE WITH THE
          LETTER M .

M,NO
14/53/07 REVIEW OF TEST SET INPUTS
14/53/10 INTEGRAL MODE
14/53/12 INPUT TEST POINT SELECTION   4
14/53/15 UPPER LIMIT   6.4   VOLT-SECONDS
14/53/20 LOWER LIMIT   3.14   VOLT-SECONDS
14/53/26 EVALUATION DELAY   1.0   SECONDS
14/53/31 INPUT TRIGGER SLOPE   TRIGGER SLOPE NEGATIVE
14/53/36 TEST SET RANGE   100.0 VOLTS
14/53/40 FIXED WIRE SWITCHES 5.
14/53/44 STIMULUS SOURCE   NO STIMULUS SELECTED
14/53/48 STIMULUS APPLICATION POINT   NO APPLICATION POINT REQUESTED
14/53/54 DO YOU WISH TO ALTER ANY OF THE SETTINGS

M,NO
14/54/53 THE MEASURED RESULT IS   -5.999 VOLT-SECONDS
14/54/57 THE VALUE IS MORE NEGATIVE THAN THE LOW LIMIT
14/55/02 DO YOU WISH TO MODIFY ANY PARAMETER OF THE TEST JUST COMPLETED

15/11/07 FOR A DESCRIPTION OF THE TEST SET TYPE THE NUMBER 1
15/11/52 FOR A GLOSSARY OF TERMS TYPE THE NUMBER 2
15/11/27 FOR A DEMONSTRATION OF THE TEST SET TYPE THE NUMBER 3
15/12/02 FOR THE AUTOMATIC MODE TYPE THE NUMBER 4
15/12/06 FOR THE SINGLE STEP MODE TYPE THE NUMBER 5
15/12/10 FOR THE REPETITIVE SINGLE STEP MODE TYPE THE NUMBER 6
15/12/16 FOR THE NEW TEST MODE TYPE THE NUMBER 7
15/12/20 FOR THE SELF TEST MODE TYPE THE NUMBER 8

M,9
15/12/54 TYPE THE NUMBER OF THE FIRST TEST STEP IN THE DESIRED SEQUENCE.
7.25
15/14/50 A TEST SET HOLD HAS OCCURED ON STEP NUMBER   0025
15/15/06 THE MEASURED RESULT OF THIS STEP IS   0.004441 VOLT-SECONDS
15/15/11 THIS RESULT IS MORE POSITIVE THAN THE HIGH LIMIT
          IS IT DESIRED THAT TESTING IN THIS SEQUENCE CONTINUE
M,YES
15/17/19 THE REQUESTED TEST SEQUENCE HAS BEEN COMPLETED.
15/17/23 THERE WERE HOLDS ON THE FOLLOWING TEST STEPS
15/17/25   0025
15/17/35 DO YOU WISH TO SELECT ANOTHER SEQUENCE
M,NO

15/17/34 TO TERMINATE THE DEMONSTRATION TYPE THE NUMBER 0
15/17/38 FOR A DESCRIPTION OF THE TEST SET TYPE THE NUMBER 1
15/17/42 FOR A GLOSSARY OF TERMS TYPE THE NUMBER 2
15/17/52 FOR A DEMONSTRATION OF THE TEST SET TYPE THE NUMBER 3
15/17/52 FOR THE AUTOMATIC MODE TYPE THE NUMBER 4
15/18/01 FOR THE SINGLE STEP MODE TYPE THE NUMBER 5
15/18/05 FOR THE REPETITIVE SINGLE STEP MODE TYPE THE NUMBER 6
15/18/10 FOR THE NEW TEST MODE TYPE THE NUMBER 7
15/18/15 FOR THE SELF TEST MODE TYPE THE NUMBER 8

M,5
15/18/57 TYPE THE NUMBER OF THE DESIRED TEST STEP.
7.25
15/19/47 THE MEASURED RESULT OF THIS STEP IS   0.000576 VOLT-SECONDS
15/19/53 THE VALUE IS MORE POSITIVE THAN THE HIGH LIMIT.
15/19/58 IS EXECUTION OF ANOTHER TEST STEP DESIRED
M,NO

15/20/11 TO TERMINATE THE DEMONSTRATION TYPE THE NUMBER 0
15/20/16 FOR A DESCRIPTION OF THE TEST SET TYPE THE NUMBER 1
15/20/21 FOR A GLOSSARY OF TERMS TYPE THE NUMBER 2
15/21/26 FOR A DEMONSTRATION OF THE TEST SET TYPE THE NUMBER 3
15/21/30 FOR THE AUTOMATIC MODE TYPE THE NUMBER 4
15/21/36 FOR THE SINGLE STEP MODE TYPE THE NUMBER 5
15/21/43 FOR THE REPETITIVE SINGLE STEP MODE TYPE THE NUMBER 6
15/21/46 FOR THE NEW TEST MODE TYPE THE NUMBER 7
15/22/12 FOR THE SELF TEST MODE TYPE THE NUMBER 8

M,5
15/22/17 TYPE THE NUMBER OF THE DESIRED TEST STEP.

15/21/05 TO TERMINATE REPETITION OF TESTING TYPE THE WORD STOP.
15/21/21 THE MEASURED RESULT OF THIS STEP IS   0.001066 VOLT-SECONDS
15/21/23   0.001066
15/21/43   0.001066
15/21/56   0.001066
                                                0.001066

M,STOP
15/22/12 DO YOU WISH TO EXECUTE ANOTHER TEST STEP IN THIS MODE

4.3.6.2   (Continued)

The language also provides access to reference material for use by the operator during testing. These references include a description of the test system and its capabilities, a glossary of terms used in the language and a list and description of the test steps available in the test system memory. The language also provides the means of generating new test steps and procedures on-line without resorting to a computer programmer.

4.3.7   Instrument Unit Design

It was assumed that the existing Saturn V instrument unit concept could be modified for use in the MLLV family. This unit would be mounted on a larger diameter and would be less complex than that required for the Saturn V when used on a single-stage-to-orbit vehicle and slightly more complex than the Saturn V instrument unit when used on the vehicles using the strap-on stages. With the addition of recent advancements in the state-of-the-art, the weight of the instrument unit is estimated to be approximately 4200 pounds. The instrument unit has been considered a part of the payload and its weight is included in the gross payload weights shown in this document. No specific instrument unit design was undertaken for this study.

The design of the Saturn V instrument unit was used to determine the resources and costs as shown in Volumes III through V of this final report.

4.3.8   Vehicle Sensitivities

This section contains (1) an analysis of the effects of payload density on vehicle loads, stress and control requirements, (2) a comparison of the single stage to orbit vehicle with the multichamber/plug propulsion system versus the single stage to orbit vehicle with a toroidal/aerospike propulsion system and (3) a comparison of the "staged" trajectory mode on payload performance with 156 and 260 inch SRM stages.

4.3.8.1   Payload Sensitivity

The design loads analysis for the MLLV main stage showed that the "worst envelope" design loads will result from operation of either the MLLV single-stage-to-orbit vehicle or the main stage plus eight 260' SRM stages plus a three module injection stage vehicle. A major portion of the main stage compressive design envelope will result from operation of the single-stage-to-orbit vehicle. The payload sensitivity study was conducted to determine the effect of decreasing payload density on the MLLV single-stage-to-orbit vehicle only.

The effect of varying payload density on main stage structural design was determined by evaluating loads at max $(q\alpha)$ due to bending. Since bending moment loads will increase for longer payload lengths, lower payload densities will result in higher bending loads. Use of higher density payloads generally reduce structural requirements assuming similar nose cone aerodynamic characteristics. The MLLV payload density of 5.0 lbs/cu ft. however, is very near the maximum attainable density for that configuration without a change in the nose cone geometry.

4.3.8.1   (Continued)

A lower density of 2.0 lbs/cu ft. was used for the payload sensitivity study. A payload weight of 500,000 pounds was used. The vehicle length will increase 59.5 feet with the decrease in payload density.

Figure 4.3.8.1-1 shows the mass characteristics of the 2.0 lbs/cu ft payload. Figures 4.3.8.1-2 and -3 show the impact of the lower payload density on the main stage compressive and tensile load envelopes respectively. Forward skirt load envelopes for operation of the single-stage-to-orbit vehicle are also shown. The compressive load envelope for the low density payload configuration will design all structure aft of the forward skirt (Figure 4.3.8.1-2). The only portion of the tension load envelope that will changed is at the forward end of the forward skirt (Figure 4.3.8.1-3) where the low density payload vehicle loads are only slightly higher than the design values.

The loads presented in Figures 4.3.8.1-2 and -3 indicate that the LH_2 tank wall and both the aft and forward skirts will require re-evaluation for lower density payloads.
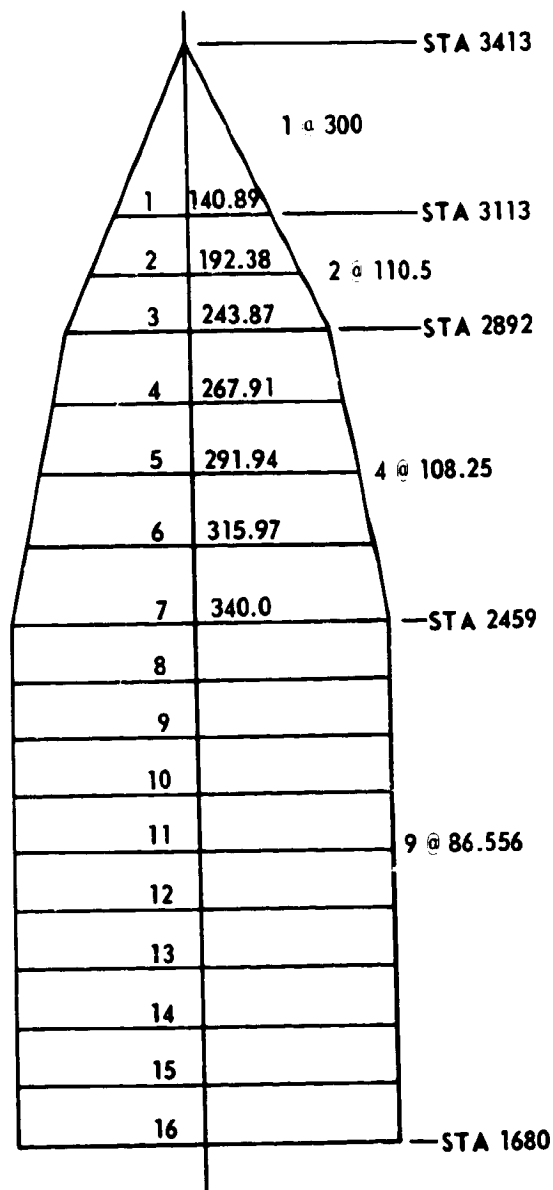
Figure 4.3.8.1-4 presents the single-stage-to-orbit vehicle control sensitivity to payload density. Higher payload densities, above five pounds per cubic foot, will result in a reduced control requirement. Higher payload densities will also provide increased times to double amplitude. For densities less than the selected design value, the required TVC deflection will increase significantly.

4.3.8.2   Comparison of Single-Stage-To-Orbit Vehicles With Multichamber/Plug Propulsion System Versus the 2000 PSIA and 1200 PSIA Toroidal/Aerospike Propulsion System

The single-stage-to-orbit vehicle configuration with the multichamber/plug propulsion system or the 1200 psia or 2000 psia toroidal/aerospike propulsion system were subjected to a comparative analysis. The differences in the propulsion system employed will impact structures, weights, control and separation, propulsion performance, pressurization, and flight performance. These areas are discussed below:

a.   Structures - A comparison of the core stage structures with either type of propulsion system indicated that all the structural components of the stage above the thrust skirt will be identical regardless of the propulsion system used. The thrust skirts will differ due to the method of reacting the engine thrust. It was assumed in the stress analysis that the toroidal/aerospike engine thrust will be uniformly distributed at the engine/skirt interface while the multichamber/plug engine thrust will consist of concentrated forces applied at 24 equally spaced points around the thrust structure periphery.

MLLV PAYLOAD WEIGHT
680 DIA.

STA 3413

1 @ 300

1	140.89

STA 3113

2	192.38

2 @ 110.5

3	243.87

STA 2892

4	267.91
5	291.94

4 @ 108.25

6	315.97
7	340.0

STA 2459

8	
9	
10	
11	

9 @ 86.556

12	
13	
14	
15	
16	

STA 1680

ITEM	CG	V_X VOLUME FT^3	V_X/V_T	WEIGHT
1	3188.0	3,446	0.0138	6,900
2	3051.1	5,620	0.0225	11,250
3	2941.9	9,599	0.0384	19,200
4	2836.2	12,889	0.0517	25,850
5	2728.1	15,422	0.0618	30,900
6	2619.9	18,182	0.0727	36,350
7	2511.8	21,169	0.0848	42,400
8	2415.7	18,182	0.0727	36,350
9	2329.2	18,182	0.0727	36,350
10	2242.6	18,182	0.0727	36,350
11	2156.1	18,182	0.0727	36,350
12	2069.5	18,182	0.0727	36,350
13	1982.9	18,182	0.0727	36,350
14	1896.4	18,182	0.0727	36,350
15	1809.8	18,182	0.0727	36,350
16	1723.3	18,182	0.0727	36,350
		250,000	1.00	500,000

DENSITY = 2.0 #/FT^3

FIGURE 4.3.8.1-1   MASS CHARACTERISTICS OF 2.0 LBS/FT^3 PAYLOAD
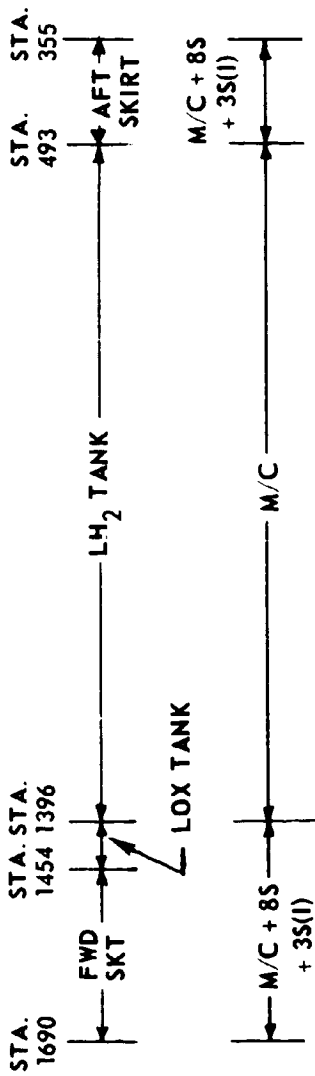
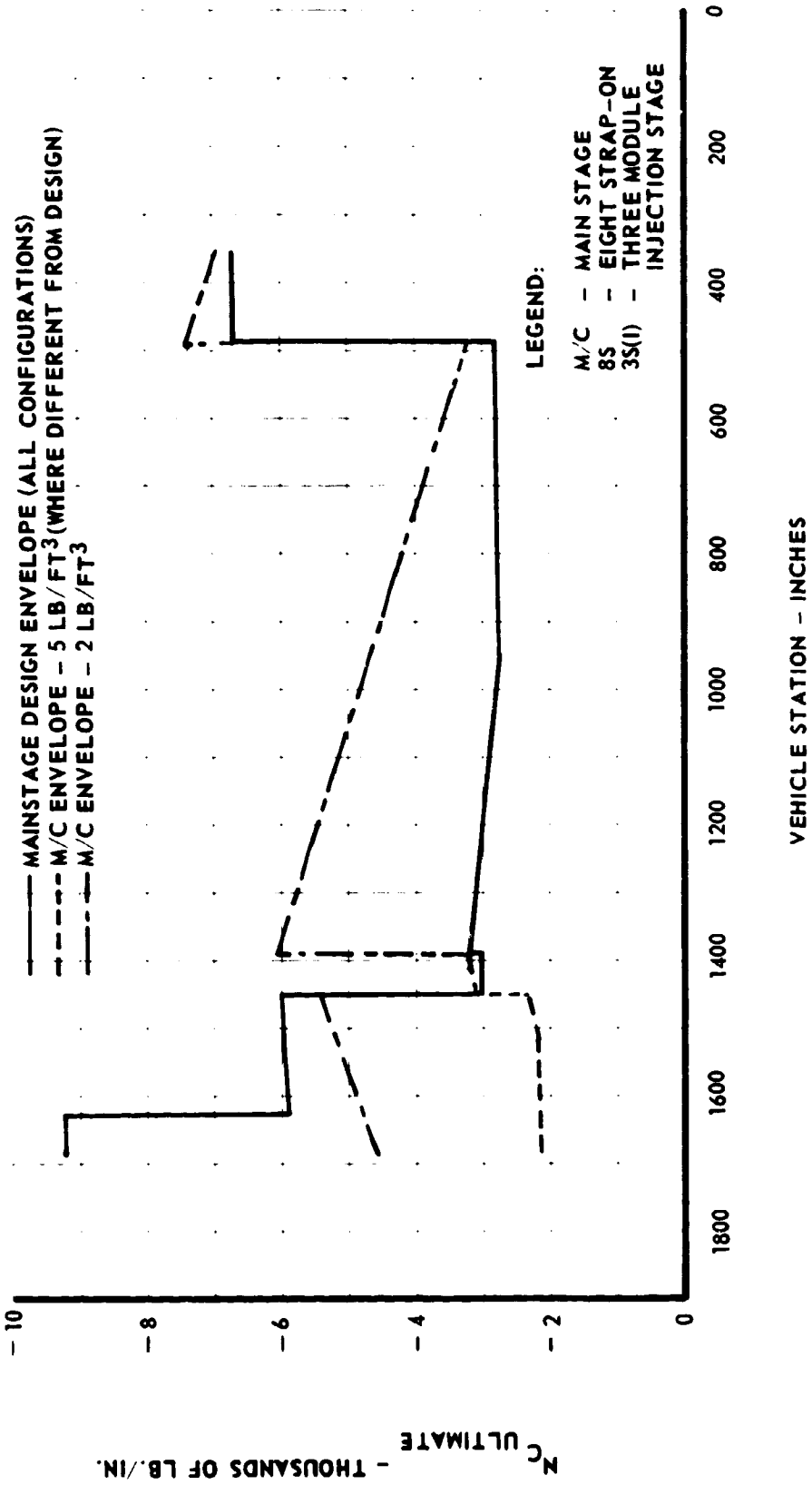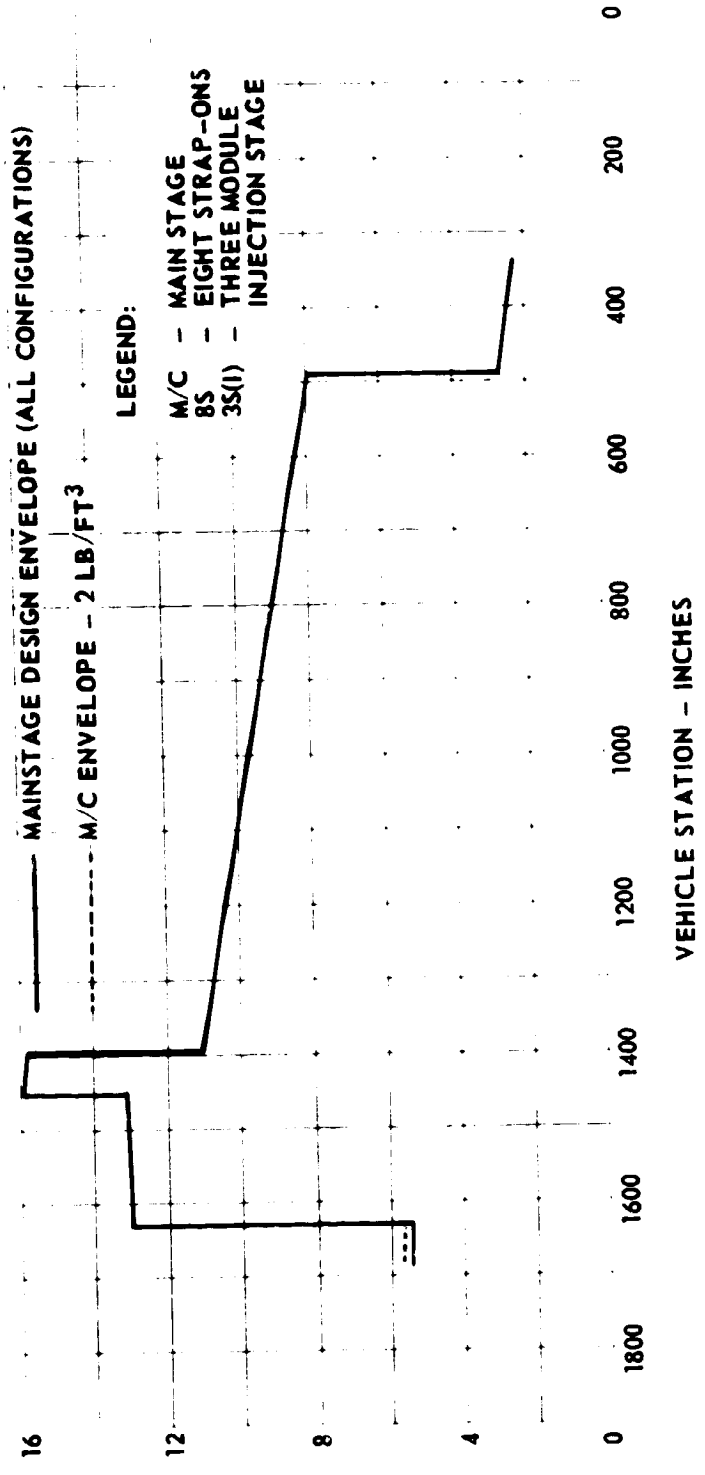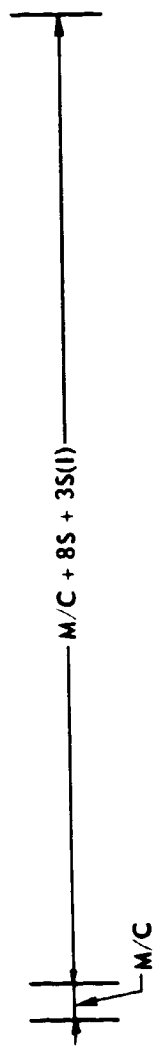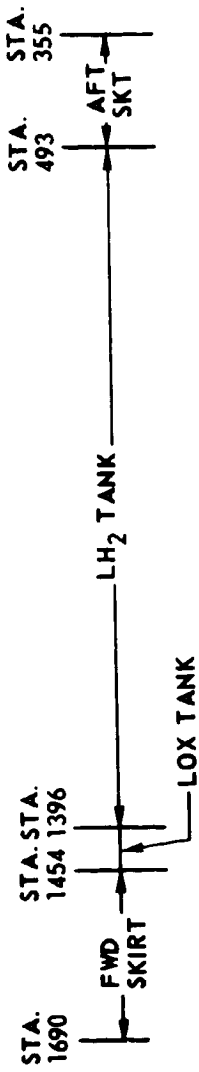FIGURE 4.3.8.1-2 ULTIMATE COMBINED COMPRESSIVE LOAD ENVELOPE – MLLV PAYLOAD SENSITIVITY CONFIGURATION – (PAYLOAD DENSITY 2.0 LB/FT^3)

FIGURE 4.3.8.1-3 ULTIMATE COMBINED TENSILE LOAD ENVELOPE – MLLV PAYLOAD SENSITIVITY CONFIGURATION – (PAYLOAD DENSITY 2.0 LB/FT³)
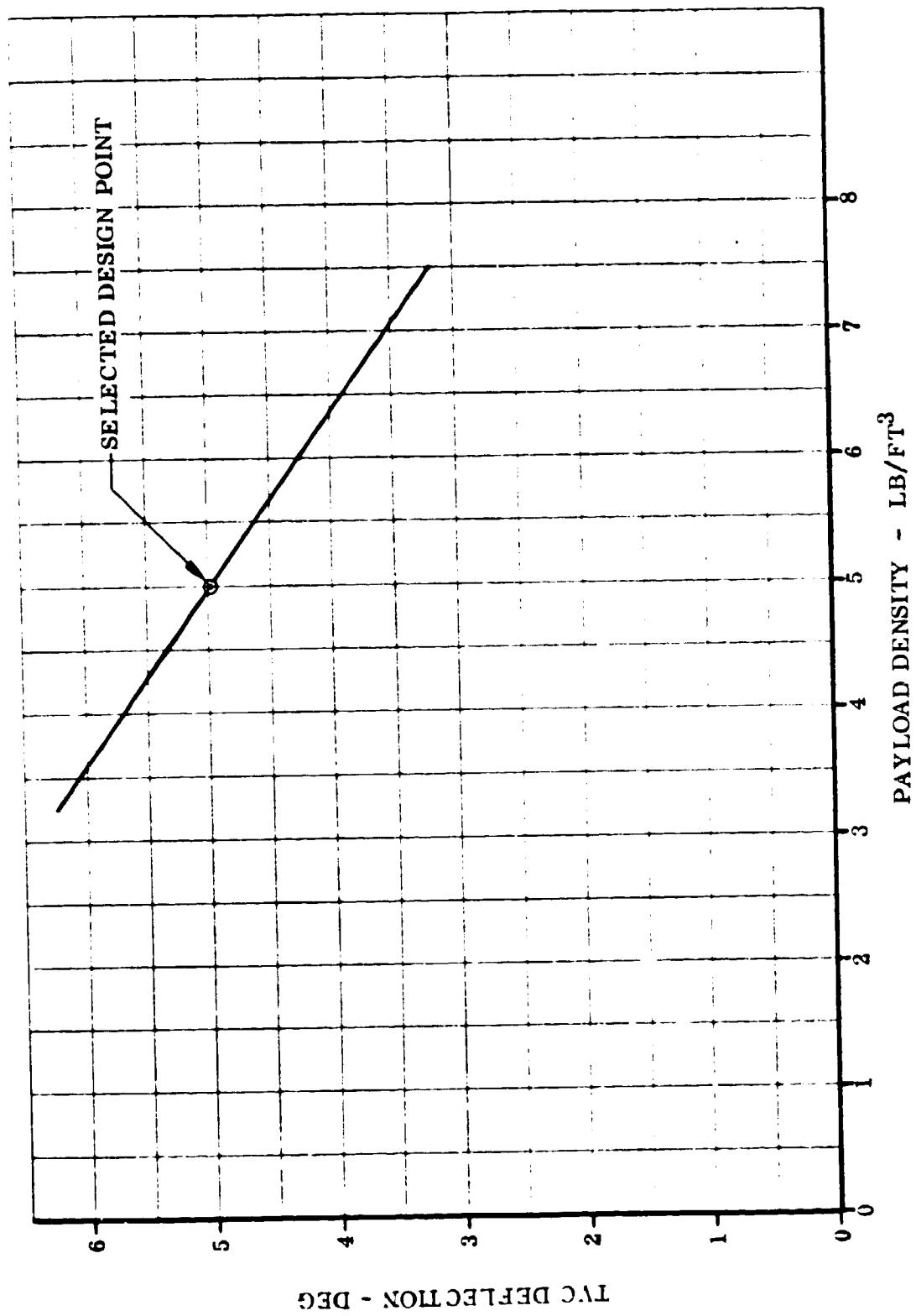
FIGURE 4.3.8.1-4   MLLV CORE TVC SENSITIVITY TO PAYLOAD DENSITY

4.3.8.2   (Continued)

The method used to design and size the multichamber/plug vehicle and the toroidal/aerospike vehicle were identical. A detail discussion of the stress analysis technique is shown in Section 4.3.3.1 and Volume VIII, Appendix B.

The toroidal/aerospike engine thrust structure was analyzed as a stiffened cylinder subjected to a uniformly distributed loading at the engine-skirt interface. The method of stability analysis was the same as that used for the multichamber/plug thrust structure. The interface between the engine and thrust structure was assumed to be a pinned connection with the rsult that no bending moment was applied to the skirt at the engine attachment.

Table 4.3.3.1-III, shown in Section 4.3.3.1, is a comparison of the MLIV aft skirt structural sizes with the toroidal/aerospike or the multichamber/ plug propulsion system.

b.   Weights - The stress analyses sized the rings, thrust posts, and the skin-stringers which comprise the aft thrust structure. The weight of the aft skirt structure for the toroidal/aerospike engine system will be 14,579 pounds and for the multichamber/plug system will be 16,768 pounds. The remainder of the main stage structure and their weights will be identical for either propulsion system.

The 2000 psia toroidal/aerospike propulsion system weights will be significantly less than those of the multichamber/plug system. The overall weight of the 2000 psia toroidal/aerospike system will be 75,050 pounds. The overall weight of the 1200 psia toroidal/aerospike will be 60,240 pounds. (Based on Rocketdyne data.)

The overall weight of the multichamber/plug system will be 116,613 pounds. The engine system weight will be 100,800 pounds for the 24 modules with the remaining weight (15,813 pounds) including the weight of the plug, plug support structure, TVC, plumbing, etc. (Based on Pratt and Whitney data.)

The combined weight of the propulsion system and aft skirt for the 2000 psia toroidal/aerospike system will be 89,629 pounds. These same structures for the 1200 psia toroidal/aerospike weigh 74,819 pounds. For the multichamber/ plug propulsion system and its aft skirt, the combined weight will be 133,381 pounds. The main stage inert weight differences are attributable to the differences in these two structures. The remainder of the main stage structure will be identical. The single-stage-to-orbit vehicle mass fraction for the multichamber/ plug propulsion system is estimated to be 0.936, the same vehicle with the 2000 psia toroidal/aerospike system is 0.943 and the same vehicle with the 1200 psia toroidal/aerospike is 0.945.

4.3.8.2 (Continued)

c. Control and Separation - The vehicle will require 3.9 degrees of thrust vector control capability for control. This capability can readily be obtained by the multichamber/plug propulsion system since the 3.9 degree requirement is less than the module design tilt angle when the module is hinged against the plug. This high TVC requirement will not impose any significant weight penalty to the multichamber/plug engine system. Roll control requirements are small and can be accomplished by deflection of the base plug bleed gases.

The toroidal/aerospike propulsion system will use fluid injection to achieve thrust vector control. As the deflection requirements increase, the injection fluid requirements increase, the injection fluid requirements increase at an increasing rate. LOX will be diverted from the engines to the fluid injection nozzles. The LOX requirements, while high during the maximum deflection (maximum dynamic pressure) regime, however, will not impose a significant weight or performance loss on the vehicle since the time for maximum deflection will be short duration and the fluid injection LOX will provide some axial impulse (though not as effectively as when used in normal engine operation). (As with the multichamber/plug, the system with the toroidal/aerospike can achieve roll control by deflection of the base bleed gases.)

Other control parameters, i.e., flight system gains and uncontrolled divergence rates will be identical regardless of the propulsion system employed.

The SRM/main stage separation requirement differs between the propulsion systems. The shape and size of main stage exhaust plume flow fields affect the separation of strap-on motors. For this reason, preliminary calculations of the extent of plume formation were made for two engine systems. These calculations are shown in the previous Section 4.2.6.1. The freeze line will be oriented at 6 degrees from the axial for the multichamber/plug propulsion system and 30 degrees from the axial for the toroidal propulsion system. The large plume of the toroidal propulsion system will require separation motors with greater impulse to prevent the solid motors from impacting the main stage exhaust plume and tumbling back into the main stage. The main stage to injection stage separation, the injection stage to payload separation and the ullage requirements are identical regardless of the propulsion system used.

d. Propulsion Performance - The propulsion performance data is strongly influenced by the differences in operating pressure. For the multichamber/plug propulsion system, a high pressure propulsion system was selected. Rocketdyne under the AMLLV Contract, (NAS2-4079) selected 2000 psi for the toroidal propulsion system. Under this MLLV contract, (NAS2-5056), Rocketdyne recommended a 1200 psia engine which can be built using existing turbopump technology. The multichamber/plug propulsion system will provide significantly higher specific

376

4.3.8.2 (Continued)

impulse than this lower pressure toroidal/aerospike propulsion system.
The latter engine system will have a significantly lower weight. These
factors will be off-setting and will result in approximately the same
payload capability for the MLLV vehicle employing either of these latter
(multichamber/plug and 1200 psia toroidal/aerospike) propulsion
systems. The 2000 psia toroidal engine system appears to offer the best
performance/weight features.

Table 4.3.8.2-I shows comparative propulsion system performance data for the
multichamber/plug and toroidal/aerospike engines. The significant data from
the table are the specific impulse and weight. The sea level specific impulse
for the Rocketdyne 2000 psi toroidal is seven seconds better than the P&W
multichamber/plug while the 1200 psi toroidal is five seconds lower than the
multichamber/plug. The toroidal propulsion will be more nearly optimized
at sea level than the multichamber/plug. However, after approximately
10 seconds of flight, the multichamber/plug will become more nearly
optimumly expanded and its specific impulse will improve rapidly. At
altitude (vacuum), the 1200 psi propulsion system specific impulse will
be 13 seconds lower than that of the P&W multichamber/plug. That of the
2000 psi engine will be two seconds lower.

Upon throttling, the toroidal/aerospike vacuum specific impulse will be reduced
2.8 percent, while the multichamber/plug engine specific impulse loss will be
reduced only 0.7 percent. Approximately 55 percent of the burn time is at the
throttled thrust. There is a 23 second specific impulse difference (Pratt and
Whitney's multichamber/plug is 23 seconds higher than Rocketdyne's 1200 psi
toroidal) during throttling. The trajectory averaged specific impulse for the
Pratt and Whitney multichamber/plug is approximately seven seconds higher
than that of the Rocketdyne 2000 psi toroidal and approximately 12 seconds more
than that of the Rocketdyne 1200 psi toroidal.

The net effect of the above, discounting engine weight attributable to the
multichamber/plug would be a significant increase in payload capability.
The multichamber/plug propulsion system weight will, however, be 66 percent
heavier than that of the 1200 psia toroidal propulsion system and 38 percent
higher than that of the 2000 psia toroidal propulsion system.

These off-setting factors will result in the multichamber/plug propulsion system
vehicle placing a greater total weight into orbit (payload plus stage). However,
the payload weight will be lower than that of the 2000 psi toroidal system.
The 1200 psia toroidal/aerospike systems lower specific impulse will not be
quite off-set by its lower weight. The payload comparison showed that the 1200
psi toroidal/aerospike and the multichamber/plug will have almost identical
payload capabilities.

TABLE 4.3.8.2-I   PROPULSION SYSTEM PERFORMANCE COMPARISON

Propulsion Contractor		Rocketdyne			Pratt & Whitney
Propulsion System		Toroidal/Aerospike		Multichamber/Plug	Multichamber/Plug
Parameter Operating Pressure		(1200)	(2000)	(Classified)	(Classified)
Sea Level Thrust, lbs		8.0M	8.0M	8.0M	8.0M
Chamber Pressure, psia		1200	2000	3000	3000
Mixture Ratio, O/F		6:1	6:1	6:1	6:1
Diameter, ft.		57	57	57	57
Nozzle Length (% of 15° Core)		10	10	20	-
Area Ratio		80	139	198	206
Engine Length, ft.		11	11	21.8	25.5
Sea Level Specific Impulse*		-5	+7	-20	0
Altitude Specific Impulse*		-13	-2	-10	0
Throttled Specific Impulse*		-23	-13	-11	0
Propulsion System Weight**		100	119.7	166.3	165.7
Number of Bell Modules		-	-	24	24
Module Area Ratio		-	-	67	67
Bell Module Length, ft.		-	-	9.6	11
Nozzle Length (10% of Isentropic Length) ft.		-	-		26

* Shown as a Delta Specific Impulse with the Pratt and Whitney Multichamber/Plug as Standard

** Shown as a Percentage of 1200 psia Toroidal/Aerospike Weight

378

4.3.8.2   (Continued)

e.   Pressurization - The pressurization system used for the MLLV core will be
    identical regardless of whether the multichamber/plug propulsion system or
    the toroidal/aerospike system are used.

    The following factors permit the use of identical systems:

    1.   Stated NPSH requirements of the toroidal and multichamber engines are identical.

    2.   The hardware forward of the engines is assumed to be the same, producing
         identical flow losses.

    3.   Trajectories of the two vehicles are similar resulting in approximately
         the same fluid acceleration head at the engine inlets.

    4.   Maximum propellant vapor pressure will be the same for both configurations.

f.   Flight Performance - Flight trajectories were flown for the single-stage-to-
    orbit vehicles with the 1200 psia and 2000 psia toroidal propulsion systems and
    the multichamber/plug propulsion system.

    The vehicles with the multichamber/plug propulsion system delivered 852,815
    pounds to 100 N. mile orbit of which 471,649 pounds were payload. The remainder
    was the stage drop weight. The stage mass fraction was 0.936.

    The vehicle with the 1200 psia toroidal propulsion system delivered 794,696
    pounds to orbit of which 472,200 pounds were payload. The remainder was
    the stage drop weignt. The stage mass fraction was 0.945.

    The vehicle with the 2000 psia toroidal propulsion system delivered 828,360
    pounds to orbit of which 491,054 pounds were payload. The remainder of which
    was stage drop weight. The stage mass fraction was 0.943.

    A comparison of the flight parameters show that the velocity, flight path angle
    accelerations and maximum dynamic pressures are approximately the same
    for each of the above vehicles.

4.3.8.3　　　Effect of Use of "Sequentially Staged" Strap-On Stages

An analysis was undertaken to determine the advantages of "sequentially staged" SRM strap-on stages to improved payload capability. Vehicles with both 156 inch and 260 inch solid motor strap-on stages were analyzed. The vehicles were launched in a modified zero stage mode. In the case of the vehicle with eight - 260" diameter SRM stages, six of the stages were ignited at launch. After the SRM propellant was expended, these stages were separated and the remaining two SRM strap-on stages were ignited. After the propellant was expended from these two stages, the stages were ejected and the main stage was ignited and used to insert the payload into orbit.

An equivalent type vehicle with 156 inch SRM stages launch in a modified zero stage mode required that 12 of the 16 strap-on stages be ignited at launch. After the propellant in the 12 SRM stages was depleted, the stages were ejected and the remaining four 156 inch SRM strap-on stages were ignited. These stages were separated after their propellant depletion and the main stage was ignited and used to insert the payload into orbit.

For this comparison, the mass fraction utilized for the 260" SRM strap-on stages was 0.90. For the 156 inch strap-on stages, a slightly lower mass fraction of 0.895 was assumed. This slightly lower mass fraction was assumed as some of the stage components such as instrumentation, electronics, TVC, nose cone, heat shields, raceways, environmental tunnels and attachment structures will not scale proportionally as SRM size is varied.

This comparison showed that the vehicle payload capability with eight 260 inch SRM strap-on launch in a "staged" trajectory mode will be approximately 1,950,000 pounds. For the vehicle with sixteen 156 inch strap-ons, also launched in a "staged" trajectory mode, the payload capability will be approximately 1,930,000 pounds.

A comparison of the vehicle with eight 260 inch SRM strap-ons launched in a "staged" mode versus the same vehicle with all strap-ons ignited at launch shows that approximately 200,000 pounds of additional payload can be delivered by the "staged" trajectory mode. This is approximately an 11 percent increase in payload capability. With the 156 inch SRM stages used in a "staged" mode, this payload increase is slightly less, i.e., 10 percent.

It was concluded that the staged trajectory mode may be a desirable launch mode which will provide additional payload capability. Additional analyses are required to assess the effects of certain vehicle environments and penalties. These effects include: drag losses, base losses, and penalties on the vehicle structure due to the SRMs not ignited at launch.

REFERENCES

1.0.0.0-1 NAS CR 73154, "Study of Advanced Multipurpose Large
Launch Vehicles", The Boeing Company, January 1968.

4.1.1.1-1 Saturn V Launch Vehicle with 260-Inch Diameter Solid Motors.
NASA Contract NAS8-21105, The Boeing Company Document
Number D5-13408.

4.1.1.1-2 Minuteman Strap-Ons for Saturn V Vehicles. NASA Contract
NAS8-5608 (TOA-36), The Boeing Company Document
D5-11424 and 2.

4.1.1.7-1 Pratt and Whitney FR-1415, "Study for Evaluation of Plug
Multichamber Configuration", NAS8-11436, Phase I Report.

4.1.3.1-3 Improved Saturn V Vehicles and Intermediate Payload Saturn V
Vehicles, NASA Contract NAS8-20266, The Boeing Company
Document Number D5-13183-3.

4.2.1.0-1 TM AE-64-16, "Results of an Experimental Investigation to
Determine the Aerodynamic Loading on Three Saturn Payloads"
Chrysler Report, 1964.

4.2.1.0-2 Tsien, Hseu - Shen, "Supersonic Flow on an Inclinded Body of
Revolution", Journal of the Aeronautical Sciences, Volume 5,
pp. 480-483, 1938.

4.2.2.1-1 Munk, M. M., "The Aerodynamic Forces on Airship Hulls",
NACA TR No. 184, 1923.

4.2.2.1-2 Pitts, Nielson, and Kaatari, "Lift and Center of Pressure of
Wing-Body-Tail Combination at Subsonic, Transonic, and
Supersonic Speeds", NACA Report 1307.

4.2.2.3-1 Schlichting, Hermann, "Boundary Layer Theory", McGraw
Hill Book Company, Inc., 1960.

4.2.2.3-2 Morgan, James, R., "Experimental Static Longitudinal Stability
and Axial Force Characteristics of the Saturn V Chemical, Rift
and Nuclear Vehicles", MSFC Memo M-AERO-E-244-63.

4.2.2.3-3 Report PWA FR 1415, Section VIII, Pratt and Whitney,
October 1965.

REFERENCES (Continued)

4.2.2.3-4   NASA TRR-6, "Experimental & Theoretical Studies of
              Axisymmetric Free Jets", by Eugene S. Love, Carl E. Grigsby,
              Louise P. Lee, and Mildred S. Woodling, dated 1959.

4.2.2.3-5   Aerojet-General Corporation Letter #SRO-68-5500C-L-98,
              September 26, 1968 (shown in Volume IX, Appendix C).

4.2.4.6-1   Boeing Document BHA-0235, "General MATRIX Manipulator
              Program", dated May 14, 1968.

4.2.4.6-2   Dynamics of Structures, Walter C. Hurty and Moshe F. Rubinstein,
              Prentice-Hall Inc., 1964.

4.2.4.7-1   Gruner, W. J., Johnston, G. D., "An Engineering Approach to
              Prediction of Space Vehicle Acoustic Environments".

4.2.4.8-1   Barrett, R. E., "Techniques for Predicting Localized Vibratory
              Environments of Rocket Vehicles". NASA Technical Note D-1836.

4.2.4.8-2   "Saturn S-IC - 503 Static Test, Vibration Acoustic Data", Boeing
              Document D5-13644-3.

4.2.4.9-1   NASA TMX-53328, "Terrestrial Environment Criteria Guidelines
              for use in Space Vehicle Development", 1966 Revision.

4.2.6.4-1   NASA TN-D-1454, "A General 7090 Computer Program for
              Computation of Chemical Equilibrium Compositions, Rocket
              Performance and Chapman-Jouguet Detonations", S. Gordon,
              October, 1962.

4.2.7.2-1   Radiation Heat Transfer, E. M. Sparrow and R. D. Cess, Brooks
              Cole Publishing Company, Belmont, California, 1966.

4.2.7.2-2   A New and Simpler Formulation for Radiative Angle Factors,
              E. M. Sparrow, Journal of Heat Transfer, Volume 85, Ser. C,
              No. 2, pp. 81-88, 1963.

4.3.3.1-1   D5-13272, "Analysis of Stability Critical Orthotropic Cylinders
              Subjected to Axial Compression", 1966.

4.3.3.1-2   Kuhn, Paul, "Stress in Aircraft and Shell Structures". McGraw-
              Hill Book Company, Incorporated, New York, 1956.

REFERENCES (Continued)

4.3.3.1-3   Shanley, F. R., "Weight Strength Analysis of Aircraft Structures".
               Dover Publications Incorporated, New York, 1960.

4.3.3.1-4   NASA-MSFC Astronautic Structures Manual.

4.3.3.2-1   "MLLV Plug Cluster Rocket Engine Performance", Pratt and
               Whitney Report No. PDS-2957, September 13, 1968.

4.3.3.2-2   "Parametric Data for Advanced 02/H2 Aerospike and Multichamber
               Plug Nozzle Engines", Enclosure 2 to Rocketdyne Letter No.
               68RC12017, dated September 13, 1968.

4.3.3.2-3   "Advanced 02/H2 Engine Data for an 8,000,000 Pound Thrust Multi-
               purpose Large Launch Vehicle (MLLV)", Enclosure 2 to Rocketdyne
               Letter No. 68RC15283, dated December 20, 1968.

4.3.5.3-1   J. G. Schumacher and B. Lincoln, Development of Design Curves for
               the Stability of Thin Pressurized and Unpressurized Circular
               Cylinders, General Dynamics Corporation, Report AZD-27-275,
               dated 8 May 1959.

4.3.3.2-4   Thrust Vector Control - Plug Cluster, Pratt and Whitney,
               Report SRM FR-2325, dated 1966.

SYMBOLS

<u>PERFORMANCE</u>

$\dfrac{B_2}{B_1}$	Burn Ratio - Propellant Consumed at Reduced Thrust Divided by Propellant Consumed at Full Thrust
Percent Throttling	Amount of Thrust Reduction, Full Thrust Minus Reduced Thrust Divided by Full Thrust Times 100
AMR	Atlantic Missile Range
COV	Calculus of Variation Steering Routine
I_{sp}	Specific Impulse
N. MI., N.M.	Nautical Mile
Q, q	Dynamic Pressure
W	Weight
T	Thrust
g's	Longitudinal Acceleration. Gravities
λ'	Mass Fraction, Useable Propellant Divided by Total Stage Weight (Useable Propellant Plus Drop Weight)

<u>Subscripts</u>

M/C	Main Stage with Multichamber/Plug Propulsion System
IS	Injection Stage
P	Propellant
S	Strap-ons
PLD	Payload
o	Value at Start Burn (i.e., W_o = Lift-Off Weight)
d	Value at Stage Burn Out, (i.e., W_D = Drop Weight)

AERODYNAMICS

A, S	Area
C P/D	Center of Pressure, Calibers
C_A	Axial Force Coefficient
C_Z	Normal Force Slope, 1/RAD
C_{DO}	Total Vehicle Drag Coefficient at Zero Angle of Attack
M	Mach number
X/D	Calibers
q	Dynamic Pressure, Pounds Per Square Foot
α	Vehicle Angle of Attack, degrees

Subscripts

∞	Free Stream

DESIGN

AMLLV	Advanced Multipurpose Large Launch Vehicle
MLLV	Half-Size Multipurpose Large Launch Vehicle
F.S.	Field Splice
I.S.	Injection Stage
L/D	Stage Length to Diameter Ratio
POD	Pressure-fed Liquid Stage
SRM	Solid Rocket Motor
STA	Vehicle Station

SYMBOLS   (Continued)

A1   Aluminum

Be   Beryllium

Ti   Titanium

STRUCTURE

G   Longitudinal Acceleration

N   Axial Load Per Inch Circumference

OASPL   Overall Sound Pressure Level

OBSPL   Octave Band Sound Pressure Level

p^2 Acoustic Pressure Power Spectral Density $(psi)^2/cps$

SO   Strap-on Stages

G^2 Response Power Spectral Density g^2/cps

db, dB   Decibel, Reference Pressure 0.0002 dynes/centimeter^2

q   Dynamic Pressure, pounds per square foot

α Angle of Attack, degrees

η Longitudinal Load Factor

λ' Mass Fraction

ω_i Modal Frequency

ϕ_i Mode Shape Matrix

$[F]$ Total Vehicle Flexibility Matrix

$[M]$ Total Vehicle Mass Matrix

$[I]$ Identity Matrix

Subscripts

c	Compression
t	Tension

PROPULSION AND PRESSURIZATION

δ	Module Gap - Distance between bell nozzle exits
GH_2	Gaseous hydrogen
GHe	Gaseous helium
I_{sp}	Specific Impulse, $\dfrac{lbf - sec}{lbm}$
NPSH	Net Positive Suction Head, feet of fluid
LH_2	Liquid Hydrogen
LOX	Liquid Oxygen
M.R.	Mixture Ratio
P_a	Ambient Pressure
P_c	Engine Chamber Pressure
T_c	Engine Chamber Temperature
PU	Tank Ullage Pressure
SRM	Solid Rocket Motor
TVC	Thrust Vector Control
T/P	Turbopump
α	Nozzle Conical Half Angle
ϵ	Nozzle Expansion Ratio
γ	Ratio of Specific Heat

CONTROL & SEPARATION

Fineness Ratio	Vehicle Length Divided by Vehicle Diameter
A_0	Attitude Gain
A_1	Attitude Rate Gain
P/L	Payload
TVC	Thrust Vector Control
β_c	Commanded Thrust Deflection Angle
ν	Prandtl-Meyer Angle
θ_e	Attitude Error
$\dot{\theta}$	Attitude Rate
σ	Standard Deviation of Population

END

DATE

FILMED

NOV 19 1969